

REPORT DOCUMENTATION PAGE

AFRL-SR-AR-TR-02-

Public reporting burden for this collection of information is estimated to average 1 hour per response, including the time for gathering and maintaining the data needed, and completing and reviewing the collection of information. Send comments to: 1215 Jefferson Davis Highway, Suite 1204, Arlington, VA 22202-4302, and to the Office of Management and Budget, Paperwork Reduction Project (0704-0188) Washington, DC 20503.

PLEASE DO NOT RETURN YOUR FORM TO THE ABOVE ADDRESS.

1. REPORT DATE (DD-MM-YYYY) 05- 28 -2002		2. REPORT DATE Final Technical Report		3. DATES COVERED (From - To) 09-01-2001 to 02-28-2002	
4. TITLE AND SUBTITLE Gas and Chemical Lasers and Intense Beam Applications III				5a. CONTRACT NUMBER	
				5b. GRANT NUMBER F49620-01-1-0488	
				5c. PROGRAM ELEMENT NUMBER 61102F	
6. AUTHOR(S) Heaven, Michael C. Davis, Steven J.				5d. PROJECT NUMBER 2303	
				5e. TASK NUMBER EX	
				5f. WORK UNIT NUMBER	
7. PERFORMING ORGANIZATION NAME(S) AND ADDRESS(ES) Society of Photo-Optical Instrumentation Engineers (SPIE) PO Box 10 Bellingham, WA 98227-0010				8. PERFORMING ORGANIZATION REPORT NUMBER Volume 4631	
9. SPONSORING/MONITORING AGENCY NAME(S) AND ADDRESS(ES) Air Force Office of Scientific Research 801 N. Randolph Street, Room 732 Arlington, VA 22203-1977				10. SPONSOR/MONITOR'S ACRONYM(S) AFOSR/NL	
				11. SPONSORING/MONITORING AGENCY REPORT NUMBER	
12. DISTRIBUTION AVAILABILITY STATEMENT Approved for Public Release					
13. SUPPLEMENTARY NOTES ISBN 0-8194-4370-0					
14. ABSTRACT This proceedings contains papers on the following topics: Oxygen-Iodine Chemical Lasers; other chemical lasers; laser systems, modeling and interactions; COIL technology development.					
15. SUBJECT TERMS Laser					
16. SECURITY CLASSIFICATION OF:			17. LIMITATION OF ABSTRACT SAR	18. NUMBER OF PAGES 296	19a. NAME OF RESPONSIBLE PERSON Janice Gaines Walker
a. REPORT Non-classified	b. ABSTRACT	c. THIS PAGE			19b. TELEPHONE NUMBER (Include area code) (360) 676-3290

PROCEEDINGS OF SPIE



SPIE—The International Society for Optical Engineering

Gas and Chemical Lasers and Intense Beam Applications III

Steven J. Davis
Michael C. Heaven
Chairs/Editors

22–24 January 2002
San Jose, USA

Sponsored by
SPIE—The International Society for Optical Engineering

Cosponsored by
AFOSR—Air Force Office of Scientific Research (USA)



Volume 4631

20020617 038



PROCEEDINGS OF SPIE
SPIE—The International Society for Optical Engineering

Gas and Chemical Lasers and Intense Beam Applications III

Steven J. Davis
Michael C. Heaven
Chairs/Editors

22–24 January 2002
San Jose, USA

Sponsored and Published by
SPIE—The International Society for Optical Engineering

Cosponsored by
AFOSR—Air Force Office of Scientific Research (USA)



Volume 4631

SPIE is an international technical society dedicated to advancing engineering and scientific applications of optical, photonic, imaging, electronic, and optoelectronic technologies.



The papers appearing in this book compose the proceedings of the technical conference cited on the cover and title page of this volume. They reflect the authors' opinions and are published as presented, in the interests of timely dissemination. Their inclusion in this publication does not necessarily constitute endorsement by the editors or by SPIE. Papers were selected by the conference program committee to be presented in oral or poster format, and were subject to review by volume editors or program committees.

Please use the following format to cite material from this book:

Author(s), "Title of paper," in *Gas and Chemical Lasers and Intense Beam Applications III*, Steven J. Davis, Michael C. Heaven, Editors, Proceedings of SPIE Vol. 4631, page numbers (2002).

ISSN 0277-786X
ISBN 0-8194-4370-0

Published by
SPIE—The International Society for Optical Engineering
P.O. Box 10, Bellingham, Washington 98227-0010 USA
Telephone 1 360/676-3290 (Pacific Time) • Fax 1 360/647-1445
<http://www.spie.org/>

Copyright© 2002, The Society of Photo-Optical Instrumentation Engineers.

Copying of material in this book for internal or personal use, or for the internal or personal use of specific clients, beyond the fair use provisions granted by the U.S. Copyright Law is authorized by SPIE subject to payment of copying fees. The Transactional Reporting Service base fee for this volume is \$15.00 per article (or portion thereof), which should be paid directly to the Copyright Clearance Center (CCC), 222 Rosewood Drive, Danvers, MA 01923 USA. Payment may also be made electronically through CCC Online at <http://www.directory.net/copyright/>. Other copying for republication, resale, advertising or promotion, or any form of systematic or multiple reproduction of any material in this book is prohibited except with permission in writing from the publisher. The CCC fee code is 0277-786X/02/\$15.00.

Printed in the United States of America.

Contents

- vii *Conference Committee*
- ix *Introduction*
- xi *Description of first COIL demonstration, December 1977*
Oxygen-iodine chemical laser, W. E. McDermott, D. J. Benard, N. R. Pchelkin, R. R. Bousek

KEYNOTE PAPER

- 1 **Historical perspective of COIL (Keynote Paper)** [4631-01]
W. E. McDermott, NASA Ames Research Ctr. (USA)

SESSION 1 THE FIRST 25 YEARS OF COIL: PART I

- 13 **Mechanism and kinetics of iodine dissociation in COIL (Invited Paper)** [4631-02]
M. C. Heaven, A. V. Komissarov, V. Goncharov, Emory Univ. (USA)
- 23 **Gain and temperature in a slit nozzle supersonic chemical oxygen-iodine laser with transonic and supersonic injection of iodine (Invited Paper)** [4631-03]
S. Rosenwaks, B. D. Barmashenko, E. Bruins, D. Furman, V. Rybalkin, A. Katz, Ben-Gurion Univ. of the Negev (Israel)
- 34 **Chemical generation of atomic iodine for COIL** [4631-04]
O. Špalek, V. Jirásek, Institute of Physics (Czech Republic) and Institute of Inorganic Chemistry (Czech Republic); J. Kodymová, M. Čenský, Institute of Physics (Czech Republic); I. Jakubec, Institute of Inorganic Chemistry (Czech Republic)
- 43 **Modeling of the chemical generation of atomic iodine in a chemical oxygen-iodine laser** [4631-05]
V. Jirásek, O. Špalek, J. Kodymová, M. Čenský, Institute of Physics (Czech Republic)

SESSION 2 THE FIRST 25 YEARS OF COIL: PART II

- 53 **German COIL efforts: status and perspectives (Invited Paper)** [4631-07]
W. L. Bohn, DLR (Germany)
- 60 **Historical perspective of COIL diagnostics (Invited Paper)** [4631-08]
S. J. Davis, Physical Sciences Inc. (USA)
- 74 **Modeling of the gain, temperature, and iodine dissociation fraction in a supersonic chemical oxygen-iodine laser** [4631-09]
B. D. Barmashenko, E. Bruins, D. Furman, V. Rybalkin, S. Rosenwaks, Ben-Gurion Univ. of the Negev (Israel)
- 86 **Contribution of the COIL Laboratory in Prague to the chemical oxygen-iodine laser research and development (Invited Paper)** [4631-10]
J. Kodymová, O. Špalek, Institute of Physics (Czech Republic)

- 101 **COIL technology development at Boeing (Invited Paper)** [4631-11]
S. C. Hurlock, The Boeing Co. (USA)

SESSION 3 2002: 25 YEARS OF COIL

- 116 **History of COIL development in Japan: 1982–2002 (Invited Paper)** [4631-19]
M. Endo, Tokai Univ. (Japan); T. Uchiyama, Keio Univ. (Japan); K. Nanri, S. Takeda, T. Fujioka, Tokai Univ. (Japan)
- 128 **High-power COIL and YAG laser welding** [4631-20]
F. Wani, T. Nakabayashi, A. Hayakawa, S. Suzuki, K. Yasuda, Kawasaki Heavy Industries, Ltd. (Japan)
- 137 **COIL development in Kawasaki Heavy Industries, Ltd.** [4631-22]
T. Takada, F. Wani, K. Yasuda, Kawasaki Heavy Industries, Ltd. (Japan)
- 145 **Spatially resolved temperature diagnostic for the chemical oxygen-iodine laser based on a variant of saturation spectroscopy** [4631-23]
G. T. Phillips, G. P. Perram, W. B. Roh, Air Force Institute of Technology (USA)
- 154 **Diagnostic development for the ElectriCOIL flow system** [4631-24]
J. T. Verdeyen, D. M. King, D. L. Carroll, CU Aerospace (USA); W. C. Solomon, Univ. of Illinois/Urbana-Champaign (USA)
- 161 **Measurement of chemical oxygen-iodine laser singlet oxygen generator parameter using Raman spectroscopy** [4631-25]
W. Zhao, F. Sang, L. Duo, F. Chen, Y. Zhang, B. Fang, Dalian Institute of Chemical Physics (China)

SESSION 4 OTHER CHEMICAL LASERS

- 167 **Tunable diode laser gain measurements of the HF(2-0) overtone transitions in a small-scale HF laser (Invited Paper)** [4631-27]
C. F. Wisniewski, G. C. Manke II, G. D. Hager, Air Force Research Lab. (USA); P. G. Crowell, Northrup Grumman Corp. (USA); C. R. Truman, Univ. of New Mexico (USA)
- 178 **Atomic fluorine source for chemical lasers** [4631-29]
S. J. Davis, D. B. Oakes, M. J. Read, A. H. Gelb, Physical Sciences Inc. (USA)
- 184 **Parametric study of $\text{NCl}(a^1\Delta)$, $\text{NCl}(b^1\Sigma)$ from the reaction of $\text{Cl}/\text{Cl}_2/\text{He} + \text{HN}_3/\text{He}$** [4631-30]
L. Duo, S. Tang, J. Li, X. Min, F. Sang, B. Yang, Dalian Institute of Chemical Physics (China)
- 192 **Review of recent experiments and calculations relevant to the kinetics of the HF laser (Invited Paper)** [4631-14]
G. C. Manke II, G. D. Hager, Air Force Research Lab. (USA)
- 209 **Tunable solid state laser for HF mirror metrology** [4631-15]
A. L. Oien, T. J. Carrig, G. J. Wagner, C. J. Urbina, Coherent Technologies, Inc. (USA); J. W. Arenberg, TRW, Inc. (USA); J. A. Keene, Coherent Technologies, Inc. (USA)
- 217 **Imaging spectroradiometer for HF laser studies** [4631-16]
W. Rawlins, D. B. Oakes, P. A. Mulhall, S. J. Davis, Physical Sciences Inc. (USA)

- 225 **Room temperature rate constant for $H+F_2$** [4631-17]
J. Han, Emory Univ. (USA); G. C. Manke II, Air Force Research Lab. (USA); M. C. Heaven, Emory Univ. (USA)

SESSION 5 LASER SYSTEMS, MODELING, AND INTERACTIONS

- 234 **IR- and UV-laser interaction with metal surfaces (Invited Paper)** [4631-31]
V. F. Tarasenko, S. B. Alekseev, A. V. Fedenev, I. M. Goncharenko, N. N. Koval, K. V. Oskomov, V. M. Orlovskii, N. S. Sochugov, M. A. Shulepov, High Current Electronics Institute (Russia)
- 244 **Energy transfer dynamics in the $A(O_u^+)$ state of Bi_2** [4631-32]
J. L. Cox, M. W. Dolezal, R. E. Franklin, G. P. Perram, Air Force Institute of Technology (USA)
- 254 **Numerical testbed for laser materials processing** [4631-33]
M. S. Gross, I. Black, Heriot-Watt Univ. (UK); W. H. Müller, Technische Univ. Berlin (Germany)
- 264 **High-power-gas-discharge- and laser-plasma-based EUV sources** [4631-38]
F. Flohrer, K. Gäbel, D. Klöpfel, P. Köhler, I. Ahmad, S. Götze, J. Kleinschmidt, V. Korobotchko, J. Ringling, G. Schriever, U. Stamm, XTREME technologies GmbH (Germany)

POSTER SESSION

- 271 **Pulsed COIL with volume generation of iodine atoms in electric discharge** [4631-06]
N. N. Yuryshev, N. P. Vagin, A. F. Konoshenko, V. S. Paziuk, P.N. Lebedev Physical Institute (Russia)
- 280 **Observation on laser-induced lens effect in sound generation under water using high-power ultrashort-pulse laser** [4631-43]
H. He, Shanghai Institute of Optics and Fine Mechanics (China); S. Feng, Shanghai Acoustics Lab. (China)
- 284 **Plasma chemical oxygen-iodine laser: problems of development** [4631-46]
A. A. Ionin, P.N. Lebedev Physical Institute (Russia); A. P. Napartovich, Troitsk Institute for Innovation and Fusion Research (Russia); N. N. Yuryshev, P.N. Lebedev Physical Institute (Russia)
- 293 *Addendum*
- 295 *Author Index*

Conference Committee

Conference Chairs

Steven J. Davis, Physical Sciences Inc. (USA)
Michael C. Heaven, Emory University (USA)

Program Committee

Willy L. Bohn, DLR (Germany)
Ernest A. Dorko, University of New Mexico (USA)
Masamori Endo, Tokai University (Japan)
Gordon D. Hager, Air Force Research Laboratory (USA)
Jarmila Kodymová, Institute of Physics (Czech Republic)

Session Chairs

- 1 The First 25 Years of COIL: Part I
Steven J. Davis, Physical Sciences Inc. (USA)
- 2 The First 25 Years of COIL: Part II
Jarmila Kodymová, Institute of Physics (Czech Republic)
- 3 2002: 25 Years of COIL
Salman Rosenwaks, Ben-Gurion University of the Negev (Israel)
- 4 Other Chemical Lasers
Willy L. Bohn, DLR (Germany)
- 5 Laser Systems, Modeling, and Interactions
Steven J. Davis, Physical Sciences Inc. (USA)
Michael C. Heaven, Emory University (USA)

Introduction

We were pleased to chair the third Conference on Gas and Chemical Lasers and Intense Beam Applications at the San Jose Convention Center from 22-25 January 2002. We had announced at the second conference in 2000 that we planned to celebrate the 25th anniversary of the invention of the Chemical Oxygen Iodine Laser (COIL) at this conference. We were very pleased with the response to this call, and many excellent papers were presented. Indeed the 25th anniversary of COIL was the centerpiece of this conference.

One of our goals was to present the history of COIL from the first concepts through the exciting research and applications of COIL. Bill McDermott, one of the four COIL inventors, kicked-off the conference with a fascinating anecdotal history of COIL. This plenary paper set the tone for the rest of the sessions. Researchers from several of the leading COIL research facilities from around the world followed with descriptions of their research, and each presented some historical perspective of their contributions to the development of COIL.

The highlight of the conference was a special banquet held on January 22. This event honored the four inventors of COIL, Nick Pchelkin, Ron Bousek, Dave Benard, and Bill McDermott, shown below.



Photo Courtesy of Prof. Masamori Endo

Left to right: Nick Pchelkin, Ron Bousek, Dave Benard, and Bill McDermott at the COIL 25th anniversary banquet.

With the generous assistance of SPIE, we were able to bring the inventors to the conference and recognize their achievements. At the banquet, Mike Berman of the Air Force Office of Scientific Research (AFOSR) and a former COIL researcher, offered some interesting comments on the history of COIL and the early chemical laser research sponsored by AFOSR. Art Guenther, Chief Scientist of the Air Force Weapons Laboratory during the time of the first COIL, delivered a brief but insightful keynote address. Richard Hoover, President of SPIE in 2001, presented plaques to each of the inventors. The attendees were then entertained with comments and perspectives from each of the COIL inventors. We hope that the current COIL researchers enjoyed interacting with the early COIL pioneers.

In addition to the photo, we have also included in the following pages a description of the first COIL demonstration written by the four inventors in December 1977. Although we could not locate the two figures referred to in the text, the rest of the draft is original and serves as an appropriate introduction to this commemorative proceedings volume. We are grateful for the efforts of the organizing committee, and we would also like to thank all the speakers and authors for a most enjoyable conference. We would like to thank SPIE for helping to arrange the banquet and plaques. We also gratefully acknowledge AFOSR for support of the conference. This conference continues to grow in its ability to attract the top laser researchers in the world and to foster collaborations. We look forward to many more such meetings in the future.

Steven J. Davis
Michael C. Heaven

OXYGEN-IODINE CHEMICAL LASER

William E. McDermott, Major, USAF

David J. Benard, GS-13, USAF

Nicholas R. Pchelkin, Captain, USAF

Ronald R. Bousek, Major, USAF

Air Force Weapons Laboratory (AFSC)
Kirtland AFB, NM 87117

INTRODUCTION

Description

The oxygen-iodine laser is the first chemical laser to operate on an electronic transition. As a result, the wavelength (1.3 microns) is shorter than that of any other chemical laser.

The laser consists of four major components: (1) A chemical reactor produces a gaseous stream of excited oxygen molecules. (2) A cryogenic trap removes undesirable components (chlorine and water) from the oxygen flow. (3) A "spray bar" injects iodine vapor into the oxygen flow. Energy is transferred from excited oxygen to iodine atoms by collisions. (4) An optical resonator extracts energy from the iodine atoms, and lasing occurs at a wavelength of 1.315 microns.

Laboratory Development

The oxygen-iodine laser project was initiated at AFWL in January 1975 although preliminary experiments had been done as early as April 1973. The in-house work was supplemented with contract work through AFOSR (3 contracts), The Aerospace Corporation, Rockwell Science Center, and the Frank J. Seiler Laboratory (USAFA). The major advance - an efficient chemical source of $O_2(^1\Delta)$ - was an extension of the Seiler Laboratory's work done by the current AFWL in-house research team. On October 1977, the first generator producing adequate $O_2(^1\Delta)$ was built. Lasing was first achieved on 1 December 1977 (4 milliwatts). A second laser was designed and built to demonstrate efficient operation. This laser produced over 100 watts of output power in July 1978. Further work will be directed towards parameterization of the laser and understanding its operational characteristics.

Significance

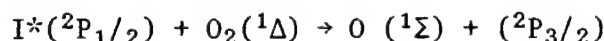
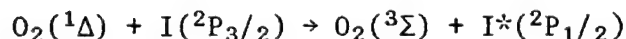
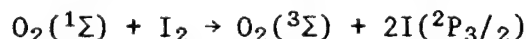
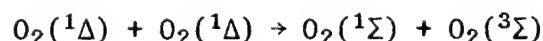
The wavelength is substantially shorter than other current high energy chemical lasers, so smaller optics and better beam focusing are possible. The efficiency is promising, so device size and weight may be smaller than for other high energy lasers.

ABSTRACT

Laser action in a purely chemically-pumped atomic iodine laser was first demonstrated at the Air Force Weapons Laboratory and has been extensively studied there. In this laser a heterogeneous chemical reaction between gaseous chlorine and a basic solution of hydrogen peroxide is used to produce a flowing stream of molecular oxygen in the excited $O_2(^1\Delta)$ electronic state. Molecular iodine is added to the flow and is dissociated into atoms by $O_2(^1\Delta)$ formed by energy pooling from $O_2(^1\Delta)$. Energy is transferred rapidly from $O_2(^1\Delta)$ to the iodine atoms, and CW lasing at 1315 nanometers occurs between electronic states of atomic iodine. Since all of the energy is supplied by a chemical reaction, this is the first demonstration of a purely chemically-pumped electronic-transition laser. Because its wavelength is shorter than that of other chemical lasers under development for high energy applications, smaller optics and better beam focusing are potential advantages. The theoretical efficiency in terms of energy per unit mass of reactants appears to be good. Computer modeling of the oxygen-iodine chemical kinetics indicates that the small signal gain profile can be suitably controlled to provide efficient lasing. The results of AFWL laser experiments and computer modeling aimed at characterizing the important parameters of the oxygen-iodine chemical laser will be discussed.

The use of a chemical reaction as a pumping mechanism for a laser was first demonstrated by Kasper and Pimentel,¹ who achieved lasing on various HCl vibrational transitions in a flash initiated H₂/Cl₂ mixture. The first pure chemical laser,² using no external power sources, was developed by Cool and Stephens. All such chemical lasers which have been developed to date operate on rotational-vibrational transitions within a single electronic state. Kasper and Pimental reported³ transient lasing on atomic iodine produced by the pulsed photolysis of CF₃I and CH₃I.

The oxygen-iodine laser is the first example of cw laser action on a transition between two distinct electronic states which is pumped only by a chemical reaction requiring no external sources of power. This laser operates on the ²P_{1/2}-²P_{3/2} transition of the iodine atom at 1315 nm and is pumped by the reaction scheme



The fourth step in this scheme is critical in that it guarantees total dissociation of the I₂ by a "positive feedback" type of kinetics. This effect is relevant since I₂ is an efficient quencher of I*(²P_{1/2}). The use of the reaction scheme (1) as a pumping mechanism for iodine was first suggested by the work of Derwent and Thrush⁴ who found that the quenching rate of O₂(¹Δ) by ground-state iodine atoms was rapid ($k = 4.6 \pm 1.5 \times 10^{13} \text{ cm}^3 \text{ mol}^{-1} \text{ sec}^{-1}$) and calculated the equilibrium constant to be 2.9. MacKnight and Modreski⁵ noted that a 15% ratio of O₂(¹Δ) to total oxygen would support an inversion in the iodine atom. Several investigators^{6,8} attempted to produce a laser using excited oxygen obtained via microwave discharge or by various chemical schemes. These authors also developed improved kinetic models which raised the necessary O₂(¹Δ) percentage required to about 25% and⁹ determined the optimum I₂ pressure. In the most recent experiments⁹ it was demonstrated by chemical pumping and energy transfer that inversion of the spin orbit states of atomic iodine had been achieved.

In¹⁰ our experiments a chemical generator based on the work of Seliger¹⁰ was used to produce $O_2(^1\Delta)$ from the reaction of chlorine with basic H_2O_2 . Figure 1 shows the generator design.

Five liters of 90% H_2O_2 and 2 liters of 6N NaOH were admitted to the reactor through the reagent feed lines at the top of the generator. During the loading operation, N_2 was continuously flowed through the bubbler to preclude liquid from entering the bubbler itself and to provide good mixing of the H_2O_2 and NaOH. The mixing of the base and peroxide is an exothermic process that can lead to a run away decomposition of the H_2O_2 if the generator temperature exceeds $60^\circ C$. To prevent this, the reagents were mixed in the generator under vacuum, so that evaporative cooling due to the pumping off of water vapor maintained an operating temperature below $30^\circ C$. This mixing process also has the advantage of concentrating the base-peroxide mixture that is used to generate the $O_2(^1\Delta)$.

The $O_2(^1\Delta)$ was generated via the reaction of Cl_2 gas with the basic H_2O_2 solution. The Cl_2 was admitted to the generator through the bubbler structure. Most of the Cl_2 was reacted in the generator and the oxygen production was approximately stoichiometric with the Cl_2 flow rate of 0.03 moles/sec. The effluent from the chemical generator was passed through a liquid nitrogen cold trap of standard reentrant design to remove water vapor and unreacted Cl_2 . The $O_2(^1\Delta)$ concentration was measured at the exit of the cold trap by monitoring the 1270 nanometer emission ($a^1\Delta \rightarrow X^3\Sigma$) with a narrow bandpass filter and a cooled intrinsic Ge detector. Typical results were approximately 35% $O_2(^1\Delta)$ at pressures of 1 torr in the laser cavity. The distance from the midplane of the generator to the inlet of the laser cavity was approximately 3 meters.

The laser section itself (Figure 2) consisted of a gradual expansion duct from 7.6 cm diameter glass pipe (cross sectional area = 45.6 cm^2) to a 50 cm x 2.54 cm (cross sectional area = 127 cm^2) rectangular duct. The rectangular section was terminated into the side of a 15 cm diameter pipe that was connected to a high capacity vacuum pump. The inner surface of the stainless steel laser cavity was coated with halocarbon grease to minimize $O_2(^1\Delta)$ wall deactivation and iodine atom recombination. The laser mirrors were mounted internally to the vacuum on tubes extending from either side of the flow region. The mirrors were separated by 1.36 meters. Each mirror tube was purged with a small flow of Argon during operation of the laser.

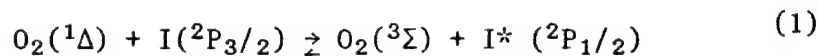
Molecular iodine was injected with a carrier flow of Ar into the oxygen flow via an I_2 bomb heated to approximately $50^\circ C$. The injector itself was a 1 cm OD. stainless steel tube with a thin (0.25 mm) slot

42 cm long milled along its length. The injector tube was centered in the rectangular flow channel approximately 6 cm upstream of the cavity axis with the slot on the downstream side. The injector tube was also resistively heated in order to prevent condensation of I₂ on the interior.

The limiting apertures in the laser cavity were the walls of the flow tube and the inside diameter of the mirror support tubes. Using a > 99.9% maximum reflectance flat back mirror and a 98.3% reflectivity (1.7% transmitting) 5m radius of curvature front mirror the laser output was sufficient to easily burn a mode pattern into a black plastic plate in a few seconds. The mode pattern was equal in size and shape to the area of the limiting aperture (2.5 cm high x 4 cm in the flow direction) and an output power of approximately 100 watts was measured using a Scientech disk calorimeter. Operation of the laser was dependent upon generator performance but was easily reproducible.

DISCUSSION

The extractable O₂(¹Δ) energy can be determined from the equilibrium constant, K, of the pumping reaction:



where

$$K = \frac{[\text{I}^*(^2\text{P}_{1/2})] [\text{O}_2(^3\Sigma)]}{[\text{I}(^2\text{P}_{3/2})] [\text{O}_2(^1\Delta)]} = 2.9(300^\circ\text{K})$$

and the zero gain condition on the inversion density:

$$\frac{\text{I}(^2\text{P}_{1/2})}{\text{I}(^2\text{P}_{3/2})} = 0.5$$

An $[O_2(^1\Delta)]/[O_2(^3\Sigma)]$ ratio of .17 is therefore required to maintain positive gain. Consequently, the extractable energy in the flow corresponds to the $O_2(^1\Delta)$ in excess of 17% of the total O_2 . Thus with 35% $O_2(^1\Delta)$, about 18% of the total O_2 can contribute to laser output. For our conditions, the extractable energy was 600 watts giving a conversion efficiency in the laser itself of 15%. In these experiments the conversion efficiency was less than 100% because, as will be shown, the laser was overcoupled resulting in inadequate saturation of the lasing medium.

The rate of stimulated emission based on the measured output power aperture size, mirror transmission, and a Doppler broadened stimulated emission cross section was $1.5 \times 10^4 \text{ sec}^{-1}$. The rate of loss of excess $O_2(^1\Delta)$, however, is given by the rate of stimulated emission times the ratio of iodine to excess oxygen. At an iodine partial pressure of 5×10^{-3} torr and the optimal lasing conditions, the rate of excess $O_2(^1\Delta)$ loss was approximately 300 sec^{-1} due to stimulated emission and energy transfer. The rate of loss of $O_2(^1\Delta)$ due to the flow through the resonator cavity is V/L ($V = 60 \text{ m/sec}$, $L = 4 \text{ cm}$) or 1500 sec^{-1} . The expected efficiency is therefore approximately $300/(1500 + 300)$ or 15%. In this analysis the energy transfer rate can be assumed to be very large in comparison to the stimulated emission rate which is then the rate limiting step. Since the forward transfer rate is approximately gas kinetic this assumption is clearly correct.

The optimum mirror outcoupling based on the estimated gain of 5% per round trip and assuming non-productive mirror losses of 0.1% is around 0.5%. Reducing the outcoupling would cause a corresponding increase in the intracavity intensity and therefore accelerate the stimulated emission rate causing greater laser output to occur as the O_2/I mixture flows through the laser cavity. Alternatively, a longer resonator section would permit greater time for extraction of the $O_2(^1\Delta)$ energy and thus increase the laser output as well.

In summary, this experiment has demonstrated the feasibility of highly efficient operation of the oxygen-iodine chemical laser. The authors wish to acknowledge the technical assistance of Gary Lee, Pat Timlin, Ken and Don Maier and Charles Fry. The authors are especially indebted to our glass blower Jan Marien, who constructed the large glass traps required for this laser demonstration.

REFERENCES

1. J.V.V. Kasper and G.C. Pimentel, Phys. Rev. Lett. 14, 352 (1965).
2. T.A. Cool and R.R. Stephens, J. Chem. Phys. 51, 5175 (1969).
3. J.V.V. Kasper and G.C. Pimentel, Appl. Phys. Lett. 5, 231 (1964).
4. R.G. Derwent and B.A. Thrush, Faraday Discuss Chem. Soc. 53, 162 (1972).
5. A.K. MacKnight and P.J. Modreski (unpublished).
6. R.D. Franklin, A.K. MacKnight, and P.J. Modreski, Electronic Transition Lasers, edited by T.I. Steinfeld (The MIT Press, Cambridge, Mass., 1976), p. 119.
7. A.K. MacKnight, R.D. Franklin, and R.L. Kerber, Electronic Transition Lasers II, edited by L.E. Wilson, S.N. Suchard, and T.I. Steinfeld (The MIT Press, Cambridge, Mass., 1977), p. 305.
8. R.F. Heidner III (unpublished).
9. A.T. Pritt, Jr., R.D. Coombe, D. Pilipovich, R.L. Wagner, D. Benard, and C. Dymek, Appl. Phys. Lett. 31, 745 (1977).
10. H.H. Seliger, J. Chem. Phys. 40, 3133 (1964).

Historical Perspective of COIL

William E. McDermott
Chief Technology Officer
Directed Energy Solutions

ABSTRACT

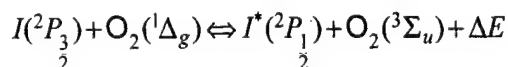
The oxygen-iodine laser was the first electronic transition chemical laser. It first lased 25 years ago at the Air Force Weapons Laboratory (now the Air Force Research Laboratory). The development started several years earlier and involved the support of many people in the laser community. I would like to describe the early thoughts, insights and even misconceptions that we had in the early days. I will also highlight the contributions of many of the people and organizations that contributed to the early development of the COIL laser.

1. A Brief Background on $O_2(^1\Delta_g)$

Chemical sources of $O_2(^1\Delta_g)$ have been known for many years. Mallet [1] first reported the red glow obtained when hypochlorite solution and hydrogen peroxide was mixed. The $O_2(^1\Delta_g)$ molecule was first identified by Herzberg in the spectrum of the sun in 1934. Groh [2] mentions the red chemiluminescence obtained when gaseous chlorine or bromine is added to basic hydrogen peroxide. Later, Groh & Kirriman [3] mixed gaseous chlorine with KOH and hydrogen peroxide and proposed that the red glow is from two $O_2(^1\Delta_g)$ molecules colliding. Later, Seliger [4] published the spectra of the hypochlorite – peroxide reaction in the red at 634 nm. For me, the seminal article on excited oxygen was Khan and Kasha [5]. Even though the chemical process that produced a metastable electronically excited species was known, the marriage of oxygen and iodine came in discharge studies.

2. Iodine and $O_2(^1\Delta_g)$

The reaction of iodine and discharged oxygen was first reported by Ogryzlo and his group [6]. They observed that when iodine was added to excited oxygen, a bright yellow glow was seen. This was recognized as I_2 B state emission. They also observed a strong emission at 1.315μ , the iodine atom $^2P_{1/2} - ^2P_{3/2}$ transition. The excitation of the iodine was attributed to the near resonant pumping by $O_2(^1\Delta_g)$. The iodine atoms were thought to be formed by the dissociation of molecular iodine by $O_2(^1\Sigma_u)$. This work didn't attract the attention of the laser community until later. In 1969, Elmer Ogryzlo went on sabbatical to Brian Thrush's laboratory in England. There he suggested the oxygen-iodine system as an interesting system for Thrush's graduate student, R. G. Derwent. The suggestion generated several papers [7], [8], [9], [10], and [11]. In their third paper, they suggested that an inversion could be achieved on the iodine atom $^2P_{1/2} - ^2P_{3/2}$ transition if a sufficient $O_2(^1\Delta_g)$ fraction could be produced. Using the equilibrium constant for the energy pumping reaction, They showed a flow containing about 15% $O_2(^1\Delta_g)$ could produce an inversion on the iodine $^2P_{1/2} - ^2P_{3/2}$ transition. It was radical to propose an equilibrium as a pumping reaction – in a two level system terminating in the ground state!



$$\Delta E = 279 \text{ cm}^{-1}$$

$$K_{eq} = 0.75e^{\frac{401.42}{T}}$$

$$\alpha = \sigma_0 \left(\left[I(^2P_{1/2}) \right] - \frac{1}{2} \left[I(^2P_{3/2}) \right] \right)$$

$$\alpha > 0 \text{ for}$$

$$\frac{O_2(^1\Delta_g)}{O_2(^1\Delta_g) + O_2(^3\Sigma_u)} > 14.5\%$$

at T = 300K

3. The Search for a Chemical Source of $O_2(^1\Delta_g)$

This paper produced a considerable amount of interest at the Air Force Weapons Laboratory (AFWL); who, like many other research organizations, had developed an interest in short wavelength chemical lasers. The first advocate was Dr. Al MacKnight who brought the Derwent and Thrush article to my attention. I had just arrived at the Air Force Academy (USAFA), where I was teaching Instrumental Analysis in the Chemistry Department. I had been selected to spend the next year as an exchange officer to the Frank J. Sieler Research Laboratory (FJSRL) – a part of the Air Force Office of Scientific Research (AFOSR) – and was looking for research projects of interest to the Air Force. I had visited the AFWL the previous year and met a number of the technical people there. In the summer of 1973, I began working on electronic transition chemical lasers. The initial funding for the effort was \$10,000 provided by Dr. Don Ball, then head of AFOSR. This money went towards purchase of an S-1 photomultiplier and electronic data recording equipment. I began to look at a number of systems including the Ba-N₂O-CO system, the reaction of SnH₄ with N₂O, and various alkali metal – oxidant systems. These were experiments in which the species were burnt in a flame or mixed in the afterglow of a microwave discharge and the spectra recorded. Nothing much of interest came from these experiments. In those days, we didn't have the Internet to browse; so I would spend hours in the library tracking down references. I was aware of the hypochlorite – peroxide method of producing $O_2(^1\Delta_g)$ since Al MacKnight was doing experiments with that system as well as microwave discharges. One day – I think it was in mid-1974 – I ran across the Khan and Kasha article. Michael Kasha was doing biomedical research on the possible role of $O_2(^1\Delta_g)$ in cancer. He had just gotten a new graduate student – A.U. Khan. Michael told me later that he wanted to see what this new guy could do in the lab, so he gave him the problem to record the spectrum of $O_2(^1\Delta_g)$. About a week later, he came back with the spectrum. Khan had built a small bubbler shaped somewhat like a saxophone (hence the name "Hirtzian device" – after Al Hirt, a famous New Orleans jazz musician) with a fritted disk at the end. He bubbled chlorine gas through a basic solution of hydrogen peroxide and recorded the spectra. In the article that I saw, a print of the spectrum of the emission in the 1.27 μ region was attached. It had been recorded on photographic film at good resolution. The text did not mention what I saw in the spectrum. It was clearly rotationally resolved! There seemed to be no continuous emission between the rotational lines. Since molecules in solution are strongly perturbed during emission by collisions, emission from molecules in solution will not show rotational structure. The emission Ahsan Khan saw was from the gas phase. At that point, I was convinced that the liquid phase reaction between chlorine and basic hydrogen peroxide could produce high yields of gaseous $O_2(^1\Delta_g)$.

4. Early Research on Chemical Sources

4.1. *Air Force Weapons Laboratory (1973 – 1977)*

At the AFWL, Al MacKnight pursued a number of approaches to establish oxygen-iodine as a laser. First, a number of flow studies were done and several attempts were made to lase using microwave excited oxygen as a source. None of the laser experiments were successful. MacKnight also tried to react gaseous hydrogen peroxide with calcium hypochlorite to produce $O_2(^1\Delta_g)$ which was also unsuccessful. The AFWL did, however, support a number of research projects to develop a COIL laser. It also encouraged AFOSR to support additional University research such as my effort at the USAFA.

4.2. *University of California, Santa Barbara (1975-1977)*

At the Quantum Institute at the University of California at Santa Barbara, Paul Lee and Warren Slafer attempted to build a chemical generator using bromine or chlorine condensed on a rotating dewar. The frozen halogen was then sprayed with basic hydrogen peroxide. It was reported to work adequately (~25%) and was delivered to the AFWL in early 1977. It didn't seem to catch the interest of the researchers there at the time.

4.3. Rockwell Science Center (1976-1978)

A more important effort was started at Rockwell Science Center by Bob Coombe and his collaborators – A. T. Pritt, I. B. Goldberg, D. Pilipovich, and R. I. Wagner. The investigation centered on the use of chlorine fluorosulfate (ClOSO_2F) and BHP. The effort was less important in the details of the chemical generation process and more important that it produced the first measurement of gain in a chemical pumped iodine system [12]. We discovered later that chlorine fluorosulfate and BHP generates chlorine gas which then reacts with the excess BHP to produce $\text{O}_2(^1\Delta_g)$. Ira Goldberg also recognized the value of EPR as a measurement standard for excited oxygen and used it in these studies.

4.4. Air Force Academy (1973-1976)

After reading the Kasha and Khan article, I embarked on devising a way to use the reaction between chlorine and BHP to produce gaseous $\text{O}_2(^1\Delta_g)$. I reasoned that the control of the gas-liquid interface was important and that the reaction would have no hope of producing a high yield of excited oxygen unless the reaction rate of chlorine with BHP was faster than the quenching rate of $\text{O}_2(^1\Delta_g)$ on BHP. The first experiment was to determine the rate of reaction of chlorine with BHP. Since funding was limited, we couldn't look at the disappearance of chlorine as it reacted with BHP; so we studied the reaction of chlorine with NaOH. We could follow that reaction with a pressure gauge. Chemically, these reactions should be about equal in rate. A recording mercury manometer was devised (we couldn't afford a capacitance manometer) to measure the pressure drop as chlorine passed over concentrated NaOH solution. John Viola, who was also teaching at USAFA, was a great help in designing and running these experiments. The apparatus is described in a note [13]. We found that the sticking coefficient of chlorine with NaOH was about 10^{-2} . We reasoned that the quenching coefficient of $\text{O}_2(^1\Delta_g)$ on BHP would be less than 10^{-5} , therefore it appeared that the system would work. The real question in my mind was how we could accurately measure the yield of excited oxygen relative to the ground state. I gave a seminar to the Physics Department in 1974 and mentioned the lack of a good method to measure the excited oxygen yield. At the end of the seminar, one of the Physics instructors, Dave Thomas, came up to me and suggested that gas phase electron paramagnetic resonance (EPR) could measure both ground state and excited oxygen. Even more important, there was an EPR in one of the Physics laboratories. With Dave's help, we soon showed that we could measure both species accurately. At this point, we built a small rotating wetted wall generator that we could attach to the EPR. It is shown schematically in Figure 1.

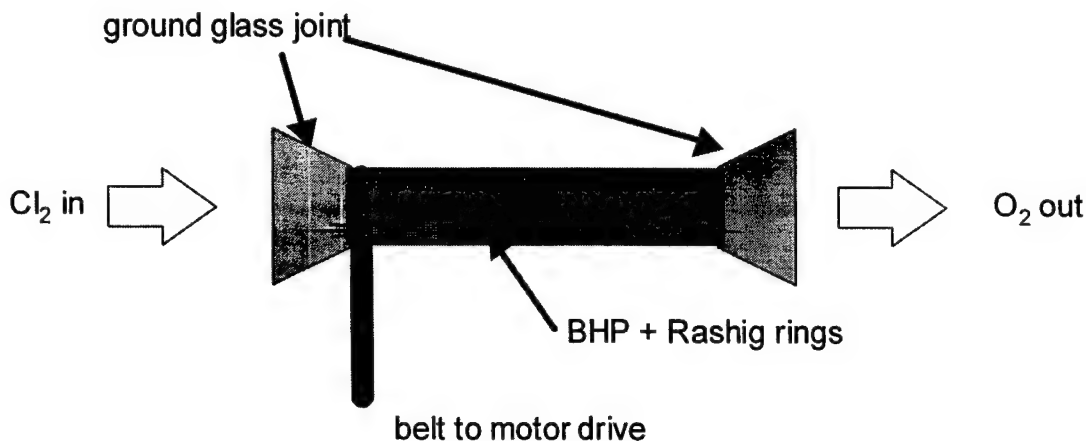


Figure 1 The first >15% chemical generator

Among the experiments I was able to do while at USAFA was observation on the EPR of $^2\text{P}_{1/2}$ iodine atoms excited by the chemical generator. This showed that the water produced by the reaction did not stop the

iodine dissociation process. The performance, a yield greater than 15% at the generator, was reported at the Second Summer Colloquium on Electronic Transition Lasers [14]. By then, I had left the USAFA and was attending a one-year Air Force middle management school. I was able to attend the conference because AFOSR provided funds. The paper did not generate any interest in the community.

It was extremely important during this early period to be able to discuss the problems of chemical lasers with many of the experts in the field. AFOSR and AFWL funding gave the researchers an opportunity to interact with many of the best scientists of the 20th century. Herb Broida and Dick Zare came to mind as people who were always available to help in anyway they could. Elmer Ogryzlo and J.C. Polyani both came to the USAFA under AFOSR funding to discuss electronic transition chemical lasers with me.

5. Early COIL Work at AFWL (1977 – 1981)

On arriving at AFWL in late 1977, there was already a well-equipped laboratory. It contained a flow system, laser cavity and EPR system. It had been configured to test the generator developed at RSC. I inherited the iodine laser team, which consisted of Nick Pchelkin, Dave Benard and a couple of technicians. Down the hall, I had access to one of the best experimental physicists in the world – Steve Davis. I had turned down Leroy Wilson's offer to work on a "real, short term, high payoff" system called ALFA. The first few months were occupied with two problems. The first was that the "system" model developed at AFWL predicted that more than 25% $O_2(^1\Delta_g)$ was required to achieve threshold. Any generator had to beat this new, higher standard. In fact, I was able to show that the model incorrectly calculated the equilibrium constant and that Derwent and Thrush were right after all [15]. The second problem was an article by two scientists at the Naval Research Laboratory who measured the branching ratio between the pumping reaction and the non-resonant branch [16]. The experiment used photodissociation of alkyl iodides as a source of $I(^2P_{1/2})$. Their value was 40%. Clearly, if that were true, there would never be a sustained inversion. I never could figure out what they did wrong. I knew their answer was inconsistent with the experiments I did at USAFA and Dave Benard's measurement of gain at RSC. Always believe the experiment that most closely duplicates what you are trying to do.

By this time, the management was getting upset with the "slow" pace of our effort to get the CFS generator running and directed me to stop advocating the chlorine – BHP reaction and immediately install a CFS system on the test stand. Being a good soldier, I called Nick Pchelkin in and asked him how long it would take to get a chlorine line plumbed into the lab. His answer was 8 AM tomorrow morning – I told him to do it. I then had a short meeting with Nick and Dave Benard to figure out what generator to start testing with. I advocated my rotating, wetted wall device. Nick didn't like that because it would take too long to build. I described the Khan and Kasha experiment and Nick was pretty excited because he could have a bubbler ready by the next day. I didn't think a bubbler would work because we didn't have a direct control of the gas-liquid interface. But you never know until you try the experiment, so I told Nick to go ahead with the bubbler. It is shown in Figure 2. We measured over 35% $O_2(^1\Delta_g)$ on the EPR the first time we turned on the device. In the experiment, I found I was able to control the gas-liquid interface by a combination of liquid depth and flow rate. In fact, the term bubbler was a misnomer. I really pumped the chlorine through the liquid at a very high rate – the flow formed conical channels and the liquid was pretty violently agitated. Chemical engineers call that a sparger.

At this point, lasing was not far off. As usual, we were still having trouble getting enough iodine into the laser, so Dave Benard redesigned the iodine source. Nick Pchelkin also rigged up a $O_2(^1\Delta_g)$ meter using a pressure tap and the photometric detector we had cross calibrated with the EPR. We were not using diluent so pressure was a measurement of total oxygen and chlorine. The "yield" was really $O_2(^1\Delta_g)$ divided by chlorine in. The detector was at the exit of the laser cavity. Dave suggested the most important diagnostic. Two IR detectors with narrow band 1.315 μ filters were placed on the laser cavity – one looking down the optical axis; the second on the side perpendicular to the laser axis. The latter measured spontaneous emission and the former laser emission. Nick had these fed to an X-Y recorder. As $O_2(^1\Delta_g)$ was added before the mirrors were aligned, the two signals tracked linearly. As we tweaked the mirrors, we could recognize a positive change by an increase in the end emission as the side emission stayed constant. On 1 Dec 1976, the end emission suddenly shot off scale for the first time announcing laser action. We also had an IR phosphor

card. It showed a distinct higher order transverse mode. It looked like the 2,6 Hermite-gaussian mode shown on page 688 of Siegman [17]. The $O_2(^1\Delta_g)$ meter normally oscillated between 35% and 40%; but when the laser turned on, it immediately dropped to a rock constant 15%. During the several minutes of 4 mW lasing, the mode actually jumped several times. It was a pretty exciting day [18].

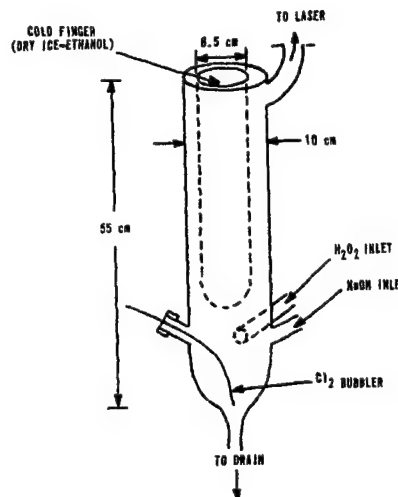


Figure 2 The first oxygen generator to power a laser.

That evening, Dave and Nick went out to dinner and designed the next laser on a napkin while waiting for their steak to be delivered. I scaled up the generator to match the transverse flow channel the next day. It would have been ready in a week if we had been able to get the laser built outside, but we were required to use the base model shop which took 6 months to build the laser cavity. In the meantime, Dave borrowed a small transverse flow cavity from Johns Hopkins that we used for flow studies. This was called COIL II. The second laser was called COIL III for that reason. It produced over 100 watts – a 25,000 times scale up [19].

The next few years were an exciting time. We had tremendous support from Pete Avizonis, the AFWL Chief Scientist, who became – and remains to this day – an ardent advocate of the COIL laser. Rick Heidner contributed the first systematic study of iodine dissociation [21]. The results were not always positive. Rick's work, coupled with some ab initio calculations done by Harvey Michaels; suggested that dissociation did not occur from the $O_2(^1\Sigma)$ channel, but through vibrationally excited molecular iodine. Quenching of the intermediate state could make scaling to higher pressures impossible. Steve Davis then began critical work to unravel this new dissociation mechanism [20]. Bob Shea took over the computer model and continually reminded me that our understanding of the kinetics was limited - motivating me to make sure we supported as many kinetic studies as we could. He was also the first to calculate the power in the flow and identify pressure scaling problems at subsonic velocity. Verne Schlie developed a gain probe for the COIL laser – a CW photolysis laser [22]. This was the first example of international cooperation – Verne spent a summer at the Max Planck Institute at Garching, Germany learning the details of photolysis lasers from the experts there. Verne also pointed out that there might be a problem with anomalous dispersion in COIL. This formed an interesting Ph.D. thesis topic for an Air Force Institute of Technology (AFIT) student named Dave Neumann. Dave and Steve Davis developed a method to measure the broadening coefficient of $^2P_{1/2}$ by oxygen and show that anomalous dispersion would not be a problem. On finishing his degree; Dave joined our little, but growing, group. He was to have a major impact on COIL development.

Not all of our effort was confined to in-house work. As a matter of fact, we gave funding to almost anyone who was interested in working on COIL lasers. Rocketdyne, Garrett AirResearch, McDonnell-Douglas Research Laboratories, and Bell Aerospace all worked on developing and understanding generators. Each also tried a laser – some worked and some didn't. We learned as much from the failures as we did from the

successes. Wayne Soloman ran the effort at Bell and is still active in the field at the University of Illinois. Al MacKnight was the leader at Garrett. I also felt that the McDonnell-Douglas effort (Ralph Richardson, Harvey Lilenfeld and Charlie Wiswall) provided key technical data [23]. Orv Sandall from the University of California at Santa Barbara, a consultant to Rocketdyne, gave us the first real chemical engineering analyses of the generator [24]. Steve Hurlock led the experimental team at Rocketdyne providing the data. Following that round, TRW and Bell Aerospace looked at characterizing and scaling the laser. I've already mentioned the work of Rick Heidner at Aerospace Corporation who continued to make major contributions to COIL kinetics. Jim Hurst at the Oregon Graduate Center made the first detailed study of the liquid phase chemistry [25]. He concluded that the intrinsic yield of $O_2(^1\Delta_g)$ in solution was near 100%.

At AFWL, we continued our scale-up efforts designing and building a multi-kilowatt subsonic laser. I left the AFWL just as that device was coming on line; leaving Gordan Hager who we had just hired from Rocketdyne and Doug Loverro, an ex-student of mine from USAFA, with the problem of getting it to work – which they did [26]. Gordan is still at the AFWL, although he is concentrating on his successful laser – the second electronic transition chemical laser, NCI-I. Bob Coombe also played an important role in the NCI-I discovery. During the same period, we had to face the problems of scaling subsonic devices – they would be large and probably exhibit poor beam quality. I asked Dave Neumann to head a technical group to develop a recommendation on the future course of COIL development. His recommendation to develop a supersonic COIL laser was critical to the current success of COIL. At that time it was quite a risk, a previous attempt had failed and no one had ever pushed $O_2(^1\Delta_g)$ through a supersonic nozzle. The proper place to inject the iodine and indeed the behavior of iodine dissociation at high pressures was a real unknown. Dave did succeed in demonstrating the first supersonic COIL laser about a year later [26]. About this time, Keith Truesdell also joined us from Rocketdyne. Keith remains one of the major drivers in COIL development.

6. An Explosion of Research

By the early 1980's, a number of groups began to exploit the potential of the COIL laser. Lasers were built in Russia, Israel, Japan, France, China, Germany and the Czech Republic. I have listed some of these lasers and their characteristics in Table 1. Some of the major advances were made during this time period. I've already mentioned Dave Neumann's successful supersonic laser. Marciel Zagidullin's invention of the jet generator was another major step [27]. Sani Yoshida's demonstration of greater than 40% laser efficiency showed COIL could be engineered to very high efficiency. Gordan Hager continued his innovative work by both frequency doubling [28] and Q-switching COIL [29]. The technical detail of COIL laser development can be found in the outstanding review by Keith Truesdell, Charlie Helms, and Gordon Hager [26]. Charlie Helms also did exceptional work on laser efficiency and mixing nozzles. I would also be amiss if I didn't mention the extraordinary work done by Mike Heaven to unravel the mystery of iodine dissociation [30], [31]. Mike will follow this address and talk in detail about his current research. We also will hear from many of the people who have contributed to COIL and I will not attempt to cover their many contributions here. I would like to highlight the importance of diagnostics – Steve Davis has been the leader in this most important effort. We will also hear about some of the commercial applications of COIL in the material processing industry. Another major application – The Airborne Laser – was reviewed yesterday by Steve Lamberson.

7. Conclusion

I would like to highlight the contributions of a few organizations whose contributions to the early development of COIL has been often overlooked. The AFOSR sponsored research in the mid-1970's was absolutely critical to the invention of COIL. Not only did it sponsor my own first efforts to develop a chemical generator, but supported technical efforts throughout the world. The AFIT also supported development by educating many of the key scientists involved in the US COIL effort. My Ph.D. was supported through the AFIT Civilian Institute Division as was my roommate – Greg Canavan, who ran the ARPA Electronic Laser program in the late 1970's. Graduates of the AFIT residence program included Nick Pchelkin and Dave Neumann. The

importance of a broad-based support for fundamental research and scientific education cannot be underestimated.

As a final note, I would like to assure you that advances in electronic transition lasers will continue to occur. Gordon Hager's session on NCI – pumped iodine is one example. At Directed Energy Solutions, I've been working with Dave Neumann on a new source of high pressure, high yield $O_2(^1\Delta_g)$. Initial experiments have produced excited oxygen concentrations in excess of an atmosphere. Such a source would reduce the weight and volume of a COIL laser by a factor of ten.

Year	Ref	Organization	Cl ₂ Flow	Power	Delta	Efficiency	Comments
			moles/s	watts	w/cm ²		
		USA					
1977	[18]	AFWL	0.004	0.004	2.00E-05	1.00E-05	longitudinal flow, subsonic
1978	[32]	AFWL	0.03	150	1.2	5%	subsonic
1982	[26]	AFWL	0.60	4600	4.6	8%	subsonic
1984	[26]	AFWL	0.15	1600	40	12%	supersonic
1989	[26]	AFWL	1.80	39000	172	24%	supersonic, ROTOCOIL
1989	[28]	AFWL					frequency doubled
1990	[29]	AFWL		630			magnetically Q switched
1991	[26]	AFPL	0.50	10000	200	22%	supersonic, RADICL
1996	[33]	AFPL	0.07	1750	197	28%	compact supersonic, VERTICOIL
1996	[34]	AFPL					mode locked COIL
1979	[23]	McD	0.02	10	0.08	1%	subsonic
1984	[35]	McD	0.02	180	0.10	10%	subsonic
1985	[36]	McD					
1981	[26]	TRW	0.20	2000	7	11%	subsonic
1984	[26]	TRW	0.30	4200	84	15%	supersonic
1981	[26]	RD	0.05	150	0.9	3%	subsonic
1985	[26]	RD	0.15	1900	58	14%	supersonic
1995	[37]	RD	0.90	17500	400	21%	supersonic, mode limited - aperture
1995	[37]	RD	0.50	13716	258	30%	supersonic
		RUSSIA					
1982	[38]	VNIIEF		0.01			subsonic
1983	[38]	VNIIEF		180			subsonic
1986	[38]	VNIIEF		900			subsonic
1990	[38]	VNIIEF		4000			subsonic
1984	[39]	Lebedev, Moscow	0.001	5			subsonic, 50% H ₂ O ₂
1989	[40]	Lebedev, Moscow					photodissociation of ozone
1991	[41]	Lebedev, Samara					jet generator
1997	[42]	Lebedev, Samara	0.01	200		22%	jet generator
		Israel					
1982	[43]	Ben Gurion U		5			subsonic
1994	[44]	Ben Gurion U		9			supersonic
1997	[45]	Ben Gurion U	0.01	177		18%	supersonic
		Japan					
1983	[46]	Nat Def Acad		10			subsonic
1987	[47]	Laser Lab, Chiba	0.002	40		21%	subsonic
1989	[48]	Laser Lab, Chiba	0.005	200		41%	subsonic
1989	[49]	Laser Lab, Chiba	0.07	1020		16%	subsonic

Year	Ref	Organization	Cl ₂ Flow	Power	Delta	Efficiency	Comments
		France					
1984	[50]	ONERA		4			subsonic, 30% H ₂ O ₂
1991	[51]	ONERA		570			
		China					
1988	[52]	Dalian Inst Chem Phys					electrical discharge, 130 mJ
1994	[53]	Dalian Inst Chem Phys	0.03	178		7%	
1995	[54]	Dalian Inst Chem Phys	0.15	1000		7%	supersonic
1996	[55]	Dalian Inst Chem Phys	0.30	5000		18%	supersonic
		Czech Rep					
1991	[56]	Inst of Physics	0.01	58		5%	subsonic
		Germany					
1997	[57]	DLR		5000			generator from AFPL

Table 1 Selected COIL Laser Devices

8. REFERENCES

1. Mallet, I., *Compt. Rend.*, 1927. **185**: p. 352.
2. Groh, M.P., *Presentation de reactions accompagnees de luminescence rouge*. Bulletin De La Societe Chimique De France, 1938. **5**: p. 12.
3. Groh, M.P.a.A.K., *Etude Spectrale d'une Reaction Luminescente*. Comptes Rendus Acad. Sci., 1942. **215**: p. 275.
4. Seliger, H.H., *Anal Biochem*, 1960. **1**: p. 60.
5. Khan, A.U.a.K., M., *J. Chem. Phys.*, 1963. **39**: p. 2105.
6. Arnold, S.J., Finlayson, N. and E. A. Orgryzlo, *Some Novel Energy-Pooling Processes Involving $O_2(^1\Delta_g)$* . *J. Chem. Phys.*, 1966. **44**: p. 2529.
7. Derwent, R.G., D.R. Kearns, and B.A. Thrush, *The Excitation of Iodine by Singlet Molecular Oxygen*. *Chem. Phys. Lett.*, 1970. **6**(2): p. 115-116.
8. Derwent, R.G. and B.A. Thrush, *Measurements on $O_2(1D)$ and $O_2(1S)$ in Discharge Flow Systems*. *Trans Faraday Soc*, 1971. **67**: p. 2036-2043.
9. Derwent, R.G. and B.A. Thrush, *The Radiative Lifetime of the Metastable Iodine Atom $I(52P_{1/2})$* . *Chem. Phys. Lett.*, 1971. **9**(6): p. 591-592.
10. Derwent, R.G. and B.A. Thrush, *Excitation of Iodine by Singlet Molecular Oxygen Part 1. - Mechanism of the I_2 Chemiluminescence*. *Journal of the Chemical Society of London, Faraday Discussions II*, 1972. **68**: p. 720-728.
11. Derwent, R.G. and B.A. Thrush, *Excitation of Iodine by Singlet Molecular Oxygen. Part 2. - Kinetics of the Excitation of the Iodine Atoms*. *Chem. Soc. Farad. Disc.*, 1972. **53**: p. 162-171.
12. Pritt, A.T.J., R.D. Coombe, D. Pillipovich, R.I. Wagner, D. Benard, and C.T. Dymek, *Appl. Phys. Letters*, 1977. **31**: p. 745.
13. McDermott, W.E.a.J.T.V., *A Recording Mercury Manometer*. *Journal of Chemical Education*, 1976.
14. McDermott, W.E., et al. *Chemical Generation of Molecular $O_2(^1\Delta_g)$* . in *Summer Colloquium on Electronic Transition Lasers 2*. 1976. Aspen, CO: MIT Press, Cambridge, MA.
15. McDermott, W.E., "On The Calculation of Thermodynamic Functions for Electronically Excited Laser Species," **Laser Digest**, 1978.
16. McDonald, J.R.a.H., J.K., *I^* Atom Bimolecular Quenching by O_2 , H_2O , H_2O_2 , and H_2* , in *NRL Memorandum Report*. 1976, Naval research Laboratory.
17. Siegman, A.E., *Lasers*. 1986, Mill Valley, CA: University Science Books.
18. McDermott, W.E., et al., *An Electronic Transition Chemical Laser*. *Appl. Phys. Lett*, 1978. **32**(8): p. 469-470.
19. McDermott, W.E., et al., *Efficient Operation of a 100-W Transverse Flow Oxygen-Iodine Chemical Laser*. *Applied Physics Letters*, 1979. **34**: p. 469-471.
20. van Bentham, M.H.a.S.J.D., *J. Phys. Chem*, 1986. **90**: p. 902.
21. Heidner, R.F., Gardner, C.E., Segal, G.I., and T.M. El-Sayed, *J. Phys. Chem.*, 1983. **87**: p. 2348.
22. Schlie, L.A. and R.D. Rathge, *Long Operating Time CW Atomic Iodine Probe Laser at 1.315 μm* . *IEEE Journal of Quantum Electronics*, 1984. **20**(10): p. 1187-1196.
23. Richardson, R.J. and C.E. Wiswall, *Chemically Pumped Iodine Laser*. *Applied Physics Letters*, 1979. **35**: p. 138.
24. Sandall, O.C., et al., *The Solubility and Rate of Hydrolysis of Chlorine in Aqueous Sodium Hydroxide at 0°C*. *AIChE Journal*, 1980.
25. Hurst, J.K., *Mechanism of Singlet Oxygen Generation by Chemical Reactions*, . 1977, Oregon Graduate Center, University of Oregon.
26. Truesdell, K.A., C.A. Helms, and G.D. Hager. *A History of COIL Development in the USA*. in *Tenth International Symposium on Gas Flow and Chemical Lasers*. 1994. Friedrichshafen, Germany: SPIE.
27. Zagidullin, M.V., et al., *Highly efficient Jet $O_2(^1\Delta)$ Generator*. *Sov. J. Quantum Electronics*, 1991. **21**(7): p. 747-753.

28. Johnson, D.E., et al., *A frequency doubled chemical oxygen iodine laser*. Applied Physics B, 1989. **B48**: p. 339-42.
29. Highland, R., P. Crowell, and G. Hager, *A 630 watt average power Q-switched chemical oxygen-iodine laser*. 1990.
30. Van Marter, T., M.C. Heaven, and D. Plummer, *Measurement of the rate constant for the quenching of $I(^2P_{1/2})$ by $O_2(X)$ at 150K*. Chemical Physics Letters, 1996. **260**: p. 201-207.
31. Lawrence, W.G., et al., *Inelastic collision dynamics of vibrationally excited $I_2(X)$* . Journal of Chemical Physics, 1997. **106**(1): p. 127-141.
32. Benard, D.J., et al., *Efficient Operation of a 100-W Transverse-Flow Oxygen-Iodine Chemical Laser*. Appl. Phys. Lett., 1979. **34**(1): p. 40-41.
33. Rittenhouse, T.L., Phipps, S. P., Helms, C. A., and Truesdell, K. A., *High efficiency operation of a 5 cm gain length supersonic chemical oxygen-iodine laser*. 1996.
34. Phipps, S.P., Helms, C. A., Copland, R. J., Rudolph, W. and K.A. Truesdell, *Mode locking of a CW supersonic chemical oxygen-iodine laser*. IEEE Journal of Quantum Electronics, 1996. **32**: p. 2045-50.
35. Wiswall, C.E., H.V. Lilenfeld, and S.L. Bragg, *Operation of an ICI Fueled Oxygen-Iodine Chemical Laser*. Applied Physics Letters, 1984. **45**: p. 5.
36. Wiswall, C.E., et al., *Moderate-Power CW Chemical Oxygen-Iodine Chemical Laser Capable of Long Duration Operation*. Journal of Applied Physics, 1985. **58**: p. 115.
37. McDermott, W.E., et al. *Operating Experience With a High Throughput Jet Generator*. in *Gas and Chemical Lasers*. 1997. San Jose, CA: SPIE.
38. Kalinovsky, V.V., et al., *High-power oxygen-iodine laser*. 1980.
39. Vagin, N.P., et al., *Chemical oxygen-iodine laser utilizing low-strength hydrogen peroxide*. Kvantovaya Elektronika, Moskva, 1984. **11**: p. 1688-9.
40. Zolotarev, V.A., et al., *Oxygen-iodine laser with a photodissociation source of excited $O_2(a^1\Delta_g)$ oxygen*. Kvantovaya Elektronika, Moskva, 1989. **16**: p. 1095-7.
41. Zagidullin, M.V., et al., *An oxygen-iodine laser utilizing a high-pressure $O_2(^1\Delta)$ generator*. Kvantovaya Elektronika, Moskva, 1991. **18**: p. 1417-18.
42. Zagidullin, M.V., et al., *Highly efficient supersonic chemical oxygen-iodine laser with a chlorine flow rate of 10 mmol/s*. Kvantovaya Elektronika, Moskva, 1997. **24**: p. 201-5.
43. Rosenwaks, S. and J. Bachar, *An efficient, small scale chemical oxygen-iodine laser*. Applied Physics Letters, 1982. **41**: p. 16-18.
44. Elor, A., et al., *A small scale, supersonic chemical oxygen-iodine laser*. Optics and Laser Technology, 1994. **26**: p. 87-89.
45. Blayvas, I., et al., *Power optimization of small-scale chemical oxygen-iodine laser with jet-type singlet oxygen generator*. IEEE Journal of Quantum Electronics, 1996. **32**: p. 2051-7.
46. Watanabe, K., et al., *Small-signal gain and saturation parameter of a transverse-flow CW oxygen-iodine laser*. IEEE Journal of Quantum Electronics, 1983. **QE**: p. 1699-1703.
47. Yoshida, S., et al., *Efficient operation of a chemically pumped oxygen iodine laser utilizing dilute hydrogen peroxide*. Applied Physics Letters, 1987. **51**: p. 1490-2.
48. Yoshida, S., et al., *Chemical oxygen iodine laser of extremely high efficiency*. Journal of Applied Physics, 1989. **65**: p. 870-2.
49. Fujii, H., et al., *Development of high-power chemical oxygen-iodine laser for industrial application*. Journal of Applied Physics, 1990. **67**: p. 3948-53.
50. Bonnet, J., et al., *Experimental analysis of a chemical oxygen-iodine laser*. Applied Physics Letters, 1984. **45**: p. 1009-11.
51. Louvet, Y., et al., *A high power chemical oxygen iodine laser*. 1991.
52. R. Zhang, et al., *A pulsed chemical oxygen-iodine laser initiated by electrical discharge*. Chinese Journal of Lasers, 1988. **15**: p. 455-7.
53. Zhou, D., et al., *Continuous wave chemical oxygen iodine laser using extracavity power output*. 1994.
54. Sang, Q.F., et al., *Supersonic COIL research activities in Dalian, China*. 1995.
55. Li, B., et al., *Supersonic cw chemical oxygen-iodine laser*. 1996.

56. Schmiedberger, J., *et al.*, *Experimental Study of Gain and Output Coupling Characteristics of a CW Chemical Oxygen-Iodine Laser*. IEEE Journal of Quantum Electronics, 1991. **27**(6): p. 1265-1270.
57. von Entress-Fursteneck, L.H., *et al.*, *Supersonic COIL operation at DLR Germany*. Proceedings of the SPIE The International Society for Optical Engineering, 1997. **3092**: p. 706-9.

Mechanism and kinetics of iodine dissociation in COIL

Michael C. Heaven*, Anatoly V. Komissarov and Vasilii Goncharov,
Department of Chemistry, Emory University, Atlanta, GA 30322

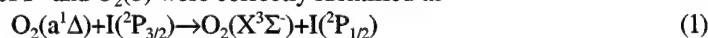
ABSTRACT

Dissociation of I_2 by $O_2(a^1\Delta)$, with subsequent excitation of I^* , was first observed by Arnold *et al.*¹ in 1966. This key discovery led to the eventual development of the chemical oxygen iodine laser (COIL). The mechanism by which I_2 is dissociated was not determined by Arnold *et al.*¹ and has remained elusive, despite many experimental attempts to unravel this question. Although the details are not known, it is apparent that a complex interplay between vibrationally and electronically excited states of I_2 is involved. Vibrationally excited states of O_2 have also been implicated. Characterization of the dissociation process is an important issue for COIL as the efficiency is impacted by the energy cost of dissociating the iodine. In this paper we provide a historical summary of work on the dissociation mechanism, and summarize the current understanding of the problem.

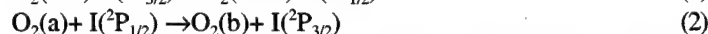
Keywords: Chemical lasers, oxygen, iodine, reaction kinetics, energy transfer.

1. INTRODUCTION

In 1966 Arnold *et al.*¹ reported the key observations that led to the eventual development of the chemical oxygen iodine laser (COIL). They found that adding I_2 to a flow of excited oxygen produced emissions from $I_2(B^3\Pi(0_u^+))$, $I(^2P_{1/2})$ (denoted as I^* in the following), and $O_2(b^1\Sigma^+)$. The reactions responsible for excitation of I^* and $O_2(b)$ were correctly identified as



and



However, Arnold *et al.*¹ were unable to resolve the question of how I_2 was initially dissociated. The energy levels of O_2 , I_2 and I that are relevant to this problem are shown in Fig. 1. As $O_2(a)$ does not carry enough energy to dissociate I_2 in a single collision, Arnold *et al.*¹ speculated that the first encounter could populate an excited state of I_2 , and a second $O_2(a)$ molecule would dissociate this excited species. This can be represented by the sequence



An alternative explanation is that $O_2(b)$ directly dissociates I_2 . Arnold *et al.*¹ demonstrated that $O_2(b)$ could be generated in a flow of $O_2(a)$ by the pooling reaction



The dissociation mechanism is a matter of importance for COIL as this process consumes an appreciable amount of energy. In a flow tube study, Alsing *et al.*² found that approximately six $O_2(a)$ molecules were needed to dissociate one I_2 molecule under optimized conditions. For less favorable reagent ratios up to sixteen $O_2(a)$ molecules were needed to dissociate one I_2 . In addition to consuming energy, the kinetics of the dissociation process can also influence the power extraction efficiency in a laser system. The time scale for dissociation determines the downstream position at which the maximum concentration of I^* will occur. If dissociation takes place too slowly the maximum I^* concentration will be achieved after the gas has left the optical cavity. Conversely, if high concentrations of I^* are formed before reaching the optical cavity, energy is lost during transport (mostly due to quenching by H_2O from the $O_2(a)$ generator). This leads to a curious situation where the conditions that give maximum power from the laser do not correspond to complete dissociation of I_2 ^{3,4}.

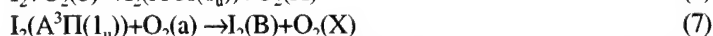
Since the seminal work of Arnold *et al.*¹ there have been several attempts to unravel the details of the dissociation mechanism. A generally accepted model was established in 1988, and optimal values for the most important rate constants were proposed^{5,6}. The model was developed using data from kinetic studies of elementary reactions and analyses of device performance characteristics. It has been used for most

* heaven@euch4e.chem.emory.edu. Phone (404) 727 6617, FAX (404) 727 6586

subsequent computational studies of COIL systems. Due to the method of construction, the model does a good job of reproducing the behavior of well-characterized devices. However, it cannot be relied upon to predict the properties of devices running under non-standard conditions (e.g., high pressures and/or novel gas mixing geometries). Consequently, computational predictions for untested conditions or new hardware cannot be trusted. As we will discuss in this article, the problems stem from the fact that we still do not have a complete understanding of the dissociation process.

2. THE FIRST QUANTITATIVE MODEL: DISSOCIATION OF I_2 BY $O_2(b)$

Derwent and Thrush⁷⁻¹⁰ used flow tube techniques to examine the oxygen-iodine system. The kinetics were followed by monitoring emissions from $I_2(B)$ and I^* . Arnold *et al.*¹ had assumed that $I_2(B)$ was formed by I^*+I+M recombination, but Derwent and Thrush⁷ were able to show that it is produced by sequential excitation of I_2 . They proposed the mechanism



but did not consider the excited states of I_2 to be important in the dissociation process. Their analysis of the kinetics led to the conclusion that I_2 was dissociated by⁸



This reaction set, along with the pooling reactions 2 and 5, provided a satisfactory representation of the observed emission signals. Derwent and Thrush¹⁰ also used the equilibrium between reaction 1 and the reverse process



to evaluate the radiative lifetime of I^* . In considering these data they realized that reaction 1 could sustain CW lasing on the $I^*\rightarrow I$ transition. The subsequent demonstration of a chemically driven $O_2(a)/I^*$ laser^{11,12} (as described in the preceding paper by McDermott¹³) stimulated further studies of O_2/I_2 kinetics.

3. THE CHAIN DISSOCIATION MECHANISM AND PROBLEMS WITH THE IDENTITY OF I_2^\dagger .

The model proposed by Derwent and Thrush^{7,8} required a gas kinetic rate constant ($\sim 2\times 10^{-10} \text{ cm}^3 \text{ s}^{-1}$) for the removal of $O_2(b)$ by I_2 . Using pulsed laser excitation of $O_2(b, v=0)$, Houston and co-workers^{14,15} made direct measurements of the removal rate constant. The value they obtained, $2\times 10^{-11} \text{ cm}^3 \text{ s}^{-1}$, was too small to account for the flow tube results. Consequently, Heidner *et al.*¹⁶ performed a careful and systematic reinvestigation of the $I_2/O_2(a)$ kinetics. Fluorescence signals from $I_2(B)$, $I_2(A)$, I^* , $O_2(b)$ and $O_2(a)$ were monitored in flowing $I_2/O_2(a)$ mixtures. The dependence of the I_2 dissociation rate on the presence of H_2O was also examined; the motivation being that H_2O was present in the flow from chemical $O_2(a)$ generators, and it was expected to have a deleterious effect on the dissociation rate. Heidner *et al.*¹⁶ established the most important characteristics of the dissociation process. They found that there was a slow initiation step followed by rapid, branched-chain dissociation of I_2 . I^* was identified as the chain carrier. Noting that the dissociation rate was dependent on the initial concentration of I_2 , they also suggested that an excited state of I_2 was the precursor to atomic iodine. The reaction scheme used to model these observations was as follows. The slow initiation step was attributed to reaction 3. This was followed by the rapid dissociation of I_2^\dagger by reaction 4. I atoms liberated by this sequence are excited by reaction 1, permitting I^* to carry the chain via the reaction



As expected, the presence of H_2O did slow the dissociation rate. It was known that both $O_2(b)$ and I^* were effectively quenched by H_2O , but when Heidner *et al.*¹⁶ modeled their results they found that these were not the primary reactions influencing the dissociation rate. Instead, the models required gas kinetic ($2\times 10^{-10} \text{ cm}^3 \text{ s}^{-1}$) deactivation of I_2^\dagger by H_2O



Heidner *et al.*¹⁶ attempted to define a sub-set of critical rate constants by fitting to their dissociation rate data. Unfortunately, several of the rate constants could not be uniquely determined as they were strongly

correlated. Two limiting rate constant sets were offered as constraints on a yet-to-be-determined set of final values. Three of the rate constants differed by more than an order of magnitude between the two models. Heidner *et al.*¹⁶ also noted that their models were not completely satisfactory, as they could not find a single set of parameters that could represent all of the data. They did find that the original Derwent and Thrush⁸ model gave acceptable results, but concluded that "the agreement with experiment is moderately good, but, based on the direct measurements of Houston and co-workers, such agreement must be fortuitous".

Hediner *et al.*¹⁶ discussed possible assignments for I_2^+ . Within the framework of their model there were two plausible alternatives. Either I_2^+ was vibrationally excited $I_2(X)$ or the metastable electronically excited species $I_2(A'^3\Pi(2_u))$. There were troubling difficulties with both of these choices. $I_2(A')$ has an excitation energy of 10,042 cm^{-1} , so it cannot be accessed by energy transfer from $O_2(a)$ ($T_0=7882 \text{ cm}^{-1}$). Near-resonant transfer from $O_2(a)$ or I^* would populate $I_2(X)$ vibrational levels in the range of $v=40-50$. Experiments performed by Hall *et al.*¹⁷ showed that I^* was rapidly quenched by I_2 ($k=3.5\times 10^{-11} \text{ cm}^3\text{s}^{-1}$), and that vibrationally excited $I_2(X)$ was formed in the process. Van Bentham and Davis¹⁸ later went on to show that vibrationally excited $I_2(X)$ was generated when I_2 was added to a flow of $O_2(a)$. The problem, with regard to assigning I_2^+ to vibrationally excited $I_2(X)$, was that Hall *et al.*¹⁷ reported rapid relaxation of $I_2(X, v=40)$ by Ar. This result appeared to be at variance with Heidner *et al.*'s¹⁶ observation that the dissociation rate was not influenced by the presence of Ar. This conflict could be resolved by recognizing that several vibrational energy transfer collisions would be needed to relax the initially formed $I_2(X, v\sim 40)$ to levels that did not have sufficient energy to be dissociated by a collision with $O_2(a)$ ($I_2(X, v<20)$). Assuming that the vibrational relaxation rate constant measured by Hall *et al.*¹⁷ corresponded to $\Delta v=-1$ transfer, David *et al.*¹⁹ used kinetic modeling to show that the vibrational cascade process would not be fast enough to impact the dissociation rate for the conditions of Heidner *et al.*'s¹⁶ experiments. With this insight it was concluded that I_2^+ is the vibrationally excited species, and Heidner *et al.*'s¹⁶ model 1 rate constants were adopted for subsequent simulations of COIL devices. However, lingering doubts concerning the identity of I_2^+ remained. Lilenfeld²⁰ compared the effects of H_2O , CO_2 , and SF_6 on the dissociation rate. He found that H_2O and CO_2 were very effective in deactivating I_2^+ , while SF_6 was about 8 times less effective than CO_2 . It was surprising to find that SF_6 was not the best deactivator, as this molecule has many vibrational modes that can accept vibrational energy from I_2 . Based on these observations Lilenfeld²⁰ favored the notion that I_2^+ is the electronically excited species $I_2(A')$. He noted that $O_2(a, v=1)$ has almost enough energy to excite $I_2(A')$, and used EPR spectroscopy to show that $O_2(a, v=1)$ was present in the flow from his singlet oxygen generator.

Several excited states of I_2 could be involved in the process where $O_2(a)$ dissociates $I_2(A')$. Emission from $I_2(B)$ is seen in $O_2(a)/I_2$ flames, and it had been suggested that reaction 7 and $I_2(A')+O_2(a)\rightarrow I_2(B)+O_2(X)$, followed by predissociation of $I_2(B)$ were the source of I atoms. Lilenfeld²⁰ was able to eliminate these channels by demonstrating that strong magnetic fields, which accelerate the $I_2(B)$ predissociation rate, do not increase the overall dissociation rate.

4. IS I_2^+ VIBRATIONALLY EXCITED $I_2(X)$? A CLOSER LOOK.

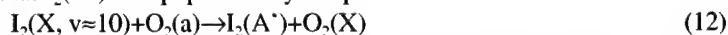
Lilenfeld²⁰ and Heidner *et al.*¹⁶ had drawn attention to the puzzling characteristics of I_2^+ deactivation. This species was rapidly removed by H_2O and CO_2 , while collisions with He or Ar were less effective by orders of magnitude. For example, in Heidner *et al.*'s¹⁶ model 1 the rate constants for deactivation of I_2^+ are (in units of $\text{cm}^3 \text{s}^{-1}$) 3×10^{-10} (H_2O), 5×10^{-11} ($O_2(X)$), and 4×10^{-12} (Ar). These trends are more typical of electronic quenching, rather than vibrational relaxation. Heaven and co-workers²¹⁻²⁴ examined the viability of equating I_2^+ deactivation with $I_2(X)$ vibrational energy transfer by studying the relaxation process under well-controlled conditions. Individual ro-vibrational levels of $I_2(X)$ in the range $22<v<43$ were populated using a pulsed stimulated emission pumping technique. The excited molecules were allowed to make a few collisions with the surrounding bath gas, and then the pulses from a probe laser were used to observe the range of levels populated by energy transfer. Fig. 2 shows results from this type of measurement. In this instance $I_2(X)$ was excited to the $v=23, J=57$ level (where J is the rotational quantum number). The upper panel in Fig. 2 shows a probe laser spectrum taken under collision free conditions. The $J=57$ population gives rise to just two spectral lines that obey the $\Delta J=\pm 1$ selection rule. The lower panels show the results of colliding $I_2(v=23, J=57)$ with Ar and H_2O . Most of the lines in these traces originate from rotationally inelastic collisions

($\Delta v=0$ transfer). The lines marked with asterisks are the result of $v=23 \rightarrow 22$ transfer. From these traces it can be seen that the probabilities for vibrational relaxation by H_2O and Ar are comparable. Modeling of these data indicates that vibrational relaxation by H_2O is about a factor of two faster than relaxation by Ar²⁴. The rate constants do not differ by a factor of 75, as required by the models of I_2^+ deactivation. The absolute magnitudes of the vibrational relaxation rate constants also pose a problem. For relaxation by H_2O the total removal rate constant was $1.6 \times 10^{-10} \text{ cm}^3 \text{ s}^{-1}$, and this was dominated by $\Delta v=-1$ transfer. This is only half of the I_2^+ deactivation rate constant, without considering the damping effect of the vibrational cascade sequence. Models of $v=40 \rightarrow 20$ relaxation²⁴ predict an overall deactivation rate constant for H_2O of $8 \times 10^{-12} \text{ cm}^3 \text{ s}^{-1}$.

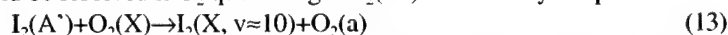
Although the vibrational relaxation rate constants were in gross disagreement with the limiting deactivation rate constants of Heidner *et al.*¹⁶, this did not mean that the identification of I_2^+ as $\text{I}_2(\text{X}, v>20)$ had necessarily been invalidated. Heidner *et al.*¹⁶ stated that their rate constant set was not unique. Consequently, Paschkewitz and Heaven²⁵ explored the possibility of re-optimizing the rate constant package with the I_2^+ deactivation rate constants constrained to values that were compatible with the vibrational relaxation rate constant measurements. The model was fit to Heidner *et al.*'s¹⁶ dissociation rate data. It was found that the value of the H_2O deactivation rate constant could be reduced to a minimum value of $4.8 \times 10^{-11} \text{ cm}^3 \text{ s}^{-1}$, but this was still too large to be consistent with vibrational relaxation. Other problems with the re-optimized model were that it could not tolerate deactivation by Ar and the dissociation rates predicted for low concentrations of H_2O were in poor agreement with the experimental data²⁵. The conclusion drawn from these efforts was that $\text{I}_2(\text{X}, v>20)$ is not the immediate precursor of atomic iodine. Although $\text{I}_2(\text{X}, v>20)$ may play an important role in the dissociation mechanism, the deactivation kinetics are governed by a different species.

5. IS I_2^+ ELECTRONICALLY EXCITED I_2 ?

Emission from $\text{I}_2(\text{A}^3\Pi(1_u), \tau_{\text{rad}}=220 \mu\text{s})$ is readily observed from $\text{O}_2(\text{a})/\text{I}_2$ flames^{16,26}, but the lowest energy electronically excited state of I_2 ($\text{A}^3\Pi(2_u)$) is very metastable, and cannot be detected by emission spectroscopy. Basics *et al.*²⁷ used laser excitation techniques to demonstrate that $\text{I}_2(\text{A}')$ was generated in $\text{O}_2(\text{a})/\text{I}_2$ mixtures. They found that $\text{I}_2(\text{A}')$ and $\text{I}_2(\text{X}, v>20)$ were present at comparable concentration levels. Barnault *et al.*²⁸ proposed that $\text{I}_2(\text{A}')$ was populated by the process



Support for this mechanism was provided by a study of the $\text{I}_2(\text{X})$ vibrational population distribution in a flowing $\text{I}_2/\text{O}_2(\text{a})$ mixture. Barnault *et al.*²⁸ observed selective depletion of vibrational levels around $v \approx 10$, indicating that this population was being removed by reaction 12. The dissociation mechanism proposed by Barnault *et al.*²⁸ was dependent upon vibrational excitation of $\text{I}_2(\text{X})$, but the kinetics were controlled by passage through the A' state. Additional kinetic schemes involving $\text{I}_2(\text{A}')$ were elaborated by Bouvier *et al.*²⁹ These models could accommodate the fact that moderate pressures of Ar or He had very little influence on the dissociation rate. Tellinghuisen and Phillips³⁰ had reported rate constants for removal of $\text{I}_2(\text{A}')$ by He and Ar of 0.94×10^{-14} and $2.8 \times 10^{-14} \text{ cm}^3 \text{ s}^{-1}$, respectively. The small rate constants were consistent with removal via collision induced dissociation. Quenching of $\text{I}_2(\text{A}')$ by molecular collision partners that could accept energy by E-E or E-V transfer was expected to be much more effective. Tellinghuisen and Phillips³⁰ observed a self-quenching rate constant of $5.5 \times 10^{-11} \text{ cm}^3 \text{ s}^{-1}$. These trends provided some indication that $\text{I}_2(\text{A}')$ could be the key intermediate, but data for the quenching of $\text{I}_2(\text{A}')$ by H_2O and $\text{O}_2(\text{X})$ were needed to further explore this possibility. Komissarov *et al.*³¹ measured these rate constants using pulsed laser pump-probe techniques. Quenching rate constants of 6.3×10^{-12} and $3.4 \times 10^{-12} \text{ cm}^3 \text{ s}^{-1}$ were obtained for $\text{O}_2(\text{X})$ and H_2O , respectively. Clearly, these collision partners were much more effective quenchers than He or Ar, but the quenching still appeared to be slower than that required for I_2^+ deactivation. Furthermore, O_2 was more effective in removing $\text{I}_2(\text{A}')$ than H_2O , in conflict with the ordering of the deactivation rate constants. Komissarov *et al.*³¹ suggested that the latter problem could be resolved if O_2 quenching of $\text{I}_2(\text{A}')$ occurred by the process



which would minimize the loss of energy and permit facile re-excitation. Conversely, it was assumed that quenching by H_2O caused irreversible deactivation to the lowest vibrational levels of $\text{I}_2(\text{X})$. The remaining problem was the low absolute magnitudes of the $\text{I}_2(\text{A}')$ quenching rate constants. This could be

accommodated in the model by reducing the rate constants for excitation and dissociation of $I_2(A')$, thereby allowing the deactivation processes to compete. The resulting kinetic scheme is illustrated in Fig. 3.

An attempt to derive rate constants for the revised kinetics package was made by modeling the data of Heidner *et al.*¹⁶ The performance of the revised model was comparable to that of Heidner *et al.*'s¹⁶ limiting case models. Once again it was found that the available data were not sufficient to define a unique set of rate constants. Komissarov *et al.*³¹ concluded that their model was capable of reproducing the dissociation rate data, and presented one set of physically reasonable rate constants as an example. Subsequently, Bruins *et al.*³² and Madden³³ have modeled the performance of COIL devices using the Komissarov *et al.*³¹ rate constants. They found poor agreement with the experimental data, primarily due to underestimation of the I_2 dissociation rate. This failure shows that the rate constant package contains errors, it does not necessarily imply that the mechanism is incorrect. The model has sufficient flexibility that fitting the rate constants to flow tube and COIL performance data would provide a parameterized model that would work as well as the standard model. However, this would be an exercise of questionable value, as it cannot be used to distinguish the true mechanism from functionally equivalent models. Further studies of the elementary reactions are needed to assess the viability of the mechanism proposed by Komissarov *et al.*³¹

6. IS VIBRATIONALLY EXCITED O_2 IMPORTANT IN THE DISSOCIATION PROCESS?

The crux of the problem with models that are dominated by the kinetics of an I_2^+ intermediate is the relative ordering of the deactivation rate constants, $k_{H_2O}^{\dagger} \approx 6k_{O_2}^{\dagger} > 75k_{Ar}^{\dagger}$. The Derwent and Thrush^{7,8} model was successful because H_2O is the most efficient quencher of $O_2(b)$. Houston and co-workers had shown that dissociation by $O_2(b, v=0)$ was untenably slow, but alternative mechanisms involving vibrationally excited $O_2(b)$ and $O_2(a)$ have been advanced. As noted above, Lilenfeld²⁰ detected $O_2(a, v=1)$ in his experiments, and suggested that $I_2(A')$ could be directly excited by this species. More recently, Azyazov *et al.*³⁴ observed $O_2(a, v=1)$ in the flow from a jet-type singlet oxygen generator. In these experiments the evidence for the presence of $O_2(a, v=1)$ was provided by detection of the $O_2(a, v=1)-O_2(a) \rightarrow O_2(X)-O_2(X)$ dimole emission band. Azyazov *et al.*³⁴ estimated that about 2% of the $O_2(a)$ in their system was vibrationally excited. They suggested possible roles for vibrationally excited O_2 in the dissociation mechanism that included $O_2(a, v>0)+I_2(X) \rightarrow O_2(X) + I_2(A')$, and gas kinetic dissociation of $I_2(X)$ by $O_2(b, v>0)$. Processes that might generate vibrationally excited O_2 include



Models based on these reactions will no doubt be able to reproduce the flow tube and laser performance data, once the rate constants have been empirically adjusted. As with the previous models, it will not be possible to evaluate the reality of the model as the required rate constants and final state distribution data are not available. Measurements of a few key rate constants should be undertaken to assess the importance of these reactions.

7. CONCLUSION

Thirty six years ago Arnold *et al.*¹ noted that "A more difficult question is how the I_2 is initially dissociated". Their comment remains valid. Important details of the dissociation mechanism have been gleaned from careful kinetic measurements, but this data set is still far from complete. Models of the dissociation process have been further elaborated and refined by fitting to laser performance characteristics. Unfortunately, the complexity of the process does not allow the mechanism to be determined by this approach. Since the establishment of the standard reaction set and rate constant package used to model COIL devices, investigations of specific reactions have shown that some of the critical rate constants are incorrect, and have called the accepted mechanism into question. At this point the standard model should be regarded as an intelligent parameterization, rather than a correct physical description.

The majority of the data used to establish the COIL kinetics package was recorded more than fifteen years ago. The generation of researchers who revealed the potential of the $I_2/O_2(a)$ system, and mapped the functional characteristics of the I_2 dissociation process, did so through elegant application of a limited set of diagnostic tools. Since that time advanced techniques for characterizing the key species in COIL systems have been developed, as described in the paper by Davis³⁵. Application of the full range of diagnostic techniques in new studies of the dissociation mechanism will lead to a final resolution of this long-standing problem. The development of truly predictive computational models for COIL devices will then be in reach.

ACKNOWLEDGMENT

Support provided by the Air Force Office of Scientific Research for work on the reaction kinetics of the $I_2/O_2(a)$ system led to the demonstration of the first COIL system. AFOSR has sustained its commitment to fundamental studies of reaction dynamics, which is reflected in the fact that the greater majority of the research described in this article was sponsored by AFOSR. The authors are grateful for the continued support of these efforts at Emory University through AFOSR grant F49620-01-1-0070.

REFERENCES

1. S. J. Arnold, N. Finlayson, and E. A. Ogryzlo, "Some novel energy-pooling processes involving $O_2(a)$ " *J. Chem. Phys.* **44**, 2529 (1966).
2. P. M. Alsing, S. J. Davis, and G. L. Simmons. "Efficiency of the dissociation of I_2 by $O_2(a)$ " unpublished preprint.
3. B. D. Barmashenko and S. Rosenwaks, "Power dependence of chemical oxygen-iodine lasers on iodine dissociation," *AIAA J.* **34**, 2569-2574 (1996).
4. C. A. Helms, J. Shaw, G. D. Hager, "Iodine dissociation in COILs," *Proc. SPIE-Int. Soc. Opt. Eng.* **2502**, 250-7 (1995).
5. G. P. Perram and G. D. Hager, "Standard chemical oxygen-iodine laser kinetics package" Air Force Weapons Lab., Kirkland AFB, NM. 1988.
6. G. P. Perram and G. D. Hager, "Standard chemical oxygen-iodine laser kinetics package, Revision" Air Force Weapons Lab., Kirkland AFB, NM. 1988.
7. R. G. Derwent and B. A. Thrush, "Excitation of iodine by singlet molecular oxygen. 1. Mechanism of the iodine chemiluminescence," *J. Chem. Soc., Faraday Trans. 2* **68**, 720-8 (1972).
8. R. G. Derwent and B. A. Thrush, "Excitation of iodine by singlet molecular oxygen. 2. Kinetics of the excitation of the iodine atoms," *Faraday Discuss. Chem. Soc. No.* **53**, 162-7 (1972).
9. R. G. Derwent, David R. Kearns, and Brian A. Thrush, "Excitation of iodine by singlet molecular oxygen," *Chem. Phys. Lett.* **6**, 115-16 (1970).
10. R. G. Derwent and B. A. Thrush, "Radiative lifetime of the metastable iodine atom $I(5^2P_{1/2})$," *Chem. Phys. Lett.* **9**, 591-2 (1971).
11. D. J. Benard, W. E. McDermott, N. R. Pchelkin, and R. R. Bousek, "Efficient operation of a 100 W transverse-flow oxygen-iodine chemical laser," *Appl. Phys. Lett.* **34**, 40-1 (1979).
12. W. E. McDermott, N. R. Pchelkin, D. J. Benard and R. R. Bousek, "An electronic transition chemical laser," *Appl. Phys. Lett.* **32**, 469-70 (1978).
13. W. E. McDermott, "Historical Perspective of COIL," *Proc. SPIE-Int. Soc. Opt. Eng.*, **4631**, (2002).
14. R. G. Aviles, D. F. Muller, and P. L. Houston, "Quenching of laser-excited $O_2(b)$ by carbon dioxide, water, and diatomic iodine," *Appl. Phys. Lett.* **37**, 358-60 (1980).
15. D. F. Muller, R. H. Young, P. L. Houston, "Direct observation of diatomic iodine collisional dissociation by $O_2(b)$," *Appl. Phys. Lett.* **38**, 404-6 (1981).
16. R. F. Heidner, III, C. E. Gardner, G. I. Segal, and T. M. El-Sayed. "Chain-reaction mechanism for molecular iodine dissociation in the $O_2(a)$ -iodine atom laser," *J. Phys. Chem.* **87**, 2348-60 (1983).
17. G. E. Hall, W. J. Marinelli, and P. L. Houston, "Electronic-to-vibrational energy transfer from excited atomic iodine ($I^*(5^2P_{1/2})$) to molecular iodine ($25 < v < 43$)," *J. Phys. Chem.* **87**, 2153-61 (1983).

18. M. H. Van Benthem and S. J. Davis, "Detection of vibrationally excited molecular iodine in the dissociation region of chemical oxygen-iodine lasers," *J. Phys. Chem.* **90**, 902-5 (1986).
19. D. David, V. Joly, and Fausse, "High vibrational levels of iodine as intermediate states in the iodine dissociation by $O_2(a)$," *Proceedings of the 7th International Symposium on Gas Flow and Chemical Lasers*, 1987.
20. H. V. Lilenfeld, "Oxygen-Iodine Laser Kinetics", Air Force Weapons Laboratory Technical Report AFWL-TR-83-1, 1983.
21. W. G. Lawrence, T. A. Van Marter, M. L. Nowlin and M. C. Heaven, "Energy transfer processes for $I_2(X)$ of relevance to COIL," *Proc. SPIE-Int. Soc. Opt. Eng.* **2702** (Gas and Chemical Lasers), 214-225 (1996).
22. M. L. Nowlin and M. C. Heaven, "Collisional relaxation of highly excited vibrational levels of $I_2(X)$," *J. Phys. IV 4* (C4, LASER M2P), C4/729-C4/737 (1994).
23. M. L. Nowlin and M. C. Heaven, "Energy transfer rate constants for highly excited rovibrational levels of molecular iodine," *J. Chem. Phys.* **99**, 5654-60 (1993).
24. W. G. Lawrence, T. A. Van Marter, M. L. Nowlin and M. C. Heaven, "Inelastic collision dynamics of vibrationally excited $I_2(X)$ " *J. Chem. Phys.* **106**, 127-141 (1997).
25. J. S. Paschkewitz and M. C. Heaven, "COIL chemical kinetics package revisited: a re-analysis of molecular iodine dissociation rate data," *Proc. SPIE-Int. Soc. Opt. Eng.* **3931** (Gas, Chemical, and Electrical Lasers and Intense Beam Control and Applications), 169-178 (2000).
26. D. Cerny, R. Bacis, A. J. Bouvier, S. Poulat, and A. Topouzkhanian, "The dissociation of molecular iodine by metastable oxygen-I. Populations of A 1u and B 0u+ iodine states through Fourier transform spectrometry analysis," *J. Quant. Spectrosc. Radiat. Transfer* **47**, 9-18 (1992).
27. M. Nota, A. J. Bouvier, R. Bacis, A. Bouvier, P. Crozet, S. Churassy and J. B. Koffend, "The dissociation of iodine by singlet molecular oxygen; role of the vibrational reservoir state A'(2u)" *J. Chem. Phys.* **91**, 1938-40 (1989).
28. B. Barnault, A. J. Bouvier, D. Pigache and R. Bacis, "Absolute measurements of the molecular iodine high vibrational levels in the oxygen-iodine reaction," *J. Phys. IV 1* (C7, Int. Conf. Laser M2P, 2nd, 1991), C7/647-C7/650.
29. A. J. Bouvier, R. Bacis, A. Bouvier, D. Cerny, S. Churassy, P. Crozet, and M. Nota, "The dissociation of molecular iodine by metastable oxygen. II. Populations of reservoir states through laser excitation spectra," *J. Quant. Spectrosc. Radiat. Transfer* **49**, 311-23 (1993).
30. J. Tellinghuisen and L. F. Phillips, "Kinetics of I_2 following photolysis at 1930 Å: Temperature dependence of A'-state quenching," *J. Phys. Chem.* **90**, 5108 (1986).
31. A. V. Komissarov, V. Goncharov, and M. C. Heaven, "Chemical oxygen-iodine laser (COIL) kinetics and mechanisms," *Proc. SPIE-Int. Soc. Opt. Eng.* **4184** (XIII International Symposium on Gas Flow and Chemical Lasers and High-Power Laser Conference), 7-12 (2001).
32. B. D. Barmashenko, E. Bruins, D. Furman, V. Rybalkin, and S. Rosenwaks, "Modeling of the gain, temperature, and iodine dissociation fraction in a supersonic chemical oxygen-iodine laser," *Proc. SPIE-Int. Soc. Opt. Eng.*, **4631** 2002.
33. T. J. Madden, private communication.
34. V. N. Azyazov, V. D. Nikolaev, M. I. Svistun, and N. I. Ufimtsev, "Luminescence of the oxygen dimole at the output of a chemical singlet-oxygen generator," *Quantum Electron.* **29**, 767-771 (1999).
35. S. J. Davis, "History of COIL diagnostics," *Proc. SPIE-Int. Soc. Opt. Eng.*, **4631**, 2002.

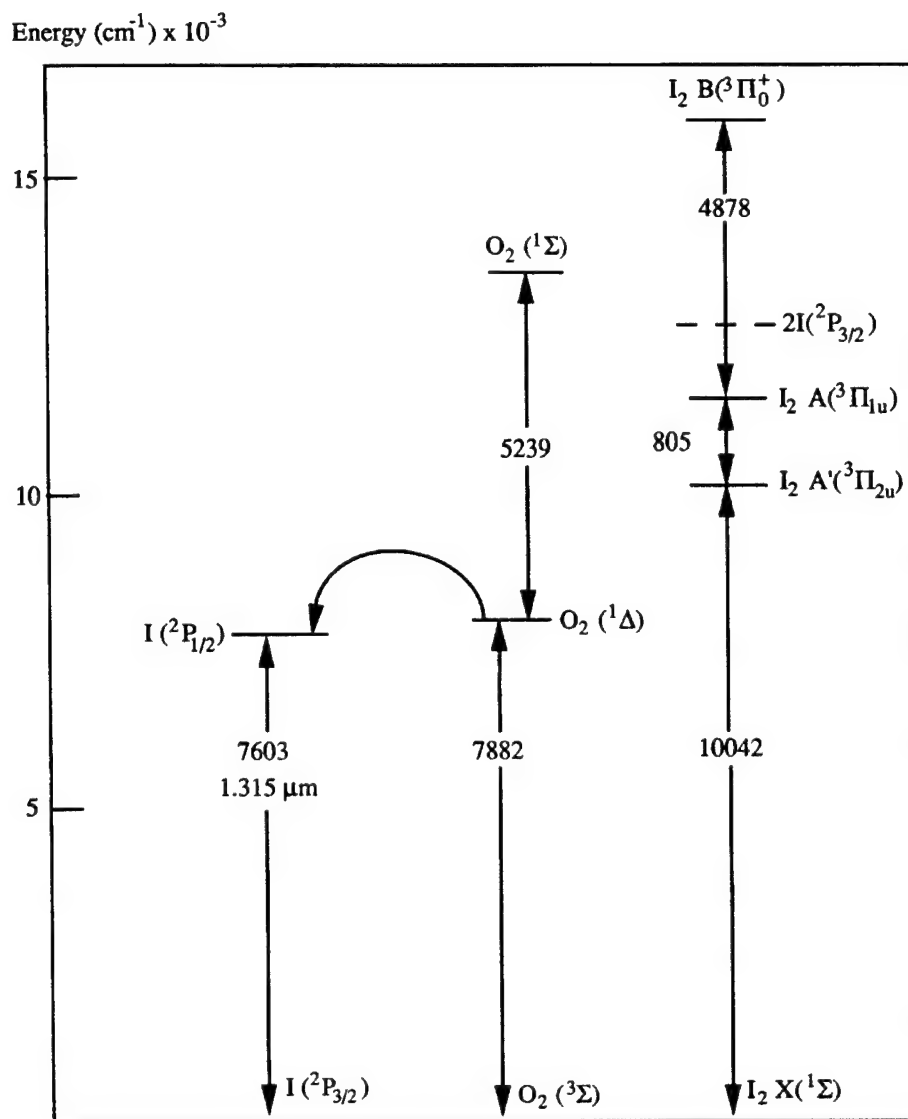


Figure 1. Energy level diagram showing the low-lying states of O₂, I₂, and I

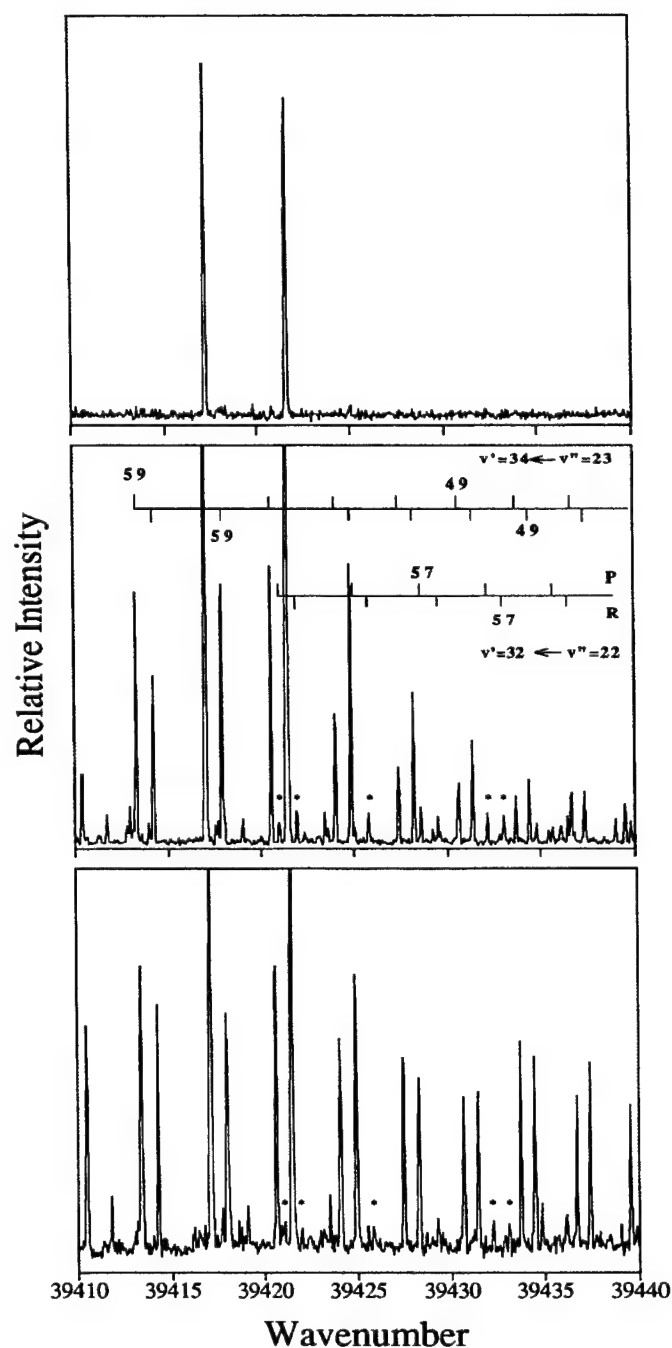


Figure 2. Spectra showing ro-vibrational level state preparation and collisional energy transfer. The upper trace demonstrates clean preparation of the $I_2(X)$ $v=23$, $J=57$ level under collision-free conditions. The middle and lower traces show the effects of ro-vibrational energy transfer induced by collisions with H_2O (middle trace) and Ar (lower trace). The peaks marked with asterisks originate from levels populated by vibrational energy transfer.

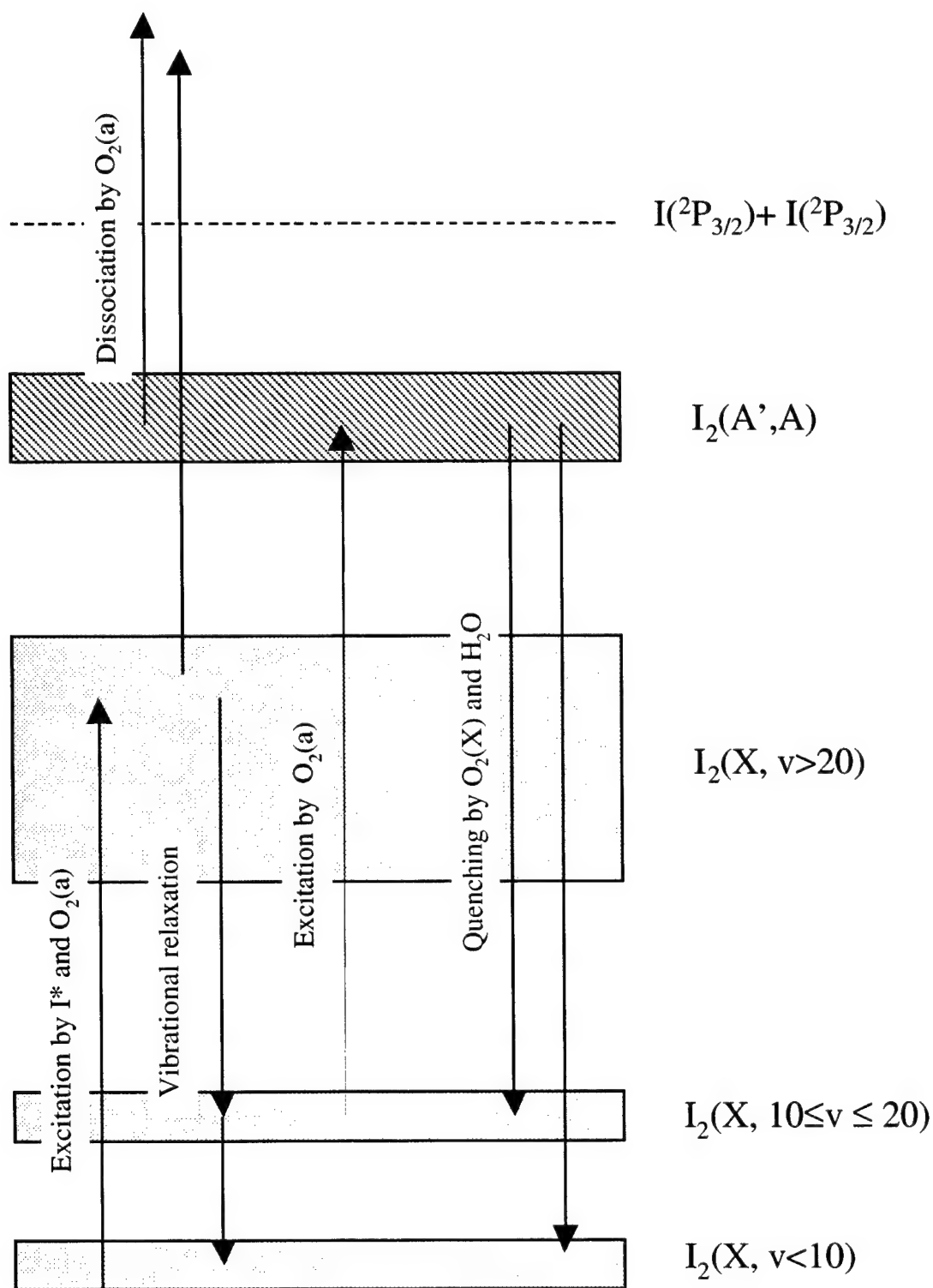


Figure 3. Schematic of the proposed dissociation mechanism proposed by Komissarov et al.³¹

Gain and temperature in a slit nozzle supersonic chemical oxygen-iodine laser with transonic and supersonic injection of iodine

S. Rosenwaks, B. D. Barmashenko, E. Bruins, D. Furman, V. Rybalkin and A. Katz
Department of Physics, Ben-Gurion University of the Negev, Beer-Sheva 84105, Israel

ABSTRACT

Spatial distributions of the gain and temperature across the flow were studied for transonic and supersonic schemes of the iodine injection in a slit nozzle supersonic chemical oxygen-iodine laser as a function of the iodine and secondary nitrogen flow rate, jet penetration parameter and gas pumping rate. The mixing efficiency for supersonic injection of iodine (~ 0.85) is found to be much larger than for transonic injection (~ 0.5), the maximum values of the gain being $\sim 0.65\%/cm$ for both injection schemes. Measurements of the gain distribution as a function of the iodine molar flow rate nI_2 were carried out. For transonic injection the optimal value of nI_2 at the flow centerline is smaller than that at the off axis location. The temperature is distributed homogeneously across the flow, increasing only in the narrow boundary layers near the walls. Opening a leak downstream of the cavity in order to decrease the Mach number results in a decrease of the gain and increase of the temperature. The mixing efficiency in this case (~ 0.8) is much larger than for closed leak.

Keywords: chemical lasers, oxygen, iodine, power lasers

1. INTRODUCTION

The chemical oxygen-iodine laser (COIL)¹ emits at $1.315\mu m$ and is the shortest wavelength and the most efficient high-power chemical laser operating to date. The laser operation is based on the transition between the spin-orbit levels of the ground state configuration of the iodine atom, $I(5p^5\ ^2P_{1/2}) \rightarrow I(5p^5\ ^2P_{3/2})$, where the upper level is populated by a near resonant energy transfer from an $O_2(a^1\Delta_g)$ molecule (produced in a chemical generator by the reaction of gaseous chlorine with basic hydrogen peroxide solution):



Mixing of the $O_2(^1\Delta)$ with I_2 molecules results in their dissociation to iodine atoms which are subsequently excited via reaction (1). Maximum values of lasing power were obtained for supersonic COILs where the primary gas ($O_2(^3\Sigma) - O_2(^1\Delta) - He (N_2)$) was brought to supersonic velocity via expansion in a converging-diverging nozzle², whereas the secondary $I_2 - He (N_2)$ flow was injected into the primary flow at some location in the nozzle, either in the subsonic, transonic, or supersonic section of the flow.

One of the most important parameters of the supersonic COIL is the mixing efficiency η_{mix} , defined as the fraction of $O_2(^1\Delta)$ mixed with iodine (see below). To achieve high lasing power P this parameter should be high. Indeed, P can be estimated with the aid of the COIL heuristic equation³

$$P = 91(kJ/mole)nCl_2U(Y_{plen} - Y_{diss} - Y_{th})\eta_{mix}\eta_{ext}, \quad (2)$$

where $91(kJ/mole)$ is the energy of $I^*(\equiv I(^2P_{1/2}))$, nCl_2 the chlorine molar flow rate, U the chlorine utilization and Y_{plen} is the $O_2(^1\Delta)$ yield just upstream of the iodine injection,

$$Y_{diss} = NF \frac{nI_2}{nCl_2\eta_{mix}} \quad (3)$$

is the $O_2(^1\Delta)$ loss during iodine dissociation, η_{ext} the optical extraction efficiency of the resonator, F the iodine dissociation fraction and N is the number of $O_2(^1\Delta)$ molecules lost in the region of iodine dissociation per I_2 molecule. Eqs. (2) and (3) show that P increases with increasing η_{mix} . To estimate η_{mix} it is necessary to know the spatial distributions of the gain g and gas temperature T across the flow at the optical axis of the resonator. Both g and T can be easily measured using diode laser based diagnostic⁴, the first measurements of the gain in supersonic COILs with subsonic injection of iodine being carried out in⁵⁻⁷. In⁶ and⁷ the gain distribution across the flow was monitored for the RADICL and VertiCOIL devices, 5 kW and 1 kW class supersonic COILs, respectively, developed at the Air Force Research Laboratory in Albuquerque, NM. These COILs use He as a buffer gas. For conditions where nitrogen buffer gas or no primary buffer gas is used, the subsonic mixing scheme is not optimal and it is reasonable to move the mixing point downstream to the transonic or supersonic part of the nozzle. This was done in^{8,9} where efficient supersonic COILs using N_2 buffer gas and applying transonic and supersonic mixing of iodine and oxygen were developed.

Recently we reported on the measurements of the gain and temperature at the flow centerline of a slit nozzle supersonic COIL operating without primary buffer gas and using transonic and supersonic schemes of iodine injection¹⁰. Comparison between the values of the gain at the flow centerline and at a point located lower than the flow centerline for transonic injection showed that the gain is strongly non-uniform in a direction perpendicular to both the flow direction and the optical axis, which means that the overall mixing is poor. To study the O_2/I_2 mixing in supersonic COILs with transonic and supersonic schemes of the iodine injection, we measured in the present work the spatial distributions of the gain and temperature as a function of the iodine and secondary nitrogen flow rate, jet penetration parameter and gas pumping rate. Using spatial distributions of g and T and the values of Y_{plen} , measured in the subsonic section of the flow as described in¹¹, we estimated the mixing efficiency η_{mix} . Flow conditions for good mixing in the COIL are found.

2. EXPERIMENTAL SETUP

The experimental setup, including a jet-type singlet oxygen generator (JSOG), is similar to that used in¹⁰. A brief description will be given here for completeness. The oxygen produced in the generator (the same as described in¹⁰) flows into a diagnostic cell with a flow cross section of $1 \times 5 \text{ cm}^2$, which serves as an interface between the generator and the iodine injectors housing. The $O_2(^1\Delta)$ yield Y_{plen} , water vapor fraction, Cl_2 utilization and the temperature of the subsonic flow are simultaneously measured in the diagnostic cell as described in¹¹.

The iodine-oxygen mixing system is located downstream of the diagnostic cell and uses slit supersonic nozzle. We study three slit nozzles (Fig. 1) with iodine injection in the transonic (nozzle No. 1) and supersonic (nozzles No. 2 and 3) sections of the nozzle. All the slit nozzles have the same critical cross sections of 2.5 cm^2 . In slit nozzle No. 1 iodine is injected at the nozzle throat (Fig. 1 a) and in nozzles No. 2 and 3 – in the supersonic section of the nozzle (Fig. 1 b and c). Nozzles 1 and 2 have two rows of injection holes in each wall (top and bottom). The first row of nozzle No. 1 has 31, 0.6-mm diameter holes and the second row 62, 0.4-mm diameter holes (this nozzle was referred to as nozzle No. 2 in¹⁰). The first row of nozzle No. 2 is located 3 mm downstream of the critical cross section and has 49, 0.5-mm diameter holes. The second row has 50, 0.4-mm diameter holes (this nozzle was referred to as nozzle No. 3 in¹⁰). Nozzles No. 1 and No. 2 have the same total cross section of the injection holes equal to 0.32 cm^2 . The angle between the directions of the primary and secondary flows is 90° and 74° for nozzles 1 and 2, respectively. In order to decrease the effect of choking the primary flow by the secondary stream, smaller angle (45°) between the directions of the primary and secondary stream is used in nozzle No. 3. This nozzle has one row of 25, 1.3-mm diameter holes, located 2 mm downstream of the critical cross section, in each wall. The total cross section of the injection holes is 0.64 cm^2 , i.e., larger than for nozzles No. 1 and 2. That is why this nozzle usually operates with secondary N_2 flow rate larger than the primary gas flow rate, which means that the operation conditions of the ejector COIL¹² can be tested using nozzle No. 3.

The laser section starts at the nozzle exit plane (flow cross section of $5 \times 1 \text{ cm}^2$) from where the floor and the ceiling diverge at an angle of 8° . The optical cavity is of 5 cm gain length. For the gain diagnostic system we replaced the laser mirrors by optical windows. The gain was measured at the optical axis of the resonator, 4.5 cm downstream of the nozzle exit plane.

The iodine diagnostic system used in the present work was developed by Physical Sciences Inc.⁴ and is described in detail in¹⁰. It is based on sensitive absorption spectroscopy by tunable near infrared diode laser monitoring the gain for the $I^*(5p^5 \ ^2P_{1/2}, F=3) \rightarrow I(5p^5 \ ^2P_{3/2}, F=4)$ transition at 1315 nm. The diode laser beam makes a single pass through the gain region of the cavity (Fig. 2). To probe the gain distribution in the direction y perpendicular to both the flow direction x and the cavity optical axis z , a collimator launching the beam from the diagnostic system into the gain region is mounted on a linear stage moving in the y direction. The gain is monitored in 50 points uniformly distributed over the flow height $H = 1.5$ cm. After passing the gain region the beam is focused onto a photodiode. The laser frequency is scanned over the I transition, monitoring the gain profile. The temperature of the gas in the cavity is found from the Doppler linewidth $\Delta\nu_D$, the later being determined by fitting the Voigt function to the experimental gain profile as described in¹⁰.

3. RESULTS AND DISCUSSION

In what follows spatial dependencies $g(y)$ and $T(y)$ are presented for different values of iodine molar flow rate nI_2 , jet penetration parameter (defined below), nozzle type and rate of pumping of the gas. Most of the measurements are done for two values of Cl_2 flow rates, $nCl_2 \sim 12$ and ~ 15 mmole/s. The mixing parameter η_{mix} , characterizing the quality of mixing in the flow, is defined and found for different flow conditions.

3.1. Jet penetration parameter

As shown in¹³ changes of secondary nitrogen molar flow rate $(nN_2)_s$ affect the depth of penetration of the N_2/I_2 jets into the primary flow. That means that the gain spatial profiles depend on the penetration parameter defined as¹³

$$\Pi = \frac{n_s}{n_p} \sqrt{\frac{\mu_s T_s p_p}{\mu_p T_p p_s}}, \quad (4)$$

where n , μ and p are the molar flow rate, molecular weight and pressure, respectively, and the subscripts "p" and "s" indicate primary and secondary flow.

Fig. 3 shows $g(y)$ dependencies for nozzle No. 1 with transonic injection of iodine, for $nI_2 = 0.25, 0.28$ and 0.36 mmole/s and $\Pi = 0.12, 0.16$ and 0.18 , respectively. Just as in⁶, for small Π , 0.12 (underpenetrated jets), the gain distribution across the flow has bimodal structure with two peaks corresponding to the centerline of the jets and located higher and lower than the flow centerline. Increase of the penetration parameter results in merging of the two peaks and the gain distribution has one peak at the flow centerline. Π equal to 0.16 and 0.18 corresponds to full penetration (when the jets injected from the opposite walls touch and the bimodal structure disappears) and overpenetration of the jets, respectively. The gain distribution for the case of overpenetration is a little narrower than for full penetration, which is probably due to the effect of the overlap of the overpenetrated jets. The maximum gain at the flow centerline is achieved for overpenetrated jets.

3.2. Nozzle No. 1 with transonic injection of iodine

The $g(y)$ distributions for nozzle No. 1 for different values of nI_2 are shown in Fig. 4a for overpenetrated jets ($\Pi = 0.26$, corresponding to maximum gain) and no primary N_2 . The gain is a non-monotonous function of nI_2 and the dependence of the gain on nI_2 at the flow centerline is different from that at the off axis locations. Fig. 4b shows dependencies of g on nI_2 at $y = 0$ (flow centerline) and $y = 0.5$ cm. It is seen that the optimal value of nI_2 at the flow

centerline is smaller than that at the off centerline location. The reason for this behavior is that the initial I_2 distribution across the flow is strongly nonuniform, the iodine being concentrated near the flow centerline. For low values of the iodine flow rate, the dissociation rate is proportional to the iodine density, hence at the flow centerline both dissociation and gain increase faster with increasing nI_2 than at the off axis location. For higher iodine flow rates the excited species, $O_2(^1\Delta)$, I^* and I_2^* , are rapidly quenched by iodine molecules which results in a decrease of the gain. The quenching rate, which is proportional to the density of I_2 , is higher at the flow centerline than at the off axis location, resulting in faster decrease of the gain at the flow centerline for large iodine flow rate. Therefore the optimal nI_2 at the flow centerline is smaller than at the off axis location.

The $T(y)$ dependencies are shown in Fig. 5a and 5b for the cases of overpenetration and underpenetration, respectively. It is seen that the temperature is distributed homogeneously across the flow for different values of the penetration parameter, increasing only in the narrow boundary layers near the walls. The fact that the temperature distribution is much more homogeneous than the gain distribution, can probably be explained by the high rate of the heat transfer across the flow. The same homogeneous temperature distributions for transonic injection are also observed for different values of the flow parameters.

Using the dependencies $g(y)$ and $T(y)$ it is possible to determine the distribution of the iodine atoms molar fraction $\chi_1(y)$ and to define the mixing parameter η_{mix} . Taking into account that the distance between the iodine injection holes is much smaller than the flow height we can assume that both the gain and temperature are uniform along the optical axis direction z . This assumption is confirmed by the fact that the intensity of the yellow emission of $I_2(B^3\Pi_0^+)$ molecules observed in the supersonic section of the flow is uniform along the z direction. In this case the relation between $g(y)$, $T(y)$, $\chi_1(y)$ and $O_2(^1\Delta)$ yield Y is

$$g = \sigma_0 \left(\frac{300}{T} \right)^{1/2} \frac{p}{kT} \chi_1 \frac{(2K_e + 1)Y - 1}{(K_e - 1)Y + 1}, \quad (5)$$

where $\sigma_0 = 1.29 \times 10^{-17} \text{ cm}^2$ is the stimulated emission cross section at $T = 300 \text{ K}$, p the pressure at the optical axis and $K_e = 0.75 \exp(402/T)$ is the equilibrium constant of reaction (1). For nI_2 much smaller than the optimal iodine flow rate we can assume that on the one hand the rate of iodine dissociation is proportional to the density of I_2^{13} , which means that the molar fraction of I_2 , $\chi_{I_2}(y)$, is proportional to $\chi_1(y)$, and on the other hand the yield Y is close to Y_{plen} , measured in the subsonic section of the flow. In this case $\chi_1(y)$ found from Eq. (5) (with $Y = Y_{plen}$) can be used to define η_{mix} :

$$\eta_{mix} \equiv \frac{\int_{-H/2}^{H/2} \chi_1(y) dy}{(\chi_1)_{\max} H}, \quad (6)$$

where $(\chi_1)_{\max}$ is the maximum value of $\chi_1(y)$. It should be noted once again that the definition (6) (with $\chi_1(y)$ calculated by (5)) makes sense only for small nI_2 . Fig. 6 shows distributions of $g(y)/g_{\max}$ and $\chi_1(y)/(\chi_1)_{\max}$ for the same flow conditions as in Fig. 4 at $nI_2 = 0.228 \text{ mmole/s}$ which is much smaller than the optimal $nI_2 = 0.38 \text{ mmole/s}$. It is seen that for transonic injection the normalized distributions of g and χ_1 are very close to each other, being different only near the duct walls. The calculated value of η_{mix} is equal to 0.52, close values of η_{mix} being found for other primary flow parameters and in particular for the primary flow diluted by N_2 buffer gas. Thus, poor mixing is achieved for transonic injection of iodine.

To increase the mixing efficiency it is necessary to decrease the pumping rate. This is achieved by opening a leak downstream of the cavity as explained in ¹⁰ and results in increase of the pressure and decrease of the Mach number in

the supersonic section of the flow. Figs. 7a and b show the $g(y)$ distributions (at different nI_2) for opened and closed leak, respectively, and the same flow rates of Cl_2 and N_2 . Figs. 8a and b show $T(y)$ for the same conditions. It is seen that maximum values of the gain at the flow centerline for opened leak are smaller than for closed leak, the gain distribution for opened leak being more homogeneous than for closed leak. This behavior is in agreement with the conclusions drawn in ¹⁰ using a simple theoretical model. The temperatures for opened leak are higher than for closed leak, which is due to weaker expansion of the gas for opened leak. Calculations of the mixing parameters using Eqs. (5) and (6) at $nI_2 \approx 0.23$ mmole/s show that η_{mix} is equal to 0.83 and 0.57 for opened and closed leak, respectively. Therefore for opened leak the mixing is much better than for closed leak, which is also in agreement with conclusions obtained in ¹⁰.

3.3. Nozzles No. 2 and 3 with supersonic injection of iodine

Figs. 9a and b show the $g(y)$ distributions for nozzles No. 2 and 3, respectively. The primary flow did not contain N_2 buffer gas and the leak downstream of the cavity was closed. Comparison between Fig. 4a and Figs. 9a and b shows that the maximum values of the gain are almost the same for transonic and supersonic injection, however, for supersonic injection the gain is distributed much more uniformly across the flow. Fig. 10 shows calculated $\chi_1(y)/(\chi_1)_{max}$ for nozzle No. 3 at $nI_2 = 0.39$ mmole/s and the same flow conditions as in Fig. 9b. Comparison between Figs. 6 and 10 shows that unlike transonic injection, where iodine is concentrated near the centerline, for supersonic injection the iodine distribution across the flow is rather uniform and weakly increases near the walls. The calculated η_{mix} is 0.82 and 0.86 for nozzles No. 2 and 3, respectively. Hence for any angle of injection the supersonic injection scheme provides for much more uniform mixing than the transonic injection scheme.

4. SUMMARY

We measured spatial distributions of the gain and temperature across the flow in a slit nozzle supersonic COIL without primary buffer gas using diode laser based diagnostic systems. This was done to estimate the oxygen/iodine mixing efficiency of the COIL, which, in turn, strongly affects the output power. The spatial distributions of the gain and temperature were studied for transonic and supersonic schemes of the iodine injection as a function of the iodine and secondary nitrogen flow rate, jet penetration parameter and gas pumping rate. The mixing efficiency for supersonic injection of iodine (~ 0.8) is found to be much larger than for transonic injection (~ 0.5), the maximum values of the gain being $\sim 0.65\%/cm$ for both injection schemes. Measurements of the gain distribution as a function of the iodine molar flow rate nI_2 were carried out. For transonic injection the optimal value of nI_2 at the flow centerline is smaller than that at the off axis location. The temperature is distributed homogeneously across the flow, increasing only in the narrow boundary layers near the walls. Opening a leak downstream of the cavity in order to decrease the Mach number results in a decrease of the gain and increase of the temperature. The mixing efficiency in this case (~ 0.8) is much larger than for closed leak.

REFERENCES

1. W. E. McDermott, N. R. Pchelkin, D. J. Benard, R. R. Bousek, "An electronic transition chemical laser," *Appl. Phys. Lett.*, vol. 32, pp. 469-470, 1978.
2. K. A. Truesdell and S. E. Lamberson, "Phillips laboratory COIL technology overview," *SPIE*, vol. 1810, pp. 476 - 492, 1992.
3. J. Hon, D. N. Plummer, P. G. Crowell, J. Erkkila, G. D. Hager, C. A. Helms, K. A. Truesdell, "Heuristic Method for Evaluating COIL Performance," *AIAA Journal*, vol. 43, pp. 1595-1603, 1996.
4. S. J. Davis, M. G. Allen, W. J. Kessler, K. R. McManus, M. F. Miller and P. A. Mulhall, "Diode laser-based sensors for chemical oxygen-iodine lasers," *SPIE*, vol. 2702, pp. 195 - 201, 1996.
5. E. Lebiush, B. D. Barmashenko, A. Elor and S. Rosenwaks, "Parametric study of the gain in a small scale, grid nozzle supersonic chemical oxygen-iodine laser," *IEEE J. Quantum Electronics*, vol. 31, pp. 903-909, 1995.
6. R. F. Tate, B. S. Hunt, C. A. Helms, K. A. Truesdell and G. D. Hager, "Spatial gain measurements in a chemical oxygen iodine laser (COIL)," *IEEE J. Quantum Electronics*, vol. 31, pp. 1632 - 1636, 1995.
7. P. B. Keating, B. A. Anderson, C. A. Helms, T. L. Rittenhouse, G. D. Hager and K. A. Truesdell, "2-D spatial gain maps in a small scale chemical oxygen-iodine laser," in *Proc. Int. Conf. Lasers '96*, Portland, OR, Dec. 1996.

8. D. Furman, B. D. Barmashenko and S. Rosenwaks, "An efficient supersonic chemical oxygen-iodine laser operating without buffer gas and with simple nozzle geometry," *Appl. Phys. Lett.*, vol. 70, pp. 2341-2343, 1997.
9. V. N. Azyazov, M. V. Zagidullin, V. D. Nikolaev and V. S. Safonov, "Chemical oxygen-iodine laser with mixing of supersonic jets," *Quantum Electronics*, vol. 27, pp. 491-494, 1997.
10. D. Furman, E. Bruins, V. Rybalkin, B. D. Barmashenko and S. Rosenwaks, "Parametric study of small signal gain in a slit nozzle, supersonic chemical oxygen - iodine laser operating without primary buffer gas," *IEEE J. Quantum Electronics*, vol. 37, pp. 174-182, 2001.
11. D. Furman, B. D. Barmashenko and S. Rosenwaks, "Diode-laser based absorption spectroscopy diagnostics of a jet-type generator for chemical oxygen-iodine lasers," *IEEE J. Quantum Electronics*, vol. 35, pp. 540-547, 1999.
12. T. T. Yang, Y. C. Hsia, L. F. Moon and R. A. Dickerson, "Advanced Mixing Nozzle Concepts for COIL," *SPIE* vol. 3931, pp. 116-130, 2000.
13. C. A. Helms, J. Shaw, G. D. Hager and K. A. Truesdell, "Iodine dissociation in COILs," *SPIE*, vol. 2502, pp. 250 - 257, 1996.

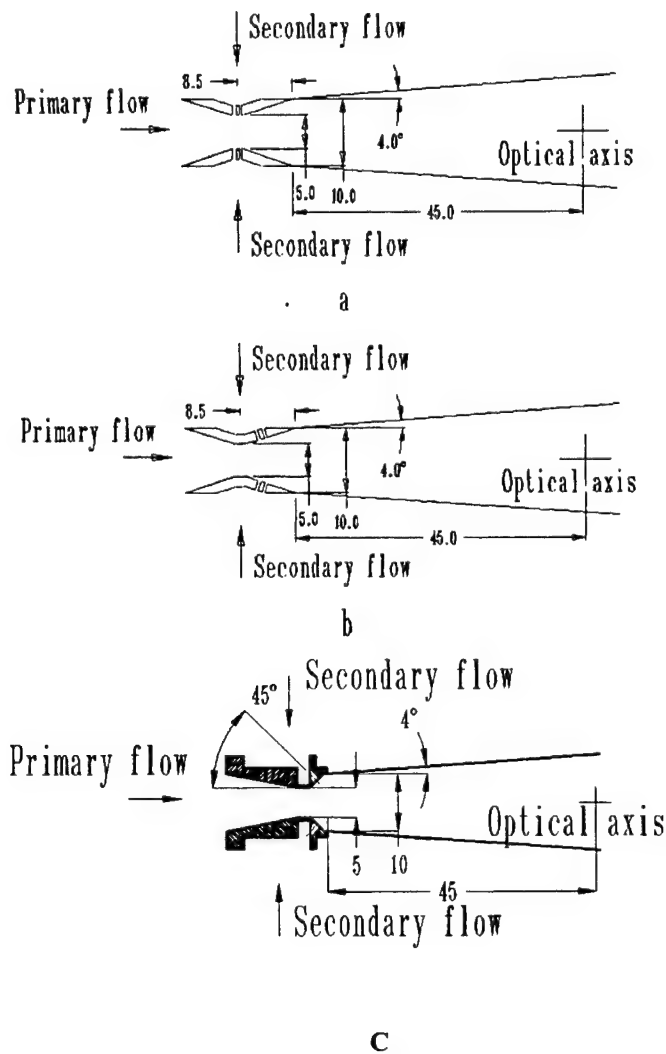


Fig. 1. Schematics of the slit nozzles; a) slit nozzle No. 1 with transonic injection of I_2 ; b) and c) slit nozzles No. 2 and 3, respectively, with supersonic injection of iodine. All measures are in millimeters.

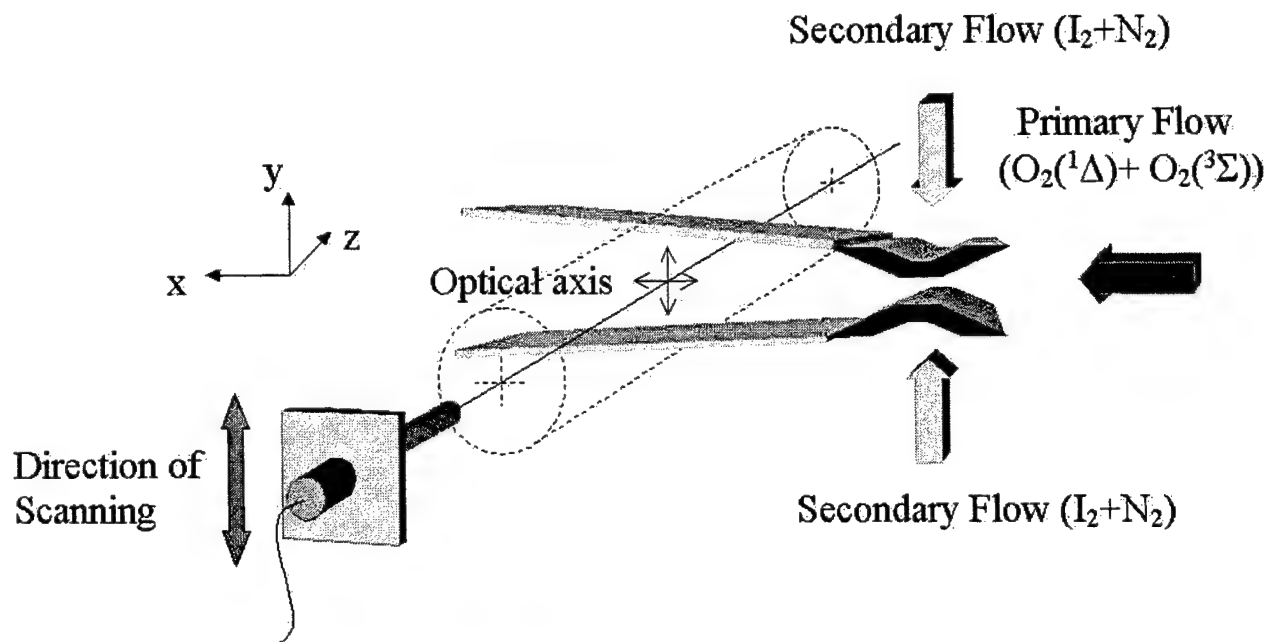


Fig. 2. Schematics of the gain scanning experiment.

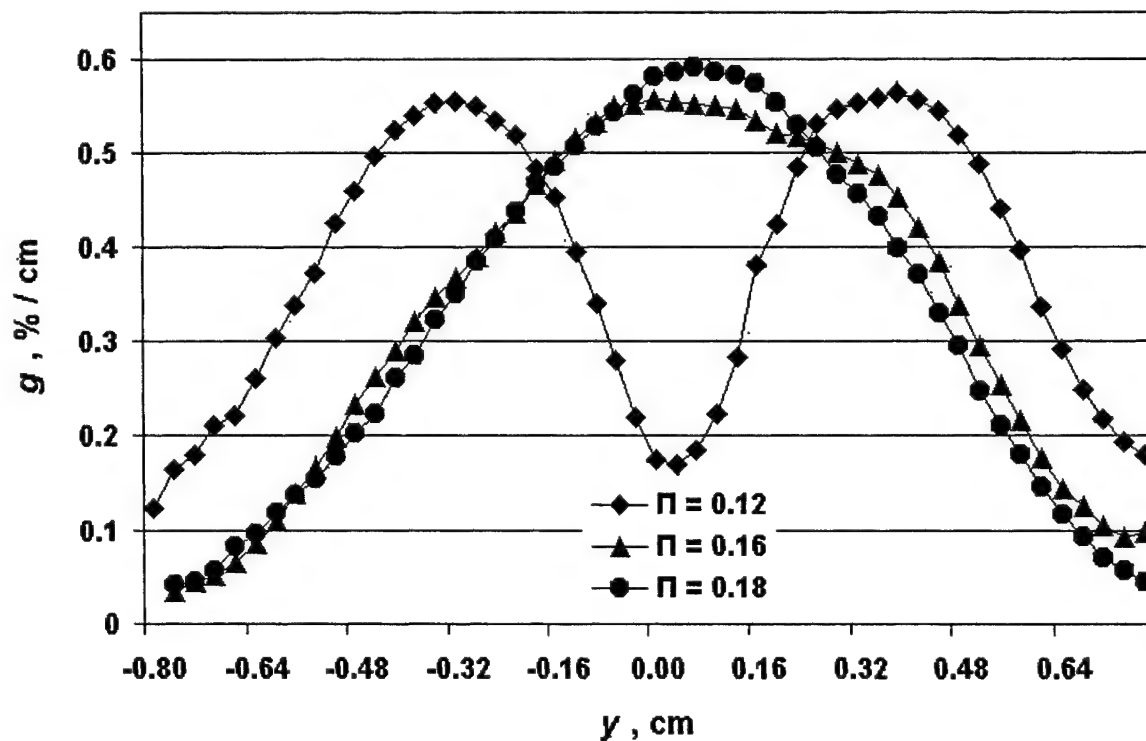


Fig. 3. The gain distributions across the flow, for $n\text{I}_2 = 0.25, 0.28$ and 0.36 mmole/s and penetration parameter $\Pi = 0.12, 0.16$ and 0.18 , respectively, for nozzle No. 1 (transonic injection). The chlorine and primary nitrogen flow rates are 14.8 and 15.2 mmole/s, respectively.

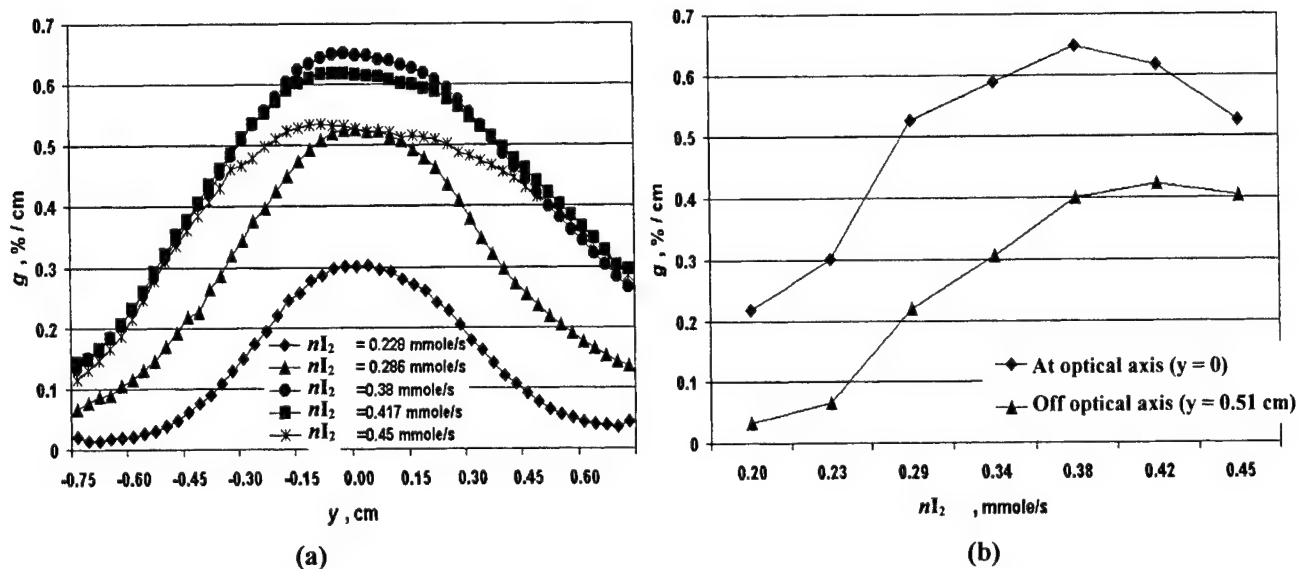


Fig. 4. (a) The gain distributions across the flow for different values of nI_2 for nozzle No. 1 (transonic injection); the chlorine, primary and secondary nitrogen flow rates are 14.4, 0 and 9.9 mmole/s, respectively, the penetration parameter $\Pi = 0.26$; (b) the gain dependencies on nI_2 at the optical axis and off the optical axis for the same flow conditions as in (a).

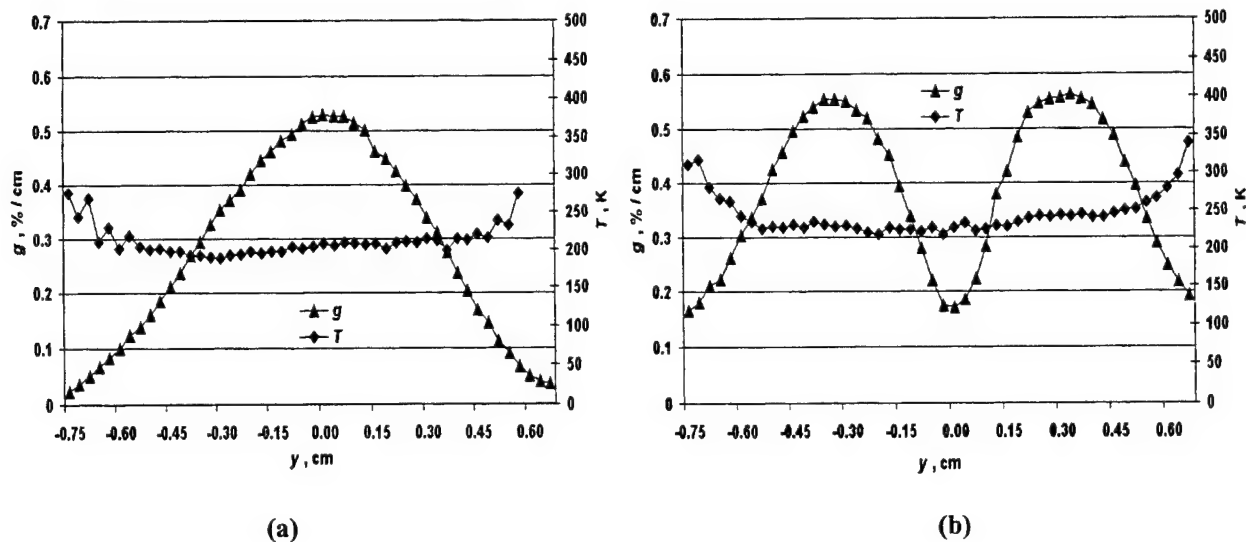


Fig. 5. The gain and temperature distributions across the flow for nozzle No. 1 (transonic injection), the chlorine, primary nitrogen and iodine flow rates are 14.8, 15.2, and 0.25 mmole/s, respectively; (a) overpenetrated jets, the penetration parameter $\Pi = 0.18$ and the secondary flow rate is 12.6 mmole/s; (b) underpenetrated jets, $\Pi = 0.12$; the secondary nitrogen flow rate is 6.4 mmole/s.

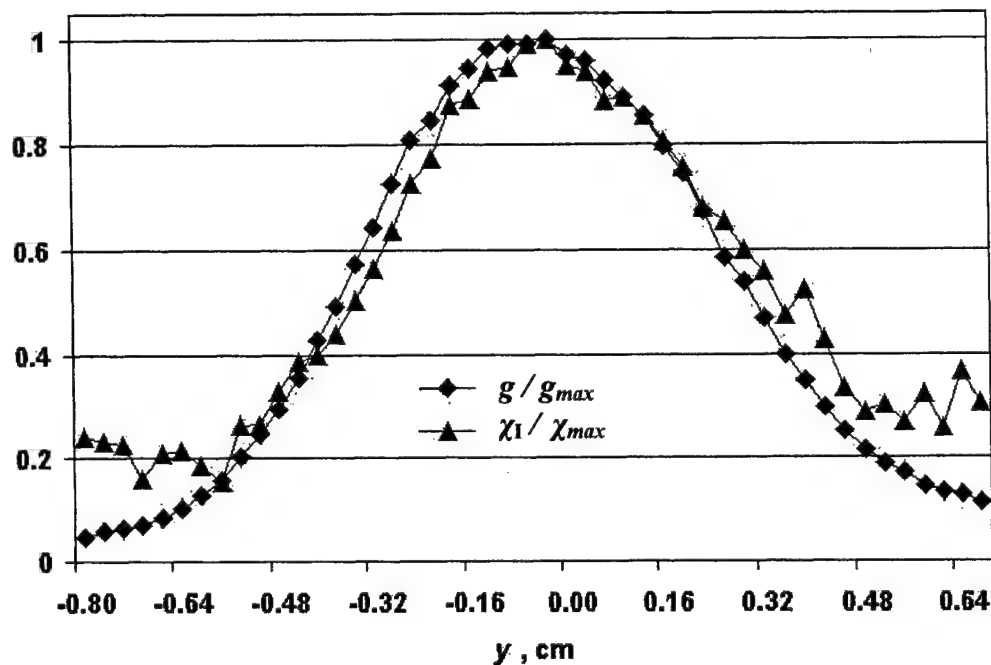
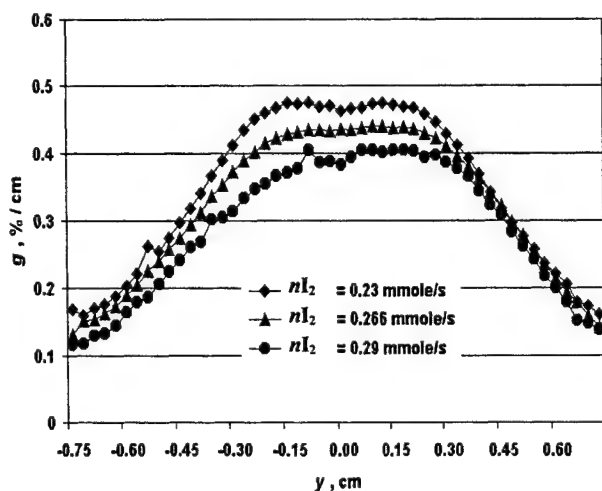
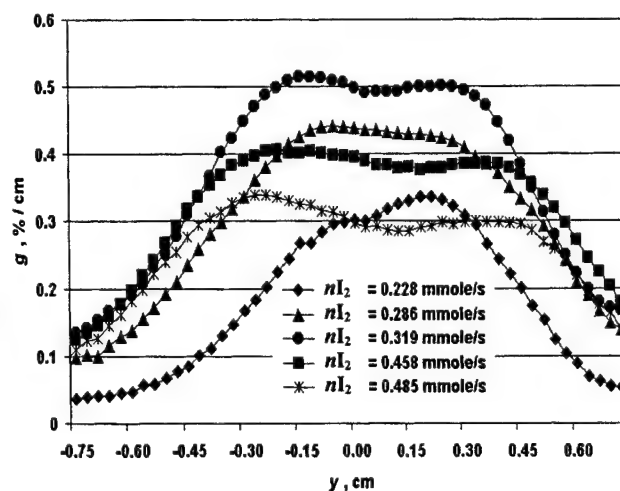


Fig. 6. Normalized gain $g(y)/g_{max}$ and iodine atoms molar fraction $\chi_I(y)/(\chi_I)_{max}$ across the flow for nozzle No. 1 (transonic injection) and the same flow conditions as in Fig. 4 and $nI_2 = 0.23$ mmole/s.

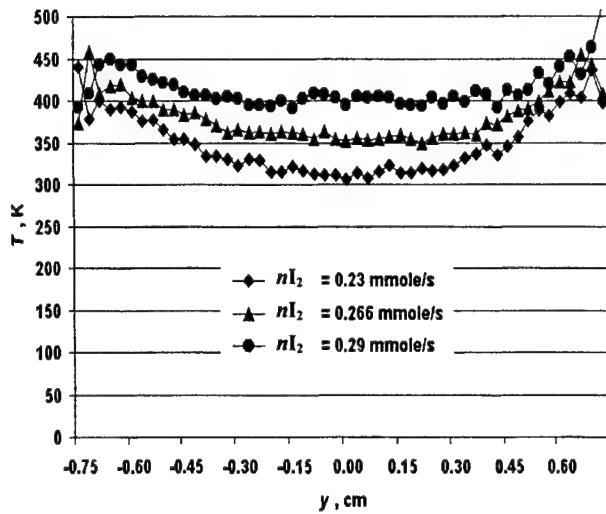


(a)

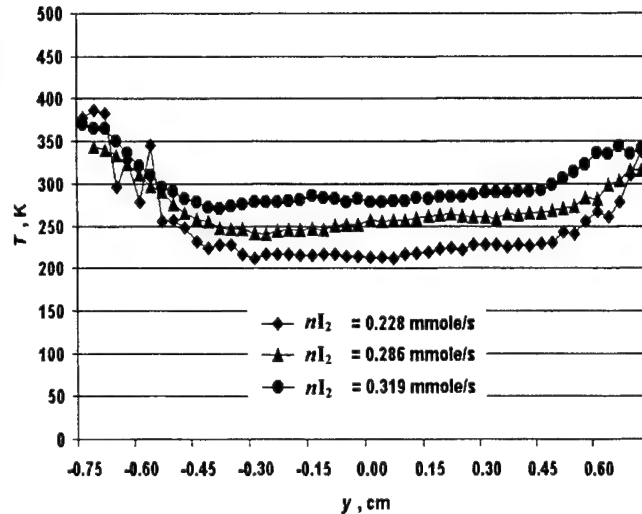


(b)

Fig. 7. The gain distribution across the flow for nozzle No.1 (transonic injection) with opened (a) and closed (b) leak downstream of the cavity; (a) the chlorine, primary and secondary nitrogen flow rates are 11.8, 0, and 4.1 mmole/s, respectively; (b) the chlorine, primary and secondary nitrogen flow rates are 14.3, 0, and 4.9 mmole/s, respectively. For both opened and closed leak the penetration parameter Π is the same (0.19).

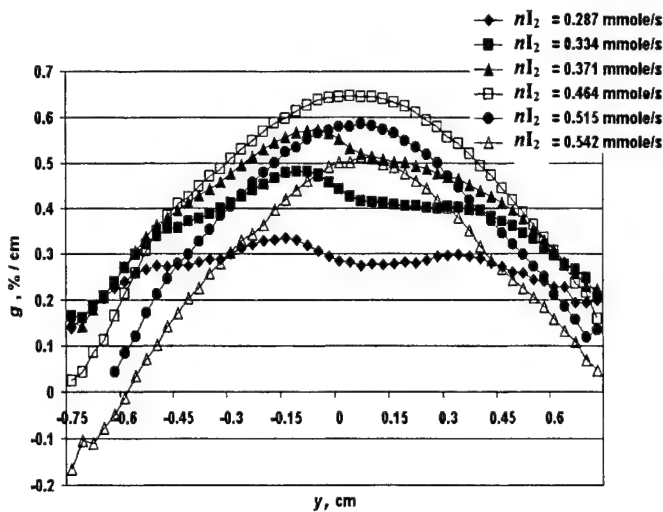


(a)

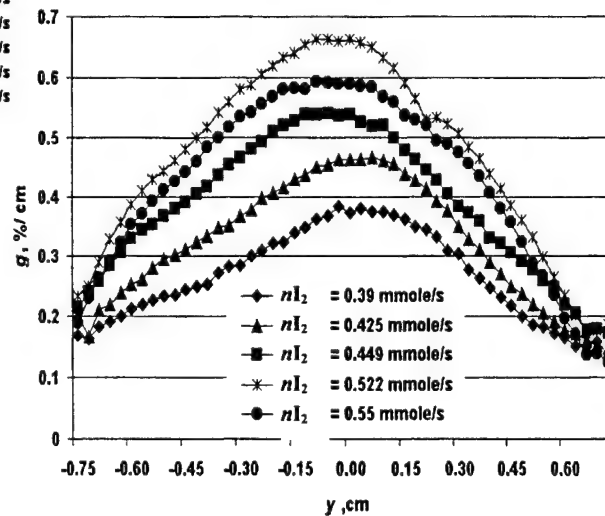


(b)

Fig. 8. The temperature distribution across the flow for nozzle No.1 (transonic injection) with opened (a) and closed (b) leak downstream of the cavity and the same flow conditions as in Fig. 7.



(a)



(b)

Fig. 9. The gain distributions across the flow for different values of nI_2 and closed leak for nozzles No. 2 (a) and 3 (b) (supersonic injection); (a) the chlorine, primary and secondary nitrogen flow rates are 15.1, 0 and 12.7 mmole/s, respectively; (b) the chlorine, primary and secondary nitrogen flow rates are 15, 0 and 20.2 mmole/s, respectively.

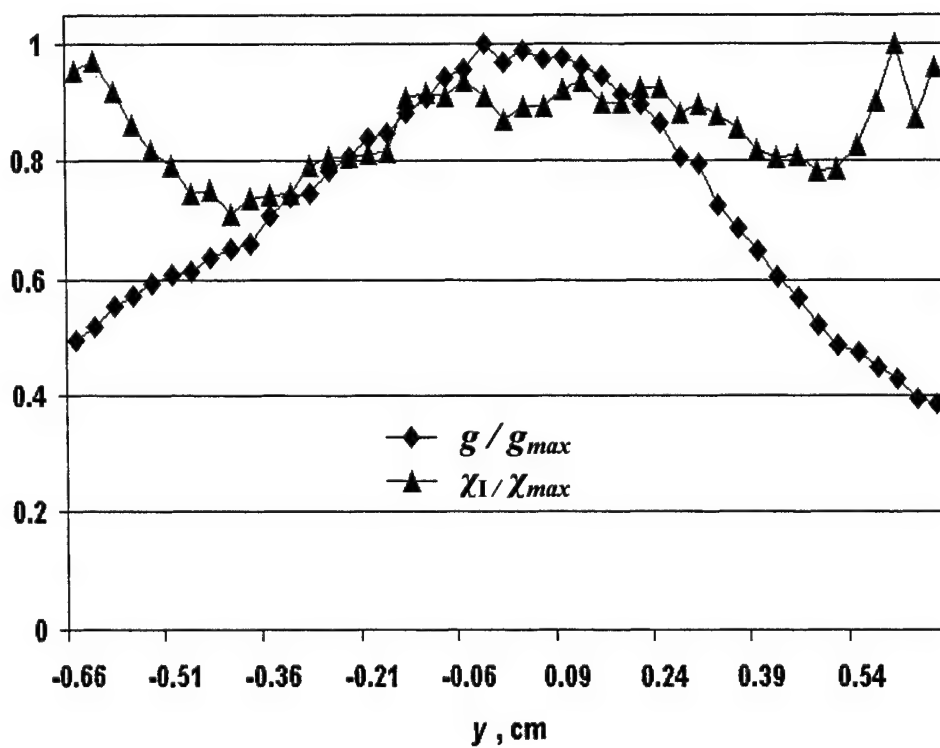


Fig. 10. Normalized gain $g(y)/g_{max}$ and iodine atoms molar fraction $\chi_1(y)/(\chi_1)_{max}$ across the flow for nozzle No. 3 (supersonic injection) and the same flow conditions as in Fig. 9b and $nI_2 = 0.39$ mmole/s.

Chemical generation of atomic iodine for COIL

Otomar Špalek^{*a, b}, Vít Jirásek^{a, b}, Jarmila Kodymová^a, Miroslav Čenský^a, Ivo Jakubec^{**b}

^aInstitute of Physics, ^bInstitute of Inorganic Chemistry, Academy of Sciences of the Czech Rep.,
Czech Republic

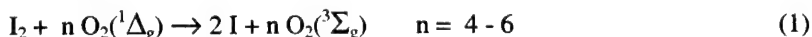
ABSTRACT

A method of the chemical production of atomic iodine aimed for application in COIL was studied experimentally. The method is based on chemical generation of chlorine atoms and their subsequent reaction with hydrogen iodide. Effects of initial ratio of reactants and the way of their mixing were investigated and interpreted by means of the developed model of the reaction system. In optimum conditions, the yield of iodine atoms, related to HI, attained 70 – 100 %.

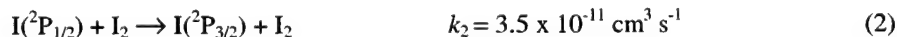
Keywords: atomic iodine, atomic chlorine, chemical oxygen-iodine laser, COIL,

1. INTRODUCTION

In conventional COIL systems, the energy of 4-6 molecules of singlet oxygen, $O_2(^1\Delta_g)$, is consumed to dissociate one iodine molecule to iodine atoms



In the case of another source of atomic iodine, this energy might be utilized for laser pumping. It was estimated that a production of atomic iodine without participation of singlet oxygen could increase a laser power by 25 %.¹ Molecular iodine as a precursor of iodine atoms in COIL introduces further drawbacks like a very fast quenching of excited iodine atoms by iodine molecules



or technical problems connected with evaporation of solid or liquid iodine and supplying iodine vapor into the laser mixing region. To avoid the process (1), methods of microwave discharge pre-dissociation of iodine molecules,² or dissociation of alkyl iodides by electrical discharge³ were investigated up to now. We proposed a method of chemical generation of atomic iodine that fit to COIL conditions.^{4,5} In this paper, results of experimental investigation are presented.

2. DESCRIPTION OF REACTION SYSTEM

The proposed method of chemical generation of atomic iodine in COIL takes advantage of the knowledge gathered during investigation of chemical HCl and HCl/CO₂ transfer lasers.⁶ It is based on a two-step process. In the first step, atomic chlorine is formed by the reaction of chlorine dioxide with nitrogen oxide, in the second step chlorine atoms react with gaseous hydrogen iodide producing atomic iodine.

* E-mail: spaleko@fzu.cz; phone +420 2 66052603; fax +420 2 86890527; Na Slovance 2, 182 21 Prague 8; Czech Republic;

** E-mail: jakubec@iic.cas.cz; 250 68 Řež, Czech Republic

2.1 Generation of chlorine atoms

The fast exothermic reaction of gaseous chlorine dioxide with nitrogen oxide



is employed to generate Cl atoms. It proceeds as a branched chain reaction consisting of the following steps



Reaction (6) is the chain-branching step since there is a net production of one chain carrier. The main reaction product is atomic chlorine for the initial NO : ClO₂ ratio equal to 2 : 1, or ClO radicals for the ratio 1 : 1, respectively. For a fast and efficient course of the above process, the chain carriers Cl and ClO must not be excessively depleted by other processes. The most important loss processes for both Cl and ClO are the termolecular reactions with nitrogen dioxide, NO₂, which is an unavoidable and stable by-product of the reactions (4) and (5)^{6,7}



2.2. Generation of iodine atoms

Iodine atoms are generated by the very fast exothermic reaction of chlorine atoms with hydrogen iodide



In this reaction, up to 70 % of the reaction exothermicity is transferred into vibrational energy of HCl* molecules.⁶ In the case of atomic iodine generation in the stream of singlet oxygen, iodine atoms will be excited in the reaction



Besides this process, recombination of iodine atoms into molecules takes place in termolecular reaction with helium ($k_{\text{He}} = 3.8 \times 10^{-33} \text{ cm}^6 \text{ s}^{-1}$), and molecular iodine ($k_{\text{I}_2} = 3.7 \times 10^{-30} \text{ cm}^6 \text{ s}^{-1}$), respectively. The most important loss process for atomic iodine, owing to a high concentration of NO₂ in the reaction mixture, is the reaction with nitrogen dioxide



followed by



The modeling neglecting a limited mass-transfer rate showed^{6,7} that simultaneous injection of HI, ClO₂ and NO is characterized by exhausting Cl atoms from the reaction mixture by the extremely fast reaction with HI, which results in deceleration of the chain reaction (3). Admixing of hydrogen iodide at a certain distance downstream from the mixing point of ClO₂ and NO was found to be more effective for atomic I production.⁷ A partitioning of NO flow between two injectors was proposed because it could also diminish a loss of produced chlorine atoms⁶. An optimum yield of iodine

atoms was obtained when the second half of NO with HI was injected 0.6 cm downstream from the first injection place (at gas velocity of 200 m s^{-1}).⁷

3. EXPERIMENTAL

The generation of atomic iodine was studied in the system with nitrogen, and some preliminary experiments were performed in the flow of singlet oxygen. A small-scale device was designed for the flow and pressure conditions that are characteristic for the subsonic flow upstream the supersonic nozzle in COIL. The setup for measurements in an excess of nitrogen is shown schematically in Fig. 1.

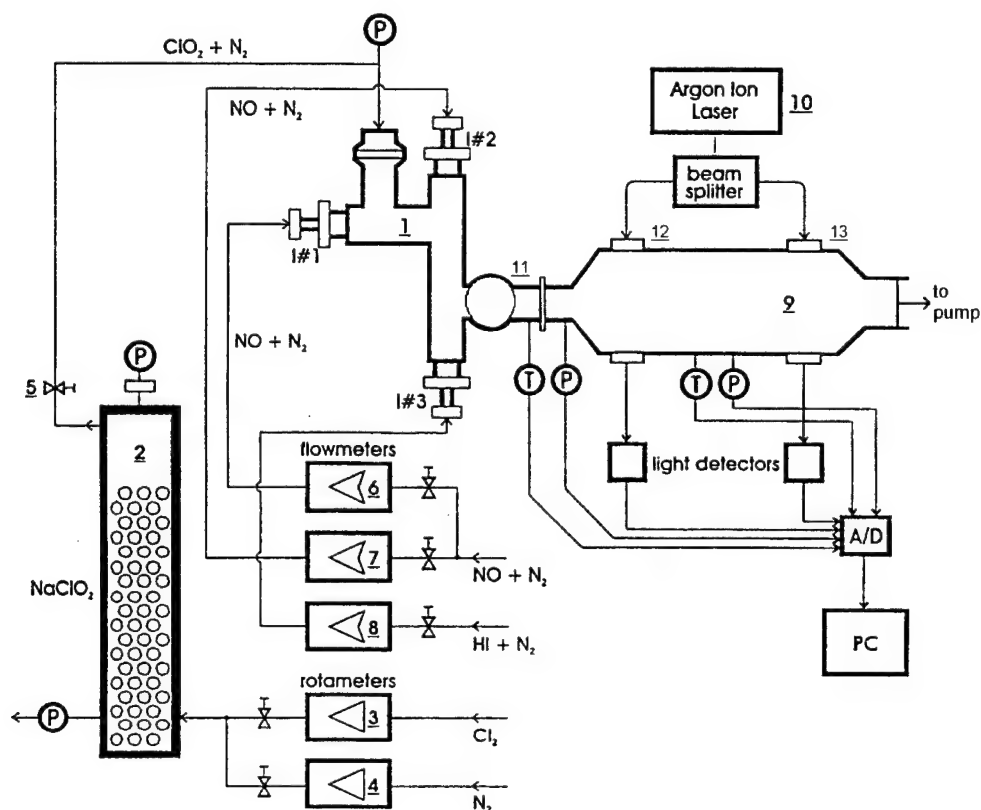


Fig. 1. Scheme of the small-scale device for atomic iodine generation. 1 – flow reactor, 2 – ClO_2 generator, 3,4 – rotameters, 5 – valve, 6 – 8 flowmeters, 9 – diagnostics cell, 10 – Ar ion laser, 11 – ISD cell, 12, 13 – VIS photometry cells

A flow-through chemical reactor 1 is made of stainless steel tube of 10 mm in inner diameter. In the reactor bends, three injectors are inserted coaxially for injection secondary gases into the primary gas. They can be moved and so allow to adjust a time span between injection of reactants. The injectors are made of stainless steel tube of 5 mm in outer diameter with one, two or three rows of openings. The reactor was designed for the flows: $0.1 \text{ mmol ClO}_2 + 5 \text{ mmol N}_2/\text{s}$ as a primary flow, $0.1 \text{ mmol NO/s} + 1 \text{ mmol N}_2/\text{s}$ through the 1st and 2nd injector, respectively, $0.1 \text{ mmol HI/s} + 1 \text{ mmol N}_2/\text{s}$ through the 3rd injector. Diameter and number of the openings in each injector were calculated so to assure the full penetration of each secondary gas into the primary flow. 24 openings of 0.4 mm in diameter were drilled in the 1st injector, 20 openings in the 2nd injector, and 16 openings in the 3rd injector. The pressure in each injector, and the

pressure before the measuring diaphragm of flowmeters 6 – 8 matched up the sonic condition in the diaphragm orifice. The pressure in the reactor was 2 – 4 kPa (15 – 30 torr) and the gas velocity 140 m s^{-1} .

The primary gas flowing into the reactor contained 4 - 10 % ClO_2 . A mixture of NO and nitrogen (10 % NO) was introduced either through the 1st and 2nd injectors simultaneously, or through one of them only. The mixture of hydrogen iodide and nitrogen (with 8 - 10 % HI) was mostly introduced through the 3rd injector. Flow rates of reacting gases were up to $240 \mu\text{mol ClO}_2/\text{s}$, $600 \mu\text{mol NO/s}$ and $500 \mu\text{mol HI/s}$.

Gaseous chlorine dioxide, the reactant for chlorine atoms formation, was produced on site by a heterogeneous reaction between gaseous chlorine and sodium chlorite⁶



This process took place in the ClO_2 generator 2, where gaseous chlorine diluted with nitrogen (in the ratio from 1 : 20 to 1 : 50) was introduced at room temperature. The generator made of PVC tube (7 cm or 11 cm of inner diameter, 1 m long) was filled with either powdered sodium chlorite, or water solution of this salt (40 % w/w). For safety reasons, the partial pressure of ClO_2 in the system should not exceed 30 torr. Flow rates of chlorine dioxide and residual chlorine were determined by chemical analysis of the solution obtained by bubbling the exiting gas through a solution of potassium iodide.

Gas mixture exiting the reactor 1 entered first the optical cell 11 used for atomic iodine detection by the Iodine Scan Diagnostics (ISD) with a tunable diode probe laser.⁸ The method is based on the sensitive absorption spectroscopy by means of tunable near infrared diode laser that monitors the gain or absorption for the $\text{I}(^2\text{P}_{1/2}) - \text{I}(^2\text{P}_{3/2})$ transition at 1315 nm. The laser frequency is scanned over the 3–4 transition in iodine atom. The probe beam passes through the optical cell 11 (11 mm in inner diameter and 45 mm of inner length) in the double pass configuration parallel to the gas flow direction. The optical cell was attached to the reactor without any connecting tube as the lifetime of iodine atoms in the studied gas mixture is rather short (0.1 – 1 ms).⁷ Due to low flow rates of reactants and produced atomic iodine, and because a sufficient absorption length was needed, the longitudinal gas flow through the cell was chosen. The gain/loss data were processed with PC on line using a special developed software. Besides this direct method for I atoms detection, an indirect method was used based on the measuring the concentration of I_2 molecules that are formed by recombination of generated iodine atoms at some distance downstream. The I_2 concentration was determined by the VIS photometry at 488 nm in two optical cells 12, and 13. The argon ion laser with a beam splitter, two silicon photodiodes, and current amplifiers were used. Signals from these diodes, signals from the gas flow meters 6 – 8, and temperature and pressure sensors were processed by AD converter and PC on line. The transport time of gas from the 3rd injector to the entrance of the cell 11 was about 0.2 ms, to the cell exit 0.8 ms, to the axis of the cell 12 – 6 ms, and to the axis of the cell 13 – 93 ms, respectively. The flow rate of produced nitrogen dioxide was evaluated from the change of 488 nm light absorption after admixing NO into the primary ClO_2 flow (before HI admixing) using the published absorption cross-section of $2.7 \times 10^{-19} \text{ cm}^2$. Gas exiting the diagnostic cell was passed through a scrubber with a bed of solid potassium hydroxide and through a liquid nitrogen trap. The system was exhausted with a rotary pump ($25 \text{ m}^3/\text{h}$).

A generation of atomic iodine in the flow of singlet oxygen was performed using the same reactor 1, into which a stream of singlet oxygen was introduced as the primary gas. A small-scale jet-type generator of the cross section $8 \times 16 \text{ mm}$ with liquid jets counter-flown by gaseous chlorine was described in detail in our earlier paper.⁹ The $\text{O}_2(^1\Delta_g)$ concentration was evaluated from $1.27 \mu\text{m}$ emission in a detection cell placed at the generator exit. The gas containing $\text{O}_2(^1\Delta_g)$ was introduced into the reactor 1 as a primary gas, the mixture $\text{ClO}_2 + \text{N}_2$ was injected through the 1st injector, $\text{NO} + \text{N}_2$ through the 2nd injector, and $\text{HI} + \text{N}_2$ through the 3rd injector.

4. RESULTS AND DISCUSSION

4.1. ClO_2 production

A solid NaClO_2 (50% w/w) was used first for ClO_2 production. The larger ClO_2 generator was filled with 10 dm^3 of powdered chlorite, and $90 \mu\text{mol}$ chlorine/s was passed through it. It produced $140 - 150 \mu\text{mol ClO}_2/\text{s}$ with the yield of 80 – 85 %, the exiting gas contained further about $15 \mu\text{mol/s}$ of residual chlorine. At higher chlorine flow rate, the ClO_2

yield was lower. The ClO_2 yield was also decreasing with "aging" the filler (e.g., only 40 % yield was measured after two months of intermittent use, even if the sodium chlorite was exhausted from 12 – 15 % only). This phenomenon, observed also by Arnold⁶, is probably caused by a layer of sodium chloride on the surface of chlorite crystals. This layer obviously hinders the chlorine diffusion and slows down the ClO_2 production. In the second arrangement, chlorine-nitrogen mixture was bubbled through 1 dm³ of chlorite solution (32 %) providing 200 – 250 $\mu\text{mol ClO}_2/\text{s}$ with the yield 81 – 85 %. The production rate was very stable for about 5 hours, which corresponded to about 90 % utilization of the chlorite. This process is substantially more effective and reproducible than the former. Some problem could introduce water in the exiting gas due to the quenching of excited iodine atoms. This effect, however, should not be too serious, as the contribution of this water is substantially lower than the amount produced by the singlet oxygen generator.

4.2. Molecular iodine formation

Besides molecular iodine formed by recombination of generated I atoms, some I_2 molecules may be formed also by other reactions. One of them is the reaction of residual molecular chlorine (coming from ClO_2 generator) with hydrogen iodide



The rate constant of this reaction $k_{15} = (3.4 \pm 1.7) \times 10^{-33} \text{ cm}^6 \text{ s}^{-1}$ was evaluated from our earlier measurements⁴ performed in the described reactor at room temperature and concentration of reactants $(2 \div 9) \times 10^{16} \text{ cm}^{-3}$. It was found by the modeling of the reaction system producing atomic iodine that the reaction (15) may have some effect on the I_2 concentration measured in the optical cell 13, but effect of this reaction on the I_2 concentration in the cell 12 is negligible. For this reason, the overall rate of atomic iodine production was calculated from the I_2 flow rate evaluated for the cell 12.

In the next experiments the ClO_2 – HI system was investigated. In the reactor 1, the secondary flow of 90 – 340 $\mu\text{mol HI/s}$ was injected through the 3rd injector into the primary flow of 200 – 250 $\mu\text{mol ClO}_2/\text{s}$. No iodine atoms were detected in ISD cell 11, but molecular iodine was measured in both cells 12 and 13. From these measurements, the rate constant of the reaction



was evaluated. It followed from the modeling of the reaction system ClO_2 –NO–HI that the reaction (16) may increase I_2 concentration measured in the cell 12. It occurred, however, only in the case of excessive HI flow rate against the rate of Cl atoms generation, i.e. at $\text{HI}/\text{ClO}_2 \geq 1$, and $\text{NO}/\text{ClO}_2 < 1$.

4.3. Atomic iodine generation in an excess of nitrogen

In Fig.2, an example of the time course of flow rates of HI and produced atomic iodine is shown for constant flow of nitrogen oxide. Atomic iodine was detected both directly by ISD, and indirectly as molecular iodine. It can be seen in this figure that the rate of generation of atomic iodine increases with increasing flow rate of hydrogen iodide. The flow rate of atomic iodine detected by ISD corresponded to the overall atomic I flow rate, however, up to about 50 $\mu\text{mol/s}$ only. With increasing HI flow rate above this limit, the ISD signal remained constant or even fell. This can be explained so that with increasing HI flow rate the rate of formation of atomic iodine also increases, and the rate of reactions (12), (13) as well. The local concentration of I atoms drops markedly with the distance from the HI injection, and the flow rate measured by ISD represents only a fraction of the overall production rate. In these conditions the concentration gradient of atomic iodine downstream the HI injector may become steeper, and the fraction of the atomic iodine flow rate detected in the cell 11 to the overall production rate smaller. Fig. 3 shows a calculated course of atomic and molecular iodine flow rate downstream the HI injection. It can be seen that the average flow rate of atomic iodine in the ISD cell is substantially lower than the maximum flow rate near the HI injector. In a real system, the concentration gradient is probably more moderate due to a limited mass transfer rate. Results of modeling showed that the overall production rate of atomic iodine corresponds better to a double value of the molecular iodine flow rate

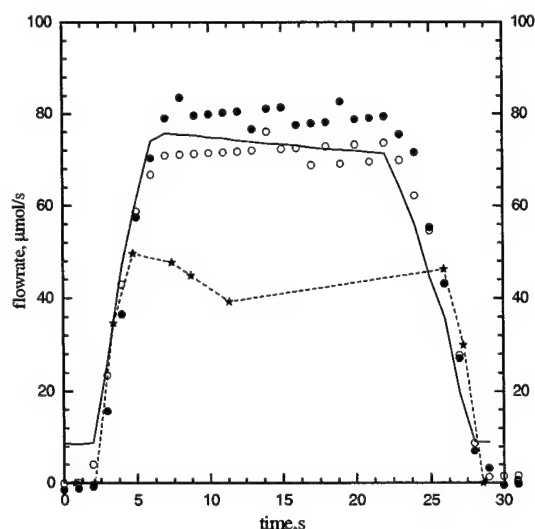


Fig. 2: Time course of HI flow rate (—), rate of formation of atomic iodine detected by ISD (---*---), and visible photometry in the cells 12 (○) and 13 (●), respectively. Total pressure 2.1 kPa, 245 $\mu\text{mol ClO}_2/\text{s}$ and 2 mmol N_2/s in the primary flow, 150 $\mu\text{mol NO/s}$ through the 1st injector, 150 $\mu\text{mol NO/s}$ through the 2nd injector, $d_{1,2}=38$ mm, $d_{2,3}=3.7$ mm, $d_{3\text{-ISD}}=10$ mm

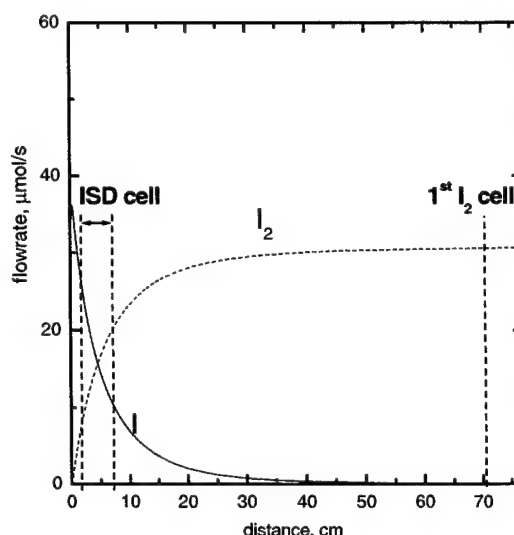


Fig. 3: Calculated course of atomic and molecular iodine flow rate on the distance from the 3rd injector at gas velocity 140 m/s, 220 $\mu\text{mol ClO}_2/\text{s}$ in primary flow, 205 $\mu\text{mol NO/s}$ (2nd injector) and 220 $\mu\text{mol HI/s}$ (3rd injector), $d_{2,3}=3.7$ mm, $d_{3\text{-ISD}}=11$ mm.

measured in the cell 12. It is valid, however, only in the case that the contribution of the reaction (16) to the I_2 concentration can be neglected.

In the next experiments, approximately the same overall amount of NO was injected into the primary flow of chlorine dioxide, but in a different way. Nitrogen oxide was introduced either through 1st or 2nd injector, or through both injectors simultaneously (see Tab.I).

Table I

Effect of the way of NO injection on atomic I production measured by ISD ($n_{\text{I}}^{\text{ISD}}$) and VIS photometry ($n_{\text{I}}^{\text{VIS}}$). Primary flow 220 $\mu\text{mol ClO}_2/\text{s}$, distance between injectors: $d_{1,2}=30$ mm, $d_{2,3}=3.7$ mm, and to ISD cell 11: $d_{3\text{-ISD}}=20$ mm.

n_{NO} (1 st inj.), $\mu\text{mol/s}$	n_{NO} (2 nd inj.), $\mu\text{mol/s}$	n_{HI} (3 rd inj.), $\mu\text{mol/s}$	$n_{\text{I}}^{\text{ISD}}$, $\mu\text{mol/s}$	$n_{\text{I}}^{\text{VIS}}$, $\mu\text{mol/s}$
320	0	100	0	18
150	150	100	50	80
0	330	100	82	98

When all NO was introduced through the 1st injector, most of Cl atoms were lost (by reactions (7) - (9)) before mixing with HI, which resulted in a low production of atomic iodine. A medium atomic iodine production was attained when NO was introduced through both 1st and 2nd injector simultaneously. Results of mathematical modeling of this system show (Fig. 4) that mostly ClO radicals are formed downstream the first injector (by the reaction (4)), and Cl atoms are generated downstream the second injector (by the non-chain mechanism). In this case, the HI injector was placed as close to the 2nd NO injector as possible so that a very small proportion of Cl atoms sufficed to be recombined in

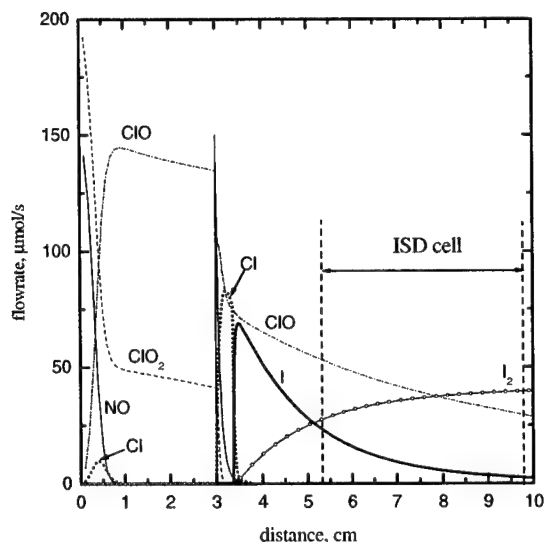


Fig.4: Calculated flow rate of reactants and products at gas velocity 140 m/s, 200 $\mu\text{mol ClO}_2/\text{s}$ in primary flow, 150 $\mu\text{mol NO/s}$ (1st injector), 150 $\mu\text{mol NO/s}$ (2nd injector) and 100 $\mu\text{mol HI/s}$ (3rd injector), $d_{1-2} = 38 \text{ mm}$, $d_{2-3} = 3.7 \text{ mm}$, $d_{3-\text{ISD}} = 20 \text{ mm}$

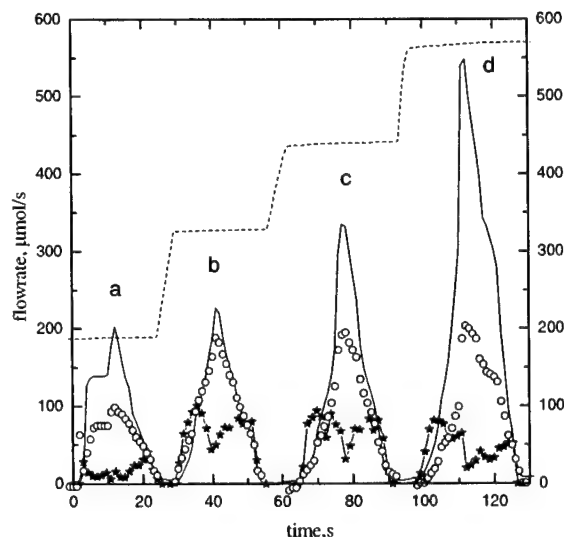


Fig.5 : Time course of NO flow rate through thr 2nd injector (.....) and HI flow rate through the 3rd injector (—), rate of formation of atomic iodine detected by ISD in the cell 11 (—★—) and visible photometry in the cell 12 (○), respectively. Total pressure 2.1 kPa, 220 $\mu\text{mol ClO}_2/\text{s}$ and 2 mmol N_2/s in the primary flow, $d_{1-2} = 38 \text{ mm}$, $d_{2-3} = 3.7 \text{ mm}$, $d_{3-\text{ISD}} = 10 \text{ mm}$.

reactions (7) - (9). This figure also shows that only a small fraction of I atoms can be detected by ISD cell. In a real system, this fraction may be higher due to a limited mass transfer rate that extends the region of iodine atoms further

downstream. It was also proved experimentally that the rate of I atoms production did not depend on the distance between the 1st and 2nd injector (in the range of 8-21 mm). This is in accordance with the calculated high stability of ClO radicals in this region (see Fig.4).

The highest yield of atomic iodine (measured by both methods) was achieved when all NO was injected only 3.7 mm upstream the HI injector. It means that the time span of 27 μs between 2nd and 3rd injector, respectively, is sufficient for an effective production of chlorine atoms formed by the chain mechanism of the reaction (3). This is in a good agreement with the time span of 35 μs system between the HI injection and the maximum concentration of Cl atoms which was obtained by the modeling (see Fig. 4 in our previous paper⁷).

In the next series, effects of distances between injectors on atomic iodine production were studied (see Tab. II).

Table II

Effect of distance between injectors, (d), on atomic I flow rate measured by ISD (n_I^{ISD}) and VIS photometry (n_I^{VIS}). Primary flow 240 $\mu\text{mol ClO}_2/\text{s}$, 1st injector: 220 $\mu\text{mol NO/s}$, 2nd injector: 220 $\mu\text{mol NO/s}$, 3rd injector: 100 $\mu\text{mol HI/s}$.

d_{1-2} , mm	d_{2-3} , mm	$d_{3-\text{cell 11}}$, mm	n_I^{ISD} , $\mu\text{mol /s}$	n_I^{VIS} , $\mu\text{mol /s}$
9	23	20	5	15
37	3.7	20	20	54
37	3.7	11	40	55

This data proved that diminishing the distance, d_{2-3} , between the second NO injector and HI injector is favorable (in spite of the longer distance between 1st and 2nd NO injection) due to a reduced loss of chlorine atoms. A diminishing of the distance between HI injection and ISD cell 11 resulted in higher concentration of I atoms measured in this cell even

though the overall rate of I generation remained unchanged. It can be explained by a lower loss of I atoms in reactions (12), (13). This result can also explain a very low ISD signal of atomic iodine measured during our initial experiments, when the ISD cell was connected with the reactor by means of a 4 cm long tube.

Another example of the measured time course of reactants and atomic iodine flow rate is shown in Fig. 5. This figure documents effects of HI and NO flow rate, respectively, on the production of atomic iodine. In accordance with the above results, a lower rate of I production was measured in the region *a*, when NO was introduced by the first and the second injector simultaneously.

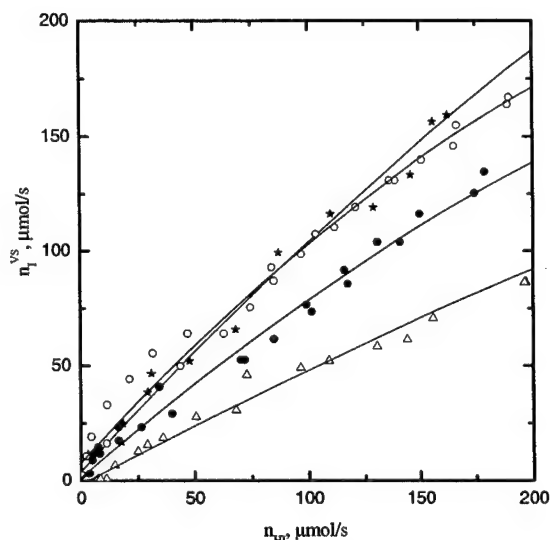
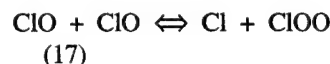


Fig. 6.: Overall flow rate of atomic iodine (in cell 12) on HI flow rate. NO flow rate: 205 $\mu\text{mol/s}$ (\star), 330 $\mu\text{mol/s}$ (\circ), 440 $\mu\text{mol/s}$ (\bullet), 560 $\mu\text{mol/s}$ (Δ), other conditions as in Fig.5.

In the next regions, with NO introduced through the second injector, the overall rate of atomic iodine production was higher at lower NO/ ClO_2 ratio. This is more obvious from the dependence of the production rate of I atoms on HI flow rate plotted for different NO flow rate (see Fig.6).

For NO/ ClO_2 ratio equal to 1 or 1.5, the yield of atomic iodine was nearly 100 % (related to HI). At higher NO/ ClO_2 ratio (2 and 2.6) the yield was substantially lower (70 and 45 %, respectively). This effect could be explained by different mechanism of atomic chlorine production in both experimental conditions. At NO/ $\text{ClO}_2 \geq 2$, chlorine atoms are formed very fast by the chain branching mechanism (4) - (6) and still before mixing with HI may be partly lost by the fast reactions with nitrogen dioxide (eqs.(7), (8)). In the case of the ratio NO/ $\text{ClO}_2 \approx 1$, more stable radicals ClO are formed, which are in equilibrium with Cl atoms and ClOO radicals⁶



This equilibrium is strongly shifted to the left ($k_{17} = 2.8 \times 10^{-14} \text{ cm}^3 \text{ s}^{-1}$ and $k_{-17} = 1.0 \times 10^{-11} \text{ cm}^3 \text{ s}^{-1}$). In the

presence of HI, chlorine atoms are consumed in the very fast reaction (10), and further chlorine atoms are produced by the reaction (17). Excessive ClOO radicals then also provide Cl atoms in the reaction⁶



The modeling of this system showed that the atomic chlorine production by the chain reaction (3) (at NO/ $\text{ClO}_2 \approx 2$) followed by atomic iodine formation (eq.(10)) proceeds much faster than the non-chain process through the reactions (4), (17), (18), and (10). In a real system, where the mixing of Cl atoms with HI occurs in a limited rate only, the second reaction path may be more effective because of lower loss of atomic chlorine in reactions (7) and (8). These loss processes proceed mostly in the regions with insufficient HI supply. The developed one-dimensional model (assuming an instantaneous mixing of reactants) of the studied reaction system, however, did not confirm quantitatively the observed effect of NO/ ClO_2 ratio on the atomic iodine production.

First experiments with atomic I generation in the flow of singlet oxygen are under way so that the preliminary results will be presented at the conference only.

4.5. Application possibilities of the method in COIL

The method of atomic iodine generation above described is planned to be applied in COIL provided that results of the study performed in the flow of singlet oxygen will be promising. Owing to a relatively short lifetime of iodine atoms in the reaction mixture (0.1 - 1 ms) at pressures typical for the subsonic part of COIL (a few kPa), an application of the proposed process is anticipated either very close to the supersonic nozzle, or with transonic mixing of reactants.

5. CONCLUSIONS

A method of the chemical production of atomic iodine, based on chemical generation of chlorine atoms and their subsequent reaction with gaseous hydrogen iodide, was studied experimentally. It is aimed to be applied in the COIL operation. The method is.

Effects of initial ratio of reactants and the way of their mixing were studied and interpreted by means of the developed model of this reaction system.

In optimum conditions, the yield of atomic iodine production was rather high, from 70 to 100 % (related to ClO_2 or HI).

The proposed process of atomic I generation is assumed to be applied in the supersonic COIL either very close to a supersonic nozzle, or with transonic mixing of reactants. It may save a significant fraction of singlet oxygen and so increase the laser efficiency.

ACKNOWLEDGMENTS

This work was supported by the USAF European Office for Research and Development (EOARD), and the Grant Agency of the Czech Republic. The authors thank to Dr. G. Hager from the USAFRL for his encouragement in this work and the AFRL for lending the diode probe laser diagnostics.

REFERENCES

1. E. Endo, D. Sugimoto, H. Okamoto, K. Nanri, T. Uchiama, S. Takeda, T. Fujioka, "Output Power Enhancement of a Chemical Oxygen-iodine Laser by Predissociated Iodine Injection", *Jpn. J. Appl. Phys.* **39**, pp. 468-474, 2000.
2. M. Endo, M. Kawakami, S. Takeda, F. Wani, T. Fujioka, "Output Power Enhancement by the Injection of Dissociated Iodine in Supersonic Chemical Oxygen-Iodine Laser", *Proc. SPIE*, Vol. **3612**, pp. 56-61, 1999
3. V.S. Pazyuk, N.P. Vagin, N.N. Yurishv, "Repetitively Pulsed Chemical Oxygen-Iodine Laser with a Discharge Generation of Atomic Iodine", *Proc. SPIE*, Vol. **2767**, pp. 206-208, 1995
4. O. Špalek, V. Jirásek, J. Kodymová, I. Jakubec, M. Čenský, "Preliminary experimental results on chemical generation of atomic iodine for COIL", *Proc. SPIE*, Vol. **4184**, pp. 111-115, 2000
5. V. Jirásek, O. Špalek, J. Kodymová, "Modeling of chemical generation of atomic iodine for chemical oxygen-iodine laser", *Proc. SPIE*, Vol. **4184**, pp. 103-106, 2000
6. J. Arnold, K.D. Foster, D.R. Snelling, R.D. Suart, "A Purely Chemical HCl Laser Employing Transverse Flow", *IEEE J. Quant. Electron.*, **QE-14**, pp. 293-302, 1978.
7. V. Jirásek, O. Špalek, J. Kodymová, M. Čenský, "Chemical generation of atomic iodine for chemical oxygen-iodine laser. I. Modelling of reaction systems", *Chem. Phys.*, **269**, pp. 167-178, 2000
8. R.F. Tate, B.S. Hunt, C.A. Helms, K.A. Truesdell, G.D. Hager, "Spatial Gain Measurements in a Chemical Oxygen Iodine Laser", *IEEE J. Quant. Electron.*, **31**, pp. 1632-1636, 1995
9. J. Kodymová, O. Špalek, "Performance Characteristics of Jet-type Generator of Singlet Oxygen for Supersonic Chemical Oxygen-Iodine Laser", *Jpn. J. Appl. Phys.*, **37**, p. 117-121, 1998

Modeling of the chemical generation of atomic iodine in a chemical oxygen-iodine laser

Vít Jirásek*, Otomar Špalek, Jarmila Kodymová, and Miroslav Čenský

ABSTRACT

The mathematical modeling of reaction systems for chemical generation of atomic iodine is presented. This process can be applied in the chemical oxygen-iodine laser (COIL), where it can save a substantial part of energy of singlet oxygen and so increase the laser output power. The parametric study of the production of atomic fluorine and subsequently atomic iodine in dependence on the pressure and dilution with inert gas was made. The calculation of the interaction between produced atomic iodine and singlet oxygen was made with four different mixing/reacting schemes.

Keywords: chemical oxygen-iodine laser, atomic iodine, modeling, gas reactions

1. INTRODUCTION

In conventional COIL systems, iodine atoms in the ground state, $I(^2P_{3/2})$, are formed from molecular iodine dissociated by the energy of singlet oxygen, $O_2(^1\Delta_g)$. The using of atomic iodine instantly prepared in other way can substantially increase the chemical efficiency of the laser. Up to now, methods of microwave discharge pre-dissociation of molecular iodine¹, and discharge dissociation of alkyl iodides² were tested to generate atomic iodine for COIL.

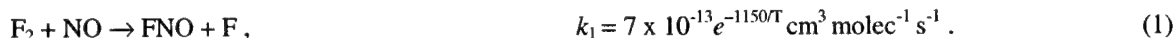
We proposed a method of chemical generation of atomic iodine for COIL based on the reaction of hydrogen iodide with chemically generated atomic fluorine or chlorine.^{3,4} Atomic iodine produced in this way can then undergo the energy transfer from singlet oxygen contained in the gas flow. Because the reaction of hydrogen iodide with both atomic fluorine and chlorine is very fast, the chemical efficiency of atomic iodine production is determined by the efficiency of the preparation of atomic fluorine (in reaction $F_2 + NO$) or chlorine ($ClO_2 + NO$). To estimate the efficiency of these processes, a simplified one-dimensional (1-D) kinetic model was proposed and numerically solved for both reaction systems.⁴ In this modeling, a constant gas velocity and constant total enthalpy were assumed, and the diffusion of species and heat transfer along the flow were neglected. The calculations were performed for the conditions that correspond with the subsonic channel, i.e., upstream the nozzle throat, in the supersonic COIL device operated in our laboratory: the total pressure of 4 kPa, temperature of 300 K, velocity of 200 m/s. The results following from this modeling showed that atomic fluorine is produced with a rate that is too slow to realize this process directly in the subsonic channel. More promising results were obtained by the modeling of the reactions with atomic chlorine, resulting in a sufficient production rate of atomic iodine. However, it is a disadvantage of this process, that the produced atoms are rapidly recombined in the presence of NO_2 . The results of 1-D modelling of this system⁴ are only in some respect in quantitative accordance with the results from the experiments.^{3,5}

The new results of modeling of the production of atomic iodine via atomic fluorine are presented in this paper, including the dependence on the initial pressure and dilution with the inert gas. The results of calculations of the interaction between produced atomic iodine and singlet oxygen are also included, considering four different mixing/reacting schemes.

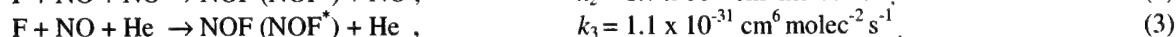
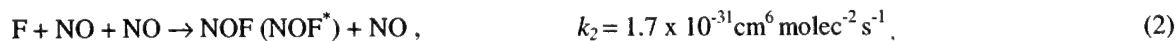
Correspondence: e-mail: jirasek@fzu.cz; phone 420-2-66052603; fax 420-2-6880729; Department of Gas Lasers, Institute of Physics of Academy of Sciences, Na Slovance 2, 182 21 Prague 8, Czech Republic

2. DESCRIPTION OF REACTION MECHANISM

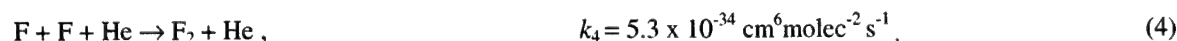
Fluorine atoms are produced by the fast exothermic reaction ($\Delta H_{298}^0 = -77$ kJ/mol) of molecular fluorine with nitrogen oxide⁶⁻⁸



The yield of F atoms is substantially influenced by several consecutive reactions, mainly the termolecular reactions of F atoms with NO and other molecules present in the reaction system (e.g., helium used as a diluent)^{9,10}

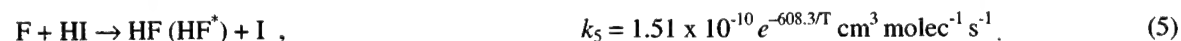


Nitrosyl fluoride, NOF, is formed either in the ground or electronically excited state. The reactions (2) and (3) are also very exothermic (for NOF ground state, $\Delta H_{298}^0 = -229.4$ kJ/mol). The three-body recombination of F atoms by the exothermic reaction ($\Delta H_{298}^0 = -158.3$ kJ/mol)¹⁰



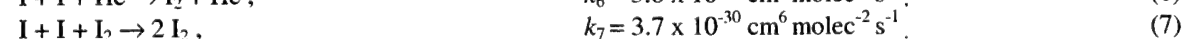
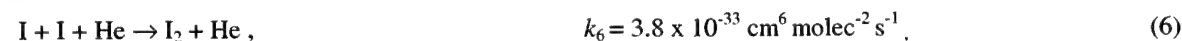
cause another loss of produced fluorine atoms. The 20-30 % efficiency of F atom production in the reaction system including reactions (1)-(4) predicted by Helms *et al.*¹¹, corresponded well with their experimental results. Hoell *et al.*¹² published the calculated F yield of 18 %.

Atomic iodine is generated by the fast reaction ($\Delta H_{298}^0 = -261.7$ kJ/mol) of F atoms with hydrogen iodide^{13,14}

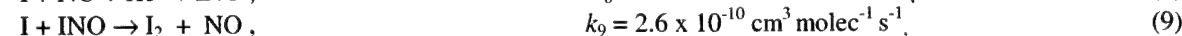
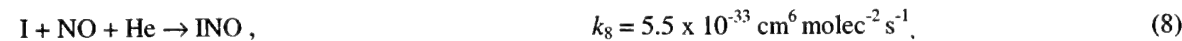


The energy liberated in this process is partly stored in vibrationally excited HF molecules. The contribution of HF* can exceed 56 %, according to Jonathan *et al.*'s study.¹³ The exoergicity of the reaction (5) may suffice even to form electronically excited iodine atoms, I(²P_{1/2}) with the branching ratio that was theoretically estimated¹⁵ up to the value of 0.5, however the experimental value obtained by using a high resolution Fourier transform spectrometer¹⁴ did not exceed the value of 0.005.

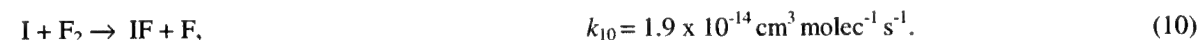
The resultant efficiency of I atom production is influenced (in addition to the above loss-processes of F atoms) by the reactions which consume I atoms, the termolecular recombination of I atoms in the presence of buffer gas (He) and molecular iodine^{16,17}



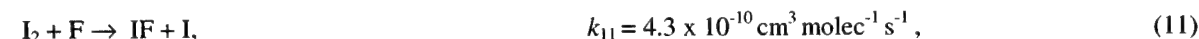
The unreacted nitrogen oxide may cause the loss of I atoms by the mechanism¹⁸



while the reaction of atomic iodine with unreacted fluorine is slow



Molecular iodine produced in the processes (6)-(9) can also react with F atoms to form atomic iodine¹⁷



where IF is formed in both ground and excited states.

3. DESCRIPTION OF MATHEMATICAL MODEL

One-dimensional numerical model used in our previous paper⁴ supposed the constant velocity of gas and consequently constant volume flowrate. However, this assumption is not valid in the case of highly exothermic reactions where temperature significantly rises along the reaction coordinate, the mixture expands and accelerates. The species concentrations are changing not only due to chemical reactions but also due to increase in volume flowrate. In the presented model, the species molar flowrates were calculated according to the differential equation

$$u \frac{d\dot{n}_j}{dx} = \sum_i \frac{k_i}{\dot{V}^{v_k+v_l-1}} \dot{n}_k^{v_k} \dot{n}_l^{v_l}, \quad (12)$$

where $u = \dot{V} / A$ is the gas velocity, x the reaction coordinate, $\dot{n}_j, \dot{n}_k, \dot{n}_l$ are the molar flowrates of species j, k, l , k_i is the rate constant of the i -th reaction, v_k, v_l are the exponents of the kinetic equation and A is the cross-section of the reaction channel.

The volume flowrate \dot{V} was evaluated according to the ideal gas equation of state:

$$\dot{V} = \frac{\sum_j \dot{n}_j RT}{p}. \quad (13)$$

Temperature and pressure changes were calculated by the simultaneous solving of the equation for the total enthalpy conservation

$$\frac{d}{dx} \left(\sum_j \int c_{p,j} dT + \frac{1}{2} \rho_m u^2 \right) = \sum_j \left(-h_j^0 + \int c_{p,j} dT \right) \frac{d\dot{n}_j}{dx}, \quad (14)$$

where $c_{p,j}$ and h_j^0 are the molar heat capacity and enthalpy of formation of species j and ρ_m is the molar density of mixture, and the dynamic equation

$$dp + M \rho_m u du = 0 \quad (15)$$

where M is the molar weight of the mixture.

This set of equations was numerically solved using the fourth-order Runge-Kutta routine.

4. MODELING OF F AND I ATOMS PRODUCTION. RESULTS AND DISSCUSION.

4.1 Production of F atoms

The production of F atoms was modeled including the reactions (1)-(4) for several values of initial pressure, helium dilution and initial concentration ratio $[\text{NO}]:[\text{F}_2]$. The results are summarized in Tab. 1. It is obvious, that the conversion of F_2 molecules to F atoms rapidly decreases and the reaction path becomes shorter with increasing of the initial pressure. The conversion substantially declines with increasing the ratio of rates of reactions (2), (3) and (1):

$$\frac{r_2 + r_3}{r_1} = \frac{k_2 [\text{F}] [\text{NO}] + k_3 [\text{F}] [\text{NO}] [\text{He}]}{k_1 [\text{F}_2] [\text{NO}]}. \quad (16)$$

Tab. 1. Production of F atoms. $\eta_F = n(F)_{max}/n(F_2)_0$ is the maximum conversion of F_2 to F, T , p , and τ are values of temperature, pressure and reaction time calculated at the place of maximum conversion.

[NO]:[F ₂]	p ₀ (kPa)	[He]:[F ₂]	η_F	T (K)	p (kPa)	τ (ms)
2	1	23	0.70	490.6	1.44	4.0
2	2	23	0.50	514.3	2.55	1.7
2	4	18	0.41	586.7	4.64	0.6
1	4	23	0.34	517.8	4.43	3.2
2	4	23	0.35	536.6	4.48	0.7
2	4	41	0.24	442.4	4.23	1.3
2	10	23	0.20	564.9	10.27	0.2

This ratio becomes higher with increasing both, the pressure and helium dilution. The conversion is not influenced by the initial ratio [NO]:[F₂], but significant amount of NO remains unreacted at [NO]:[F₂] > 1. The effect of residual content of F₂ or NO on the I^{*} quenching is discussed in Sec. 5.

The expression (16) depends also on the temperature. The constants k_2 , k_3 are taken as temperature independent, but k_1 increases with temperature (eq.(1)). Consequently, as the mixture temperature rises due to the exothermic reactions, the production rate of F atoms increases too. The calculated increase in temperature ($\Delta T = 140 - 260 K$) probably results also in the increase of the rates of reactions (2) and (3). The temperature dependence of these reactions was not measured, but is supposed to be relatively small.⁹

The concentration profiles for the conditions typical for the subsonic part of the COIL (4 kPa) are shown in Fig. 1.

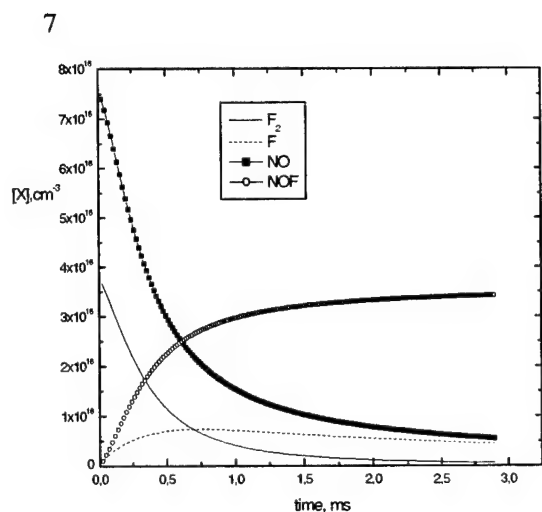


Fig. 1. Fluorine atoms production. Time development of concentrations of different species. Initial concentration ratio [F₂]:[NO]:[He]=1:2:23, initial pressure 4 kPa, initial temperature 300 K.

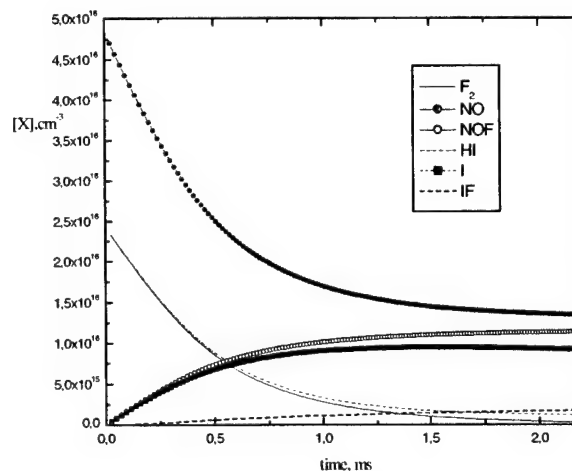


Fig. 2. Iodine atoms production. Time development of concentrations of different species. Initial concentration ratio [F₂]:[NO]:[HI]:[He]=1:2:1:36, initial pressure 4 kPa, initial temperature 300 K.

The conversion does not overcome 35 %. In accordance with the previous modeling⁴, it can be concluded that the production of F atoms is too slow under these conditions. Then, assuming the gas velocity of 200 m/s, HI will have to be introduced into the flow channel at the 20 cm distance from the F₂/NO injection.

The other possibility is to produce F atoms in a separate reactor and then to introduce them together with HI into the O₂(¹Δ_g) flow, as described in Sec. 5.1.

4.2 Production of atomic iodine

In recent modeling⁴ it was found, that simultaneous admixing of F₂, NO, and HI can give promising results in atomic iodine production efficiency. In this case, hydrogen iodide reacts instantly with formed F atoms, and reduces the rate of the loss reactions (2) and (3). This process was modeled including the reactions (1) - (11) under the assumptions described in Sec. 3. The results are summarized in Tab. 2.

Tab. 2. Production of I atoms. $\eta_I = n(I)_{max}/n(F_2)_0$ is the maximum conversion of F₂ to I, T, p, and τ are values of temperature, pressure and reaction time calculated at the place of maximum conversion.

[NO]:[F ₂]	p ₀ (kPa)	[He]:[F ₂]	η_I	T (K)	p (kPa)	τ (ms)
2	1	9	0,86	1373	1.00	5.5
2	1	18	0.88	976	1.00	5.8
2	1	36	0.89	692	1.00	9.9
1	1	37	0.68	611	1.00	10
2	4	36	0.84	652	4.57	1.5
2	10	36	0.64	642	10.0	0.5

The effect of helium dilution on the conversion of F₂ to I atoms is very small on the contrary to the F atoms production. The conversion is higher by 20% at the initial concentration ratio [NO]:[F₂]=2:1 against 1:1. The time course of concentrations for the initial pressure of 4 kPa is shown in Fig. 2. It can be seen that the reaction time for reaching the maximum conversion is approximately two times longer in comparison with F atom generation. It could be ascribed to the additional process producing I atoms in reaction (11).

The degree of the conversion of F₂ to F atoms (in the system F₂+NO), and F₂ to I atoms (in the system F₂+NO+HI) in dependence on the initial pressure is shown in Fig. 3. It follows from the comparison of the two dependencies that the conversion to F atoms rapidly decreases with increasing pressure, while the conversion to I atoms is less pressure dependent. This is caused by the suppression of the loss reactions (2) and (3), so the ratio (16) is much less pressure dependent.

The calculated increase in temperature for both, the F and I atoms production is independent on the initial pressure. The heating of the mixture is, of course, dependent on the dilution by helium. The temperature does not exceed 550 K in the case of F atoms production and 700 K in the case of I atoms production, if there is a sufficient dilution with inert gas (the dilution ratio [F₂]:[He] = 1:30 corresponds to the amount of helium contained in the COIL primary gas).

It should be noted, that the calculations included only particles in the ground electronic state. The excited particles NOF*, HF*, and IF* are also formed and hence the reaction enthalpy is partly transformed to the excitation energy. The resulting reaction temperature should be therefore lower then the values presented in Tables 1 and 2.

The results of the modeling of F and I atoms production were used in calculations of the I* production when produced atoms were introduced into the stream of singlet delta oxygen.

5. MODELING OF I* PRODUCTION

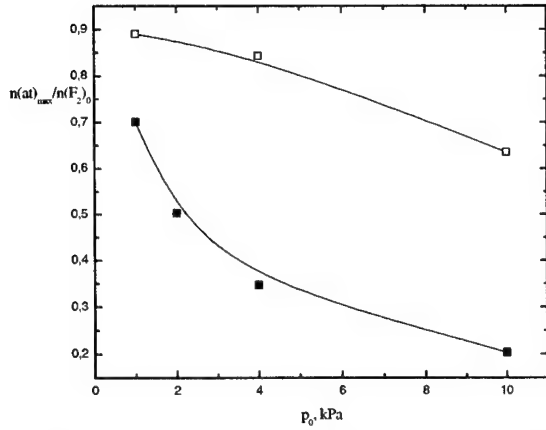


Fig. 3. Conversion of F_2 to F atoms in the mixture of F_2 and NO (solid symbols) and conversion of F_2 to I atoms in the mixture of F_2 , NO and HI (open symbols) in dependence on the initial pressure. Helium dilution $[F_2]:[He] = 1:30$.

5.1 Description of reaction conditions

The 1-D modeling of reactions between primary and secondary gases in COIL can describe the real three-dimensional process only approximately and must include some additional terms which make the correction on the limited rate of gases mixing.^{19, 20} Nevertheless, for the first estimation of this process they can be neglected. Our aim is to compare the suggested mixing schemes from the kinetic point of view with a special interest on the lifetime of I^* atoms. The reactions between F, HI and $O_2(^1\Delta_g)$ in the first series and between I and $O_2(^1\Delta_g)$ in the second series are modelled. The calculations start from the results of F or I atoms production process including all reactants and products occurred in the reactions (1)-(11) (secondary gas). The initial values for the primary gas are taken from the typical composition of the gas exiting the singlet oxygen generator, i.e:

$[O_2]:[He] = 1:2$, $[O_2(^1\Delta_g)]:[O_2(^3\Sigma_g^-)] = 3:2$ and 3 % of H_2O . The reactions between $O_2(^1\Delta_g)$ and I, I_2 are taken from the reference.²¹

The subsonic mixing conditions include the initial pressure of 4 kPa and temperature of 300 K and the

supersonic mixing assumes the pressure of 0.5 kPa and temperature of 200 K. The results of F/I atoms production at 10 kPa are used in the case of subsonic mixing and results for F/I atoms production at 1 kPa in the case of supersonic mixing (see Fig. 4).

The constant temperature was assumed in this modelling, with aim to save the computer time.

The initial concentration ratio of F or I atoms and $O_2(^1\Delta_g)$ was chosen according to the known optimal ratio $[I_2]/[O_2] = 1:50$ for COIL operation, i.e.:

$$\frac{[I]_0}{[O_2(^1\Delta)]_0} = \frac{2}{50 - N}, \quad (17)$$

where N is the number of molecules of $O_2(^1\Delta_g)$ consumed for the dissociation of one I_2 molecule. In the following calculation, the value $N=5$ was assumed.

5.2. Results and discussion

5.2.1 F + HI + $O_2(^1\Delta_g)$ system

Time development of the concentration of iodine $I(^2P_{1/2})$ state at the subsonic conditions is shown in Fig. 5 (solid line). The concentration rises up to 0.13 ms and then slowly decreases. Assuming the average gas velocity of 200 m/s, the maximum concentration is attained at a distance of 2.6 cm. Under the supersonic conditions, the excitation rate is very low (see Fig. 6, solid line). If the supersonic gas velocity of 1000 m/s is assumed, the maximum concentration is attained at the distance of 1 m.

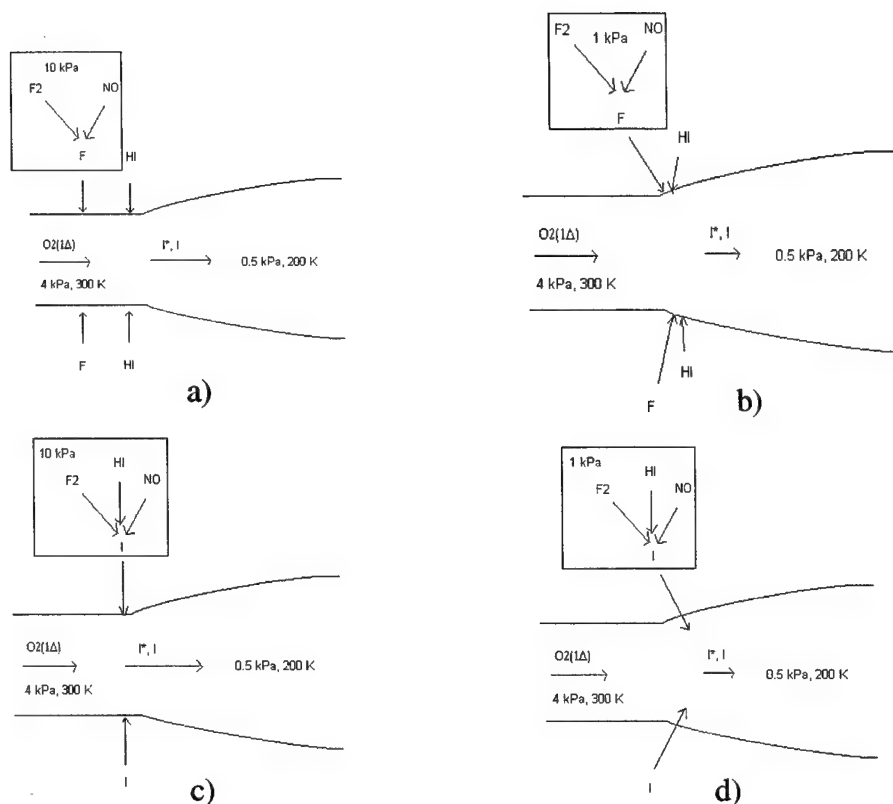


Fig. 4.: Different mixing schemes for I^* generation: a) the subsonic mixing of F, HI and $O_2(^1\Delta_g)$, b) the supersonic mixing of F, HI and $O_2(^1\Delta_g)$, c) the subsonic mixing of I and $O_2(^1\Delta_g)$, d) the supersonic mixing of I and $O_2(^1\Delta_g)$

5.2.2 $I + O_2(^1\Delta_g)$ system

Time development of the concentration of iodine $I(^2P_{1/2})$ state at the subsonic conditions is shown in the Fig. 5 (dashed line). The concentration rises up to 0.04 ms and then rapidly falls. Assuming the average gas velocity of 200 m/s, the maximum concentration is attained at a distance of 8 mm. If the mixing delay is taken into account, the loss of excited iodine in the subsonic channel should not be serious if the injection is placed right before the nozzle throat.

Under the supersonic conditions, the concentration rapidly rises and attains its maximum value before 0.03 ms, which corresponds to a distance of 3 cm (see Fig. 6, dashed line). Then the concentration slowly decreases: for example, 80 % of the maximum value is attained at a distance of 38 cm.

The calculations of the two above mentioned methods were performed with the same initial concentrations of atoms introduced into the flow channel, F atoms in the first method and I atoms in the second one. However, the energy transfer from singlet oxygen to atomic iodine is faster than the reaction (5). That is why the maximum concentration of $I(^2P_{1/2})$ is higher in the case of $I + O_2(^1\Delta_g)$ system and, on the other hand, its subsequent decrease is faster.

The described process of the production of I atoms brings many new species into the laser mixture, that can quench produced excited atomic iodine and singlet oxygen as well. According to the known values of rate constants for quenching of singlet delta oxygen⁴, the influence of the components coming from atomic iodine production is very small.

The known rate constants for quenching of $I(^2P_{1/2})$ are summarized in Tab. 3 (for references, see⁴). The comparison of the quenching by different species calculated from the initial concentrations of reactants provides an interesting insight into the $I(^2P_{1/2})$ lifetime. The initial rates divided by initial I^* concentration for $I + O_2(^1\Delta_g)$ system under subsonic and

Tab. 3. Quenching of $I(^2P_{1/2})$ by components present in the reaction system for I atoms generation

NO	5×10^{-17}
HI	5×10^{-14}
HF	3×10^{-12}
H ₂ O	2.3×10^{-12}
I ₂	3.5×10^{-11}
F ₂	5.0×10^{-14}
O ₂ (¹ Δ _g)	1.1×10^{-13}
IF	1.3×10^{-11}

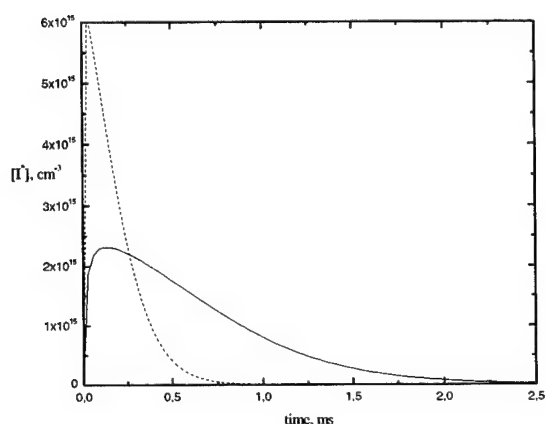


Fig. 5. Concentration profiles of excited iodine for subsonic conditions. Mixing of F, HI and O₂(¹Δ_g) (—), mixing of I and O₂(¹Δ_g) (-----).

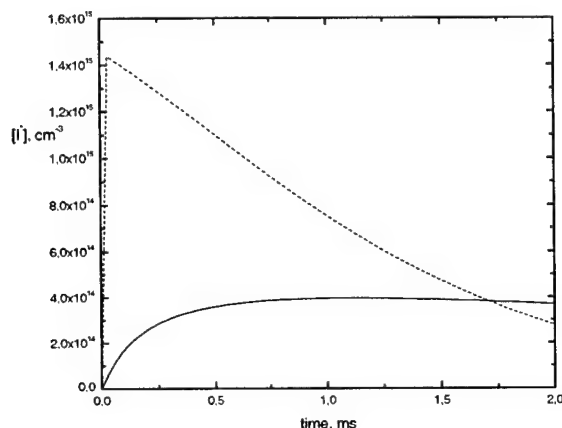


Fig. 6.: Concentration profiles of excited iodine for supersonic conditions. Mixing of F, HI and O₂(¹Δ_g) (—), mixing of I and O₂(¹Δ_g) (-----).

supersonic conditions are shown in Fig. 7a,b. The most effective quenchers are IF and HF molecules. Their quenching effect is two/three times higher than the effect of H₂O molecule that is the well-known serious quencher in COIL medium.²² It must be noted, that the above-mentioned values are valid under the assumption of ground electronic state of IF and HF produced. As mentioned in Sec. 3, these particles are formed partly in the excited state, but the rate constants of $I(^2P_{1/2})$ quenching by IF^{*} and HF^{*} were not published. Ground and excited NOF molecule could be also a serious quencher of $I(^2P_{1/2})$, but the appropriate quenching constant is not known as well. The quenching effect of NO and F₂ is small, so that the residual content of these species should not bring any complications.

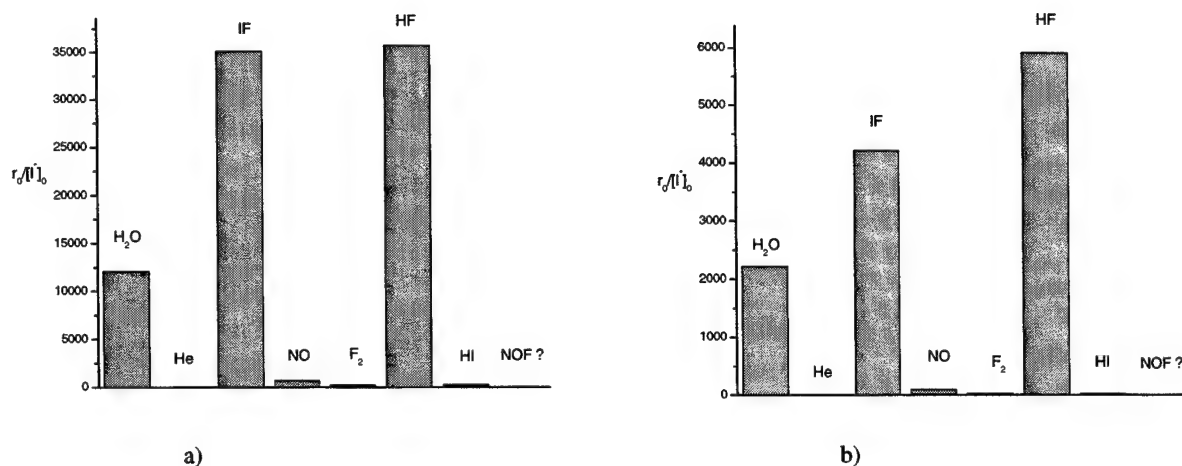


Fig. 7a,b. I^* quenching by different molecules. a) subsonic mixing of I and $O_2(^1\Delta_g)$,
b) supersonic mixing of I and $O_2(^1\Delta_g)$

5. CONCLUSIONS

The detailed 1-D mathematical modeling of the chemical production of atomic fluorine and atomic iodine, subsequently, was made. The dependencies of the conversion of F_2 to F or I atoms on the initial pressure and concentration ratios were calculated. It was confirmed that the reaction path for F or I atoms production is too long to be realised directly in the subsonic laser part. In the newly suggested process, F or I atoms are produced in a separate reactor and they are introduced into the stream of $O_2(^1\Delta_g)$. The four different mixing/reacting schemes for reaction between F, HI and $O_2(^1\Delta_g)$ in one case and I and $O_2(^1\Delta_g)$ in the second case were modeled. The supersonic mixing of I and $O_2(^1\Delta_g)$ seems to be the most advantageous process, where atomic iodine is produced separately with good efficiency and the energy transfer from $O_2(^1\Delta_g)$ to atomic iodine is fast at the beginning of the supersonic nozzle. The other possible processes are the subsonic mixing of F, HI and $O_2(^1\Delta_g)$ or I and $O_2(^1\Delta_g)$. The supersonic mixing of F, HI and $O_2(^1\Delta_g)$ gives an insufficient rate of I^* production.

ACKNOWLEDGEMENTS

This work was supported by the USAF European Office for Aerospace Research and Development (EOARD) and Grant Agency of the Czech Republic.

REFERENCES

1. E. Endo, D. Sugimoto, H. Okamoto, K. Nanri, T. Uchiyama, S. Takeda and T. Fujioka, "Output power enhancement of a chemical oxygen-iodine laser by predissociated iodine injection", *Jap. J. Appl. Phys.* **39**, pp.468-474, 2000.
2. V.S. Pazyuk, N.P. Vagin and N.N. Yuryshv, "Repetitively pulsed chemical oxygen-iodine laser with a discharge generation of atomic iodine", *Proc. SPIE* Vol. **2767**, pp.206-208, 1995.
3. O. Špalek, V. Jirásek, J. Kodymová, I. Jakubec, and M. Čenský, "Preliminary experimental results on chemical generation of atomic iodine for a COIL", *Proc. SPIE* Vol. **4184**, pp.111-115, 2000
4. V. Jirásek, O. Špalek, J. Kodymová, and M. Čenský, "Chemical generation of atomic iodine for chemical oxygen-iodine laser. I. Modeling of reaction systems", *Chem.Phys.* **269**, pp.167-178, 2001

5. O. Špalek, V. Jirásek, J. Kodymová, M. Čenský, and I. Jakubec, "Chemical generation of atomic iodine for COIL", *Proc. of this conference* (submitted for publication)
6. S. Johnston and H. J. Bertin, "Heat of formation of nitrosyl fluoride", *J. Am. Chem. Soc.* **81**, p.6402, 1959.
7. C.E. Kolb, "Resonance fluorescence study of the gas phase reaction rate of nitric oxide with molecular fluorine", *J. Chem. Phys.* **64**, pp.3087-3090, 1976.
8. T.L. Pollock and W.E. Jones, "Gas phase reactions of fluorine atoms", *Can. J. Chem.* **51**, pp.2041-2046, 1973.
9. E.G. Skolnik, S.W. Veysey, M.G. Ahmed, and W.E. Jones, "Rate constants for the reaction of fluorine atoms with nitric oxide in the presence of various third bodies", *Can. J. Chem.* **53**, p.3188-3193, 1975.
10. P. Kim, D.I. MacLean and W.G. Valance, *Abstr. 164th National Meeting Am. Chem. Soc.*, pp.3188-3193, N.Y., 1972.
11. C.A. Helms, L. Hanco, K. Healey, G. Hager and G.P. Perram, "Generation of high-number densities of iodine monofluoride in a supersonic flow", *J. Appl. Phys.* **66**, pp.6093-6097, 1989.
12. J.M. Hoell, F. Allario, O. Jarrett, and R.K. Seals, "Measurements of F₂, NO, and ONF Raman cross sections and depolarisation ratios for diagnostics in chemical lasers", *J. Chem. Phys.* **38**, pp.2896-2901, 1973.
13. N. Jonathan, C.M. Melliar-Smith, S. Okuda, D.H. Slater and D. Timlin, "Initial vibrational energy level distributions determined by infrared chemiluminescence. II. The reaction of fluorine atoms with hydrogen halides", *Mol. Phys.* **22**, pp.561-547, 1971.
14. J.P. Sung and D.W. Setzer, "Electronic and vibrational energy disposal in the reactions of fluorine atoms, with hydrogen bromide and hydrogen iodide", *Chem. Phys. Lett.* **48**, pp.413-419, 1977.
15. U. Dinur, R. Kosloff, and R.D. Levine, "Analysis of electronically nonadiabatic chemical reactions: An information theoretic approach", *Chem. Phys. Lett.* **34**, pp.199-205, 1975.
16. T.T. Yang, D.A. Copeland, A.H. Bauer, V. Quan, W.E. McDermott, R.A. Cover and D.M. Smith, *AIAA* **97-2384**, pp.1-28, 1997.
17. P.P. Bemand, M.A.A. Clyne, and R.T. Watson, *J.C.S. Faraday Trans. I* **69**, p.1356, 1973.
18. H. van den Bergh and J. Troe, "Kinetic and thermodynamic properties of INO and INO₂ intermediate complexes in iodine recombination", *J. Chem. Phys.* **64**, p.736, 1976.
19. B.D. Barmashenko, A. Elior, E. Leibush, S. Rosenwaks, "Modeling of mixing in chemical oxygen-iodine lasers: Analytic and numerical solutions and comparison with experiments", *J. Appl. Phys.* **75**, pp.7653-7664, 1994.
20. J. Beránek, K. Rohlena, J. Kodymová, O. Špalek, "A 1D kinetic model of COIL applied to experimental data", *SPIE Vol.* **3092**, pp.569-572, 1996
21. J. Paschkewitz, J. Shang, J. Miller, T. Madden, "An assessment of COIL physical property and chemical kinetic modeling methodologies", *AIAA* **2000-2574**, pp.1-16, 2000
22. D. H. Burde and R.A. McFarlane, *J. Chem. Phys.* **64**, p.1850, 1976

German COIL Efforts: Status and Perspectives

Willy L. Bohn*

DLR Institute of Technical Physics, D-70569 Stuttgart, Germany

ABSTRACT

Historically, COIL research in Germany has started with microwave excitation of an oxygen flow. But soon all efforts have been devoted to the chemical generation of excited singlet oxygen and have eventually given rise to a supersonic 10 kW class rotating disk driven device. A diode based diagnostic provides data of small signal gain and cavity temperature which emphasize the role of iodine injection for different penetration conditions. Heat release can lead to substantially higher temperatures as expected from adiabatic expansion. Power extraction is found to be in good agreement with theoretical predictions. Alternatively, small scale liquid jet generator experiments show encouraging 60 % efficiency. Besides air defense related applications and a study on space debris removal, results are given which are pertinent to the decommissioning of nuclear installations. In particular, laser cutting of concrete at 1.3 μm is demonstrated and theoretically scaled up to relevant power levels.

Keywords: chemical lasers, oxygen, iodine, power extraction, decommissioning

1. INTRODUCTION

Historically, it all started in 1987 with a helium and oxygen gas mixture flowing thru a 2.45 GHz microwave discharge. At that time the laboratory was heavily involved in different types of electrically excited lasers with special emphasis on CO_2 and CO lasers. Therefore, it seemed quite natural to investigate the possibility to electrically excite the oxygen molecule; an idea that has become very popular, recently. The historic device is shown in Fig. 1. At that time the efficiency of electrically generating $\text{O}_2(^1\Delta)$ was so low that no further attempt was undertaken to start real laser

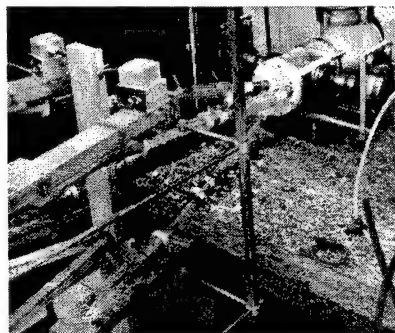


Fig. 1: Historic microwave discharge in oxygen.

experiments. Encouraged by the results obtained with the chemical excitation of $\text{O}_2(^1\Delta)$ in the U.S. the decision was taken in Germany to redirect the research to the chemical excitation as well and to abandon the electric discharge scheme. From there on all major efforts have been aimed at the investigation of a 10 kW rotation disk driven device. Major achievements on that road will be reviewed in chapter 2.1. More recently growing interest has been given to the liquid jet oxygen generator and its scaling potential as compared to the rotating disk concept. The second part of this paper addresses present and future applications. Since most applications require high beam quality this particular issue will be discussed in chapter 3.1. Subsequently, three different application areas will be described: the tactical air defense, the laser supported space debris removal, and the laser decommissioning of nuclear installations. This also includes a comparison of investment and running costs of COIL as compared to its major laser competitors.

2. COIL LASER RESEARCH AND DEVELOPMENT

2.1 Review of German 10 kW class COIL investigations

Most of the work has been concentrated on a rotating disk driven device using a nozzle bank with 20 elements and subsonic iodine injection¹. For base line conditions the laser is operated with a chlorine mass flow of typically 0.5 mol/s and a $\text{He}:\text{Cl}_2$ ratio of 3. The Mach number after the supersonic expansion is close to 2. As shown in Fig. 2 the O_2H^+ molarity and rotation speed of the disk pack have been varied over a wide range and the utilization approaches typically

* contact thru: Tel.: +49 711 6862 772; Fax: +49 711 6862 788; E-mail: Willy.Bohn@dlr.de

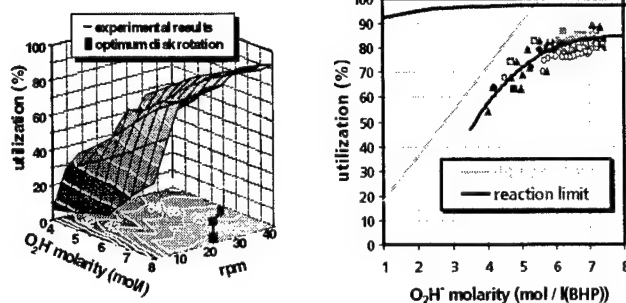


Fig. 2: Utilization as a function of O_2H^+ and rpm (left) and compared to diffusion and reaction limits (right).

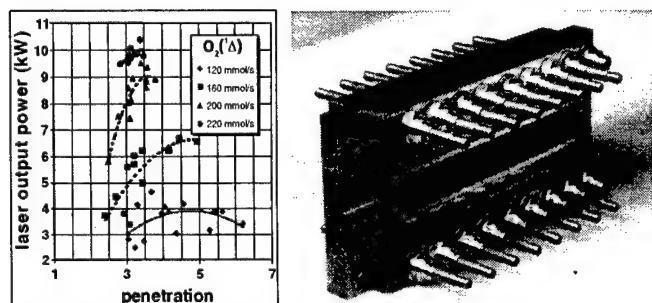


Fig. 3: Laser power as a function of penetration (left); nozzle bank (right).

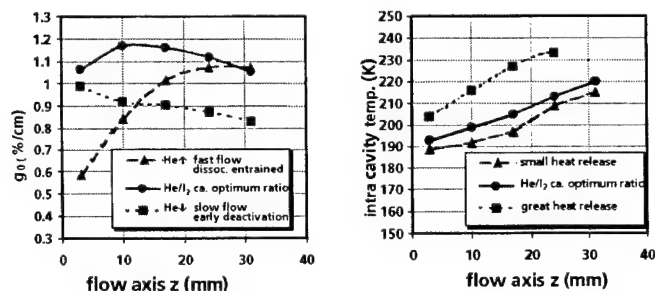


Fig. 4: a) Small signal gain, and b) cavity temperature in flow direction with $I_2 = \text{const.}$

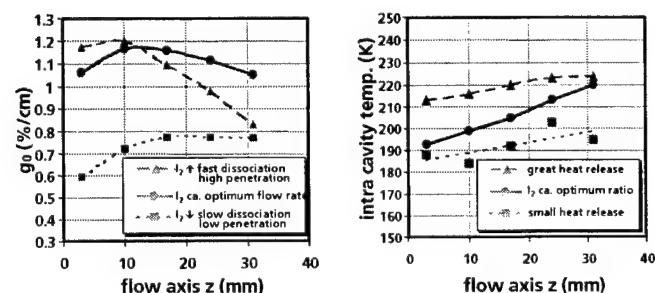


Fig. 5: a) Small signal gain, and b) cavity temperature in flow direction with $He/I_2 = \text{const.}$

90% for optimum operating conditions. On the right part of Fig. 2 a collection of data points demonstrates the transition from a diffusion limited to a reaction limited model as a function of the O_2H^+ molarity in the BHP. For power optimization one of the most important issues is the influence of iodine penetration: the latter basically reflects the ratio of the momentum of the iodine flow to the main flow. As can be seen in Fig. 3 the maximum laser output power is obtained within a narrow range of penetration values at high singlet oxygen flow rates. This behavior is much more relaxed at lower singlet oxygen flow rates. The nozzle bank used in all those experiments is shown on the right hand side of Fig. 3.

A considerable step in COIL research and understanding occurred with the advent of more sophisticated diagnostic tools, in particular the diode based optical diagnostics as provided by the PSI Corporation². An appropriate example is given by the measurements³ of small signal gain and temperature along the flow axis. The major goal was to investigate the impact of the secondary flow by excursion of parameters with respect to optimum lasing conditions which will be represented by a full line in the following figures.

In the first case, we keep the iodine concentration constant and vary the helium flow rate. Increasing the latter accelerates the flow and leads to a very substantial entrainment of the dissociation, and accordingly, to the small signal gain along the flow axis as shown in Fig. 4a. On the other hand, decreasing the helium flow rate decelerates the flow and the small signal gain readily starts with a high value at the nozzle exit plane but early deactivation occurs and thus the small signal gain decreases monotonically. Fig. 4b shows how this behavior translates to the cavity temperature: whereas the fast flow exhibits a small heat release the slow flow is governed by a quite substantial heat release and thus the cavity temperature increases dramatically along the flow axis and exceeds 230 K 25 cm after the nozzle exit plane.

In the second case we keep the He/I_2 ratio constant while changing the iodine flow rate. Increasing the iodine flow rate leads to a fast dissociation and thus the small signal gain exhibits highest values at the nozzle exit plane but sharply decreases thereafter due to deactivation. This situation reflects a high iodine penetration. Decreasing the iodine flow rate limits the small signal gain to rather low values and characterizes a low penetration situation (Fig. 5a).

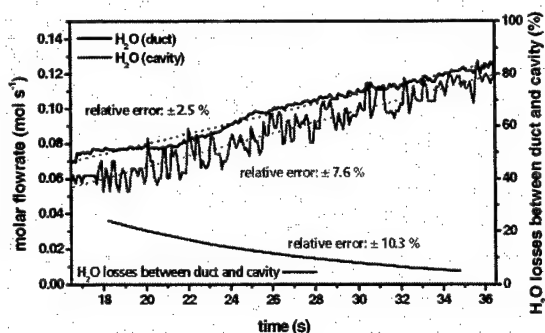


Fig. 6: Water vapor in transport duct and cavity (upper traces); H₂O losses (bottom trace).

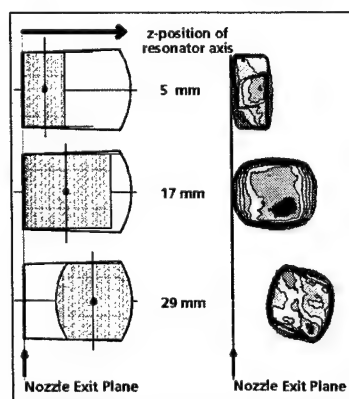


Fig. 7: Beam pattern for different outcoupling configurations.

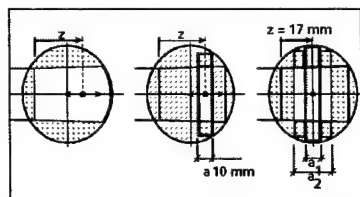


Fig. 8: Schematic of outcoupling geometries.

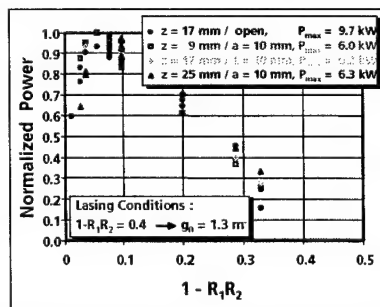
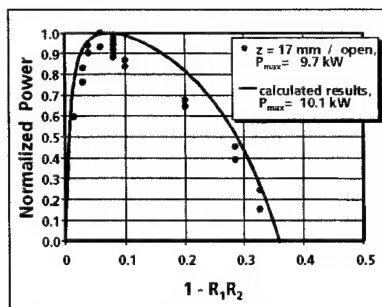


Fig. 10: Rigrod plot for a) an open resonator, and b) an obscured resonator aperture.

Accordingly, great heat release occurs for high penetration and small heat release with temperatures ranging between 190 K and 200 K is found for low penetration, as shown in Fig. 5b.

Another example relates to the water vapor measurement. Using the PSI diagnostic water vapor concentration is measured in the transport duct prior to the nozzle bank and in the cavity: the upper curve in Fig. 6 corresponds to the duct measurement and the lower curve which is characterized by substantial fluctuations corresponds to the cavity measurement. The fluctuations arise because of the lower signal to noise ratio obtained in the cavity measurement. At the bottom of Fig. 6 the total water vapor losses between duct and cavity positions is shown as a function of time: they range from about 20 % to 5 % within the measured time interval. This measurement strongly suggests that water condensation is not negligible during the expansion of the laser active gas.

Power extraction has been studied⁴ using a variable slit aperture in front of the outcoupling mirror. Fig. 7 shows a two-dimensional burn pattern for three different resonator outcoupling configurations: for a small aperture resonator optically centered at 5 mm from the nozzle exit plane, for a fully opened resonator centered at 17 mm, and for a resonator centered at 29 mm but limited by the downstream cavity structure. A more detailed measurement of the power extraction is obtained by either varying the width of the slit aperture or by translating a constant aperture slit along the flow axis. The corresponding geometry is schematically shown in Fig. 8. Increasing the width of the slit in front of the outcoupling mirror leads, as expected (and shown in Fig. 9), to a higher fraction of the normalized laser output power: for a slit width of 30 mm the maximum

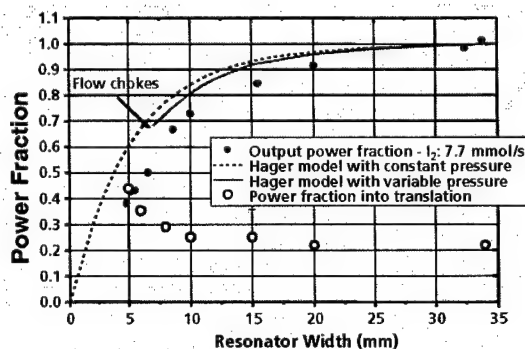


Fig. 9: Laser power fraction as a function of resonator width.

available output power has already been reached. For smaller widths the power fraction decreases down to 40 %. At that point the laser operation is discontinued and the flow in the cavity chokes: all the remaining power is converted into translational energy as shown by the open dots. This experimental situation is supported by a saturated gain model first derived by Hager⁵ of the AFRL: whereas the dotted line reflects the model with constant pressure the full line corresponds to the same model but with variable pressure. Its validity is, of course, limited

to the point where the laser active flow chokes. In general, Fig. 9 demonstrates a rather good agreement between theory and experimental data.

Rigrod analysis is another way to investigate power extraction properties. Fig. 10a exhibits an experimental and theoretical Rigrod plot obtained with an open resonator optically centered at 17 mm downstream of the nozzle exit plane. For a laser power of about 10 kW a fairly good agreement is obtained between experimental dots and the calculated solid line. In order to interrogate the active flow with respect to possible gradients, a 10 mm wide slit has been positioned at 9, 17 mm and 25 mm downstream of the nozzle exit plane, respectively. Results are compared with the fully opened resonator (open circles) and, since no significant deviations are found this leads to the conclusion that the flow conditions are fairly constant within the optical cavity.

2.2 Liquid jet singlet oxygen generator

In recent years considerable effort has been devoted to the investigation and development of so-called jet-type oxygen generators invented by Russian researchers at the Samara Branch of the Lebedev Institute. In order to derive a figure of merit for the jet generator the efficiency of all published devices has been plotted in Fig. 11 as a function of the reaction time of the BHP jets with the chlorine gas. However, 22 different data points do not really exhibit any characteristic behavior. In conclusion, the reaction time is not the expected figure of merit; thus this unanswered question remains to be considered in all the efforts dedicated to the development of jet generators. In Germany, a small scale generator with 49 liquid jets of 0.5 mm \varnothing and a

typical length between 10 cm and 15 cm has been investigated. A picture of the experimental device is shown in Fig. 12.

Utilization, yield, and generator efficiency have been plotted in Fig. 13 as a function of distance from the exit of the generator. At a total pressure of 90 mbar for a helium/oxygen mixture, efficiencies of up to 60% have been demonstrated at the generator exit. Further investigations with special emphasis on scaling properties are under way.

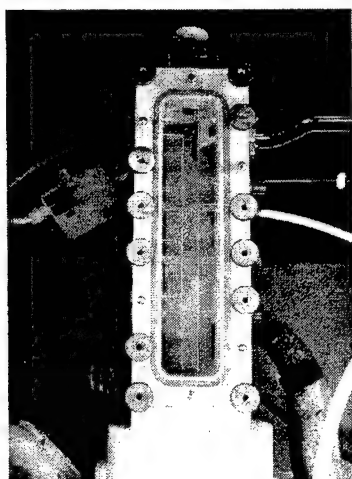


Fig. 12: Jet generator device.

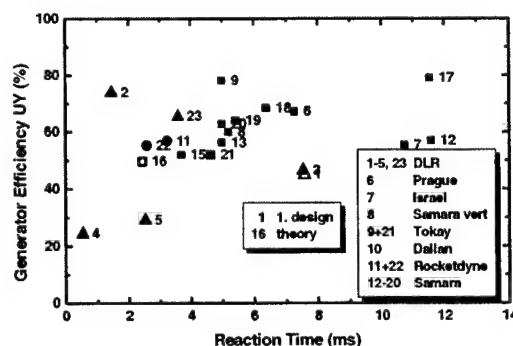


Fig. 11: Survey of jet generator efficiency.

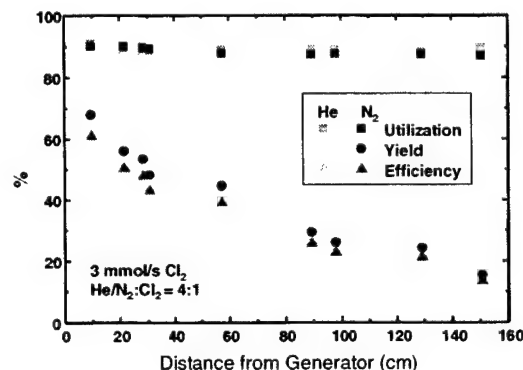


Fig. 13: Performance data of jet generator.

3. PRESENT AND FUTURE APPLICATIONS

3.1 Beam quality issue

Since most of the laser applications require high beam quality a survey is given in Fig. 14 of the beam quality factor, M^2 , related to either commercially available lasers (full symbols) or laboratory devices (open symbols). The data collection covers CO_2 gas lasers, lamp and diode pumped solid state lasers, fiber lasers, and a novel thin disk solid state laser. As the output power increases only CO_2 lasers keep a beam quality better than 10 times the diffraction limit. For comparison two COIL beam quality values have been added: one has been reported by the Dalian Group in China and the other one has been advertised (but never officially published) by the AFRL in the U.S. Fig. 14 very clearly shows the lack of brightness property of present solid state lasers and the huge brightness potential suggested by COIL technology. In order to overcome the problem of small signal gain in moderate sized COIL devices we currently

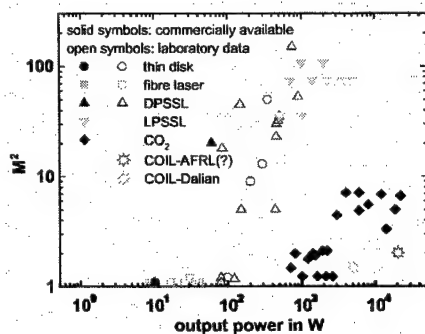


Fig. 14: Beam quality factor survey.

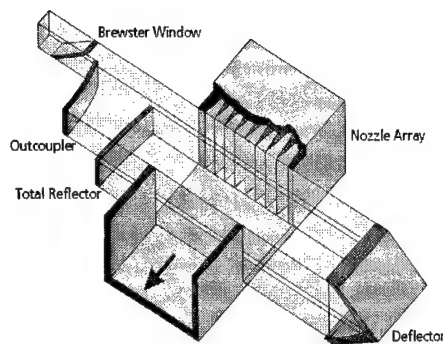


Fig. 15: Layout of folded hybrid resonator.

investigate a folded hybrid resonator scheme as shown in Fig. 15. This resonator is unstable in flow direction and stable in the direction of the nozzle exit plane. A folded beam path should sustain enough gain in order to efficiently operate the laser. First experimental investigations have not yet been successful due to the high alignment sensitivity associated with this particular resonator concept.

3.2 Tactical air defense

Germany has engaged into a national demonstrator program based on the technology reviewed in chapter 2.1. This effort is a container based approach aimed at the evaluation of COIL technology for future air defense applications. The system covers all the necessary infrastructure for proper laser operation, a target acquisition system, and a tracking and pointing system including atmospheric turbulence corrections using adaptive optics. This program is primarily carried out by German industrial companies and supported by the German government.

3.3 Space debris removal

Considering the pulsed operation capability of COIL a study has been undertaken to define the potential of a larger COIL system for spaced debris removal from ground. Enhanced peak power by gain switching a 3 kW CW COIL has been demonstrated by Hager⁶ et al. in 1994. The demonstrated enhancement factor was about 13 with respect to the CW value. Assuming a slightly more optimistic enhancement factor of 15 and a mechanical coupling coefficient of $C_m = 3$ for repetitively pulsed laser operation vs. $C_m = 1$ for CW operation we have derived COIL requirements for space debris removal. In Fig. 16 the minimum average power is plotted as a function of the diameter of the beam director. Two different debris removal scenarios have been considered. Firstly, the ORION⁷ scenario which is aimed at removing the debris at an altitude of 1000 km. In the ORION concept suggested by Phipps et al. a 20 kW average power beamlet fusion laser is being used; the dotted lines exhibit the power requirement of a repetitively pulsed COIL assuming a mechanical coupling of 3 and 1, respectively. Secondly, the Falcon⁸ scenario is intended to remove debris at an altitude of 450 km using a 5 MW CW nuclear pumped laser. In contrast, a repetitively pulsed COIL requires average powers as shown by the two full lines with different mechanical coupling coefficients. In summary, a scaled up COIL technology provides an interesting alternative to the space debris removal issue as compared to the ORION and Falcon concepts, respectively⁹.

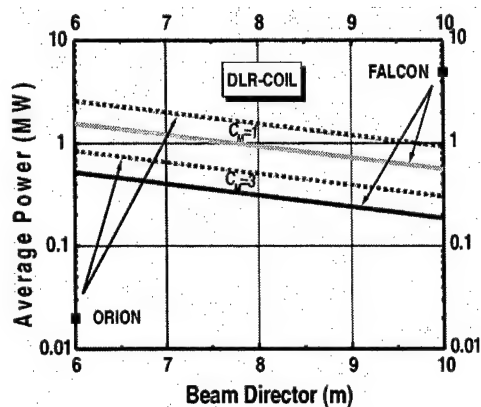


Fig. 16: Required average COIL power for debris removal.

3.4 Decommissioning of nuclear installations

The potential COIL advantages for applications in the area of decommissioning are obvious:

- scalable in power
- high beam quality
- fiber optic beam delivery
- robotic/remote processing capability
- efficient material interaction due to short wavelength.

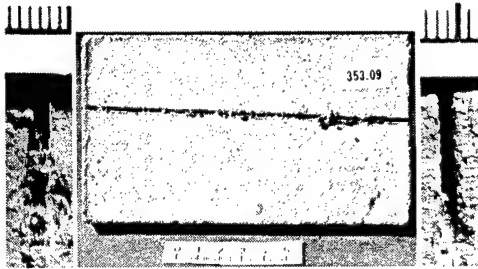


Fig. 17: Cutting concrete at 1.3 μm

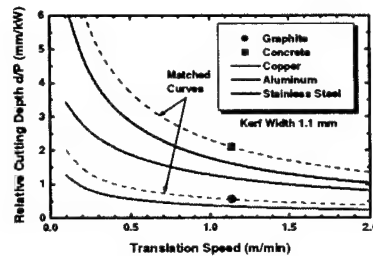


Fig. 18: Modeling of cutting speed for different materials.

Whereas the three last positions are valid for present solid state lasers, the two first positions may only be matched by COIL technology in the near future. First experiments have been undertaken with the 10 kW DLR COIL in order to demonstrate its capability of cutting

Laser	Investment Costs 1000 € / kW	Running Costs (incl. Depreciation) € / kWh
CO ₂	60	10
Nd:YAG (lamp)	125	20
Nd:YAG (diode)	1000	110
COIL	170	50

Fig. 19: Figures for the marketplace.

concrete. A sample is shown in Fig. 17 with a cutting depths of about 5 cm. Using available models we have tried to predict COIL cutting performance in materials relevant to decommissioning applications. Since no data base is available for those materials we have derived our calculations by anchoring the model to our experimental points. As deduced from Fig. 18 a 70 kW COIL would be capable of cutting 30 cm of concrete at a speed of 0.4 m/min. In order to further assess the future industrial potential of COIL in the area of decommissioning a comparison of costs with respect to other industrial laser candidates has been undertaken. A brief summary of the results is highlighted in Fig. 19. Although the CO₂ laser appears to be the most attractive low

cost candidate it should be mentioned that its wavelength is not suited for fiber optic beam delivery and, thus, he is not a candidate to be seriously considered for the application discussed here. The lamp pumped Nd:YAG laser is still cheaper than COIL but its scalability to high power levels has yet to be demonstrated.

4. CONCLUSIONS AND OUTLOOK

Successful operation and understanding of COIL at relevant power levels has been achieved. COIL technology has matured to the point that it basically can support an effort aimed at the development of an air defense demonstrator. Furthermore, COIL technology is being considered for future civilian applications, as well.

However, some fundamental issues are presently still unresolved: the iodine dissociation is satisfactorily described in the existing devices but no universal nor scalable model is presently available. Although high beam quality is generally anticipated it needs to be demonstrated along with efficient laser operation. And finally the question arises if the high brightness leading edge of COIL will prevail over the considerable improvements that may occur in solid state laser research for the years to come.

ACKNOWLEDGEMENTS

The author thanks F.Duschek, K.Gruenewald, J.Handke, W.O.Schall, C.Schreiber and F.Waiblinger for providing all the experimental material and H.-A.Eckel for his support by editing this paper.

REFERENCES

1. J. Handke, A. Werner, W.L. Bohn, W.O. Schall, "Multikilowatt Supersonic Oxygen Iodine Laser", Proc. GCL 10th International Symposium, SPIE Vol:2502 (1994), p.266
2. S.J. Davis, W.J. Kessler, M. Bachmann, "Collisional broadening of absorption lines in water vapor and atomic iodine relevant to COIL diagnostics", Gas and Chemical Lasers and Intense Beam Applications II, Vol 3612, pp. 157-166, San José, 1999

3. J. Handke, K. Gruenewald, F. Duschek, "Comparative studies on small signal gain and output power for COIL systems", Proc. XIII International Symposium on Gas Flow and Chemical Lasers and High Power Laser Conference, SPIE Vol. 4184 (2001) p. 45
4. J. Handke, K. Gruenewald, W.O. Schall, "Power extraction investigations for a 10 kW-class supersonic COIL", 12th GCL/HPL St. Petersburg (1998), SPIE Vol. 3574 p. 309
5. G.D. Hager, C.A. Helms and K.A. Truesdell, D. Plummer, J. Erkkila and P.Crowell, "A Simplified Analytic Model for Gain Saturation and Power Extraction in the Flowing Chemical Oxygen Iodine Laser", IEEE Journal of Quantum Electronics, Vol.32 No.9, Sept. 1996, p.1525
6. G.D. Hager and D. Kopf, "The repetitively pulsed chemical oxygen iodine laser", 25th AIAA Plasmadynamics and Laser Conference, June 20-23 (1994), Colorado Springs, CO
7. C.R. Phipps, G. Albrecht, H. Friedmann, D. Gavel, E.V. George, J. Murray, C. Ho, W. Priedhorsky, M.M. Michaelis and J.P. Reilly, "ORION. Clearing near earth debris", Laser and Particle Beams (1996), Vol. 14 No 1 p. 1
8. D.K. Monroe, "Space debris removal using a high-power ground-based laser" in Laser Power Beaming, SPIE Vol. 2121 (1994), p.276
9. W.L. Bohn, "High power supersonic chemical oxygen iodine laser", Proc. of the Conference on High-Power Laser Ablation, Santa Fe, NM (1998), SPIE Vol. 3343 p. 119

Historical perspective of COIL diagnostics

Steven J. Davis*
Physical Sciences Inc.

ABSTRACT

In this paper, I present a history of the development of diagnostic techniques for the chemical oxygen iodine laser (COIL). Several established optically based techniques have been applied to COIL including: visible and near infrared chemiluminescence, resonance absorption, and laser induced fluorescence. I trace the history of these developments using the diagnostic methods as the overall theme. In many cases a variant of an established diagnostic was used to probe for some key kinetic rate or mechanism. Indeed, the goal of developing the now well established COIL kinetic rate package was responsible for the introduction of new diagnostic methods. I discuss diagnostics both before and after the demonstration of the first COIL device.

Keywords: Chemical Oxygen Iodine Laser, optical diagnostics, development history

1. INTRODUCTION

During this commemorative session on the 25th anniversary of the invention of COIL, we are recounting the history of the development of this unique laser system.¹⁻³ The excellent reviews of the laser development and COIL kinetics by Bill McDermott⁴ and Mike Heaven⁵ earlier in this volume provide ample motivation for a discussion of diagnostics.

In the following pages I have described some of the developments that led to the present diagnostic toolbox now available to COIL researchers. Before launching into a detailed discussion of COIL diagnostics it is important to at least mention the important species and parameters relevant to COIL development. I will be brief here since others have already covered much of this earlier in these proceedings.

Although numerous diagnostic methods have been developed and applied to COIL, it is important to emphasize that this has not been an isolated journey. In many cases, some kinetic rate or elucidation of a reactive mechanism was needed. This led either to a variation of an existing diagnostic or the development of a new method. Most frequently it was the former, and this is entirely reasonable; application of a well-proven technique to a new problem is often a prudent approach.

In this brief overview, I will attempt to trace the highlights of COIL diagnostic development. I have been privileged to be part of this area during and after the demonstration of the first COIL. While I have tried to provide a historical background, the reader will note that my review is not entirely chronological. Rather, I chose to frame the review around several general, optical and even non-optical techniques. I hope that this does not trouble the reader, but it is how I mentally categorized the history of COIL diagnostics.

There now exists a fairly extensive toolbox of diagnostics available to the COIL developer, and these are listed in Table 1. In the following survey, I will highlight the development of several of these "tools".

* sdavis@psicorp.com; phone 1 978 689 0003; fax 1 978 689 3232; <http://www.psicorp.com>; Physical Sciences Inc., 20 New England Business Center, Andover, MA, USA 01810-1077

Table 1. "Toolbox" of diagnostics that have been applied to COIL

Method	Species/Parameter	Method	Species/Parameter
• Near-IR chemiluminescence	$\left\{ \begin{array}{l} \text{O}_2(a^1\Delta) \\ \text{I}(^2\text{P}_{1/2}) \\ \text{I}_2(A^3\Pi_1) \end{array} \right\}$	• Laser-induced fluorescence	$\left\{ \begin{array}{l} \text{Mixing} \\ \text{Reaction layers} \end{array} \right\}$
• Visible chemiluminescence	$\left\{ \begin{array}{l} \text{O}_2(b^1\Sigma) \\ \text{I}_2(B^3\Pi_0) \\ \text{O}_4^* \\ \text{Temperature} \end{array} \right\}$	• Raman spectroscopy	O_2^* yield
• Electron spin resonance	$\left\{ \begin{array}{l} \text{O}_2(X^3\Sigma) \\ \text{O}_2(a^1\Delta) \\ \text{I}(^2\text{P}_{3/2}, ^2\text{P}_{1/2}) \end{array} \right\}$	• Pressure meters	Species concentration
• Resonance absorption	$\left\{ \begin{array}{l} \text{I}(^2\text{P}_{3/2}, ^2\text{P}_{1/2}) \text{ (gain)} \\ \text{O}_2(X^3\Sigma) \text{ (yield)} \\ \text{H}_2\text{O} \\ \text{Temperature} \\ \text{I}_2 \text{ mass flow} \\ \text{I}_2 \text{ dissociation} \\ \text{Cl}_2 \text{ mass flow} \end{array} \right\}$	• Mass flow meters	"Fuel" flows
		• Power meters	Laser output power

The history of when these various diagnostic tools were developed and/or applied to COIL related research is summarized in Fig. 1. This figure is only intended to be a rough guide.

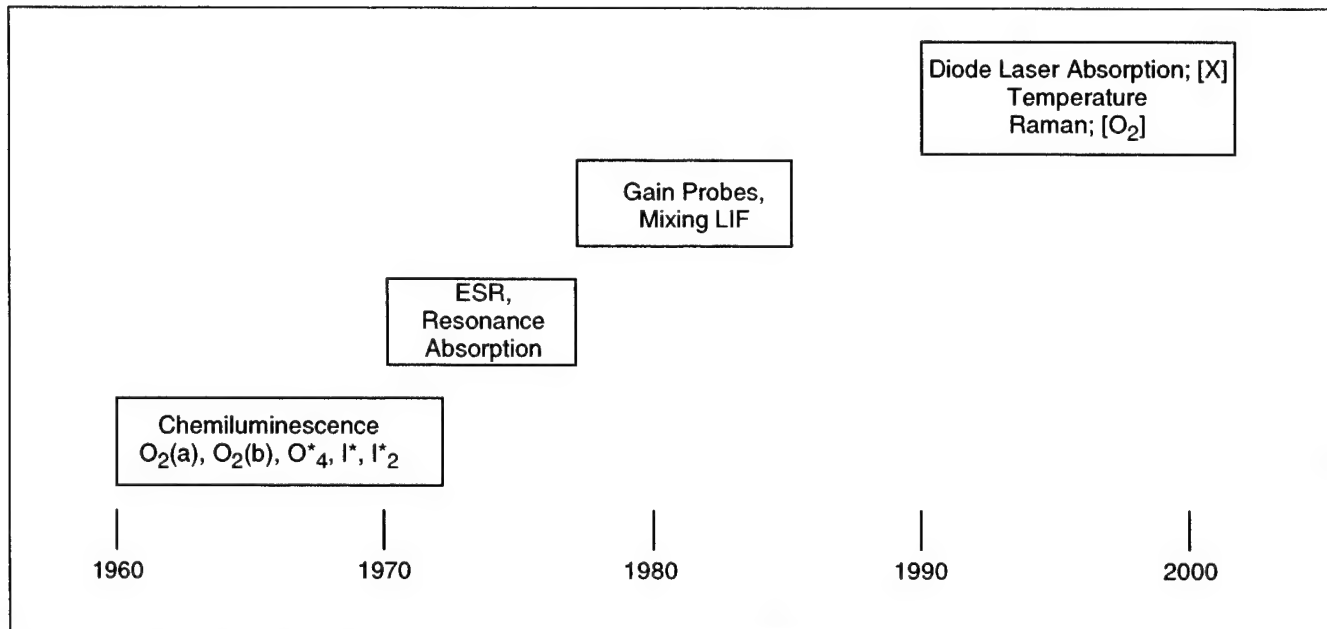
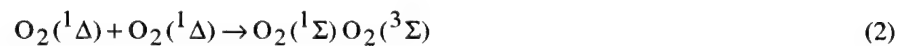


Fig. 1: History of COIL diagnostic development.

The overall COIL kinetics are well documented and we only present the essential features here. In brief, the system is described by Eqs. (1) through (3).



The equilibrium condition for inversion of the atomic iodine in COIL is given by Eq. (4)

$$K_{eq} = \frac{k_f}{k_r} = 0.75 \exp(402/T) \quad (4)$$

At room temperature, the atomic iodine lasant species can be inverted with about 18% of the oxygen in the $O_2(^1\Delta)$ state. The fraction of the oxygen required to invert the iodine is less at lower temperatures. This means that any additional singlet delta oxygen can be used to derive output power from the COIL device.

The reader will note that I have neglected the dissociation process in the reactions listed above. This was discussed in detail in Mike Heaven's paper earlier in this volume.⁵ From the above, we can deduce that knowledge of the concentrations of $O_2(^1\Delta)$, $O_2(^3\Sigma)$, $I(^2P_{1/2})$, $I(^2P_{3/2})$, and temperature are crucial. In addition, monitors for $O_2(^1\Sigma)$ and H_2O were target species early in COIL development because of their potential roles in the molecular iodine dissociation. Water vapor is a known quencher of the upper laser level $I(^2P_{1/2})$ in COIL.

2. EARLY DEVELOPMENTS

2.1 Chemiluminescence

Chemiluminescence often provides a convenient method for tracking excited state species, but it provides no information on the ground states of the relevant emitters since only spontaneous emission is observed. Knowledge of excited state lifetimes can in principle be used to determine the concentrations of the emitting states. However, calibration of the detection system and taking proper account of the viewing geometry often introduce considerable error into the chemiluminescence method. In general, determination of excited state species by absolute chemiluminescence methods is accurate to only about $\pm 40\%$. In spite of these issues, chemiluminescence is often the most sensitive and efficient diagnostic tool for initial assessment of a candidate chemical laser system.

Elmer Ogyzlo et al.⁶ used chemiluminescence to monitor $O_2(^1\Delta)$, $O_2(^1\Delta)_2$, $I(^2P_{1/2})$ and $O_2(^1\Sigma)$. Indeed, in this strikingly brief, yet succinct paper, they described several of the key issues related to COIL. These include energy transfer from $O_2(^1\Delta)$ to I atoms, energy probing of two $O_2(^1\Delta)$ molecules, and ominous comments about the still not completely understood I_2 dissociation mechanism.

Derwent and Thrush⁷⁻⁹ also used chemiluminescence to probe the products of the interaction of $O_2(^1\Delta)$ and $O_2(^1\Sigma)$ with I_2 . In a series of seminal papers they described the results of several key experiments. For example, in Fig. 2 we show the vibrational distribution in $I_2B(^3\Pi)$ produced in the interaction of both $O_2(^1\Sigma, ^1\Delta)$ with I_2 .

They used these and similar data to suggest kinetic mechanisms, and some of these ideas are still valid. By using chemiluminescence to derive populations of $O_2(^1\Delta)$ and $O_2(^1\Sigma)$, and establishing the equilibrium constant, they predicted that an atomic iodine laser pumped by $O_2(^1\Delta)$ would be possible.

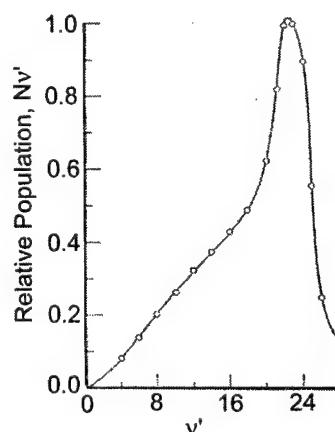


Fig. 2: Vibrational distribution within $I_2(B)$ produced by singlet oxygen pumping and obtained by Derwent and Thrush from visible chemiluminescence.

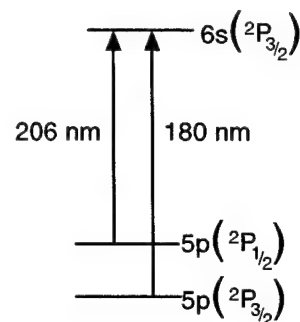


Fig. 3: Low lying energy levels of atomic iodine.

2.2 Resonance absorption and fluorescence

The atomic structure of the lower levels of atomic iodine are not only favorable for laser oscillation but are also readily probed via strong optical transitions in the UV region. In Fig. 3 we show the spin orbit terms ($^2P_{3/2}$) and ($^2P_{1/2}$) of the groundstate $5s^2p$ configuration. Since these two states arise from the same configuration, the $^2P_{1/2}$ level is metastable with respect to $^2P_{3/2}$ via LaPorte's rule.

In contrast (as shown in Fig. 3), the strong, radiatively allowed transition to the analogous state of the $5p^46s$ configuration provides sensitive probes for the $^2P_{1/2,3/2}$ states. Husain and coworkers^{10,11} took full advantage of this and reported a long series of kinetic measurements of the $^2P_{1/2}$ state. This early work provided not only important kinetic rate coefficients and estimates of the radiative lifetime of the $^2P_{1/2}$ state, but also laid the foundation for a diagnostic crucial to COIL.

2.3 The first gain measurement

Dave Benard led a group from the Air Force Weapons Laboratory (AFWL), the Rockwell Science Center and Rocketdyne Inc. in a key demonstration experiment.¹² The setup is shown in Fig. 4. Rocketdyne had developed a singlet oxygen generator using the reaction of chlorofluorosulfate (CFS) with H_2O_2 and had measured singlet oxygen yields of 35%.

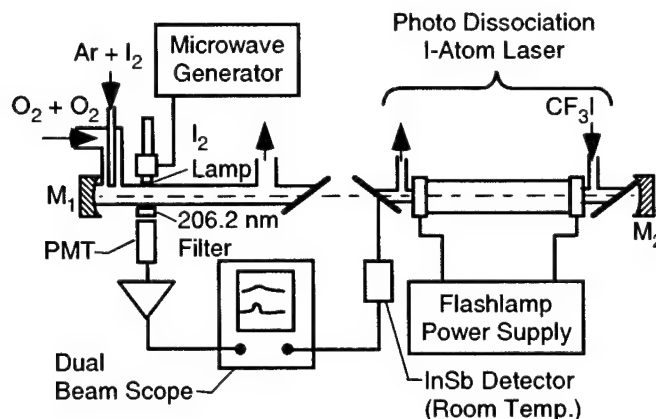


Fig. 4: Experimental arrangement for the first gain measurement in COIL.

The idea behind the diagnostic was to saturate the $I(^2P_{1/2} \leftarrow ^2P_{3/2})$ transition with a strong pulse from an I atom photolysis laser. If the $^2P_{1/2}$ state is inverted with respect to the $^2P_{3/2}$ then the saturation pulse will drive population down from the $^2P_{1/2}$ state to the $^2P_{3/2}$ state. The relative population of the $^2P_{1/2}$ and $^2P_{3/2}$ states was monitored with a resonance lamp operating at 206 nm (see Fig. 4). Using this sensitive double resonance approach, Benard and coworkers¹² were able to demonstrate weak, but certain positive gain in a singlet oxygen pumped iodine atom flow system. This provided the crucial data needed to maintain the focus and the program to produce a chemically pumped short wavelength laser.

2.4 "First light"

Recognition of the fundamental differences in the spatial and directional distributions between spontaneous and stimulated emission led to the key optical diagnostic that guided the first successful COIL laser demonstration. The basic idea is shown in Fig. 5. Two Ge detectors were positioned next to the longitudinal flow cavity region. Detector A probed along the optical axis and detector B examined the light emitted normal to the optical axis. Consequently, detector A was sensitive to stimulated emission directed along the resonator axis, and detector B detected spontaneous emission emitted normal to the optical axis. The approach to laser oscillation in any laser includes a buildup of stimulated emission intensity along the resonator axis. Thus one expects that the end detector A will show a faster rise than the side viewing detector B. This is exactly what was seen on the first COIL. The end detector initially became noisier than the side detector as the intensity along the optical axis grew due to stimulated emission. Finally, as laser threshold was reached, the end detector "pegged." A power meter showed 4 mW output. Transverse mode structure was observed on an IR sensitive card, confirming laser oscillation.¹

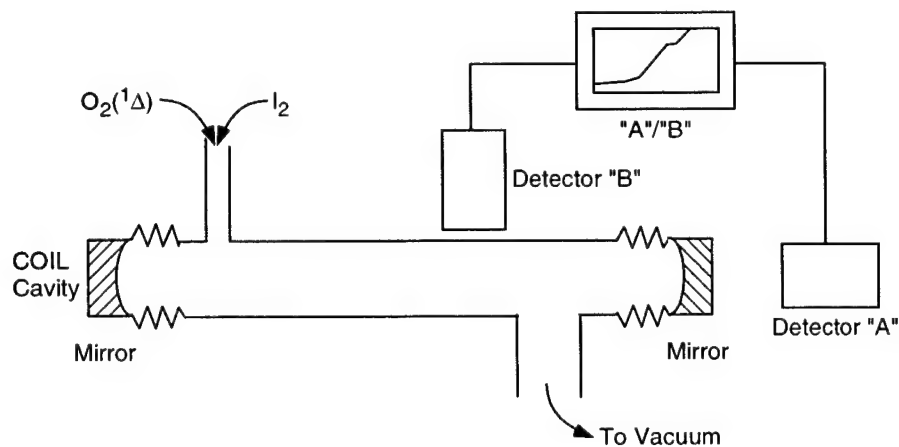


Fig. 5: Experimental arrangement for the first COIL gain measurement.

3. POST LASER DEMONSTRATION DIAGNOSTICS

3.1 Introduction

The laser demonstration¹ of 1 December 1977 was a defining moment in the history of COIL diagnostics. In general, the diagnostics prior to December 1, 1977 were developed to support this key milestone. Subsequent to the laser event, it was clear that the COIL kinetic mechanisms and rates needed serious development. This led to a renaissance of kinetics studies that has not been equaled since that time. Premier federal, industrial, and academic laboratories were focused on this system for a period of about 5 years.

3.2 Chemiluminescence

Soon after the first demonstration of COIL, the group at Aerospace Corp headed by Rick Heidner began a systematic and detailed series of experiments to determine key kinetic mechanisms and rate coefficients.^{13,14} Using a microwave source for excited oxygen and a temperature controlled flow reactor, they produced kinetic data that are used to this day. From these data they developed possible mechanisms for the molecular iodine dissociation that were discussed earlier by Mike Heaven.⁵ These data have withstood the test of time for nearly two decades and comparisons continue to be made between new models for the dissociation to the data-base produced by this excellent work.

At AFWL (now the Air Force Research Laboratory), my research group was involved with an active program to examine candidates for short wavelength chemical lasers. We were already involved in developing diagnostics for COIL. These diagnostics included both passive (chemiluminescence) and active (resonance absorption and fluorescence) techniques. Before describing some of the active techniques, I want to discuss some of the interesting results that we obtained from the chemiluminescence work.

The dissociation of molecular iodine had been an elusive problem for many years. Using a small flow tube and a microwave discharge to produce singlet oxygen, we made some initial probes into the efficiency of the dissociation process by monitoring the number of singlet oxygen molecules consumed to dissociate one iodine molecule.¹⁵ The experiment was relatively simple: measure the consumption of singlet oxygen as a function of the added I_2 . We used an optically based mass flow meter to measure the iodine mass flow. In Fig. 6 we show results from that experiment that imply that the dissociation efficiency increased as the molecular iodine was increased. While not defining a mechanism or producing kinetic rates, this early experiment did imply that iodine itself might be active in the dissociation process.

We also developed a Fabry-Perot interferometer to examine the collisional broadening of the hyperfine components of the $I(^2P_{1/2} \rightarrow ^2P_{3/2})$ transition, again using chemiluminescence.¹⁶ A microwave production source produced $O_2(^1\Delta)$, and this flow was added to a small flow tube reactor that also mixed in I_2 . We spectroscopically examined the hyperfine components of the atomic iodine chemiluminescence emission as shown in Fig. 7.

Examination of these spectra as a function of added oxygen yielded the first broadening data under COIL conditions and demonstrated that the prior concerns about an anomalously large oxygen broadening of the COIL laser transition were unfounded. We concluded that under COIL conditions, the reduction in the line center gain on the (3,4) transition caused by oxygen collisional broadening would be minimal.

There are several possible methods for determining the flow temperature. Thermocouples can be used, but the metastable oxygen leads to errors in thermocouple measurements due to deactivation of the excited oxygen on the thermocouples. In addition, thermocouple measurements are notoriously inaccurate in rarified, supersonic gas flows

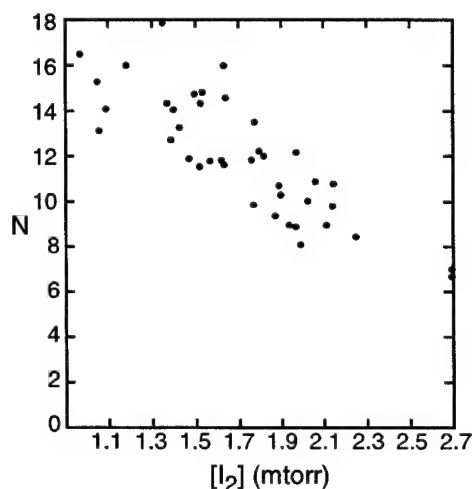


Fig 6: Plot of the number of singlet oxygen molecules required to dissociate an I_2 as a function of the I_2 concentration.

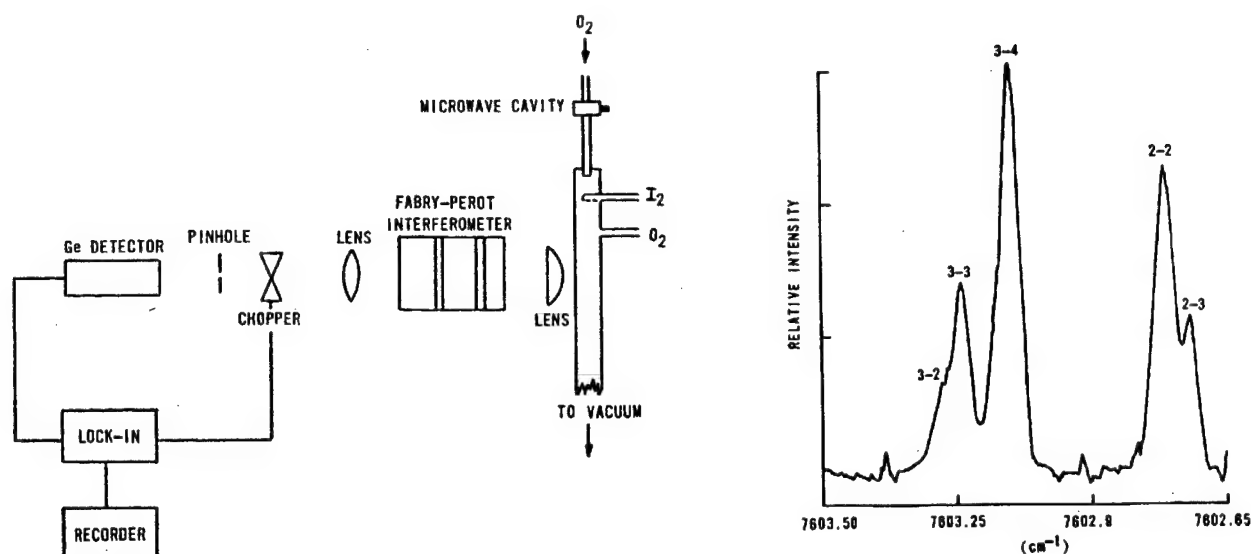


Fig. 7: Partially resolved hyperfine structure from atomic iodine produced by the interaction of molecular iodine with singlet oxygen and recorded with a Fabry-Perot interferometer.

such as in COIL. Other potential methods include measurement of the rotational temperature of species in the flow such as the rotational manifold of oxygen. Van Benthem and Davis¹⁷ demonstrated a variant of this approach by monitoring the rotationally resolved emission on the $O_2(b \rightarrow X)$ system produced in chemical oxygen generators used in COIL. We determined the temperature $T = 310$ K over a large sparger singlet oxygen generator on the AFWL COIL IV. While potentially useful, one must be assured that the rotational manifold of the electronically excited $O_2(b)$ state is at the translational flow temperature, and this may not be true at typical low pressure COIL conditions.

3.3 Resonance absorption

Most "active" diagnostics developed for COIL during this period used resonance absorption and fluorescence. Interestingly, several diagnostics that we developed used the optical ($B \leftarrow X$) transition in I_2 . Indeed, at least four diagnostics were based on this absorption band:

- I atom probe laser
- I_2 dissociation fraction
- I_2 mass flow meter
- Laser induced fluorescence for flow mixing.

The relevant energy levels of the $I_2(B-X)$ system are shown in Fig. 8. The B state correlates to one excited and one ground state atom. For excitation wavelengths longer than about 501 nm, strong, visible fluorescence is produced. In contrast, when excited by optical wavelengths less than 500 nm, the visible fluorescence is dramatically reduced. However, strong emission from the excited $I(^2P_{1/2})$ is produced. We used this selective process to produce the first I atom laser based upon photolysis of I_2 .¹⁸ This has distinct advantages over photolysis of alkyl-iodides such as CF_3I , because I_2 regenerates itself from I atom recombination. We used this simple, dye laser pumped I atom laser to probe for gain on COIL IV, and it identified a chemically induced coating problem on the COIL cavity mirrors.

Len Hanco and I developed an iodine mass flow meter based on the continuum absorption near 490 nm from the ground state of I_2 .¹⁹ The concentration of molecular iodine in a cell can be determined directly from such a measurement. If the cell is in line with the iodine delivery system in a COIL, then one can use this approach to determine the mass flow of the iodine. One needs to measure the mass flow rate and pressure of the carrier gas in the same cell, but these parameters can be readily measured with a mass flow meter and capacitance manometer respectively.

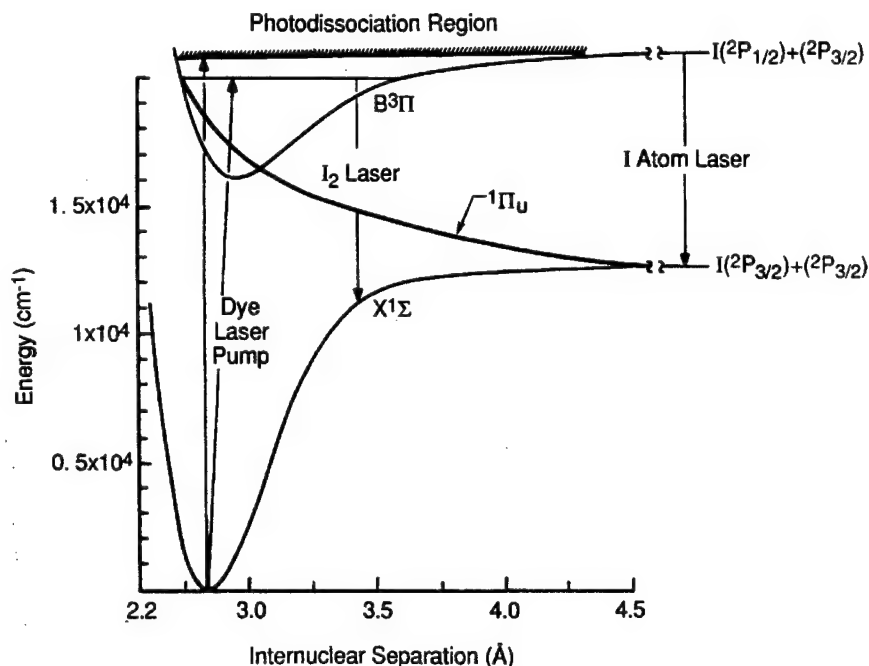


Fig. 8: Energy levels in I_2 relevant to several COIL diagnostics.

Iodine dissociation fraction measurements in the cavity of COIL devices are made using an analogous strategy. One monitors the absorption on a bound-bound transition of the B-X system. As the iodine is dissociated, the absorption is reduced, and this provides a direct measurement of the dissociation fraction.

Hall, Marinelli, and Houston²⁰ completed an important experiment in 1983 that conclusively demonstrated that highly vibrationally excited I_2 was a major product of the quenching of $I(^2P_{1/2})$ by molecular iodine. They detected $I_2(X; 25 \leq v'' \leq 43)$ using laser induced fluorescence to probe the products of this quenching process. Following up on this excellent work, we used laser induced fluorescence to probe the dissociation region in a flow of singlet oxygen and molecular iodine and observed a similar distribution of vibrationally hot ground state I_2 .²¹ This combined with the prior chemiluminescence results of Heidner,^{13,14} Lilenfeld,^{22,23} and Alsing,¹⁷ confirmed that iodine was an active participant in its own dissociation.

Finally, with respect to visible wavelength resonant absorption techniques, I should mention the flow field visualization that Larry Rapagnani and I developed for studying mixing in subsonic and supersonic chemical laser flow fields.²⁴ We injected iodine vapor into the plenum of a cw, HF chemical laser run without fuels. The nozzle was a CL II supersonic device. We used an argon ion laser operating at 514.5 nm to excite the $v'=43$ level in $I_2(B)$ at several selected locations downstream of the nozzle. A photograph of the planar laser induced fluorescence emitted by the excited iodine molecules is shown in Fig. 9. The LIF originates from the argon ion laser beam slightly downstream of the nozzle exit bank and persists for about 2 cm, consistent with the Mach 3 flow and the radiative lifetime of the $I_2(B)$ excited state. With the advent of CCD cameras, this method progressed from a qualitative demonstration to a quantitative technique to study mixing in chemical lasers. Numerous COIL development facilities have used this LIF technique to assess mixing in advanced nozzles.

3.4 Electron paramagnetic resonance

The group at MDRL led by Harvy Lilenfeld completed a comprehensive series of kinetics measurements that used chemiluminescence, EPR, spectroscopy, and LIF.^{22,23,25} They used these tools to excellent advantage and produced a series of reliable and important kinetics rates, many of which are now in the Air Force standard rate package for COIL. They also made significant contributions to the understanding of important kinetic mechanisms including the dissociation process.



Fig. 9: LIF image of nozzle effluent pattern in a Mach 3 chemical laser flowfield. The image is from laser excited molecular iodine. Flow is down in the picture.

3.5 Diode laser sensors

With the advent of reliable, near IR laser diodes, a new class of diagnostics based on resonance absorption became feasible. The telecommunications industry was the main catalyst for the development of these new lasers that are now used as sources for wavelength division multiplexing (WDM) and dense wavelength division multiplexing (DWDM) applications. Low loss and low dispersion fiber optics in the 1.3 to 1.65 μm spectral region led to the development of superior lasers in this spectral window for telecommunications. Narrow and controllable wavelengths from the diode lasers is crucial for DWDM, and distributed feedback (DFB) lasers were developed for this purpose. At Physical Sciences Inc. (PSI) we recognized that this could lead to a new class of sensitive diagnostics for COIL including singlet oxygen yield, water vapor, iodine atoms, and translational temperature. In 1991, we began to investigate room temperature diode lasers as sensors for numerous gases, and have demonstrated monitors for over 30 gases since that time. Some of these were relevant to COIL, and we developed modules^{26,27} for three important species:

- Ground state oxygen
- Water vapor
- Iodine atoms.

The DFB lasers developed for telecommunications offer several advantages for rugged, fieldable COIL diagnostics. First, they produce narrow band (5 to 30 MHz), output that is rapidly (kHz rates) tunable over isolated rovibrational or rovibronic lines of the target species. Secondly, these lasers can be directly coupled to single mode fiber optic cables. This greatly simplifies the interface to COIL systems. Finally, as we discuss below, since the diode laser can scan an entire lineshape, the measurement becomes independent of both pressure and, to a large extent, temperature in the measurement volume.

The typical diode laser based sensor contains the diode laser, fiber optic delivery system, a room temperature solid state detector such as Si or InGaAs, and a PC controlled data acquisition and analysis system. A standard installation on a COIL device is shown in Fig. 10. Use of a fiber splitter allows us to produce several output fiber legs that can probe different regions of the COIL flow simultaneously.

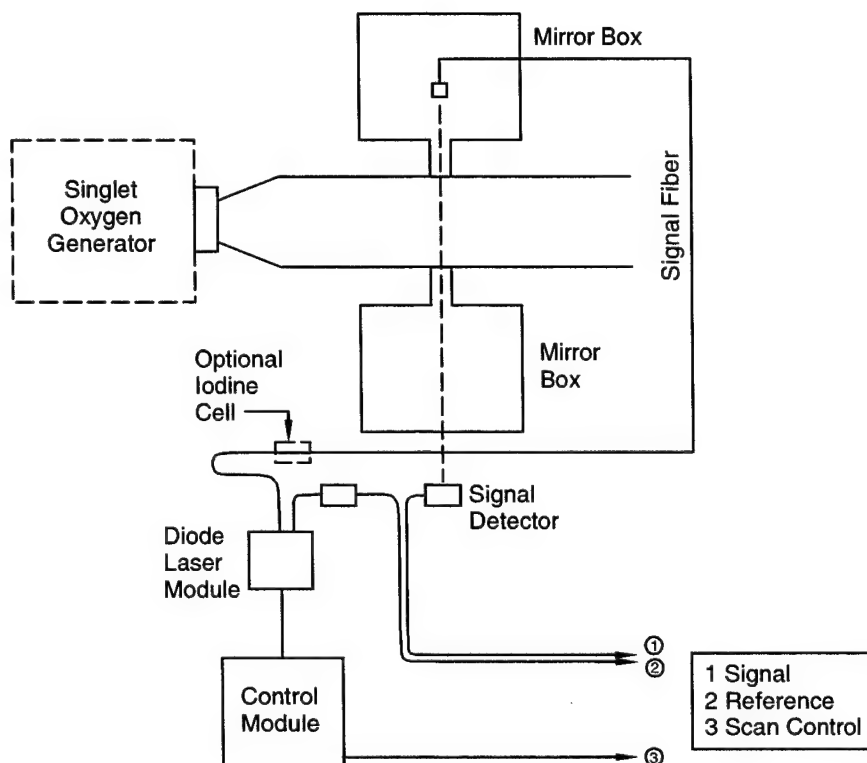


Fig. 10: Typical installation of a diode laser based COIL diagnostic. An Iodine Scan system is shown.

These systems use Beer's law to determine the concentration, N , of the target species as described in Eq. (5).

$$N = \frac{1}{S_T \ell} \int \ln \left(\frac{I_{0,v}}{I_v} \right) dv \quad (5)$$

where

S_T is the absorption linestrength

ℓ is the absorption pathlength

and $I_{0,v}$ and I_v are the initial and transmitted light intensities.

Note that since we scan the diode laser over the entire absorption feature, the integrated absorption is independent of the pressure because the integral under any absorption line is constant for constant number density of absorbers. The peak absorption is reduced as the pressure is increased, while the line broadens and the integral remains constant. Likewise, as the temperature increases, the Doppler width increases, but the integral under the absorption line remains constant. The absorption linestrength (S) has a temperature dependence due to the Boltzmann population distribution within the absorbing state. However, we have selected lines that have a minimal temperature dependence for typical COIL conditions.

The actual shape of the absorption curve is described by the lineshape function, $g(v)$. The lineshape function contains all the information with respect to the spectral shape of the absorption feature. In general, the lineshape can be described by a Voigt function which is a convolution of a Gaussian and a Lorentzian. Systematic fitting of the observed absorption lineshape will provide the Gaussian and Lorentzian full widths at half maximum (FWHM). The Gaussian FWHM can be used to determine the translational temperature in the measurement region. We have discussed this in prior

presentations and do not repeat it here.²⁸⁻³⁰ Several papers in this conference discuss temperature measurements using this approach.

In order to increase the accuracy of temperature measurements by this method, it is best to know the Lorentzian component of the linewidth. One can then deconvolve the Lorentzian to obtain the Gaussian component. To assist in this goal, we have made a series of detailed measurements of the collisional broadening coefficients²⁸⁻³⁰ of relevant absorption lines in oxygen, water vapor, and atomic iodine. Note that we define our measured broadening coefficients in terms of full width at half maximum (FWHM); i.e., (MHz/Torr). These are provided in Tables 2 through 4 below.

Table 2. Broadening coefficients for selected O₂(b←X) lines used in the Oxygen Scan diagnostic

Bath Gas	Oxygen Transition	Broadening Coefficient (MHz/Torr)	Line Shift Coefficient (MHz/Torr)
Oxygen	P5 P5	4.2	0.21
Oxygen	P19 P19	3.3	0.23
Helium	P5 P5	3.1	0.04
Neon	P5 P5	3.2	0.12
Argon	P5 P5	3.7	0.31
Nitrogen	P5 P5	4.1	0.29
Carbon dioxide	P5 P5	4.7	0.17
Chlorine	P5 P5	5.2	0.34
Water vapor	P9 Q8	5.0	---

Table 3. Broadening coefficients for the 1.3925 μ m water vapor line used in the Water Scan diagnostic

Collision Partner	Broadening Coefficient (MHz/Torr)
H ₂ O	31.2
CO ₂	14.8
NH ₃	23.8
He	1.8
Ar	3.7
O ₂	4.8
N ₂	8.8
Air	7.6
Propane (C ₃ H ₈)	10.2
Ethane (C ₂ H ₆)	8.9
Ethane (C ₂ H ₄)	13.8
Propylene (C ₃ H ₆)	7.4
Methane (CH ₄)	7.6

Table 4. Broadening coefficients for several relevant gases on the (3,4) hyperfine line of atomic iodine

Bath Gas	Broadening Coefficient (MHz)
He	3.2
N ₂	5.5
O ₂	5.0

We have also measured the temperature dependence of the collisional linebroadening of the (3,4) hyperfine line in atomic iodine for both He and O₂ over the temperature range 300 to 775K. These values are:

$$(\Delta\nu/\Delta P_{\text{He}})_T = (3.2 \pm 0.3) \times (296/T)^{0.36}$$

and

$$(\Delta\nu/\Delta P_{\text{O}_2})_T = (5.5 \pm 0.6) \times (296/T)^{0.70}$$

These values can be used in the data reduction of absorption lineshapes including those in the cavity region where the temperatures are considerably lower than 300 K.

3.6 Raman spectroscopy

Gylys and Rabin³¹ have recently reported a complementary method for measuring the yield of singlet oxygen using Raman scattering. This method provides a direct measurement of the concentrations of both O₂(¹Δ) and O₂(³Σ) since the Raman cross sections for both these species are known. The typical set up is shown in Fig. 11. Since the Raman cross section is low, the method requires a high power laser and sensitive, wavelength dispersing optical detectors. Despite these potential drawbacks, Gylys and Rabin have demonstrated impressive results. There also a paper in this meeting that discussed Raman as an oxygen diagnostic for COIL.³²

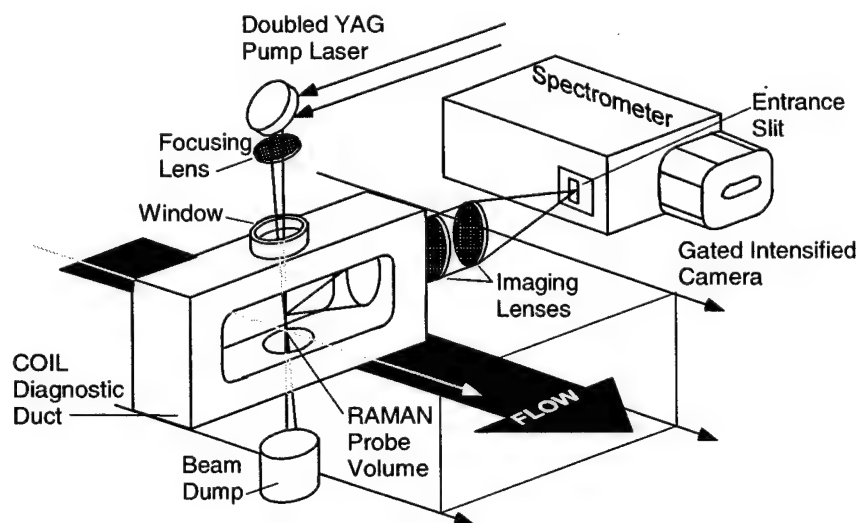


Fig. 11: Experimental setup for Raman imaging in COIL.

4. SUMMARY AND CONCLUSIONS

In this brief survey of the history of COIL diagnostics, I have attempted to provide a perspective of progress and recent developments. It is clear that we have all come a long way in developing tools to help investigate key aspects of COIL. We have seen a progression from the earliest chemiluminescence probes that led to the discovery of COIL to approaches that allow probing of ground state species, small signal gain, temperature, and spatially resolved parameters. These diagnostics, whatever flavor, will continue to aid the further development of advanced and more efficient COIL devices. Until the present time, most sensitive COIL diagnostics have been used to gain a better understanding of how this system operates, i.e. kinetic mechanisms and rates. Chemiluminescence-based diagnostics have been used for many years on active COIL devices as system "health" monitors. I suggest, that a fruitful path for future work in the diagnostics area would be to incorporate both passive and active diagnostics as part of a suite of open- and closed- loop feed back control systems to enhance the stability and reliability of COIL. Of course, this will require considerable engineering, but that is consistent with the high level of maturity that COIL has attained.

I would be remiss if I did not at least mention that advanced diagnostics might someday assist in the eventual resolution of the molecular iodine dissociation mystery. We may yet have some science to discuss at the 50th anniversary of COIL!

ACKNOWLEDGMENTS

I have had the privilege of working with many talented researchers in the field of COIL diagnostics and kinetics. I have already mentioned several in the body of the paper. In addition to them I would like to acknowledge Bob Shea and Dave Neumann, who were actively involved in some of the early diagnostics development work at AFWL. I would also like to mention Art Guenther and Pete Avizonis who recognized the value of advanced diagnostics and were very supportive. Don Ball, former director of AFOSR Chemical and Molecular Sciences, deserves a special thanks for generous and continual support during much of the period discussed. Gordon Hager of AFRL also has been very supportive of the diode laser diagnostics development. Finally, I would also like to thank my many colleagues at PSI including Bill Kessler, Phil Mulhall, Phil Keating, and Mark Allen for assisting in the development of the diode laser sensors.

REFERENCES

1. W.E. McDermott, N.R. Pchelkin, D.J. Benard, and R.R. Bousek, "An Electronic Transition Chemical Laser", *Appl. Phys. Lett.* **32**, 469, 1978.
2. D.J. Benard, W.E. McDermott, N.R. Pchelkin, and R.R. Bousek, "Efficient Operation of a 100-W Transverse Flow Oxygen Iodine Chemical Laser", *Appl. Phys. Lett.* **34**, 40, 1979.
3. R.J. Richardson and C.E. Wiswall, "Chemically Pumped Iodine Laser", *Appl. Phys. Lett.* **35**, 138, 1979.
4. W.E. McDermott, "Historical Perspective of COIL", SPIE Paper 4631-01, Gas and Chemical Lasers and Intense Beam Applications IV, San Jose, CA, January 2002.
5. M.C. Heaven, A.V. Komissarov, and V. Goncharov, "Mechanism and Kinetics of Iodine Dissociation in COIL", SPIE Paper 4631-02, Gas and Chemical Lasers and Intense Beam Applications IV, San Jose, CA, January 2002.
6. S.J. Arnold, N. Finlayson, and E.A. Ogryzlo, "Some Novel Energy-Pooling Processes Involving $O_2(^1\Delta_g)$ ", *J. Chem. Phys.* **44**, 2529, 1966.
7. R.G. Derwent and B.A. Thrush, "Excitation of Iodine by Singlet Molecular Oxygen", Part I, Mechanism of the I_2 Chemiluminescence", *J.C.S. Faraday II* **68**, 720, 1972.
8. R.G. Derwent and B.A. Thrush, "Excitation of Iodine by Singlet Molecular Oxygen", Part II, Kinetics of the Excitation of Iodine Atoms", *Discs. Faraday Soc.* **53**, 162, 1972.
9. R.G. Derwent and B.A. Thrush, "Measurements of $O_2(^1\Delta_g)$ and $O_2(^1\Sigma_g)$ in Discharge Flow Systems", *Trans. Faraday Soc.* **67**, 2036, 1971.
10. R.J. Donovan, F.G.M. Hathorn, and D. Husain, "Study of Electronically Excited Atoms, $I(5^2P_{1/2})$ in the Presence of Alkyl Iodides", *Trans. Faraday Soc.* **64**, 1, 1968.
11. J.J. Deakin and D. Husain, "Temperature Dependence of Collisionally induced Spin Orbit Relaxation of Electronically Excited Iodine Atoms, $I(5p^5^2P_{1/2})$ ", *J.C.S. Faraday II*, **68**, 1603, 1972.
12. A.T. Pritt, R.D. Coombe, D. Pilipovich, R. Wagner, D. Benard, and C. Dymek, "Chemical Generation of a Population Inversion Between the Spin Orbit States of Atomic Iodine", *Appl. Phys. Lett.* **31**, 746, 1977.
13. R.F. Heidner, C.E. Gardner, G.I. Segal, and T.M. El-Sayed, "Chain Reaction Mechanism for I_2 Dissociation in the $O_2(^1\Delta)$ I-atom Laser", *J. Phys. Chem.* **87**, 2348, 1983.
14. R.F. Heidner, C.E. Gardner, T.M. El-Sayed, and G.I. Segal, "Temperature Dependence of $O_2(^1\Delta) + O_2(^1\Delta)$ and $I(^2P_{1/2}) + O_2(^1\Delta)$ Energy Pooling," *J. Chem. Phys.* **74**, 5618, 1981.
15. P.M. Alsing, G. Simmons, and S.J. Davis, "Observations Concerning the Efficiency of the I_2 Dissociation by $O_2(^1\Delta)$ ", Laser Digest, AFWL TR- 82-88, 1982.
16. D.K. Neumann, P.K. Clark, R.F. Shea, and S.J. Davis, " O_2 Pressure Broadening of the Iodine $^2P_{1/2} \rightarrow ^2P_{3/2}$ Transition", *J. Chem. Phys.* **79**, 4680, 1983.
17. S.J. Davis and M.H. VanBenthem, "A Temperature Measurement Technique for COIL-IV", Laser Digest, AFWL TR-84-76, 1985.
18. S.J. Davis, "Dye Laser Pumped Atomic Iodine Laser", *Appl. Phys. Lett.* **32**, 656, 1978.
19. S.J. Davis and L. Hanco, "An I_2 Flow Rate Diagnostic for the Oxygen Iodine Laser", Laser Digest, AFWL-TR-79-104, 1979.

20. G.E. Hall, W.J. Marinelli, and P.L. Houston, "Electronic to Vibrational Transfer from $I^*(5^2P_{1/2})$ to $I_2(25 < V < 43)$ ", *J. Phys. Chem.* **87**, 2153, 1983.
21. S.J. Davis and M. VanBenthem, "Detection of Vibrationally Excited I_2 in the Iodine Dissociation Region of Chemical Oxygen-Iodine Chemical Lasers", *J. Phys. Chem.* **90**, 902, 1986.
22. H.V. Lilenfeld, "Oxygen Iodine Laser Kinetics", AFWL TR-83-01, Kirtland AFB, NM, 1983.
23. H.V. Lilenfeld, G.R. Bradburn, and F.E. Hovis, "Oxygen Iodine Laser Kinetics", AFWL-TR-84, 1984.
24. N.L. Rapagnani and S.J. Davis, "Laser Induced Fluorescence Measurements in a Chemical Laser Flowfield", *AIAA Journ.* **17**, 1402, 1979.
25. H.V. Lilenfeld and R.J. Richardson, "The ESR Spectrum and Linewidth Measurements of Atomic Iodine", *J. Chem. Phys.* **70**, 3859, 1979.
26. M.G. Allen, K.L. Carleton, S.J. Davis, W.J. Kessler, and K.R. McManus, AIAA 25th Plasmadynamics and Lasers Conference, Colorado Springs, CO, June 1994.
27. S.J. Davis, M.G. Allen, W.J. Kessler, K.R. McManus, M.F. Miller and P.A. Mulhall, "Diode Laser-based Sensors for Chemical Oxygen Iodine Chemical Lasers", SPIE paper 2702-17, OE-Lase Conference, San Jose, CA, 1996.
28. S.J. Davis, W.J. Kessler, , and M. Bachmann, "Collisional Broadening of Absorption Lines in Water Vapor and Atomic Iodine Relevant to COIL Diagnostics," SPIE Paper No. 3612-25, The International Society for Optical Engineering, San Jose CA, 1999.
29. S.J. Davis, W.J. Kessler, M. Bachmann, P.A. Mulhall, "Collisional Broadening Coefficients for Oxygen and Water Absorption Lines Used in COIL Diagnostics," SPIE Paper 3268-80, Gas and Chemical Lasers and Intense Beam Applications, San Jose, CA, 1998.
30. S.J. Davis, W.J. Kessler, and P.K. Keating, "Progress in the Development of Sensors for COIL Devices", Paper 3931-24, SPIE Gas Phase and Chemical Lasers and Intense Beam Interactions, San Jose, CA, 2000.
31. V.T. Gyls and L.F. Rubin, "Direct Measurement of $O_2(a^1\Delta)$ and $O_2(X^3\Sigma)$ in Chemical Oxygen Iodine Lasers with use of Spontaneous Raman Imaging", *Appl. Opt.* **37**, 1026, 1998.
32. W. Zhao, F. Sang, and L. Duo, "Measurement of Chemical Oxygen Iodine Laser Singlet Oxygen Generator Parameter using Raman Spectroscopy", Paper 4631-25, Gas and Chemical Lasers and Intense Beam Applications IV, San Jose, CA, January 2002.

Modeling of the gain, temperature, and iodine dissociation fraction in a supersonic chemical oxygen-iodine laser

B. D. Barmashenko, E. Bruins, D. Furman, V. Rybalkin and S. Rosenwaks
Department of Physics, Ben-Gurion University of the Negev, Beer-Sheva 84105, Israel

ABSTRACT

We report on a simple one-dimensional model developed for the fluid dynamics and chemical kinetics in the chemical oxygen iodine laser (COIL). Two different I_2 dissociation mechanisms are tested against the performance of a COIL device in our laboratory. The two dissociation mechanisms chosen are the celebrated mechanism of Heidner and the newly suggested mechanism of Heaven. The gain calculated using Heaven's dissociation mechanism is much lower than the measured one. Employing Heidner's mechanism, a surprisingly good agreement is obtained between the measured and calculated gain and temperature over a wide range of the flow parameters. Other predictions of the model (larger mixing efficiency and higher temperature with a leak opened downstream of the resonator and gain decrease along the flow) are also in agreement with the experimental observations.

Keywords: chemical lasers, oxygen, iodine, power lasers

1. INTRODUCTION

The chemically driven oxygen iodine laser (COIL) ¹ is the only known example of a high power chemically driven electronic transition laser. The laser transition, at 1.315 microns, takes place between the spin-orbit levels of the ground state configuration of the iodine atom, $I(5p^5\ ^2P_{1/2}) \rightarrow I(5p^5\ ^2P_{3/2})$. The iodine atoms are pumped by a near resonant energy transfer from oxygen molecules in the excited singlet-delta state, $O_2(a^1\Delta_g)$



$O_2(^1\Delta)$ is produced in a chemical generator by the reaction of gaseous chlorine with a basic hydrogen peroxide solution (BHP). Mixing of the $O_2(^1\Delta)$ with I_2 molecules results in their dissociation to iodine atoms which are subsequently excited via reaction (1).

To understand the kinetic and mixing processes in COILs and optimize the output power it is necessary to have reliable models describing the COIL operation and, in particular, the small signal gain, iodine dissociation fraction and gas temperature in the resonator. One and quasi-two-dimensional models of supersonic COILs accounting for both chemical reactions and mixing processes were developed in ²⁻⁶. The calculated values of the power and gain are in reasonable agreement with experimental measurements performed for a small scale supersonic COIL developed in our laboratory ^{3,7} and for the RADICL device, a 5 kW class supersonic COIL, developed at the Air Force Research Laboratory in Albuquerque, NM ^{8,9}. More sophisticated three-dimensional (3-D) computational fluid dynamics (CFD) models were developed in ¹⁰⁻¹³ to take into account non-uniform distribution of the gain and temperature across the flow and, in particular, the three-dimensional horseshoe structure of the jets injected into the cross flow, shocks and turbulence that can not be directly modeled using the one and quasi-two-dimensional approaches. These 3-D models, however, are complex, need very long computation time and to the best of our knowledge are often inapplicable to parametric studies of the COIL when input parameters are changed continuously over a wide range. At the same time it appears that one- and quasi-two-dimensional models are able to reproduce most of the essential features of the chemical kinetics, mixing and hydrodynamics in the active medium of the COIL ^{5,6}. Although these models give distributions of the small signal gain, temperature and density of $O_2(^1\Delta)$ only in the flow direction, the computation time is very short and it is possible to quickly predict performance over a wide range of input parameters (chemical flow rates, position of the mixing point and stagnation temperature). Since the values of some of the input parameters (the $O_2(^1\Delta)$ yield, flow rates of the

chlorine and water, stagnation temperature in the subsonic section of the flow and mixing efficiency) were previously known with very low accuracy it was very difficult to compare the results predicted by the aforementioned one-dimensional models with experimental data.

Recently we reported on diagnostic measurements in a slit nozzle supersonic COIL with transonic mixing, operating without primary buffer gas and with secondary N_2 ¹⁴. Using diode laser based diagnostics we measured the gain and temperature in the resonator, the $O_2(^1\Delta)$ yield and water vapor fraction in the subsonic section of the flow. In addition, the chlorine utilization and gas temperature at the generator exit were measured. In the present paper a simple one-dimensional model of the supersonic COIL with transonic injection of iodine is developed and used to simulate the experimental results obtained in¹⁴. This model is similar to the leaky stream tube model developed in³. The input parameters of the model were taken from the aforementioned measurements¹⁴. The objective of the present modeling is to provide for accurate calculations of chemical kinetics processes, rather than gas dynamics in the COIL. That is why most of the gas dynamics properties of the flow such as spatial distributions of the static pressure, static temperatures in the "cold" runs without chemical reactions, mixing efficiencies and stagnation pressures and temperatures, were also taken from the experiment. Calculations of the gain, temperature and iodine dissociation fraction along the flow as a function of the iodine flow rate, the most important parameter affecting both the gain and dissociation fraction, were carried out. The changes in iodine flow mainly affect the rates of chemical reactions and gas temperature and have only weak, indirect (via temperature changes) effect on the flow hydrodynamics. In particular, the iodine jets penetration into the primary flow (proportional to the momentum of the jet at the sonic injection hole and hence to the stagnation pressure of the secondary flow) is changed by less than 10-15% (depending on the iodine injector geometry) over the characteristic range of the iodine flow (0 – 0.4 mmole/s), which means that the iodine flow has a weak influence on the penetration. Our recent measurements¹⁵ of the gain distribution across the flow also confirm that the penetration is almost unaffected by the iodine flow. Indeed, for small values of the penetration parameter the gain distribution has bimodal structure with two peaks located higher and lower than the flow centerline and corresponding to the centerlines of the iodine jets. We observed that the peak positions and hence the iodine penetration, are almost independent of the iodine flow rate.

Comparison between the calculated and experimental dependencies of the gain and temperature on the iodine flow rate permits to determine which of the proposed kinetic schemes and sets of rate constants for I_2 dissociation,¹⁶ or¹⁷, fits better to the experimental results. The model was run for different flow rates of chlorine and secondary nitrogen and different positions of the optical axis along the flow and compared with the experimental results¹⁴.

2. OUTLINE OF THE MODEL

2.1 General assumptions of the model

The model considers a typical configuration of a supersonic COIL¹⁴ in which I_2 premixed with nitrogen (secondary flow) is injected perpendicularly into the main flow (primary flow) composed of O_2 [partially excited to $O_2(^1\Delta)$], H_2O and Cl_2 (see Fig. 1). The injection occurs in the transonic part of the supersonic slit nozzle through injection holes in each side (top and bottom). After the injection the gas is brought to supersonic velocity via expansion in the nozzle and flows through the duct with the floor and the ceiling diverging at an angle of 8° towards the optical resonator. As shown in² the perpendicular injection of the jets into the primary flow results in jets bending, merging of each series of single jets (injected from the same wall) to form a thin plane jet and jet-induced entrainment of some fraction of the primary gas into the jets. However, unlike our previous models^{2,3} the present model does not deal with the form and trajectory of the I_2/N_2 jets. Instead, just as in⁴ and⁶, an approach based on description of the injection and penetration processes by parallel streams is used. It is assumed that after the jets' bending is completed the two parallel streams are formed in the critical cross section of the nozzle, the O_2 primary stream and the mixed stream containing the entire I_2/N_2 secondary flow and fraction α_p of the primary flow instantly mixed with the secondary flow (see Fig. 2). In what follows this initial stage of mixing will be referred to as "premixing". Then the streams undergo supersonic expansion accompanied by chemical reactions in the mixed stream and gradual entrainment of the primary flow into the mixed stream (due to diffusion process). This process continues towards the optical resonator where the fraction of the primary flow entrained into the secondary stream due to diffusion process is indicated as β_p . The total mixing at the optical

axis is defined as the sum of α_p and β_p , determined below using the experimentally measured gain spatial profile across the flow. The model is divided into two main parts:

1. The first part of the model calculates the initial conditions in the primary and mixed streams at the critical cross section of the flow. The primary stream parameters before mixing with the secondary stream are equal to the critical flow parameters for Mach number equal to unity, the critical pressure of the primary flow being calculated from the measured stagnation pressure in the subsonic part of the flow. The stagnation pressure of the secondary flow before injection holes is found from the given flow rates of the iodine, nI_2 , nitrogen, nN_2 , and the stagnation temperature T_{s0} of the secondary flow, taking into account the injection holes discharge coefficient, $C_N \sim 0.7 - 0.8$ ¹⁸. The expansion of the jets is assumed to be adiabatic, but non-isentropic due to shock waves and viscosity. Due to irreversible effects, the stagnation pressure drops whereas the stagnation temperature remains unchanged for an adiabatic flow, the stagnation pressure losses PO_{L1} being 0.75- 0.9¹⁸. The exact value of PO_{L1} in this range has a very small effect on the calculated values of the gain and temperature. Parameters of the secondary stream before the “premixing” (temperature, velocity and cross section) are found from the given secondary flow rates, nI_2 and nN_2 , and the stagnation pressure (corrected by the loss factor PO_{L1}) and temperature of the secondary flow assuming equal static pressures in the primary and secondary streams. The secondary stream before the “premixing” is, as mentioned above, assumed to be parallel to the primary stream.

Flow parameters of the primary and mixed streams just after the “premixing” (see Fig. 1) are found from mass, momentum and energy conservation conditions assuming that the static pressure after premixing is equal to that before the “premixing”. The constant static pressure approximation during “premixing” is inaccurate since the pressure in the supersonic expansion changes rapidly away from the sonic line at the nozzle throat. However, this approximation has a very small effect on the calculations of the gain and temperature in the supersonic section of the flow because most of the chemical reactions start downstream of the throat.

2. In the second part of the model the mass flow rates $\omega_{m(p)}(Z)$ of species Z , the temperature $T_{m(p)}$ and the velocity $U_{m(p)}$ (the sub indexes “m” and “p” indicate mixed and primary streams, respectively) are calculated by solving the conservation differential equations, considering the supersonic expansion of the primary and mixed streams, the entrainment of the primary gas into the mixed layer and the chemical reactions occurring in the mixed layer. The final conditions of the primary and mixed streams after the “premixing”, as calculated in the first part of the model, serve as the initial conditions for the differential equations. In order to calculate the dynamical and chemical conditions at every point until the optical resonator, we assume a spatial dependence of the pressure along the flow. This dependence is based on the pressures measured at three points in the supersonic section of the flow and the critical pressure, calculated by the first part of the model. We assume the pressure to change linearly between successive points. In order to take into account non isentropic effects during the expansion in the slit nozzle (shock waves and boundary layers) we assumed that, just as for the jet expansion described in the first part of the model, the stagnation pressure in both the primary and secondary streams drops in the diverging section of the nozzle (from our calculations an exact position of the pressure drop location has a negligibly small effect on the calculated parameters). Like the loss factor PO_{L1} , the stagnation pressure loss factor PO_{L2} is 0.75- 0.9. It should be noted that with $PO_{L1(2)}$ equal to unity the calculated values of T_{mc} are smaller than the measured temperatures.

The above-mentioned first-order differential equations are solved numerically using “ode15s” Matlab computer program for stiff differential equations with relative error tolerance of 10^{-3} . The output of the program contains the values of the specific densities, temperature (T_m) and the flow parameters along the flow. The gain g and iodine dissociation fraction F are given by¹⁹

$$g = \frac{7}{12} \sigma ([I(^2P_{1/2})]_m - 0.5[I(^2P_{3/2})]_m), \quad (2)$$

and

$$F = 1 - \omega_m(I_2) / \omega_{m0}(I_2), \quad (3)$$

respectively, where $\sigma = 1.29 \times 10^{-17} (300/T_m)^{1/2} \text{ cm}^2$ is the stimulated emission cross section for the strongest transition $F = 3 \rightarrow F = 4$ between the hyperfine sublevels of the iodine atom and $\omega_{m0}(I_2)$ is the initial mass flow rate of I_2 before injection. Since the pressures at the optical axis are smaller than 2 Torr, Doppler approximation for the gain profile is used in Eq. (2). Running the program with different values of the input parameters gives the dependence of the gain, temperature and iodine dissociation fraction on these parameters.

2.2 Chemical reaction schemes

The model uses two different sets of chemical reactions suggested in ^{16, 17}. The first set of reactions is based on the mechanism of iodine dissociation suggested by Heidner et al. ¹⁶. This set of reactions was adopted in the standard kinetics package ^{20, 21} which is used for most computational simulations of COIL devices. Heidner's mechanism assumes that vibrationally excited $I_2(X)$ is the immediate precursor to atomic iodine in COIL systems and hence that the dissociation is a two step process requiring at least two $O_2(^1\Delta)$ molecules to dissociate one I_2 .

Recent kinetic measurements and modeling studies carried out by Heaven et al. ¹⁷ indicate that these assumptions are invalid, and that electronically excited $I_2(A')$ is the I atom precursor. Heaven et al. ¹⁷ suggested a new model of iodine dissociation where both $I_2(A')$ and vibrationally excited $I_2(X)$ are significant dissociation intermediates. This model requires at least three $O_2(^1\Delta)$ molecules to dissociate one I_2 . The second set of reactions used in our calculations is based on Heaven's mechanism of iodine dissociation.

3. CALCULATED RESULTS AND COMPARISON WITH EXPERIMENTAL MEASUREMENTS

3.1 Input parameters of the model

The input parameters of the model were measured in the experiment described in ¹⁴. Those parameters are the flow rates of the different species of primary and secondary flows, the temperature and pressure of both flows in the subsonic part and the pressure at three different points downstream of the supersonic nozzle exit plane. The cross-sections of the primary flow in the subsonic part (5 cm^2) and of the secondary flow in the sonic part (0.2 cm^2 and 0.34 cm^2 for transonic injectors No. 1 and 2, respectively, described in detail in ¹⁴), are fixed parameters.

There are three unknown parameters (explained in section 2.1) of the model: (1) the mixing parameter, α_p , or the total mixing efficiency $\eta_{mix} = \alpha_p + \beta_p$, (2) the losses in stagnation pressure of the secondary flow when injected into the primary flow, $P0_{L1}$, and (3) the losses in stagnation pressure of the flows during the supersonic expansion, $P0_{L2}$. The values of $P0_{L1}$ and $P0_{L2}$ are established in the following way: (a) the temperature of the gas mixture at the optical axis in the "cold runs", i. e., in the absence of iodine flow, is found by extrapolating the measured temperatures to nI_2 corresponding to zero gain as described in ¹⁴; (b) then, values for $P0_{L1}$ and $P0_{L2}$ are selected by which the calculated temperature of the mixed flow at the optical axis, for zero nI_2 , is equal to the extrapolated temperature. The previous procedure is based on the assumption that the iodine flow rate, which is very small compared to the total flow rate, does not affect the flow dynamics but has a strong effect on the chemical kinetics and hence the pressure losses for any nI_2 are the same as in the "cold runs". The parameter α_p is chosen to give the best fit to the experimental results. In section 3.3 we estimate the parameter α_p from experimental measurements of the gain spatial profile across the flow and compare it to the result obtained for α_p from the model. The input parameters of the model are shown in Table 1.

3.2 Comparison of calculated and experimental results

Figs. 3 and 4 show calculated dependencies of g , T_m and F on nI_2 for Heidner's and Heaven's mechanisms of iodine dissociation, respectively, for run 1 (Table 1) with $nCl_2 = 20$ mmole/s and the first position of the optical axis located 5 cm downstream of the injection point. The same figures show experimental dependencies of g and T_m on nI_2 obtained in ¹⁴. It should be mentioned that F is not measured during the experiment and therefore only the calculated results for F are presented. It is seen (Fig. 3) that a good agreement is obtained between the calculated and experimental results for the dissociation mechanism of Heidner. For the model including the dissociation mechanism of Heaven (Fig. 4) the gain obtained is much smaller than that measured in the same run. The reason for that is that the calculated values of F for Heaven's model are much smaller than for Heidner's model, e. g., for $nI_2 = 0.33$ mmole/s, corresponding to the maximum measured gain, the values of F are 0.4 and 0.76, for these models, respectively. Calculations show that good fit between the experimental and calculated results for Heaven's dissociation mechanism could not be obtained for other values (between 0 and 1) of the unknown input parameters of the model. In the remainder of this section we will use only the model which includes Heidner's mechanism.

In Fig. 3 the dashed lines are the gain and temperature calculated for large diffusion and as can be seen there is only a slight difference from the results calculated for small diffusion, the total mixing efficiency η_{mix} being the same for both cases. Therefore, from now on we will restrict ourselves to the case of small diffusion, which gives a slightly better fit.

Fig. 5 shows the gain and temperature as calculated for the second position of the optical axis, 9 cm downstream of the injection point, for the same conditions as in Figs. 3 and 4. As there are no sufficient experimental results for these conditions, only the calculated results are shown. Comparison between Fig. 5 and 3 shows that the gain decreases as the optical axis is moved downstream from the first position and the temperatures increase due to higher losses. This trend is also observed experimentally in ¹⁴.

Figs. 6 and 7 show that there is a good agreement between the calculated and experimental results for smaller values of nCl_2 (runs 2 and 3, Table 1). Fig. 8 shows the calculated and experimental results for an opened leak downstream of the cavity. As explained in ¹⁵, opening of the leak results in smaller pumping rate and Mach number in the cavity. It should be noted that to reach an agreement between the calculated and measured values of the gain we assumed (see Table 1) that the mixing efficiency η_{mix} for opened leak (~ 0.8) is larger than for closed leak (~ 0.5). This assumption is in good agreement with both estimates of η_{mix} using experimental measurements of the gain spatial profile across the flow presented below in section 3.3 and the conclusions of Ref. 14. The reason for larger mixing for opened leak is that the Mach number is smaller in this case, resulting in a larger time for mixing. It is worth noting that the values of the static pressure for opened leak are about 1.5 times larger than for closed leak due to higher back pressure introduced by the leak. Measurements of the pressure in the supersonic section of the flow show that the pressure decreases monotonically along the flow which means that there are no jumps in pressure caused by strong shock waves and only weak oblique shock waves may be present in the flow. These shock waves are therefore not taken into account in our one-dimensional model. Comparison between Fig. 8 and 3, 6 and 7 shows that the values of T_m and F for opened leak are higher than for closed leak, which is due to longer residence time of the flow between the injection point and the optical axis.

3.3 Estimate of the mixing parameter

To estimate the value of η_{mix} , experiments were carried out where the gain was measured as a function of the height y perpendicular to the direction of flow ¹⁵. Fig. 9 shows the dependencies $g(y)$ for the cases of closed and opened leak and the same flow conditions as in runs 1 and 4 (Table 1), respectively. It is seen that for the opened leak the gain is distributed more homogeneously along y than for closed leak.

η_{mix} can be defined as

$$\eta_{mix} \equiv \frac{\int_0^H g \cdot dy}{g_{max} H}, \quad (4)$$

where H is the height of the flow duct and g_{max} is the maximum value of the gain. Expression (4) does not take into account that the gain decreases near the walls not only because of the incomplete mixing but also due to increase in the gas temperature as a result of the heat transfer from the walls and wall deactivation of I^* . The later two processes occur in the thin boundary layers near the walls, hence Eq. (4) is a good approximation for η_{mix} ¹⁵. The values of η_{mix} estimated using Eq. (4) are 0.46 and 0.73 for closed and opened leak, respectively. These values are in excellent agreement with the values of η_{mix} used in the model, 0.48 (run 1) and 0.76 (run 4) for closed and opened leak, respectively.

4. SUMMARY

We tested the one-dimensional model presented in this paper against the performance of the COIL device in our laboratory. The celebrated Heidner's mechanism of iodine dissociation gives good agreement between the experimental and calculated results. The gain calculated using the newly suggested Heaven's dissociation mechanism is much lower than measured experimentally. It is shown that the rate of I_2 dissociation for Heaven's mechanism is smaller than that calculated using Heidner's mechanism. A possible reason is that the rate constants for Heaven's mechanism, obtained in¹⁷ by fitting the calculated to the experimentally measured times of iodine dissociation, are not accurate enough. It is worth noting that the set of rate constants given in¹⁷ are suggested to model the flow tube results of Heidner et al.¹⁶. This set, as noted in¹⁷, is not unique and may not model conditions of experiments with the supersonic COIL, lying outside the range of the data for which it was derived. Although good results are obtained for Heidner's mechanism, it suffers from inconsistencies, as discussed in¹⁷. It is very important therefore to measure experimentally the iodine dissociation fraction in order to decide which dissociation mechanism is closer to reality. But this is not an easy task as the absorption of I_2 molecules in the supersonic portion of the flow is very small, in particular when the gain length is short, as in our laser (5 cm).

The agreement obtained between the measured and calculated results over a wide range of the flow parameters is surprisingly good. Other predictions of the model (larger mixing efficiency and higher temperature with a leak opened downstream of the resonator and gain decrease along the flow) are also in agreement with the experimental observations.

REFERENCES

1. W. E. McDermott, N. R. Pchelkin, D. J. Benard and R. R. Bousek, "An electronic transition chemical laser," *Appl. Phys. Lett.*, vol. 32, pp. 469-470, 1978.
2. B. D. Barmashenko, A. Elior, E. Lebiush and S. Rosenwaks, "Modeling of mixing in chemical oxygen-iodine lasers: Analytic and numerical solutions and comparison with experiments," *J. Appl. Phys.*, vol. 75, pp. 7653-7655, 1994.
3. A. Elior, B. D. Barmashenko, E. Lebiush, and S. Rosenwaks, "Experiment and modeling of a small-scale, supersonic chemical oxygen-iodine laser," *Appl. Phys. B*, vol 61, pp. 37 - 47, 1995.
4. D. L. Carroll, "Modeling high-pressure chemical oxygen-iodine lasers," *AIAA Journal*, vol. 33, pp. 1454-1462, 1995.
5. B. D. Barmashenko and S. Rosenwaks, "Power dependence of chemical oxygen-iodine lasers on iodine dissociation," *AIAA J.*, vol. 34, pp. 2569-2574, 1996.
6. T. T. Yang, D. A. Copeland, A. H. Bauer, V. Quan, W. E. McDermott, R. A. Cover, D. M. Smith, "Chemical Oxygen-Iodine Laser Performance Modeling," in *AIAA 28th Plasmadynamics and Lasers Conf.*, Atlanta, GA, June 23-25, 1997, paper 97-2384.

7. E. Lebiush, B. D. Barmashenko, A. Elior and S. Rosenwaks, "Parametric study of the gain in a small scale, grid nozzle supersonic chemical oxygen-iodine laser," *IEEE J. Quantum Electronics*, vol.31, pp. 903-909, 1995.
8. C. A. Helms, J. Shaw, G. D. Hager and K. A. Truesdell, "Iodine dissociation in COILs," *SPIE*, vol. 2502, pp. 250 – 257, 1996.
9. R. F. Tate, B. S. Hunt, C. A. Helms, K. A. Truesdell and G. D. Hager, "Spatial gain measurements in a chemical oxygen iodine laser (COIL)," *IEEE J. Quantum Electronics*, vol.31, pp. 1632 - 1636, 1995.
10. T. G. Madden, W. C. Solomon, "A detailed comparison of a computational fluid dynamic simulation and a laboratory experiment for a COIL laser" in *AIAA 28th Plasmadynamics and Lasers Conf.*, Atlanta, GA, June 23-25, 1997, paper 97-2387.
11. T. G. Madden, G. D. Hager, A. I. Lampson and P. G. Crowell, "An investigation of supersonic mixing mechanism for the chemical oxygen-iodine laser (COIL)," in *AIAA 30th Plasmadynamics and Lasers Conf.*, Norfolk, VA, June 28- July 1, 1999, paper 99-3429.
12. W. Masuda, M. Hishida and N. Azami, "Mixing/reacting zone structure and small signal gain coefficient of a supersonic flow chemical oxygen-iodine laser," *SPIE*, vol. 3092, pp. 573 – 576, 1997.
13. M. Suzuki, T. Suzuki and W. Masuda, "Numerical simulation of throat-mixing system for supersonic flow chemical oxygen-iodine laser," *SPIE*, vol. 4184, pp. 99 – 102, 2001.
14. D. Furman, E. Bruins, V. Rybalkin, B. D. Barmashenko and S. Rosenwaks, "Parametric study of small signal gain in a slit nozzle, supersonic chemical oxygen - iodine laser operating without primary buffer gas," *IEEE J. Quantum Electronics*, vol. 37, pp. 174-182, 2001.
15. S. Rosenwaks, V. Rybalkin, E. Bruins, D. Furman, B. D. Barmashenko and A. Katz, "Spatial Distribution of the Gain and Temperature across the Flow in a Slit Nozzle Supersonic COIL with Different Schemes of Iodine Injection," presented at the COIL R&D Workshop Prague 2001, Prague, Czech Republic, 2001.
16. R. F. Heidner III, C. E. Gardner, G. I. Segal, , T. M. El-Sayed, "Chain reaction mechanism for I_2 dissociation in the $O_2(^1\Delta)$ -I atom laser," *Journal of Physical Chemistry*, vol. 87, pp. 2348-2360, 1983.
17. A. V. Kommissarov, V. Goncharov and M. C. Heaven, "Chemical oxygen iodine laser (COIL) kinetics and mechanisms," *SPIE*, vol. 4184, pp. 7 – 12, 2001.
18. A. H. Shapiro, *The Dynamics and Thermodynamics of Compressible Fluid Flow*. New York: Ronald, 1953, vol. 1, pp. 73-110.
19. N. N. Yuryshev, "Chemically pumped oxygen-iodine laser," *Quantum Electronics*, vol. 23, pp. 583 - 600, 1996.
20. G. P. Perram, "Approximate analytic solution for the dissociation of molecular iodine in the presence of singlet oxygen," *Int. J. Chem. Kinet.*, vol. 27, pp. 817-828, 1995.
21. G. P. Perram and G. D. Hager, "The standard chemical oxygen-iodine laser kinetics package," U. S. Air Force Weapons Lab., AFWL-TR-88-50, Kirtland AFB, NM, Oct. 1988.

Table 1. Input parameters of the model for different runs. The values are taken from the measurements of Ref. 14, except $P_{0,L1}$, $P_{0,L2}$ and η_{mix} which are fitting parameters

Run No. (Fig. No)	Nozzle type	nCl_2 [mmole/s]	nN_2 [mmole/s]	Leak	p_{sub}^* , [Torr]	p_{res}^* , [Torr]	Y	$P_{0,L1}$	$P_{0,L2}$	η_{mix}
1(3)	No. 2	20.1	8.7	closed	16.9	1.4	0.52	0.75	0.75	0.48
2(6)	No. 2	15.1	7.1	closed	12.7	1.1	0.56	0.75	0.85	0.51
3(7)	No. 2	11.8	5.1	closed	8.5	1	0.6	0.9	0.9	0.6
4(8)	No.1	11.7	3	opened	8.7	1.4	0.5	0.75	0.75	0.76

*Pressure measured in the subsonic section of the flow.

** Pressure measured at the optical axis of the resonator.

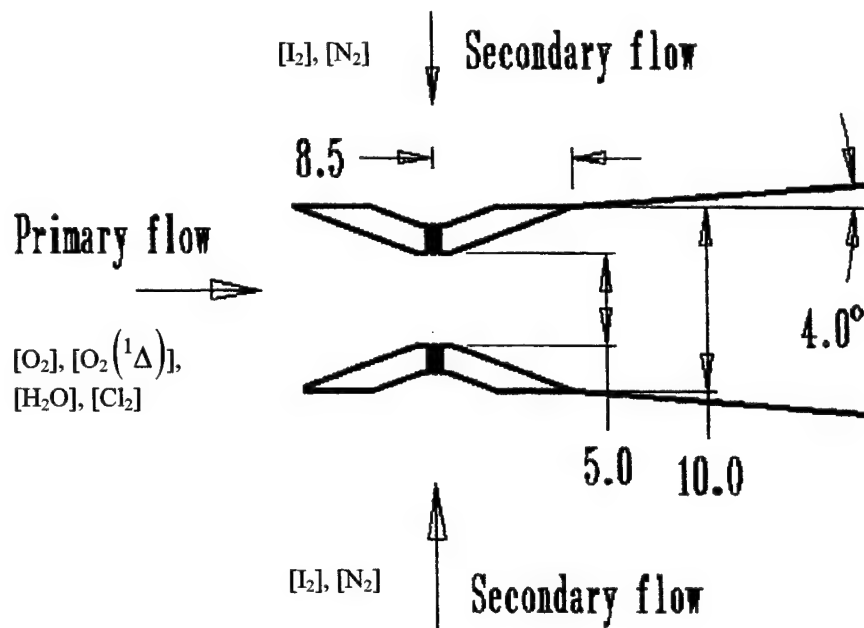


Fig. 1 Schematic of the supersonic nozzle with transonic injection of I₂ (measures are in millimeters).

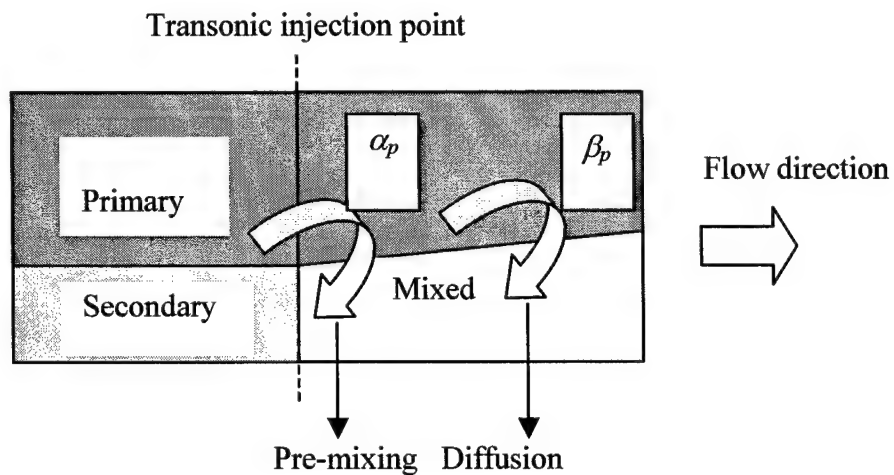


Fig. 2 Schematic of the mixing concept in the model. α_p is the fraction of the primary flow “premixed” with the secondary flow; β_p is the fraction of the primary flow at the optical axis obtained due to gradual mixing with the secondary flow during the supersonic expansion.

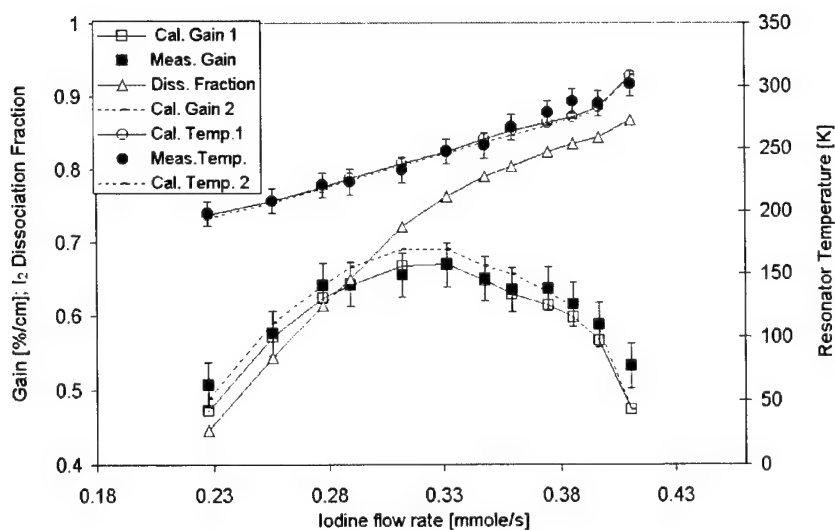


Fig. 3 Calculated (using Heidner's model) and measured gain g , temperature T_m and iodine dissociation fraction F at the first position of the cavity optical axis (5 cm downstream of the injection point) as a function of the iodine flow rate. The chlorine and secondary nitrogen flow rates are 11.7 and 8.7 mmole/s, respectively, the leak downstream of the cavity is closed (run No. 1, Table 1). Calculated gains and temperatures indicated by 1 (solid line) and 2 (dashed line) correspond to the slow and fast diffusion, respectively, the total mixing efficiency η_{mix} being the same for both cases.

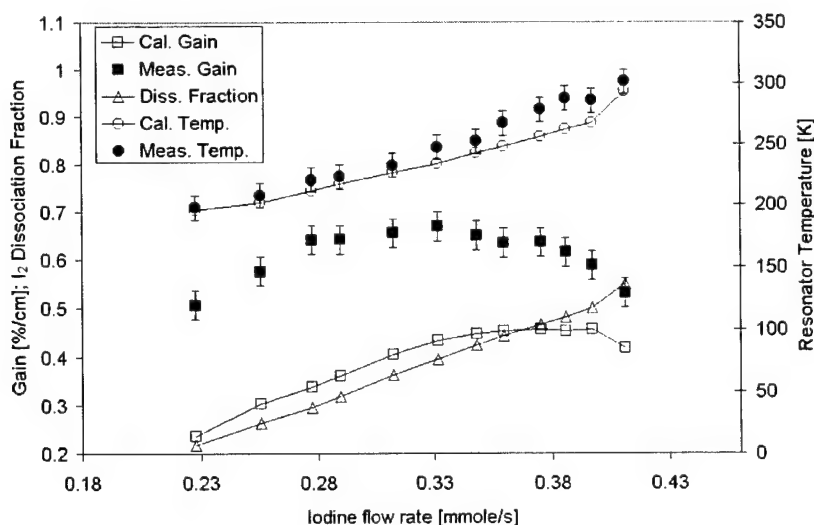


Fig. 4 Calculated (using Heaven's model) and measured gain g , temperature T_m and iodine dissociation fraction F for the same conditions as in Fig. 3 (run No. 1, Table 1)

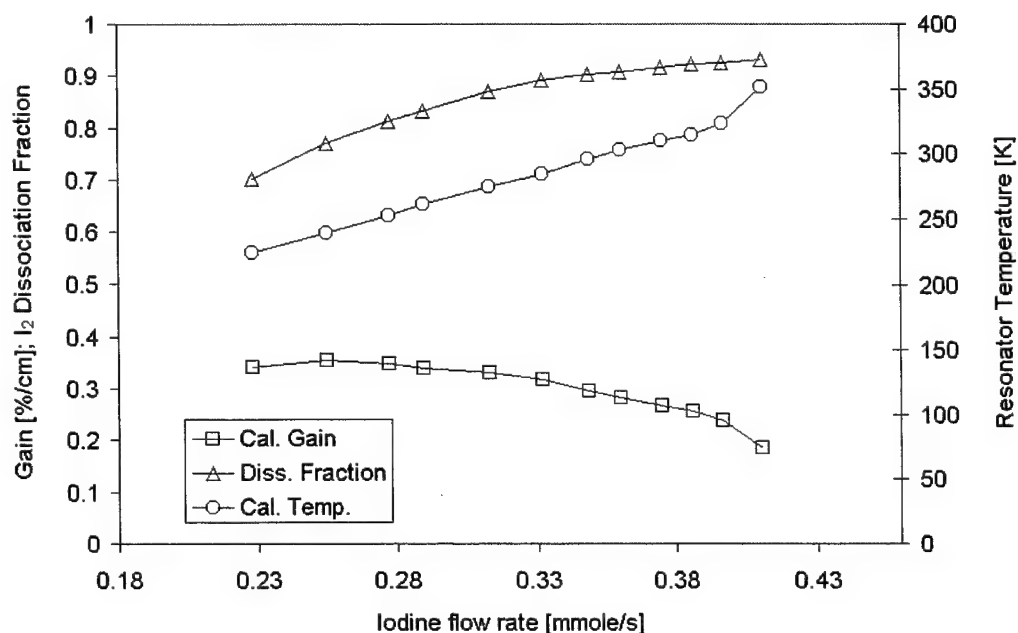


Fig. 5 Calculated (using Heidner's model) gain g , temperature T_m and iodine dissociation fraction F at the second position of the cavity optical axis (9 cm downstream of the injection point) for the same conditions as in Fig. 3 (run No. 1, Table 1)

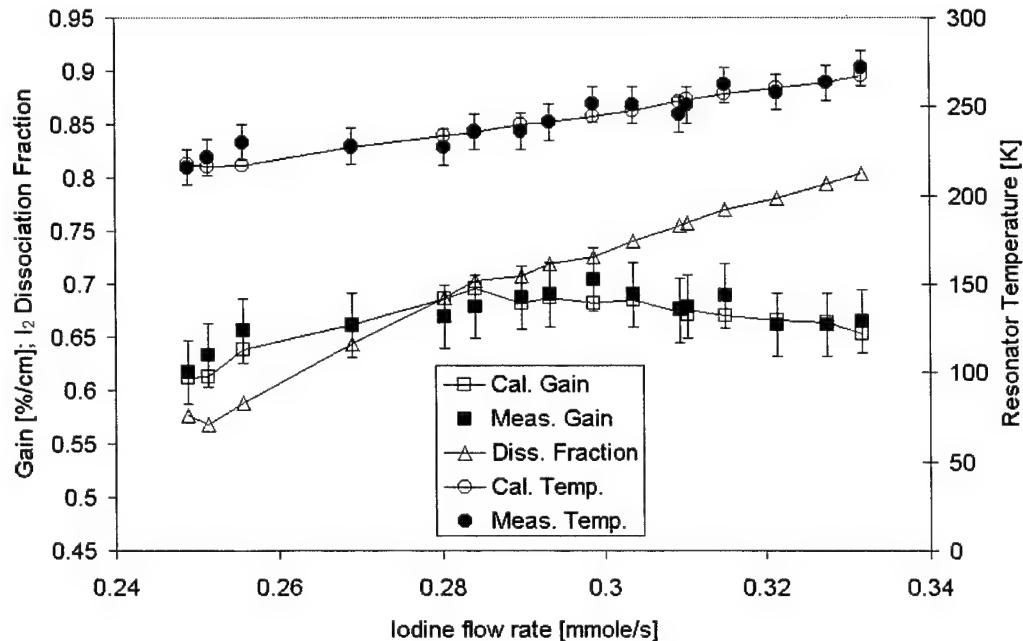


Fig. 6 Calculated (using Heidner's model) and measured gain g , temperature T_m and iodine dissociation fraction F at the first position of the cavity optical axis (5 cm downstream of the injection point) as a function of the iodine flow rate. The chlorine and secondary nitrogen flow rates are 15.1 and 7.1 mmole/s, respectively, the leak downstream of the cavity is closed (run No. 2, Table 1)

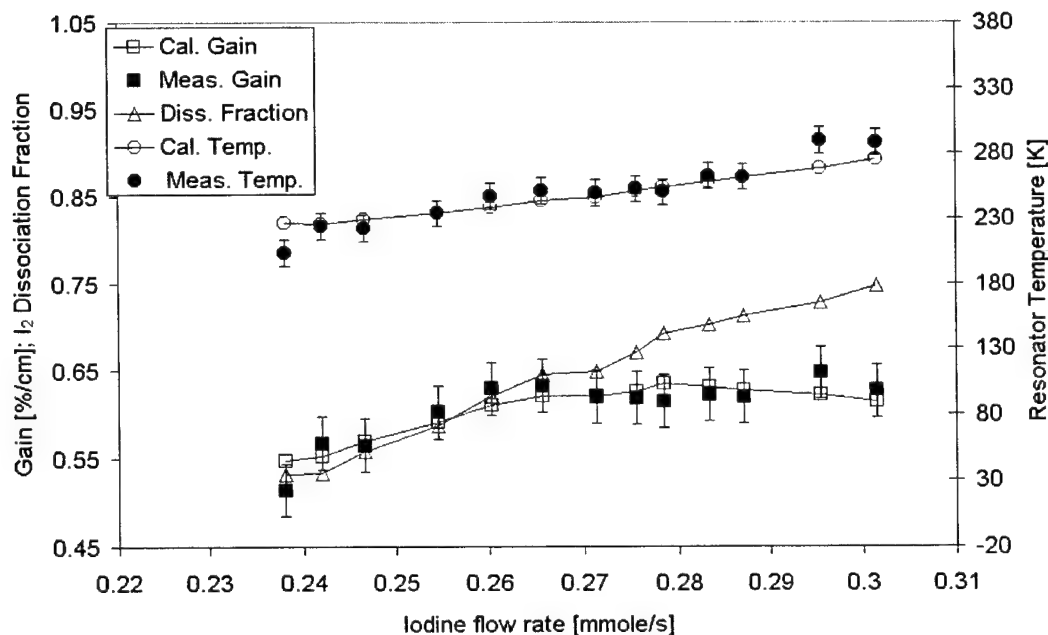


Fig. 7 Calculated (using Heidner's model) and measured gain g , temperature T_m and iodine dissociation fraction F at the first position of the cavity optical axis (5 cm downstream of the injection point) as a function of the iodine flow rate. The chlorine and secondary nitrogen flow rates are 11.8 and 5.1 mmole/s, respectively, the leak downstream of the cavity is closed (run No. 3, Table 1)

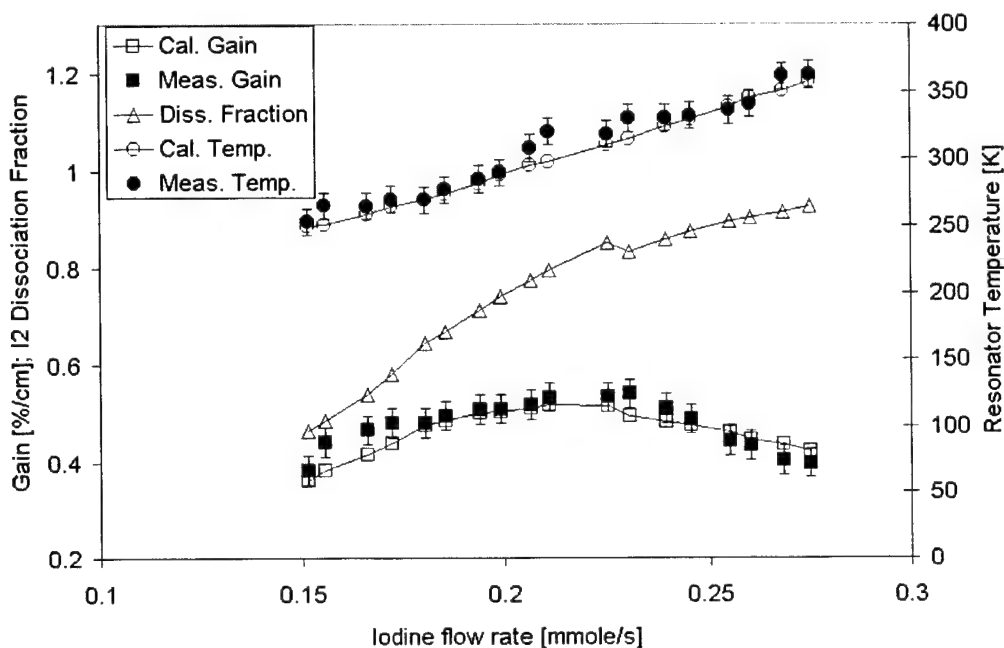


Fig. 8 Calculated (using Heidner's model) and measured gain g , temperature T_m and iodine dissociation fraction F at the first position of the cavity optical axis (5 cm downstream of the injection point) as a function of the iodine flow rate. The chlorine and secondary nitrogen flow rates are 11.7 and 3 mmole/s, respectively, the leak downstream of the cavity is opened (run No. 4, Table 1).

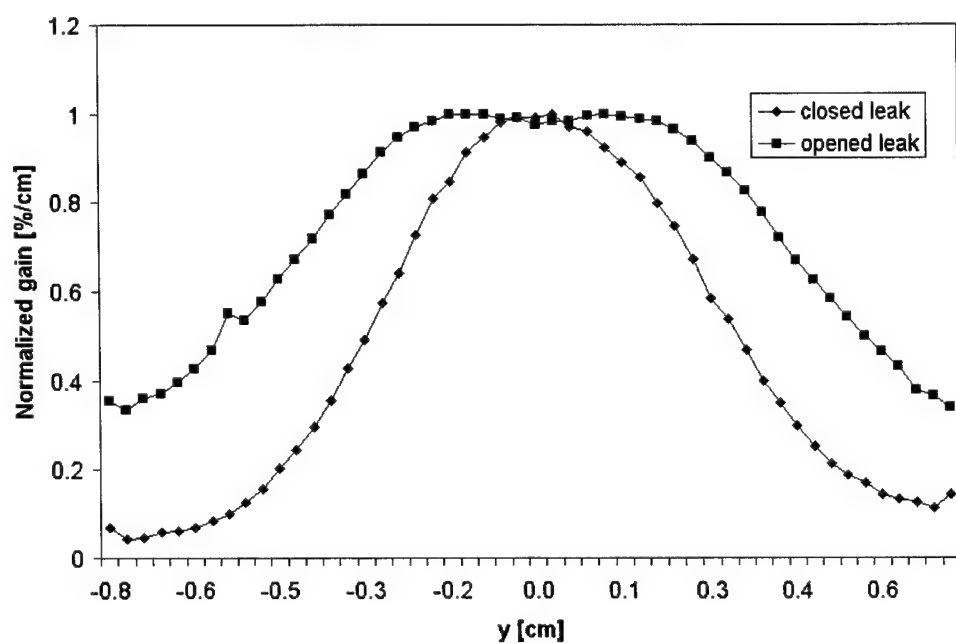


Fig. 9 Measured gain distribution in the y direction across the flow for closed and opened leak.

A contribution of COIL Laboratory in Prague to the Chemical Oxygen-Iodine Laser research and development

Jarmila Kodymová* and Otomar Špalek
Department of Gas Lasers, Institute of Physics of Academy of Sciences
Prague, Czech Republic

ABSTRACT

The key results gathered in the COIL Laboratory of the Institute of Physics AS in the Czech Republic since 1985 to date on the experimental and theoretical investigation of Chemical Oxygen-Iodine Laser (COIL), and related problems are reviewed in a certain context of historical perspective of the COIL research and development.

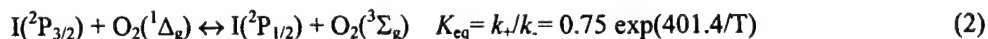
Keywords: chemical lasers, oxygen-iodine laser, singlet oxygen, atomic iodine

1. INTRODUCTION

Laser emission at 1.315 μm from magnetic-dipole transition between spin-orbit levels of the ground state configuration of iodine atom



was first observed during flash photolysis of alkyl iodides, and since its discovery by Kasper and Pimentel¹ in 1964, the iodine photodissociation laser has been developed into systems capable of very high energies. The Prague Asterix Laser System (PALS) is currently one of the largest such facilities in the world, delivering on the target a focused power density up to 10^{16} W/cm^2 in 400 ps (at the fundamental wavelength).² Lasing mechanism of the Chemical Oxygen-Iodine Laser (COIL) follows the same physical principle, only the $^2P_{1/2}$ upper level is pumped via the energy of singlet delta state of molecular oxygen, $\text{O}_2(^1\Delta_g)$. Unique physical and chemical properties of this metastable species³ that is able to transfer its energy to iodine atom in a near-resonant process, and can be generated chemically with very high efficiency have brought about the exceptional position of COIL among other chemical lasers. The pumping mechanism discovered by Derwent *et al.*⁴ in the seventies, is represented by the reverse reaction process with temperature dependent equilibrium constant



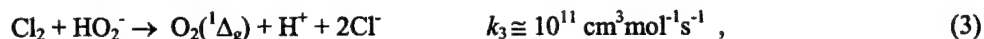
Twenty-five years have passed in 2002 since McDermott and his colleagues⁵ from the Air Force Weapons Laboratory (the Air Force Research Laboratory nowadays) demonstrated the first COIL generation on the milliwatt level. A multihundred-kilowatt version of the COIL facility has been developed and tested for the Airborne Laser program⁶ since that time. In the meantime, a tremendous theoretical and experimental work has been devoted to understand comprehensively this laser system to bring it to the present technological level. The Prague laboratory joined this investigation in 1985. Theoretical and experimental efforts have been focused on partial problems in the COIL operation that have concerned, for example, the $\text{O}_2(^1\Delta_g)$ generation for both subsonic and supersonic COIL, the chemical generation of atomic iodine for a COIL, laser performance characteristics in CW and pulsed regime, etc. A brief cross-section through results of this investigation is presented below.

* Correspondence: Na Slovance 2, 182 21 Prague 8, Czech Republic
Email: kodym@fzu.cz; Tel.: +420 2 66052699; Fax: +420 2 86890527

2. SINGLET OXYGEN GENERATION

2.1. Mechanism of $O_2(^1\Delta_g)$ loss in a low-pressure chemical generator

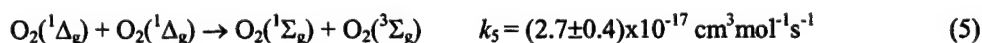
The 25th commemorative COIL session permits mentioning the interesting result following from our "pioneer" work done on the $O_2(^1\Delta_g)$ generation by the reaction⁷



and the mechanism of $O_2(^1\Delta)$ loss in a low-pressure bubbler-type (sparger) generators⁸⁻¹⁰ employed for driving the COIL in subsonic flow regime. The $O_2(^1\Delta_g)$ formed in the liquid film surrounding the bubbled chlorine through the BHP has to diffuse into the gas bubble during the time that the bubble is moving up through the head of liquid (basic solution of hydrogen peroxide, BHP). The gas pressure (consisting of reacting chlorine and formed singlet oxygen) within the two-phase (g-l) bubbling mixture in the reactor column is substantially increased due to a hydrostatic pressure of the liquid column than in the gas space above the liquid head. For example, if the O_2 pressure in the generator plenum is 1 Torr, then the 8 cm liquid head provides the hydrostatic pressure of 8 Torr on gas bubbles at the reactor bottom. By this effect, the loss of $O_2(^1\Delta_g)$ in gas bubbles at the bottom is 64 times higher. A mathematical model for estimation of these loss-processes in sparger-type generators was developed considering a variation in the volumetric fraction of gas in g-l mixture with a distance from reactor bottom, as well as the effect of water vapour pressure in gas bubbles on the $O_2(^1\Delta_g)$ loss.⁹ This simplified model is based on the mass balance for $O_2(^1\Delta_g)$ over a differential layer dy of the g-l mixture following from the relation

$$-N_A n d\eta = r_4 \beta S dy \quad (4)$$

N_A - the Avogadro constant, n - molar flow rate of chlorine or oxygen, η - $O_2(^1\Delta_g)$ yield from layer dy (y - vertical coordinate specifying the distance from reactor bottom), S - reactor cross section, r_4 - rate constant of reaction (5).¹¹



The β factor is the volumetric fraction of gas in the g-l mixture evaluated from the height of two-phase (foamy) mixture (h) and a liquid height without gas in the reactor (h_0), $\beta = 1 - h_0/h$. There are two main $O_2(^1\Delta_g)$ deactivation processes in these generators. First, the $O_2(^1\Delta_g)$ in the bubble diffuses back to the liquid surrounding it, is attached and deactivated. Secondly, a deactivation/pooling $O_2(^1\Delta_g)$ self-quenching process occurs in the gas phase (bubble) itself by the reaction (5). This process is pressure dependent (quadratic in $O_2(^1\Delta_g)$ concentration), and consequently strongly accelerated within g-l mixture due to the hydrostatic pressure of liquid (in the above given example, by two orders of magnitude). Contrariwise, if the bubble residence time in BHP is too short, not all Cl_2 is converted into $O_2(^1\Delta_g)$ and generator yield is also low. The results of this research are remembered in Fig. 1.

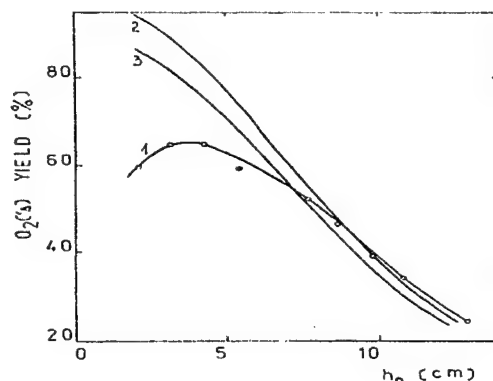


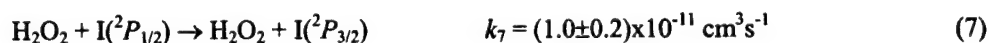
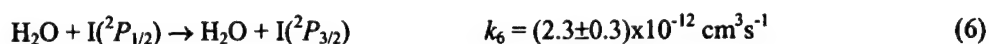
Fig. 1. $O_2(^1\Delta_g)$ yield as a function of BHP height in reactor. 1 - experimental curve, 2 - calculated curve including $O_2(^1\Delta)$ loss by reaction (5), 3 - calculated curve including another $O_2(^1\Delta)$ losses (in liquid phase, quenching on reactor wall, transport in duct)

It is evident that this type of singlet oxygen generator can operate at moderate/low pressure, and only way to achieve high mass flow is to increase the generator surface area resulting in a larger O₂ collection plenum. This finding was afterwards considered in designs of sparer-type generators.

2.2. Generation of O₂(¹Δ_g) in a high-pressure jet SOG

Development of the supersonic COIL during early ninetieth called for a high-pressure O₂(¹Δ_g) generators. We concentrated on the investigation of the jet-type SOG that was set up first in the Samara COIL laboratory.¹² A large surface area of liquid in the form of liquid jets for performing the reaction (3) allowed a substantial reduction of the generator volume (dimensions), and consequently the O₂(¹Δ_g) loss in the gas phase. Velocity of liquid jets is very high (5-20 m/s), which ensures a fast renovation of the gas-liquid boundary, and so minimizes HO₂⁻ ions depletion from the surface layer. It contributes to lowering the O₂(¹Δ_g) loss also in the liquid phase. Our effort in the investigation of this generator was focused on some problems in operation of this generator.¹³⁻¹⁶ Experimental results obtained on the small-scale pilot device concerned, for example, the influence of different configurations and diameters of holes (0.3, 0.5, and 0.8 mm) in the BHP injector on the jets stability, and a detailed investigation of water vapour estimation in gas exiting the generator. We searched for conditions, at which the water vapour content was minimized.

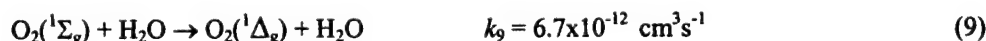
Water formed during O₂(¹Δ_g) generation causes together with peroxide vapor a significant problem in the COIL operation because it quenches the excited state of atomic iodine in very fast processes¹⁷



In a supersonic laser, water can cause also undesirable fluid-dynamic effects due to its condensation during the gas expansion cooling.¹⁸ Water vapor concentration in gas was estimated by the relation (8) derived from the mass balance of O₂(¹Σ_g) state.¹⁹

$$c_{\text{H}_2\text{O}} = k_4 c_{\Delta}^2 / k_9 c_{\Sigma} \quad (8)$$

This species is formed in the pooling reaction (5), and is very efficiently quenched by water molecule.²⁰



Water partial pressure was evaluated from the emissions of O₂(¹Σ_g) and O₂(¹Δ_g) states for different BHP composition, BHP jets temperature, varying Cl₂ flow rate, and different BHP injector configurations. The experimentally obtained data were compared with calculated values of the saturated water vapour pressure above the BHP (for given BHP compositions and temperatures). The both values were nearly the same. The relative water vapour content was well decreasing on increasing the generator pressure. It was the experimental proof that employing the high-pressure jet SOG in the COIL operation reduces a detrimental effect of water.

2.3. The Einstein coefficient for O₂(¹Δ_g) fundamental emission

Work on the development of high-pressure jet-type chemical generator of O₂(¹Δ_g) and the above-described parametric investigations, and simultaneously in the literature opened discussions on the right value of the Einstein coefficient for O₂(¹Δ_g) emission at 1.27 μm (*A*-coefficient) triggered our interest in verification of this coefficient. Mlynchak and Nesbit²¹ challenged the Badger *et al*'s²² value of 2.58 × 10⁻⁴ s⁻¹ when they reported a new value of 1.47 × 10⁻⁴ s⁻¹. The radiative lifetime of O₂(¹Δ_g), τ_Δ^{rad}, ~65 min (a half-lifetime ~45 min) considered so far in the COIL, increased to ~113 min. A detailed insight into this problem revealed that published values of the Einstein *A*-coefficient evaluated by means of various theoretical approaches and experimental techniques varied in a wide range resulting in τ_Δ^{rad} from ~53 to ~151 min.^{23,24} This fact could make the evaluation of O₂(¹Δ_g) concentration in COIL questionable.

To verify a rightness or faultiness of the *A*-value used so far, the way of employing two independent experimental techniques simultaneously was chosen.²⁵ The electron paramagnetic resonance (EPR) spectroscopy was one method, and the optical emission spectroscopy was the second one supplemented with the mathematical model developed for the

evaluation of $O_2(^1\Delta_g)$ concentration from the emission measurements. In this model, we assumed that $O_2(^1\Delta_g)$ molecules are distributed uniformly in the optical cell emitting photons in all directions with a rate, r ,

$$r = A_{\Delta} c_{\Delta}^{ES} = A_{\Delta} P_{\Delta} / RT \quad (10)$$

A_{Δ} - Einstein coefficient for spontaneous emission of $O_2(^1\Delta_g)$, P_{Δ} - $O_2(^1\Delta_g)$ partial pressure.

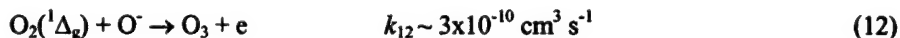
The $O_2(^1\Delta_g)$ concentration, c_{Δ}^{ES} , was evaluated from the measured signal of the fundamental emission at 1.27 μm and declared sensitivity of the photodiode, and the calculated ratio of the $O_2(^1\Delta_g)$ emission detected by the photodiode and the emission of all $O_2(^1\Delta_g)$ molecules present in the detection cell. The proposed mathematical model was used to evaluate this ratio, in which a photocurrent of the photodiode was directly proportional to a value of the Einstein A -coefficient substituted into relation (10).²⁵ A quantitative evaluation of the $O_2(^1\Delta_g)$ concentration by means of the EPR spectroscopy was based on the "double integral method" of EPR spectra processing by the relation²⁵

$$c_{\Delta}^{EPR} = k_{\Delta} \int_{-\infty-\infty}^{\infty} \int_{-\infty-\infty}^{\infty} y_{\Delta} \, dB \, dB \quad (11)$$

By comparison of the $O_2(^1\Delta_g)$ concentrations obtained contemporary by both experimental methods and supplemented by the mathematical model, a new value of the Einstein A -coefficient of $(2.24 \pm 0.4) \times 10^{-4} \text{ s}^{-1}$ was obtained. The corresponding $O_2(^1\Delta_g)$ radiative lifetime is $\sim 74 \text{ min}$. Shortly after our first reporting this result, Newman *et al.*²⁶ published the value of $(2.19 \pm 0.07) \times 10^{-4} \text{ s}^{-1}$ giving the $\tau_{\Delta}^{rad} \sim 76 \text{ min}$.

2.4. Generation of $O_2(^1\Delta_g)$ in a discharge plasma

The theoreticians of our department performed during the eightieth the fundamental investigation on the physical kinetics of high-frequency (hf) glow discharge in oxygen with respect to generation of the $a^1\Delta_g$ state for pumping the iodine laser.²⁷ Coming out from the properties of the electron gas described by solution of the Boltzmann equation for the electron distribution function, the $O_2(^1\Delta_g)$ concentration in the plasma was calculated with precondition that population of this electronic level is driven by electron collisions only. The upper concentration limit of $O_2(^1\Delta_g)$ achievable in this reaction system was evaluated from the statistical balance between the production and loss processes. The calculated relative population of $a^1\Delta_g$ state, X_{Δ}/N , is shown in Fig. 2 as a function of the hf field parameters E_{eff}/N and ω (E_{eff} - effective value of hf field, N - concentration of neutral molecules, ω - frequency). It can be seen that the yield of $O_2(^1\Delta_g)$ in hf discharge plasma in pure oxygen can hardly exceed 15% in the chosen range of parameters. Moreover, it is the maximum $O_2(^1\Delta_g)$ concentration that might be still reduced by collisions with negative ions present in the plasma, e.g.²⁷



Outside the region of active discharge, the relative $O_2(^1\Delta_g)$ concentration is even lower (only 3 to 10% in the pressure range of 1-10 Torr). According to this studies, the hf discharge unlikely might produce the $a^1\Delta_g$ state in the amount sufficient to sustain the operation of iodine laser pumped by the energy of such generated singlet oxygen. This conclusion was supported by a subsequently performed analysis by Swift²⁸ of the kinetic processes that accompany the $O_2(^1\Delta_g)$ generation in microwave discharge plasma in pressure range of 1-10 Torr. By these calculations, a maximum attainable relative concentration of $O_2(^1\Delta_g)$ was 10%.

A current experimental research on plasma discharge generation of $O_2(^1\Delta_g)$ for pumping the iodine laser (Discharge Oxygen-Iodine Laser, DOIL) is performed by our colleague J. Schmiedberger in his long-time co-operation with Japanese Institutes. The last results were obtained with the generation of radio-frequency plasma of O_2+N_2+NO mixture in the hollow electrode jet generator.²⁹ The generator is schematically shown in Fig. 3. The plasma jet was extra chilled reactively with transversely injected mixture of $Ar+NO_2$. Adding NO to oxygen enhanced the $O_2(^1\Delta_g)$ production up to 20% through the energy transfer from electronically excited state of NO molecule to O_2 . Another increase was achieved when NO_2 was injected into the reaction system, which caused via certain kinetic processes a lowering in a content of O

and O_3 species in the gas mixture. The $O_2(^1\Delta_g)$ with 32% yield was generated at pressure of 0.43 Torr. In combination of this rf plasma generator with a transversally injected molecular iodine, atomic iodine emission at 1.315 μm was detected at the laser output mirror by the spectrum analyser. This emission was recalculated to the output power of $\sim 3 \text{ nW}$.²⁹

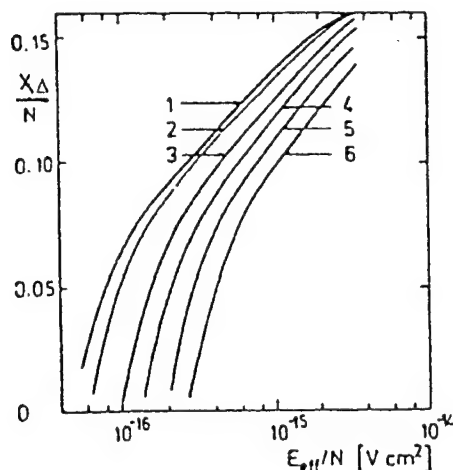


Fig. 2. Calculated relative concentration of the $O_2(^1\Delta_g)$ as a function of E_{eff}/N for several values of the parameter ω/N : 1 – 2.65×10^{-8} ; 2 – 4.7×10^{-8} ; 3 – 9.4×10^{-8} ; 4 – 1.33×10^{-7} ; 5 – 1.88×10^{-7} ; 6 – $2.65 \times 10^{-7} [\text{cm}^3 \text{s}^{-1}]$.

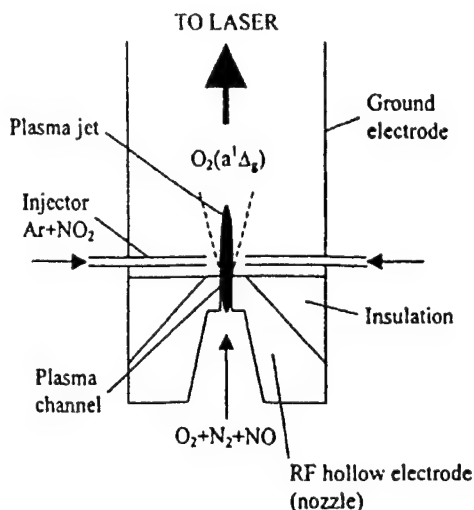
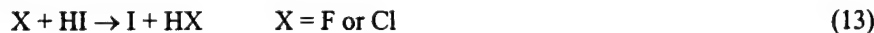


Fig. 3. Radio-frequency plasma jet generator of $O_2(^1\Delta_g)$

3. ATOMIC IODINE GENERATION

A generation of atomic iodine in the ground state, $I(^2P_{3/2})$, directly in the COIL medium to replace its conventional production from dissociated molecular iodine by $O_2(^1\Delta_g)$ opens up a way for potential improvement of the COIL performance. The first is the removal of the $O_2(^1\Delta_g)$, energy to dissociate I_2 , allowing this energy to be extracted as power. The second is the decrease in the molecular weight of the injectant, allowing for faster diffusive mixing, and avoiding negative effect of I_2 on the $I(^2P_{1/2})$ quenching. Also the technical problems induced by special treatment of I_2 vapour could be diminished.

With these needs in mind, our efforts has been focused currently on the gas phase chemical method of atomic iodine generation employing a principal reaction



The reaction (13) represents in fact a multiple gas phase chemical processes that occur in the overall reaction system. It involves initially the generation of F and Cl atoms, respectively, in the reaction of molecular fluorine, F_2 , or chlorine dioxide, ClO_2 , with nitrogen oxide, NO. Additionally, each of these processes is composed of multiple individual chemical reactions describing production and loss processes, including species contained in the COIL medium. And finally, this set of processes occurs within a flowing gas with the exothermicity of the reactions, which brings into the system a complication with coupling the chemical kinetics to the fluid dynamics.

The goals of our work on this problem are: 1/ to provide an overview of the current theoretical understanding of the two complex reaction systems, and to fit them to experimental conditions characteristic for a COIL, 2/ to test experimentally the both reaction systems in a flow reactor (a pilot small-scale device) to prove their suitability for a realistic COIL, and 3/ to test prospectively the developed method of atomic iodine generation directly on an adapted supersonic COIL device built in our laboratory. Work towards the first goal has involved, to date, a model based on the generalized one-

dimensional (1-D) flow development, exploring the chemical processes within the reaction systems. The calculations have been performed for physical conditions (pressure, temperature, and flow rates) applicable to a subsonic region (i.e., upstream of the nozzle throat) of the 1kW-class supersonic COIL operated in our laboratory. The effects of initial concentration ratio of reactants and different configuration of reactants injection were considered. A rate of I atoms generation has been investigated in a flow of nitrogen (as a buffer gas), and a reactive stream containing $O_2(^1\Delta)$. A reaction mechanism for the kinetics of I atoms generation in the $(Cl+HI+O_2(^1\Delta))$ and $(F+HI+O_2(^1\Delta))$, respectively, system has been developed and sensitivities to key processes in this mechanism have been considered. The modeling provided the concentration profiles of all relevant reaction components and the temperature profile along the reaction path. The results of this relatively rough estimation showed that I atoms can be generated via F atoms with the yield of up to 70%, however, on a rather long reaction path (20-40 cm). The reaction system via Cl atoms provided by these calculations I atom yield 80% on substantially shorter reaction path (~4 cm). For this reason, the later system would meet better the COIL mixing conditions. Atomic iodine could be generated near the critical nozzle plane of the supersonic COIL or during the transonic mixing. The chemical kinetics of fluorine system is however simpler, and all reactants are commercially available in gas cylinders. A detailed description of results on the 1-D modeling of both reaction paths for chemical generation of atomic iodine, and their interpretation were partly published^{30,31}, and some advanced results can be found in the paper of this Proceedings.³² A more sophisticated estimation of optimal conditions for I atoms generation needs the 2-D or 3-D modeling, involving also the fluid dynamics effects. This work is planned for a near future.

Work towards the second goal above has involved to date the experimental investigation of I atoms generation via Cl reaction system. A design of the small-scale flow reactor, and the experimental conditions were developed on the basis of the results of the above-mentioned modeling. Preliminary experiments provided atomic iodine with the molar flow rate up to 160 $\mu\text{mol/s}$, and I yield over 70% (in nitrogen).³³ Effects of initial ratio of reactants, and the way of their mixing were studied during the following on investigation. The yields of atomic iodine in the range of 70-100% (related to HI or ClO_2 flow rates) were attained. Some advanced results can be found in the paper of this Proceedings.³⁴ The experiments on atomic iodine generation in the $O_2(^1\Delta)$ stream are under way.

4. REPETITIVELY PULSED SUBSONIC COIL

A period of the early ninetieth signified one of the meaningful millstones in the COIL R&D – a demonstration of ability to operate a COIL in the pulsed regime. A prestige of COIL among other laser systems, particularly technological ones, so has increased. The magnetic gain modulation in a COIL could make possible, e.g., a more efficient non-linear conversion of the wavelength 1.315 μm to the second and higher harmonics. A slow (non-pulsed) control of 3-4 gain could be utilized for a continuous regulation of CW power (within 0-100% of the maximum value) without any change of flow or other operation parameters. Further, it could be employed as a method of the output power stabilization by means of the negative feedback controlling the magnetic field intensity in the gain region.

Besides previously investigated pulsed methods applicable to the COIL, like a pulsed UV photolysis of alkyl iodides in gas containing singlet oxygen³⁵, and electric discharge initiation of I atoms production from alkyl iodides³⁶, a Q-switching technique either mechanical³⁷ or magneto-optical³⁸ was also applied to a COIL. The optical switching utilizes the phenomenon of suppressing the gain on the basis of the Zeeman effect.³⁹ Owing to a low gain, low output coupling, and near threshold generation in a COIL, the Q-switching showed a disadvantage due to an increase in intracavity losses.

The pulsed technique investigated in our laboratory is also based on principle of the magnetic suppression (modulation) of gain, but the Zeeman effect is induced by externally applied magnetic field on the gain region.⁴⁰ The small signal gain on the strongest spectral line 3-4 observed in the laser generation in zero magnetic field is weakened in growing magnetic field, and due to above-mentioned physical characteristics of COIL, rather low magnetic fields are needed to quench the laser generation at 1.315 μm . Such a threshold or under-threshold condition can be expressed by the relation⁴¹

$$(2 g_{34}(B) L) / (\delta_0 + \delta_e) \leq 1 \quad (14)$$

$g_{34}(B)$ - small-signal gain at magnetic field B , L - gain length, δ_0 - intracavity losses, δ_c - resonator output coupling. Peak power enhancement over cw power can be achieved in the pulsed mode when pulsed power extraction times are short compared to the time that it takes to fill the outcoupled gain volume with fresh "fuel" (in a subsonic system usually $\sim 10^{-3}$ s). Energy of the single pulse is given by the average CW power (with zero magnetic field), and the optimal repetition rate. A pulsed length and its enhancement over CW power depend also on a switching off rate of the magnetic field. The gain volume, from which power can be extracted, is limited by deactivation rate of both the singlet oxygen and excited atomic iodine. Provided that this rate is fixed for a particular temperature in the cavity region, the way to increase this volume and thus increase the peak power enhancement is to increase the velocity of the flowing laser gases, and so to increase the concentrations of $O_2(^1\Delta_g)$ or atomic iodine or both. Experimental verification of the proposed pulsed technique was performed on the small-scale subsonic COIL device generating the CW output power up to several tenth watts. It was modified to apply magnetic field to the gain cavity from two rectangular coils attached to the laser body made of Plexiglas (see Fig. 4).

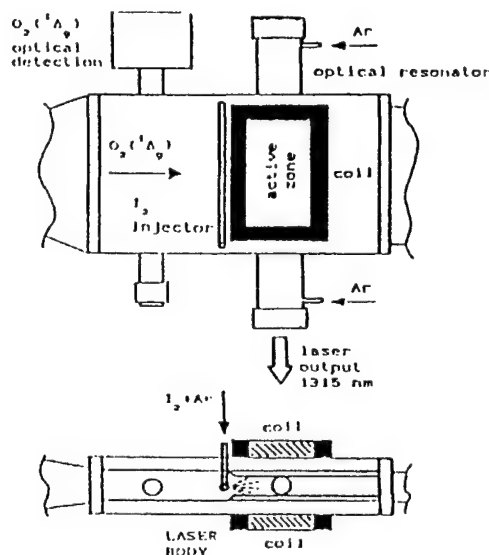


Fig. 4. Scheme of set up for magnetic pulsed regime of COIL

A typical oscillogram of the periodically pulsed COIL is shown in Fig. 5 that was recorded for 15 W of the average CW power. The peak enhancement corresponded to the power of 48 W, i.e., the enhancement ratio was 3.2. A length of single pulse was ~ 200 μ s at the rate of magnetic field pulsing of 0.5 G/ μ s.⁴¹ A maximum peak power enhancement achieved on this experimental configuration was ~ 3.5 only with the repetition rate of ~ 1 kHz. It was given by the relatively long switching off time of the used magnetic field generator. Consequently, extraction of the pulse power could not be fully developed.

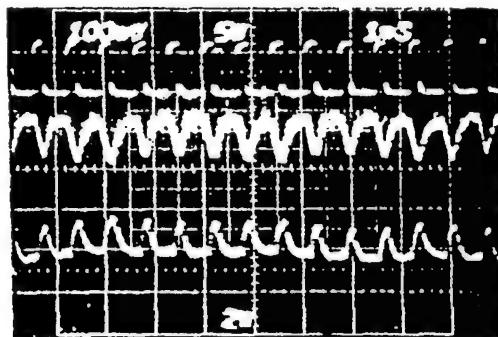


Fig. 5. Oscillogram of the repetitively pulsed COIL.
upper trace – pulsed magnetic field (1 ms/div, peak current 250 A);
lower trace – laser pulsed power (CW power 15 W, pulsed power 48 W)

Concurrently with our work, the magnetic field nullified-switched gain technique was developed at the AFRL by Hager *et al.*⁴² This technique works on principle of the gain suppressing below the lasing threshold by a static magnetic field that is followed by applying a fast rising current pulse to cancel the cavity magnetic field. A switching off the magnetic field was very fast in this way ($\sim 0.5 \mu\text{s}$) resulting in the laser pulse extraction with duration less than $20 \mu\text{s}$, and a peak-CW power enhancement ratio of 12.7.

Experimental data on estimation of the "3-4 gain quenching" magnetic field intensity, called a threshold magnetic field, were also collected during this investigation. It is defined as $g(B_{th}) = g_{th}(B=0)$.⁴³ The magnetic field was continuously increased up to level when the output laser power quenched. The values of $g(B_{th})$ evaluated in dependence on iodine molar flow rate in the cavity, and for several values of output coupling parameter are plotted in Fig. 6. This dependence showed a linear character in the overall tested parameters, even though the dependence of laser power, as well as output coupling, on iodine molar flow rate, showed generally maximum for a certain value of iodine concentration in the cavity.

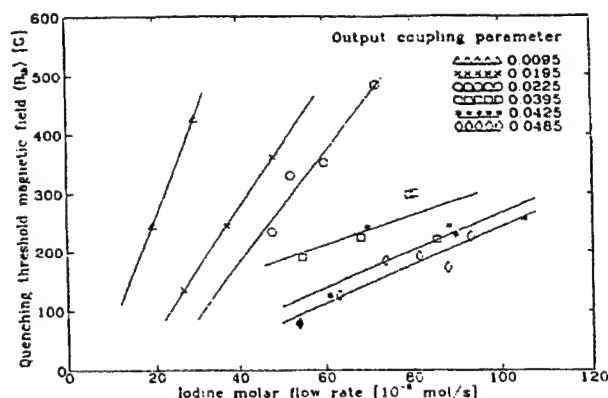


Fig. 6. Dependence of threshold magnetic field on iodine molar flow rate for different output couplings

It can be concluded from these results that a certain value of threshold magnetic field is affected by a set of physical and operation parameters together, particularly by iodine molar flow rates, small signal gain, threshold gain, and output couplings. In spite of the fact that a mutual relation among these parameters is rather complex, we proposed using a dimensionless parameter, the normalized gain defined as the ratio of threshold and small-signal gain (g_{th}/g), to evaluate from the experimental data the threshold magnetic field for given conditions. The threshold gain includes the effect of output coupling, intra-resonator losses, and gain length. Iodine flow rate, Doppler and pressure broadening of the laser transition, and also mixing efficiency affect the small signal gain. The dependence of normalized gain on the threshold magnetic field is shown in Fig 7.

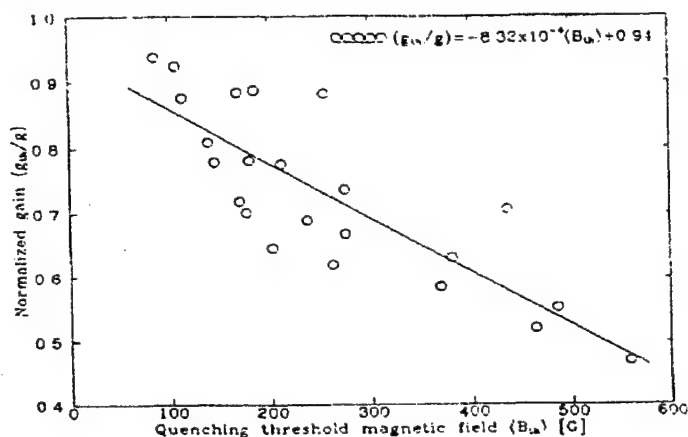


Fig. 7. Normalized gain (g_{th}/g_0) in relation to threshold magnetic field

5. OPERATION OF 1 kW-CLASS SUPERSONIC COIL

5.1. Performance characteristics

A small-scale 5-cm gain length supersonic chemical oxygen iodine laser driven by a jet singlet oxygen generator (jet SOG) with a closed-loop liquid flow system has been developed since 1996, and laser characteristics have been investigated. Parameters of the principal device parts are similar to the VertiCOIL developed in the AFRL except the rotating disks generator. The PC on-line with designed hardware and software nearly fully automatically controls the all system and records 32 essential laser parameters. An iodine vapour in helium is injected into the primary oxygen/helium flow in a subsonic region 5 to 7 mm upstream from the nozzle throat plane. A single horizontal slit configuration of nozzle is used for the adiabatic expansion of gas flow. A distance between the sonic plane and optical axis of the laser resonator is adjusted from 35 to 55 mm. A stable configuration of the resonator with 5 cm-diameter inner mirrors is employed. The mirrors are protected by helium atmosphere. The nozzle ramps and mirrors holders limit the multimode output beam size to 3.7 cm in the flow direction by 1.5 cm between the ramps.

Few experimental results are shown to represent state of the art of the investigation performed on this device to date. The jet SOG is operated typically at pressure 7.5 to 9.0 kPa (60 to 70 torr), with helium admixed to chlorine in the ratio mostly 1:2. A pressure in the generator, and consequently $O_2(^1\Delta_g)$ yield could be easily controlled by throttling the gas at the generator exit. It can be seen from one example of the generator performance record shown in Fig. 8. An increase in the yield with pressure decreasing results from a shorter residence time of gas in the generator, and also a lower $O_2(^1\Delta_g)$ partial pressure. Both effects diminish $O_2(^1\Delta_g)$ loss in the self-quenching/pooling reactions¹¹

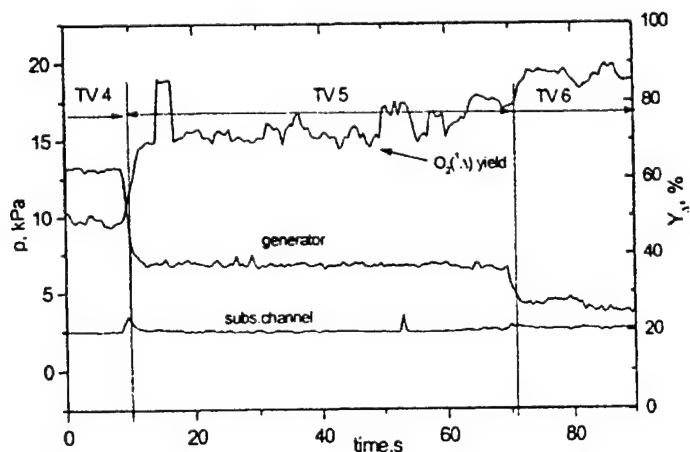
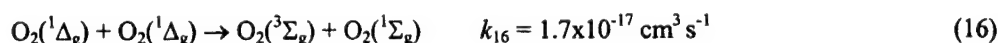
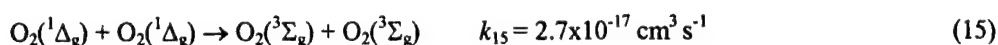


Fig. 8. Pressure in jet generator and $O_2(^1\Delta_g)$ yield controlled by gas throttling at generator exit. Position of throttle valve flap in tens of degrees is denoted by TV numbers (TV0 - closed, TV9 - opened entirely). Cl_2 flow rate of 40 mmol/s, He_{prim} flow rate of 40 mmol /s.

The jet SOG driving the supersonic COIL provided typically rather high $O_2(^1\Delta_g)$ yields (see Table1).

Tab. 1

P_{gen} , kPa	7	8	9	10
$O_2(^1\Delta_g)$ yield, %	80	77	70	63

Gas dynamic conditions in the whole laser system were tested during a „cold flow run“, i.e., with gaseous nitrogen instead of chlorine was introduced into the primary flow. The average Mach number, M_1 , for a subsonic flow ahead of the sonic throat, and the supersonic flow in the resonator region, M_2 , were evaluated from pressure ($P_{1,2}$) in the respective regions of the device, gas molar flow rates, (n), physical properties of the flowing gas (molecular weight, MW , and adiabatic constant, κ), stagnation temperature, and the flow cross section.⁴⁴ The local Mach number, M_2' , in the supersonic region was evaluated from the pressure ratio P_{stat}/P_{Pit} (P_{stat} - static pressure measured at the cavity wall, P_{Pit} - stagnation pressure measured by the Pitot tube in the cavity centreline placed 55 mm from sonic throat).⁴⁵ The results are summarized in Table 2.

Tab. 2

n_{N_2} , mmol/s	n_{He} , mmol/s	P_1 , Pa	P_2 , Pa	P_{Pit} , Pa	MW , kg/mol	κ	M_1	M_2	M_2'
21	90	2055	174	1457	8.6×10^{-3}	1.57	0.41	1.94	2.37

Laser output power was investigated at various iodine flow rates and output couplings. One example of such dependence is shown in Fig. 9. A simplified Rigrod theory⁴⁶ for saturation intensity was employed to estimate the small signal gain and saturation intensity from these experimental data. The gain of $1.29 \times 10^{-2} \text{ cm}^{-1}$, and the saturation intensity of 5.4 kW/cm^2 were evaluated.

The effect of titration ratio $[I_2]/[O_2(^1\Delta_g)]$ on laser power was searched also for different output couplings. Fig. 10 illustrates it for two values of generator pressure. The highest power was mostly achieved for $[I_2]/[O_2(^1\Delta_g)] = (5 \pm 1)\%$. The optimum value of 1.7% obtained on the VertiCOIL system⁴⁷ was significantly lower, however this discrepancy diminishes to 3.1% when the titration ratio is recalculated by dividing the total $[O_2]$ in VertiCOIL with $O_2(^1\Delta_g)$ yield (0.55).

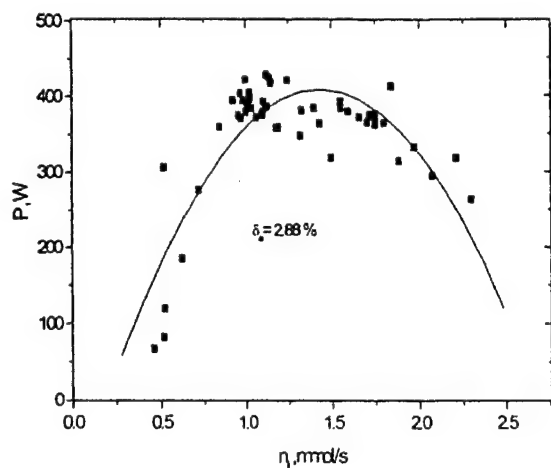


Fig. 9. Laser power as a function of iodine flow rate. Output coupling 2.83% ($T_1 + T_2$), 40 mmol Cl_2/s , 80 mmol He_{prim}/s , 40 mmol He_{sec}/s .

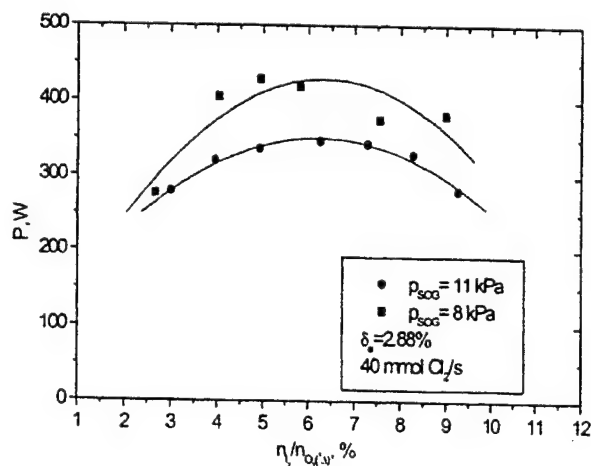


Fig. 10. Laser power as a function of titration ratio $[I_2]/[O_2(^1\Delta_g)]$ at two pressures in generator

The optimum dilution ratio, $[He_{sec}]/[I_2]$, at maximum attainable laser power was found in the range from 1:30 to 1:70. These measurements were directed to get efficient mixing of the primary gas flow, $O_2(^1\Delta_g) + He_{prim}$, and the secondary gas flow, $I_2 + He_{sec}$. It was estimated by means of the relative penetration factor, $\pi_{rel} = \pi/\pi_{full}$. The penetration parameters, π and π_{full} , describing the mixing both gas flows are evaluated from their physical properties, and hardware parameters of the device.⁴⁸

$$\pi = (n_s/n_p) [(M_s T_s P_p) / (M_p T_p P_s)]^{1/2} \quad (17)$$

$$\pi_{full} = (d A_s) / 5 D A_p \quad (18)$$

n - flow rate, M - molecular weight of gas mixture, T - temperature, P - pressure, d - height of primary flow channel, A - flow cross-section, D - orifice diameter of secondary flow (index p – primary flow, index s – secondary flow). The best mixing conditions resulting in the maximum output power were at the values of π_{rel} between 0.8-1.0.

State of the art of the performance characteristics of the COIL device operated in our laboratory are summarized in Table 3. The laser operation has not been assessed as enough efficient yet. The reason for a rather low chemical efficiency (measured output power) is most probably a bad quality of the resonator mirrors used so far in this laser system.

Tab. 3.

Laser power	430 W
Running time	1.5 min
Chlorine flowrate	37.8 mmol/s
Primary helium diluent	80 mmol/s
Generator pressure	8 kPa (60 Torr)
Chlorine utilization	0.97
Starting BHP molarity	6.7 M HO ₂ ⁻
O ₂ (¹ Δ _g) measured yield	0.72
Pressure upstream the nozzle	3.8 kPa (28.5 Torr)
Laser cavity pressure	380 Pa (2.8 Torr)
I ₂ / O ₂ flow rate ratio	0.029
Mirrors reflectivity	0.9995/0.981
Mode length	3.7 cm
Small signal gain (Rigrod)	0.013 cm ⁻¹
Saturation intensity	5.4 kW/cm ²
Chemical efficiency	0.12

5.2. Small signal gain distribution and cavity temperature evaluation

A spatial distribution of the small signal gain, and evaluation of cavity temperature was investigated by means of the Iodine Scan Diode Probe diagnostics developed for a COIL at the PSI⁴⁹, and used first at the AFRL.⁵⁰ The line-shape of the COIL gain profile was scanned in frequency by a diode laser of narrow line width operating in the region of the COIL transition frequency. The small signal gain, $g(\nu_0)$, was determined using the equation⁴⁷

$$I(\nu_0) = I_0(\nu_0) \exp(g(\nu_0) L) \quad (19)$$

$I_0(\nu_0)$ - line-center probe laser intensity entering the gain region, $I(\nu_0)$ - line-center intensity after amplification through the gain region, L - gain length.

The temperature in terms of the Doppler full width at half-maximum, $\Delta\nu_D$, was evaluated from the relation⁴⁷

$$\Delta\nu_D(T) = 2 \nu_0 / c \{ \ln 2 (2 k T / M) \}^{1/2} \quad (20)$$

ν_0 - central frequency, c – light velocity within medium, k - the Boltzmann's constant, M - mass of medium species.

Performed mapping of the gain distribution through the gain region was aimed at the inspection of mixing conditions in the cavity at different experimental conditions, and bearing out our guess at the reason of rather low chemical efficiency of this device (mirrors quality). The results presented below were gathered for the primary gas flow of 40 mmol Cl₂/s

and 80 mmol $\text{He}_{\text{prim}}/\text{s}$, the secondary gas flow of 40-80 He_{sec} mmol/s and 1-2 mmol I_2/s . The plenum pressure was 3.4 - 4 kPa (25-30 Torr), the cavity pressure measured at the upper wall in the location of the resonator axis was 300-390 Pa (2.2-2.8 torr). The 2.5 mm i.d.-beam of the probe laser was passed through the gain medium parallel to the optical axis. A two-pass configuration of the probe beam was chosen for the data extraction. The probe beam emitter/detector unit and the mirror system for beam alignment were mounted on an assembly of the motorized linear positioning equipment that allowed fast and precise movements either in horizontal direction (x axis) along the gas flow or vertical direction (y axis) perpendicular to the gas flow. The grid of measuring positions is presented in Fig. 11.

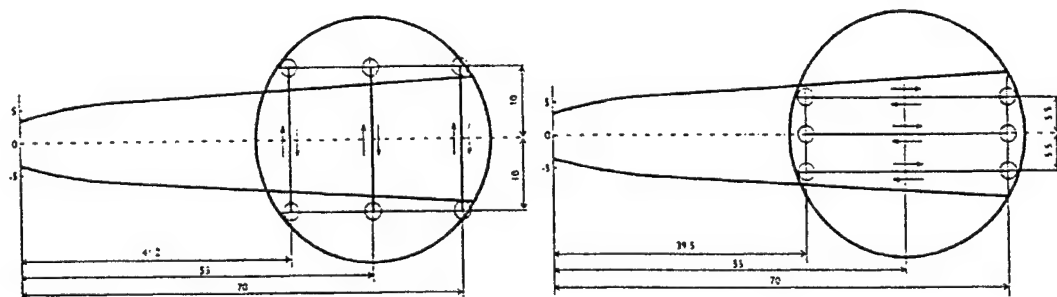


Fig. 11. Scheme of probe beam scanning in vertical and horizontal position

Duration of each scan was 13.3 seconds, and the gain data were recorded within 60-100 seconds' hot runs. One example of the gain distribution curves cross the gain region in the vertical direction measured at three values of I_2 flow rate is illustrated in Fig. 12. A parabolic shape of the gain distribution curve indicates that the gas flow velocity across the gain region was inhomogeneous resulting in a slower gas flow at boundary layers (0.5 to 1.5 mm thick) along the cavity walls. In these layers, a remarkable quenching of excited I atoms occurred. Molecular iodine may be also present in these layers which may consume $\text{O}_2(^1\Delta_g)$ in its dissociation. The maximum gain was attained at the iodine flow rate of 1.5 mmol I_2/s . Similar parabolic distribution of gain was obtained for different distance from the nozzle, but the maximum gain values were attained at different iodine flow rates under constant other conditions. An insufficient mixing of primary and secondary flows (inefficient penetration) could be easily detected by this diagnostics (see Fig. 13). The gain distribution record in this case (40 mmol $\text{He}_{\text{sec}}/\text{s}$ only) showed two peaks and minimum located in the cavity center, which can be explained by a shortage of iodine is in the center of the cavity.

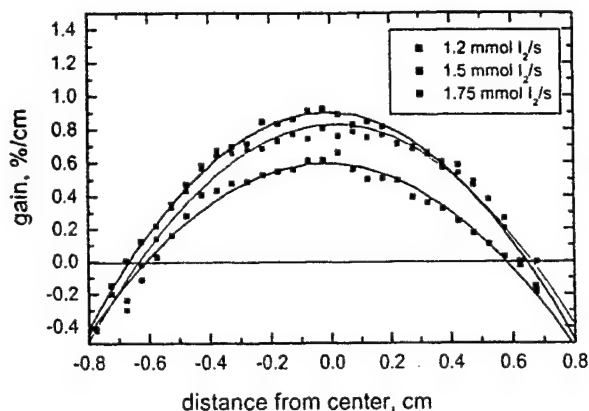


Fig. 12. Gain distribution in vertical direction, 5.5 cm downstream nozzle throat (resonator axis); for three I_2 flow rates; 80 mmol $\text{He}_{\text{sec}}/\text{s}$.

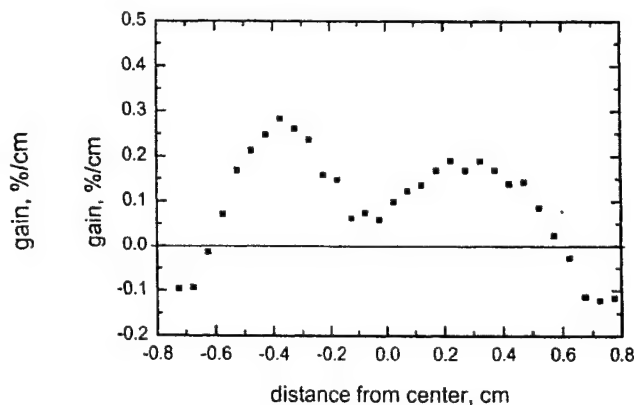


Fig. 13. Gain distribution in vertical direction, 5.5 cm downstream nozzle throat (resonator axis); 1.5 mmol I_2/s , 40 mmol $\text{He}_{\text{sec}}/\text{s}$.

A plot of measured gain on evaluated relative penetration factor is shown in Fig. 14. The small signal gain of $\sim 1\%/\text{cm}$ was typical for the supersonic COIL device operated in our laboratory at optimal mixing conditions. Comparing it, for

example, with the gain attainable on the RADICL device (~ 1.2 %/cm), and considering also twice higher cavity pressure in this laser system (5.8 Torr), there is a prospect to enhance the gain of our COIL driven by jet SOG when the cavity pressure is increased.

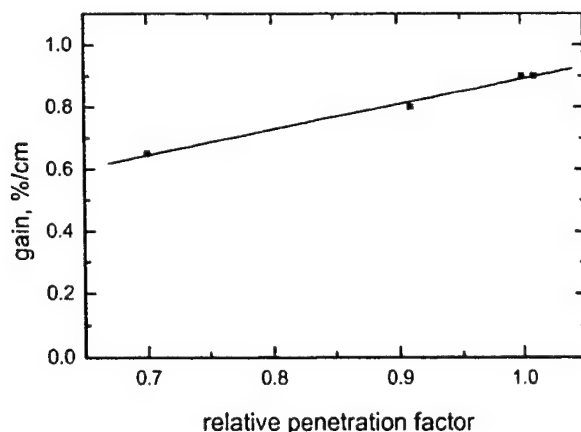


Fig. 14. Gain in the cavity center in relation to calculated relative penetration factor; 5.5 cm from the nozzle throat (resonator axis), 1.5 mmol I_2 /s, 80 mmol H_{sec} /s.

The gas temperature calculated from these measurements was not homogeneous across the whole cavity. In the boundary layers when the probe beam recorded weak emission or even absorption, the gas temperature was much higher (>350 K) than in the cavity center (175 – 205 K). A low gas velocity and high rate of exothermic processes per unit length in the boundary layers near the walls to the cavity center can explain it.

6. SUMMARY

The above-presented results have been extracted from a number of publications and reports that have come out from the COIL Laboratory in Prague. We hope that our current and future research on COIL related problems contributes and will contribute to the advanced COIL technology.

ACKNOWLEDGMENTS

The authors wish to recognize all colleagues who played significant roles in the presented research over the years. This work was partly done as a research program within the contracts with the USAF EOARD, partly in the framework of the Research Laser Centre at the Institute of Physics supported by the Ministry of Education (project LN00A100 and ME442).

REFERENCES

1. J.V.V. Kasper and G.C. Pimentel, "Atomic iodine photodissociation laser", *Appl. Phys. Lett.* **5**, pp. 231-233, 1964.
2. K. Rohlena, B. Rus, L. Juha, J. Skála, B. Králiková, K. Jungwirth, J. Ullschmied, K.J. Witte, H. Baumhacker, "Prague Asterix Laser System (PALS) and its upgrade", *Proc. SPIE* **4184**, pp. 132-136, 2000.
3. D.R. Kearns, "Physical and chemical properties of singlet molecular oxygen", *Chem. Review* **71**, pp. 395-427, 1971.
4. R.G. Derwent, D.R. Kearns, and B.A. Thrush, "The excitation of iodine by singlet molecular oxygen", *Chem. Phys. Lett.* **6**, pp. 115-116, 1970.
5. W.E. McDermott, N.R. Pchelkin, D.J. Benard, and R.R. Bousek, "An electronic transition chemical laser", *Appl. Phys. Lett.* **32**, pp. 469-470, 1978.

6. S.E. Lamberson, "The Airborne Laser", *Proc. SPIE* **4184**, pp. 1-6, 2000.
7. R.J. Richardson, J.D. Kelley, and C.E. Wiswall, " $O_2(^1\Delta_g)$ generation mechanism in the chemically pumped iodine laser", *J. Appl. Phys.* **52**, pp. 1066-1071, 1981.
8. O. Špalek, J. Kodymová, and A. Hiršl, "Influence of hydrostatic pressure on $O_2(^1\Delta_g)$ yield in a bubbler-type chemical generator", *J. Appl. Phys.* **62**, 2208-2211, 1987.
9. O. Špalek, J. Kodymová, and A. Hiršl, "Theoretical modelling of singlet oxygen bubbled generator for chemical oxygen-iodine laser", *Proc. SPIE* **1031**, pp. 319-323, 1988.
10. J. Kodymová, O. Špalek, and A. Hiršl, " $O_2(^1\Delta_g)$ loss-mechanism in bubbler-type chemical generators", *Proc. Int. Workshop on Iodine Lasers*, Bechyně, Czech Republic, pp. 230-235, 1986.
11. A.I. Didjukov, Yu.A. Kulagin, L.A. Shelepin, and V.N. Yarygina, "Analysis of processes rate in presence of singlet oxygen molecule" (in Russian), *Quantum Electronics* **16**, pp. 892-904, 1989.
12. N.F. Balan, R.M. Gizadullin, M.V. Zagidullin, A.Yu. Kurov, V.D. Nikolaev, V.M. Pitchkasov, and M.I. Svistun, *Quantum Electron.* **16**, pp. 2197-2200, 1989.
13. O. Špalek and J. Kodymová, "Influence of arrangement of liquid jets on operation of jet singlet oxygen generator", *Proc. SPIE* **2767**, pp. 237-244, 1995.
14. O. Špalek and J. Kodymová "Optimization of jet singlet oxygen generator", *Proc. SPIE* **3092**, pp. 565-568, 1996.
15. O. Špalek and J. Kodymová, "Singlet oxygen generator for a supersonic chemical oxygen-iodine laser. Parametric study of recovery of chemicals", *Proc. SPIE* **2987**, pp. 131-136, 1996.
16. J. Kodymová and O. Špalek, "Performance characteristics of jet-type generator of singlet oxygen for supersonic chemical oxygen-iodine laser", *Jpn. J. Appl. Phys.* **37**, pp. 117-121, 1998.
17. D.H. Burde and R.A. McFarlane, "Collisional quenching of excited iodine atoms $I(^5P_{1/2})$ by selected molecules", *J. Chem. Phys.* **64**, pp. 1850-1851, 1976.
18. R. Dickerson, J. Hon and J. Blauer, "Modeling the rotating disk generators", *AIAA* **92-3007**, pp. 1-13, 1992.
19. J. Bonnet, D. David, E. Georges, B. Laporcq, and C. Verdier, "Experimental analysis of chemical oxygen-iodine lasers", *Appl. Phys. Lett.* **45**, pp. 1009-1011, 1984.
20. R.G. Aviles, D.F. Muller, and P.L. Houson, "Quenching of laser-excited $O_2(b^1\Sigma_g^+)$ by CO_2 , H_2O , and I_2 ", *Appl. Phys. Lett.* **37**, pp. 358-360, 1980.
21. M. G. Mlynčzak and D.J. Nesbitt, "The Einstein coefficient for spontaneous emission of the $O_2(^1\Delta_g)$ state", *Geophys. Res. Lett.* **22**, pp. 1381-1384, 1995.
22. R.B. Badger, A.C. Wright, and R.T. Whitloch, "Absolute intensities of the discrete and continuous absorption bands of oxygen gas at 1.26 and 1.065 μ and the radiative lifetime of the $^1\Delta_g$ state of oxygen", *J. Chem. Phys.* **43**, pp. 4345-4350, 1965.
23. O. Špalek, J. Kodymová, V. Bálek, P. Stopka, and I. Miček, "Attempt to verify experimentally Einstein A-coefficient used for $O_2(^1\Delta_g)$ determination in COIL", *Proc. SPIE* **3574**, pp. 550-559, 1998.
24. J. Kodymová and O. Špalek, " $O_2(^1\Delta_g)$ radiative lifetime: Contribution to discussion on the Einstein A-coefficient used in COIL for $O_2(^1\Delta_g)$ determination from fundamental emission", *Proc. SPIE*, **3612**, pp. 92-99, 1999.
25. O. Špalek, J. Kodymová, P. Stopka, and I. Miček, "Experimental verification of the Einstein A-coefficient used for evaluation of $O_2(^1\Delta_g)$ concentration in the chemical oxygen-iodine laser", *J. Phys. B: At. Mol. Opt.* **32**, pp. 1885-1892, 1999.
26. S. M. Newman, I.C. Lane, A. J. Orr-Ewing, D.A. Newnham and J. Ballard, "Integrated absorption intensity and Einstein coefficients for the $O_2\ a^1\Delta_g - X^3\Sigma_g^- 0,0$ transition: A comparison of cavity ringdown and high resolution Fourier transform spectroscopy with a long-path absorption cell", *J. Chem. Phys.* **110**, pp. 10749-10757, 1999.
27. K. Mašek and K. Rohlena, "Physical kinetics of a hf glow discharge in oxygen. Generation of the $a^1\Delta_g$ state for pumping in an iodine laser", *Czech J. Phys.* **B34**, pp. 1227-1234, 1984.
28. K. Swift, "Microwave excitation of oxygen $O_2(^1\Delta)$ for an oxygen-iodine laser", *Forschungsbericht, DFVLR Institute für Technische Physik*, Stuttgart, **89-23**, pp. 1-39, 1989.
29. J. Schmiedberger and H. Fujii, "Radio-frequency plasma jet generator of singlet delta oxygen with high yield", *Appl. Phys. Lett.* **78**, pp. 2649-2651, 2001.
30. V. Jirásek, O. Špalek, J. Kodymová, "Modelling of chemical generation of atomic iodine for chemical oxygen-iodine laser", *Proc. SPIE* **4184**, pp. 103-106, 2000.
31. V. Jirásek, O. Špalek, J. Kodymová, and M. Čenský, "Chemical generation of atomic iodine for chemical oxygen-iodine laser. I. Modelling of reaction systems.", *Chem. Physics* **269**, pp. 167-178, 2001.

32. V. Jirásek, O. Špalek, J. Kodymová, and M. Čenský, "Modeling of the chemical generation of atomic iodine in a chemical oxygen-iodine laser", *Proc. SPIE of this conference* (submitted for publication).
33. O. Špalek, V. Jirásek, J. Kodymová, I. Jakubec, and M. Čenský, "Preliminary experimental results on chemical generation of atomic iodine for a COIL", *Proc. SPIE* **4184**, pp. 111-115, 2000.
34. O. Špalek, V. Jirásek, , M. Čenský, J. Kodymová, and I. Jakubec, "Chemical generation of atomic iodine for COIL", *Proc. SPIE of this conference* (submitted for publication).
35. N.G. Basov, N.P. Vagin, P.G. Kryukov, D.Kh. Nurligareev, V.S. Pazyuk, and N.N. Yuryshev, " CH_3I and $\text{n-C}_3\text{F}_7\text{I}$ as donors of iodine atoms for a pulsed oxygen-iodine chemical laser", (in Russian), *Quantum electronics* **11**, pp. 1893-1894, 1984.
36. R. Zhang, F. Chen, X. Song, Q. Xu, C. Huan, Q. Zhuang, and C. Zhang, "Photolysis/electrical discharge initiated pulsed chemical oxygen-iodine lasers using alkyl iodides as the iodine source", *Proc. SPIE* **1031**, pp. 308-311, 1988.
37. F. Matsuzaka, T. Ohga, M. Imachi, and T. Uchiyama, "Q-switching operation of chemical oxygen-iodine laser", *Proc. 12th Int. Conference on Laser Applications*, New Orleans, LA, pp. 223-227, 1989.
38. R. Highland, P. Crowell, and G. Hager, "A 630 watt average power Q-switched chemical oxygen-iodine laser", *Proc. 12th Int. Conference on Laser Applications*, New Orleans, LA, pp. 228-236, 1989.
39. I.M. Belousova, B.D. Bobrov, V.M. Kiselev, V. N. Kurzenkov, and P.I. Krepostnov, " I^{127} atom in a magnetic field" *Optika i Spektroskopia* **37**, pp. 38-47, 1974.
40. J. Schmiedberger, J. Kodymová, J. Kovář, O.Špalek, and P. Trenda, "Modulation of oxygen-iodine laser", *Patent No. 276690*, 1990 (Czech Republic), *Patent No. 5*, 199,041, 1993 (USA).
41. J. Schmiedberger, J. Kodymová, J. Kovář, O.Špalek, and P. Trenda, "Magnetic modulation of gain in a chemical oxygen-iodine laser", *IEEE J. Quant. Electron.* **27**, 1262-1264, 1991.
42. G.D. Hager, D. Kopf, D. Plummer, T. Salsich, and P. Crowell, "Demonstration of a repetitively pulsed magnetically gain switched chemical oxygen-iodine laser", *Proc. SPIE* **1810**, pp. 509-551, 1992.
43. J. Schmiedberger, O. Špalek, J. Kodymová, and J. Kovář, "Experimental study of magnetic quenching of laser generation in COIL", *Proc. SPIE* **1810**, pp. 521-524, 1992.
44. A.H. Shapiro, *The Dynamics and Thermodynamics of Compressible Fluids Flow*, Vol. I. p. 82, 1953.
45. L. Horwath, *Modern Development in Fluid Dynamics High Speed Flow*, (in Russian) Vol. II, 1956.
46. W.W. Rigrod, "Gain saturation and output power of optical masers" *J. Appl. Phys.* **14**, pp. 2602-2609, 1963.
47. T.L. Rittenhouse, S.P. Phipps, and Ch.A. Helms, "Performance of a high-efficiency 5-cm gain length supersonic chemical oxygen-iodine laser", *IEEE J. Quant. Electronics* **35**, pp. 857-866, 1999.
48. J.E. Scott, J.L.R. Shaw, K.A. Truesdell, G.D. Hager, C.A. Helms, "Design considerations for the chemical oxygen-iodine supersonic mixing nozzle" *AIAA paper* 94-2436, pp. 1-7, 1994.
49. S.J. Davis, M.G. Allen, W.J. Kessler, K.R. McManus, M.F. Miller, and P.A. Mulhall, "Diode laser-based sensors for chemical oxygen-iodine lasers", *Proc. SPIE* **2702**, pp. 195-201, 1996.
50. R.F. Tate, B.S. Hunt, C.A. Helms, K.A. Truesdell, and G.D. Hager: "Spatial Gain measurements in a Chemical Oxygen Iodine laser (COIL)", *IEEE J. Quant. Electronics* **31**, pp. 1632-1636, 1995.

COIL technology development at Boeing

Stephen C. Hurlock*, The Boeing Company, Canoga Park, CA

ABSTRACT

The historical COIL contributions at the McDonnell Douglas Research Laboratory, the Rocketdyne Division of Rockwell International and Boeing's Laser and Electro-Optic Systems organization are briefly described. The latter organization now contains the capabilities of the two heritage organizations. Boeing's new high pressure sealed COIL is also described.

1. INTRODUCTION AND HISTORICAL BACKGROUND

Two industrial organizations participating in the early COIL developments were the McDonnell Douglas Research Laboratory and the Rocketdyne Division of Rockwell International. Both of these are now part of The Boeing Company and their laser and electro-optics capabilities have been incorporated into Boeing's Laser and Electro-Optic Systems organization. MDRL was the first industrial organization (and second only to the Air Force weapons Laboratory¹) to report a successful COIL². Rocketdyne was the first industrial organization to win a competitive award for COIL development³. This heritage has continued unbroken over the intervening years and many contributions to COIL technology have been made by the individual and combined organizations. Boeing continues to be a major force in the COIL community, advancing the technology both incrementally and discontinuously through experiments, testing, and analysis sponsored by U.S. Government contracts and by Company discretionary resources. This paper gives a brief account of that historical background, provides a summary of the highlights of some of Boeing's contributions, and then proceeds to describe Boeing's recent work, which has resulted in the development and demonstration of a new type of COIL laser system.

2. HIGHLIGHTS OF TECHNOLOGY DEVELOPMENT AT BOEING

Over the years since 1978, the organizations and individuals belonging to what is now Boeing's Laser and Electro-Optic Systems organization have explored and developed a huge number of concepts for advancing COIL technology in virtually every aspect of the laser and a broad range of applications. The paragraphs below present a brief sampling of this activity.

2.1 Oxygen Generators

Both at MDRL and Rocketdyne, just about every conceivable type of gas-liquid contact device was explored for $O_2(^1\Delta)$ generators, from spargers, through wetted wall devices, aerosols, and jets, with many variants along the way. Novel chemistry as well as detailed parametric characterization of BHP- Cl_2 chemistry was examined. A recent innovation eliminates the solids formation in BHP, which has plagued many researchers⁴.

The first $O_2(^1\Delta)$ generator developed at Boeing used a refrigerated rotating surface as a support for the gas-liquid contact surface. Similar to the modern rotating disk generators, this device had a scraper to remove spent liquid from the rotating surface³. Another wetted wall generator configuration which was very successful in the early years employed static commercial mixers with relatively high surface area wetted by flowing BHP, with co-flow or counter-flow Cl_2 , with or without diluent. These were scaled by over 1000x in Cl_2 flow and achieved 90% Cl_2 utilization and > 70% BHP utilization in a single pass. A small-scale version of one of these devices, with N_2 diluent added at the exit, was the first to report $O_2(^1\Delta)$ yields in excess of 70%. Boeing also explored a variety of aerosol configurations, coupled to a variety of separators. More recently, the full gamut of high-pressure jet generators with He diluent was explored, with counter-flow configurations being the most successful⁵. The generator used in our new laser is a diluent-free cross-flow jet generator which delivers ~ 20 Torr of O_2 at ~ 65% yield, ~ 90% Cl_2 utilization, and ~ 1 Torr of H_2O . The gas-liquid separation allows only ~ 2% of the gas to exit with the liquid, while the gas product is effectively liquid-free.

2.2 Nozzles

Over the past 25 years, COIL nozzle development has not seen as much attention as $O_2(^1\Delta)$ generator development. The "Classical COIL Nozzle" was developed at Boeing in 1981-83 and has been the standard for helium-diluted COILs. It remains in use virtually unchanged today. The nozzle which we developed for our new laser is a totally different approach, designed for use with heavier diluents, where it can lead to significant improvements in system pressure recovery performance. The two approaches and their differences are illustrated later in this paper.

2.3 Pressure recovery

Conventional and advanced pressure recovery technologies have been developed and used at Boeing over the years. Bank blowers at the outboard ends of the nozzle is a technology that has been successfully adapted to COILs from Gas Dynamic Laser (GDL) and HF/DF chemical laser technology. Likewise, conventional diffusers, with and without sidewall energizers, have been adapted to COIL. Boeing successfully developed an advanced normal shock diffuser technology and applied it to COIL^{6,7}. All of these approaches were applied to COILs using helium diluent. With our new laser, the pressure recovery potential of the cavity exit flow is at least 100 Torr, using conventional diffuser technology.

2.4 Exhaust management

Boeing has used mechanical pumps and ejectors for much of the laboratory development work with COILs. More recently, a large, evacuated catch vessel has proved effective and convenient, and works especially well with a laser like ours, which has a relatively high diffuser exit pressure. In the early years, chemical pump technology based on a variety of reactive materials was explored. Our new laser includes a sealed exhaust system in which cryogenically cooled zeolite is used to adsorb the laser exhaust^{8,9}.

3. HIGH PRESSURE SEALED COIL

3.1 Introduction

We refer here to the conventional or classical approach to COIL as that in which the Cl_2 in the generator is diluted by He at significant levels and the I_2 is injected into the generator effluent in the subsonic region of slit nozzles. The injection is accomplished via an array of penetrating jets of I_2 diluted and carried by He. Mixing occurs in the subsonic, transonic and supersonic regions of the nozzle and cavity flow, with much of the mixing completed by the nozzle exit plane. Nozzle expansion typically leads to velocities near Mach 2 in this technology¹⁰. This approach was developed first at Boeing in the early '80s under company and then U.S. Air Force sponsorship. It has been the basis of most supersonic COIL work until recently. A schematic of a typical COIL based on this technology is shown in Figure 1, where it is described as low pressure COIL technology, based on the diffuser exit pressure of 10-20 Torr.

In contrast, the newer technology described here, developed at Boeing in 1997-99, uses an $O_2(^1\Delta)$ generator with no diluent. The generator effluent is expanded to approximately Mach 1 as it enters the laser cavity. There, I_2 is introduced along with N_2 as a diluent in a supersonic nozzle, which expands the flow to Mach 5 under our typical conditions. This flow, in addition to introducing the I_2 , mixes with and transfers momentum to the Mach 1 generator flow and accelerates it, resulting in a mixed Mach number of 3 – 3.5 at the cavity exit. A schematic of a typical COIL based on this technology is shown in Figure 2, where the diffuser exit pressure is shown as 100-200 Torr, leading to the designation of high pressure COIL technology. In addition to the obvious advantages of much higher recovery pressure, this technology also results in a significantly lower static temperature in the cavity, providing kinetic and threshold enhancements to power extraction.

3.2 CFD analysis of nozzle mixing

Although this new technology appears very attractive, it presents a real challenge in achieving good mixing in the short times (and thus short flow distances) required by COIL kinetics. Our approach to developing a solution to this challenge has been to define conceptual nozzle designs and then use iterative CFD analysis and other analyses to determine the best configuration. Slit nozzles were selected to minimize boundary layer losses. Our design goal was to have a nozzle that achieved reasonably good mixing within 8-10 cm of flow length and essentially complete mixing by 20 cm, which was a

nominal power extraction distance. Figure 3 shows the parameters of the selected design in terms of upstream and downstream flows as well as the framework of the calculations.

In order to meet the stringent mixing length target, mixing aids were needed, and their dimensionality was varied to achieve the goal. The nozzle which was designed using this approach is shown in Figure 4. A CFD result for this nozzle is shown in Figure 5, where it is seen that the goal of good mixing by 8-10 cm was achieved. Using flow composition parameters from Figure 3, complete mixing would be represented when the N_2 fraction is 0.83. More detailed discussion of the design analysis has been reported previously ¹¹.

3.3 Cold flow testing of selected nozzle

As a design validation, a test article was fabricated and tested in cold flow. The nozzle bank, shown in Figure 6, contained three ejector nozzles of the same length, spacing, and manufacturing methods as the full laser nozzle. The oxygen generator was represented by a plenum upstream of the nozzle bank. The bank included two full and two half oxygen nozzles to feed the downstream cavity, which was a rectangular duct with no divergence, followed by a diffuser section with straight sidewalls and 6° divergence top and bottom. Pitot probe scans were made in the horizontal direction at three downstream locations. Vertical scans were also made. Some horizontal scan data are included in Figure 6, and show high peak pressures and significant structure at the upstream location (3.2 cm downstream of the nozzle exit plane), while the structure has been largely removed at the most downstream (20.7 cm) location. Elimination of spatial variation in the Pitot pressure is interpreted as indicative of completeness of mixing. This work has been described in more detail previously ¹².

In addition to the Pitot scans to evaluate mixing, experiments were conducted to evaluate pressure recovery potential. In these experiments, the valve connecting the experiment to the facility vacuum system was gradually closed while monitoring the pressure at the diffuser exit and the pressure in the straight-walled duct representing the laser cavity. Results are presented in Figure 7, where the cavity pressure is seen to remain constant at about 10 Torr until the diffuser breaks back and the cavity unstarts, which occurs at back pressures between 90 and 100 Torr for the two test cycles shown. This indicates a pressure recovery of 100 Torr, achieved with very conventional diffuser technology. This work has also been reported previously ¹².

3.4 Laser system description

Incorporating the selected nozzle design, a hypersonic COIL laser test bed was designed, fabricated, installed and tested ¹³. The device, seen in Figure 8, was designated as the 1 mole laser, because the target generator flow was 1 gmol/s of Cl_2 , with no diluent. Testing results led to 0.9 gmol/s as the optimum flow for this device. Because the new nozzle concept requires a high pressure iodine source, a new high pressure I_2 vaporizer was developed under contract by General Atomics. This system, capable of delivering I_2 at 100 psia and higher is shown in Figure 9. The exhaust from this new laser contains only O_2 and N_2 , with small amounts of H_2O , Cl_2 and I_2 . This composition, unlike that from the low pressure technology, which contains large amounts of helium, can be adsorbed by commercial adsorbents. Boeing exploited this feature by adding an adsorber bed to the system, resulting in a sealed laser with no exhaust. The adsorber selected was cryogenically cooled zeolite, also referred to as molecular sieve material. The sealed exhaust system may be seen in Figure 10.

3.5 Laser system testing

The system was highly instrumented, including a large number of pressure and temperature measurements to measure the reactant and diluent flows as well as to characterize the gas and liquid flow through the generator, nozzle, cavity, diffuser and exhaust management system. Flow visualization employed video cameras. A suite of chemical diagnostics helped to characterize the flow composition. Another suite of optical diagnostics was used to measure the outcoupled beam characteristics.

Measurements at the generator exit included P, T, $[O_2(^1\Delta)]$, $[O_2(^1\Sigma)]$, $[Cl_2]$, and $[H_2O]$, which allowed chlorine utilization and $O_2(^1\Delta)$ yield to be determined. Another measurement in the BHP effluent allowed its gas content to be determined. Optical emissions at the generator exit and in the laser cavity were collected using the fiber bundle arrangement shown in Figure 11, which allowed simultaneous recording of filtered emission (in-band emission) for $O_2(^1\Delta) - O_2(^3\Sigma)$, $O_2(^1\Sigma) - O_2(^3\Sigma)$, as well as resolved emission using visible and infrared optical multichannel analyzers (OMAs). Some spectra

from these OMAs are shown in Figure 12. The performance of the oxygen generator, averaged over all of the 0.9 gmol/s tests, is summarized in Figure 13.

Optical bundles were also positioned to collect emission from the cavity and an example visible wavelength OMA spectral record with time evolution is shown in Figure 14. Early in the test, the same O_2 emission features as shown in Figure 13 are evident. As the I_2 is turned on and its flow ramped up, the $I_2(B)-I_2(X)$ emission dominates this spectral region, but the influence of pooling on $[O_2(^1\Sigma)]$ can be seen.

The diagnostic suite to outcouple a beam and to characterize the beam included a resonator, a calorimeter, a fast flux monitor, and a mode footprint monitor. These may be seen in the layout of Figure 15 and the photographs of Figure 16. The laser resonator was a half-symmetrical stable resonator with a partially transparent dielectric on a transparent flat substrate and a high reflectivity dielectric on a transparent spherical substrate. Total energy in the high power beam was measured using a full-beam, full-power calorimeter. A full-beam sample of the power leaking through the high reflectivity mirror was measured by a fast flux monitor, whose signal was converted to power by normalization of the integrated signal to the energy measured by the calorimeter. The mode footprint (beam footprint) was recorded using an infrared video camera viewing a diffuse scatter plate located behind the high reflectivity resonator mirror.

Representative power vs. time records for four tests are shown in Figure 17. Three of the tests involved increasing the I_2 flow and show attendant power increases. In the fourth, the I_2 flow was constant and the sealed exhaust system was operating. In some of the power records, transient events are seen. These were determined to be transient increases in extracted power and indicate that significantly more power is available in the flow than we were able to extract in a steady-state fashion. Comparisons of the new laser performance with helium diluent results for other lasers are shown in Figure 18, where chemical efficiency is plotted against the well-known $P\cdot\tau$ parameter. The steady-state performance is comparable with the best of the helium data base, while the transient results, if they could be achieved in steady state, would represent a significant improvement.

Finally, the new laser, because of the I_2 delivery and injection method, results in mixing within the supersonic cavity flow, in contrast to the conventional low-pressure helium diluent technology, where the flow enters the cavity in a nearly premixed state. This latter condition has required developers to deal with the well known sugar-scoop intensity problem. The mode footprint images, shown in Figure 19, reveal that the new laser has a uniform beam intensity and does not exhibit a sugar-scoop effect.

4. SUMMARY

Boeing's Laser and Electro-Optical Systems organization, and its predecessor Rockwell International and McDonnell Douglas organizations, have been contributing to COIL technology advancements for only slightly less than the 25 years being commemorated by this session. These contributions have come in nearly every aspect of the technologies needed to bring this laser from the laboratory to useful application in a variety of areas. A few of these contributions in the oxygen generator, nozzle, pressure recovery and exhaust management areas were highlighted at the beginning of this paper. The conventional low-pressure subsonic-injection nozzle is probably the most enduring of these earlier contributions.

The ejector nozzle, recently developed for the high pressure sealed COIL, represents both a continuation of Boeing's legacy as the leader in COIL nozzle development as well as a departure from the past, enabling COIL applications that would not have been possible with the earlier technologies. At the same time, Boeing's high pressure sealed COIL represents integration and demonstration of a COIL system incorporating a very advanced high pressure, high performance $O_2(^1\Delta)$ generator; the new nozzle; and a sealed exhaust system. The result is an operating laser system test bed that is new from end to end. The performance of this laser, measured by chemical efficiency, is competitive with the best of the low-pressure helium-based technology, and indications are that significantly more power is available.

* Stephen Hurlock is retired from Boeing and can be reached at (805) 527-8865

REFERENCES

1. W. E. McDermott, N. R. Pchelkin, D. J. Benard, R. R. Bousek, *Appl. Phys. Lett* **32**, 469-470 (1978).

2. R. J. Richardson, C. E. Wiswall, *Appl. Phys. Lett.* **35**, 138-139 (1979).
3. S. C. Hurlock, H. O. Laeger, R. I. Wagner, "Chemically Pumped Iodine Laser" AFWL-TR-79-52 (Rocketdyne Division, Rockwell International, 1979).
4. D. Stelman, U.S. Patent 6,224,786, May 1, 2001.
5. W. E. McDermott, J. C. Stephens, J. Vetrovec, R. A. Dickerson, "Operating experience with high throughput jet generator", SPIE Proc. Vol. 2987, SPIE (SPIE, 1997).
6. J. A. Davis, L. F. Moon, U.S. Patent 4,487,366, December 11, 1984.
7. S. E. Rodriguez, J. P. Maddox, R. J. Netzer, A. Z. Ullman, U.S. Patent 5,735,469, April 7, 1998.
8. J. Vetrovec, U.S. Patent 6,154,478, November 28, 2000.
9. J. Vetrovec, Chemical Oxygen-Iodine Laser with a Cryosorption Vacuum Pump, Photonics West Conference, San Jose (SPIE, 2000).
10. J. Hon, et al., *AIAA Journal* **34**, 1595-1603 (1996).
11. T. T. Yang, Y. C. Hsia, L. F. Moon, R. A. Dickerson, Advanced Mixing Nozzle Concepts for COIL, Gas and Chemical Lasers and Intense Beam Applications III, 2000, San Jose CA (SPIE, 2000).
12. T. T. Yang, R. A. Dickerson, L. F. Moon, Y. C. Hsia, AIAA 2000-2425 High Mach Number, High Pressure Recovery COIL Nozzle Aerodynamic Experiments, 30th Plasmadynamics and Lasers Conference, Denver, CO (AIAA, 2000).
13. T. T. Yang, S. C. Hurlock, R. A. Dickerson, L. F. Moon, Y. C. Hsia, High Efficiency, High Pressure Recovery, High Mach Number Nitrogen Based Chemical Oxygen Iodine Laser, International Conference on Lasers LASERS 2000, Albuquerque, NM (STS Press, McLean VA, 2000).

FIGURES

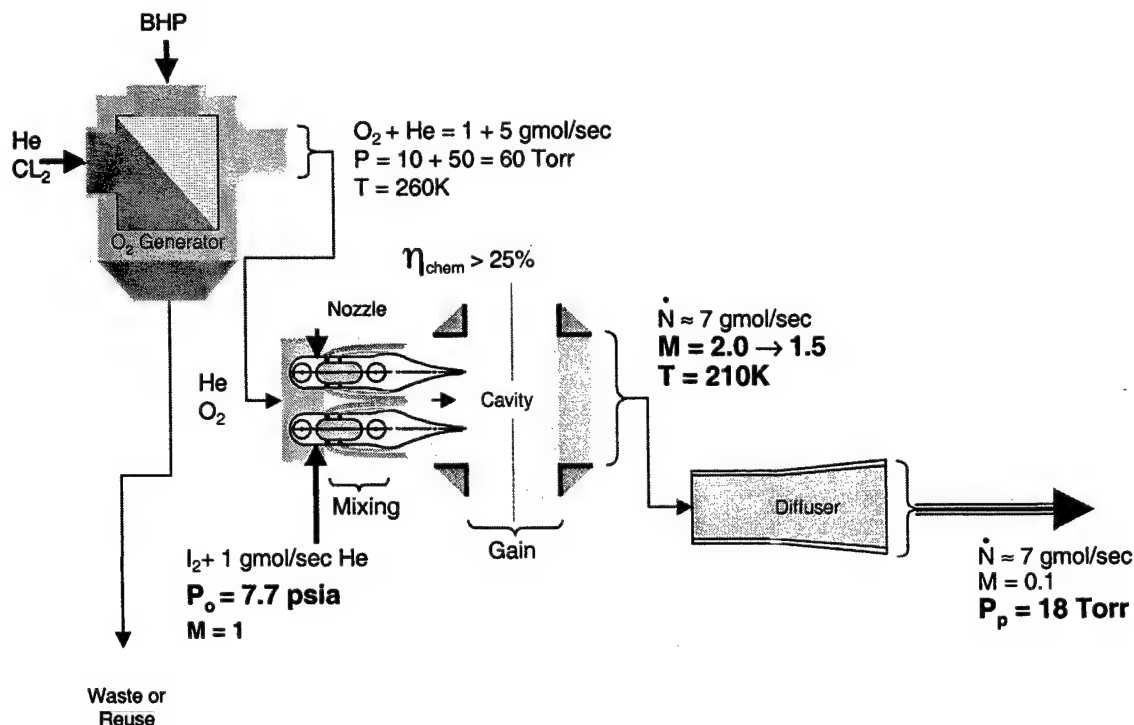


Figure 1. Laser System Based on Low Pressure COIL Technology

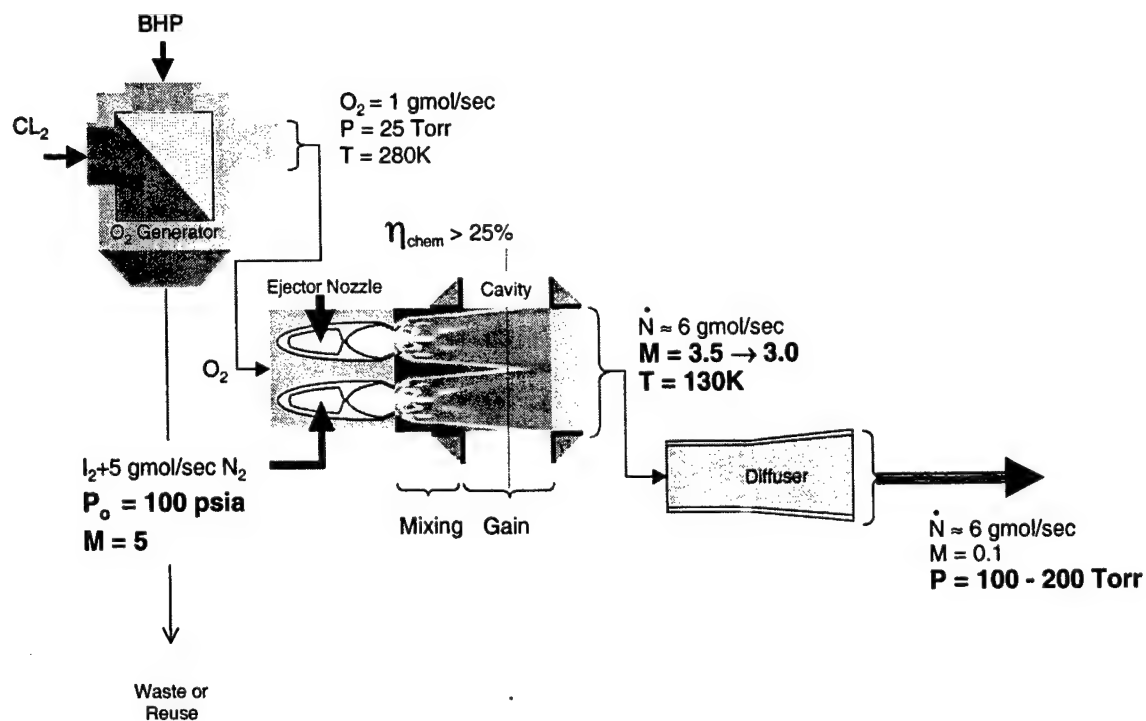
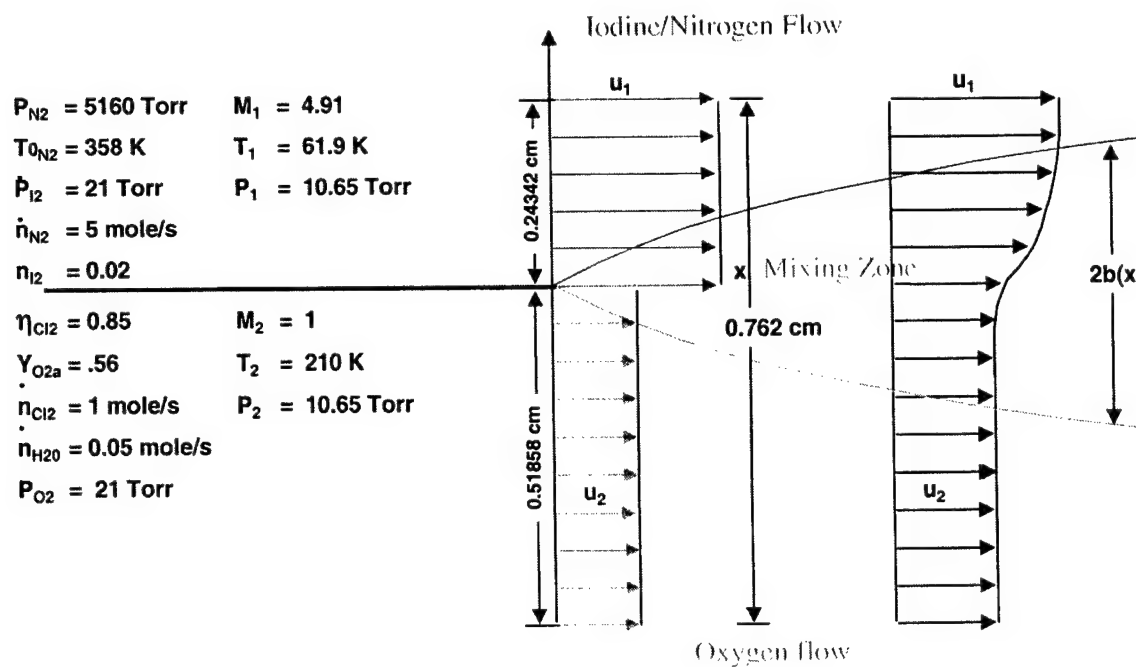


Figure 2. Laser System Based on Next Generation COIL High Pressure Technology



3/97-TTY-045rb

Figure 3. Supersonic Shear Layer Mixing in High Pressure N_2 Diluent COIL

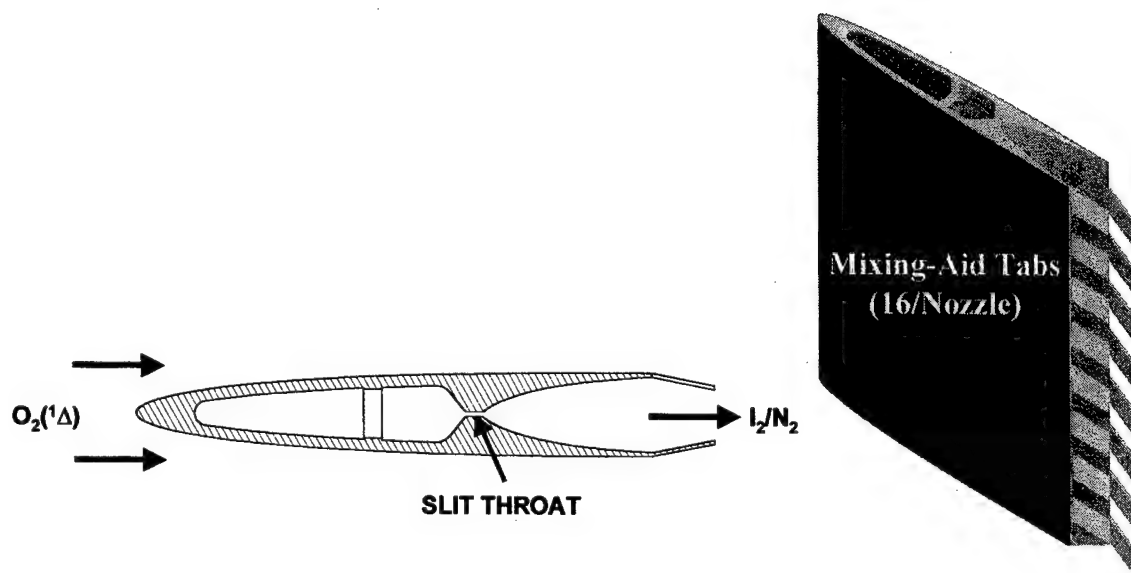


Figure 4. Nozzle Design Based on CFD Analysis

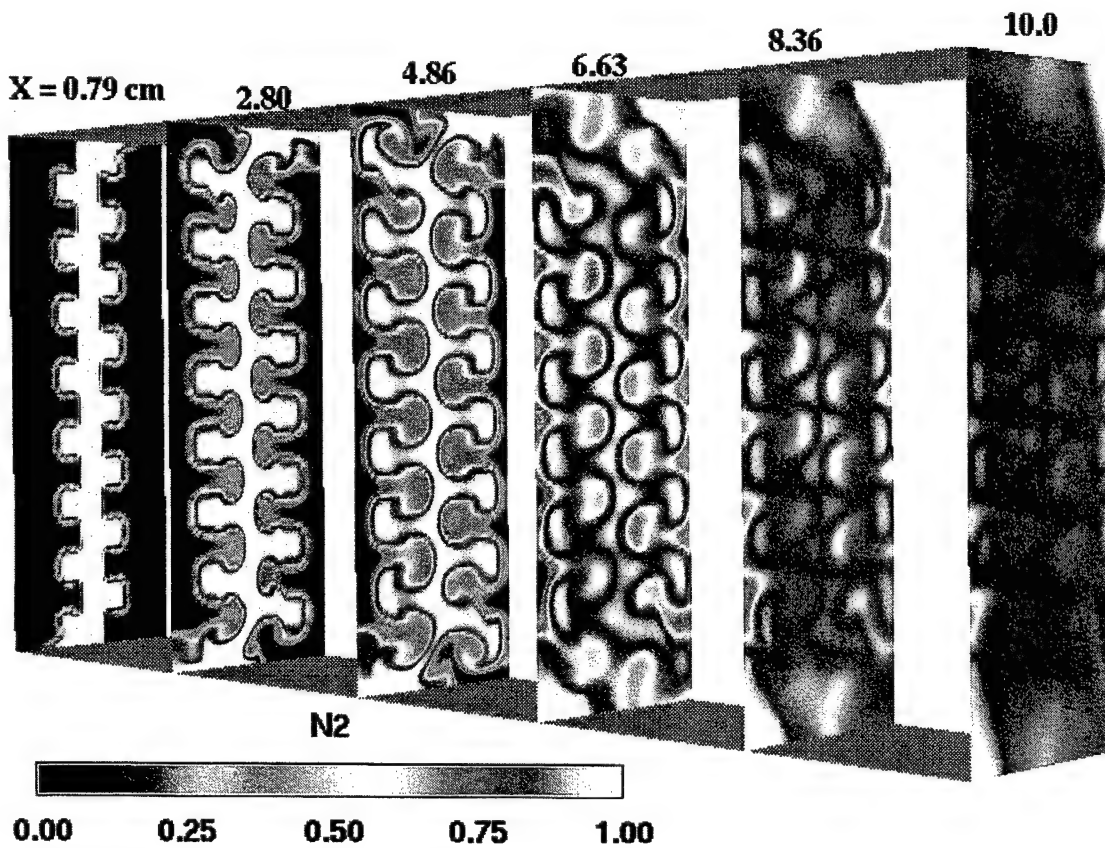
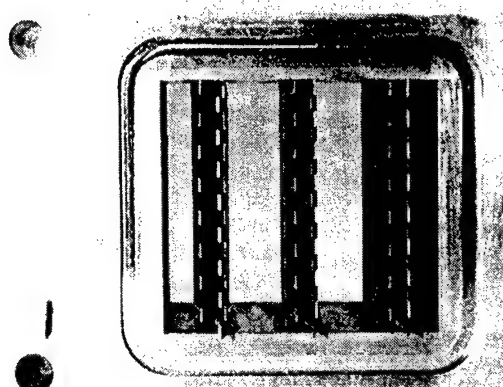


Figure 5. CFD Results for Selected Nozzle Show Excellent Mixing



O₂ & N₂ Exit Side

Horizontal Pitot Scans Downstream of Nozzle Exit Plane

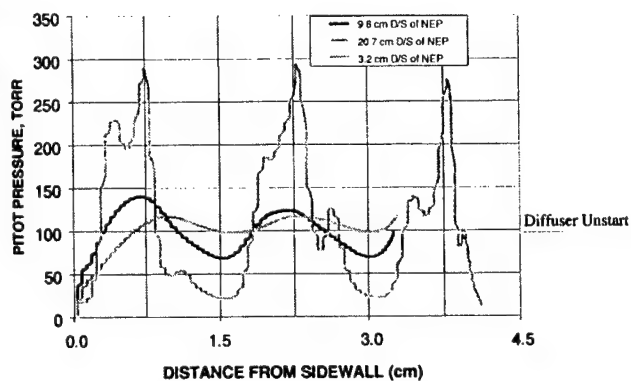


Figure 6. Cold Flow Testing of 3 Blade Test Article Confirms CFD Mixing Results

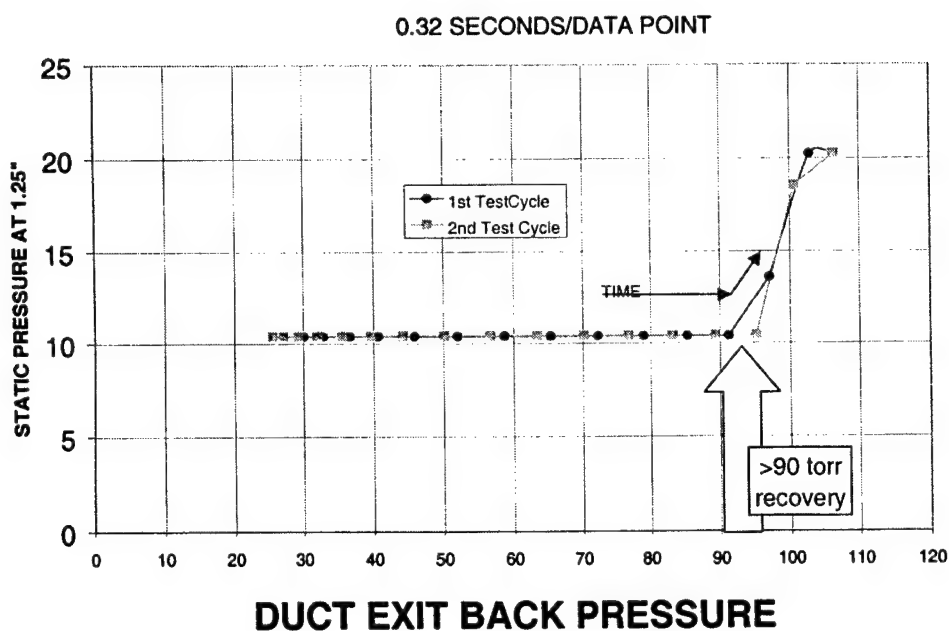


Figure 7. Diffuser Unstart Tests Show ≈ 100 Torr Pressure Recovery

JET OXYGEN GENERATOR

MACH 5 IODINE INJECTION NOZZLE

**PARALLEL WALL
OPTICAL CAVITY**

TRANSITION DUCT

**DIFFUSER
95 TORR RECOVERY**

OPTICAL TUNNEL (2)

**OPTICAL ISOLATION
VALVE (2)**

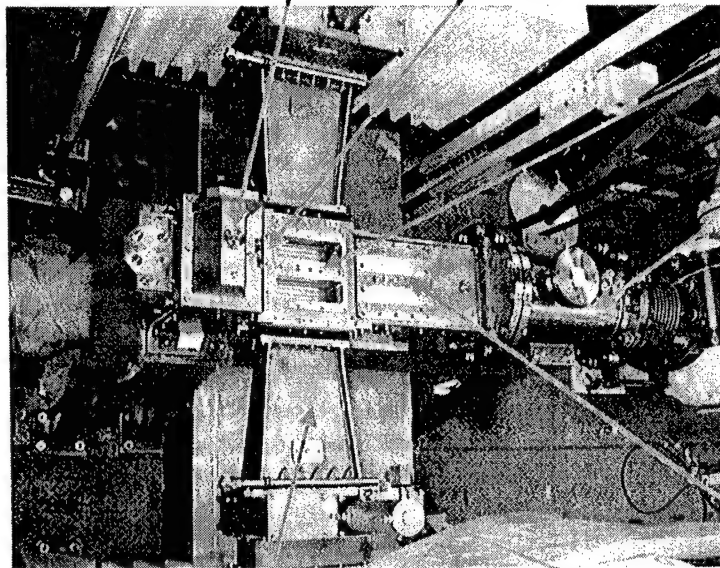


Figure 8. Boeing's New High-Pressure, High Mach Number COIL

Vaporizer (Outside)

Vaporizer (Inside)

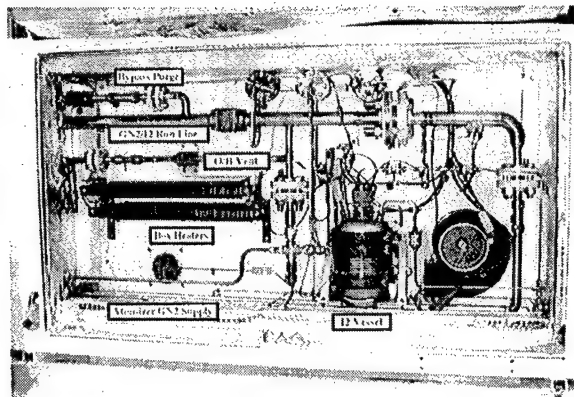
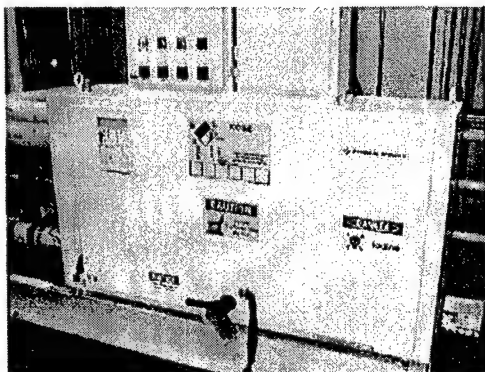


Figure 9. High Pressure Iodine Supply System, Developed for Boeing by General Atomics

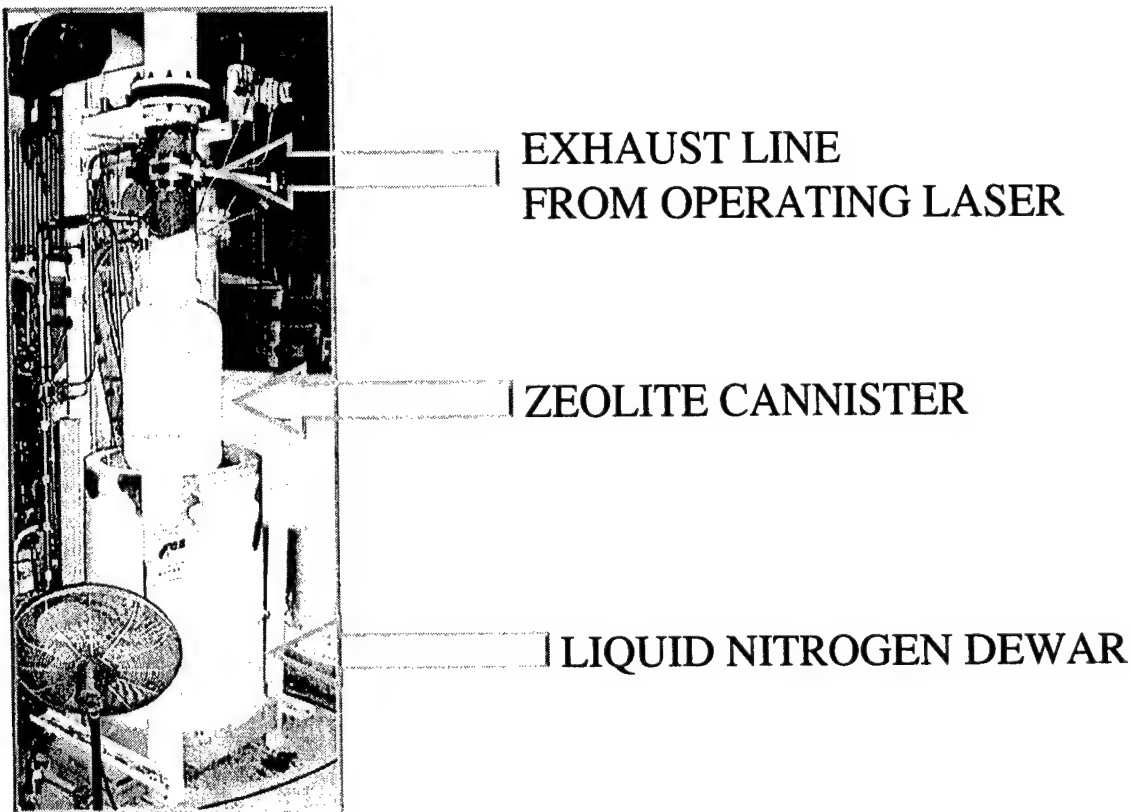


Figure 10. Sealed Exhaust System for Boeing's New High Pressure Sealed COIL

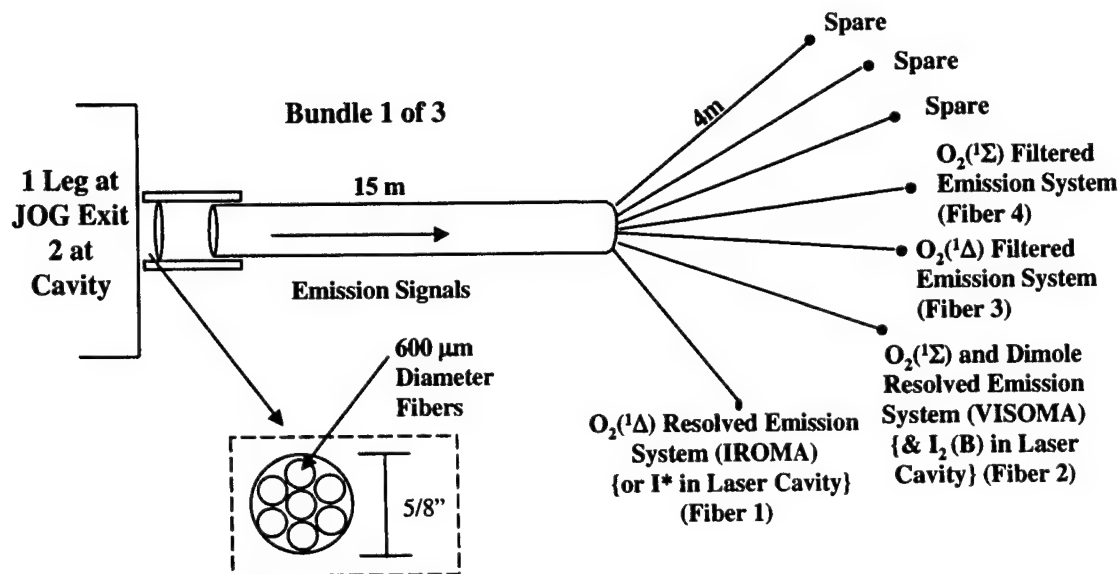


Figure 11. Fiber Bundle Approach for Simultaneous, Co-located Chemical Diagnostic Measurements

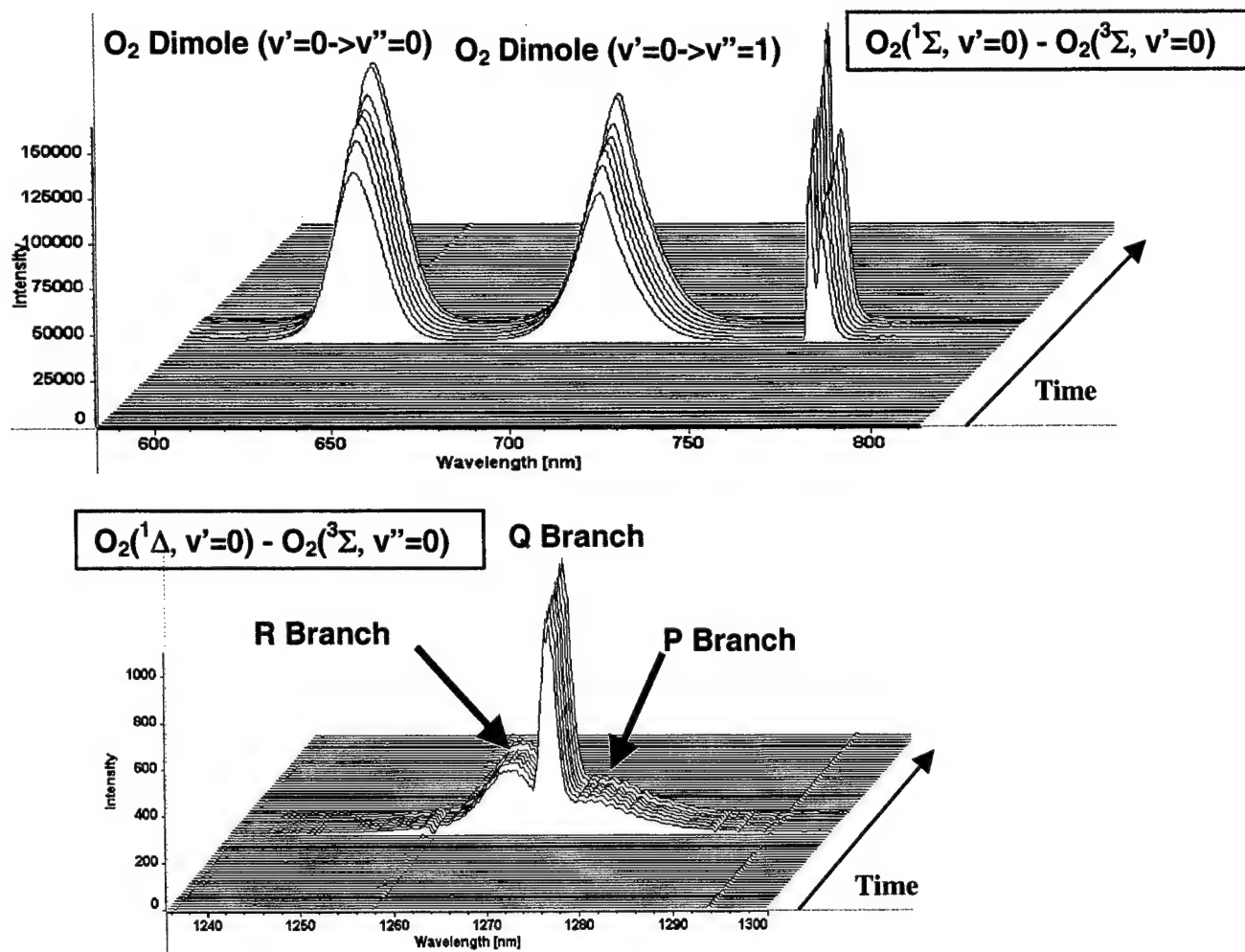


Figure 12. Visible and Infrared Optical Multichannel Analyser Spectra of Generator Outlet

- Outlet Pressure = 21 Torr, Controlled by Nozzle
- Outlet Temperature = 342 K
- Chlorine Utilization = 0.89, Cl₂ Pressure = 2.2 Torr
 - From absorption/scatter measurements: average windows, average T
 - Consistent with BHP temperature rise
 - Consistent with mass spectrometry via O₂ / N₂
- O₂($^1\Delta$) Yield \approx 0.6 - 0.7
 - From filtered and OMA emission: average [Cl₂], average T
 - Consistent with JOG Raman measurements: 0.64
- H₂O pressure = 1.4 Torr (1 Torr Typical)
 - From absorption measurements: average T
- Gas Bypass with BHP Effluent, \leq 2%
- Liquid Content of Gas Product - nil

Figure 13. O₂($^1\Delta$) Generator Performance Averaged Over All 0.9 gmol/s Tests

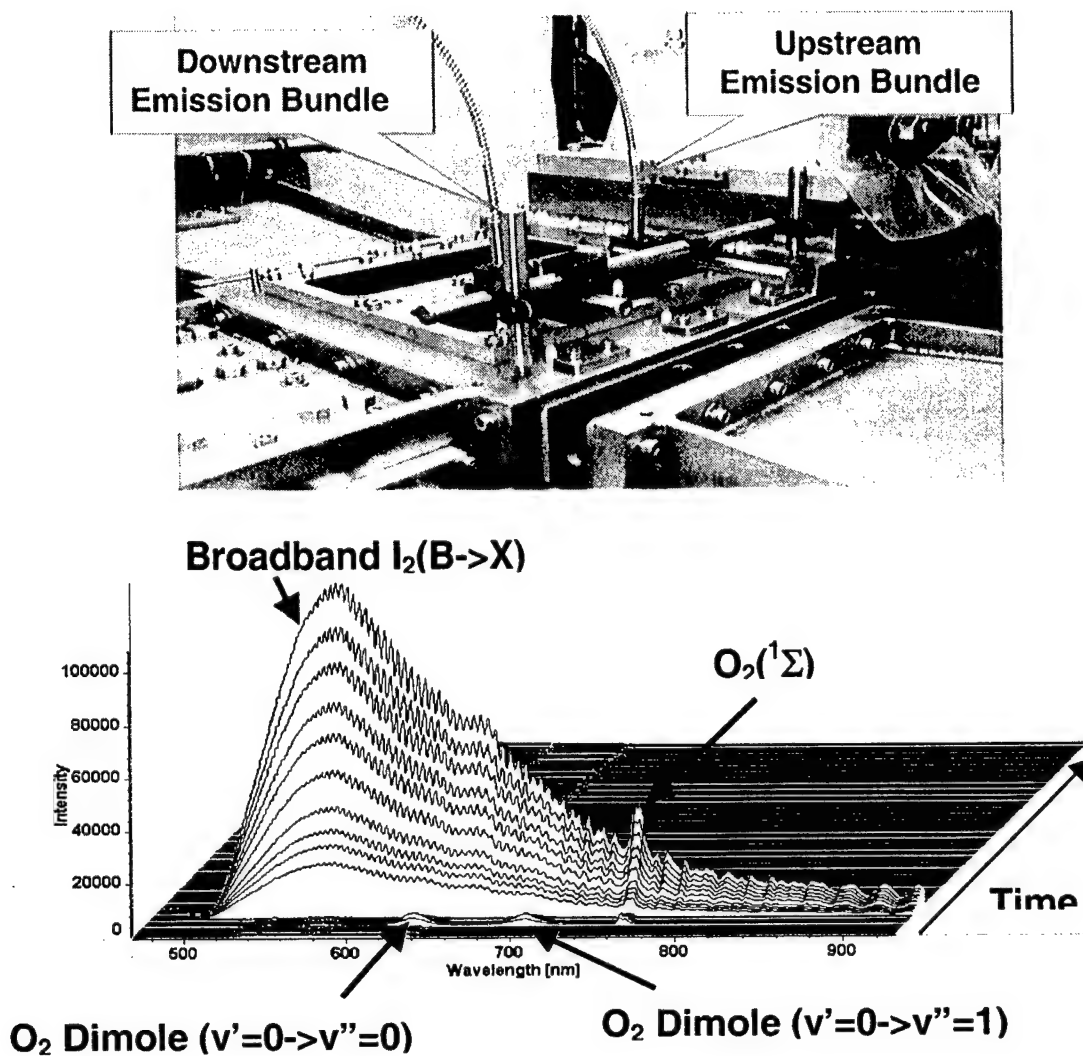


Figure 14. Cavity Visible Emission Spectra

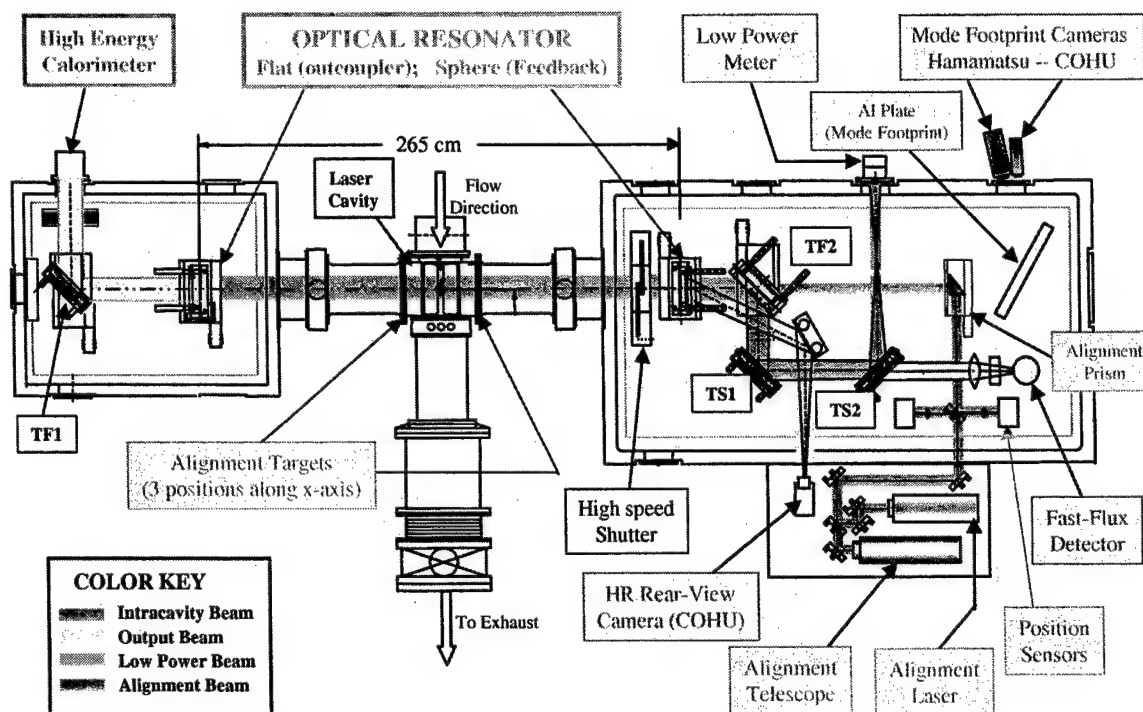


Figure 15. Layout of Optical Diagnostics System, Including Resonator

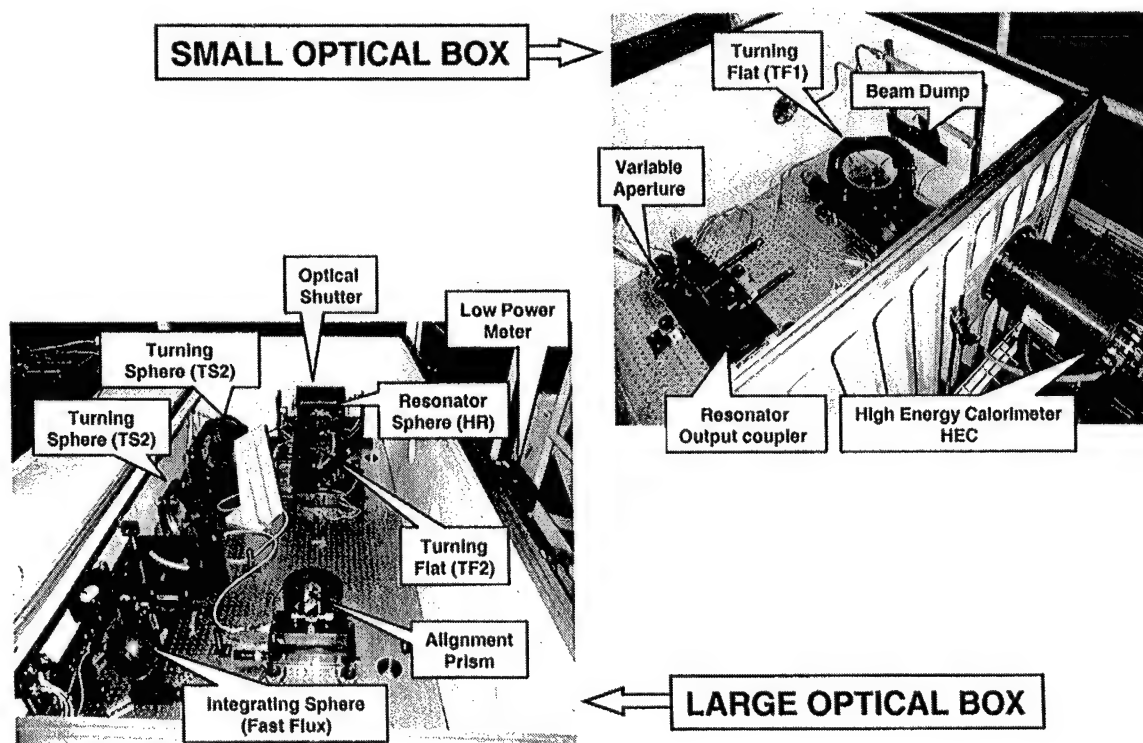


Figure 16. Interior of Optical Boxes, Showing Optical Diagnostics

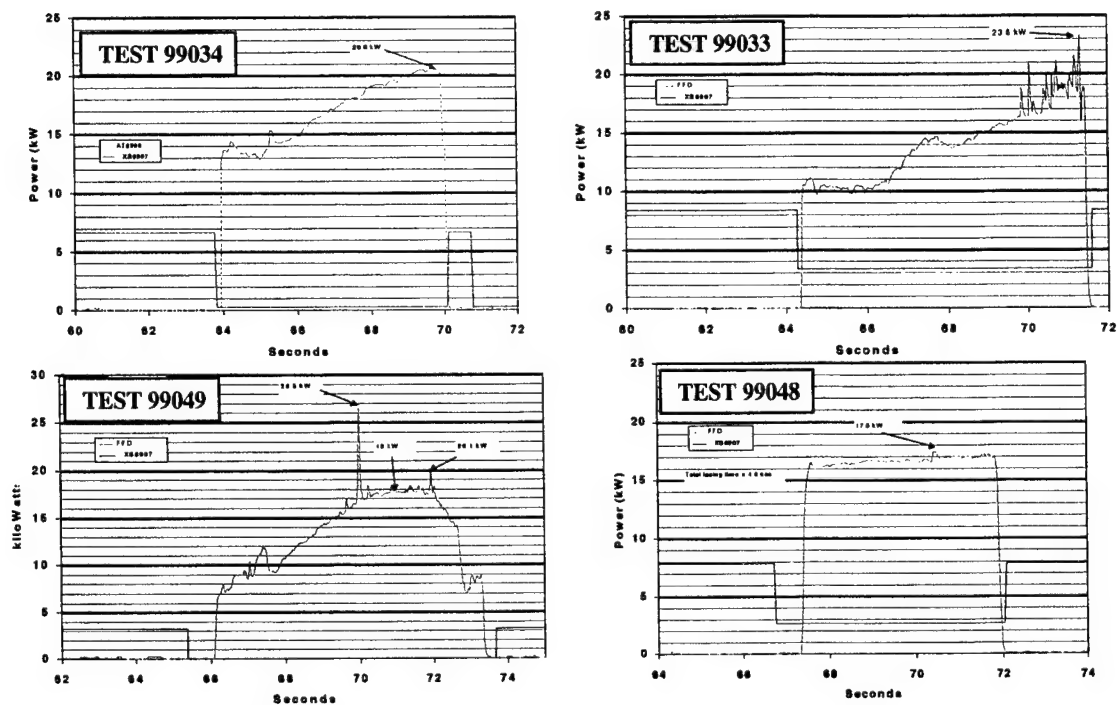


Figure 17. Some Typical Power vs. Time Scans from the Fast Flux Monitor

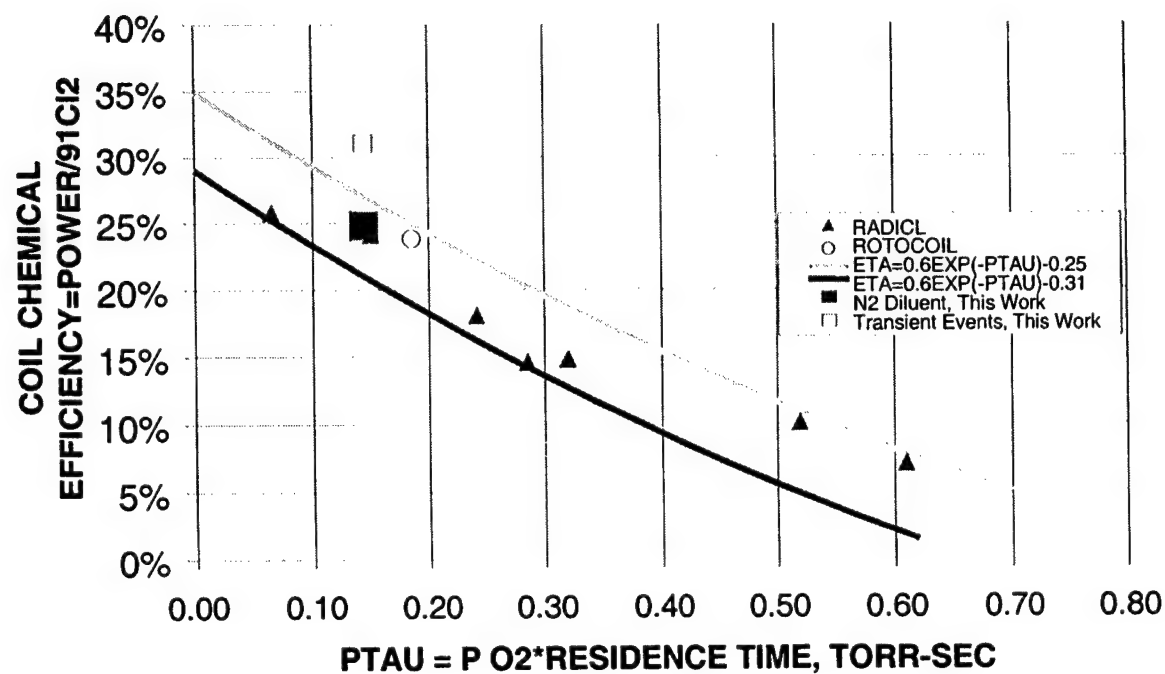


Figure 18. New N₂ Laser Performance is Comparable with Helium Diluent Chemical Efficiency

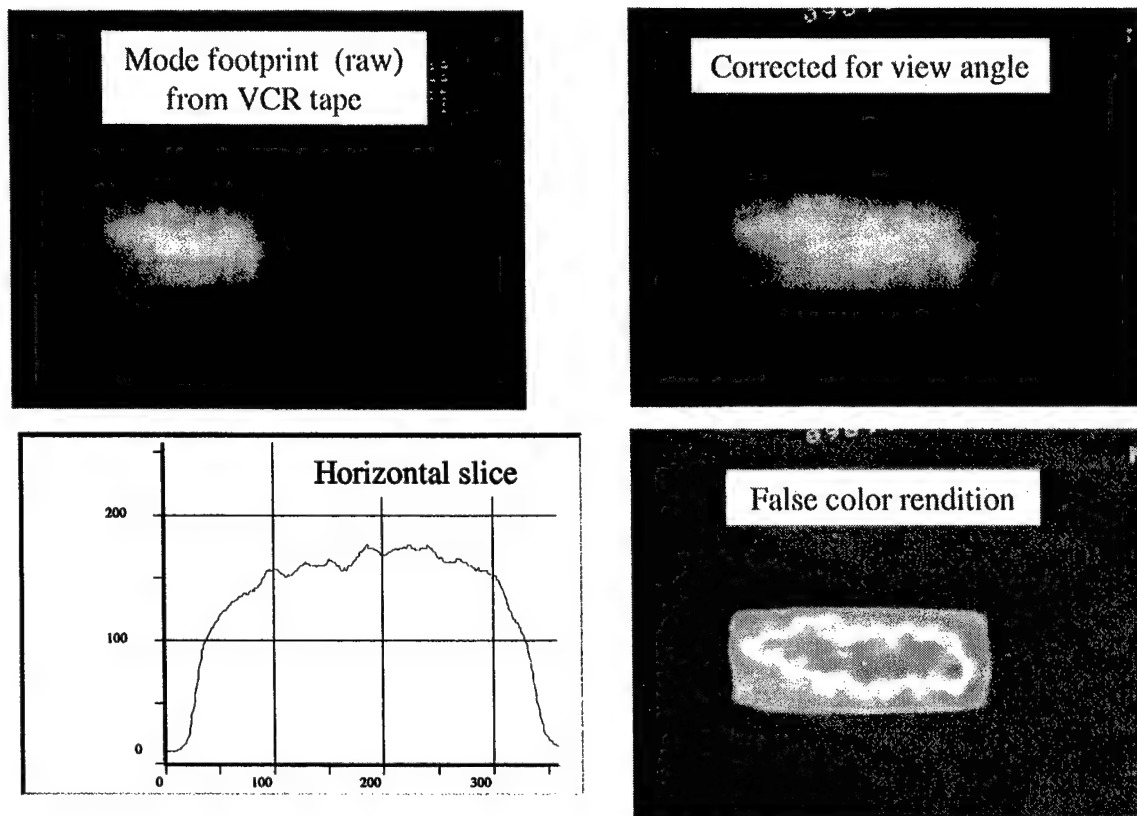


Figure 19. Results from Mode Footprint Camera Show Uniform Beam Intensity

History of COIL development in Japan: 1982-2002

Masamori Endo^{♦A}, Taro Uchiyama^B, Kenzo Nanri^A,
Shuzaburo Takeda^C and Tomoo Fujioka^A

^ADepartment of Physics, Tokai University, 1117 Kita-Kaname,
Hiratsuka City, 259-1292, Japan.

^BDepartment of System Design Engineering, Keio University,
3-14-1, Hiyoshi, Kohoku-ku, Yokohama, 223-8522, Japan.

^CDepartment of Electro-Photo Optics, Tokai University

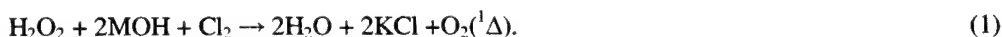
ABSTRACT

A twenty-years of COIL researches and developments in Japan are reviewed. The researches of four major sites, namely, Keio University, Industrial Research Institute, Kawasaki Heavy Industries and Tokai University are presented in order of time. Epoch-making works are highlighted, and the significance of those works in the industrial COIL development is discussed. Finally, current status of COIL researches in Japan is introduced.

Keywords: iodine laser, COIL, Japan, history

1. INTRODUCTION

Chemical oxygen-iodine laser (COIL) is a continuous-wave chemical laser operating at 1.3μm. The principle of COIL is briefly described as follows. Hydrogen peroxide is mixed with some alkali (normally KOH or NaOH) and prepared in a vessel. The solution is called a BHP (basic hydrogen peroxide). Cl₂ gas is provided in it to produce singlet oxygen O₂(¹Δ) by the following reaction,



Water vapor is released from BHP together with O₂(¹Δ) and should be removed since it is a strong quencher of the lasing species, I(²P_{1/2}). Singlet oxygen is then mixed with iodine molecule vapor. Iodine is dissociated by the collisional energy transfer from O₂(¹Δ). The iodine atom is then excited to the first electronically excited state by the subsequent collision with O₂(¹Δ), and lasing is obtained between (²P_{1/2}) - (²P_{3/2}) levels of iodine. The I₂/O₂ ratio of typical COIL is a few percent and an iodine atom is excited many times in the laser cavity. The reactions are summarized as follows,



Chemical efficiency is defined by the following formula,

$$\eta_c = \frac{[\text{LaserOutput(W)}]/h\nu}{[\text{Cl}_2 \text{ mol flow(mol/s)}]N_A} \times 100 \quad [\%]. \quad (5)$$

♦ Correspondence: Email: endo@tokai.ac.jp; Telephone: +81-463-58-1211 Ext. 3721;

In principle, a Cl_2 molecule produces an $\text{O}_2(^1\Delta)$ (eq.1) and that excites an iodine atom (eq. 3), then it produces a laser photon (eq. 4). Therefore, chemical efficiency is the quantum yield of the comprehensive chemical processes involved in COIL. It is very often used to measure the performance of a COIL device.

2. BEGINNING – EARLY 1980'S

The Faculty of Science and Technology, Department of Electric Engineering, Keio University has a long history of research in gas lasers that goes back to 1960's. At the time when the laser laboratory was led by Fujioka, one of his interests was the photochemical iodine laser. Therefore, it was a natural consequence that he started the research of COIL shortly after the first demonstration of lasing by the United States Air Force.¹

Although the COIL was considered as a candidate of directive energy weapons (and is going to be realized soon), Fujioka was aware of its usefulness as an industrial laser from the very beginning of the COIL history. At the same time, Watanabe, who was a graduate student of Keio University Laser Laboratory, started his career at the National Defense Academy in Japan with the research of COIL, too. Japanese COIL history started with a race between a teacher and his student.

The student reached the finish line first. The first oscillation of COIL was obtained by Watanabe *et al.*² in 1982. Shortly after, Keio University also succeeded in lasing by Serizawa, Uchiyama and Fujioka *et al.*³ Figure 1 shows the singlet oxygen generator (SOG), water vapor trap, and optical cavity of the Watanabe's apparatus. The constructions of the both COILs were so-called Bachar-Rosenwaks type,⁴ which was the typical design in the early 80's. According to the Watanabe's first report, the output power was 12W and chemical efficiency was 4.4%. Watanabe measured the property of the laser medium by the variable-loss optical cavity.⁵

Keio group's interests were oriented to the industrial applications from the very beginning of their studies. It must be emphasized on that in the early 80's, the use of COIL as an industrial laser was not widely accepted and Keio University pioneered the industrial COIL development. They have already demonstrated the optical fiber transmission of COIL output in 1983.⁶ To say the chemical efficiency, their early apparatus obtained 16.8% at an output of 105W from a $25 \times 1 \text{ cm}^2$ flow duct.⁷

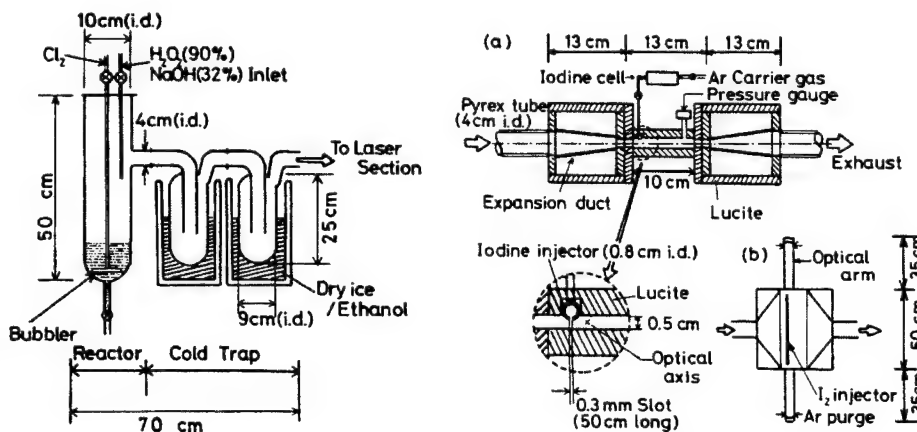


Fig. 1: The first COIL in Japan²

3. KHI & IRI – LATE 1980'S

There was a remarkable movement in Japanese COIL history in 1986. Fujioka resigned Keio University and started-up a laser research center at Industrial Research Institute (the institute renamed itself as Institute of Research and Innovation in 1989). One of the objectives of the IRI Laser Laboratory was to offer the research site for national research programs of high-power industrial lasers. The well-known 20kW CO laser for decommissioning and dismantlement of nuclear power plants (D&D)⁸ was originated here. A five-year project of industrial COIL development also started up at the IRI Laser Laboratory, and the program was shared with Kawasaki Heavy Industries

(KHI). The goal of the project was the development of the world's first industrial COIL at 1kW output, all-day-long operation capability.

Initially, the research program was led by Yoshida. Yoshida modified the bubbler type SOG to improve the performance of the SOG that used dilute hydrogen peroxide. Although eq. (1) produces singlet oxygen at an efficiency of 100%, not all the oxygen is yielded in the ($^1\Delta$) state because of the quenching reactions in the liquid phase. It was believed that dense ($>60\%$) H_2O_2 should be used for the efficient yield of $O_2(^1\Delta)$.

The use of dilute hydrogen peroxide is crucial for industrial applications. In Japan, the hydrogen peroxide of equal to or less than 35wt% was much less restricted for usage, storage, and conveyance. Figure 2 shows the IRI's first COIL apparatus.⁹ Dense array of bubbler tubes close to the BHP surface is seen. Finally, Yoshida claimed (and not widely believed) that a 40% of chemical efficiency was obtained at an output power of 200W, using a 35wt% hydrogen peroxide.¹⁰

The IRI COIL apparatus was scaled up to a 1kW device,¹¹ then the know-how was transferred to KHI to make a commercial COIL device. The COIL research at IRI Laser Laboratory ceased in 1991.

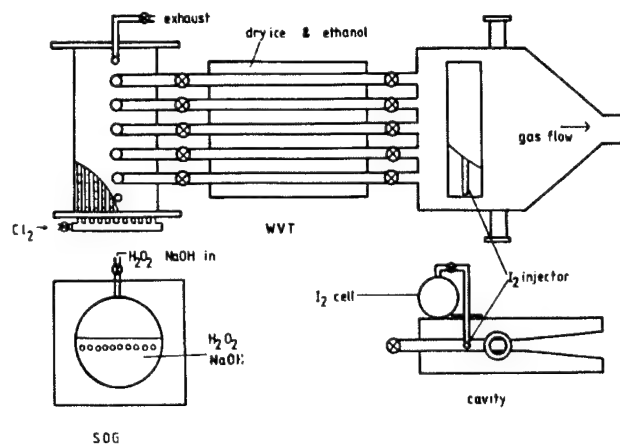


Fig. 2: IRI's first COIL: the origin of the commercial COIL.⁹

4. KEIO UNIVERSITY – 1990'S

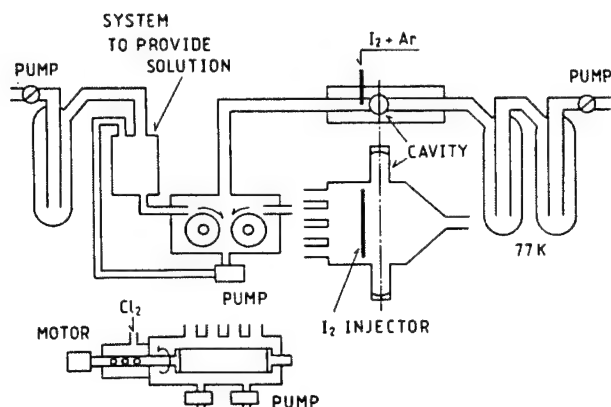


Fig. 3: Porous pipe SOG and COIL without a water vapor trap¹³
the porous pipe SOG and COIL without a water vapor trap. An output power of 87W with a chemical efficiency of 7.8% was obtained.^{13,14}

The unique porous-pipe SOG led Uchiyama to another application: pulsed high-pressure SOG. The principle of the pulsed SOG is as follows; first, the surface of the porous pipe is kept wet with BHP in a closed chamber. Then Cl_2 gas is injected to the inside of the porous pipe at a blast. The Cl_2 gas penetrates to the surface, react with the BHP at the surface of the pipe, and fill the chamber instantaneously with $O_2(^1\Delta)$. In this way, a 35Torr $O_2(^1\Delta)$ pressure was

It can be said that Keio group rather stepped aside the main stream of the industrial COIL development in 1990's. Nevertheless, a number of unique works have been done during this decade.

In the early COIL devices, the unwanted byproduct of the SOG, water vapor, was removed by the cold trap (see Figs. 1 and 2). Uchiyama considered that the necessity of the water vapor trap inevitably prevents long-term operation of COIL, and should be removed. Uchiyama's strategy was the deep cooling of BHP (close to $-30^\circ C$), and use of a porous pipe SOG¹² that was effective at very low BHP temperature. Figure 3 shows the schematic of

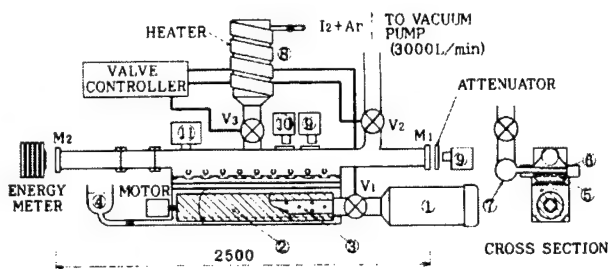


Fig. 4: Pulsed COIL.¹⁶ 1:Cl₂ tank 2:Porous pipe 3:Perforated inner tube 4:Solution (H_2O_2+KOH) 5:Air filter 6:Iodine injectors 7:Manifold 8:Prechamber 9:Ge photodiode 10:Si photodiode 11:Pressure gauge

observed in a very short period.¹⁵ The world's first pulsed COIL was developed using this SOG.¹⁶ An ambitious study, observation of lasing from $O_2(^1\Delta)$ directly, was tried using this pulsed SOG.¹⁷ According to the theoretical calculation, a 6-m active volume length should produce a realistic positive gain even $O_2(^1\Delta)$ to $O_2(^3\Sigma)$ is a strictly prohibited transition. However, the experiment resulted in unsuccessful.

Q-switching¹⁸ and magnetic gain switching¹⁹ were studied at Keio University. Because COIL is an energy transfer laser, the lasing species has only a few percent of the extractable energy. Therefore, those switching methods do not work as efficient as say, CO_2 laser. Nevertheless, an 11 times enhancement in Q-switching regime, and a 3.3 times enhancement in magnetic gain switching were obtained respectively.

Intracavity second harmonic generation was studied at Keio University. The objective of this study was to get the more valuable visible light than infrared at an efficiency of 100%. The idea of the intracavity SHG is to place a SHG crystal inside the laser cavity and use dichroic mirrors (total reflector for fundamental and transparent to the second harmonic) for optical cavity. Because only the converted light can escape from the optical cavity, the SHG crystal acts as an output coupler. Therefore, 100% conversion efficiency is expected. The obtained output power was 16.1W in TEM_{00} mode,^{20,21} and the conversion efficiency was estimated to be nearly 100%. It means that the second harmonic output was the same as the fundamental output in which an optimized partial reflector was used and the SHG crystal was removed.

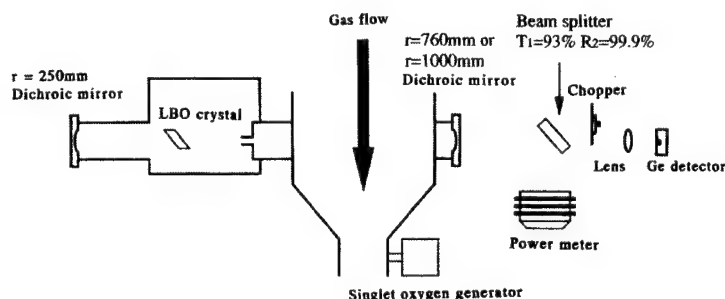


Fig. 5: Intracavity SHG of COIL²¹

Iodine predissociation was studied at Keio University. In the first step of the oxygen-iodine reactions (see eq. 2), approximately 10% of the $O_2(^1\Delta)$, that have the capability of pumping iodine, is used merely to dissociate iodine molecules to atoms. Therefore, substituting the dissociation with external energy enhances the output power of COIL because more $O_2(^1\Delta)$ survives to the laser cavity than conventional COIL. The point is that the theoretical limit of enhancement is not limited to 10% because there is an oscillation threshold of $O_2(^1\Delta)$ yield in COIL same as the other lasers. The extractable power P_{ext} from the singlet oxygen flow can be expressed as

$$P_{ext} = \dot{m} E \eta_q (Y - Y_{th} - Y_{dis}), \quad (6)$$

where \dot{m} is the oxygen flow rate [mol/s], E is the energy of singlet oxygen per unit quantity [J/mol], η_q is the quantum efficiency of the energy transfer (0.97), Y is the yield of the oxygen, Y_{th} is the lasing threshold yield, and Y_{dis} is the part of the singlet oxygen necessary for iodine dissociation. Y is 0.4 to 0.6 for the typical SOGs. We assume Y to be 0.5, Y_{th} to be 0.2 (for subsonic COIL), and Y_{dis} to be 0.1. In this case, the extractable power comes to $P_{ext} = 0.2\dot{m}E\eta_q$. If we completely substitute the dissociation energy with the external source, Y_{dis} is no longer subtracted and the extractable power becomes $P_{ext} = 0.3\dot{m}E\eta_q$. Therefore, approximately 50% of output power enhancement is expected by the external iodine dissociation.

Uchiyama used an RF discharge to dissociate iodine and applied the technique to their subsonic COIL. As a result, chemical efficiency was improved from 4% to 12%.²²

5. KHI – 1990'S

KHI started the development of industrial COIL with IRI in the late 80's.^{23,24} The national project delivered the world's first commercial COIL in 1992.²⁵ The device was sold to the Applied Laser Engineering Center (ALEC), and it is still available for value. The remarkable capability of the device was the eight hours of long-term operation at a stable

($\pm 2\%$) output power of 1kW. To cope with the water vapor trap clogging, KHI developed a breakthrough disk type water vapor trap as seen in Fig. 6. Because the ice deposited on the surface of the disks are continuously removed by the scraper, the cross section of the gas flow duct is kept constant. As far as we know, this device is still holding the continuous-operation time record.

After the successful end of the national project, KHI continued the development of COIL. It was the time that the U. S. Air Force demonstrated the supersonic COIL operation.²⁶ The application of supersonic expansion has significant advantages for industrial COIL, too. Especially, high output power scalability and high output power per unit width of the flow duct leads to a realistic industrial device at an output range of >10kW. In addition, the requirement of the high-pressure SOG operation removed the necessity of the water vapor trap, because the water vapor pressure is limited to the saturation vapor pressure of water in spite of the increased operating pressure. However, the traditional bubbler type SOG could not operate at higher pressure than a few Torr. KHI have selected the application of transverse type jet SOG for their supersonic COIL. In 1996, they have obtained an output power of 10kW.²⁷ and 12kW was recorded in 1999. This remarkable output was obtained with a very high efficiency, $\eta_c=26\%$. Moreover, the output power was stable for more than 30 minutes.

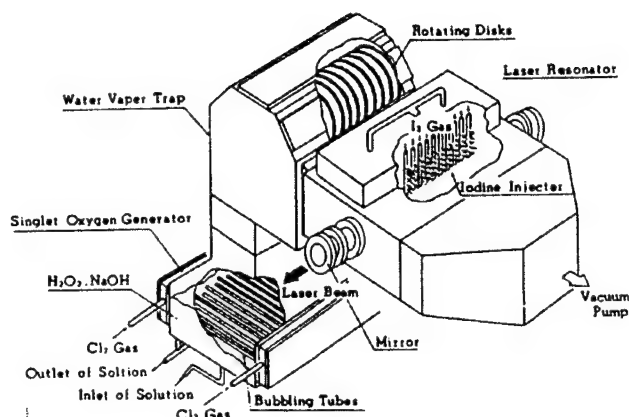


Fig. 6: KHI's subsonic COIL with a rotating-disk type water vapor trap.²³

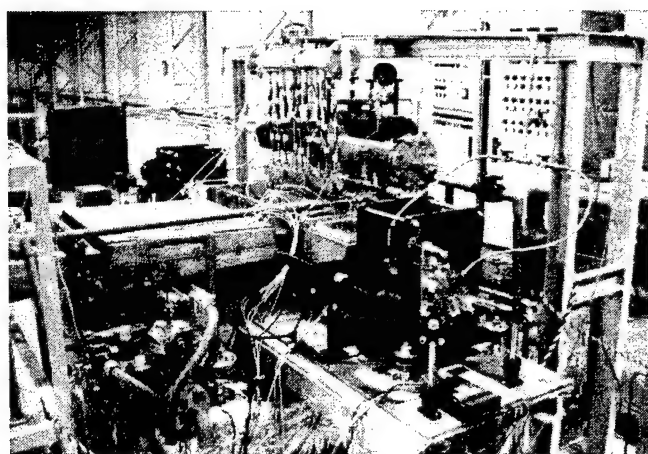


Photo 1: KHI's supersonic COIL operating at 12kW.

to D&D is obvious. In addition, the wavelength of $1.3\mu\text{m}$, that is ideal for optical fiber delivery, is suitable for remote, unmanned cutting. Needless to say that the high-power capability and high beam quality of COIL is advantageous for cutting of thick steel or concrete. KHI conducted number of studies²⁸⁻³⁰ for material processing of COIL. They have proposed an empirical formula that predicts the cutting performance of very thick materials.³¹

Recently, KHI demonstrated an underwater cutting of thick steel specimen by the COIL through optical fiber delivery.³² At an output power of 7kW, cutting capability for stainless steel workpiece was up to 80mm of thickness.

It was not only the COIL development itself but also the applications of COIL that were pursued at KHI. Because COIL is a chemical laser, its application to the D&D is very promising. Since no high-power electricity is required for COIL and the nuclear power plants are usually settled in remote places, its advantage

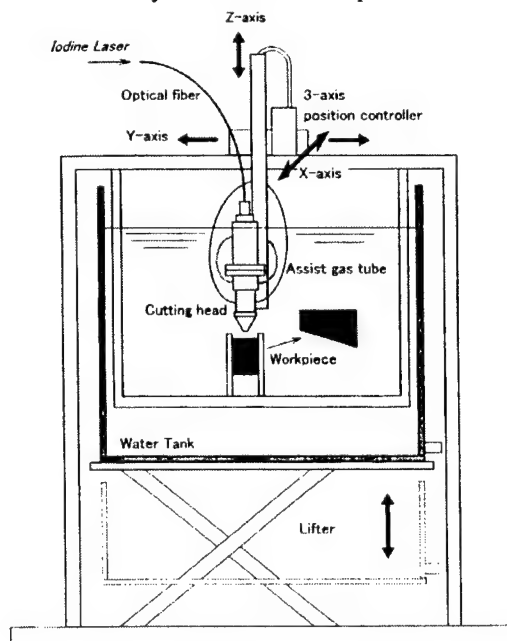


Fig. 7: Experimental setup of the COIL D&D – underwater cutting with optical fiber delivery of laser power.³²

6. TOKAI UNIVERSITY - 1996~

The history of COIL research at Tokai University began in 1996, shortly after Fujioka moved to Tokai University and started up a laser research laboratory. Tokai University COIL research group took up a research program sponsored by NEDO (New Energy and Industrial Technology Development Organization) together with KHI. The goal of the program was to show the feasibility of the "Optical Power System"³³ (See Fig. 8). The name implies the use of laser power like today's electricity. High-efficiency operation of supersonic COIL, output power enhancement by using microwave discharge, output power control, optical fiber transmission, high beam quality resonator, and reuse of BHP were studied.

To start up COIL research at Tokai University, Zagidullin was invited and their counter-flow jet type SOG technology³⁴ was transferred. It was soon after the start-up of the project that the very high chemical efficiency (23.4%) of the supersonic COIL using nitrogen as buffer gas was obtained.³⁵ At that time, supersonic COILs were operated using helium as buffer gas to

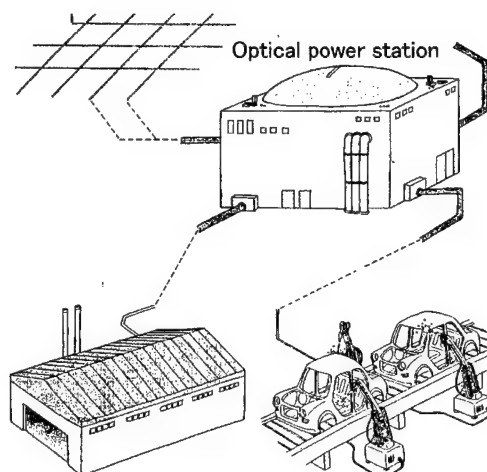


Fig. 8: Schematic drawing of the "Optical Power System".³³

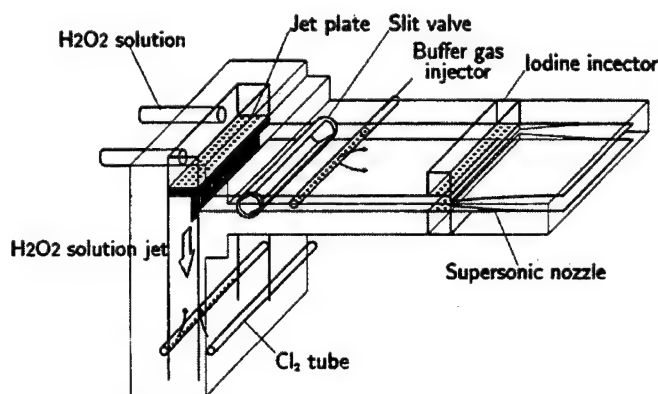


Fig. 9: SOG, iodine injector and supersonic nozzle of the Tokai University's first COIL.³⁵

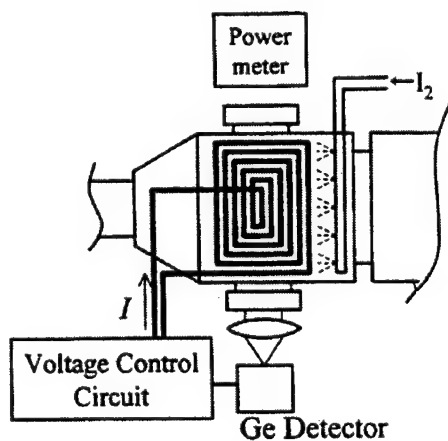


Fig. 10: Output power stabilizing system of COIL.³⁶

obtain supersonic expansion. The result showed that inexpensive nitrogen could be also used for supersonic COIL and that could dramatically reduce the operation cost. Figure 9 shows the first version of Tokai University's COIL apparatus.

Sugimoto demonstrated the output power stabilization and modulation of COIL for the first time using Zeeman effect. Figure 10 shows the schematic. The laser power is monitored by a photodetector, whose output signal is compared to a reference signal to produce an actuating error signal. The actuating error signal is then fed into the control unit of the variable dc power supply connected to the electromagnet, to change the magnetic field intensity. In this manner, the feedback system attempts to reduce the actuating error signal in order for the output power to follow the reference signal.

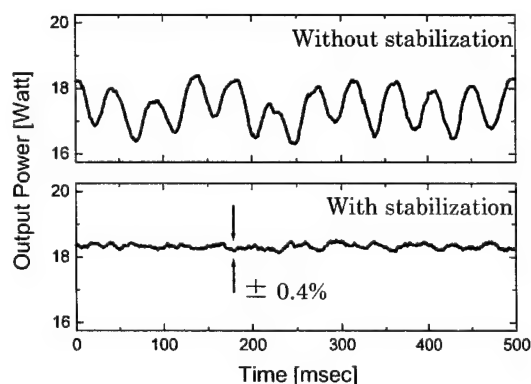


Fig. 11: Output power stabilization of COIL. Top: Fluctuated output by the added vibration. Bottom: Stabilized output.³⁶

Therefore, one can stabilize or actively modulate the output power to an arbitrary waveform. Figure 11 shows the typical result. An artificially generated output power fluctuation was stabilized within 0.4%.³⁶ COIL output was modulated to an triangular waveform at 20Hz.³⁷

Wani demonstrated the operation of COIL in a high-pressure subsonic regime.^{38,39} Although the supersonic operation was the major breakthrough of the COIL, the requirement of larger vacuum pump than subsonic regime is undesirable for many applications. Especially, the major advantage of COIL over electrically excited lasers, the mobility may be deteriorated by the large vacuum pump. The motivation of the high-pressure subsonic operation was the drastic reduction of vacuum pump by means of increasing the operation pressure of COIL and reducing the amount of buffer gas that was necessary to operate COIL in supersonic regime. The high-pressure operation capability of jet SOG was helpful for this operation regime. The main advantage of high-pressure subsonic regime to the good old subsonic COIL is device size and water vapor trap requirement. Thanks to the high-pressure operation of SOG, no water vapor trap was required upstream the laser cavity. The area of the flow duct per output power was the same as the supersonic COIL because the high pressure compensated the slow flow velocity. In fact, the subsonic COIL that used the same flow duct as the supersonic COIL obtained a higher output. The pressure at the laser cavity was 6Torr, and the chemical efficiency reached to 25%. Finally, the subsonic operation at 12Torr using a larger device was demonstrated.⁴⁰

In 1997, Tokai University and VNIIEF (Russian Federal Nuclear Center) conducted a joint research of a unique SOG, twisted aerosol SOG (TA-SOG).⁴¹ That was a part of ISTC (International Science and Technology Center) program. It was demonstrated that the TA-SOG had the potential to obtain much higher operating pressure than jet SOG without BHP mist entrainment. Now VNIIEV group demonstrated a quite high-efficiency ($\eta_c \sim 30\%$) operation of COIL using TA-SOG.⁴²

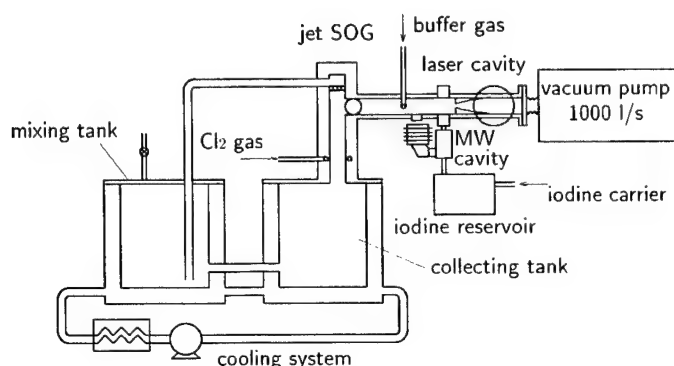


Fig. 12: Output power enhancement of COIL with a microwave discharge.⁴³

trying an elaborated mixing scheme proposed by Masuda,⁴⁵ however, not yet successful to obtain as good output power as conventional supersonic COIL.

Possible applications of COIL were discussed at Tokai University. Sugimoto conducted the drilling of some nonmetallic materials (concrete, wood, rock, etc...) to assess the capability of COIL for the use of civil engineering and rescue for the disaster.⁴⁶ Tei discussed the conceptual design of a D&D COIL based on the current COIL technology.⁴⁷

7. DEVELOPMENT OF SOG

Singlet oxygen generator has been extensively studied from the very early days of COIL research in Japan. The very high efficiency operation of COIL with dilute BHP¹⁰ owed to the Yoshida's modified bubbler SOG. Yoshida also studied an aerosol type SOG.⁴⁸ Although he obtained a good singlet oxygen yield (80%), the problem of the aerosol separation from the gas flow was left unsolved.

The predissociation of the iodine molecule was studied at Tokai University, too. In the early research Endo pointed out theoretically that the supersonic COIL with subsonic mixing regime is unsuitable for the predissociation of iodine, because the dissociated iodine is a very fast quencher of $O_2(^1\Delta)$ and iodine must be in molecular state before the expansion. Soon after that, Endo demonstrated the transonic mixing of dissociated iodine⁴³, and supersonic injection of dissociated iodine⁴⁴ to reduce the mixing point pressure, and enjoy the effect of the predissociation in the supersonic COIL. However, another problem arose. The complete mixing of primary flow (oxygen) and secondary flow (iodine) is much more difficult in the supersonic mixing regime. Tokai University is

Takehisa (Keio Univ.) developed the unique porous pipe SOG.¹³ The successful operation of COIL without a water vapor trap greatly owed to the porous pipe SOG. The porous pipe SOG technology was applied to the realization of the pulsed SOG, which generated a 35Torr of singlet oxygen.¹⁵ Currently, Keio University group is studying some jet SOG variation. One of the ideas was the jet SOG with guide plates.⁴⁹

KHI's COIL development started with the modified bubbler SOG that was developed in IRI, and the world's first commercial COIL²⁵ utilized it. Soon after that they developed the transverse-flow jet SOG for supersonic COIL. The property of their transverse jet SOG is the extraordinary stability; it can operate stably for more than an hour. It should be noted that the long-term operation of jet SOG is still an up-to-date topic of COIL development. Tokai University started COIL researches with the jet SOG that was transferred by Nikolaev and Zagidullin³⁴ in 1997. Since then, Tokai University's jet SOGs are following Zagidullin's design criteria. In 1997, VNIIEF's original SOG, TA-SOG was tested at Tokai University, and its high performance was demonstrated.⁴¹ Now Tokai University is developing a new type of SOG, mist SOG.⁵⁰ (Fig. 13). The goal of the mist SOG development is the stoichiometric usage of BHP at a single pass of the reaction zone. The unique counter-flow concept is the key technology to separate the BHP mist from the gas flow.

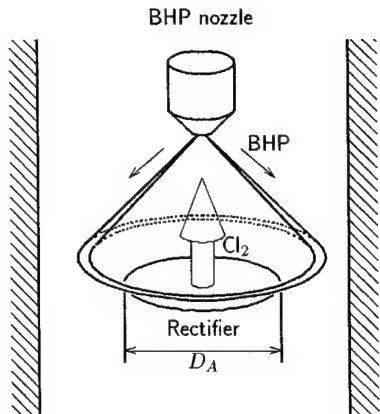


Fig. 13: Schematic drawing of the mist SOG reaction zone.⁵⁰

Fujii's group at Anan National College of Technology is studying a completely different SOG, discharge type SOG.⁵¹ Now the yield of the singlet oxygen is very close to the oscillation threshold. Table I shows the timetable of SOG development in Japan.

Table I: SOG developments in Japan.

Year	1986	1988	1990	1992	1994	1996	1998	2000	2002
IRI	Aerosol		Modified bubbler						
Keio University			Porous pipe (pulse)		Jet variation				
	Porous pipe (continuous)				Modified bubbler				
KHI					Cross-flow jet				
			Modified bubbler						
Tokai University					Modified bubbler		Mist		
							Counter-flow jet		
							♠TA-SOG		
Anan College							Discharge		

8. THEORETICAL WORKS

Numerical simulation of COIL was mainly conducted at the Nagaoka University of Technology. A three-dimensional, Navier-Stokes code including chemical reactions was developed by Masuda. The problem of supersonic COIL attracted him because it is a unique problem from the viewpoint of fluid dynamics, since the Reynolds Number is much lower than the well-studied supersonic flows. Their studies began with the diagnostics of the duct flow⁵², and followed by the

discussion of the chemical reactions at the mixing nozzles^{53,54}. The results were fed back to the KHI-COIL. The role of the water vapor condensation and heat release to the laser medium property was theoretically discussed.^{55,56} The optical resonator was modeled using a one-dimensional wave optics, and the result was compared with a geometric optics model.⁵⁷ The Q-switch operation of COIL was discussed from the viewpoint of fluid dynamics.^{58,59}

The possibility of the nuclear fusion driver using pulsed COIL was theoretically discussed by Endo^{60,61} and he predicted a new energy extraction regime, "quasi-cw energy extraction" with a 10ns pulse in the very high-pressure oxygen-iodine laser medium.

Endo discussed the possibility of the direct lasing from $O_2(^1\Delta)$.¹⁷ The point-source model included the estimation of the transition probability from each rotational level based on the Hönl-London factor, time-dependent $O_2(^1\Delta)$ number density of each rotational level, and pressure dependent line broadening. According to the calculations, the highest gain was obtained at the $^0Q(9)$ transition ($9 \rightarrow 9,9$), and the expected small signal gain from a 30Torr SOG was $3 \times 10^{-6} \text{ cm}^{-1}$.

At Tokai University, Endo developed a numerical code that did not include the numerical fluid dynamics. The rather simple code was however very helpful to assess the behavior of the laser medium of the iodine predissociation,⁴⁴ magnetic gain switching, and high-pressure subsonic operation.³⁹

9. NOW AND FUTURE – 2000~

The fruits of NEDO project conducted by Tokai University and KHI are now taken over to a private company, Miki-pulley. The company is known for the power transmission equipments, electric crutches, brakes, and so on. Their demand for a new product in their new business plan matched Fujioka's passion of industrial COIL development, and a five-year research project funded by JST (Japan Science and Technology Corporation) had started from FY2000. The goal of the program is the development of the first commercial supersonic COIL whose output is 5kW. A prototype is very close to the first light at the end of 2001. Tokai University participated in the program as a technical advisor.

In the last few years, KHI concentrated their studies on the applications of COIL. One of their research programs is a part of the national project, "Photon Project". High-speed welding of very thick aluminum alloy was demonstrated. The results of the KHI's latest work is presented elsewhere.⁶²

10. SUMMARY

A twenty-years of researches and developments of COIL in Japan were reviewed. The history of COIL in Japan originated at Fujioka's laboratory in Keio University. The first oscillation was recorded at National Defense Academy in Japan, and Keio University obtained lasing shortly after that. In 1986, IRI (Industrial Research Institute) and KHI (Kawasaki Heavy Industries) received a national project for development of the world's first commercial COIL. Now the product is working at ALEC (Applied Laser Engineering Center). Through the 90's, Keio University conducted number of unique COIL studies such as COIL without water vapor trap, porous pipe SOG, Q-switching, magnetic gain switching, intracavity second harmonic generation, pulsed operation, and so on. Tokai University COIL group started in 1996, founded by Fujioka. They obtained a high-efficiency (23.4%) operation of supersonic COIL with nitrogen as buffer gas, high-pressure subsonic operation, output power stabilization, and output power enhancement by the predissociation of iodine. Now the hottest COIL research program is conducted at Miki-Pulley. The goal of the project is the development of a commercial supersonic COIL at 5kW output.

REFERENCES

1. W. E. McDermott, N. R. Pchelkin, D. J. Benard and R. R. Bousek, "An Electronic Transition Chemical Laser", Appl. Phys. Lett. 32, pp. 469-470, 1978.

2. K. Watanabe, S. Kashiwabara, K. Sawai, S. Toshima and R. Fujimoto, "Performance characteristics of a transverse-flow, oxygen-iodine chemical laser in a low gas-flow velocity", *J. Appl. Phys.* 54(3), pp. 1228-1231, 1983.
3. K. Serizawa, A. Otsuka, H. Murata, T. Uchiyama and T. Fujioka, "Experimental and theoretical studies on chemically-pumped iodine laser", *Proc. Int. Conf. LASERS '83*, pp. 389-392, 1983.
4. J. Bachar and S. Rosenwaks, "An efficient, small scale chemical oxygen-iodine laser", *Appl. Phys. Lett.* 41(1), pp. 16-18, 1982.
5. K. Watanabe, S. Kashiwabara, K. Sawai, S. Toshima and R. Fujimoto, "Small-signal gain and saturation parameter of a transverse-flow CW oxygen-iodine laser", *IEEE J. Quantum Electron.* 19(11), pp. 1699-1703, 1983.
6. H. Murata, A. Otsuka, K. Serizawa, T. Uchiyama and T. Fujioka, "Chemically-pumped iodine laser and its application to optical power transmission", *Inst. Phys. Ser. No. 72, Proc. Int. Conf. of 5th GCL*, pp. 163-168, 1994.
7. H. Yoshimoto, H. Yamakoshi, Y. Shibukawa and T. Uchiyama, "A highly efficient, compact chemical oxygen-iodine laser", *J. Appl. Phys.* 59(12), pp. 3965-3967, 1986.
8. A. Saishu, S. Abe and T. Inoue, "Applying Laser Technology to Decommissioning for Nuclear Power Plant", *Proc. SPIE 3887*, pp. 118-127, 2000.
9. S. Yoshida, H. Fujii, T. Sawano, M. Endo and T. Fujioka, "Efficient operation of a chemically pumped oxygen iodine laser utilizing dilute hydrogen peroxide", *Appl. Phys. Lett.* 51(19), pp. 1490-1492, 1987.
10. S. Yoshida, M. Endo, T. Sawano, S. Amano and T. Fujioka, "Chemical oxygen iodine laser of extremely high efficiency", *J. Appl. Phys.* 65(2), pp. 870-872, 1989.
11. K. Shimizu, T. Sawano, T. Tokuda, S. Yoshida and I. Tanaka, "High-power stable chemical oxygen iodine laser", *J. Appl. Phys.* 69(1), pp. 79-83, 1991.
12. K. Takehisa, N. Shimizu and T. Uchiyama, "Singlet oxygen generator using a porous pipe", *J. Appl. Phys.* 61(1), pp. 68-73, 1986.
13. K. Takehisa, T. Kikuchi and T. Uchiyama, "Lasing operation of chemical oxygen-iodine laser without water-vapor trap", *J. Appl. Phys.* 63(5), pp. 1785-1786, 1988.
14. T. Kikuchi, T. Tsuruyama and T. Uchiyama, "Performance characteristics of a chemical oxygen-iodine laser without a water vapor trap", *J. Appl. Phys.* 64(6), pp. 2873-2878, 1988.
15. M. Endo, K. Kodama, Y. Handa, and T. Uchiyama, "Performance Characteristics of a High-Pressure Pulsed Singlet Oxygen Generator", *J. Appl. Phys.* 71(12), pp. 5760-5767, 1992.
16. M. Endo, K. Shiroki and T. Uchiyama, "Chemically pumped atomic iodine pulse laser", *Appl. Phys. Lett.* 59(8), pp. 891-892, 1991.
17. M. Endo, K. Kodama, Y. Handa, and T. Uchiyama, "Chemically Pumped O₂(a-X) Laser", *Appl. Phys. B*(56), pp. 71-78, 1993.
18. F. Matsuzaka, T. Ohga, M. Imachi and T. Uchiyama, "Q-switching operation of chemical oxygen iodine laser", *International Conference on Lasers '89, Houston, Dec. 1989*.
19. N. Miura, R. Kotegawa, M. Matsuo and T. Uchiyama, "Magnetic gain switching operation of Chemical Oxygen-Iodine Laser", *Proc. SPIE 1980*, pp. 186-190, 1992.
20. T. Baba, T. Tezuka, D. Ito and T. Uchiyama, "Intracavity second-harmonic generation of chemical oxygen-iodine laser emission using a LBO crystal", *Appl. Phys. B* 60(4), pp. 369-373, 1995.
21. T. Tezuka, K. Chen, K. Hashimoto and T. Uchiyama, "Intracavity Second Harmonic Generation of Chemical Oxygen-Iodine Laser Using Brewster Cut LBO Crystal", *Rev. of Laser Eng.* 24(9), pp. 1006-1012, 1996 (in Japanese).
22. T. Wakazono, K. Hashimoto, T. Takemoto, T. Uchiyama and M. Muro, "The study of Chemical Oxygen-Iodine Laser using RF discharge dissociation of I₂", *Proc. SPIE 3574*, pp.290-294, 1998.
23. H. Fujii, S. Yoshida, M. Iizuka and T. Atsuta, "Long-term stability in the operation of a chemical oxygen-iodine laser for industrial use", *J. Appl. Phys.* 66(3), pp. 1033-1037, 1989.
24. H. Fujii, S. Yoshida, M. Iizuka, T. Atsuta, "Development of high-power chemical oxygen-iodine laser for industrial application", *J. Appl. Phys.*, 67(9) Pt.1, pp. 3948-3953, 1990.
25. H. Fujii and T. Atsuta, "Current Status of Industrial COIL Development", *Proc. SPIE 1980*, pp.148-152, 1992.
26. K. A. Truesdell, C. A. Helms and G. D. Hager, "A History of COIL development in the USA", *Proc. SPIE 2502* pp. 217-237, 1994.
27. N. Naito, F. Wani and T. Nagai, "Industrial COIL in Japan", *AIAA 97-2392, AIAA 28th Plasmadynamics and Lasers Conference (Atlanta, GA, June 1997)*.

28. K. Yasuda, T. Atsuta, T. Sakurai, H. Okado, A. Hayakawa and J. Adachi, "Study on material processing of Chemical Iodine Laser", Proc. of 3rd JSME/ASME Joint Int. Conf. On Nuclear Eng. (April 23-27, 1995, Kyoto, Japan).
29. T. Sakurai, K. Yasuda, T. Osaki, E. Tada, K. Koizumi and M. Nakahira, "Study on Material Processing and Fiber Transmittance of COIL", Proc. of ICALEO, p.28, 1996.
30. K. Tsurumaki, H. Miyao, H. Tomioka, J. Adachi, K. Yasuda, H. Okado, A. Hayakawa and S. Yoshizawa, "Development of remote dismantling of components in nuclear reactor with laser transmitted through optical fiber", Proc. of ICON 5, (May 26-30, 1997, Niece, France).
31. J. Adachi, N. Takasaki, K. Yasuda and T. Atsuta, "Application of Chemical Oxygen-Iodine Laser (COIL) for Dismantling of Nuclear Facilities", Progress in Nuclear Energy 32, pp.517-522, 1998.
32. H. Okado, T. Sakurai, J. Adachi, H. Miyao and K. Hara, "Underwater cutting of stainless steel with the laser transmitted through optical fiber", Proc. SPIE 3887, pp. 152-160, 2000.
33. M. Endo, S. Takeda, F. Wani, D. Sugimoto and T. Fujioka, "Chemical Oxygen-Iodine Laser for Industrial Applications" 32nd ISATA, 99NM025 (Vienna, Austria, June 1999).
34. M. Zagidullin, V. D. Nikolaev, M. I. Svistun, V. S. Safonov and N. I. Ufimtsev, "The Study of Buffer Gas Mixing with Active Gas on Chemical Oxygen-Iodine Laser Performance with Jet Type SOG", Proc. SPIE 2702, pp. 310-319, 1996.
35. M. Endo, S. Nagatomo, S. Takeda, M. V. Zagidullin, V. D. Nikolaev, H. Fujii, F. Wani, D. Sugimoto, K. Sunako, K. Nanri and T. Fujioka, "High-Efficiency Operation of Chemical Oxygen-Iodine Laser Using Nitrogen as Buffer Gas" J. IEEE J. Quantum Electron. 34(3), pp.393-398, 1998.
36. D. Sugimoto, M. Endo, K. Nanri, S. Takeda and T. Fujioka, "Output Power Stabilization of a Chemical Oxygen-Iodine Laser with an External Magnetic Field" IEEE J. Quantum Electron. 34(9), pp.1526-1532, 1998.
37. D. Sugimoto, T. Kawano, M. Endo, S. Takeda and T. Fujioka, "Waveform Shaping of a Chemical Oxygen-Iodine Laser Utilizing the Zeeman Effect" Jpn. J. Appl. Phys. 38(9A), pp.5105-5108, 1999.
38. F. Wani, M. Endo and T. Fujioka, "High-Pressure, high-efficiency operation of a chemical oxygen-iodine laser" Appl. Phys. Lett. 75(20), pp.3081-3085, 1999.
39. F. Wani, M. Endo and T. Fujioka, "High-Pressure Subsonic Mode Operation of Chemical Oxygen-Iodine Laser" Appl. Phys. B 70(2), pp.225-230, 2000.
40. M. Endo, K. Tei, D. Sugimoto, S. Takeda, K. Nanri, T. Uchiyama and T. Fujioka, "Development of a prototype COIL for decommissioning and dismantlement", Proc. SPIE 4181, pp.23-26, 2000.
41. F. Wani, M. Endo, B. Vyskubenko, S. Ilyn, I. Krukovsky, S. Takeda and T. Fujioka, "Parametric Study of a Twisted Aerosol-Type Singlet Oxygen Generator" IEEE J. Quantum Electron. 34(11), pp.2130-2137, 1998.
42. B. A. Vyskubenko, A. A. Adamenkov, Yu. N. Deryugin, S. P. Ilyin, Yu. V. Kolobyanin, I. M. Krukovsky and E. A. Kudryashov, "High Pressure Oxygen Iodine Laser Driven by Twisted Flow Singlet Oxygen Generator", AIAA-2001-3009, AIAA 32nd Plasmadynamics and Lasers Conference (Anaheim, CA, June 2001).
43. M. Endo, D. Sugimoto, H. Okamoto, K. Nanri, T. Uchiyama, S. Takeda and T. Fujioka, "Output Power Enhancement of a Chemical Oxygen-Iodine Laser by Predissociated Iodine Injection", Jpn. J. Appl. Phys. 39(2A), pp. 468-474, 2000.
44. H. Okamoto, T. Hirata, K. Shinoda, D. Sugimoto, M. Endo, T. Fujioka and S. Takeda, "Supersonic Chemical Oxygen-Iodine Laser with Microwave Predissociation of Iodine", AIAA-2000-2492, AIAA 31st Plasmadynamics and Lasers Conference (Denver, CO, June 2000).
45. W. Masuda, M. Hishida and Y. Abe, "Mixing and Reacting Zone Structure in a Supersonic Mixing Chemical Oxygen-Iodine Laser with Ramp Nozzle Array", JSME Int. J. Ser B (Jpn Soc Mech. Eng.) 42(3), pp. 362-368, 1999.
46. D. Sugimoto, M. Endo, K. Sunako, K. Nanri and T. Fujioka, "Cutting and Drilling of Inorganic Materials for Civil Engineering using a Chemical Oxygen-Iodine Laser", Rev. Laser Eng. 28(3), pp.171-175, 2000.
47. K. Tei, D. Sugimoto, M. Endo, S. Takeda and T. Fujioka, "Chemical oxygen-iodine laser for decommissioning and dismantlement of nuclear facilities", Proc. SPIE 3887, pp.162-169, 1999.
48. S. Yoshida, H. Saito, T. Fujioka, "New singlet oxygen generator for chemical oxygen-iodine lasers", Appl. Phys. Lett, 49(18), pp. 1143-1144, 1986.
49. S. Shinoda and T. Uchiyama, "Study of Multi-Guideplate Singlet Oxygen Generator", Proc. SPIE 4184, pp. 87-90, 2000.
50. S. Muto, T. Kawano, M. Endo, K. Nanri, S. Takeda and T. Fujioka, "Parametric study of a mist singlet oxygen generator", Proc. SPIE. 4181, pp.91-94, 2000.

51. T. Kobayashi, N. Satoh, M. Ishibashi and N. Fujii, "An Efficient Excitation of Iodine Atoms by Mixing of Two Microwave Discharged Flows of I_2 and Oxygen Containing Singlet Oxygen", *Jpn J. Appl. Phys. Part 1* 36(1)A, pp. 354-355, 1997.
52. M. Inoue, M. Masuda, M. Furukawa and M. Muraishit, "Diagnosis of three-dimensional transonic flow fields with laser-induced iodine fluorescence", *SME FED (Am Soc Mech. Eng. Fluids Eng. Div.)* 218, pp. 163-170, 1995.
53. W. Masuda, M. Hishida, S. Hirooka and N. Azami, "Three-Dimensional Mixing/Reacting Zone Structure in a Supersonic Flow Chemical Oxygen-Iodine Laser", *JSME Int. J. Ser B (Jpn Soc Mech. Eng.)* 40(2), pp. 209-215, 1997.
54. W. Masuda, M. Hishida and N. Azami, "Effects of Wall Catalysis on the Reacting Zone Structure of a Supersonic Flow Chemical Oxygen-Iodine Laser", *JSME Int. J. Ser B (Jpn Soc Mech. Eng.)* 41(3), pp. 674-679, 1998.
55. W. Masuda, M. Satoh, "Effects of Water Vapor Condensation on the Performance of Supersonic Flow Chemical Oxygen-Iodine Laser", *JSME Int. J. Ser B (Jpn Soc Mech. Eng.)* 39(2), pp. 273-279, 1996.
56. W. Masuda and M. Satoh, "Numerical Simulation of a Supersonic Flow Chemical Oxygen-Iodine Laser Solving Navier-Stokes Equations", *JSME Int. J. Ser B (Jpn Soc Mech. Eng.)* 40(1), pp. 87-92, 1997.
57. W. Masuda, M. Hishida and K. Iwamoto, "Characteristics of Radiation from a Supersonic Flow Chemical Oxygen-Iodine Laser", *JSME Int. J. Ser B (Jpn Soc Mech. Eng.)* 41(4), pp. 966-974, 1998.
58. M. Hishida, K. Kominato, W. Masuda and J. Schmiedberger, "Numerical Simulation of Q-switched Operation in a Supersonic flow Chemical Oxygen-Iodine Laser", *Pap. Am. Inst. Aeronaut. Astronaut.*, pp. 12, 1999.
59. W. Masuda, M. Hishida, K. Kominato, "Characteristics of Radiation from a Q-Switched Supersonic Flow Chemical Oxygen-Iodine Laser", *JSME Int. J. Ser B (Jpn Soc Mech. Eng.)* 43(1), pp. 36-45, 2000.
60. M. Endo, K. Kodama, Y. Handa and T. Uchiyama, "Theoretical Study of a Large Scale Chemically Pumped Pulsed Iodine Laser Amplifier", *Proc. SPIE* 1810, pp. 532-535, 1992.
61. M. Endo, K. Kodama, Y. Handa and T. Uchiyama, "Theoretical Study of a New Energy Extraction Scheme of a Chemically Pumped Pulsed Iodine Laser Amplifier", *Appl. Phys. B*, 56(6), pp. 379-384, 1993.
62. F. Wani, T. Nakabayashi, A. Hayakawa, S. Suzuki and K. Yasuda, "High-power COIL and YAG welding", *Proc. SPIE* 4631, to be published.

High-power COIL and YAG laser welding

Fumio Wani, Tokuhiro Nakabayashi, Akiyoshi Hayakawa, Sachio Suzuki, and Kozo Yasuda
Technical Institute, Kawasaki Heavy Industries, Ltd.

ABSTRACT

We have constructed a laser welding system, which enabled high-power laser welding by combining three laser beams of 1 μm wavelength. Its wavelength enables optical silica fibers transmission and the flexible system. The heart of this system consists of a 4 kW and a 6 kW Nd:YAG lasers and a 10 kW Chemical Oxygen-Iodine Laser (COIL). The average power of the combined beam is up to over 20 kW. The effects of various welding parameters were investigated, such as the laser power, pulse modulation, and so on. The 10 kW COIL has a very good beam quality which is 64 mm·mrad. The beam spot diameter is 0.48 mm at the focal point. On the contrary the beam quality of Nd:YAG laser is worse, but it has the function of pulse modulation which the COIL does not have. As a result of the welding test with the 6 kW Nd:YAG laser, it was clarified that the pulse wave (PW) has good efficiency of deeper penetration at low welding speed. When the combined beam with CW COIL and PW Nd:YAG laser was used, 20 mm penetration on the stainless steel could be achieved at a welding speed of 1 m/min.

Keywords: Laser welding, thick plate welding, COIL, YAG, combined laser beam

1. INTRODUCTION

Laser welding has come into general use in various manufacturing processes because laser welding has many beneficial features such as deep penetration, low distortion and low thermal damage in material processing due to the small beam spot with high-power density^{1,2}. In addition, the laser, whose wavelength is located in 1 μm region, enables flexible optical silica fiber transmission of the output power. This attribute brings substantial production advantages over the other industrial lasers, especially CO₂ laser. In particular, this flexibility weighs with the heavy industry in which the products are made of thick and large metal parts. The technological innovations of the lamp-pumped Nd:YAG laser had raised the possibility several years ago, but as it was difficult because of the expensive running cost and unreliability. Therefore, the Japanese national R&D project "Advanced Photon Processing and Measurement Technologies" was started in 1997. In this project, the technologies of laser diode (LD) pumped 10 kW Nd:YAG laser and also the advanced processing which will use it are being developed. We secured a contract for the development of the advanced laser processing, namely, "Macroscopic processing technology", and had started the development of highly reliable laser welding technology. The goal of this contract is to establish the technology for laser welding of 30 mm thick steel plates and 20 mm thick aluminum alloy plates at a welding speed of higher than 1 m/min, providing high aspect ratio and equivalent or better strength than the base material. In order to realize it, we developed the laser welding system composed of a beam combining system, in-process monitoring sensors, Nd:YAG lasers and a COIL and many beneficial findings were obtained^{3,4,5}. In this paper, we report the high-power laser welding results with this system.

2. EXPERIMENTAL APPARATUS

The schematic diagram of our laser welding system is shown in Fig. 1. The heart of this system consists of a 4 kW and a 6 kW Nd:YAG lasers and a 10 kW class supersonic COIL. This system is equipped with in-process monitoring sensors, photo diodes and CCD cameras. It makes defect free welding by controlling welding parameters based on monitoring information from the sensors. This series of experiments were conducted by using the 6 kW Nd:YAG laser and the 10 kW COIL mostly. The photographs and specifications of both lasers are shown in Fig. 2. The maximum

output power of COIL is 12 kW. On the other hand, the Nd:YAG laser has a function of pulse modulation which the COIL does not have. The peak power is 12 kW at a pulse duty of 50 % and the pulse frequency is CW or 40~500 Hz.

Figure 3 shows the welding apparatus of the flat position welding. The COIL beam was delivered by a bending mirror and focused by using a 200 mm focal length lens. The shielding gas, N₂, Ar or He gas, was flowed through a coaxial nozzle whose diameter was 8 mm. A standoff height of the nozzle was set up in 8 mm. When the laser output power were 7.5 kW and 11 kW, the measured beam diameters at the focal point were 0.3 mm and 0.36 mm, respectively.

Figure 4 shows the welding apparatus of the horizontal position welding. The COIL beam and the Nd:YAG laser beam were delivered by bending mirrors into a beam combining system. The beam combining system contained two focal lenses, whose focal lengths were 300 mm for each beam, and one dichroic mirror. The system was assembled on an optical table; this setup gives an easiness to maintain the optical parts. In the beam combining system, laser beams were focused and

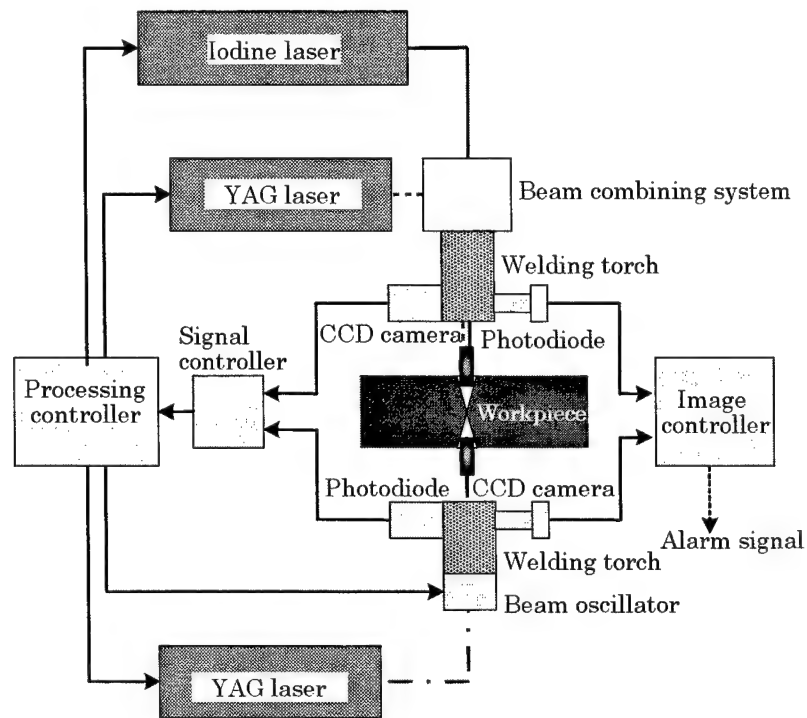


Fig. 1: Schematic diagram of the developed laser welding system

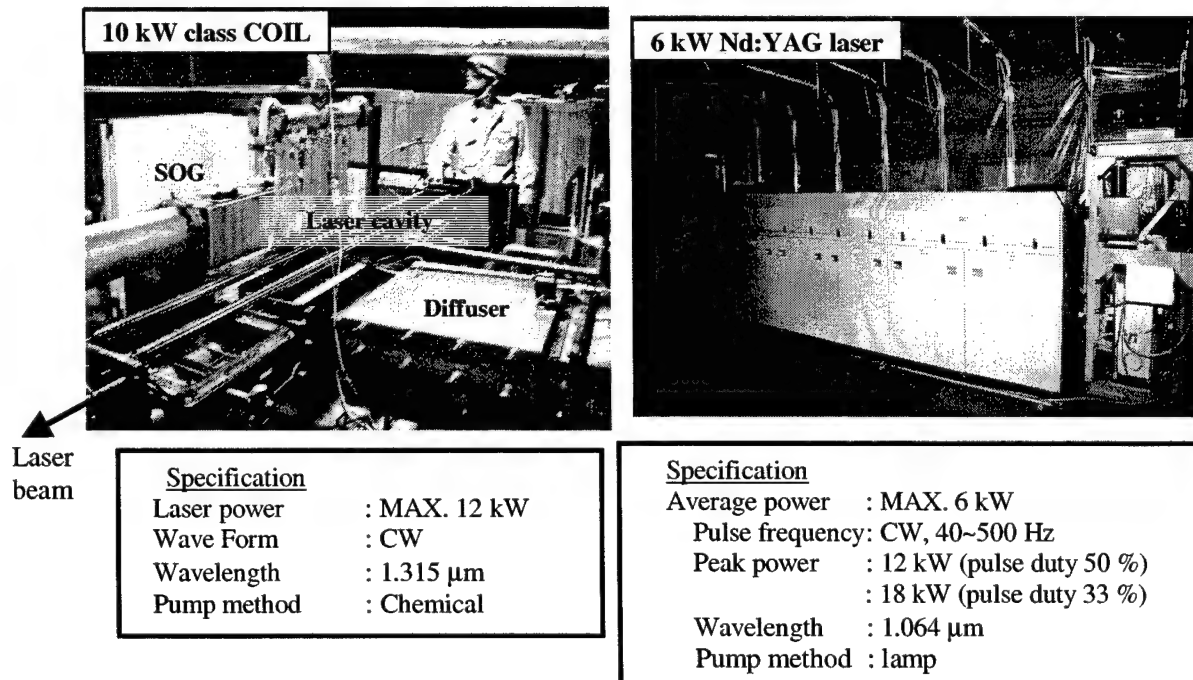


Fig. 2: Photographs and specifications of the 6 kW Nd:YAG laser and the 10 kW class COIL

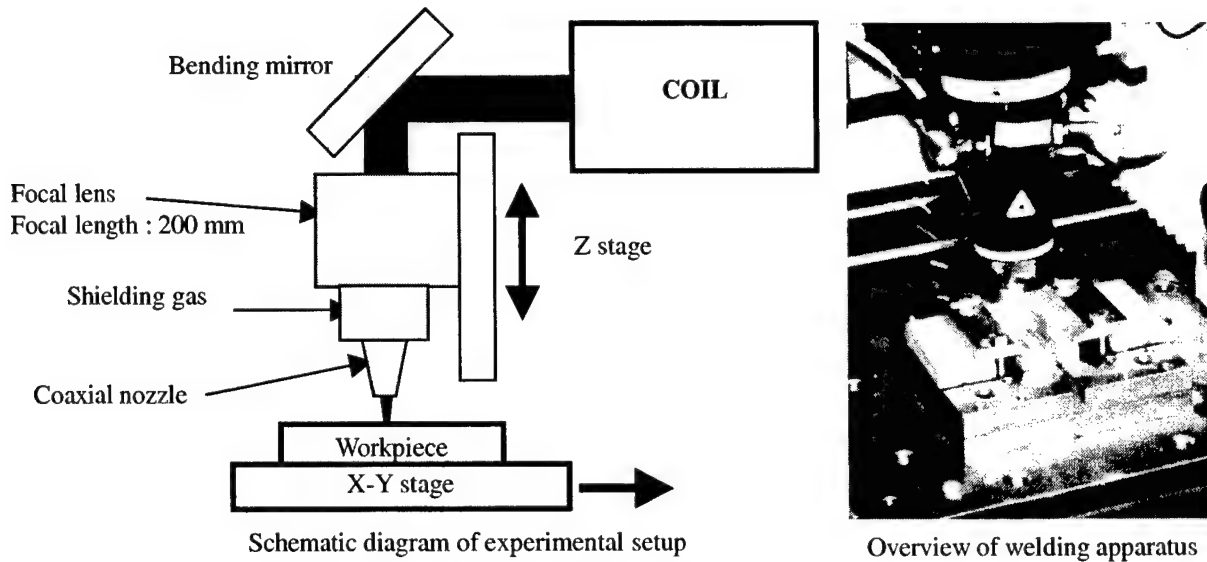


Fig. 3: Welding apparatus of the flat position welding

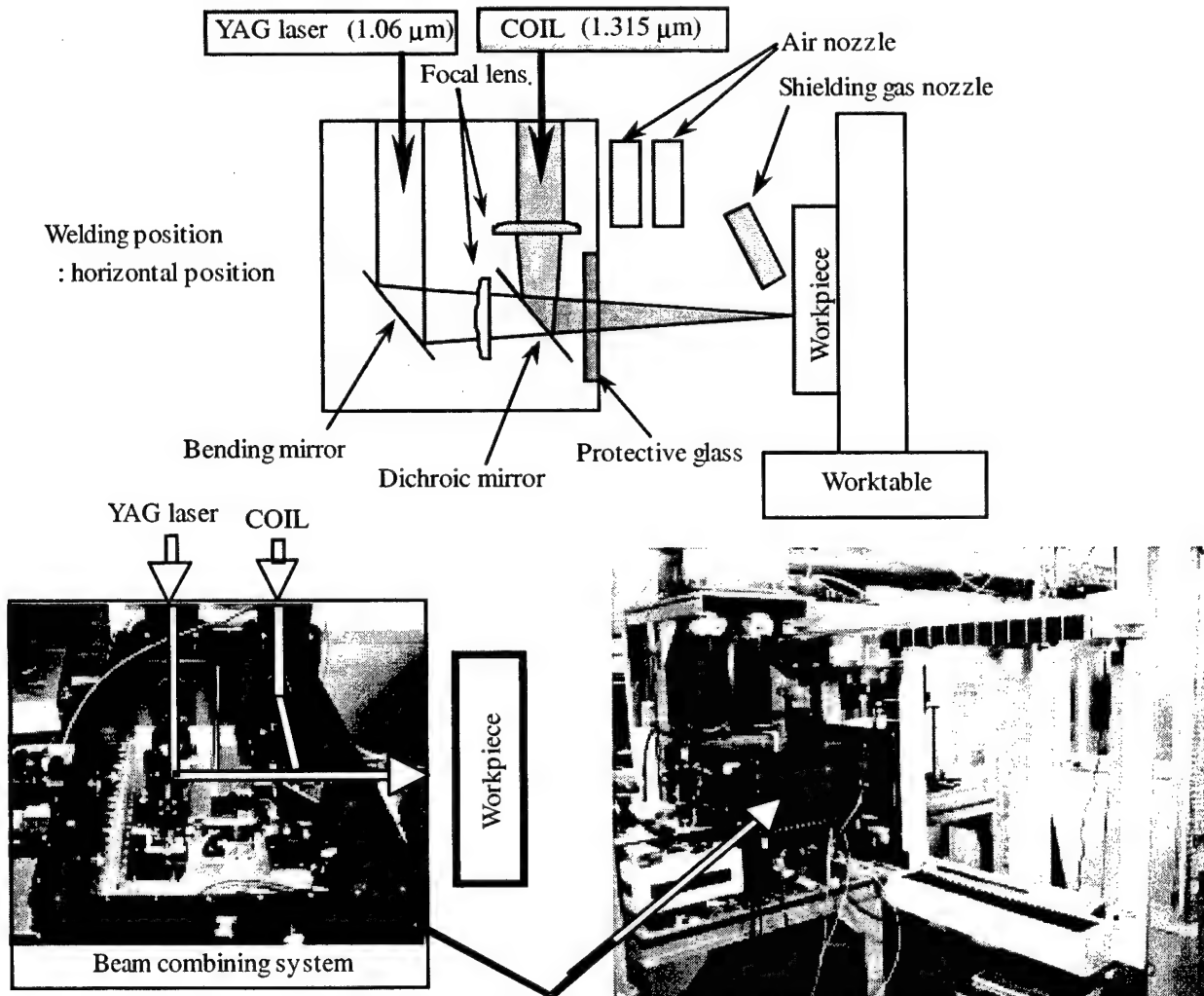


Fig. 4: Welding apparatus of the horizontal position welding

then combined to the same optical axis. The combined laser beam was irradiated to a workpiece horizontally. The shielding gas, N_2 or Ar gas, was flowed through a side nozzle whose diameter was 10 mm. A standoff height and an angle of the nozzle were set up in 10 mm and 45 degrees, respectively. Two air nozzles were set before the protective glass in order to remove spatter. The beam profiles near the focal point were measured by PROMETEC laser scope UFF100. Figure 5 shows the beam profiles of COIL and Nd:YAG laser. The measured diameters of each beam at the focal point were 0.48 and 0.88 mm respectively, at the COIL power of 12 kW and the Nd:YAG laser power of 6 kW. The COIL beam had smaller spot size than the Nd:YAG laser beam because the beam quality of COIL was very good.

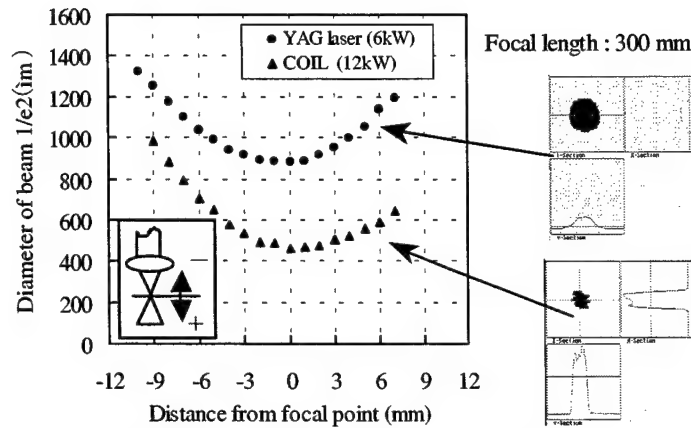


Fig. 5: Beam profiles of COIL and Nd:YAG laser

3. RESULTS AND DISCUSSION

3.1 WELDING CHARACTERISTICS WITH HIGH-POWER COIL

To understand the basic welding performance of the 10 kW class COIL, bead-on plate welding tests were carried out at laser power of 8.5 kW and 11 kW in flat position. The welding speed was varied from 0.5 to 1.5 m/min. A focal lens whose focal length was 200 mm was used and the beam focal point was set at the workpiece surface. N_2 gas was used as the shielding gas and the flow rate of it was set at 20 liter/min. Figure 6 shows cross sections of the welded bead at a constant laser power of 11 kW. Figure 7 shows the relationship between welding speed and penetration depth. Full penetration welding with the high aspect ratio in type 304 stainless steel of plate thickness 15 mm was achieved at a laser power of 11 kW and a welding speed of 0.5 m/min.

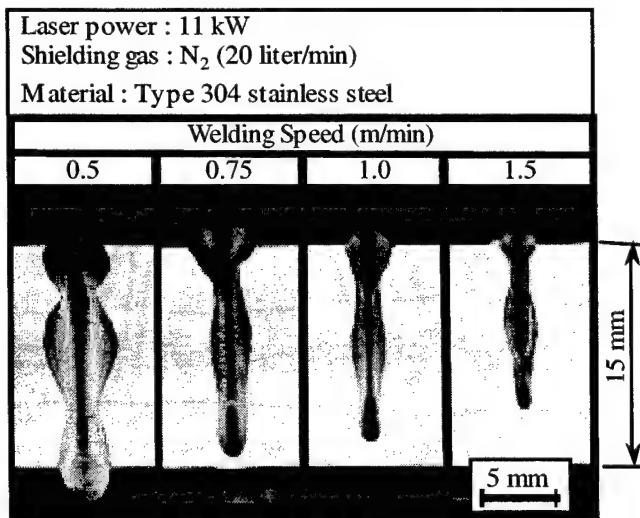


Fig. 6: Cross sections of laser welded beads

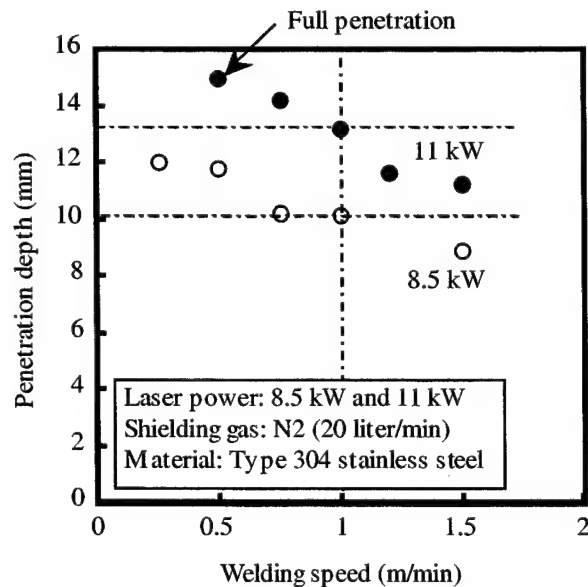


Fig. 7: Penetration depth as a function of the laser power

To confirm the effect of defocus distance of COIL, welding tests were carried out with a constant laser power of 10.8 kW and a constant welding speed of 1 m/min. As a result, the deepest penetration was obtained at a defocus distance of -3 mm as shown in Fig. 8.

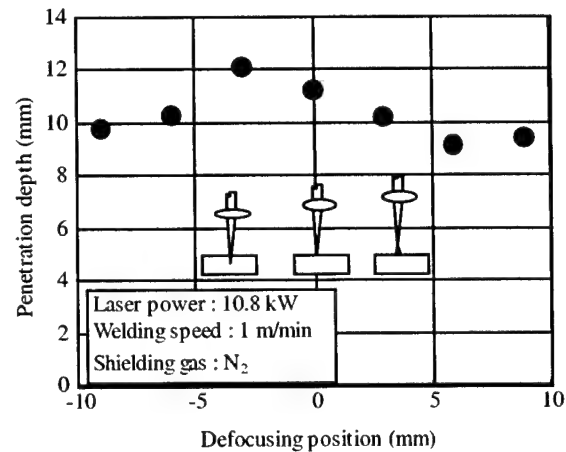


Fig. 8: Penetration depth as a function of the defocusing position

3.2 WELDING CHARACTERISTICS WITH PULSE WAVE OF YAG LASER

Bead-on-plate welding tests were carried out on stainless steel plates with thickness of 15 mm to examine the welding characteristics of the 6 kW Nd:YAG laser. The pulse duty was varied from 33 to 100 % at a constant average power of 6 kW. In these tests, the welding speed and the pulse frequency were kept to 1 m/min and 40 Hz respectively. Figure 9 shows the relationship between the pulse duty and the penetration depth. The deepest penetration was obtained at a pulse duty of 50 %. As the pulse duty increased, the bead shape became shallower and wider, and the bead appearance became better. In the range of pulse duty lower than 40 %, many spatters were generated and the penetration depth became shallower. This is attributable to the insufficient optimization of welding parameters for welding speed and pulse frequency.

The pulse frequency was varied from continuous wave to 500 Hz at a constant average power of 6 kW. This series of tests was conducted with a constant pulse duty of 50 % and a welding speed of

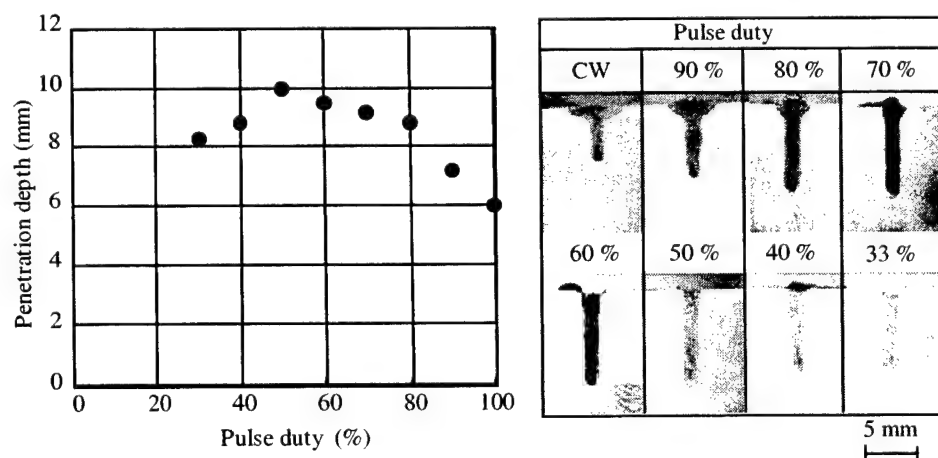


Fig. 9: Relationship between pulse duty and penetration depth

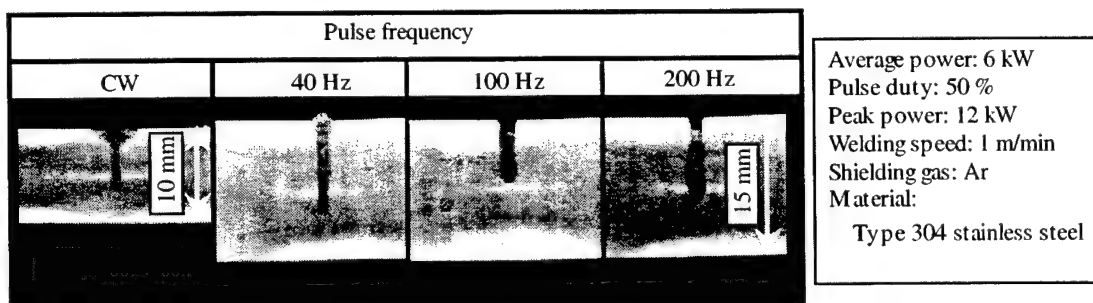


Fig. 10: Cross section of welded bead as a function of pulse duty

1 m/min. Figure 10 shows the cross section of welded bead. The bead shapes of pulse wave conditions were deeper and narrower than of a continuous wave condition. The spatters of molten metal increased as the pulse frequency increased. In the range of higher pulse frequency, underfills appeared in the weld bead surface and penetration depth fluctuated on one bead. As a result, the best frequency condition was 40 Hz.

The defocusing distance was varied from -15 to +10 mm at a constant average power of 6 kW. The series of tests was conducted with a constant pulse frequency of 40 Hz and a welding speed of 1 m/min; waveform conditions were a pulse duty of 50 % and continuous. Figure 11 shows the relationships between defocusing distance and penetration depth. The deepest penetration was obtained at defocusing distance -6 mm in both cases.

The welding speed was varied from 0.2 to 3 m/min under the best welding condition: the average power of 6 kW, the pulse duty of 50 %, the pulse frequency of 40 Hz, the welding speed of 1 m/min and the defocus distance of -6 mm. To compare the welding characteristics with those of continuous wave, a series of welding tests was also carried out with continuous wave. Figure 12 shows the relationship between welding speed and penetration depth. As welding speed became lower, the penetration depth with pulse wave became deeper than that with continuous wave. The values of penetration depth with pulse wave were 1.5 and 2 times as deep as those of continuous wave at welding speed 1 and 0.2 m/min, respectively. From this result, the deeper penetration with pulse wave at low welding speed can be explained by the high peak power and the high cooling effect of the pulse wave.

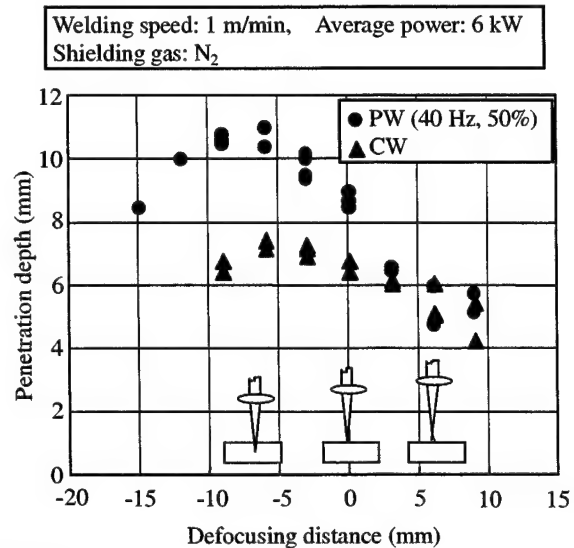


Fig. 11: Penetration depth as a function of the defocusing position

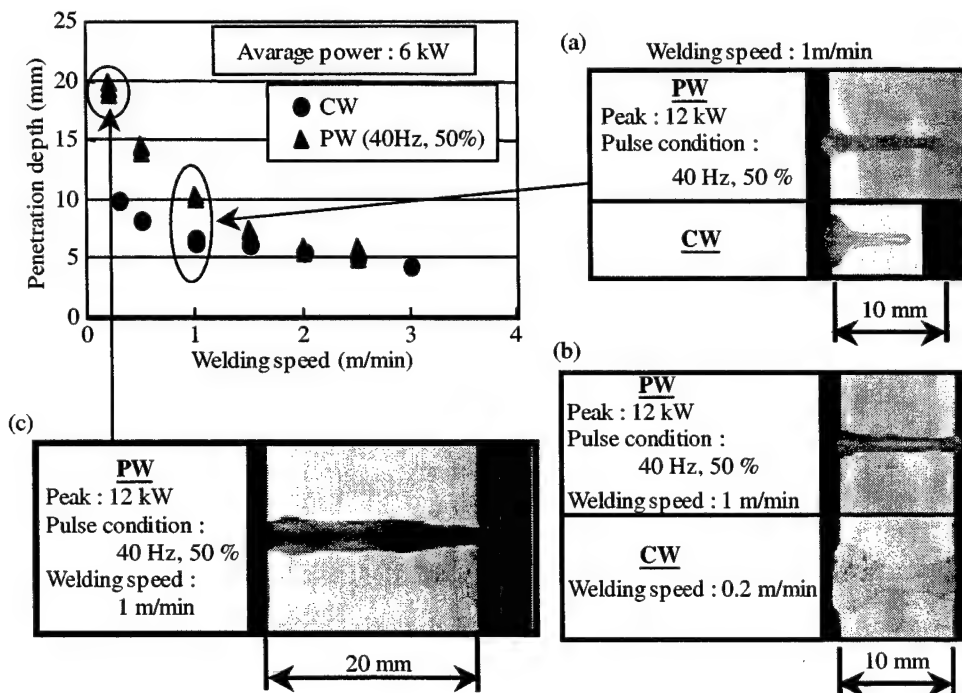


Fig. 12: Relationship between welding speed and penetration depth

3.3 LASER WELDING CHRACTERISTICS WITH HIGH-POWER COMBINED BEAM

Bead-on-plate welding tests were carried out with combining beam. Relationships between penetration depth and welding speed for various laser beam parameters are summarized in Fig. 13. As welding speed was decreased, bead shape was deeper and wider. It is confirmed that the penetration depth at combining beam of continuous wave is nearly equal to additional value of those at each single beam.

Figure 14 shows the comparison of bead shape between pulse modulation and continuous wave. At combining beam of continuous and welding speed 0.5 m/min, 20 mm penetration depth was obtained, but the heat effect was so large that welded metal was dropped. On the other hand, by using combined beam with the pulse modulation of Nd:YAG laser, 20mm penetration depth was achieved in high aspect ratio at a welding speed of 1m/min. It was confirmed that pulse modulation was effective for deeper penetration.

In addition, welding tests for square groove butt joint were conducted with the combined beam. Figure 15 shows the results of butt joint welding in type 304 stainless steel of plate thickness 20 mm. One-side and double-side welding was conducted, then defect-free and full-penetration welding was obtained in the both cases, as shown in Fig. 15. Butt joint welding tests for 30 mm thickness stainless steel plates were also carried out. Defect-free and full-penetration welding was also obtained in the cases of both side welding at a welding speed of 1 m/min. The cross section of welded plate is shown in Fig. 16.

We also conducted various welding experiments in aluminum alloy to realize the defect-free welding in aluminum alloy of plate thickness 20 mm. It was difficult

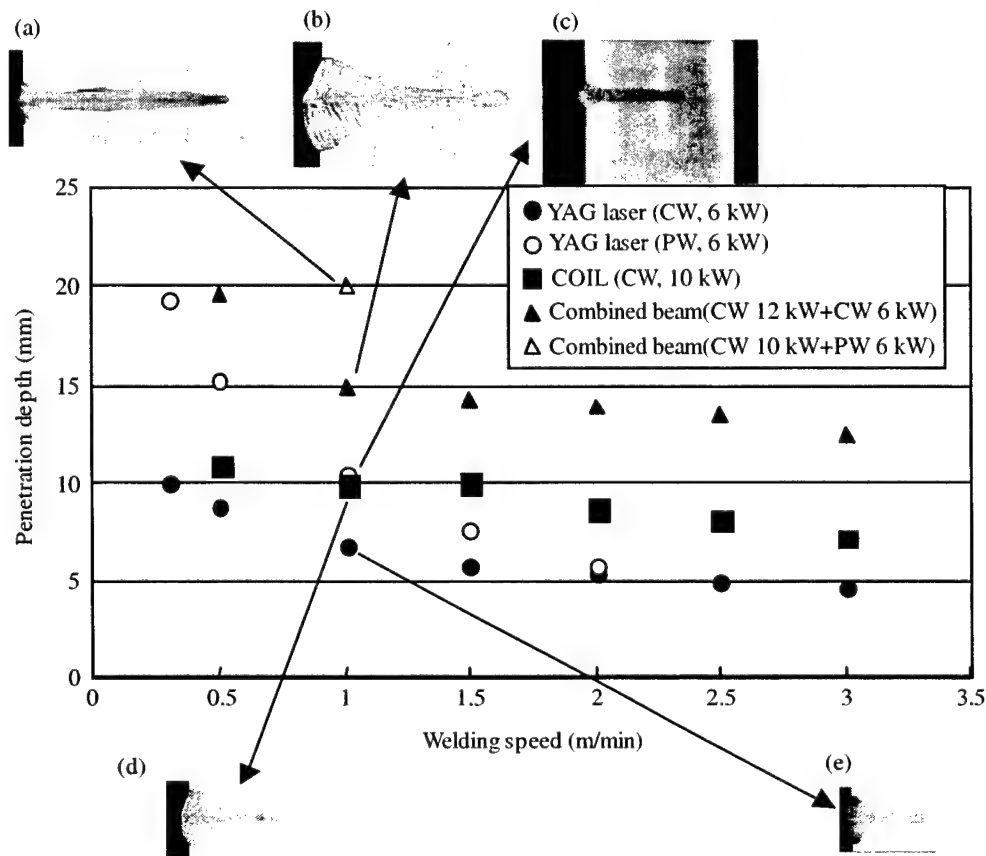


Fig. 13: Relationship between welding speed and penetration depth

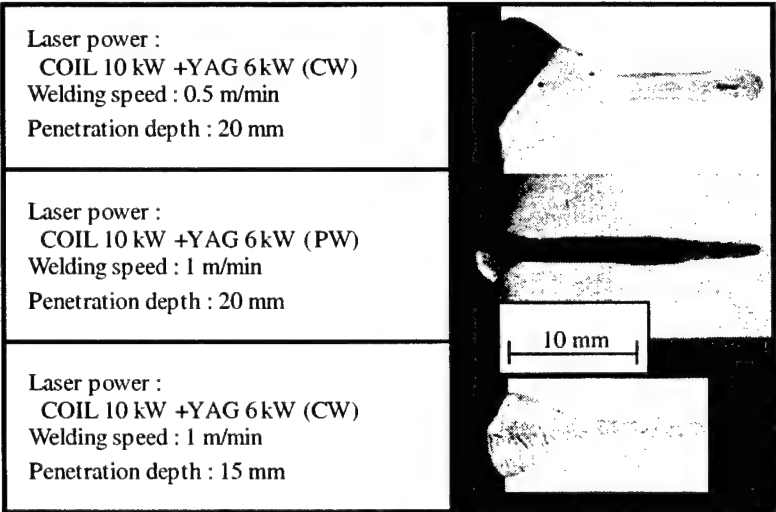


Fig. 14: Welded beads with combined beams (type 304 stainless steel)

to obtain the defect-free welding in aluminum alloy compared to steel because of the vaporization of volatile alloying additions such as magnesium. To clarify the optimum welding conditions in aluminum alloy, bead-on-plate welding tests were conducted with combined beam and single COIL beam. The defocusing distances of both beams were varied individually. The typical cross sections of welded aluminum alloy (A5083) plates are shown in Fig. 17. A penetration depth of 11.6 mm was attained with the combined beam, whose total laser power was 10 kW (COIL) + 6 kW (CW, Nd:YAG), at a welding speed of 1 m/min. In the COIL single beam welding, a penetration depth of 9.1 mm was obtained with the laser power of 10 kW at same welding speed. Now we are trying to achieve the full penetration welding with good welding quality in aluminum alloy (A5083) of plate thickness 20 mm.

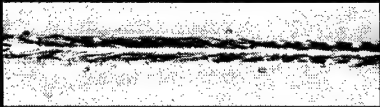
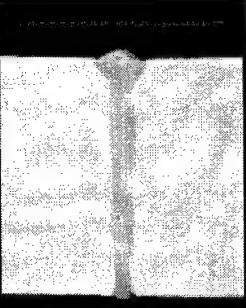


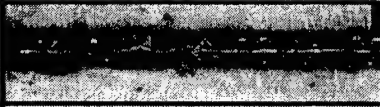
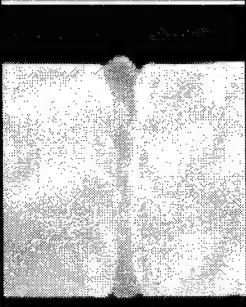

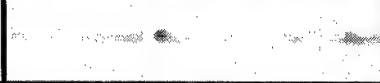

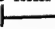
<u>One-side welding</u> Power : 10 kW COIL + 6 kW YAG YAG Pulse condition : 40 Hz, 50 % Welding speed : 0.8 m/min	Front side		
	Reverse side		
	Radiograph		
<u>Double-side welding</u> <u>Front side</u> Power : 10 kW COIL + 6 kW YAG YAG Pulse condition : 40 Hz, 50 % <u>Reverse side</u> Power : 6 kW YAG YAG Pulse condition : 40 Hz, 80 % Welding speed : 1.5 m/min	Front side		
	Reverse side		
	Radiograph		
		10 mm 	5 mm 

Fig. 15: Welding results in type 304 stainless steel butt joints of plates thickness 20 mm

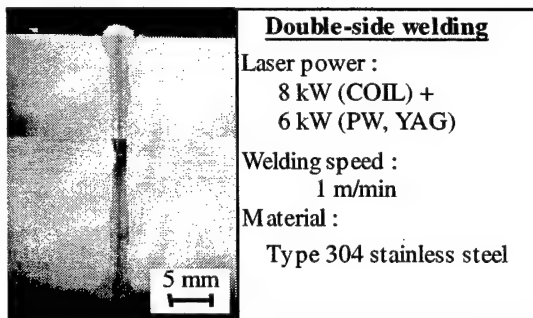


Fig. 16: Welding results in type 304 stainless steel butt joints of plates thickness 30 mm

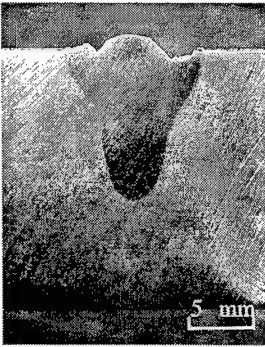

Welding speed: 1 m/min, Shielding gas: Ar gas, 20 liter/min	
	
COIL + Nd:YAG laser Laser power 10 kW + 6 kW Defocusing distance: 18 mm, 8 mm	COIL Laser power 10 kW Defocusing distance : 8 mm

Fig. 17: Welding results in A5083 of plates thickness 20 mm

CONCLUSION

We are developing the highly reliable laser welding technology with high-power lasers whose wavelengths are located in 1 μm region. To establish the technologies for the thick plate laser welding, we carried out various welding experiments and obtained following results.

The beam combining system with beams of 6 kW Nd:YAG laser and 10 kW-class COIL was developed. By using this system, abundance of valuable results about high-power laser welding were obtained. Full penetration welding with good welding quality in type 304 stainless steel of plates thickness 20 mm (one-side welding) and 30 mm (double-side welding) was achieved at a welding speed of 1 m/min.

ACKNOWLEDGMENTS

This work was partially conducted in the program "Advanced Photon Processing and Measurement Technologies" of the National Institute of Advanced Industrial Science and Technology, the Ministry of Economy, Trade and Industry, consigned to the R&D Institute for Photonics Engineering from the New Energy and Industrial Technology Development Organization (NEDO).

REFERENCES

1. K. Minamida, "High-power laser application in Nippon Steel Corporation", *Proc. SPIE* **3888**, pp. 533-542, 1999.
2. T. Ishide, S. Tsubota, M. Nayama, S. Yoshiaki, T. Nagashima, and K. Okimura, "10-kW-class YAG laser application for heavy components", *Proc. SPIE* **3888**, pp. 543-550, 2000.
3. T. Nakabayashi and M. Muro, "High power chemical oxygen-iodine laser welding", *Proc. SPIE* **3887**, pp. 359-366, 2000.
4. T. Nakabayashi, F. Wani, H. Okado, A. Hayakawa, S. Suzuki, and K. Yasuda, "Laser welding characteristics with high power combining beam", *Proc. ICALEO 2001*, **Section A-302**, 2001.
5. H. Okado, T. Nakabayashi, F. Wani, A. Hayakawa, S. Suzuki, and K. Yasuda, "Beam operation for thick plate laser welding", *Proc. the 7th Int. Symp.*, pp. 491-496, 2001.

COIL development in Kawasaki Heavy Industries, Ltd.

Tomohito Takada^{*a}, Fumio Wani^{**b}, Kozo Yasuda^{**b}

^aAerospace Company, Kawasaki Heavy Industries, Ltd.;

^bTechnical Institute, Kawasaki Heavy Industries, Ltd.

ABSTRACT

The Chemical Oxygen-Iodine Laser (COIL) has been studied for military use because it has many excellent features. These features count with not only the military but also the industry. The wavelength of COIL 1.315 μm , is a significant features of the industrial laser because it is located in a minimum loss transmission region for optical silica fibers. Therefore, we started the COIL development for industrial use in 1986. In the first stage, we developed a subsonic type. In 1992, the first 1 kW class commercial COIL was delivered. This system was successfully operated for several hours, and its output beam was delivered through the optical silica fiber of 0.3 mm core diameter. But the subsonic COIL has the disadvantage that the device size is relatively large. To solve this problem, the supersonic COIL has been introduced and developed. In 1994, 1 kW supersonic output power was attained. On the basis of this technology, we constructed a 10 kW class in 1996. This system achieved over 12 kW output power and chemical efficiency of 26 %.

Keywords: COIL, iodine laser, chemical laser, gas laser, chemical efficiency

1. INTRODUCTION

The first COIL lasing was demonstrated at the U.S. Air Force Weapons Laboratory in 1977¹. The attractive characteristics of the COIL, the short wavelength, narrow emission line, etc., motivated many researchers to develop the military COIL. On the other hand, in Japan, the COIL drew a great deal of interest to the industrial application because of its following excellent features. The wavelength of COIL is 1.315 μm and its absorption on the surfaces of material is higher than that of CO₂ laser. The optical silica fiber transmission loss of COIL is very low as same as that of Nd:YAG laser. The beam quality of COIL is very good as same as that of CO₂ laser because the laser medium is low pressure gas. The COIL can be called the laser having merits of CO₂ and Nd:YAG lasers. The COIL research in Japan was started in 1982 on basic experiment and theoretical studies at Keio Univ. The extensive studies of Keio Univ.² accelerated the study of industrial COIL and led to the joint research program of Industrial Research Institute (IRI) and us.

We have started the development of the industrial COIL in 1986. In the first stage of our COIL research, a subsonic type was studied and developed. After the joint research with IRI for several years, we have completed a 1 kW class proto-type subsonic COIL³. On the basis of this technology, the first 1kW class commercial COIL for material processing was delivered to the Applied Laser Engineering Center in Japan^{4,5}. It was successfully operated for several hours and proved the possibility of the industrial COIL. But the subsonic COIL has the disadvantage that the device size is relatively large compared with the laser power. The gain length of the 1 kW commercial COIL was about 1 m. In the early 1990's, our study of COIL has shifted to the supersonic type. And the target laser power has been pulled up to compete against the other industrial laser, especially Nd:YAG laser. In 1994, 1 kW supersonic output power was attained^{6,7}. We have constructed the 5 kW class supersonic COIL in 1995⁸ and the 10 kW class supersonic COIL in 1996^{9,10} by use of this base supersonic COIL technology. We could get gratifying COIL performance and conducted a lot of laser processing tests by use of them. A historical overview of our researches for these past 16 years about the COIL devices and its applications are discussed.

* takada_tomohito@khi.co.jp; phone 81 583 82-8129; fax 81 583 82-4269; <http://www.khi.co.jp>; Kawasaki Heavy Industries, Ltd, 1 Kawasaki-cho Kakamigahara, Gifu, 504-8710 Japan; ** wani_f@khi.co.jp; phone 81 471 24-0269; fax 81 471 24-5917; <http://www.khi.co.jp>; Kawasaki Heavy Industries, Ltd, 118 Futatsuzuka, Noda, Chiba, 278-8585 Japan

2. DEVELOPMENT OF SUBSONIC COIL DEVICE

The early study of the subsonic COIL from 1986 was conducted with IRI for several years. In this joint study, we constructed a couple of small-scale systems to study efficient operation¹¹, and long term continuous operation¹². In Ref. 11, we demonstrated a maximum chemical efficiency of 40 %. In Ref. 12, we succeeded in operating a 100 W class system for over 3 hrs by continuously replenishing the Basic Hydrogen Peroxide (BHP). In addition to those small-scale devices, we constructed a high-power version prototype and succeeded in achieving an output power of 1 kW. The 2nd version prototype, equipped with a fuel replenishing system, was constructed on the basis of these results in succession. The maximum output power of 1.1 kW, and a continuous operation time of more than 2 hr with a power of over 500 W were achieved by this system³. Based on this long-standing effort, we brought the first 1kW class commercial COIL for material processing to completion^{4,5}.

Figure 1 shows the photograph of the 1 kW commercial COIL system. The major specifications of this system are summarized in Table 1. The laser beam of the COIL can be delivered by mirror optics or an optical silica fiber. By using this system, the use of 0.3 mm core diameter optical silica fiber of 200 m length was succeeded to transmit the 1 kW output power COIL beam with low transmission loss of about 4.6 dB/km in 200 m distance⁸.

Figure 2 shows the schematic diagram of the main construction. This COIL system has some specific facilities for long time stable oscillation, such as the fuel recirculation system, pressure control system at the laser cavity, the iodine evaporator with the halogen lamp heater for coping with quickly to the laser power variation, and the water vapor trap of rotating disk type. In the fuel recirculation system, the composition and temperature of BHP are controlled automatically for stabilizing the excited oxygen generation. And the waste solution of after reaction is utilized to melt the ice which scraped off from the disk surfaces of the water vapor trap. This molten water is continuously discharged to outside the vacuum line by means of the ice discharge pump. Thus the operation could be continued stably for long time. The performance of this COIL system is over 1 kW

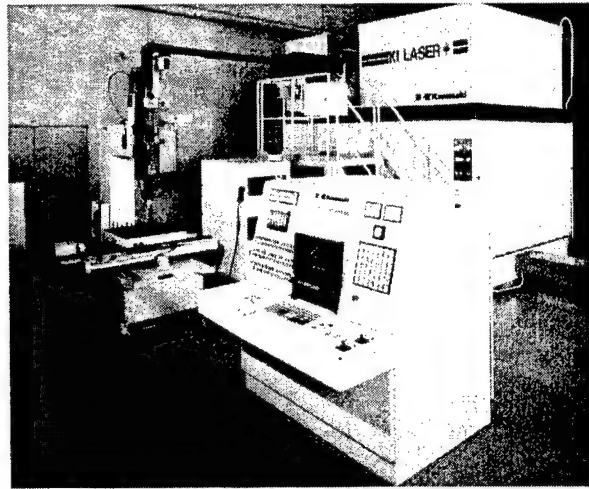


Fig. 1: 1 kW commercial COIL

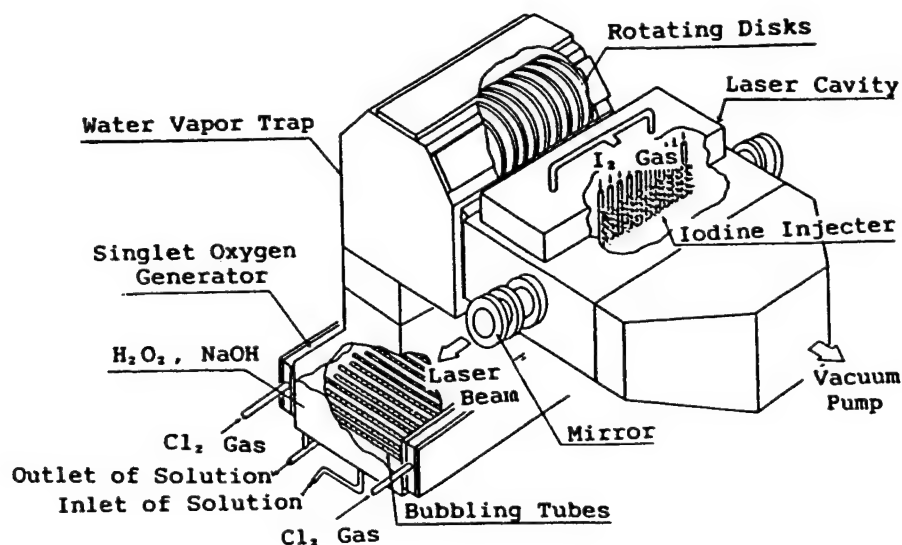


Fig. 2: The main construction of 1 kW commercial COIL

output power within ± 2 % power fluctuation with 30 % chemical efficiency. This system is in good running order to date.

3. DEVELOPMENT OF SUPERSONIC COIL DEVICE

In the early 1990's, kW class Nd:YAG laser had been brought to the market. The target range of COIL output power was gradually shifted to high-power to maintain its competitive edge by using the easy output power scalability of COIL's as leverage. In order to realize the high-power and compact industrial COIL, our study of COIL has shifted to the supersonic type. In 1994, 1 kW supersonic output power was attained as a result of several years research^{6,7}.

On the basis of this research, we have constructed the 5 kW class supersonic COIL, shown in Fig. 3, in 1995⁸. The major specifications of this 5 kW class COIL are summarized in Table 1. This system mainly consists of a jet-type singlet oxygen generator (J-SOG), a water vapor trap and others. The design specification was cleared, successfully, and it was used for quite a number of material processing tests. However, this system has a serious issue which is the short run length, because it is difficult to operate the water vapor trap continuously for a long stretch of time in the supersonic operation mode owing to the high gas pressure.

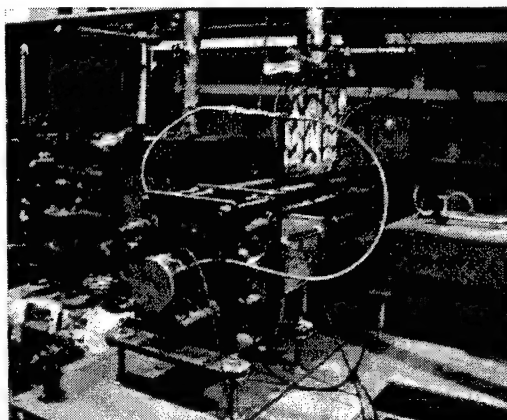


Fig. 3: 5 kW class supersonic COIL

The important factor in the industrialization of COIL is long term operation, not to mention cost. The long term operation is difficult for the former supersonic COIL, since there are two factors which are the water vapor trap and maintaining the BHP composition. We had solved these problems by further studies, and so the 10 kW class supersonic COIL had been completed in 1996^{9,10}. The main construction and the outside view of this 10 kW system are shown in Fig. 4 and 5, respectively. The major specifications of this system are summarized in Table 1.

This COIL mainly consists of a J-SOG, a supersonic cavity and a BHP circulation system. The schematic diagram of the main construction is shown in Fig. 6. In the J-SOG, singlet oxygen is generated by the chemical reaction between gaseous chlorine and BHP which is produced by mixing KOH with H_2O_2 . A mixture chlorine is introduced transversely to the BHP jet flow. The supersonic cavity is divided into three parts: iodine injectors, supersonic nozzles and a resonator. To obtain good mixing of the iodine with the primary flow of the mixture gas, the iodine is injected transversely and diagonally by the iodine injectors in the subsonic region just up stream of the supersonic nozzle throat.

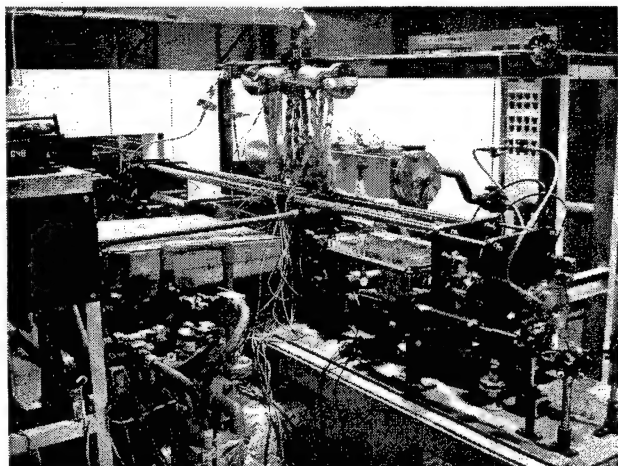


Fig. 4: The main construction of 10 kW COIL

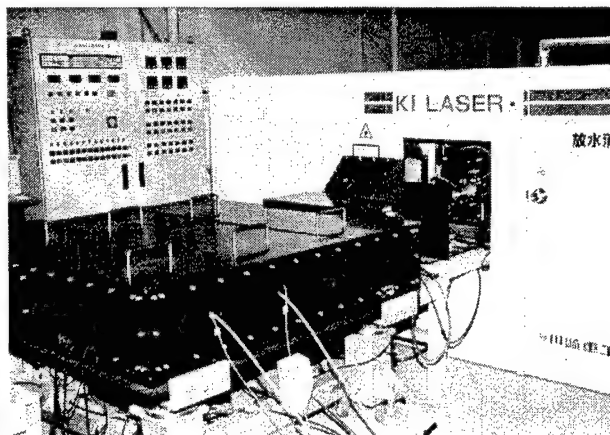


Fig. 5: The outside view of 10 kW COIL

Then the laser gas, which is composed of the mixture gas and the iodine, is expanded and accelerated to a laser gas velocity of about Mach 2 through the supersonic nozzle. The supersonic nozzle is made up of many small nozzles with vertical nozzle blades, and the area ratio of the nozzle throat to the nozzle exit plain is 1 to 2.3. To attain high efficiency and good beam quality, a Z-folded resonator configuration was adopted to this system, which makes maximum 3 paths through the gain region and the total cavity length was 5.2 m at that setting. The maximum gain length was 3.2 m per a round trip. The BHP circulation system is made

up of a BHP circulation pump, a heat exchanger and a chiller. The heat generated by the chemical reaction between gaseous chlorine and BHP is continuously removed from the BHP solution and the BHP inlet temperature is maintained at 255 K to minimize the generation of water vapor, which promises long-term operation over 30 minutes.

The experimental results with helium diluent gas about the dependence of the laser power on the mirror transmission are shown in Fig. 7. In the folded resonator configuration (2 paths), about 11 kW output was attained, and its beam shapes was 25 mm by 17 mm. The operation was conducted over a chlorine flow rate of 0.67 mol/s, a primary helium flow rate of 1.5 mol/s and a secondary helium flow rate of 0.75 mol/s. The upstream beam path in the gain medium was set in the distance of 30 mm from the supersonic nozzle outlet. The downstream beam path was set in the distance of 120 mm from the nozzle outlet. The typical measured values of the 10 kW COIL small signal gain are shown in Fig. 8. We made certain of the enough gain, 60 % of the upstream one, at the downstream side. This 10 kW COIL system can be also operated with nitrogen diluent gas instead of helium gas to curb the running cost because helium gas is very expensive, more than 5 times as expensive as nitrogen, in Japan. The output power of 5.3 kW was attained at a chlorine flow rate of 0.37 mol/s, a primary nitrogen flow rate of 0.97 mol/s and a secondary nitrogen flow rate of 0.57 mol/s. But the output

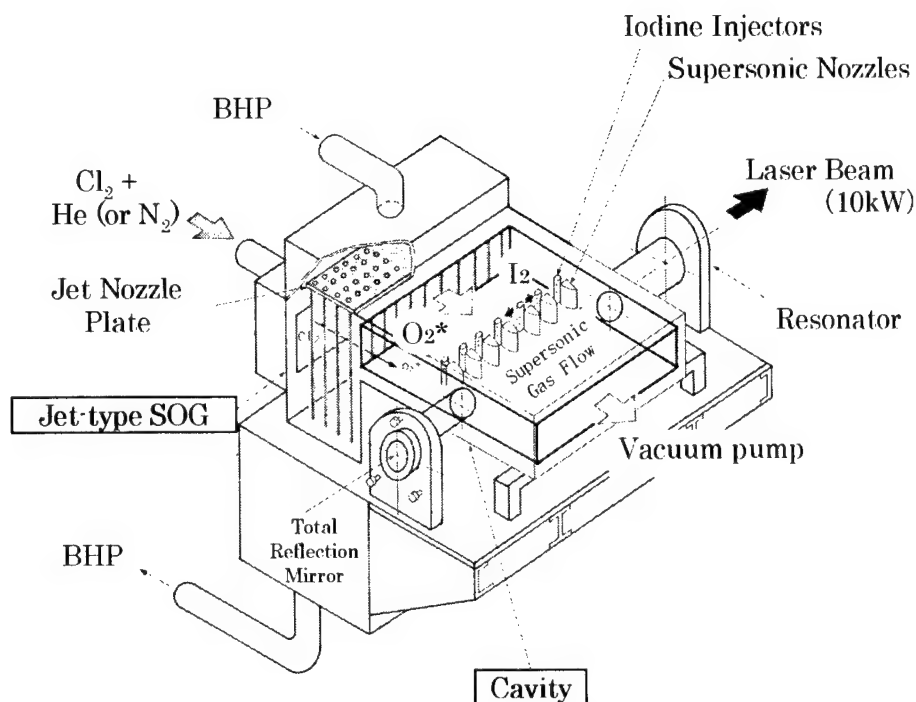


Fig. 6: Schematic diagram of the 10 kW COIL main construction

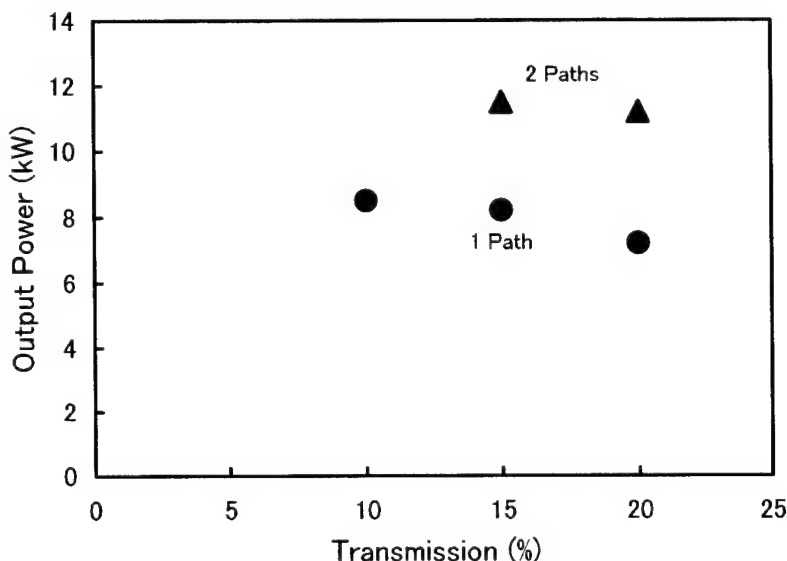


Fig. 7: Dependence of output power on mirror transmission

laser power with nitrogen diluent gas is limited to about a half of that with helium diluent to maintain the same total pressure with helium diluent gas in the J-SOG. By further studies, iodine injection technique etc., we obtained a maximum output power of 12 kW and a maximum chemical efficiency of 26 % at 3 paths configuration with helium diluent gas in 1999. This 10 kW system is operated 1-2 days a week for the laser processing at the present day.

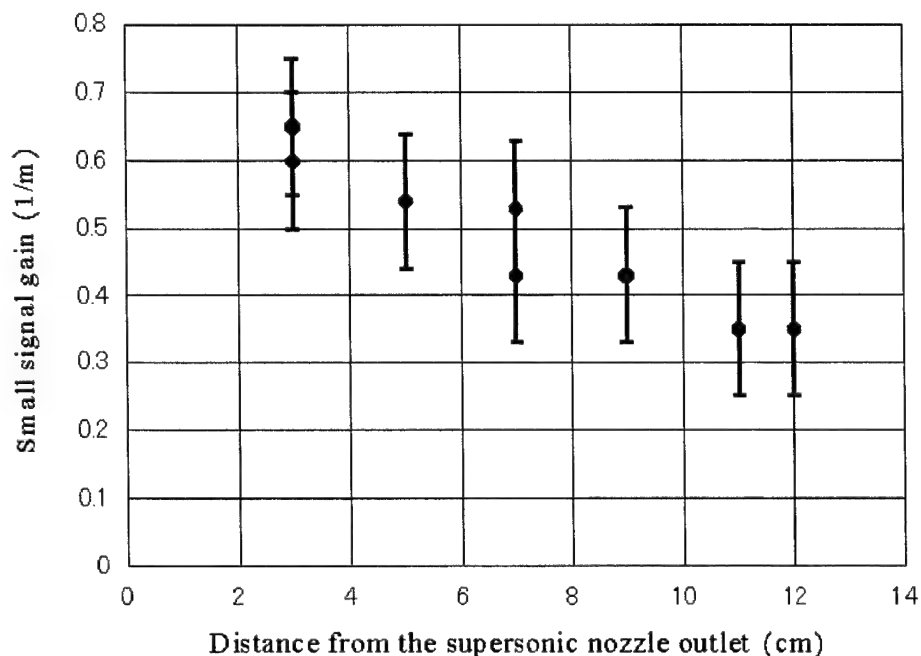


Fig. 8: Measured results of the 10 kW COIL small signal gain

Table 1: The major specifications of KHI's COILs

	1 kW (ALEC)	5 kW class	10 kW class
Operation mode	Subsonic	Supersonic	Supersonic
SOG type	Bubbler	Jet	Jet
Output power (kW)	1-2	-5	-12
Water vapor trap type	Rotating disk	Fin	Non
Chemical efficiency (%)	30	15	20-26
Cavity length (m)	2.2 (1 path)	5.1 (3 paths)	5.2 (3 paths)
Beam quality (mm*mrad)	86	60-80	60-80
Focused beam spot diameter at $1/e^2$ (μm)	280	300	220
Focal length of the focusing lens (mm)	77	84	82
Delivered fiber core diameter (mm)	0.3	0.6-0.8	0.6-0.8

4. STUDY OF COIL APPLICATIONS

The above-mentioned excellent COIL characteristics enable us to apply the laser processing to wide application fields. To examine the feasibility of the promising COIL application, we conducted various laser welding and cutting tests by using a fiber-transmitted high-power COIL beam. Especially, we conducted the study bent upon the laser remote dismantling system and the laser welding system for thick plates.

The COIL is of great advantage to application to the dismantling of the nuclear facilities, considering low transmission loss in radiation-proof optical silica fibers, high beam quality, high-power, and large energy absorption on the material surface. Figure 9 shows the concept of this COIL dismantling system. In dismantling of nuclear facilities, components of many different materials, shapes, dimensions or places need to be cut in the high radiation field so as to minimize secondary rad-wastes produced by cutting. Therefore, the cutting system for it is desired to be multipurpose, flexible, radiation-proof and easy in treatment. The laser cutting method can minimize the secondary rad-wastes because of a small beam size compared with other thermal cutting ones, and the treatment of the laser cutting devices is easy since the laser cutting head is smaller than the mechanical ones. The remote cutting system with a laser, especially COIL, transmitted through an optical silica fiber is promising for dismantling of activated in-vessel components and pressure vessels. Therefore, we conducted the empirical study of the remote laser dismantling system from 1994 to 2000^{13,14}. The laser cutting tests were conducted under the water because the operation has the matter of preventing radioactive contamination. This series of tests was carried out by use of the 1 kW subsonic commercial COIL, the 5 kW and 10 kW class supersonic COILs.

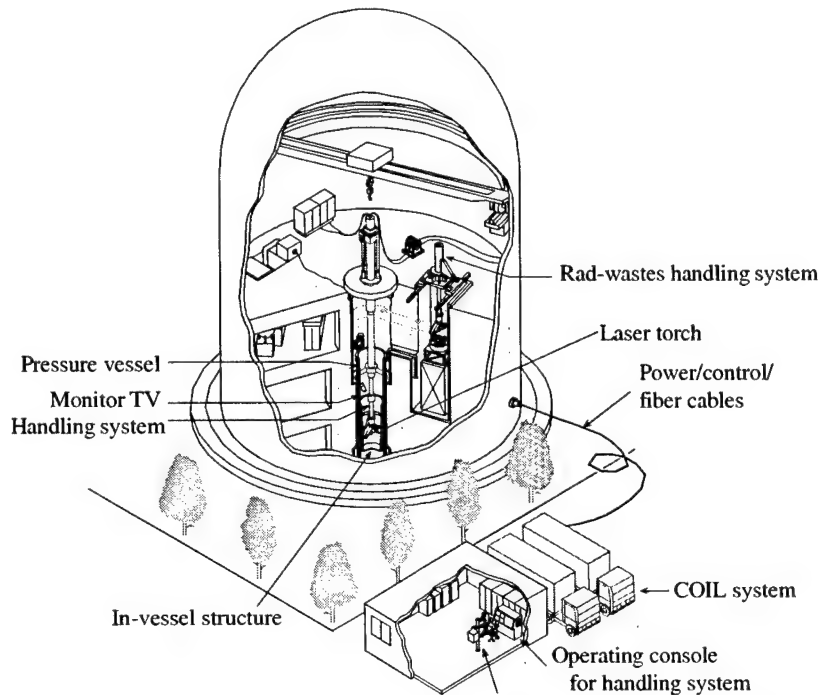


Fig. 9: Concept of remote dismantling system of nuclear reactor with COIL

We also conducted the laser welding study with COIL, energetically. Especially, the study of high-power laser welding has been accelerated under the Japanese national R&D project "Advanced Photon Processing and Measurement Technologies" since 1997. The aims of this project are to develop the technologies for generating high-power, high-quality lasers of high efficiency and low cost and also the advanced processing and measurement technologies which will use them. We secured a contract for the development of the advanced laser processing, namely, "Macroscopic processing technology", and had

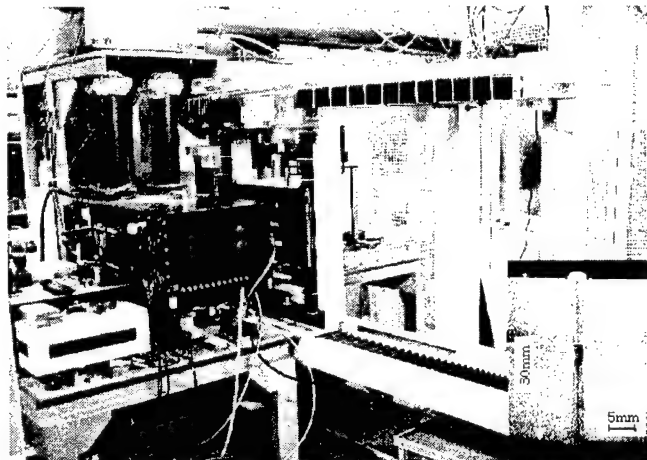


Fig. 10: Laser processing machine and welded sample of stainless steel

started the development of highly reliable laser welding technology. The goal of this contract is to establish the technology for laser welding of 30 mm thick steel plates and 20 mm thick aluminum alloy plates at a welding speed of higher than 1 m/min, providing high aspect ratio and equivalent or better strength than the base material. The laser processing machine and a cross section of the welded stainless steel are shown in Fig. 10. This study is carrying out with high-power lasers, 4 kW and 6 kW Nd:YAG lasers and the 10 kW class COIL, and many beneficial findings are obtained^{15,16,17}. The detail discussion of this study is yielded to another paper of ours¹⁸.

CONCLUSION

In this paper, we have reviewed our study of the industrial COIL from 1986 to date. As a result of long-standing study of the industrial COIL for the last 16 years, we have successfully completed the 10 kW COIL system. This system is used for the investigation of the various laser processing fields which are difficult to study by use of the conventional industrial lasers, and produces a lot of exciting results.

In the United States, the practical application of COIL is coming out true as the airborne laser (ABL). To realize a practical application in Japan, too, we will step up efforts toward the development of COIL. We hope that the brilliant features of COIL and the strenuous efforts of its researchers throughout the world will work out the broad application fields of it in the early 21st century.

ACKNOWLEDGMENTS

The development of highly reliable laser welding technology was partially conducted in the program "Advanced Photon Processing and Measurement Technologies" of the national Institute of Advanced Industrial Science and Technology, the Ministry of Economy, Trade and Industry, consigned to the R&D Institute for Photonics Engineering from the New Energy and Industrial Technology Development Organization (NEDO).

REFERENCES

1. W. E. McDermott, N. R. Pchelkin, D. J. Benard, and R. R. Bousek, "An electric transition chemical laser", *Appl. Phys. Lett.* **32**, pp. 469-470, 1978.
2. H. Yoshimoto, H. Yamakoshi, Y. Shibukawa, and T. Uchiyama, "A highly efficient, compact chemical oxygen-iodine laser", *J. Appl. Phys.* **59**, pp. 3965-3967, 1986.
3. H. Fujii, S. Yoshida, M. Iizuka, and T. Atsuta, "Development of high-power chemical oxygen-iodine laser for industrial application", *J. Appl. Phys.* **67**, pp. 3948-3953, 1990.
4. F. Wani, N. Naito, T. Nagai, M. Iizuka, H. Tsuji, and H. Fujii, "Development of 1 kW CW Iodine Laser for Industrial Use", *Proc. Laser Advanced Material Processing (LAMP'92)*, pp. 127-132, 1992.
5. H. Fujii, "COIL Development in Japan", *Proc. AIAA* **94-2419**, 1994.
6. N. Naito, F. Wani, T. Nagai, T. Nakabayashi, and H. Fujii, "High power COIL development", *Proc. CLEO/Pacific Rim'95*, pp. 160, 1995.
7. F. Wani, T. Nakabayashi, and H. Fujii, "High-pressure singlet oxygen production using a jet-type generator", *Proc. CLEO/Pacific Rim'95*, pp. 160, 1995.
8. T. Sakurai, K. Yasuda, T. Osaki, E. Tada, K. Koizumi, and M. Nakahira, "Study on material processing and fiber transmittance of COIL", *Proc. ICALEO 1996, Section E*, pp. 28-37, 1996.
9. F. Wani, N. Naito, T. Nagai, and H. Fujii, "Achievement of 10 kW oscillation of the industrial chemical oxygen iodine laser", *Proc. CLEO/Pacific Rim'97*, pp. 99, 1997.
10. N. Naito, F. Wani, T. Nagai, and H. Fujii, "Industrial COIL in Japan", *Proc. AIAA* **97-2392**, 1997.

11. S. Yoshida, M. Endo, T. Sawano, S. Amano, H. Fujii, and T. Fujioka, "Chemical oxygen iodine laser of extremely high efficiency", *J. Appl. Phys.* **65**, pp. 870-872, 1989.
12. H. Fujii, S. Yoshida, M. Iizuka, and T. Atsuta, "Long-term stability in the operation of chemical oxygen-iodine laser for industrial use", *J. Appl. Phys.* **66**, pp. 1033-1037, 1989.
13. K. Tsurumaki, H. Miyao, H. Tomioka, J. Adachi, K. Yasuda, H. Okado, A. Hayakawa, and S. Yoshizawa, "Development of remote dismantling of components in nuclear reactor with laser transmitted through optical fiber", *Proc. ICONE 5-2074*, 1997.
14. H. Okado, T. Sakurai, J. Adachi, H. Miyao, and K. Hara, "Underwater cutting of stainless steel with the laser transmitted through optical fiber", *Proc. SPIE 3887*, pp. 152-160, 2000.
15. T. Nakabayashi and M. Muro, "High power chemical oxygen-iodine laser welding", *Proc. SPIE 3887*, pp. 359-366, 2000.
16. T. Nakabayashi, F. Wani, H. Okado, A. Hayakawa, S. Suzuki, and K. Yasuda, "Laser welding characteristics with high power combining beam", *Proc. ICALEO 2001*, **Section A-302**, 2001.
17. H. Okado, T. Nakabayashi, F. Wani, A. Hayakawa, S. Suzuki, and K. Yasuda, "Beam operation for thick plate laser welding", *Proc. the 7th Int. Symp.*, pp. 491-496, 2001.
18. F. Wani, T. Nakabayashi, A. Hayakawa, S. Suzuki, and K. Kozo, "High-power COIL and YAG laser welding", *Proc. SPIE 4631*, 2002, to be published.

Spatially-resolved temperature diagnostic for the chemical oxygen-iodine laser based on a variant of saturation spectroscopy

Grady T. Phillips, Glen P. Perram, and Won B. Roh
Air Force Institute of Technology

ABSTRACT

The Chemical Oxygen-Iodine Laser (COIL) depends upon a supersonic mixing nozzle to produce optical gain on the $^2P_{1/2} - ^2P_{3/2}$ atomic iodine transition at $\lambda = 1.315 \mu\text{m}$. The translational temperature in the gain generator is particularly important, as the yield of singlet oxygen required to reach lasing threshold decreases from 17% at room temperature to 6% at $T=150\text{K}$. We have demonstrated an optical technique for measuring the gas temperature in the COIL supersonic expansion region with a spatial resolution of less than 12 mm^3 using a novel variant of saturated laser spectroscopy. The sub-Doppler hyperfine spectrum of the visible $\text{I}_2 \text{ X}^1\Sigma_g^+ \rightarrow \text{B}^3\Pi(0_u^+)$ transition exhibits 15 or 21 transitions and has been recorded using laser saturation spectroscopy with a resolution of about 10 MHz. Pressure broadening of the hyperfine components and cross-relaxation effects have been studied and depend significantly on rotational level. By altering the saturation spectroscopy apparatus so that the pump and probe beams are nearly co-propagating, a Doppler profile, limited to the iodine sample in the volume of the overlapped beams, is obtained. Temperature, as derived from the Doppler profile, is spatially resolved and used to examine the flow from a small supersonic nozzle assembly.

Keywords: saturation spectroscopy, iodine, hyperfine spectrum, linewidth, pressure broadening, temperature diagnostic, Chemical Oxygen-Iodine Laser (COIL), cross-relaxation, velocity-changing collisions

1. INTRODUCTION

Since the first demonstration of a Chemical Oxygen-Iodine Laser (COIL) in 1978,¹ the technology has advanced significantly to supersonic laser devices with high output power and excellent beam quality.²⁻⁴ The Chemical Oxygen-Iodine Laser operates on the hyperfine components of the $5^2P_{1/2} - 5^2P_{3/2}$ transition in atomic iodine and is chemically pumped through energy transfer from the metastable $\text{O}_2(a^1\Delta)$. The $\text{O}_2(a^1\Delta)$ and $\text{I}(^2P_{1/2})$ states are nearly resonant with an energy defect of only 279 cm^{-1} . Several excellent reviews of the laser hardware, chemistry, laser physics, and fluid dynamics of these devices are available.²⁻⁴

The COIL device employs a supersonic mixing nozzle to: (1) inject, mix and dissociate molecular iodine to produce the lasing, atomic iodine, (2) produce a spatially uniform gain and a region of uniform index of refraction for good beam quality, (3) increase the laser power for a given flow cross-sectional area, and (4) reduce the gas temperature in the gain cavity. The translational temperature is particularly important for COIL, as the yield of singlet oxygen required to reach lasing threshold decreases from 17% at room temperature to 6% at $T=150\text{K}$.²

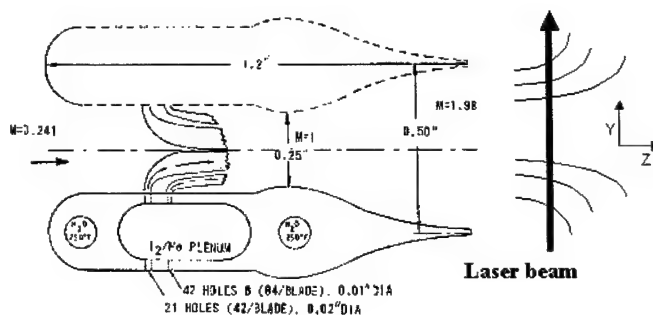


Figure 1. RotoCOIL mixing nozzle.²

Spatial distributions of the small signal gain and cavity temperature at the exit of the supersonic mixing nozzle of Chemical Oxygen-Iodine Lasers (COIL) have been measured previously by diode laser spectroscopy on the $^2P_{1/2}(F^{\circ}=3) -$

¹glen.perram@afit.edu; phone 1 937 255 3636 x 4504; Fax 1 937 255 2921; <http://www.afit.edu>; Air Force Institute of Technology/ENP, 2950 P Street, Wright-Patterson AFB, OH 45433-7765

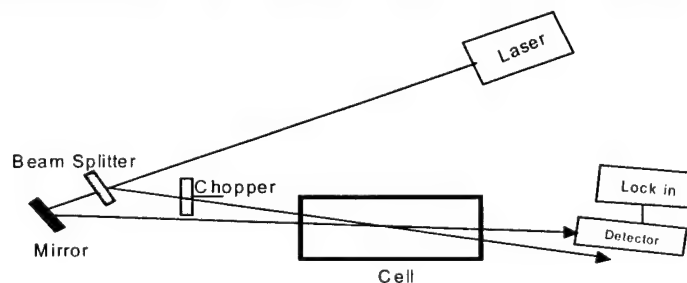
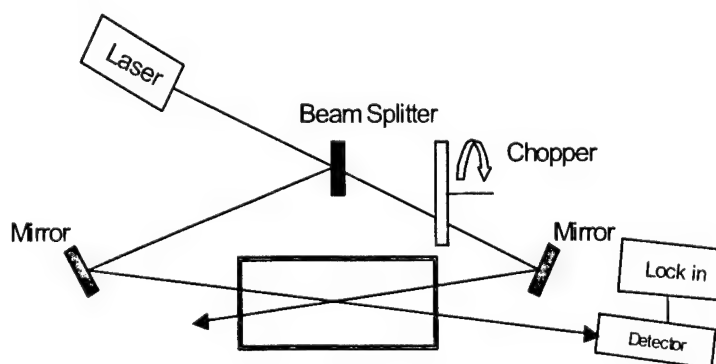
$^2P_{3/2}(F=4)$ transition in atomic iodine.⁵ The resulting cavity temperatures of about 200 K is significantly higher than the predicted temperature of the supersonic expansion of about 150 K. The technique is limited to measuring an average temperature along the direction of the diode laser beam propagation and may be biased due to the directed flow resulting from symmetrical turbulent vortices, as illustrated in Figure 1. An optical technique for measuring the three-dimensional temperature flow field at the exit plane of the supersonic nozzle is required to fully assess nozzle efficiency and chemical heat release during I_2 dissociation. The focus of the present work is to exploit a novel variant of laser saturation spectroscopy to develop a temperature diagnostic with spatial resolution of less than 12 mm^3 .

2. EXPERIMENT

Laser saturation spectroscopy is a well established technique for obtaining sub-Doppler resolution in gas phase spectroscopy.⁶ The technique depends on the selection of a subgroup of molecules with a small range of velocities near $v=0$ using a narrow linewidth laser source.⁶ In particular, saturation spectroscopy is based on the selective saturation of an inhomogeneously broadened transition. A laser source "burns a hole" into the population distribution of the absorbing state by exciting a corresponding peak in the same velocity component in the upper state. Such a hole can be detected by frequency scanning a second laser source through resonance with the first source and monitoring the attenuation of the transmitted beam.

If the output from a single laser is split into two beams which are arranged to counter-propagate in the same media (see Figure 2), then two holes will be burned symmetrically about the line center. The two beams interact with the same velocity groups only when the laser is tuned to line center. The absorption of one of the beams (probe beam) will diminish at line center if the intensity of the second beam (pump beam) is sufficiently intense (near saturation) to alter the population distribution in the absorbing state. This dip in the probe beam absorption at line center due to the counter-propagating pump beam is termed the *Lamb Dip*. One technique for using this Lamb Dip to perform sub-Doppler spectroscopy involves modulating the amplitude of the pump beam and monitoring the modulated portion of the transmitted probe beam. A non-zero signal is obtained only when the two beams interact with the same velocity group ($v=0$) in the region where the two beams are overlapped. The observed linewidth is reduced to the homogeneous (Lorentzian) limit. Such sub-Doppler spectroscopy has been demonstrated for molecular iodine,⁷ and other atomic and molecular species.⁶

In the current paper we demonstrate a novel variant of the laser saturation spectroscopy which retains the Doppler-limited lineshape, but provides spatial resolution. A schematic diagram for these experiments is shown in Figure 3. By arranging the pump and probe beam to cross each other with a small, but finite angle, the two beams can be made to simultaneously interact only with a small volume of gas. Since the two beams propagate in the same direction, they always interact with the same velocity group, and the full Doppler profile is retained. The Doppler profile can then be utilized to determine the translational temperature for the absorbing medium in the crossing volume. The width, Δv_D , (FWHM) for a single Doppler broadened line is related to the temperature, T , according to the relationship:



$$\Delta\nu_D = \sqrt{\frac{8kT \ln 2}{Mc^2}} \nu_o \quad (1)$$

where ν_o is the line center and M is the mass of the absorbing atom or molecule. By fitting the theoretical spectrum to the experimental spectra, using the temperature as the fitting parameter, one can determine the local temperature of the absorbing medium.

Molecular iodine, I_2 , is a convenient candidate for laser saturation spectroscopy in the COIL device. The saturation intensity is low and many ro-vibrational transitions of the B-X system are accessible in the red portion of the visible spectrum. The near coincidence of several rotational features, possible from different vibrational levels may aid in temperature determination, as the intensities of the rotational features are given by the statistical distribution:

$$\frac{N(J)}{N_{tot}} = \left(\frac{hcB_v}{kT} \right) (2J+1) e^{-J(J+1)hcB_v/kT} \quad (2)$$

where B_v is the rotational constant and J is the rotational quantum number.

In the present study, a Coherent model 899 ring dye laser pumped by a Spectra Physics Model 2080 Ar^+ laser at 514.5 nm was used as the laser excitation source. Exciton Rhodamine 590 dye was used to cover the spectral region 16260.16–18083.18 cm^{-1} . The intensity of the transmitted probe beam was monitored with a Hamamatsu S2281 silicon photodiode. The side fluorescence was detected with a Burle Photomultiplier Tube model C31034A02. The laser beam was amplitude modulated with a Model SR540 mechanical chopper at 0–4000 Hz and the phase sensitive detection was accomplished using a Stanford Research Systems model SR850 lock-in amplifier. A static glass cell (41.5 cm long) was evacuated to < 16 mTorr using a Alcatel 2015 C2 rotary vane pump. Iodine and added buffer gas pressures were monitored with MKS pressure transducers: MKS Model 390HA for < 1 Torr and a MKS Model 690A for 1 to 1000 Torr; both utilizing a MKS Type 270 signal conditioner.

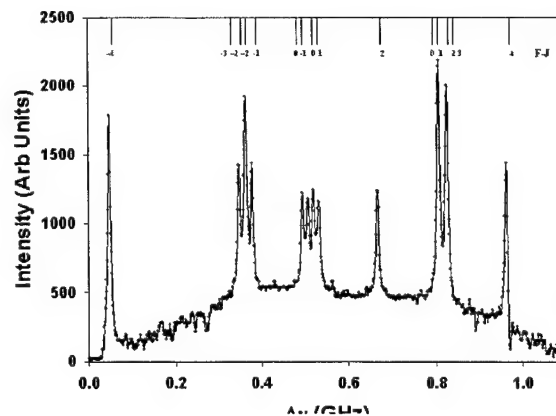
3. RESULTS

3.1 Hyperfine Spectrum

The sub-Doppler laser saturation spectrum of the isolated (171) P(70) line of the $I_2 X^1\Sigma_g^+ - B^3\Pi(0_u^+)$ transition at $\nu=17339.8187 \text{ cm}^{-1}$ is shown in Figure 4. The spectrum is composed of a set of either 15 or 21 hyperfine spectral components, depending on the parity of the rotational state. The hyperfine components are labeled according to value of F-J, as discussed below.

The Hamiltonian for the nuclear electric quadrupole interaction is:

$$\hat{H}_{NEQ} = -eQq \left(\frac{3(\vec{I}_1 \cdot \vec{J})^2 + \frac{3}{2}(\vec{I}_1 \cdot \vec{J}) - |\vec{I}_1|^2 |\vec{J}|^2}{2(2J+3)(2J-1)I_1(2I_1-1)} + \frac{3(\vec{I}_2 \cdot \vec{J})^2 + \frac{3}{2}(\vec{I}_2 \cdot \vec{J}) - |\vec{I}_2|^2 |\vec{J}|^2}{2(2J+3)(2J-1)I_2(2I_2-1)} \right) \quad (3)$$



where Q is the electric quadrupole moment, q_j is the average E-field gradient along the J direction, e is the electron charge, J is the sum of the spin and orbital angular momentum of the molecule, and $I_1=I_2=5/2$ is the atomic iodine nuclear spin angular momentum. The Hamiltonian for the nuclear magnetic dipole interaction is

$$H_m = \mu \frac{G}{I_1} (\vec{I}_1 \cdot \vec{J}) \quad (4)$$

where $\mu G/I_1$ is the spin rotation coupling constant. Finding energy eigenvalue solutions to the Hamiltonian involves the diagonalization of a nontrivial matrix. However, approximate solutions can be found for $J \gg 1$ of the form:⁸

$$E = E_{NEQ} + E_M$$

$$E_{NEQ} \cong -\frac{eQq}{8I_1(2I_1-1)} \left\{ (M_1^2 + M_2^2) + \frac{3}{J} M_1 \left[M_1(M_1+1) - I_1(I_1+1) + \frac{1}{2} \right] + \frac{3}{J} M_2 \left[M_2(M_2+1) - I_1(I_1+1) + \frac{1}{2} \right] - 2I_1(I_1+1) \right\} \quad (5)$$

$$E_M \cong \frac{\mu G}{I_1} (M_1 + M_2) J$$

Table I provides an evaluation of equation (5) for $v'=21$, $J'=116$ line using the values $eQq=-2900$ MHz and $G/I_1=0.049$ MHz. For $I_1=I_2=5/2$, the possible values from the projection along the internuclear axis are $-5/2 \leq M_1, M_2 \leq +5/2$. The Pauli exclusion principle requires the total wave function of a homonuclear diatomic molecule with a half integer nuclear spin remain antisymmetric under an exchange of the nuclei. As a consequence the $M_1 = M_2$ combinations are forbidden for $J'=\text{odd}$, but included for $J'=\text{even}$. The relative line positions for $v'=21$ for a broad range of rotational states based on the approximate solution of equation (5) is provided in Figure 5.

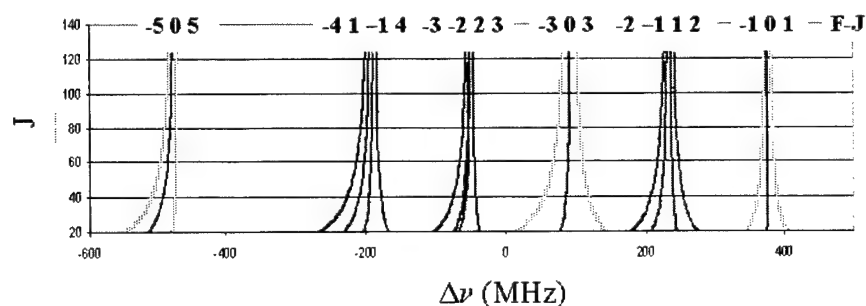


Figure 5. Predicted hyperfine splitting within $v'=21$.

Table I
Hyperfine splitting for $v'=21$, $J'=116$.

M_1	M_2	F-J	F	$E_{NEQ}+E_m$
2.5	2.5	5	122	755.989
2.5	1.5	4	121	307.820
2.5	0.5	3	120	87.375
2.5	-0.5	2	119	89.078
2.5	-1.5	1	118	307.352
2.5	-2.5	0	117	736.619
1.5	1.5	3	120	-140.349
1.5	0.5	2	119	-360.794
1.5	-0.5	1	118	-359.091
1.5	-1.5	0	117	-140.817
1.5	-2.5	-1	116	288.450
0.5	0.5	1	118	-581.238
0.5	-0.5	0	117	-579.535
0.5	-1.5	-1	116	-361.262
0.5	-2.5	-2	115	68.005
-0.5	-0.5	-1	116	-577.832
-0.5	-1.5	-2	115	-359.559
-0.5	-2.5	-3	114	69.708
-1.5	-1.5	-3	114	-141.286
-1.5	-2.5	-4	113	287.981
-2.5	-2.5	-5	112	219.592

3.2 Pressure Broadening

The hyperfine components are well represented by pressure dependent Lorentzian lineshapes. In Figure 6, the hyperfine spectrum is shown for two argon buffer gas pressures. Significant broadening is evident for low pressures. A set of Lorentzian lineshapes with common widths have been fit to the type of hyperfine data of Figure 6 for a variety of argon buffer gas pressures where the I2 pressure was fixed at .1635 Torr. The resulting linewidths are shown in Figure 7. The fit includes a Gaussian baseline, which is described below in the velocity cross-relaxation discussion.

The intercept in Figure 7 indicates a zero-pressure broadening of 9.40 ± 0.16 MHz, which corresponds to natural broadening with a lifetime of $0.67 \mu\text{s}$. The collisionless lifetime ($1/\tau_0 = 1/\tau_{\text{rad}} + 1/\tau_{\text{nr}}$) for this state is $\tau_0 = 1.08\text{-}1.14 \mu\text{s}$.⁹

The slope in Figure 7 provides a pressure broadening rate of 8.14 ± 0.30 MHz/Torr. This result is somewhat higher than the value of 6.6 MHz/Torr reported from Doppler limited absorption studies,¹⁰ and significantly larger than the (v,J) dependent rates of 0.31 – 2.96 MHz/Torr reported from fluorescence depolarization studies.¹¹ Further studies are in progress to examine the pressure broadening rates for a wide variety of collision partners.

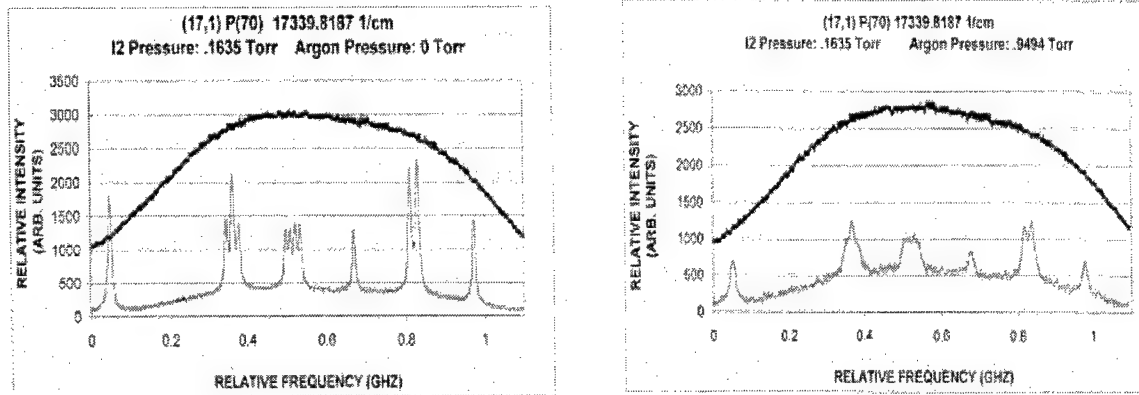


Figure 6. Pressure broadened hyperfine spectrum for the (17,1) P(70) line.

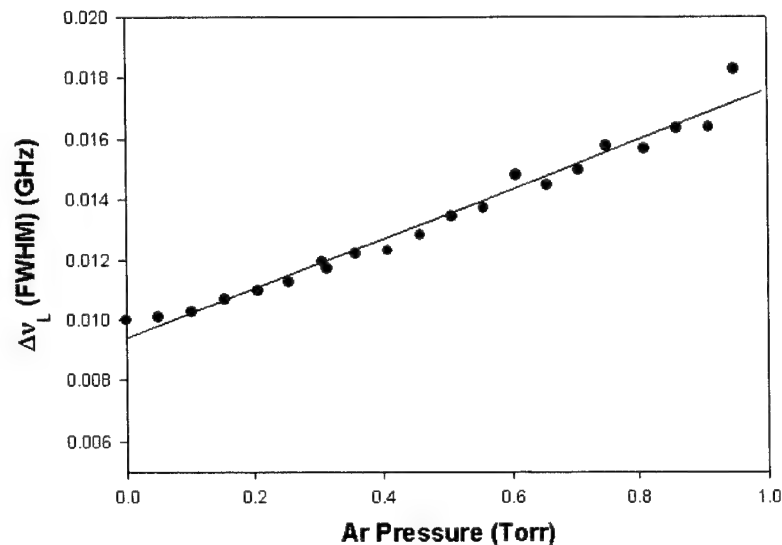


Figure 7. Pressure broadening rate for (17,1) P(70) line with argon collision partner.

Pressure broadening at higher pressures can be obtained from the laser excitation spectra. Figure 8 illustrates the side fluorescence intensity as a function of laser frequency and represents the convolution of 15 Voigt broadened hyperfine levels. To extract the pressure broadening rates, a fit of the hyperfine lines is performed. The spectrum of Figure 8 is fit to the convolved lineshape function:

$$g_V(\nu) = \sum_{i=1}^{15 \text{ or } 21} \text{Voigt}(\nu; I_i, \nu_{oi}, \Delta\nu_D, \Delta\nu_L) e^{-c \sum_{i=1}^{15 \text{ or } 21} \text{Voigt}(\nu; I_i, \nu_{oi}, \Delta\nu_D, \Delta\nu_L)} + a + b\nu \quad (6)$$

where a and b represent the background baseline, c is required to model the self absorption of the pump beam by the I_2 gas, the relative intensities of the hyperfine components, I_i , are constrained by their statistical weights, $2F+1$, ν_{oi} is the

hyperfine component line center positions as determined from the sub-Doppler spectrum, $\Delta\nu_D$ is the common Doppler width (FWHM), and $\Delta\nu_L$ is the common Lorentzian width (FWHM). The fit shown in Figure 8 was performed with the Doppler width constrained by the known sample temperature at $T=292.6$ K, and the Lorentzian width defined by the intercept in Figure 7 and the self broadening rate of $\gamma_{I_2} = 8$ MHz/Torr.¹² A complete analysis of these laser excitation spectra lineshapes at high pressure for a wide variety of collision partners is in progress. A fit to the I_2 side fluorescence broadened by Ar buffer gas is shown in Figure 9 where the Doppler width is constrained as mentioned and the Lorentzian is defined additionally by the Ar pressure broadening rate from Fig. 7.

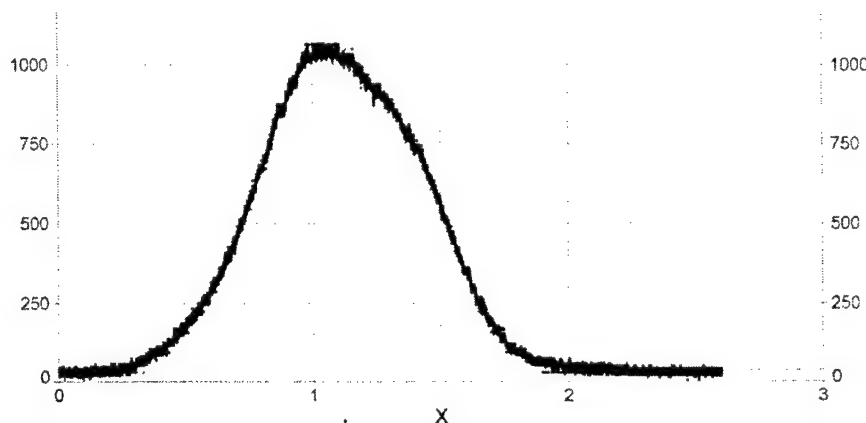


Figure 8. Laser excitation spectrum of (17,1) P(70) line at 36.5 mTorr I_2 .

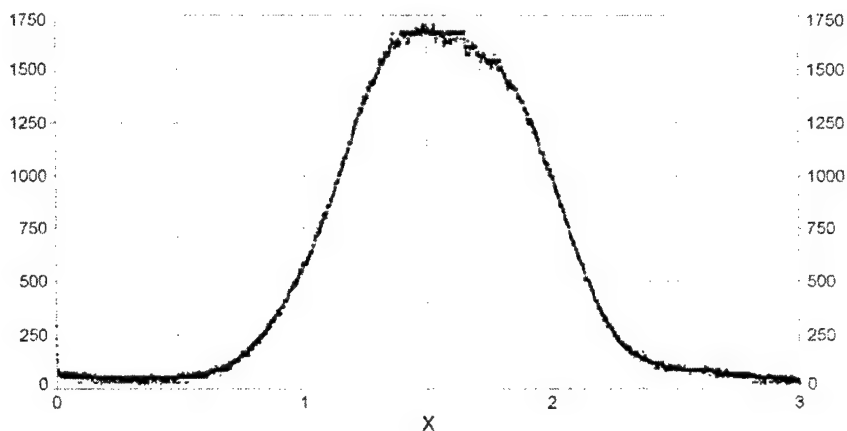


Figure 9. Laser excitation spectrum of (17,1) P(70) line at 163.5 mTorr I_2 and 3.1 Torr Ar.

3.3 Velocity Cross-Relaxation

The sub-Doppler laser saturation spectra exhibit a broader feature upon which the hyperfine structure is superimposed. The amplitude of this feature depends on rotational level, J , pressure, and modulation frequency, as shown in Figure 10. Two, closely spaced rotational lines with significantly different rotational states are overlapped in these 2 GHz scans. The broader feature is much more intense for the lower rotational level. The intensity of the broad feature relative to the intensity of the hyperfine resolved components decreases with modulation frequency (as shown in Figure 10b) and total pressure. Similar affects have been observed previously and attributed to velocity cross-relaxation dynamics.⁷

To further illustrate these collisional dynamics, consider the following example. An I_2 non-zero velocity group, v_g , interacts with the pump beam and then suffers a collision that converts the velocity group to $-v_g$. The probe beam is then in resonance with the new velocity group, and as long as the collision occurs during the same modulation cycle, the probe laser intensity is correlated with chopping frequency. Since such collisions can occur for any velocity group, v_g , a broad feature with Gaussian shape is obtained. At higher pressures and lower modulation rates, more collisions occur and contribute to a more intense feature. Apparently, the dynamics are dominated by rotationally inelastic collisions, yielding a strong dependence on rotational state. Multiple collisions would be required for R-T events, to return the population to the initial state and contribute to the observed lineshape.

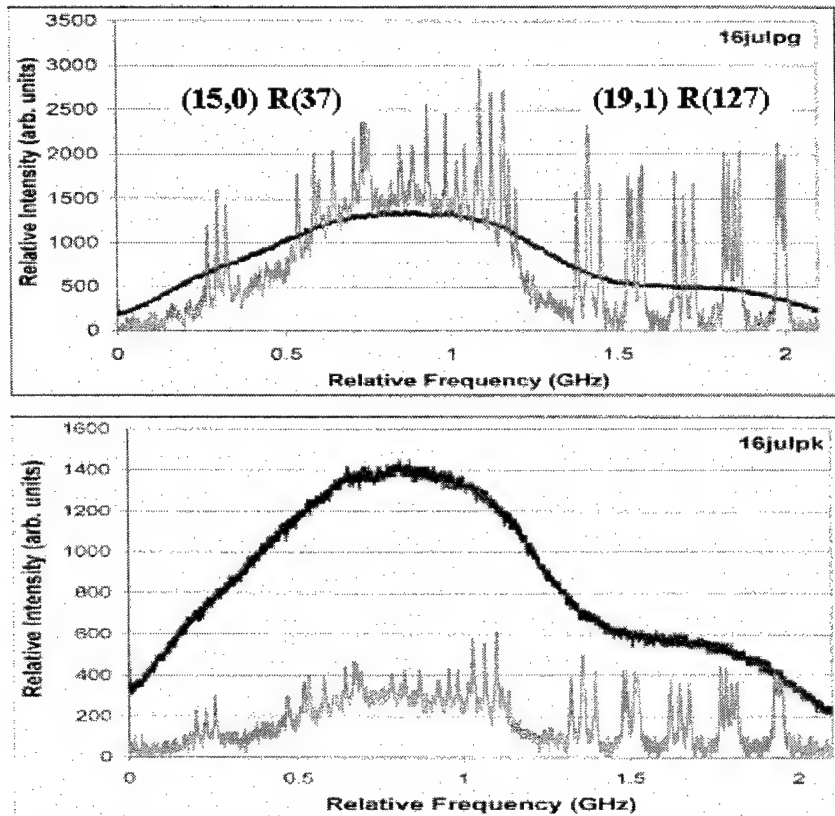


Figure 10 Upper spectrum taken at a chopping frequency of 1000 Hz. Lower spectrum taken at a chopping frequency of 3754 Hz.

3.3 Spatially-Resolved Temperature Diagnostic

The Doppler limited laser saturation spectrum for the (17,1) P(70) line using the apparatus described in Figure 3 is shown in Figure 11.¹³ For these studies, a static I_2 cell with differential heating was employed. The hot end of the cell was maintained at $T = 523$ K. The pump and probe beams were co-propagated with a small crossing angle of 3.8 degrees, resulting in a crossing volume of 12 mm^3 . Three spectra were recorded; near the hot end, in the center and near the colder end of the 0.5" diameter by 6" length cell. The width of the observed lineshapes increases with increasing cell temperature, establishing the feasibility of extracting spatially resolved temperatures. The lineshape studies discussed above are essential to extracting accurate temperatures.

Figure 12 predicts the lineshapes for temperatures in increments of 50 K from 50 - 400K. The sensitivity of the diagnostic is improved at lower temperatures, and we are pursuing the application of the technique in a supersonic

expansion as discussed below. The uncertainty in extracted temperatures may be further enhanced by using several closely spaced lines associated with different rotational levels as shown in Figure 10. The rotational Boltzmann distribution of equation (2) can be used to further constrain the temperature.

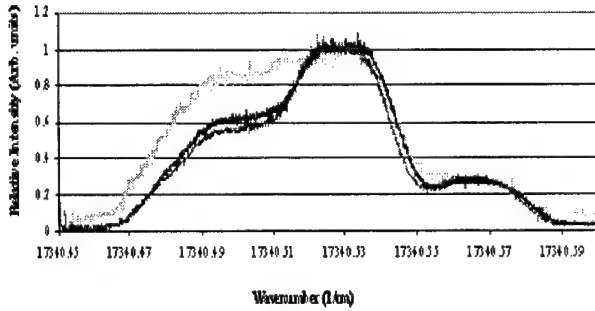


Figure 11. Doppler-limited saturation spectra at three locations in a differentially heated cell.

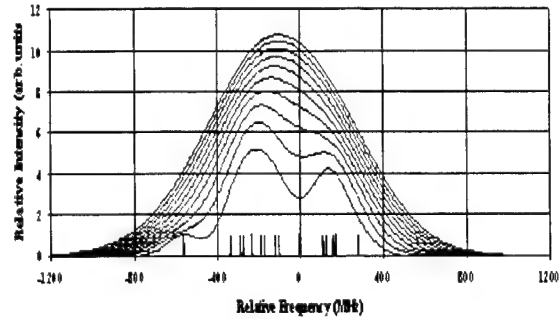


Figure 12. Predicted Doppler-limited saturation spectra at T=50 – 400 K in 50K increments.

A Laval nozzle designed by the Air Force Research Laboratory will be used to simulate the conditions in a COIL supersonic nozzle. The Laval nozzle produces a flow at the exit with constant Mach number.¹⁴ A schematic of the nozzle is shown in Figure 12. A diffuser is located after the gas inlet to establish a near-zero net hydrodynamic velocity. After the diffuser, there is a convergent section where the flow begins to accelerate and then passes through the throat, to reach its maximum velocity. The Mach number at any point in the along the nozzle can be obtained from the expression for the area ratio:¹⁴

$$\frac{A}{A^*} = \frac{1}{M} \left[\left(\frac{2}{k+1} \right) \left(1 + \frac{k-1}{2} M^2 \right) \right]^{\frac{k+1}{2(k-1)}} \quad (7)$$

where A^* is the cross-sectional area of the throat, $k=c_p/c_v$ is the ratio of the heat capacity at constant pressure to the heat capacity at constant volume, and M is the Mach number. At the throat, the Mach number is 1. Assuming the flow is accelerated to a uniform Mach number, the drop in temperature and pressure can be computed from:¹⁴

$$\frac{T_o}{T} = 1 + \frac{k-1}{2} M^2, \quad (8)$$

and

$$\frac{p_o}{p} = \left(1 + \frac{k-1}{2} M^2 \right)^{\frac{k}{k-1}}, \quad (9)$$

where T_o , and p_o are the temperature and pressure in the pre-expansion stagnation region. Assuming the stagnation temperature $T_o=298.15$ K, the temperature at the point where the nozzle widens to 0.7 cm is $T \approx 183$ K .

4. CONCLUSIONS

A novel variant of laser saturation spectroscopy to diagnose the temperature in the supersonic nozzle of a Chemical Oxygen-Iodine Laser has been demonstrated. Accurate temperature measurements require high signal-to-noise spectral lineshapes and detailed characterization of hyperfine line positions, pressure broadening rates, and self-absorption. Initial studies of the sub-Doppler lineshapes have been reported. The sub-Doppler spectra exhibit features related to

velocity cross-relaxation which may be used to study rotationally inelastic collisions. The extension of this technique to supersonic flows is in progress.

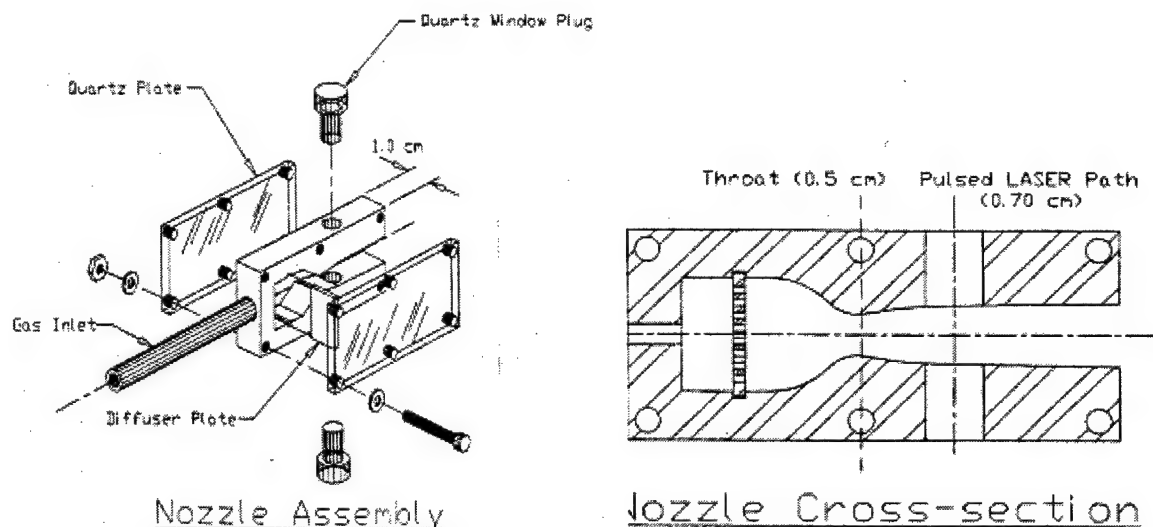


Figure 13. Laval nozzle for demonstration of spatially resolved temperature measurement at low temperatures.

REFERENCES

1. McDermott, W.E., N.R. Pchelkin, D.J. Benard, and R.R. Bousek, "An Electronic Transition Chemical Laser," *App. Phys. Lett.* **32** 469 (1978).
2. N. Bloembergen and C.K.N. Patel (Co-chairs, APS Study Group), *Rev. Mod. Phys.* **59**, S1 (1987).
3. K.A. Truesdell, S.E. Lamberson, and G.D. Hager, *AIAA* **92**, 3003 (1992).
4. P.V. Avizonis, G. Hasen, and K.A. Truesdell, *SPIE* **1225**, 448 (1990).
5. P.B. Keating, C.A. Helms, B.T. Anderson, T.L. Rittenhouse, K.A. Truesdell, and G.D. Hager, "Two-Dimensional Gain and Cavity Temperature Maps of a Small-Scale Supersonic COIL," in *Proceedings of the International Conference on Lasers '96*, Ed. Pp 194-201, V.J. Corcoran and T.A. Goldman, editors, STS Press, McLean, VA, 1997.
6. Demtroder, Wolfgang. *Laser Spectroscopy*, Berlin: Springer, 1998.
7. Morinaga, A. "Cross-relaxation Effects on the Saturation of the Visible Absorption Lines of the Iodine Molecule," *J. Opt. Soc. Am. B*, **4** (6): 906-909 (June 1987).
8. Levenson, M. D., and A.L. Schawlow, "Hyperfine Interactions in Molecular Iodine," *Physical Review A*, **6** 10-20 (July 1972).
9. Capelle, Gene A., and H.P. Broida, "Lifetimes and Quenching Cross Sections of $I_2(B^3\Pi_{Ou}^+)^*$," *The Journal of Chemical Physics*, **58** 4212-4222 (15 May 1973).
10. S.V. Kireev, S.L. Shnyrev, and Yu.P. Zaspas, *Optics and Spectroscopy*, **78** 550 (1995).
11. M. Berjot, L. Bernard, and T. Theophanides, *Can J Spectrosc* **18** 128 (1973).
12. Sorem, M.S., and A.L. Schawlow, "Saturation Spectroscopy in Molecular Iodine by Intermodulated Fluorescence," *Optics Communications*, **5** 148-151 (1972).
13. Myers Jr., James W. *Spatially Resolved Temperature Determination in I_2 Gas Using Doppler-Limited Saturation Spectroscopy*. MS Thesis, AFIT/GAP/ENP/00M-03. Graduate School Engineering and Management, Air Force Institute of Technology (AU), Wright-Patterson AFB OH, March 2000.
14. Shapiro, Ascher H. *The Dynamics and Thermodynamics of Compressible Fluid Flow, Vol. I*. New York: John Wiley & Sons, 1953, p.86.

Diagnostic development for the ElectriCOIL flow system

J. T. Verdeyen^{*a}, D. M. King^{*a}, D. L. Carroll^{*a} and W. C. Solomon^{**b}

^aCU Aerospace; ^bUniversity of Illinois at Urbana-Champaign

ABSTRACT

Detailed studies of mechanisms for producing electrically initiated COIL lasers were previously presented. Results of those studies along with more recent experimental results show that electric excitation is a very complex process that must be investigated with advanced diagnostics. Theoretical studies indicate that fractions of $O_2(^1\Delta)$ may be produced in the discharge that will permit lasing of an ElectriCOIL system. Recent kinetic studies indicate a range of useful operating parameters for ElectriCOIL that are analogous to those achieved in the all-chemical device. This can be accomplished at E/N 's in the range of 10^{-16} Volt-cm². An experimental test bed has been built up to allow detailed diagnostic measurements of the discharge efficiencies and other experimental parameters. Results of early experiments are presented.

Keywords: chemical oxygen-iodine laser, COIL, ElectriCOIL, RF excitation of oxygen, singlet-delta oxygen

1. INTRODUCTION

Researchers at CU Aerospace (CUA) and University of Illinois at Urbana-Champaign (UIUC) have been operating chemical lasers (HF/DF, Overtone HF, and COIL) for a number of years. The classical chemical oxygen-iodine laser (COIL) [McDermott, 1978] operates on the electronic transition of the iodine atom at 1315 nm, $I(^2P_{1/2}) \rightarrow I(^2P_{3/2}) + h\nu$. The population inversion is maintained by the near resonant energy transfer between the excited singlet oxygen $O_2(^1\Delta)$ molecule and the I atom ground state $I(^2P_{3/2})$ as follows: $O_2(^1\Delta) + I(^2P_{3/2}) \rightarrow O_2(^3\Sigma) + I(^2P_{1/2})$. Traditionally, this pumping reaction has been fed by a liquid chemistry singlet oxygen generator (SOG). Workers at CUA and UIUC are now addressing the engineering issues associated with an electrical COIL system (**ElectriCOIL**) [Carroll, 2001; King, 2001].

AFRL demonstrated that significant quantities of excited iodine atoms can be produced using an all gas phase generator. The excited species which transfers its energy to Iodine atoms, in this case $NI(^1\Delta)$, can be produced without a liquid phase and has provided a recent lasing demonstration (AGIL) [Henshaw, 2000]. We believe that it is possible to construct a highly efficient electric generation scheme to provide the precursor energy donor species $O_2(^1\Delta)$ and that the ElectriCOIL concept can subsequently be realized.

Workers in Japan [Itami, 1999], Russia [Ivanov, 1999], and in the U.S. [King, 2001] have shown that flowing discharge tubes containing ground state oxygen can produce significant quantities of the desired, $O_2(^1\Delta)$ precursor molecules. We believe this work suggests that one can transform such research into a practical laser system. Atomic iodine injection rather than molecular iodine injection will give added benefit to the ElectriCOIL laser. Figure 1 illustrates the limitations of existing COIL technology as well as the possible improvement from the implementation of ElectriCOIL technology. An electronically produced $O_2(^1\Delta)$ generator could be even more effective if implemented simultaneously with atomic iodine injection.

Fujii [Fujii, 1994] reported good success, 17% yield of $O_2(^1\Delta)$, with a small RF generator. More recently, workers in Japan [Itami, 1999] from Fujisaki Electric provided some evidence that they could produce 21% $O_2(^1\Delta)$ in a microwave discharge. The experiments were carried out in subsonic axial flow at 2 Torr in a 30 cm long tube with window attachments for observation. Hill [Hill, 2001] reported a value of 16%. Schmiedberger [Schmiedberger, 2001] reported a 32% yield under low-pressure conditions (0.43 Torr) with an RF discharge. We have recently obtained an $O_2(^1\Delta)$ yield of $\approx 16\%$ in our flowing RF discharge experiments at a pressure of 2 Torr and $\approx 15\%$ of 3.6 Torr.

We choose chemical efficiency as a way of relating classic COIL performance to our ElectriCOIL concept. Even an ElectriCOIL that provides 20% chemical efficiency (shown in Fig. 1) is an enormous improvement to the classic COIL

*cuaerospace@cuaerospace.com; phone 1-217-333-8274; fax 1-217-244-7757; <http://cuaerospace.com>; CU Aerospace, 2004 S. Wright St. Ext., Urbana, IL, 61801; **wsolomon@uiuc.edu; phone 1-217-244-7646; fax 1-217-244-0720; <http://www.aae.uiuc.edu>; Univ. of Illinois, 306 Talbot Lab, 104 S. Wright St., Urbana, IL 61801.

design because it will lead to a significant reduction of weight on a large weapons class laser, simpler operation procedures, and reduce the overall risk.

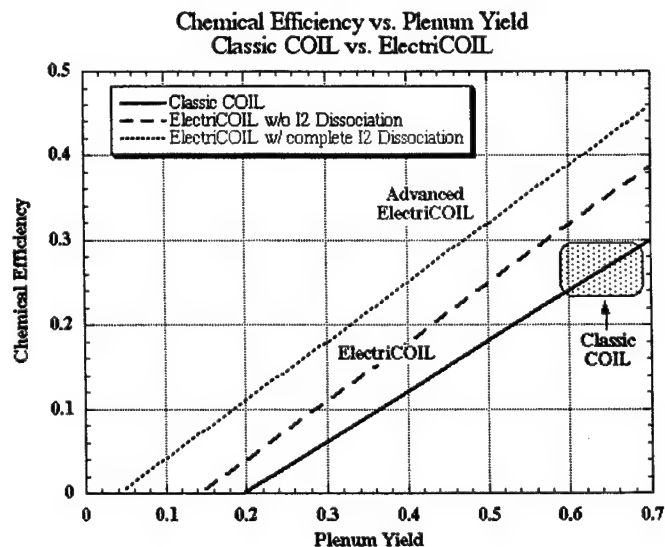


Fig. 1. A comparison between classic COIL technology and the performance possibilities for an ElectriCOIL device are illustrated here. Results based upon a heuristic equation [Hon, 1996].

Calculations using the Blaze II chemical laser model [Sentman, 1977; Carroll, 1995] support the qualitative conclusions drawn from a heuristic equation [Hon, 1996], Figs. 1 and 2. The advantage of the ElectriCOIL concept is immediately realized when examining the gain curve with and without molecular iodine pre-dissociation, Fig. 3. The gain curve, with a 20% yield and no pre-dissociation, is very low and would not make an efficient laser. However, when the molecular iodine is completely pre-dissociated, then the gain curve, even with a 20% yield, compares very favorably with the classic COIL type gain curve having a 67% yield.

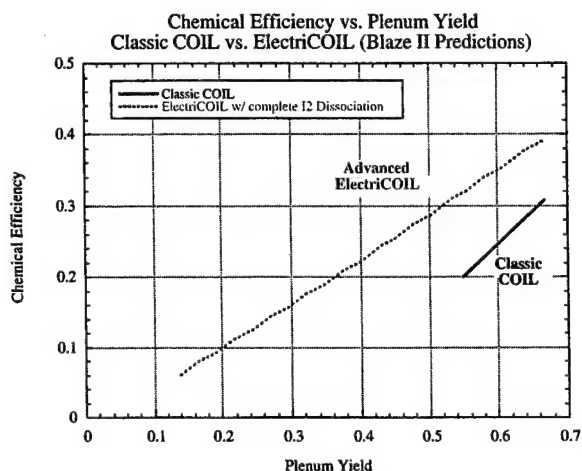


Figure 2. Blaze predictions comparing classic COIL technology and the performance possibilities for an ElectriCOIL device are illustrated. While ElectriCOIL may not be able to match the plenum yield of today's COIL system, significantly smaller yields are capable of matching current chemical efficiencies.

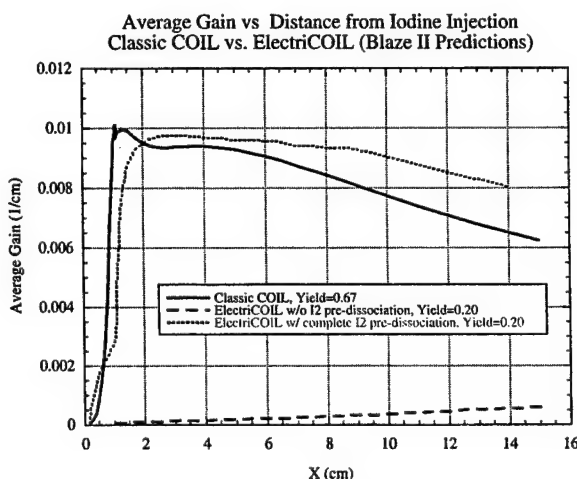


Fig. 3. Blaze predictions of the average gain as a function of distance from the iodine injection position for classic COIL with a yield of 0.67, ElectriCOIL with and without molecular iodine pre-dissociation. Helium diluent was used for these calculations.

Figure 3 also illustrates the innovative concept of combining both electrically produced singlet delta oxygen and pre-dissociated iodine. Each of these concepts have been demonstrated individually, but not in combination; when both ideas are implemented together it is possible to obtain significant gain and laser power with a mere 20% yield; this yield has already been generated in experiments conducted by Schmiedberger [Schmiedberger, 2001]. Experimental work in the area of iodine pre-dissociation has been conducted by Endo and Fujioka's group in Japan [Endo, 1999]. They reported nearly total dissociation from interaction of an Iodine/N₂ stream within the microwave cavity. Iodine pre-dissociation has also been investigated using three-dimensional CFD computations by Madden *et al.* [Madden, 1998]; Madden's results indicated that the injection of atomic iodine slightly downstream of the throat would enhance the power output of a classic COIL device. Recently, CUA and UIUC implemented an LIF experiment that showed 50% dissociation downstream from a dc electric discharge and about 95% in an RF discharge.

2. THEORETICAL BACKGROUND AND MODELING

The motivation for the use of an electrical discharge for the production of O₂(¹Δ) and O₂(¹Σ) states is provided by Figures 4 and 5. These are the predictions from a Boltzmann Equation solver [Kushner, 2000] which tracks the fraction of electrical power utilized for each electron energy loss process. Shown here is the fraction used to excite the O₂(¹Δ) state (0.977 eV/exc.) and the fraction used to excite the O₂(¹Σ) state (1.627 eV). In both the pure O₂ and 1:1 mixture of Helium and O₂, nearly 50% of the electrical power can be used to produce O₂(¹Δ_g) molecules and 20% can be used for the production of the O₂(¹Σ_g) state at an E/N of about 8x10⁻¹⁷ volt-cm².

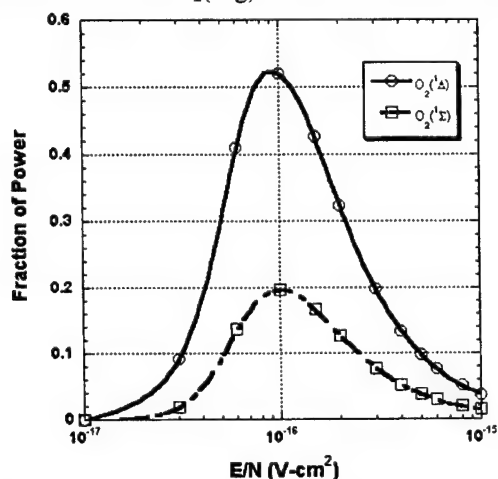


Figure 4: Results of Boltzmann calculation for pure O₂.

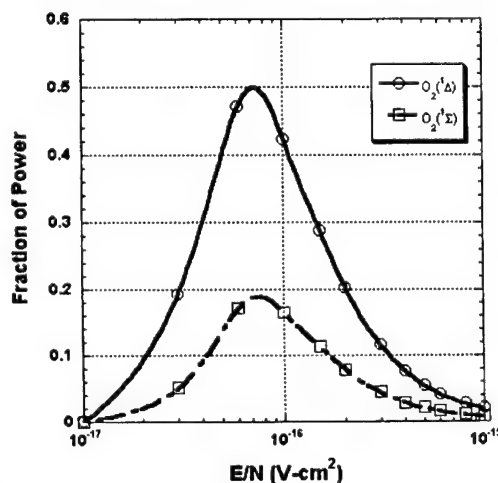


Figure 5: Boltzmann calculation with mix of He:O₂ = 1:1.

Obviously, the efficiency and yield of O₂(¹Δ_g) molecules are critically dependent on the field (E) to neutral gas density N, or E/N, with the dependence of the use of electrical power shown in Figures 4 and 5. Although these graphs show a clear maximum at E/N ~ 10⁻¹⁶ V-cm², there is no guarantee that the discharge will, in fact, operate at that value. Fortunately, experiments with a simple DC discharge (upstream from the RF one) indicated an E/N of ~1.5 - 2.0x10⁻¹⁶ V-cm² and obeyed the simple scaling laws for the positive column. Thus we feel that this is a reasonable estimate for spatially averaged value for the induction discharge used in our latest experiments. In such a discharge, the field is a maximum at the walls and zero on the axis. Recent calculations suggest an effective E/N of 1.2x10⁻¹⁶ V-cm² at 4.2 Torr and 300 Watts.

Thus, if we assume that 45% of the baseline 300 Watts of RF power is used for the production of O₂(¹Δ_g) in the cylindrical tube (R=2.54 cm and length of 10 cm) with a volume of 200 cm³ at 4.2 torr of pure O₂, then the production rate for O₂(¹Δ_g) is:

$$\frac{d[{}^1\Delta_g]}{dt} = + \frac{135W}{Vol. = 200cm^3} \times \frac{1}{0.9775eV} \times \frac{1}{1.6 \times 10^{-19} J/eV} = 4.27 \times 10^{18} cm^{-3} / s. \quad (1)$$

For the conditions used in Fig. 10, the flow velocity is approximately 2×10^3 cm/s and thus the lifetime of the molecules in the discharge region is 5 ms. Thus, this simple theory would predict an exit density of $O_2(^1\Delta_g)$ of 2.13×10^{16} cm $^{-3}$ or a yield of 16.4%. Given the simplicity of the theory, it is in reasonable agreement with our measured yields of ≈ 15 -16% (see Section 3).

A similar calculation can be done for the $O_2(^1\Sigma_g)$ density, and it yields a smaller density by about a factor of $3 \times 1.66 = 4.98$. The factor of 3 arises because of using only $\sim 15\%$ of the power (as opposed to 45% for a $^1\Delta_g$) and the factor of 1.66 because it costs 1.627 eV to produce $b^1\Sigma_g$ state as opposed to 0.9775 eV for the $a^1\Delta_g$ state. The origin of the factor of 3-4 (in Figs. 4 and 5) is a consequence of the fact that the cross-section for electron impact production of is at least 4 times that for $b^1\Sigma_g$ for virtually all electron energies of significance. This ratio is in close agreement with current experimental results.

More detailed theoretical calculations of an inductive discharge utilizing Maxwell's equations (not presented for brevity) were also made. These calculations indicate that the effective E/N for typical flow conditions in our laboratory setup (10 mmol/s of pure oxygen, corresponding to a number density of 1.3×10^{17} cm $^{-3}$) should be approximately 1.2×10^{-16} V-cm 2 at a RF coil current of 30 amps (rms); note that this is very close to optimum, Fig. 4.

3. RECENT EXPERIMENTAL RESULTS

CUA and UIUC are currently developing the ElectriCOIL device. A two-inch flow tube experiment was constructed to demonstrate generation of $O_2(^1\Delta)$ and $O_2(^1\Sigma)$ by electrical means [King, 2001]. Key flow and electrical parameters were varied to characterize the system performance. Figure 6 depicts a block diagram of the experimental setup. RF power is transferred to the flow through a "Pi" matching network driven by a 1-kW ENI OEM-12A RF power amplifier at 13.56 MHz. Diagnostics play a critical role in developing an understanding the ElectriCOIL system; as such, a great deal of care has been taken to implement high quality diagnostics for evaluating the flow properties emerging from the discharge region.

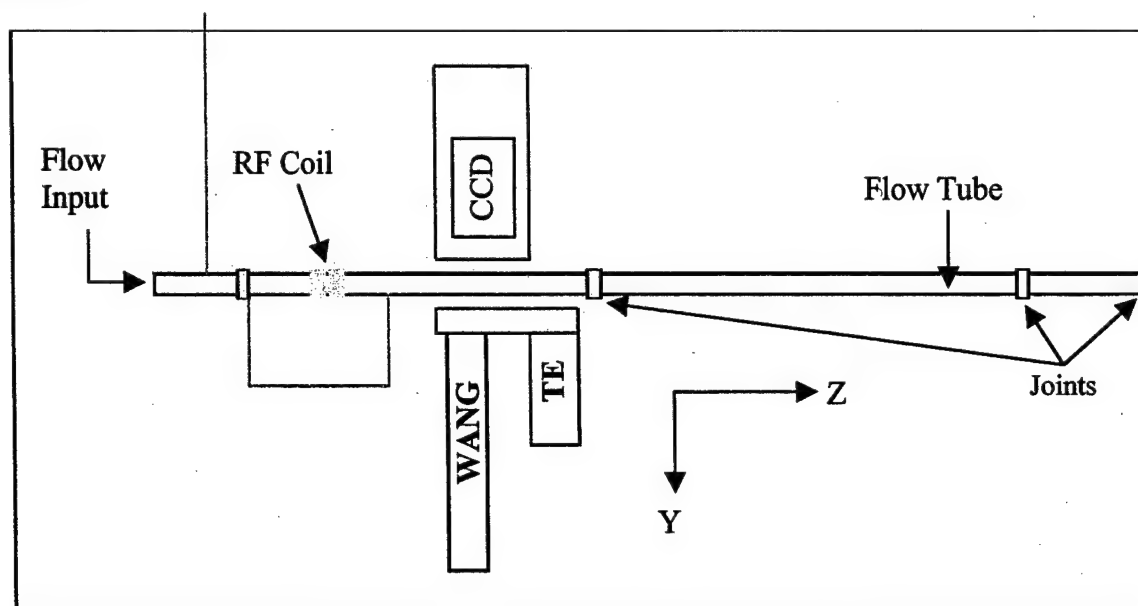


Figure 6: ElectriCOIL experimental setup at UIUC.

One of the primary measurements on the ElectriCOIL experiment is a spectrographic determination of $[O_2(^1\Sigma)]$ from its emission at 760 nm. Studies were performed to investigate the effect of oxygen and diluent flow rates, diluent type, system pressure, RF power levels, and axial flow position. The results of some of the parametric studies are presented in Fig. 7. Axial distance is measured from the end of the discharge section. Differing diluent species yielded considerably

different behaviors on the $O_2(^1\Sigma)$ levels. In Fig. 7 it is seen that the $O_2(^1\Sigma)$ level drops exponentially in the flow direction. It is of interest that the amount of Helium diluent added affects not only the concentration of the $O_2(^1\Sigma)$, but it also decreases the spatial decay downstream, an effect attributed to the increased flow velocity.

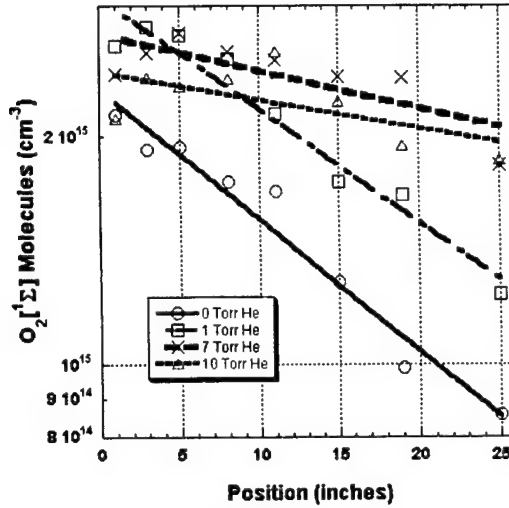


Figure 7: Effect of Helium flow rate (1.2 mmol/s of He per 1 Torr He) on $O_2(^1\Sigma)$ level with varying position for 7 mmol/s of oxygen flow. Separation of the peaks of the P and R branches of the emission indicated a gas temperature of approximately 340 K.

The next key measurement is that of the $O_2(^1\Delta) \rightarrow O_2(^3\Sigma)$ emission at 1268 nm. Results from a test setup using a sensitive Wang LN₂-cooled germanium detector and measuring the spectra with a spectrometer are shown in Fig. 8; this spectral measurement definitively verified the presence of significant percentages of $O_2(^1\Delta)$ evolving from RF discharge flows. It should be noted that the addition of NO to the discharge created a pedestal to the spectra shown in Fig. 8, but did not significantly enhance integrated $O_2(^1\Delta)$ spectra above that base. Recent measurements of the concentration of $O_2(^1\Delta)$ have been performed using a Wang detector, filtered by a CVI 1268 nm narrow bandpass filter. A great deal of care has been taken in the calibration of this measurement using two different calibrated light sources to insure the accuracy of these difficult measurements, however these are absolute intensity measurements that are inherently very difficult; the results presented in this paper are our best estimates that we believe are good to within a factor of two. Figure 9 shows that these recent measurements indicate an $O_2(^1\Delta)$ concentration of $\approx 1.9 \times 10^{16} \text{ cm}^{-3}$ in a 10 mmol/s, 3.6 Torr ($1.27 \times 10^{17} \text{ cm}^{-3}$) flow of pure oxygen, which corresponds to a yield of $\approx 15\%$; these results are consistent with the $O_2(^1\Sigma)$ concentrations in the discharge, Fig. 7.

Based upon the laser system modeling results (Figs. 1 and 2), this measured yield of $\approx 15\%$ is already at the minimum required for the ElectriCOIL system to achieve lasing. Other operating conditions have produced yields of $\approx 16\%$. Work to improve this value is continuing.

It is important to note that these yield numbers are relative to the total oxygen flow rate that is run through the discharge region. Thus, the yield as discussed so far does not reflect the fact that there is production of $O_2(^1\Sigma)$ and O atoms. Since the forward and backward reactions for the production of I^* in the laser cavity region depend only upon excited $O_2(^1\Delta)$ and ground state $O_2(^3\Sigma)$ (excluding any other reactions new to the ElectriCOIL kinetics), it may be more appropriate to define an "effective yield" that is output from such discharges.

$$Y_{eff} = \left\{ \frac{[O_2(^1\Delta)]}{[O_2(^1\Delta)] + [O_2(^3\Sigma)]} \right\}_{generator\ output} \quad (2)$$

Measurements by Ivanov [Ivanov, 1999] suggest that the concentration of O atoms is approximately the same as that of $O_2(^1\Delta)$. Hence, for the aforementioned 3.6 Torr case ($1.27 \times 10^{17} \text{ cm}^{-3}$), if we account for dissociation and assume that $1 \times 10^{16} \text{ cm}^{-3}$ of O_2 has been converted to $2 \times 10^{16} \text{ cm}^{-3}$ of O atoms, assume a concentration of approximately $2.5 \times 10^{15} \text{ cm}^{-3}$ for $O_2(^1\Sigma)$, then a yield of $\approx 15\%$ rises to an effective yield of $\approx 17\%$.

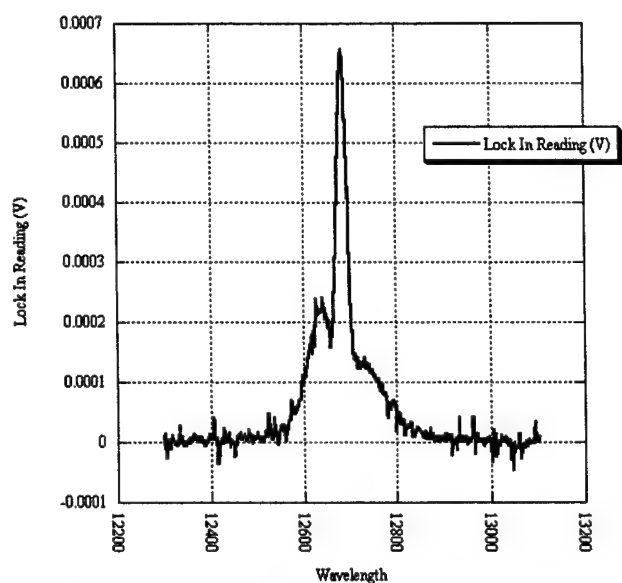


Figure 8. $O_2(^1\Delta)$ spectra taken from the ElectriCOIL RF-pumped system.

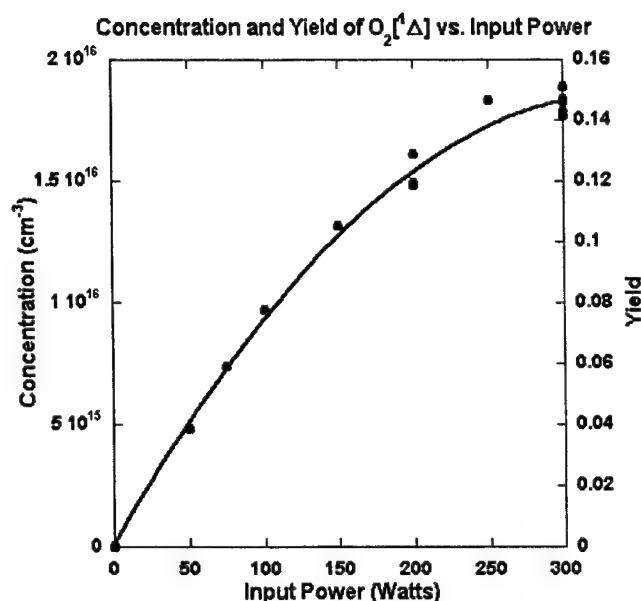


Figure 9. $O_2(^1\Delta)$ concentration data taken from the ElectriCOIL RF-pumped system at a flow rate of 10 mmol/s of pure oxygen.

Further very promising results from this research were obtained when molecular iodine was injected into the flow tube downstream of the oxygen discharge section. Two experiments were run. The flow rate of molecular iodine was approximately 0.006 mmol/s. The first had a simple 1/8" tube that was partially inserted into the flow to inject a single crossflow jet into the primary oxygen flow, Fig. 10. The second test utilized a 1/8" tube with 6 small holes drilled in the side; molecular iodine was injected in a direction parallel to the primary oxygen flow, Fig. 11. In both cases, the yellow glow from the $I_2(B) \rightarrow I_2(x)$ transition was immediately observed. The yellow glow is definitive evidence of the presence of significant concentrations of $O_2(^1\Delta)$.



Figure 10. Single jet iodine injection.



Figure 11. Multi-jet iodine injection.

4. SUMMARY

Advanced chemical iodine laser technology will logically include novel all gas phase generation techniques for an iodine energy donor and the injection of atomic rather than molecular iodine. A candidate method, RF excitation, has been

investigated in this paper. It is seen that both the singlet-sigma $O_2(^1\Sigma)$ and singlet-delta $O_2(^1\Delta)$ excited states of the oxygen molecule may be readily created via electrical excitation in the laboratory. Generally an RF discharge alone is sufficient to bring about this excitation. However, at higher flow rates (>15 mmol/s) it has been found that both an ac discharge used in tandem with the RF discharge is important to achieve high levels of excitation [King, 2001]. We believe that it may be possible to successfully supplant the two-phase elements (liquid BHP and a chlorine/helium/nitrogen gas mixture) of the classical COIL SOG using the ElectriCOIL prototype system.

Diagnostics play a critical role in developing an understanding the ElectriCOIL system; as such a great deal of care has been taken to implement high quality diagnostics for evaluating the flow properties emerging from the discharge region. Recent measurements indicate an $O_2(^1\Delta)$ concentration of approximately $2 \times 10^{16} \text{ cm}^{-3}$ in a 10 mmol/s, 3.6 Torr ($1.3 \times 10^{17} \text{ cm}^{-3}$) flow of pure oxygen, which corresponds to a yield of $\approx 15\%$; these results are consistent with measured $O_2(^1\Sigma)$ levels of $2.5 \times 10^{15} \text{ cm}^{-3}$ in the discharge and theoretical estimates. Other operating conditions have produced yields of $\approx 16\%$. We are planning to conduct experiments with additional advanced diagnostics in the near future.

ElectriCOIL will reduce weight and simplify both military and commercial chemical iodine laser systems. Potential cost and weight savings are also envisioned as the massive quantities of liquid chemicals will be completely eliminated from the device operation. Difficulty will certainly be encountered when searching for a yardstick to predict ElectriCOIL performance. Typical measures such as chemical efficiency must be redefined (or eliminated) to account for changes in the chemistry and parameters like the electrical power absorbed by the flow from the RF discharge. Sets of diagnostics and analysis are planned to take advantage of the recent progress in our laboratories.

ACKNOWLEDGEMENTS

This work was supported by the Air Force Research Laboratory's Directed Energy Directorate SBIR contract F29601-01-C-0007. We would also like to thank M. Kushner for the Boltzmann calculations, J. Laystrom, M. Sexauer, L. Skorski, B. Woodard and S. Zimmer for their assistance in the lab.

REFERENCES

- Carroll, D. (1995). *AIAA Journal*, **33**, 8, 1454.
- Carroll, D.L., and Solomon, W.C. (2001) *SPIE* **4184** 40.
- Endo, M., Sugimoto, D., Okamoto, H., Takeda, S., and Fujioka, T. (1999). "Performance characteristics of the microwave assisted chemical Iodine oxygen laser", AHPLA'99 SPIE conference, Osaka, November 1999.
- Fujii, H. (1994). "COIL in Japan," AIAA Paper 94-2419, Colorado Springs, CO, June 1994.
- Henshaw, T.L., Madden, T.J., Manke, G.C., Anderson, B.T., Tate, R.F., Berman, M.R., and Hager, G.D. (2000). AIAA Paper 2000-2424.
- Hill, A.E (2001). *Proc. of the International Conf. on Lasers 2000*, STS Press, McClean, VA, 249.
- Hon, J., Hager, G., Helms, C., and Truesdell, K. (1996). *AIAA Journal*, **34**, 8, 1595.
- Itami, S., Nakamura, Y., Nakamura, A., Shinagawa, K., Okamura M., and Fujii, H. (1999). AHPLA '99, Osaka, Nov 1999.
- Ivanov, V.V., Klopovsky, K.S., Lopaev, D.V., Rakhimov, A.T., and Rakhimova, T.T. (1999). *IEEE Trans. on Plasma Science*, **27**, p. 1279.
- King, D.M., Carroll, D.L. Carroll, and Laystrom J. K., Verdeyen, J.T., Sexauer, M. S., and Solomon, W.C. (2001). *Proceedings of the International Conf. on Lasers 2000*, STS Press, McClean, VA, 265.
- Kushner, M.J. (2000). Private communication.
- Madden, T., Hager, G., Lampson, A., and Crowell, P. (1998). *Proceedings of the International Conf. on Lasers 1998*, STS Press, McClean, VA, 287.
- McDermott, W., Pchelkin, N., Benard, D., and Bousek, R. (1978). *Appl. Phys. Lett.* **32**, 8, 469.
- Schmiedberger, J., Hirahara, S., Ichinoche, Y., Suzuki, M., Masuda, W., Kihara, Y., Yoshitani, E., and Fujii, H. (2001). *SPIE* **4184** 32.
- Sentman, L., Subbiah, M., and Zelazny, S. (1977). "Blaze II: A Chemical Laser Simulation Computer Program," Bell Aerospace Textron, Buffalo, NY, T.R. H-CR-77-8.

Measurement of chemical oxygen-iodine laser singlet oxygen generator parameter using Raman spectroscopy

Weili Zhao, Fengting Sang, Liping Duo, Fang Chen, Yuelong Zhang and Benjie Fang
Dalian Institute of Chemical Physics, the Chinese Academy of Sciences, PO Box 110, Dalian
116023, China

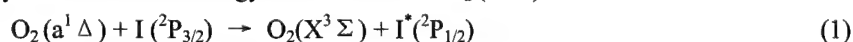
ABSTRACT

Using a doubled Nd: YAG laser as a spontaneous vibrational Raman scattering source, and a single intensified CCD array at the exit of an imaging monochromator, the Raman scattering system is used to directly measure the concentrations of the $O_2(a^1\Delta)$ and the $O_2(X^3\Sigma)$ in the chemical oxygen-iodine laser singlet oxygen generator in real time. We present the results from the tests that conducted on a 0.1-mol singlet oxygen-iodine generator. With the current reported uncertainty of the Raman cross-section, the error in the yield measurement is calculated to be less than 8%.

Keywords: chemical oxygen-iodine laser, singlet oxygen generator, Raman spectrum, yield

1. INTRODUCTION

The chemical oxygen-iodine laser is the first chemical laser based on the electronic transitions. It emits at 1315nm on the transition between the spin-orbit levels of the ground state configuration of the iodine atom. The upper level is populated by a near-resonant energy transfer from an $O_2(a^1\Delta)$ molecule to an atomic iodine atom¹⁻³.



The output power of this laser strongly depends on the yield of $O_2(a^1\Delta)$ in singlet oxygen generator^{4,5}.

$$Y = \frac{[O_2(a^1\Delta)]}{[O_2(a^1\Delta)] + [O_2(X^3\Sigma)]} \quad (2)$$

To predict the COIL performance, it is very important to measure the exact values of the yield of $O_2(a^1\Delta)$ at the exit of the singlet oxygen generator. Usually, the $O_2(a^1\Delta)$ density is measured by monitoring the $O_2(a^1\Delta)$ emission at 1270nm with a calibrated detector^{6,7}. However, the detector is difficult to calibrate and the results exhibit low absolute accuracy in the yield.

Recently, the spontaneous Raman scattering technique has been developed that it can be used to directly monitor the singlet oxygen generator by measurement both the concentrations of the $O_2(a^1\Delta)$ and $O_2(X^3\Sigma)$ simultaneously using spontaneous Raman imaging⁸. It has several advantages over other methods because it allows one to monitor both the $O_2(a^1\Delta)$ and $O_2(X^3\Sigma)$ simultaneously in the same measurement volume. Because common experimental problems such as dirty windows, fluctuations in laser power, and aerosol scattering can be ratioed out, this technique greatly

simplifies modeling and data reduction.

A Raman scattering experimental system was set up. We used it to measure the species in air and in a singlet oxygen generator. In this paper, we report the result of air and the application of Raman spectrum to measure the $O_2(a^1\Delta)$ yield at the exit of a jet-type singlet oxygen generator for COIL. The results are from the tests that conducted on a 0.1-mol singlet oxygen generator.

2. EXPERIMENT

We used the experimental setup shown in Fig. 1. A doubled Nd: YAG laser (Spectra Physics, Quanta-Ray) was used to be laser pump with a 10Hz pulse repetition rate and a 20ns pulse duration. And each pulse had a pulse energy of 400-500mJ. The output laser was elliptically polarized, and the line width was less than 1.0cm^{-1} . The laser beam has been focused into the flow cell of singlet oxygen generator through a coated quartz window by an f/6.7 lens. The Raman scattering light which was collected perpendicularly to the propagation of the laser beam was focused throughout a Kaiser Inc. holographic $\lambda = 532\text{nm}$ notch-filter onto the slits of an f/6.5 Acton Spectrapro 500 spectrograph by a coated f/1.6 lens. The scattered Raman light was dispersed by a 1200-grooves/mm and $BLZ=500\text{nm}$ grating and focused onto a 256×1024 ICCD array, the size of each pixel was $23\mu\text{m} \times 23\mu\text{m}$. The ICCD chip was cooled

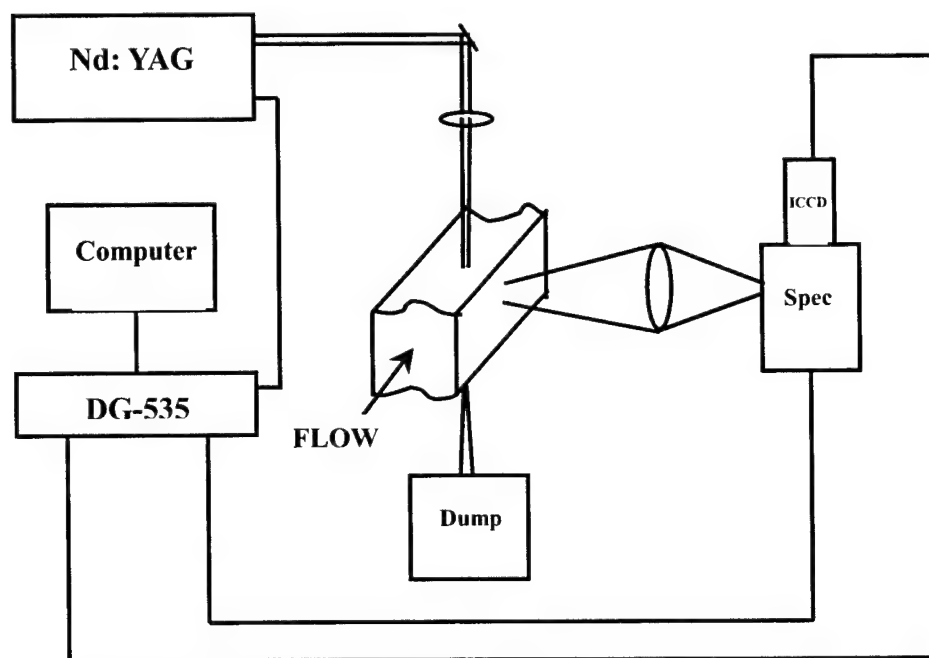


Fig.1 Schematic illustration of experimental setup

to -30°C to minimize the dark current. The DG-535 was triggered by the laser Q-Switch Sync output. At the same time, we used the computer to control DG-535 time delay so accurate that the photocathode of the image intensifier tube would be opened when the Raman scattering signal came. The detector microchannel intensifier had a gate width of 25ns. It was confirmed that this gate width could overlap each laser pulse by a 500MHz oscilloscope. The Raman cell was blacked to reduce the influence of unorderly light on optical systems.

3. RESULTS AND DISCUSSION

We used this Raman system to measure the species of air. The Raman spectrum was shown in Fig. 2. It is obtained by focusing the laser beam onto a measurement point in air. In this case, the laser output energy is about 250mJ/pulse. It is less than the energy we used in the chemical generator. The low laser output energy is needful because it can reduce the probability of optical breakdown in air. The integration time is 4 seconds. If a higher repetition rate laser were used, the same sensitivity would be obtained in shorter integration time.

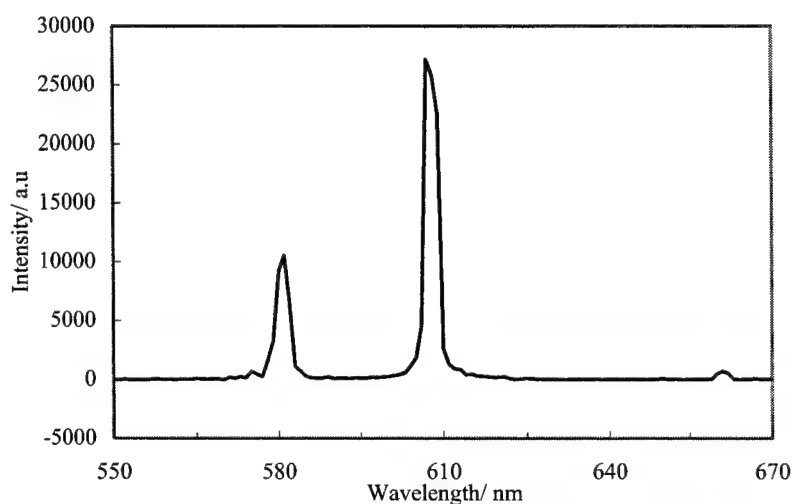


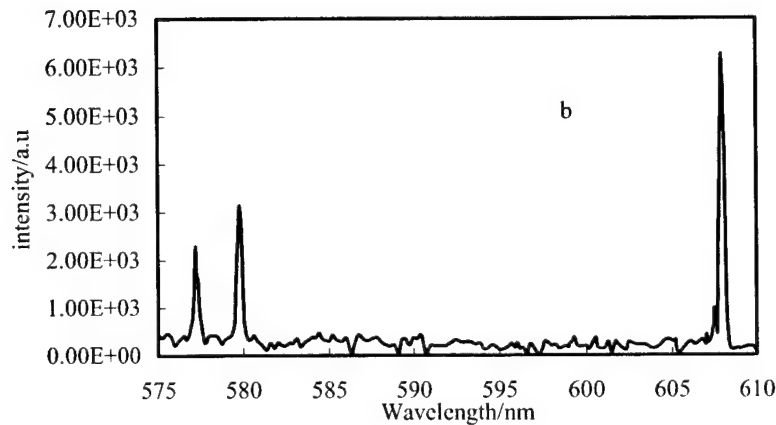
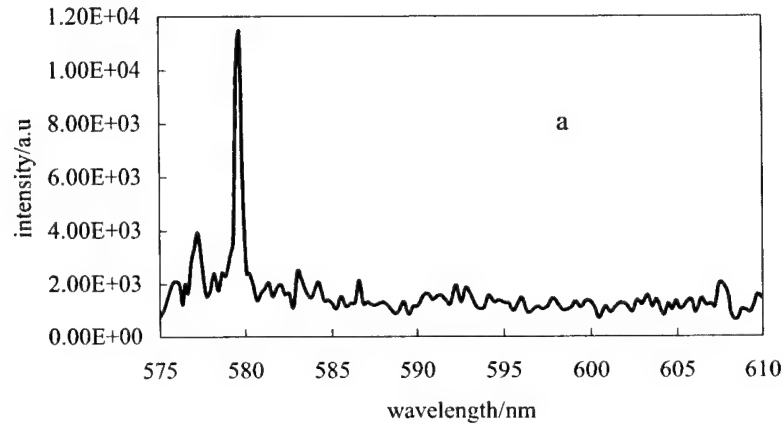
Fig. 2 The Raman spectrum of air

The typical Raman spectrums of the species in the singlet oxygen generator were shown in Fig. 3 (a) and (b). We had got each of them in 20 seconds. The Raman signal of gas in low pressure is so feeble because of the fact that Raman cross section are extremely low ($\sim 10^{-34}\text{m}^2\text{sr}^{-1}$) that it is very important enhancing the collecting efficiency. In addition, the Raman light should be collected at suitable angles. Which is the best angle is decided by the polarization direction of laser beam. In our tests, we collected the Raman signal perpendicularly to the propagation of the laser beam.

The yield can be calculated by using the expression

$$\begin{aligned}
Y &= \frac{[O_2(a^1\Delta)]}{[O_2(a^1\Delta)] + [O_2(X^3\Sigma)]} \\
&= \frac{O_2(a^1\Delta) / \sigma_{O_2(a)}}{O_2(a^1\Delta) / \sigma_{O_2(a)} + O_2(X^3\Sigma) / \sigma_{O_2(X)}} \\
&= \frac{O_2(a^1\Delta)}{O_2(a^1\Delta) + O_2(X^3\Sigma)(\sigma_{O_2(a)} / \sigma_{O_2(X)})} \quad (3)
\end{aligned}$$

where $O_2(a^1\Delta)$ and $O_2(X^3\Sigma)$ are the area under respective peaks of the $O_2(a^1\Delta)$ and $O_2(X^3\Sigma)$ Raman spectrum, σ is the Raman cross-section. $\sigma_{O_2(a)} / \sigma_{O_2(X)}$, the Raman cross-section ratio of the $O_2(a^1\Delta)$ and $O_2(X^3\Sigma)$ was determined by a series of experiments⁹ to be 0.45.



(a) $N_2:Cl_2 = 0:106$, 30Torr (b) $N_2:Cl_2 = 117:110$, 18Torr

Fig. 3 The Raman spectrum of a sparger flow

The results from the tests that conducted on a 0.1-mol singlet oxygen-iodine generator had been obtained. A table of the values of a series of experiments is presented in Table 1. The differences of the optical components at the $O_2(a^1\Delta)$ and $O_2(X^3\Sigma)$ wavelengths, such as grating, detector, and notch-filter, were ignored because of the closeness of the Stokes shifts (1508 and 1580 cm^{-1} , respectively). The accuracy of the area under peak is mainly due to the signal-noise ratio. However, the yield of the $O_2(a^1\Delta)$ is in the 50% range.

Table 1 The values of a series of experiments

No.	Pressure (Torr)	N_2	Cl_2	Y (%)
1	30	0	106	39
2	35	117	106	42
3	25	117	106	45
4	25	117	106	46
5	18	117	110	54
6	9	117	104	59

It is obvious that the yield is increasing via the reducing of generator pressure in the experimental range at fixing flux, and advisable gas is desirable to be the carrier. So we should keep the singlet oxygen generator pressure lower for the sake of obtaining higher $O_2(a^1\Delta)$ yield at suitable flux. The result of experiment No. 6 is the best in Table 1. The yield is approximately 60%. With the current reported uncertainty of the Raman cross-section, the error is calculated to be less than 8%.

The sources of error in the yield measurement is as follows:

the error in the grating calibration	0.6%
the error in determining the area under the peak	2%
the error in the cross section	5%

So the total error in the yield measurement is less than 8%.

4. SUMMARY

Using a doubled Nd: YAG laser as a spontaneous vibrational Raman scattering source, and a single intensified CCD array at the exit of an imaging monochromator, the spontaneous Raman spectroscopy can be used to directly measure the singlet oxygen generator parameter of chemical oxygen-iodine lasers. The yield of $O_2(a^1\Delta)$ is in the 50% range when the flux of N_2 and Cl_2 is approximately 1:1. With the current reported uncertainty of the Raman cross-section, the error is calculated to be less than 8%. It is the most important sources of error in the yield measurement that the ratio of signal to noise is lower. It should be improved by enhancing the repetition rate, lengthening the pulse duration, improving the polarization of the laser. Reducing the unorderly light is better method to improve the ratio of signal to noise. Increased sensitivity and accuracy can be obtained with further work.

5. ACKNOWLEDGEMENTS

The authors would like to thank Ms. Yongxiang Song , Mr. Qingguo Li and Mr. Xiangde Min for their contributions to this work.

6. REFERENCES

1. W. E. McDemott, N. R. Pchelkin, D. J. Benard, and R. R. Bousek, "An electronic transition chemical laser," Appl. Phys. Lett., Vol. 32, p469-470 (1978).
2. K. A. Truesdell and S. E. Lamberson, "Philips Laboratory COIL technology overview," Proc. SPIE, Vol. 1810, p476-492 (1992).
3. P. V. Avizonis, "Chemical pumped electronic transition lasers," in Gas and Chemical Lasers, M. Onorato, ed. (Plenum, New York), p1(1982).
4. B. D. Barmashenko, A. Elier, E. Lebiush, and S. Rosenwaks, "Modeling of mixing in chemical oxygen-iodine lasers: Analytic and numerical solutions and comparison with experiments," J. Appl. Phys., Vol. 75, p7653-7655 (1994).
5. N. N. Yuryshev, "Chemically pumped oxygen-iodine laser," Quantum Electron., Vol. 23, p583-600 (1996).
6. A. Elier, B. D. Barmashenko, E. Lebiush, and S. Rosenwaks, "Experiment and modeling of a small-scale, supersonic chemical oxygen-iodine laser," Appl. Phys. B, Vol. 61, p37-47(1995).
7. L. P. Duo, T. J. Cui, Z. Q. Wang, W. W. Chen, and F. T. Shang, "Obsolute $O_2(a^1\Delta)$ concentration measurement in singlet oxygen generator using the piston source method," High power laser and particle beams, Vol. 12(s0), p25-30 (2000). (in Chinese)
8. V. T. Gylys and L. F. Rubin, "Direct measurement of $O_2(a^1\Delta)$ and $O_2(X^3\Sigma)$ in chemical oxygen-iodine lasers with use of spontaneous Raman imaging," Appl. Optics, Vol. 37, p1026-1031(1998).
9. L. F. Rubin and V. T. Gylys, "Measurement of the Raman cross section of $O_2(a^1\Delta g)$," Optics Lett., Vol. 22, p1347-1349 (1997).

Tunable Diode Laser Gain Measurements of the HF(2-0) Overtone Transitions in a Small Scale HF Laser

Charles F. Wisniewski^a, Gerald C. Manke II^{*a}, Gordon D. Hager^a,
Peter G. Crowell^b, and C. Randall Truman^c.

^aAir Force Research Laboratory, Directed Energy Directorate; ^bLogicon/Northrup Grumman;

^cDepartment of Mechanical Engineering, University of New Mexico.

ABSTRACT

A tunable diode laser was used to probe the overtone gain medium of a small-scale HF laser. Two-dimensional, spatially resolved small signal gain and temperature maps were generated for the P(3) ro-vibrational transition in the first HF overtone band.

1. INTRODUCTION

The fundamental HF laser was invented in the mid to late 1960's¹⁻⁵. While the first HF lasers were pulse initiated^{2,5}, continuous wave HF lasers were also demonstrated prior to 1970⁶⁻⁸. Over the last 30 years, HF laser technology has advanced to the point where megawatt class lasers can be constructed. It is widely recognized that the fundamental HF laser, which operates from 2.7 - 3.0 μm , has limited utility for low altitude, long-range propagation applications due to strong absorptions in the atmosphere. Subsonic demonstrations of HF overtone lasers, which operate at a wavelength that is more amenable to long-range, low-altitude applications, were first reported in the mid-1970's by Hon⁹ and Bashkin¹⁰. However, the demonstrations were not particularly impressive due to poor efficiency. A more modern and scalable concept for an HF overtone laser was demonstrated in 1984 by Jeffers¹¹. This demonstration was especially notable because of the significantly enhanced efficiency; the overtone power was 20 - 30% of the fundamental. Improved mirrors and combustion driven HF laser technology were the keys to demonstrations of multi-kW HF overtone lasers in the mid- to late-1980's¹²⁻¹⁴. In general, the small signal gain of an HF overtone laser is approximately 2 orders of magnitude smaller than the fundamental HF laser. The development and scaling of the HF overtone lasers (i.e. $\Delta v = -2$) has been limited by the availability of mirror coatings which simultaneously suppress fundamental lasing and enable overtone oscillation. As the ability to produce such optics has improved, so too have the prospects of high-power HF overtone lasers.

Another impediment to the development of HF overtone lasers has been the lack of high fidelity small signal gain probes that can be used to directly measure the small signal gain of individual HF ro-vibrational lines with full spectral and spatial resolution. While it is possible to use a commercial Helios arc-driven HF laser as a probe, this device can be difficult and expensive to operate. In most cases, the Helios laser cavity is stabilized and locked to the line center of one of a limited number of HF overtone lines. Alternatively, a plot of extracted laser power vs. mirror reflectivity can be used to determine the threshold gain (g_{th}) according to the equation

$$g_0 = g_{th} = -\frac{1}{2L} \ln R_1 R_2 \quad [1]$$

where R_1 and R_2 are the mirror reflectivities and L is the path length. As the outcoupling mirror reflectivity decreases and the outcoupled power approaches zero the small signal gain (g_0) equals the threshold gain. However, this technique cannot generate spatially resolved gain or temperature maps. Since the efficiency of an HF laser is usually dominated by the rate of mixing, the need for spatial resolution is acute. Furthermore, this method cannot be used to measure gain on individual ro-vibrational lines because the measured threshold gain is only associated with the strongest line in the multi-line overtone spectrum. Finally, neither of these techniques can provide information about the gas temperature or any other data related to the spectral lineshape of the transition.

In principle, the lack of precise lineshape information may lead to ambiguous or deceptive answers when making comparisons with computational fluid dynamics calculations. In particular, while the gain of a laser may be directly measured, extraction of the inversion density requires knowledge of the spectral lineshape function. The definition of gain is

$$\text{gain}(cm^{-1}) = \ln \left(\frac{I(v_0)}{I_0(v_0)} \right) z^{-1} = \sigma_{stim}(v_0) \left[N_u - \frac{g_u}{g_l} N_l \right] \quad [2]$$

where z is the optical path length and N_u , N_l , g_u , and g_l are the upper and lower state number densities and degeneracies, respectively. The stimulated emission cross section is given by

$$\sigma_{stim}(v_0) = \frac{\lambda^2 A(v, J)}{8\pi} f(v_0) \quad [3]$$

where λ is the center wavelength, $A(v, J)$ is the Einstein emission coefficient, and $f(v_0)$ is the lineshape function. If the lineshape is assumed to be Gaussian, and is actually a Voigt or some other more complex function, the calculated value for the inversion density may be significantly in error. Pressure broadening coefficients (2γ) for HF^{15, 16} range from 0.75 MHz Torr⁻¹ for HF + He to 53.05 MHz Torr⁻¹ for HF + HF. Under most HF supersonic laser conditions (low pressure, mostly He), pressure broadening is not an issue, but an explicit check for it would be prudent.

Because of their narrow linewidth and tunability, External Cavity Diode Lasers (ECDLs) are ideal tools for measuring small signal gain. These devices have previously been implemented for measuring the gain in the Chemical Oxygen Iodine Laser (COIL)¹⁷ and the All Gas-phase Iodine Laser (AGIL)¹⁸. In fact, the same commercially available (New Focus, model 6300) 1.3-micron diode laser used for AGIL and COIL was also used to measure gain on our HF overtone laser test bed. As we have done in the past^{17, 18}, we have generated spatially resolved, small signal gain and temperature maps of the active medium for comparison with CFD modeling results¹⁹.

2. EXPERIMENTAL METHODS

A small-scale HF laser was constructed to generate an inversion on the first overtone of HF at 1.27 - 1.40 μm . The laser consisted of a 5 cm wide supersonic slit nozzle, where F atoms generated by a Helios discharge tube reacted with molecular hydrogen to generate vibrationally excited HF²⁰. Our nozzle design and experimental conditions are very similar to those of Sentman and co-workers^{21, 22}. The two most important differences are that we used a slit nozzle rather than a nozzle bank, and our discharge used 20% F_2 in helium rather than $SF_6 + O_2$ as the F atom source. Schematic representations of our experimental apparatus are shown in Figure 1a-b. Figure 1b shows the view from the downstream end of the nozzle looking into the plenum region. Helium is added through the first row of injection holes, while the second row was used for the addition of H_2 . The injected helium acts as a shield for the injected H_2 , with the goal of preventing reaction prior to the nozzle exit plane. A pair of He shroud flows were placed at the nozzle exit plane (NEP) to reduce recirculation of the laser media and a pair of bank blowers were located on either side of the active medium to reduce expansion of the corrosive gas flow into the mirror tunnels. The 0.9 cm long slit nozzle expands from the 3 mm throat with a 20 degree angle (relative to the center line) to 0.9 cm at the NEP. The nozzle design also provides for area relief via a large 1 cm step (top and bottom) at the NEP. A small base purge flow of He could be added to prevent recirculation in the base region.

A Helios DC discharge tube was used to generate a flow of fluorine atoms from molecular fluorine (20% in He, Matheson) diluted in helium. High purity H_2 (99.99%, Matheson) and He (Air Products) were added without additional purification. Table 1 lists the typical range of reagent flow rates, device pressures and thermocouple temperatures. The plenum pressure was typically 24 Torr and the static pressure (measured at the wall 3 cm downstream of the NEP) was ~2 Torr. A series of pitot tube measurements established the Mach number and total pressure, ~2.5 and 20 Torr, respectively.

The diode laser used to probe the absorption/gain on the $HF(v=0) \rightarrow HF(v=2)$ vibrational transition has been described previously^{18, 23, 24}. In this case, the laser was tuned to individual HF ro-vibrational lines instead of the $I(^2P_{3/2}) - I(^2P_{1/2})$ spin-orbit transition. The frequency of the laser was repetitively scanned over approximately 6GHz at a 50Hz rate. The I/I_0 signal was averaged for approximately 1 second (i.e. 50 scans) to improve the signal to noise ratio.

Spatially resolved emission spectra were generated with a 0.3 m Acton monochromator and a Near Infrared Optical Multi-channel Analyzer (NIR OMA) (Roper Scientific, OMA V). The 512 pixel array of InGaAs detectors generates the spectra with resolution well suited for our application. Fiber optic bundles were used to deliver the chemiluminescence to the monochromator. The small solid angle viewed by lens attached to the fiber optic bundle allows for spatially resolved emission spectra. While the lens - flow reactor separation used in these experiments does not allow resolution of the vertical profile, we can easily resolve the streamwise profile in 2 - 3 cm steps.

3. RESULTS AND DISCUSSION

A typical HF overtone gain measurement is shown in Figure 2. The HF(2-0) P(3) line was chosen because it should have the highest gain at our experimental conditions ($H_2 = 27 \text{ mmols sec}^{-1}$, $F_2 = 1 \text{ mmols sec}^{-1}$, $P(\text{static}) = 1.5 \text{ Torr}$, and $T \sim 200 \text{ K}$). For the sake of clarity, only every other data point is shown. The peak gain is 0.07 % cm^{-1} and

the peak width (FWHM) = 515 MHz. Also shown in Figure 2 is the Gaussian lineshape function fit to the data. The residuals for the Gaussian fit are shown in the lower panel. Note that the residuals plot has no structure, indicating that no pressure-related line broadening or narrowing effects are evident^{15, 16}. The spectral linewidth corresponds to $T = 198$ K.

Figures 3a - 3c show spatially resolved small signal gain measurements. The data were generated by moving the diode laser along the vertical (y) and streamwise (x) axes of the reactor. To reduce the number of experiments, we assumed symmetry across the centerline. Hence, the data points below the centerline are identical to the measured values from above the centerline. Each panel corresponds to one of three positions along the x-axis (1, 5, and 9 cm downstream, relative to the NEP) and the three sets of data in each panel correspond to one of three H_2 flow rates (5, 10, or 27 mmols sec^{-1}). The solid vertical lines in each panel indicate where the top and bottom base purge regions begin. For $x = 1$ cm downstream of the NEP, the gain peaks at approximately the same position (relative to the centerline) as the H_2 injectors. This strongly suggests that molecular hydrogen has not penetrated into the center of the flow stream. The double peaked profile is less pronounced but still persists 5 cm downstream of the NEP. At $x = 9$ cm, the peak gain is along the centerline of the flow, demonstrating that, albeit somewhat slowly, the H_2 does eventually penetrate into the center of the flow. The vertical profiles at 1 and 5 cm downstream show significant expansion of the flow into the base purge regions.

The highest observed small signal gain was $\sim 0.1 \% cm^{-1}$. This result compares well with the results of Sentman and coworkers' Parallel Slit Nozzle (PSN)^{25,27} and HYSIM lasers^{21, 22}. It is important to note, however, that in both cases they did not directly measure the small signal gain. Rather, they report the product $g_0 L_e$, (where L_e is the effective path length) based on plots of the outcoupled power vs. mirror reflectivity. In the case of the PSN device, if an effective path length of 14.9 cm is assumed for the PSN device (i.e. the path length predicted by CFD calculations of the size of the active medium), then the small signal gain is $0.085 \% cm^{-1}$. If, on the other hand, the geometric path length (30 cm) is used, the small signal gain is a factor of 2 smaller. Our result (which assumes $L = 5$ cm for our slit nozzle) is more consistent with Sentman if we adopt the assumption that $L_e = 14.9$ cm. Considering the strong similarities between our hardware and Sentman's, the apparent agreement with our result is not surprising.

Figure 4 shows the corresponding spatial temperature measurements. The uncertainty of the temperature in most cases is substantial because the signal to noise ratio is poor, and the lineshape is ill defined. In such cases where a reliable linewidth is not possible, only the small signal gain (which depends on the spectral area) is reported. In general, the temperature varies approximately 100 K from the centerline to the middle of the base purge region, peaking where the gain is highest.

The small signal gain was probed for several lines in addition to P(3). Figure 5 shows a few examples for HF(2-0) P(2) and P(4). While chemiluminescent spectra indicate that positive gain may also exist on several HF(3-1) lines, we could not directly probe these transitions due to the limited frequency range of the diode laser. Emission spectra of the flow at $z = 1 - 12$ cm are shown in Figure 6. According to the Boltzmann equation,

$$\ln \left[\frac{Intensity(v, J)}{A(v, J) * g(J)} \right] = \frac{-B_v * [J * (J + 1)]}{kT} \quad [3]$$

(where B_v is the rotational constant) a plot of the left hand side vs. $J(J+1)$ is linear if rotational equilibrium exists, and the slope is equal to B_v/kT . A linear plot was obtained for each vibrational level, and the temperatures are indicated in panels a-e. The vibrational distribution is also indicated. The relative vibrational population is calculated from equations [4]

$$P(v) = \frac{I(v, J)}{P(J) * A(v, J)} \quad [4]$$

and [5]

$$P(J) = \frac{g(J) * \exp(-B_v * [J * (J + 1)] / kT)}{Q_{rot}} \quad [5]$$

where Q_{rot} is the rotational partition function. The rotational temperatures are slightly higher than, but not inconsistent with the spectroscopically determined translational temperatures. Both types of temperature tend to increase slightly as the flow progresses downstream. Finally, we note that the vibrational distribution for $P_2 - P_3$ also relaxes along the length of the reactor.

4. CONCLUSIONS

A tunable diode laser has been used to measure the small signal gain of a small-scale supersonic HF overtone laser. Unlike previous measurements of the overtone gain, our technique is direct, and can be both spatially and spectrally resolved. This data is complemented by spatially resolved overtone emission spectra that confirm that each vibrational state is in rotational equilibrium. These data are ideal for 2D and 3D computational fluid dynamics (CFD) calculations. When combined with the results of the CFD calculations¹⁹, this experiment should represent the most comprehensive characterization and analysis of an HF overtone laser reported to date.

5. ACKNOWLEDGMENTS

The authors wish to acknowledge helpful discussions with Prof. L. H. Sentman regarding the construction and operation of the HYSIM nozzle, Prof. R. K. Hanson (Stanford University) for advice on HF overtone lineshape analysis, Dr. D. L. Carroll (CU Aerospace, LLC) regarding advice on preliminary CFD calculations, and Applied Research Associates, Inc. for computer time used to perform the preliminary CFD calculations. We are especially grateful to Brian Anderson (AFRL/DE) for assistance with the diode laser.

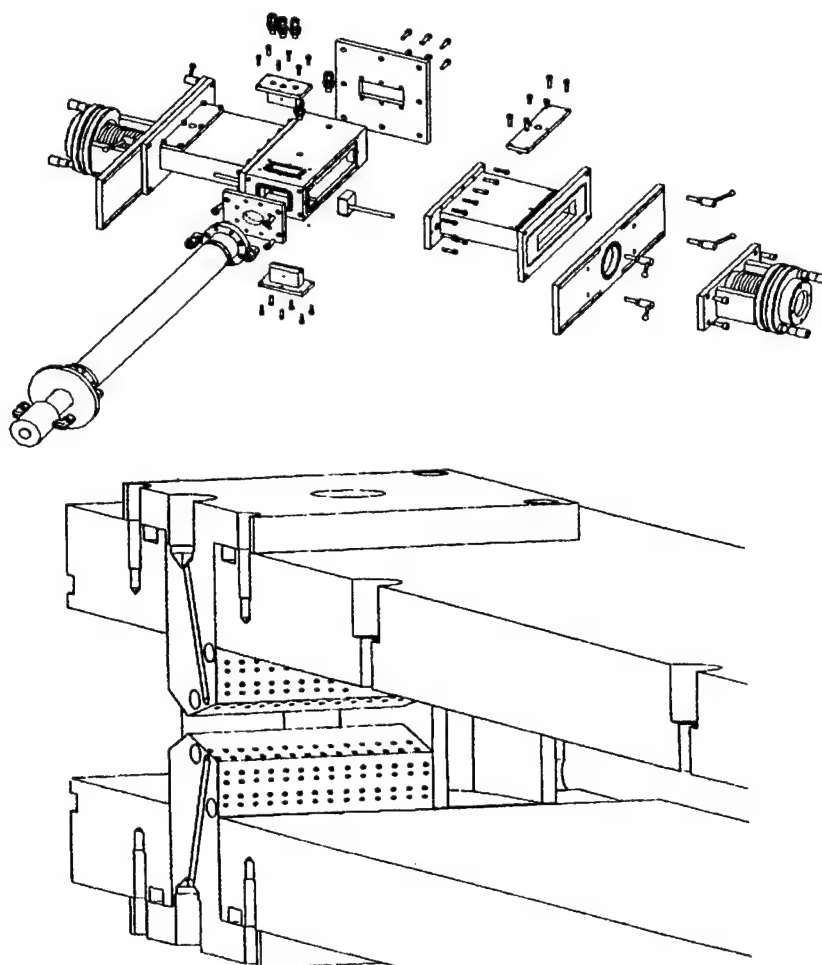
6. REFERENCES

1. Rolf W. F. Gross and Jerry F. Bott, *Handbook of chemical lasers*, Wiley, New York, 1976.
2. K. L. Kompa and G. C. Pimentel, *J. Chem. Phys.*, **47**, 857, 1967.
3. T. F. Deutsch, *Appl. Phys. Lett.*, **10**, 234, 1967.
4. O. M. Batovskii, G. K. Vasil'ev, E. F. Makarov and V. L. Tal'rose, *JETP Lett.*, **9**, 200, 1969.
5. N. G. Basov, L. V. Kulakov, E. P. Markin, A. I. Nikitin and A. N. Oraevsky, *JETP Lett.*, **9**, 375, 1969.
6. R. W. F. Gross, R. R. Giedt and T. A. Jacobs, *J. Chem. Phys.*, **51**, 1250, 1969.
7. J. R. Airey and S. F. McKay, *Appl. Phys. Lett.*, **15**, 401, 1969.
8. D. J. Spencer, T. A. Jacobs, H. Mirels and R. W. F. Gross, *Int. J. Chem. Kinet.*, **1**, 493, 1969.
9. J. F. Hon and J. R. Novak, "Chemically pumped hydrogen fluoride overtone laser", *IEEE J. Quant. Elect.*, **QE-11**, 698 - 699, 1975.
10. A. S. Bashkin, V. I. Igoshin, Yu. S. Leonov, A. N. Oraevskii and O. E. Porodinkov, "An investigation of a chemical laser emitting due to an overtone of the HF molecule", *Sov. J. Quantum Electron.*, **7**, 626 - 627, 1977.
11. W. Q. Jeffers, "Short Wavelength Chemical Lasers", *AIAA Journal*, **27**, 64 - 66, 1988.
12. W. Duncan, S. Patterson, B. Graves and M. Holloman, "Recent Progress in Hydrogen Fluoride Overtone Chemical Lasers", AIAA-91-1480, 1991.
13. W. Duncan, M. Holloman, B. Rogers and S. Patterson, "Hydrogen Fluoride Overtone Chemical Laser Technology", AIAA-89-1903, 1989.
14. W. A. Duncan, S. P. Patterson, M. E. Holloman and J. L. Sollee, *Progress in Hydrogen Fluoride Overtone Chemical Lasers*, 1990.
15. S. I. Chou, D. S. Baer and R. K. Hanson, "Diode laser measurements of He-, Ar-, and N₂-broadened HF lineshapes in the first overtone band", *J. Mol. Spectrosc.*, **196**, 70-76, 1999.
16. S. I. Chou, D. S. Baer and R. K. Hanson, "Spectral Intensity and lineshape measurements in the first overtone band of HF using tunable diode lasers", *J. Mol. Spectrosc.*, **195**, 123-131, 1999.
17. R. F. Tate, B. S. Hunt, C. A. Helms, K. A. Truesdell and G. D. Hager, "Spatial Gain Measurements in a Chemical Oxygen Iodine Laser (COIL)", *IEEE J. Quant. Elect.*, **31**, 1632 - 1636, 1995.
18. J. M. Herbelin, T. L. Henshaw, B. D. Rafferty, B. T. Anderson, R. F. Tate, T. J. Madden, G. C. Manke and G. D. Hager, "The measurement of gain on the 1.315 μ m transition of atomic iodine in a subsonic flow of chemically generated NCl(a¹ Δ)", *Chem. Phys. Lett.*, **299**, 583-588, 1999.
19. C. F. Wisniewski, G. C. Manke II, G. D. Hager, C. R. Truman and P. F. Crowell, "in preparation", 2002.
20. G. C. Manke II and G. D. Hager, "A Review of Recent Experiments and Calculations Relevant to the Kinetics of the HF Laser", *J. Phys. Chem. Ref. Data*, **30**, 713 - 733, 2001.
21. L. H. Sentman, A. J. Eyre, J. T. Cassibry and B. P. Wootton, "Studies of cw HF Chemical Laser Performance", AAE TR 99-01, UILU ENG 99-0501, 1999.
22. L. H. Sentman, A. J. Eyre, B. P. Wootton and J. T. Cassibry, "Comparison of cw HF Laser Performance for Several Nozzles", AIAA 99-3469, 1999.
23. G. C. Manke II, T. L. Henshaw, T. J. Madden, J. M. Herbelin, B. D. Rafferty and G. D. Hager, "Characterizing fluorine and chlorine atom flow rates using iodine atom spectrometry", *AIAA Journal*, **39**, 447 - 454, 2001.

24. Thomas L. Henshaw, Gerald C. Manke II, Timothy J. Madden, Michael R. Berman and Gordon D. Hager, "A new energy transfer chemical laser at 1.315 μm ", *Chem. Phys. Lett.*, **325**, 537 - 544, 2000.
25. L. H. Sentman, P. T. Theodoropoulos, T. Nguyen, D. L. Carroll and R. E. Waldo, "An Economical Supersonic cw HF Laser Testbed", AIAA Paper 89-1898, 1989.
26. D. L. Carroll, L. H. Sentman, P. T. Theodoropoulos, R. E. Waldo and S. J. Gordon, "Experimental Study of Continuous Wave Hydrogen-Fluoride Chemical Laser Overtone Performance", *AIAA Journal*, **31**, 693 - 700, 1993.
27. D. L. Carroll, L. H. Sentman, P. T. Theodoropoulos, R. E. Waldo, S. J. Gordon and J. W. Otto, "Experimental and Theoretical Study of cw HF Chemical Laser Overtone Performance", AAE TR 92-02, UILU ENG 92-0502, 1992.

Table 1: Typical Experimental Conditions

Parameter	Range
Flow Rates	
F ₂	1 mmols sec ⁻¹
H ₂	0 - 30 mmols sec ⁻¹
He(primary)	90 mmols sec ⁻¹
He(secondary)	15 mmols sec ⁻¹
He(base purge)	15 mmols sec ⁻¹
Cavity Pressure, Temperature	
Pressure (static)	1.5 - 2.0 Torr
Pressure (total)	~20 Torr
Temperature (plenum / cavity wall)	370 / 290 K
Mach #	2.1 - 2.4



Figures 1a & 1b. HYSIM slit nozzle configuration. (a). A construction diagram for the HYSIM slit nozzle is shown. Fluorine atoms are generated by the DC discharge and enter the plenum region before passing through the 3 mm high slit nozzle. Laser mirrors or glass windows can be mounted along the sides of the reactor to accommodate laser demonstrations or gain measurements, respectively. (b). Downstream view of the supersonic slit nozzle. The first two rows of injectors just downstream of the slit are for secondary (trip jet) He and H₂ injection, respectively. A 1 cm step (top and bottom) occurs at the Nozzle Exit Plane (NEP), 0.9 cm downstream of the nozzle throat. Additional He is added to purge this region and prevent recirculation.

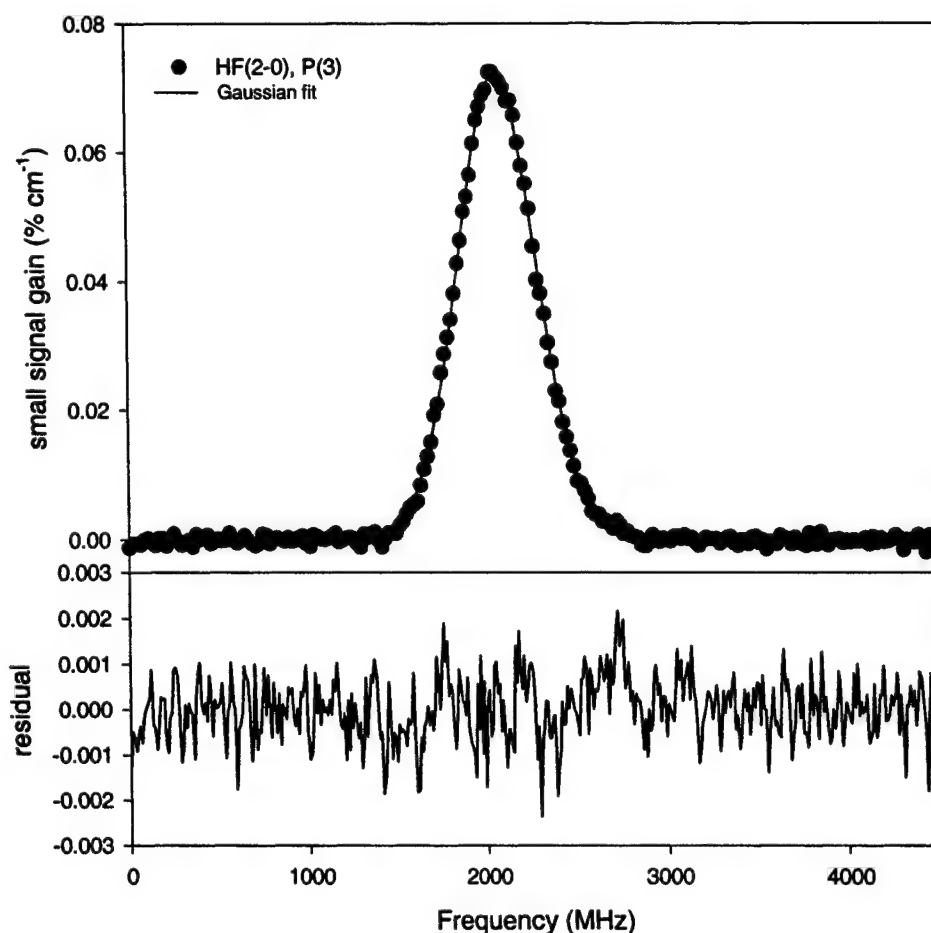
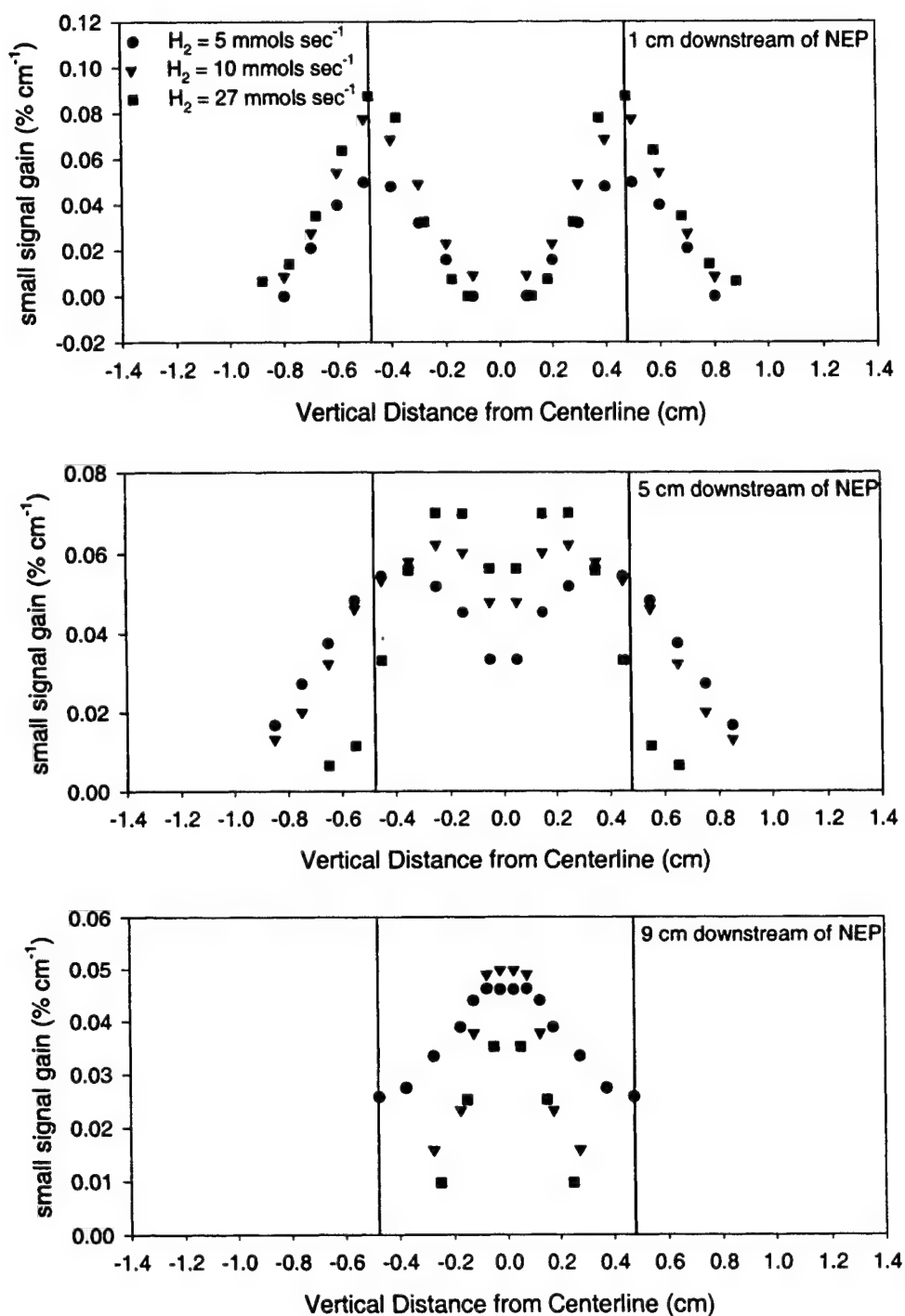
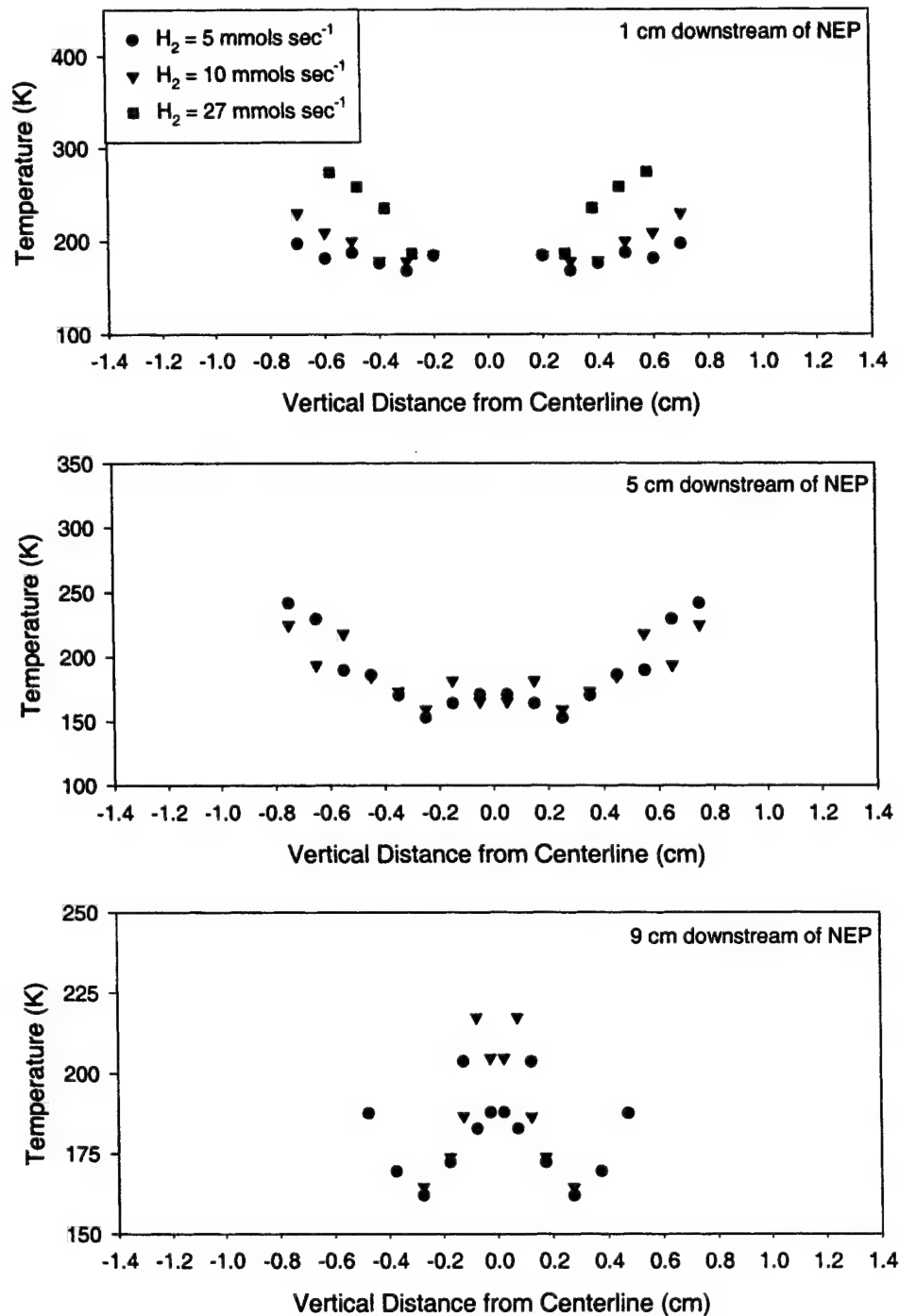


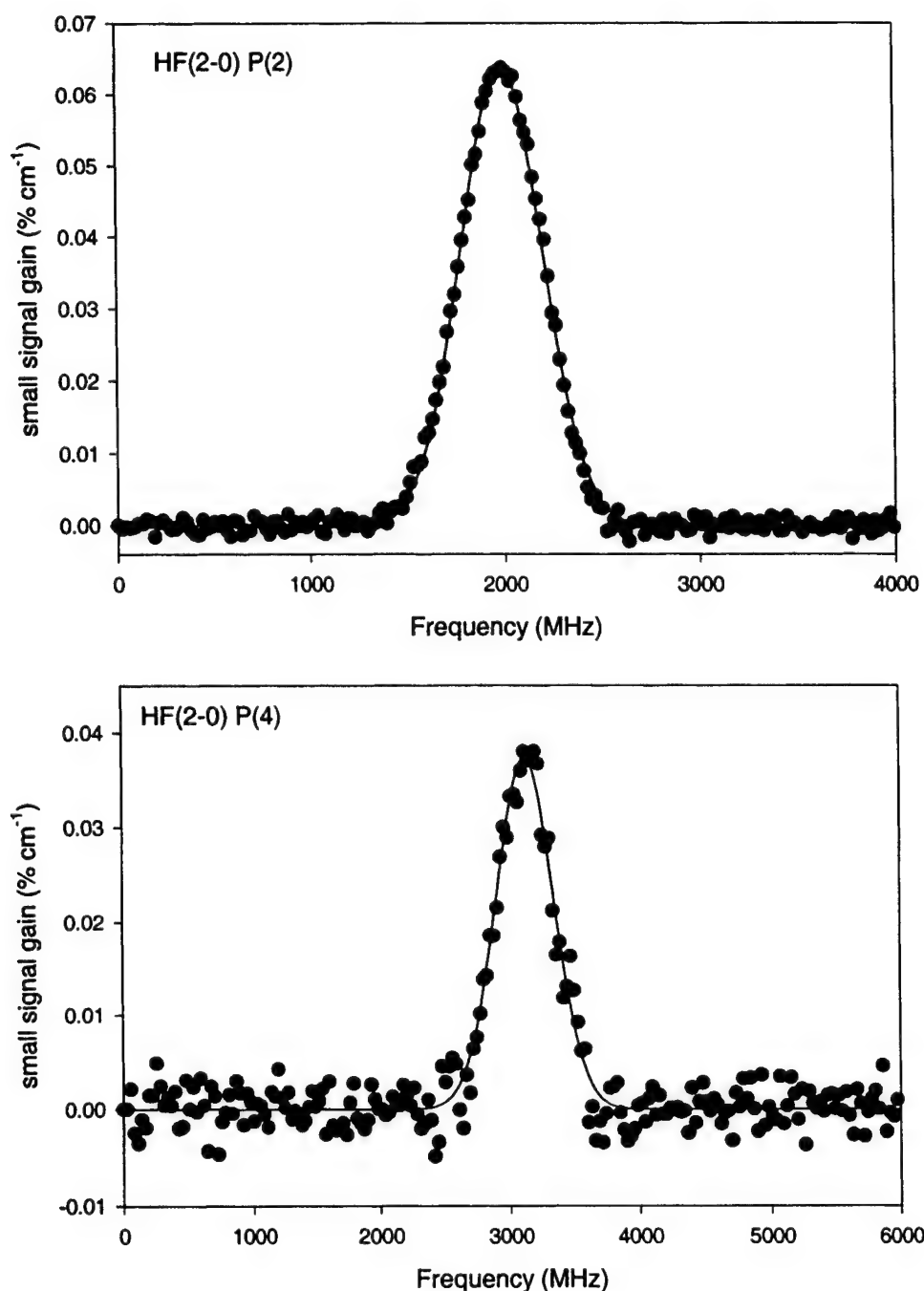
Figure 2. Small signal gain on HF(2-0) P(3). A sample HF overtone small signal gain spectrum is shown. The experimental conditions for the upper panel are $F_2 = 1 \text{ mmol sec}^{-1}$, $H_2 = 27 \text{ mmols sec}^{-1}$, $P \sim 2 \text{ Torr}$, $x = 5 \text{ cm}$ downstream of the NEP, and $y = 0.25 \text{ cm}$ above the centerline. For purposes of clarity, only every other data point is shown. The spectrum is fit by a Gaussian function which gives area = 39.6, width(FWHM) = 515.2 MHz, and peak gain = 0.072 \% cm^{-1} . The linewidth corresponds to $T = 198 \text{ K}$. A residual plot is shown in the lower panel, demonstrating that the Gaussian line function adequately fits the entire lineshape. If pressure broadening had been present, the residual plot would have non-random structure.



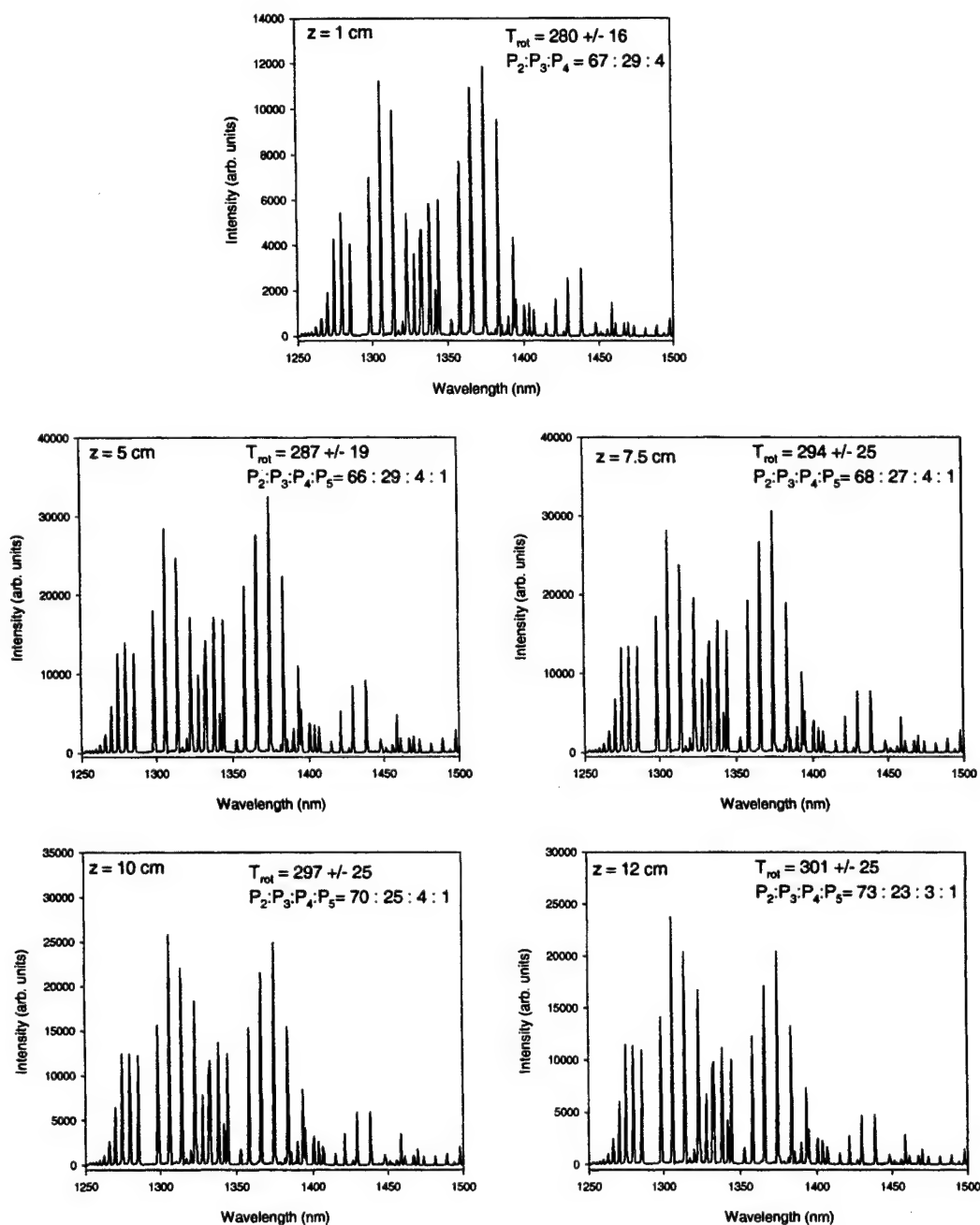
Figures 3a-c. Vertical small signal gain profiles. The diode probe laser was scanned along the vertical (y) and streamwise (x) axes of the reactor. The solid lines indicate the edges of the top and bottom base purge regions. The vertical small signal gain profile measured 1 cm downstream of the NEP indicates poor penetration of hydrogen and significant expansion of the flow into the base purge region. The mixing into the center of the flow channel improves as the flow marches downstream of the NEP, but the peak gain decreases from 0.08 % cm⁻¹ at 1 cm to 0.05 % cm⁻¹ at 9 cm.



Figures 4 a - c. Vertical temperature profiles. The diode probe laser was scanned along the vertical (y) and streamwise (x) axes of the reactor. The uncertainty of the temperature in some cases is substantial because the signal to noise ratio is poor and a reliable peak width could not be determined. Hence, fewer data points appear than in Figures 3 a-c. The temperature varies approximately 100 K from the centerline to the middle of the base purge region, peaking where the gain is highest.



Figures 5 a - b. Small signal gain for HF(2-0) P(2) and P(4). In addition to measuring the small signal gain on HF(2-0) P(3), the diode laser can scan across several other overtone ro-vibrational lines. The HF(2-0) P(2) and P(4) lines are shown in the upper and lower panels, respectively. The experimental conditions for the upper panel are $F_2 = 1 \text{ mmol sec}^{-1}$, $H_2 = 27 \text{ mmols sec}^{-1}$, $P \sim 2 \text{ Torr}$, $x = 5 \text{ cm}$ downstream of the NEP, and $y = 0.25 \text{ cm}$ above the centerline. The Gaussian function fit to P(2) spectrum corresponds to area = 33.4, linewidth(FWHM) = 490.3 MHz, and peak gain = 0.064 \% cm^{-1} . The experimental conditions for the lower panel are $F_2 = 1 \text{ mmol sec}^{-1}$, $H_2 = 27 \text{ mmols sec}^{-1}$, $P \sim 2 \text{ Torr}$, $x = 1 \text{ cm}$ downstream of the NEP, and $y = 0.4 \text{ cm}$ above the centerline. The Gaussian function fit to P(4) spectrum corresponds to area = 20.8, linewidth(FWHM) = 523.8 MHz, and peak gain = 0.037 \% cm^{-1} .



Figures 6a - e. HF overtone emission spectra. A Near Infrared Optical Multi-channel Analyzer (NIR OMA) was used to collect the HF overtone spectra shown above. Using fiber optic delivery to the monochromator, spatially resolved emission spectra can be generated. A Boltzmann analysis of the overtone spectra (see text) shows that rotational equilibrium has been achieved, that the rotational temperature increases slightly and the vibrational distribution relaxes as the flow progresses downstream. The experimental conditions for all panels are $F_2 = 1 \text{ mmol sec}^{-1}$, $H_2 = 27 \text{ mmols sec}^{-1}$, and $P \sim 2 \text{ Torr}$. Although the fiber optic lens collects chemiluminescence from a small solid angle, it was positioned such that the entire vertical profile is observed simultaneously ($y = \text{centerline} \pm 0.5 \text{ cm}$).

Atomic fluorine source for chemical lasers

S.J. Davis*, D.B. Oakes, M.E. Read, and A.H. Gelb
Physical Sciences Inc.

ABSTRACT

We present results from the early development of an F atom source appropriate for HF and AGIL chemical laser research. The system uses high power microwaves to produce a high enthalpy plasma that thermally dissociates molecular species such as SF₆ and F₂. Results of the characterization of the flow are presented.

Keywords: hydrogen fluoride lasers, combustors, halogen atom sources, microwave discharges

1. INTRODUCTION

Chemical lasers offer the obvious advantage that the population inversion is produced by selective chemical reactions, e.g., HF lasers¹ or energy transfer from chemically produced metastable species such as the Chemical Oxygen Iodine Laser (COIL)² and All Gas-Phase Iodine Laser (AGIL).³⁻⁶ Often, however, one must supply energy sources to obtain the chemical species required for the selective reactions to occur. For example the reactants that produce the HF laser are F and H₂. Consequently, production of F atoms is a key element in HF chemical lasers. Several methods for F atom production have been used: DC electric discharge, photolysis, electrical arc heating, and chemical combustors. Large, high power HF lasers use chemical combustors to produce the enthalpy necessary to thermally dissociate either F₂ or NF₃. The combustors can be driven by the reaction of H₂ and F₂. For small, laboratory-scale HF lasers DC electric discharge is often used.

In this paper we discuss a new, alternate dissociation source for F atom production that may be suitable for HF and other chemical lasers that require F atoms such as HF and the new AGIL system. Our source is based on a device called the Microwave Induced Plasma Jet (MIDJet™). The MIDJet™ device can be considered to be a thermal dissociation source of atomic species. In effect, it is an efficient electrical combustor. The MIDJet™ is shown schematically in Fig. 1. It consists of a coaxial microwave line feeding a TM₀₁ microwave cavity formed by an outer cylinder and an inner

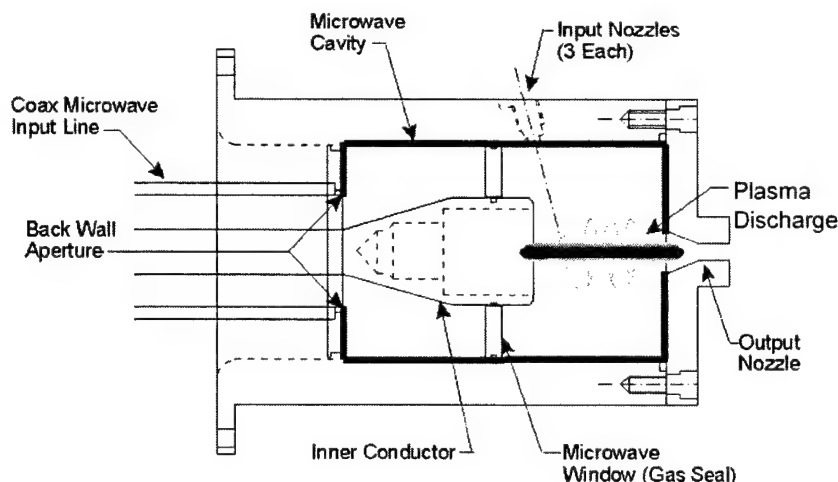


Fig. 1: Schematic of a MIDJet™ device.

*sdavis@psicorp.com; phone 1 978 689-0003; fax 1 978 689 3232; <http://www.psicorp.com>; Physical Sciences Inc., 20 New England Business Center, Andover, MA, USA 01810-1077

conductor. Microwave power is injected via a coaxial line. The inner conductor is continued into the cavity, forming a coaxial structure that allows the diameter to be significantly smaller than would be possible with an open cavity. A discharge is produced on axis, where the RF electric field is locally maximum. The input gas is introduced via nozzles in the outer wall, with nozzles angled to produce an azimuthal (vortex) flow. This flow produces a radial acceleration that results in hot gas being pushed inward. The discharge produced by the high RF electric field on axis is thus confined to a small cylindrical volume. The gas exits through a nozzle. The output flow can be subsonic, sonic, or supersonic, depending on the pressure difference between the torch and the ambient environment, and the design of the nozzle. The MIDJet™ can be operated with internal pressures from slightly sub-atmosphere to more than 10 atm, producing supersonic and subsonic flows even into the atmosphere.

2. EXPERIMENT

We assembled the apparatus shown in Fig. 2 to test the MIDJet™ as an F-atom source appropriate for chemical laser research. The MIDJet™ head was connected to a chamber with three pumping stages. The chamber was a six port cross with each port 20 cm in diameter. As indicated in Fig. 2, for some tests we used a mass spectrometer to analyze the effluents from the MIDJet™ head to measure the dissociation fraction of the molecular fluorine. This spectrometer can make measurements up to 300 amu with 1 amu resolution. Two stages of differential pumping are used to handle the high mass flow rates of the MIDJet™. Greater than 99% of the flow is pumped from the first stage by a 400 cfm Roots Blower. A 0.5 mm diameter graphite skimmer is used to separate the first pumping stage from the second. This skimmer is well downstream of the Mach disk which forms about 2 cm from the MIDJet™ exit nozzle. Beyond the Mach disk the flow is subsonic. A second skimmer separates the second differential chamber from the first and provides the entrance path for gas to be analyzed by the mass spectrometer.

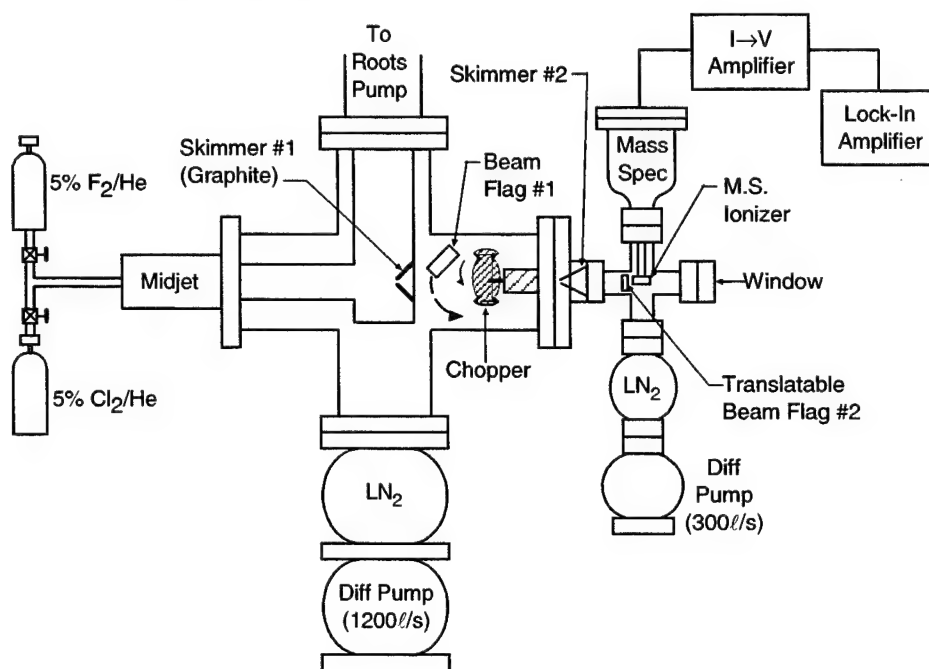


Fig. 2: Schematic of the apparatus used for the beam composition measurements.

The beam composition is measured by monitoring the mass 19 (F atom) and 38 (F₂) signals. To convert the raw signals into values that are proportional to the concentration of F and F₂ in the flow we must take into account the following: 1) F signal resulting from F₂ cracking in the mass spectrometer ionizer, 2) the relative ionization cross section by electron beam impact for F and F₂, and 3) the transmission function (sensitivity versus mass) of the mass spectrometer. For the fluorine beam the atomic content of the fluorine component of the beam (%F, neglecting the helium diluent) is given by Eq. (1).

$$\% \text{ F atoms} = \frac{N_F}{(N_F + N_{F2})} \times 100\% \quad (1)$$

where:

$$\begin{aligned} N_F &= (S_F - S_F^{F2}) T_F^{-1} C_F^{-1} \\ N_{F2} &= S_{F2} T_{F2}^{-1} C_{F2}^{-1} \end{aligned} \quad (2)$$

and:

- N_F = Value proportional to # of F atoms in beam
- N_{F2} = Value proportional to # of F_2 molecules in beam
- S_F = The $m/e = 19$ signal (Volts)
- S_{F2} = The $m/e = 38$ signal (Volts)
- S_F^{F2} = The contribution to the $m/e = 19$ signal due to the cracking of F_2
- T_F = The transmission function for $m/e = 18$
- T_{F2} = The transmission function for $m/e = 38$
- C_F = The relative ionization cross section for atomic fluorine
- C_{F2} = The relative ionization cross section for F_2 .

We obtained references reporting measurements of the absolute cross section for ionization of F and F_2 by electron impact at 70 eV (our electron energy).^{7,8} We also measured the relative transmission function for the mass spectrometer from mass (m/e) 20 to 40. The relative Ar^+ ($m/e = 40$) and Ar^{++} ($m/e = 20$) signals in our mass spectrometer formed by electron impact of argon were compared to the published cross section for the formation of Ar^+ and Ar^{++} by electron impact of argon. This comparison led to values of the relative transmission function between mass 19 and 38. Finally the contribution of F_2 cracking to the F signal was measured by turning the MIDJet™ plasma off and measuring the relative $m/e = 38$ to 19 signals for the cold flow. A summary of all the parameters necessary for the calculation of the atomic composition of the fluorine beam is presented in Table 1.

Table 1: Summary of the Parameters Used to Determine the Fluorine Beam Composition

Beam	Transmission Function (Relative)		Ionization Cross Section ($\times 10^{-16} \text{ cm}^2$)		Fraction of Parent Signal that Contributes to Atom Signal
	Atom	Parent	Atom	Parent	
Fluorine	1.00	0.763	0.87	1.10	0.210

3. RESULTS

MIDJet™ beams were made from the 5% F_2 /Helium mixture with discharge powers ranging from 1860 to 3610 W. The results of the beam composition analysis are plotted as % F_2 dissociation versus Power/Flow ratio in Fig. 3.

Fig. 3 shows that the maximum F atom content of the fluorine flow obtained in these experiments was 81%. Equilibrium calculations predict that the fluorine in the 5% F_2 /He beam will be essentially fully dissociated for Power/Flow ratios greater than 40 W/slm. We are therefore observing less dissociation than expected based upon the equilibrium prediction. However, as expected, at a fixed discharge power the data does show a correlation between F atom content and increasing Power/Flow ratio.

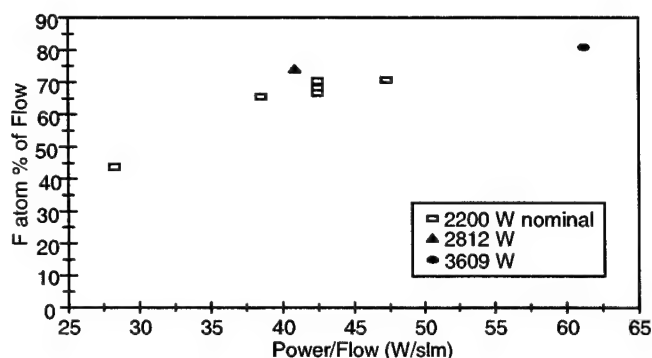


Fig. 3: F atom % of the flow versus Power/Flow (W/slm) ratio for the beams formed from the 5% F₂/helium mixture.

We estimated that the effects of gas phase recombination in the chamber are negligible. However, recirculation flows which result in background gas reaching and passing through the first skimmer would have a high recombination fraction due to substantial interaction with the chamber walls. A summary of a few composition measurements are shown in Table 2.

Table 2: Summary of the Conditions and Results for Three of the Composition Experiments Included in Fig. 3

Coupled Discharge Power (W)	Power/Flow (W/slm)	Formation Chamber Pressure (Torr)	Atomic F % of Flow	F Atom Fluence (/s)	F Atom Fluence (mmoles/s)
1880	42.5	2.80	68.2	1.02×10^{21}	1.8
2810	40.9	4.05	74.2	1.82×10^{21}	3.0
3610	61.2	3.67	80.7	1.79×10^{21}	3.0

Since the MIDJet™ device can operate at pressures of an atmosphere or greater, it is appropriate to consider it as a driver for a subsonic or supersonic chemical laser nozzle. One could consider the downstream side of the device as a plenum. The gases would then flow through a mixing nozzle as indicated in Fig. 4.

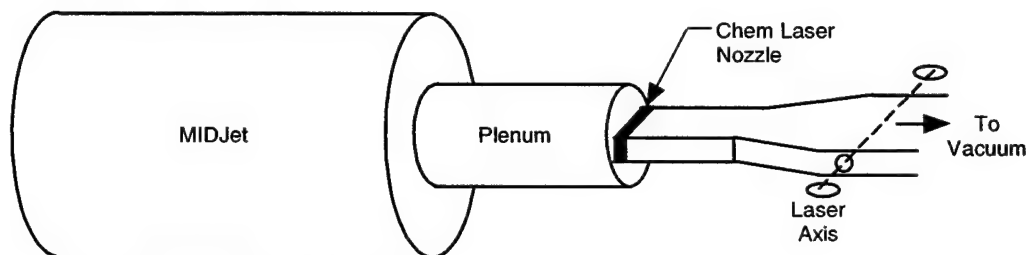


Fig. 4: Concept for a MIDJet™ driven chemical laser.

3.1 Scaled MidJet™

We have designed and are building a scaled device that will deliver 25 kW of microwave power to the flow. Equilibrium calculations indicate that such a system will be able to produce nearly 50 mmoles of F atoms. For example, in Figs. 5 and 6 we show results from an equilibrium calculation for a flow of 16 mmoles/s of F₂ and NF₃ in a flow of 700 mmoles of He. The equilibrium calculations use the heat capacities of the gases and predict dissociation fractions as a function of temperature. Fig. 5 indicates that 25 kW of absorbed power will dissociate greater than 95% of the F₂ in the flow. For NF₃ (see Fig. 6), greater than 90% of the NF₃ will be dissociated into F atoms.

The expected dissociation products from NF₃ are indicated in Fig. 7.

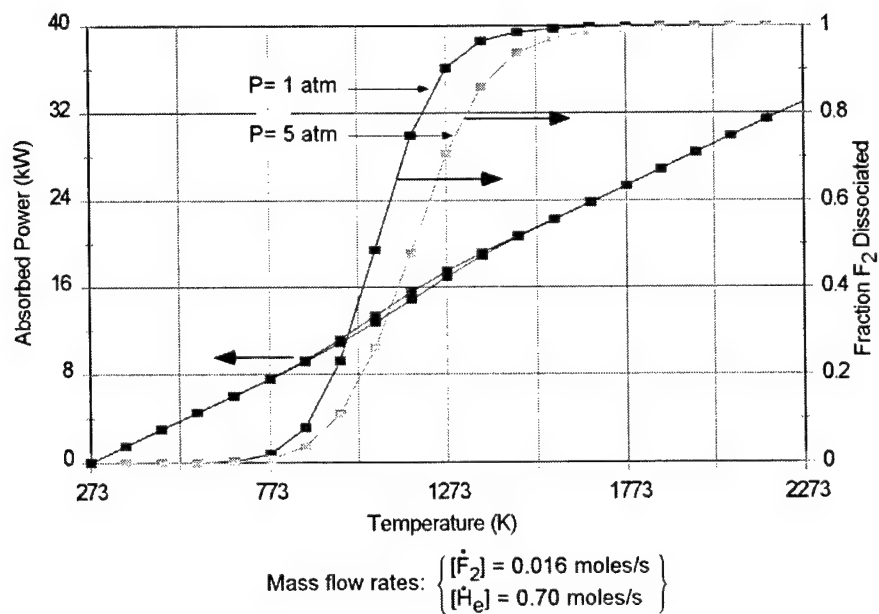


Fig. 5: Equilibrium code predictions of dissociation fraction of F_2 for a mix of F_2/He .

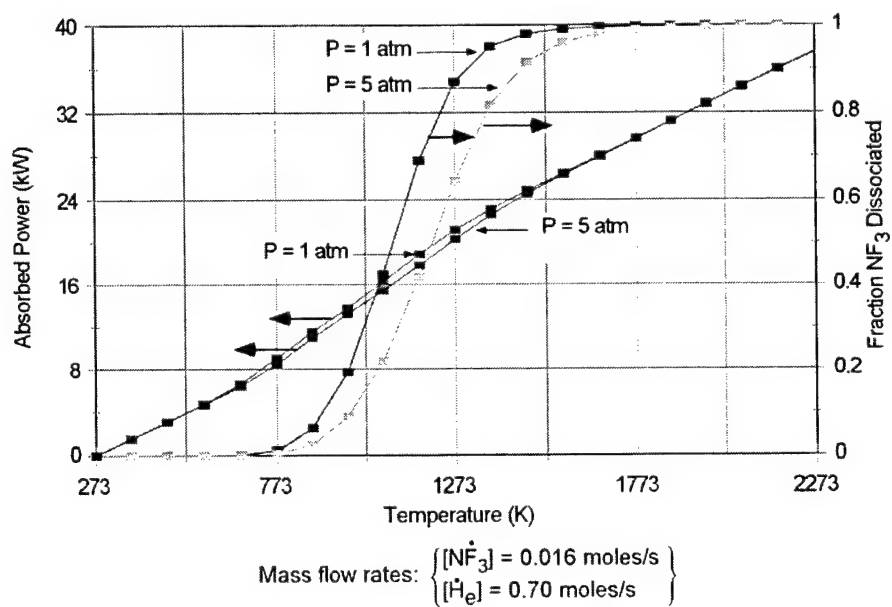


Fig. 6: Equilibrium code prediction of dissociation fraction of NF_3 for a mix of NF_3/He .

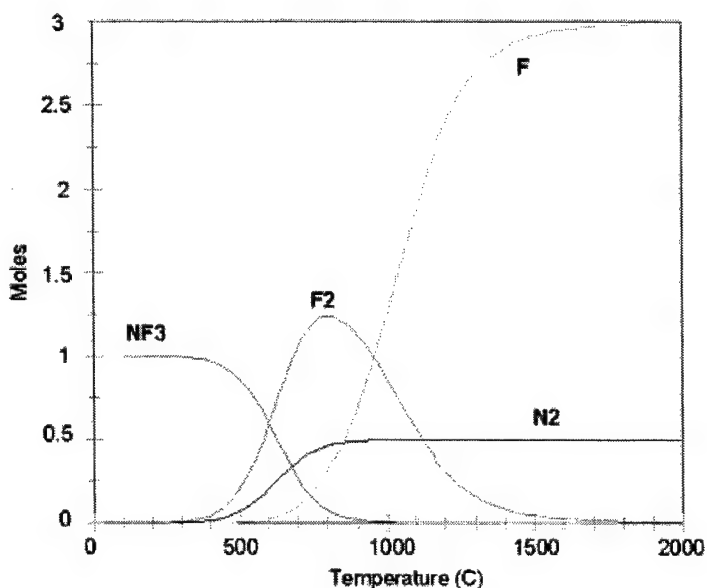


Fig. 7: Equilibrium calculation for NF_3 at 1 atm.

4. SUMMARY

We have described a novel, electrically based source for halogen atoms that may be a convenient source of F atoms for HF chemical laser research. We have characterized a device that delivers up to 3.5 kW to the gas flow and have demonstrated F atom fluences of 3 mmoles/s for a 5% mix of F_2 in He. A scaled device is under construction.

ACKNOWLEDGMENT OF SUPPORT AND DISCLAIMER

This material is based upon work supported by the United States Air Force Research Laboratory, Directed Energy Directorate, Contract No. F29601-00-C-0053. We gratefully acknowledge this support.

REFERENCES

1. R.W.F. Gross and J.F. Bott, *Handbook of Chemical Lasers*, John Wiley & Sons, New York, 1976.
2. W.E. McDermott, N.R. Pchelkin, D.J. Benard, and R.R. Bousek, "An Electronic Transition Chemical Laser," *Appl. Phys. Lett.*, **32**, 469, 1978.
3. J.M. Herbelin, T.L. Henshaw, B.D. Rafferty, B.T. Anderson, R.F. Tate, T J. Madden, G.C. Manke II, and G.D. Hager, "The Measurement of Gain on the 1.315 μm Transition in Atomic Iodine in a Subsonic Flow of Chemically Generated $\text{NCl}(a^1\Delta)$," *Chem. Phys. Lett.*, **299**, 583, 1999.
4. T.T. Yang, V.T. Gyls, R.D. Bower, and L.F. Rubin, "Population Inversion Between $\text{I}(^2\text{P}_{1/2})$ and $\text{I}(^2\text{P}_{3/2})$ of Atomic Iodine Generated by Excitation Transfer from $\text{NCl}(a^1\Delta)$ to $\text{I}(^2\text{P}_{3/2})$," *SPIE*, **1871**, 1993.
5. A.J. Ray and R.D. Coombe, "Energy Transfer from $\text{NCl}(a^1\Delta)$ to Iodine Atoms," *J. Phys. Chem.*, **97**, 3475, 1993.
6. A.J. Ray and R.D. Coombe, "An I^* Laser Pumped with $\text{NCl}(a^1\Delta)$," *J. Phys. Chem.*, **99**, 7849, 1995.
7. T.R. Hayes, R.C. Wetzel, and R.S. Freund, "Absolute Electron-Impact-Ionization Measurements of the Halogen Atoms," *Phys. Rev. A*, **35**(2), 578, 1987.
8. F.A. Stevie and M.J. Vasile, "Electron Impact Ionization Cross Sections of F_2 and Cl_2 ," *J. Chem. Phys.*, **74**(9), 5106, 1981.

Parametric Study of $\text{NCl}(a^1\Delta)$, $\text{NCl}(b^1\Sigma)$ from the reaction of $\text{Cl}/\text{Cl}_2/\text{He} + \text{HN}_3/\text{He}$

Liping Duo, Shukai Tang, Jian Li, Xiangde Min, Fengting Sang, Bailing Yang
Short Wavelength Chemical Laser Laboratory, Dalian Institute of Chemical Physics
Chinese Academy of Sciences, Dalian 116023, China

ABSTRACT

By means of Microwave generator chlorine diluted by helium is dissociated to chlorine atoms that subsequently react with hydrogen azide to produce excited states of $\text{NCl}(a^1\Delta)$ and $\text{NCl}(b^1\Sigma)$. In this paper, the intensity of $\text{NCl}(a^1\Delta)$ and $\text{NCl}(b^1\Sigma)$ emission dependent on the flow rates of different gases is studied. Moreover, the production of $\text{NCl}(a^1\Delta)$ and $\text{NCl}(b^1\Sigma)$ along the reaction tube is also investigated. By using a simple titration method, we obtain the dissociation efficiency of molecular chlorine up to 100% at the flow rates of chlorine no more than 1mmol/s. We also achieve the quenching rate of $\text{NCl}(a^1\Delta)$ by Cl_2 is about $4 \times 10^{-13} \text{ cm}^3/\text{sec} \cdot \text{molec}$ with excess flow rates of chlorine. Finally, the optimum parameters for $\text{NCl}(a^1\Delta)$ and $\text{NCl}(b^1\Sigma)$ production are summarized.

Key words: $\text{NCl}(a^1\Delta)$ and $\text{NCl}(b^1\Sigma)$, $\text{Cl}/\text{Cl}_2/\text{He} + \text{HN}_3/\text{He}$

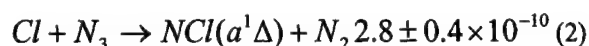
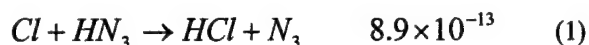
1. INTRODUCTION

Being the shortest wavelength chemical laser and the only laser based on electronic transition, the chemical oxygen-iodine laser (COIL) is of great interest owing to its potential applications in both industrial and military fields^[1]. As the energy source of the laser, $\text{O}_2(a^1\Delta)$ is produced by the reaction of gaseous chlorine with liquid basic hydrogen peroxide (BHP) in the singlet oxygen generator (SOG) which is a main part of the COIL and occupy the most of COIL in size and weight, so power-volume or power-weight efficiency is limited by the gaseous-liquid reaction. Moreover, there are the strong quenchers for excited atomic iodine, for example, water vapor and hydrogen peroxide produced in singlet oxygen generator (SOG). Consequently, it is necessary to look for metastable particles instead of $\text{O}_2(a^1\Delta)$ to pump iodine atoms.

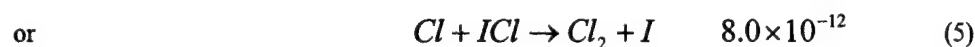
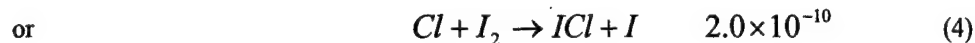
Bower and Yang^[2] reported the nearly resonant energy transfer from metastable $\text{NCl}(a^1\Delta)$ to atomic iodine in 1990 and obtained the reactive rate of $>1 \times 10^{-10} \text{ cm}^3 \text{ s}^{-1}$ which is much faster than that of $\text{O}_2(a^1\Delta)$ to atomic iodine. The concept of $\text{NCl}(a^1\Delta)/\text{I}$ as a newly possible laser system is becoming a hot point. Many papers^[3-7] about $\text{NCl}(a^1\Delta)$ energy transfer and quenching kinetics were reported. T.L.Henshaw^[8] and his group at Air Force Research Laboratory measured the gain on the 1315nm transition of atomic iodine in a subsonic flow of chemically generated $\text{NCl}(a^1\Delta)$ in 1999 and subsequently showed an output power of 180mW from a new energy transfer chemical iodine laser pumped by $\text{NCl}(a^1\Delta)$ at 1315nm in 2000^[9].

The mechanism of the system for a chemical atomic iodine laser pumped by $\text{NCl}(a^1\Delta)$ is general as following:

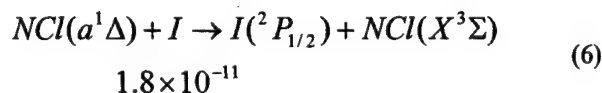
Production of $\text{NCl}(a^1\Delta)$



Production of atomic iodine

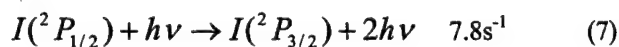


Production of excited atomic iodine

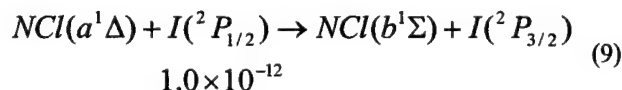
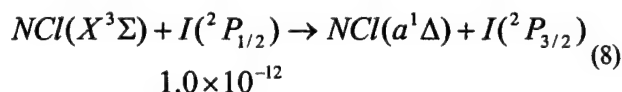


The above reactive rates are in units of cm³/sec molec..

Lasing



In addition, there is a sharp increase of NCl(b¹Σ) emission upon iodine being injected into the system of NCl(a¹Δ)/Cl/He/Cl₂/HN₃, that is, a potential chemical laser at visible^[10] is based on



In this paper, the intensity of NCl(a¹Δ) and NCl(b¹Σ) emission dependent on the flow rates of different gases was studied. Moreover, the production of NCl(a¹Δ) and NCl(b¹Σ) along the reaction tube was also investigated. The results were presented and discussed and the quenching rate of NCl(a¹Δ) by Cl₂ is obtained. The optimum parameters for NCl(a¹Δ) and NCl(b¹Σ) production were given finally.

2. EXPERIMENTAL

The diagram of the setup we used was shown in Figure 1. The reaction tube that was made of silica glass and had a length of 1.2m, the Microwave generator of 1000W, the gas supply system, OMA4 and the pumping system were indicated. The mixture of chlorine measured by a flow meter and helium measured by a flow meter flowed through the MW generator to produce chlorine atoms that then mixed and reacted with the mixture of hydrogen azide and helium at the ratio of 1:10. The chlorine and helium we used have a purity of 99.99%. HN₃ was produced by the method described in reference [2] and stored in an 180L steel container in which helium was input till the ratio of

He/HN₃ at 10:1. The pressure of the reaction tube was about 10 Torr and the linear velocity of the gases in the tube was around 100m/s. NCl(a¹Δ) and NCl(b¹Σ) emission was collected by OMA4 and processed by a computer.

3. RESULTS AND DISCUSSION

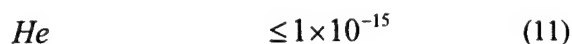
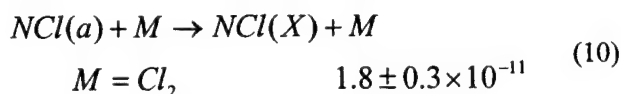
3.1 Spectrum of NCl(a¹Δ) and NCl(b¹Σ) emission

Upon HN₃/He being injected into Cl/Cl₂/He, the red fluorescence can be seen immediately. Spectra of NCl(a¹Δ) and NCl(b¹Σ) emission recorded by OMA4 are shown in Figure 2. The peaks of NCl(a¹Δ) emission around 1077nm and NCl(b¹Σ) emission around 665nm are the same with the results in the reference [11].

The OMA4 was calibrated by a standard tungsten lamp at 665nm and 1077nm and the coefficients were $5.73 \times 10^7 \text{ s}^{-1} \text{ Counts}^{-1}$ and $2.99 \times 10^8 \text{ s}^{-1} \text{ Counts}^{-1}$, respectively. By means of Einstein emission coefficients, the solid angle and the collected volume, we obtained that the densities of NCl(a¹Δ) and NCl(b¹Σ) at the experimental parameters were in the range of $10^{10 \sim 11} \text{ cm}^{-3}$ and $10^{7 \sim 8} \text{ cm}^{-3}$, respectively. The ratio of densities of NCl(a¹Δ) and NCl(b¹Σ) was about $10^{3 \sim 4}$ which is well accordant with the results of 6500 in reference [10]. However, it is the fact that the intensity counts of NCl(b¹Σ) emission looks like much stronger than that of NCl(a¹Δ) emission (reference Figure2). This is completely due to that the Einstein emission coefficient of NCl(b¹Σ) is much larger than that of NCl(a¹Δ) and the sensitivity of OMA4 is more sensitive at visible than IR range.

3.2 NCl(a¹Δ) and NCl(b¹Σ) emission along the reaction tube

The intensity of NCl(a¹Δ) and NCl(b¹Σ) emission along the reaction tube is shown in Figure 3. It can be seen that there is a maximum at the range of 4-5cm along the reaction tube at the experimental conditions of the helium flow rate of 19.7SLM, chlorine of 0.42SLM, HN₃/He mixture of 1.6SLM and the pressure of the reactor at 10Torr. This is easily understood because the production of NCl(a¹Δ) and NCl(b¹Σ) increases with the mixing which is better and better with the distance and on the other hand the quantity of NCl(a¹Δ) and NCl(b¹Σ) decreases with the distance owing to the quenching by many particles, for example, NCl(a¹Δ) quenched by the following particles.



Considering reaction formulas of (1), (10), (11), (12) and denoting [Cl₂], [He], [Cl] as [M], we can obtained the following kinetics equation,

$$\begin{aligned} \frac{d[\text{NCl}(a^1\Delta)]}{dt} &= k_1[\text{Cl}][\text{HN}_3] \\ &\quad - \sum k_m[M][\text{NCl}(a^1\Delta)] \end{aligned} \quad (13)$$

Input the linear velocity of the gas (denoted as u), the equation can be written as a function of the distance

(denoted as x),

$$\frac{d[NCl(a^1\Delta)]}{dx} = \frac{1}{u} \{k_1[Cl][HN_3] - \Sigma k_m[M][NCl(a^1\Delta)]\} \quad (14)$$

Assuming $[HN_3]$, $[M]$ and the reactive rates of k_1 and k_m as constants, and integrating the above equation as follows,

$$[NCl(a^1\Delta)] = \frac{A}{B} \cdot (1 - e^{-Bx}) \quad (15)$$

$$\text{Where, } A = \frac{1}{u} (k_1[HN_3]_0[Cl]), \quad B = \frac{1}{u} (\Sigma k_m[M])$$

If only considering the dominant reaction step (1), we can obtain that $[Cl]$ goes down with the distance according to the reaction kinetics equation,

$$\frac{d[Cl]}{dx} = -\frac{1}{u} \{k_1[Cl][HN_3]\}$$

So,

$$[Cl] = [Cl]_0 e^{-cx} \quad (16)$$

$$\text{Where } c = \frac{1}{u} k_1[HN_3]_0$$

So equation (15) becomes

$$[NCl(a^1\Delta)] = \frac{A_0}{B} \cdot e^{-cx} \cdot (1 - e^{-Bx}) \quad (17)$$

$$\text{Where } A_0 = \frac{1}{u} (k_1[HN_3]_0[Cl]_0)$$

The maximum of $NCl(a^1\Delta)$ along the distance can be easily obtained based on making the differential equation of formula (17) equal zero.

Also, both profiles have almost the same trend and the emission of $NCl(a^1\Delta)$ and $NCl(b^1\Sigma)$ spreads all over the tube inside according to spectrum measurements as well as sights. In the following we studied the relationship of intensity of $NCl(b^1\Sigma)$ emission and parameters of gaseous flow rates since $NCl(a^1\Delta)$ has the same trend with $NCl(b^1\Sigma)$ and the OMA4 has a higher signal-noise ratio at the visible.

3.3 $NCl(a^1\Delta)$ and $NCl(b^1\Sigma)$ emission dependent on ratio of He and Cl_2

The intensity of $NCl(b^1\Sigma)$ emission dependent on the ratios of He and Cl_2 was studied at the position of 5cm and indicated in Figure 4. The ratio of He and Cl_2 was changed by adjusting the flow rates of chlorine at a fixed flow rate of helium. The intensity of $NCl(b^1\Sigma)$ emission is almost completely stronger at the ratios of He and Cl_2 more than 30:1 in several flow rates of helium cases. In more detail, it also can be seen that the ratio of He and Cl_2 for the maximum intensity of $NCl(b^1\Sigma)$ emission increases with the flow rates of He. Even so, the ratio of helium and

chlorine at 30 is enough to protect atomic chlorine since it is not easy to charge for more diluent helium by means of the microwave generator.

3.4 NCl(a¹Δ) and NCl(b¹Σ) emission dependent on Cl₂

The intensity of NCl(b¹Σ) emission dependent on the flow rates of Cl₂ is shown in Figure 5 in which the maximum intensity of NCl(b¹Σ) emission was in the range of 0.25—0.4SLM for the flow rate of chlorine. More or less chlorine can cause to decrease the production of NCl(a¹Δ) and NCl(b¹Σ) because less chlorine only produces less chlorine atoms and consequently produces less excited particles, in contrast, excessive chlorine can quench the excited particles of NCl(a¹Δ) and NCl(b¹Σ). The relationship of the density of NCl(a¹Δ) and the density of Cl₂ is display in Figure 6. Now we only consider the quenching by Cl₂ since k_{He} is much less than k_{Cl2} and the atomic chlorine is much less, the kinetics equation can be written as,

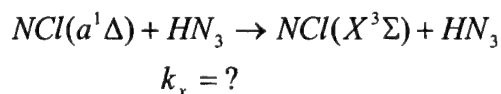
$$\frac{d[NCl(a^1\Delta)]}{dx} = \frac{1}{u}(-k_{Cl_2}[Cl_2][NCl(a^1\Delta)])$$

$$[NCl(a^1\Delta)] = [NCl(a^1\Delta)]_0 \cdot e^{-\frac{1}{u}k_{Cl_2}x[Cl_2]} \quad (18)$$

Fitting the experimental data in Figure 6, the exponential coefficient of $\frac{1}{u}k_{Cl_2}x$ is simulated as 2×10^{-16} . Based on the linear velocity of ca. 10000cm/s and the collecting position of 5cm, the quenching rate of NCl(a¹Δ) by chlorine (denoted as k_{Cl2}) is around 4×10^{-13} cm³/sec molec which is in good agreement with the result in reference [4].

3.5 NCl(a¹Δ) and NCl(b¹Σ) emission dependent on HN₃/He

The intensity of NCl(b¹Σ) emission dependent on the flow rate of HN₃/He at different flow rates of helium and chlorine is shown in Figure 7 in which it can be seen that the maximum NCl(b¹Σ) was produced at the flow rate of 2.5—3.5SLM of HN₃/He. Excess or less HN₃/He can cause the decrease of the production of NCl(a¹Δ) and NCl(b¹Σ) because less hydrogen azide only produces limited excited particles and extra hydrogen azide similarly quench the excited particles of NCl(a¹Δ) and NCl(b¹Σ) though the reaction rate of NCl(a¹Δ) quenched by HN₃ is unknown to us so far.



$$\frac{d[NCl(a^1\Delta)]}{dt} = k_1[Cl][HN_3] -$$

$$k_x[HN_3][NCl(a^1\Delta)] + k_m[M][NCl(a^1\Delta)]$$

Recently, we have done a series of experiments about changing the ratios of hydrogen azide over chlorine in another reactive device, the results are shown in Figure 8. If assuming the mixing efficiency is unity, we can obtain that the dissociation efficiency of chlorine based on the maximum flow rate of hydrogen azide,

$$\eta_{diss} = \frac{[HN_3]_{max}}{[Cl_2]}$$

is 60%~100%

In summary, the optimum operating parameters for the present setup are listed in Table 1.

4. CONCLUSION

Through the parametric study of NCl(a¹Δ) and NCl(b¹Σ) emission, it can be seen that the branch ratio of NCl(a¹Δ) and NCl(b¹Σ) is about 10³⁻⁴ in the reaction system of Cl/Cl₂/He + HN₃/He. The ratio of helium and chlorine about 30 is enough to protect atomic chlorine since it is not easy to charge for more diluent helium by means of the microwave generator. Also, we obtained that the optimum parameters for the production of NCl(a¹Δ) and NCl(b¹Σ) were the flow rates of chlorine in the range of 0.25—0.4SLM, hydrogen azide in the range of 0.25—0.35SLM, helium in the range of 11—14SLM and the pressure of the reaction tube at about 10Torr in our presently experimental conditions. More, the quenching rate of NCl(a¹Δ) by Cl₂ is about 4×10⁻¹³ cm³/sec molec. The dissociation efficiency of molecular chlorine can be up to 100% at the flow rates of chlorine no more than 1mmol/s.

REFERENCES

- [1] Zhuang Q.; Sang F.; Zhou D., "Short wavelength Chemical Laser", The Publishing House of the National Defense and Industry, 1st ed., June 1997 (in Chinese)
- [2] Yang T.T.; and Bower R.D. SPIE proceeding 1990, Vol.1225, 430
- [3] Henshaw T.L.; Herrera S.D.; and Schlie L.A., "Temperature Dependence of the NCl(a)+I(²P_{3/2}) Reaction from 300 to 482K", J. Phys. Chem. A 1998, 102, 6239
- [4] Mankell G.C and Setser D.W., "Kinetics of NCl(a and b) Generation: The Cl+N₃ Rate Constant, the NCl(a) Product Branching Fraction, and Quenching of NCl(a) by F and Cl Atoms", J. Phys. Chem. A 1998, 102, 7257
- [5] Henshaw T.L.; Herrera S.D.; Haggquist G.W.; and Schlie L.A., "Kinetics of NCl(a) via Photodissociation of ClN₃", J. Phys. Chem. A 1997, 101, 4048
- [6] Hewett K.J.; Manke II G.C.; Setser D.W.; and Brewood G., "Quenching rate constants of NCl(a) at room temperature", J. Phys. Chem. A 2000, 104, 539
- [7] Mankell G.C.; Henshaw T.L.; Madden T.J.; Hager G.D., "Temperature Dependence of the Cl+HN₃ Reaction from 300 to 480K", SPIE proceeding 2000, Vol.3931,A-12
- [8] Henshaw, T.L.; Madden, T.J.; Herbelin, J.M.; Mankell, G.C.; Anderson, B.T.; Tate, R.F.; and Hager, G.D., "Measurement of gain on the 1.315um transition of atomic iodine produced from the NCl(a)+I energy transfer reaction", SPIE proceeding 1999, Vol.3612, 147
- [9] Henshaw, T.L.; Mankell, G.C.; Madden, T.J.; Berman, M.R.; Hager, G.D. Chem. Phys. Lett. 2000, 325, 537
- [10] Yang T.T. SPIE proceeding 1994, Vol.2119, 122
- [11] Pritt, A.T.; and Coombe, R.D. Int. J. Chem. Kinetics 1980, Vol.XII, 741

*Correspondence: Email: dlp@dicp.ac.cn Tel: 86-411-4671991 ext.843 Fax: 86-411-4679766

Postal address: P.O.Box 110, Dalian, 116023, China

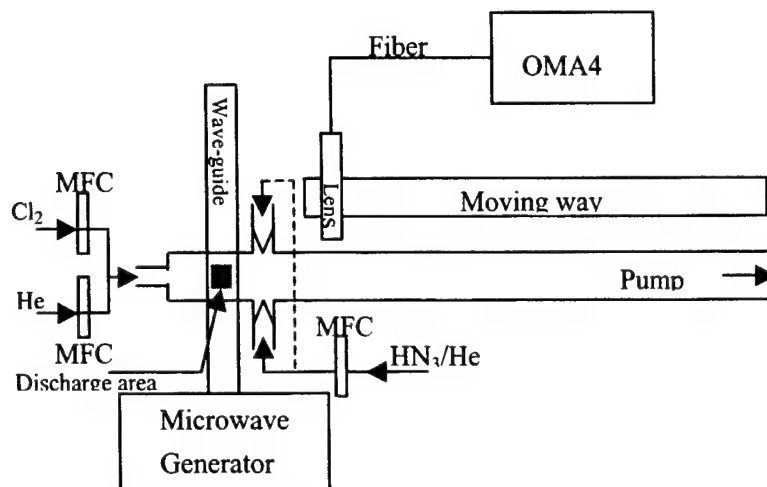


Figure 1 The schematic of the experimental setup

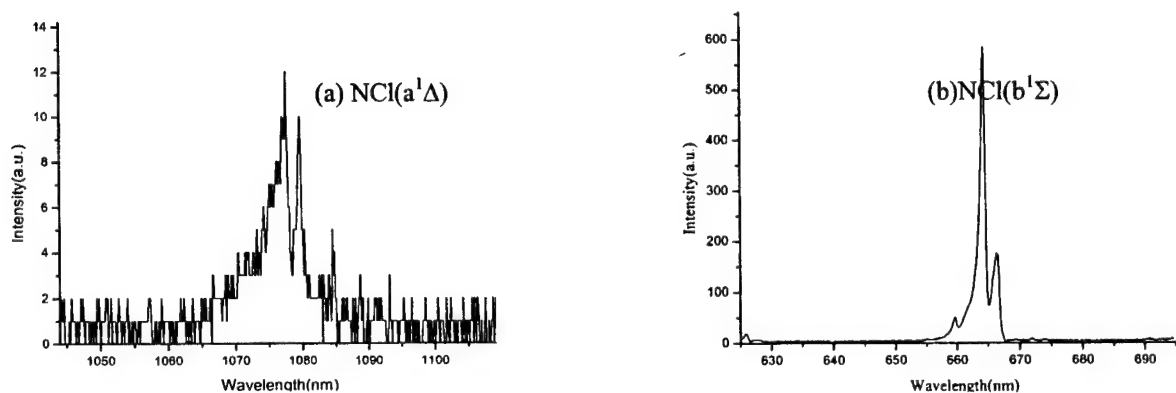


Figure 2 Spectra of $\text{NCl}(a^1\Delta)$ and $\text{NCl}(b^1\Sigma)$ emission

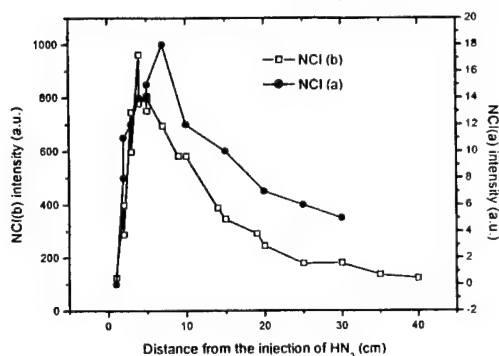


Figure 3 The intensity of $\text{NCl}(a^1\Delta)$ and $\text{NCl}(b^1\Sigma)$ emission along the reaction tube

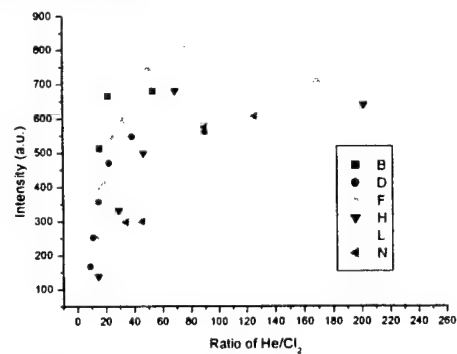


Figure 4 The intensity of $\text{NCl}(b^1\Sigma)$ emission dependent on the ratios of He and Cl_2 ,

B: He:4.8SLM; $\text{HN}_3/\text{He}(1:10)$:0.5SLM; D:He:8.1SLM ; $\text{HN}_3/\text{He}(1:10)$:1SLM;
 F: He:18.6SLM; $\text{HN}_3/\text{He}(1:10)$:2.5SLM; H: He:24.2SLM; $\text{HN}_3/\text{He}(1:10)$:1SLM;
 L: He:30SLM; $\text{HN}_3/\text{He}(1:10)$:1SLM; N: He:39.2SLM; $\text{HN}_3/\text{He}(1:10)$:2SLM

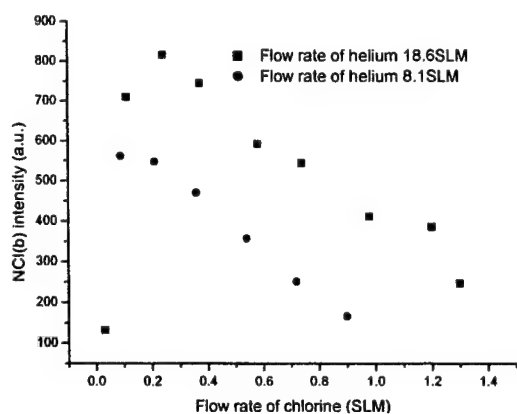


Figure 5 The intensity of $\text{NCl}(b^1\Sigma)$ emission dependent on the flow rates of Cl_2

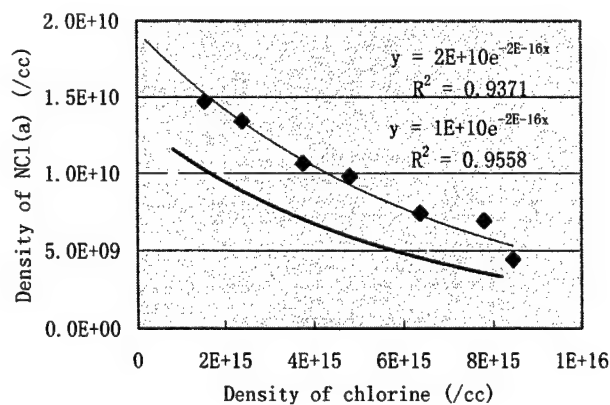


Figure 6 The dependence of density of $\text{NCl}(a^1\Delta)$ on the density of Cl_2

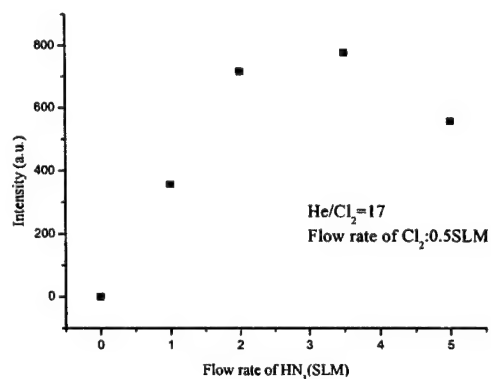


Figure 7 The intensity of $\text{NCl}(b^1\Sigma)$ emission dependent on the flow rate of HN_3/He

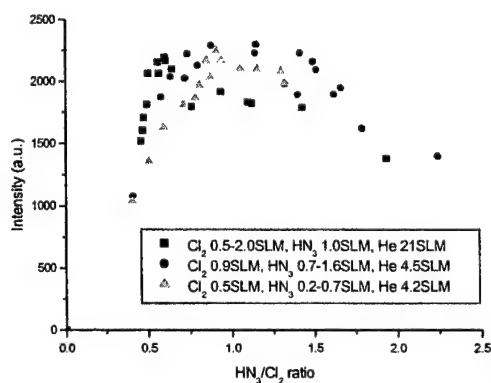


Figure 8 The relationship of the emission intensity of $\text{NCl}(b^1\Sigma)$ and the ratio of HN_3/Cl_2

Table 1 the optimum operating parameters for the present setup

HN_3 flow rate (SLM)	0.25—0.35
Cl_2 flow rate (SLM)	0.25—0.4
He flow rate (SLM)	11—14
Pressure (Pa)	1330
Diameter of the tube (cm)	2
Cl_2 dissociation efficiency (%)	60—100
Linear velocity (m/s)	100

A review of recent experiments and calculations relevant to the kinetics of the HF laser

Gerald C. Manke II* and Gordon D. Hager
Air Force Research Laboratory
Directed Energy Directorate
Kirtland AFB, NM 87117

ABSTRACT

An abbreviated review of rate coefficients relevant to HF laser kinetics modeling is presented. The literature has been surveyed from the last published review in 1983 to the present. Updated HF Einstein emission coefficients are tabulated. This brief summary of a more detailed review addresses rate coefficients relevant to HF generation, reactive quenching, self-relaxation, and vibrational relaxation by a selection of atoms and molecules. In addition, a review of recent experiments and theoretical calculations relevant to the role of rotational non-equilibrium in HF lasers is presented. A list of recommended temperature dependent expressions for critical reaction rate coefficients is given.

1. INTRODUCTION

Since its invention in the mid-1960's, the HF laser system has been extensively studied and developed to the point where megawatt-class devices can be built. In fact, most of the research in the recent past has focused on large-scale laser technology demonstrations. Despite the enormous effort expended to accomplish this, a complete understanding of all facets of HF laser performance is still evolving and is not complete. For example, research continues into the role of reagent mixing and heat transfer between the fluids and the construction material of the device. Combustor instabilities and other complex, transient, fluid dynamical features also impede our understanding of the laser's performance.

The only way to achieve insight into the details of the HF laser is to employ computational fluid dynamical (CFD) codes that can integrate the complex fluid properties with the myriad chemical reactions that occur in the laser cavity. Unfortunately (although perhaps not surprisingly considering the complexity of the problem), CFD codes have had limited success at accurately modeling real HF laser systems. As a result, both the laser performance data and the reaction rate constants used to baseline the models have come under increased scrutiny in recent years. This scrutiny has uncovered serious questions about the kinetics package that have yet to be answered conclusively. These questions include the importance of rotational nonequilibrium, the magnitude of various quenching processes, the role of three body and heterogeneous fluorine atom recombination, and other fundamental properties such as Einstein coefficients.

The main topics of this report (in order of their presentation) are Einstein coefficients and relevant kinetic measurements. It is not within the scope of this document to discuss fluid dynamics issues, such as recently developed 3 dimensional computational fluid dynamics (CFD) codes or new algorithms to model mixing or optical resonators.

2. EXPERIMENTS AND CALCULATIONS RELEVANT TO HF LASER MODELING

2.1 Einstein Coefficients

The Einstein coefficients used by most HF CFD codes are based on the values found in the Handbook of Chemical Lasers¹ (which are in turn, based on the empirical calculations of Herbelin and Emanuel²), and have not been updated in over 25 years. Table 1 gives a representative sample of the Handbook's HF vibration-rotational Einstein emission coefficients as well as the more recent (and preferred) results of Setser and co-workers³, see below. While the agreement is generally good for the first 3 vibrational levels, large differences are apparent as the vibrational quantum number increases. In 1991, Zemke⁴ and co-workers published a potential surface based on the spectroscopically determined potential of Coxon and Hajigeorgiou⁵, adjusted to reproduce the proper long-range behavior by including both dispersion and exchange effects⁶. In the same publication, Zemke and co-workers provided an *ab initio* dipole moment function that spanned the same range of internuclear distances as the complete potential energy curve. The resulting Einstein coefficients should be the most reliable theoretical values. Shortly after the publication of Zemke's results, Setser and co-workers produced an extensive set of vibration-rotational Einstein A coefficients for HF/DF and HCl/DCI³. Their calculations used an RKR potential and the *ab initio* dipole moment function of Ogilvie⁷. Their results are in excellent agreement with Zemke.

Considering the importance of the Einstein A coefficients in calculating the stimulated emission cross section and the gain, the most accurate values available should be employed. Unfortunately, Zemke and co-workers calculations were only for a limited number of rotational quantum numbers. We recommend that the HF CFD codes be updated with the results of Arunan, Setser, and Ogilvie³.

2.2 HF Kinetics

Most modern day HF CFD codes have kinetics packages that are based on a 1976 Aerospace Corporation technical report by N. Cohen & J. Bott⁸. This report and its 1977 supplement⁹ contained a thorough review of contemporary literature results up to 1977 and recommendations for rate constants related to the HF laser. An update was published 5 years later in 1982¹⁰, and a few relevant reactions were reviewed again in 1983 by Cohen & Westberg¹¹. Beyond these reports, there have only been a handful of critical evaluations of kinetic data relevant to the HF laser. A 1982 review article by Leone summarizes hydrogen halide vibrational energy transfer and contains rate coefficients relevant to the HF laser system¹². In 1983, George Hart of the Naval Research Laboratory reviewed the pulsed DF chemical laser codes and the corresponding kinetic database¹³. Although his report was specifically for DF, it contains a wide variety of relevant and helpful evaluations for the HF laser. The following paragraphs summarize the most recent and reliable calculations and experiments relevant to HF generation and quenching.

2.2.1 HF Generation - $H + F_2$ and $F + H_2$

The generation of HF(v) in the HF laser can proceed via one of two reactions, $H + F_2$ or $F + H_2$, which have significantly different product vibrational distributions. The reaction of atomic hydrogen with molecular fluorine (often referred to as the "hot" HF generation reaction) produces highly vibrationally excited HF, while $F + H_2$ (the "cold" HF generation reaction) produces only moderate vibrational excitation, see below. The vibrational distribution for $H + F_2$ peaks at $v = 6$ and extends up to $v = 9$. Table 3 summarizes the vibrational distributions recommended by the Cohen and Bott⁸⁻¹¹ reviews as well as the measured distributions from a variety of experiments. Most experimental measurements, particularly those of Polanyi¹⁴, Jonathan¹⁵, and Tardy¹⁶ analyzed their data using Einstein coefficients that have since been shown to be inaccurate^{2, 17, 18}. Hence, corrected distributions using the recommended set of A coefficients³ are shown in parentheses in Table 3.

In general, the available experimental results are in reasonable agreement for the HF(v) distribution. The only uncertainty concerns the nascent population of $v \geq 8$. On the low end, the fast flow reactor studies of Setser¹⁹ and Kaufman²⁰ found no $P_8 - P_{10}$, while on the high end the pressure-pulse chemiluminescence mapping experiments of Tardy¹⁶ found substantial populations for $v = 8 - 9$. The presence of at least some $P_8 - P_{10}$ is supported by the infrared chemiluminescence studies of Polanyi and Jonathan, who reported minor $P_8 - P_{10}$. The nascent vibrational populations from recent theoretical calculations²¹ are in satisfactory agreement with experiment but have slightly narrower distributions with small but nonzero population of $v = 8 - 10$.

Surprisingly, the Cohen and Bott reviews recommend no initial population of $v = 0 - 2$, even though all of the experimental measurements (most of which were available at the time) indicate small, but nonzero P_1 and P_2 . Clearly, some initial population of $v = 1 - 2$ is indicated by the experimental evidence, and in light of this, we recommend the distribution given in the final column of Table 2. This distribution attempts to encompass the general observation that $v = 8 - 9$ is present but at lower populations than suggested by Tardy. The recommended values for $v = 1 - 6$ are simply the average and one standard deviation from the 5 experimental measurements. Recommendations for $v = 0, v = 7 - 10$ are estimates based on the experimental values and have significantly larger error bars ($\pm 50\%$ or more). Our distribution is similar in shape to the DF(v) distribution generated by the $D + F_2$ reaction^{16, 22}, which falls off rapidly beyond the peak at $v = 9 - 10$.

The total rate constant for $H + F_2$ has not been firmly established. The 1982 Cohen & Bott review¹⁰ gives $k(T) = 5.0 \times 10^{-15} T^{1.5} \exp(-845/T) \text{ cm}^3 \text{ molecule}^{-1} \text{ s}^{-1}$ and the 1983 Cohen & Westberg recommendation¹¹ is essentially the same, $4.8 \times 10^{-15} T^{1.4} \exp(-667/T) \text{ cm}^3 \text{ molecules}^{-1} \text{ s}^{-1}$. In both cases, the recommended value was based on the experiments of Homann and co-workers²³ and unpublished transition state theory calculations of Westberg and Cohen²⁴. The 1981 Baulch kinetic²⁵ database recommends $k = 1.46 \times 10^{-10} \exp(-1210/T) \text{ cm}^3 \text{ molecule}^{-1} \text{ s}^{-1}$ for $T = 290 - 570 \text{ K}$ and points out that Homann's result is significantly smaller (approximately a factor of 2 at 300 K) than previous results by Rabideau²⁶, Vasil'ev²⁷, and Goldberg²⁸. A new measurement of the total H atom removal rate constant and the nascent HF distribution was performed recently by Heaven and co-workers²⁹. They report $k = 2.4 \pm 0.4 (2\sigma) \times 10^{-12} \text{ cm}^3 \text{ molecule}^{-1} \text{ s}^{-1}$.

The $F + H_2$ reaction is a prototypical system for fundamental reaction dynamics, and as such, has been a favorite subject for both theoretical and experimental state-to-state reactive scattering studies. The reaction is particularly amenable to molecular beam studies and vibrationally state resolved differential cross sections have been measured³⁰⁻³⁶.

Corresponding high level *ab initio* calculations and simulations^{37,38} have achieved very good agreement with experiment. The vibrational distribution remains unchanged from the 1982 Cohen & Bott report¹⁰, 0.00 : 0.15 : 0.55 : 0.30 for $v = 0 - 3$.

A recent review by Persky & Kornweitz³⁹ has refined the overall rate constant for the $F + H_2$ reaction. Following a detailed examination of relevant publications they recommend $k(T) = 1.1 \pm 0.1 \times 10^{-10} \exp(-(450 \pm 50)/T) \text{ cm}^3 \text{ molecule}^{-1} \text{ s}^{-1}$ over the 190 - 376 K temperature range, and $2.43 \pm 0.15 \times 10^{-11} \text{ cm}^3 \text{ molecule}^{-1} \text{ s}^{-1}$ at 298 K. This compares reasonably well with literature reviews published in 1983¹¹ ($k(T) = 4.5 \times 10^{-12} T^{0.5} \exp(-319/T)$) and $k_{298} = 2.66 \times 10^{-11} \text{ cm}^3 \text{ molecule}^{-1} \text{ s}^{-1}$), 1992⁴⁰, and 1997⁴¹ ($k(T) = 1.4 \times 10^{-10} \exp(-(500 \pm 200)/T)$ and $k_{298} = 2.6 \pm 0.6 \times 10^{-11} \text{ cm}^3 \text{ molecule}^{-1} \text{ s}^{-1}$), as well as the Cohen & Bott reviews of 1977⁹ ($k(T) = 2.7 \times 10^{-10} \exp(-805/T)$ and $k_{298} = 1.8 \times 10^{-11} \text{ cm}^3 \text{ molecule}^{-1} \text{ s}^{-1}$) and 1982¹⁰ ($k(T) = 4.32 \times 10^{-12} T^{0.5} \exp(-307/T)$ and $k_{298} = 2.7 \times 10^{-11} \text{ cm}^3 \text{ molecule}^{-1} \text{ s}^{-1}$). The most recent review by the IUPAC Subcommittee on Gas Kinetic Data Evaluation for Atmospheric Chemistry⁴² adopted the Persky recommendation³⁹. Unfortunately, the limited temperature range of the Persky expression is problematic for HF laser modeling, since the laser typically operates at substantially higher temperatures. To date, there has been only one experiment that has measured $k(F + H_2)$ above 376 K. Heidner and co-workers⁴³ monitored the time-resolved infrared emission of product HF following multi-photon dissociation of SF_6 in the presence of H_2 over the 295 - 765 K temperature range. The resulting Arrhenius expression for $k(F + H_2)$ is $2.2 \pm 0.4 \times 10^{-10} \exp(-(595 \pm 50)/T) \text{ cm}^3 \text{ molecule}^{-1} \text{ s}^{-1}$, just 7 % smaller than Persky's at room temperature but 40% larger if Persky's expression is extrapolated to 765 K. Persky & Kornweitz³⁹ considered Heidner's results "problematic with regard to the calculated kinetic isotope effect." Indeed, the Heidner experiment gave a temperature independent kinetic isotope effect while the accepted value is

$$\frac{k_{F+H_2}}{k_{F+D_2}} = 1.04 \pm 0.02 \exp((186 \pm 5)/T). \quad [1]$$

In lieu of more data for $T > 376$, we recommend the conclusions of Persky and Kornweitz³⁹ for the 190 - 376 K temperature range and the expression of Heidner and co-workers⁴³ for $T > 376$ K.

Some CFD codes⁴⁴ include F atom reactions with vibrationally excited H_2 even though this process was not included in the original Cohen and Bott compilations. There have been no specific experimental measurements to support or refute this assumption and we do not recommend inclusion of reactive processes that involve vibrationally hot H_2 . In any case, it is unlikely that inclusion of these reactions will have any effect on the overall performance of the laser because $[H_2(v > 0)]$ should be extremely small.

2.2.2 Reactive Quenching

Vibrationally excited HF can be removed by hydrogen atoms by V-R,T inelastic collisions or by chemical reaction to give molecular hydrogen and an F atom:



In principle, microreversibility enables one to calculate the rate constant for [2] from the extensive data available for the well-studied $F + H_2$ reaction. In fact, numerous theoretical studies have attempted to do this using the $F + H_2$ potential energy surface⁴⁵⁻⁴⁹. According to these calculations the barrier to F atom transfer is large, $\sim 33 \text{ kcal mol}^{-1}$, and reaction [2] should be slow for $v < 3$ ⁵⁰⁻⁵². This is consistent with the experimental results of Heidner and co-workers⁵³⁻⁵⁵ who measured $HF(v)$ deactivation by H atoms directly using HF laser induced fluorescence, and the flow tube measurements of Kwok & Wilkins⁵⁶. These experiments report a large change in the $HF(v)$ removal rate constant for $v = 1-2$ vs. 3. This change is generally attributed to the opening of the reactive channel for $v \geq 3$. However, according to Heidner^{54,55} only a fraction of the total $H + HF(3)$ encounters that result in removal of $HF(3)$ proceed via chemical reaction and the upper limit for reactive quenching, $k(H + HF(3) \rightarrow H_2 + F)$, is $5.0 \times 10^{-11} \text{ cm}^3 \text{ molecule}^{-1} \text{ s}^{-1}$.

The 1981 Baulch kinetics database²⁵ makes no recommendation for k_2 because the experimental evidence available at the time was inconsistent with the data for the well established forward reaction, $F + H_2$. While there have been no new experiments (for thermal collisions) since the work of Heidner and Bott⁵³⁻⁵⁵, the available theoretical calculations support their slower reaction rate constants^{8,57}.

2.2.3 HF Self-Relaxation

One of the most active areas of HF kinetics research in the past 15 years has been in the study of HF self-relaxation and vibrational energy transfer. The importance of these processes is acute because this is the dominant relaxation pathway in the HF laser. Unfortunately, a consensus regarding the magnitude of the rate constants had not been reached prior to 1982. For example, the 1977 Cohen and Bott⁹ compilation contains moderate to large rate constants for single- and multi-quantum V-R,T deactivation of HF by ground state HF



while the 1982 Cohen and Bott package¹⁰ includes only single quantum deactivations. Significant differences also exist for the HF V-V energy transfer reactions such as



Implicitly included in reaction [3] are the V-R redistribution processes that produce highly rotationally excited HF:



As will be discussed in detail below, this quenching process is of special interest because it has the potential to contribute significantly to rotational nonequilibrium.

Shortly after the publication of the 1982 review¹⁰, the Crim group at the University of Wisconsin⁵⁸⁻⁶² and the Kaufman group at the University of Pittsburgh^{20, 63-66} undertook a major effort to characterize the total self-relaxation rate constants and the mechanism for HF self-relaxation. Crim's group used a double resonance type of experiment where the vibrationally excited HF molecules were prepared in discrete ro-vibrational states by a pulsed laser. The time resolved fluorescence and/or $\Delta v = 1$ absorption signals were analyzed to determine total quenching rates and relaxation mechanisms. Kaufman, on the other hand, prepared vibrationally excited HF in a flow reactor where dilute flows of H or F atoms (generated by a microwave discharge) were reacted with a variety of F or H atom donors. The IR emission was collected with an InSb detector and circularly variable filter. A modified Stern-Volmer analysis was applied to the quenching data. Table 3 compares the experimentally determined rate constants for HF self-relaxation with a variety of other experiments⁶⁷⁻⁷⁸, relevant calculations⁷⁹⁻⁸³, and the standard kinetics packages⁸⁻¹¹. The agreement for $v = 1 - 7$ is, in general, excellent and k_3 is well established. The experimental relaxation rates scale as $v^{2.9}$ and are independent of the initial rotational quantum number.

In addition to total quenching rate constants, the Crim and Kaufman laboratories also determined the relaxation mechanism. Kaufman's group argued strongly for a V-T,R mechanism (rather than V-V energy transfer) based on Lambert-Salter plots^{20, 63-66} and the magnitude of the rate constants. In particular, they pointed out that if the predominant mechanism were V-V energy transfer, (eg. $\text{HF}(7) + \text{HF}(0) \rightarrow \text{HF}(6) + \text{HF}(1)$) then the rate constant for the exothermic reverse process would be 100 times greater than the gas kinetic limit. Crim's double resonance experiments were able to quantify the role of V-V energy transfer. They found that the fraction of inelastic $\text{HF}(v) + \text{HF}(0)$ room temperature encounters that proceed via V-T,R relaxation, is 1.0, 0.41 ± 0.10 , 0.56 ± 0.05 , 0.84 ± 0.05 , and 0.98 ± 0.19 for $v = 1 - 5$, respectively^{59, 60, 62}. For $v > 3$, vibrational energy transfer to the ground state collision partner plays a relatively minor role in the relaxation process. Both Crim and Kaufman agree that multi-quantum relaxation is unimportant^{62, 63} even though work by Pimentel and Thompson (see below) suggested the possibility of multi-quantum V-R transfer with Δv as large as 5. Crim probed the role of multi-quantum deactivations directly and found that 0.98 ± 0.19 and 0.87 ± 0.21 of the relaxed $\text{HF}(4)$ and $\text{HF}(5)$ molecules, respectively, appear in the next lower vibrational level⁶². It is important to note that Crim and co-workers' results are based on the assumption that V-T,R processes that produce metastable high rotational states (which would not be detected in their experiment) can be neglected. The invariance of the vibrational relaxation rate constant with initial rotational quantum number and the work of Leone (see below) tend to validate this assumption.

Finally, Crim and co-workers found that the rate constants for HF self-relaxation are inversely dependent on temperature^{59, 61}. Crim and co-workers interpret their temperature dependent data in terms of relaxation probabilities. The functional form of the fitting function suggests that long-range forces dominate the relaxation process:

$$P_v(T) = AT^{-m} \quad [6]$$

where $P_v = k_v/k_c$ (k_c is the gas kinetic rate constant for a collision diameter of 0.25 nm) and A and m are fitting parameters. Strangely, the A values determined by our fits (where $m = 1.3$ was fixed) vary significantly from Crim's analysis⁶¹: $A(\text{Crim}) = 22, 370, 880$, and 1850 for $v = 1, 3, 4$, and 5 respectively, while $A(\text{this work}) = 12, 315, 764$, and 1610 for the same v levels. Nonetheless, considering the overall agreement in the literature for $v = 1 - 7$ and the accuracy of double resonance technique, we recommend Crim's HF self-quenching rate constants⁶¹. The temperature dependence of $v \geq 6$ has not been measured. If the temperature dependence found for $v = 1 - 5$ (i.e. $k_v = P_v * k_c = k_c * A * T^{-1.3}$) is applied, then $A(6) = 3107$ and $A(7) = 4339$ are calculated from the measured room temperature values²⁰.

2.2.4 HF Relaxation and V-V Energy Transfer with H_2

There have been several studies of $\text{HF}(v)$ relaxation by a variety of molecular quenchers. Table 4 summarizes the results for $\text{Q} = \text{H}_2$, which are the most relevant to HF laser kinetics^{20, 71, 75, 84-87}. With the exception of the work by Poole and Smith⁷⁵, the agreement for the total quenching rate constants is good for $v = 3 - 5$. The mechanism for the quenching is generally believed to be V-T,R for $v = 3 - 5$ for two important reasons. First, V-V energy transfer from $\text{HF}(v)$ to H_2 is endothermic for all single vibrational quantum changes in HF:



In fact, due to the anharmonicity of HF, the energy gap between HF($\Delta v = -1$) and H₂(0-1) increases with vibrational quantum number ($\Delta E_{v,v} = -198 \text{ cm}^{-1}$ for HF(1) and -1171 cm^{-1} for HF(7)). Secondly, if the endothermic V-V process were the dominant mechanism, then the exothermic reverse process



would be several times larger than the gas kinetic limit. Only for HF(1) does a V-V process seem possible, and indeed, vibrational energy transfer is the most likely mechanism for $v = 1$. For $v > 1$, however, the V-T,R process



should be the dominant mechanism.

The 1982 Cohen and Bott review¹⁰ contains temperature and vibration dependent expressions for reactions [13] and [15] even though there is no convincing evidence for a temperature dependent quenching process⁸⁵.

$$k_7(\text{ref. 11}) = 2.4 \times 10^{10} v^{0.35} T^{0.5} e^{(407 - \Delta E_v)/RT} \text{ cm}^3 \text{ mol}^{-1} \text{ s}^{-1} \quad [10]$$

$$k_9(\text{ref. 11}) = v^{2.7} (0.6 \times 10^{12} T^{-1} + 1.0 \times 10^4 T^{2.28}) \text{ cm}^3 \text{ mol}^{-1} \text{ s}^{-1} \quad [11]$$

For example, in 1973 Cohen & Bott measured the temperature dependence⁷¹ ($T = 295, 450 - 1000 \text{ K}$), of HF(1) deactivation by H₂ and found that the total deactivation ($k_7 + k_9$) rate was independent of temperature (see Figure 4 of ref⁷¹). A year later Bott re-measured the temperature dependent quenching of HF(1) from 440 - 690 K and the data showed considerable scatter and only a weak temperature dependence⁸⁴. Finally, in 1980 Bott and Heidner measured HF(1) and HF(3) quenching by H₂ at 295 and 200 K and found deactivation rate coefficients that were constant vs. T within their experimental error⁸⁵. Clearly, there is not sufficient evidence to support a T dependent quenching rate constant.

Cohen & Bott's expression⁹ for k_9 significantly underestimates the measured values at room temperature, see Table 4. In fact, the 1982 package¹⁰ eliminates the energy transfer reactions from H₂(2) and H₂(3) as well as the $\Delta v > 1$ exchanges contained in the 1977 Cohen and Bott package because there is no specific experimental justification for them. We recommend the rate constant values listed in Table 4 for the V-T,R quenching of HF by H₂ and assign a T^0 temperature dependence. The HF(v) + H₂(v') V-V energy transfer reactions (reaction [8]) are calculated from detailed balance.

2.3 Rotational Non-equilibrium

The question of rotational non-equilibrium for the HF laser system has been the subject of considerable controversy for many years^{88, 89}. The presence of rotational non-equilibrium in the HF laser was first suggested by pulse initiated HF laser experiments by Pimentel and co-workers⁹⁰⁻⁹³ which generated lasing on HF rotational transitions with J as high as 33 in the $v = 1$ manifold and $J = 29$ in the $v = 0$ manifold. The observation of rotational laser emission is an extremely sensitive method for studying rotational occupancies because the population inversions needed to produce the laser emission are 100 times lower than for ro-vibrational transitions⁹³. Pimentel's analysis of the transient behavior of the laser emission suggested that collisional V-T,R energy transfer reactions that populate the high rotational states were responsible for the observed positive gain, rather than direct pumping by the initiating reaction. A remarkably similar phenomenon was observed by Robinson and co-workers in their work with HF⁹⁴, OH⁹⁵, and NH⁹⁶. Further experimental observations of emission from high J states following HF(v) quenching by CO, CO₂, and HCN^{97, 98} as well as quasiclassical trajectory calculations^{99, 100} also support the assertion that high rotational states are produced in the V-T,R relaxation process.

The evidence is clear that the principal HF(v) relaxation mechanism in the HF laser environment is HF self-relaxation, and that the relaxation proceeds via V-T,R energy transfer. There are two important questions, however, that remain:

1) What are the specific products of the V-T,R process? Figure 1 summarizes the possible relaxation / energy transfer routes for HF($v = 2$). The possible mechanisms include "true" V-T,R relaxation (the solid arrow) where the loss of a vibrational quantum results in some small amount of rotational and translational energy transfer to the HF($v = 0$) quencher or near-resonant V-R redistribution (the broken arrows), where the quenched HF molecule relaxes to a lower vibrational state with a high rotational quantum number and very little energy is transferred to the quencher.

2) Are the high- J HF molecules produced by the self-relaxation process "metastable"? In general, rotational relaxation rate constants ($k \sim 10^{-10} - 10^{-9} \text{ cm}^3 \text{ molecule}^{-1} \text{ s}^{-1}$) are 10 - 100 times larger than vibrational deactivation rate constants ($k \sim 10^{-12} - 10^{-10} \text{ cm}^3 \text{ molecule}^{-1} \text{ s}^{-1}$). However, because the separation between HF rotational levels is large, it is possible that $k_{R-R,T} \approx k_{V-R,T}$ for sufficiently high J levels. If so, the vibrational relaxation process could significantly perturb the equilibrium rotational distribution and considerable errors could be realized when attempting to model real HF laser devices.

2.3.1 Relevant Experimental Studies

As was discussed above, the self-relaxation measurements of Crim⁶², Kaufman⁶³, and Moore⁷⁷ all concluded that multi-quantum deactivations were not important. In particular, Crim determined that 0.98 ± 0.19 and 0.87 ± 0.21 of the relaxed

HF(4) and HF(5) molecules, respectively, appear in the next lower vibrational level⁶². Kaufman came to the same conclusion and suggested that multiquantum relaxation processes account for less than 1% of the total measured relaxation rate constants⁶³. Thus, any high-J states that are produced by the HF(ν) self-relaxation process will almost certainly be found in the $J = 0 - 20$ range of the next lower vibrational level.

The role of V-T,R relaxation reactions that populate high rotational states of the next lower vibrational level was addressed directly by the work of Haugen, Pence, and Leone¹⁰¹ who measured the time dependent population of HF($\nu = 0, J = 10 - 14$) following pulsed generation of HF($\nu = 1, J = 6$). They concluded that a substantial fraction of the relaxation of $\nu = 1$ occurs through the high lying rotational levels of $\nu = 0$ (~20 - 40% of the total $\nu = 1$ relaxation rate). The total phenomenological self-relaxation rate constant for HF($\nu = 1$) (which by definition for $\nu = 1$ is purely V-T,R) that they measured was identical to that determined in the double resonance experiments of Crim & co-workers⁵⁸, ($k = 1.46 \pm 0.1 \times 10^{-12} \text{ cm}^3 \text{ molecule}^{-1} \text{ s}^{-1}$).

There has been a significant effort in the last 20 years to measure and predict rotational relaxation rate constants. Most recently, Muyskens, Copeland, and Crim¹⁰²⁻¹⁰⁶ have measured rotational relaxation rate constants for HF($\nu = 2 - 4, J = 0 - 4$) with a variety of colliders. Their results generally confirm the standard view that rotational relaxation is 10 - 100 times faster than vibrational relaxation, particularly for the lower rotational quantum numbers ($J = 0 - 8$). In addition to probing the role of V-T,R relaxation, the Leone group¹⁰¹ has also measured rotational relaxation rate constants for $\nu = 0, J = 10 - 14$. They found no experimental evidence of bottleneck effects and concluded that R-R,T rates always exceed the V-T,R rate by one or two orders of magnitude, even for $J = 10 - 13$. While their initial report¹⁰¹ recommended R-R,T rate constants for $\nu = 0, J = 10 - 14$ which range from $\sim 1.2 \times 10^{-10} - 6 \times 10^{-11} \text{ cm}^3 \text{ molecule}^{-1} \text{ s}^{-1}$, subsequent measurements in the same laboratory suggested even larger values^{107, 108}. The dominance of R-R,T relaxation over V-T,R and V-V energy transfer extends to other colliders besides HF. Taatjes and Leone, for example, measured the rotational relaxation rate constants for HF with a variety of collision partners (Ar, He, Ne, Kr, Xe, H₂, and D₂)¹⁰⁷ and found that while rotational relaxation by atomic species is very inefficient relative to HF, H₂, and D₂ the rotational relaxation rate constants for atomic quenchers exceed the vibrational deactivation rate constants by several orders of magnitude: $k(\text{R-R,T}) \geq 10^{-12}$ and $k(\text{V-R,T}) = 10^{-17} - 10^{-18} \text{ cm}^3 \text{ molecules}^{-1} \text{ s}^{-1}$. Leone and co-workers extended their measurements to non-ambient temperatures¹⁰⁸ and found that the HF V-T,R and R-R,T self relaxation reactions have a negative temperature dependence. The negative temperature dependence for rotational relaxation of HF($\nu = 0, J = 13$) is dramatic, $T^{-1.57}$.

In addition to the direct experimental measurements, there have also been attempts to extrapolate the low-J results to high-J using scaling laws and approximations such as the exponential energy gap law (EEG), the power law model (PLM), and the energy corrected sudden (ECS) approximation. Most of these efforts are summarized elsewhere^{88, 89}, and while the accuracy of the models for predicting accurate R-R,T rates is the subject of some controversy, two general conclusions may be drawn from the relevant literature. 1) The PLM and ECS models give the most reliable results when compared to the existing high J and low J data. The EEG model consistently underestimates $k(\text{R-R,T})$, in some cases by several orders of magnitude. 2) The rate constants for rotational relaxation, $k(\text{R-R,T})$, are large, $\geq 10^{-11} \text{ cm}^3 \text{ molecules}^{-1} \text{ s}^{-1}$.

One noteworthy pair of reports^{109, 110}, which claim to use a "more reliable form of the power scaling law" to calculate rotational energy transfer rate constants for $\nu = 1 - 2, J = 0 - 20$ give $k(\text{R-R,T})$ values on the order of $10^{-11} - 10^{-10} \text{ cm}^3 \text{ molecule}^{-1} \text{ s}^{-1}$, even for $J = 20$. On the other hand, their results suggest that rotational relaxation rates actually *increase* with vibrational energy, contrary to the results of Crim and coworkers¹⁰²⁻¹⁰⁶. The reliability of their model is, as the authors themselves admit, "an open discussion."

2.3.2 Relevant Theoretical Studies

No review of the role of rotational equilibrium for the HF laser would be complete without some discussion of quasiclassical trajectory calculation results, most notably those of Wilkins and Kwok^{79, 80, 111, 112}, Thompson^{99, 100, 113, 114}, and Billing^{83, 115-117}. Billing's calculations found no evidence of high rotational state population, while the calculations by Wilkins and Thompson indicate that vibrational-rotational energy transfer is a relatively efficient process and that multiquantum deactivations occur on a fairly regular basis. In particular, Thompson^{99, 100} calculated state-to-state collision cross sections for HF($\nu = 4, J = 20$) relaxation by He and reported 3.3, 6.7, 10.7, 18.5, and 38.24 a.u.² for $\Delta\nu = 4, 3, 2, 1$ and 0, respectively. Calculations of this sort are usually very sensitive to the details of the potential surface on which the trajectories run, and unfortunately the requisite state-to-state cross sections required to evaluate the reliability of the theoretical calculations have yet to be measured. In general, the available experimental data does not support multiquantum deactivations.

In summary, the majority of the available evidence supports single vibrational quantum V-T,R relaxation which populates the high rotational states of the next lower vibrational state. There is no specific experimental evidence supporting multiquantum vibrational V-T,R relaxation. There is no doubt that near-resonant V-T,R relaxation plays an

important role in the HF chemical laser system and successful quantitative modeling depends on its inclusion. However, the available experimental evidence clearly shows that $k(V-T,R) \ll k(R-R,T)$, and in light of this, it is doubtful that high J states can act as "reservoirs" for near-resonant lasing levels. It seems more likely that the $V-T,R$ process simply reduces the gain of the (1-0) and (2-1) transitions by reducing the population of the upper state while simultaneously increasing the population of the lower state.

3. CONCLUSIONS

Table 5 summarizes the recommendations of this report. Overall, many of the expressions found in the 1982 review by Cohen & Bott¹⁰ remain valid today, in particular, the elimination of multi-quantum deactivation reactions that were a key feature of the 1977 kinetics package. These kinds of relaxation processes have been demonstrated to be very slow and can be safely neglected. Other areas of agreement include the total HF generation rate constants and the relaxation rate constants for collisions with molecular and atomic quenchers. A new measurement of the H atom removal rate constant for the "hot" reaction, $H + F_2$, would be particularly useful.

The major changes that we suggest occur in the Einstein coefficients, HF self-relaxation, and the nascent distribution for $H + F_2$. While in many cases these changes are minor, they may ultimately have significant effects to CFD calculation results due to enormous complexity of the HF laser system.

Clearly, there are some aspects of the HF kinetics package that should be re-examined experimentally. For example, in the case of $HF(v) + F, H, Ar, \text{ and } He$, the recommended expressions are based on only a handful of measurements at a narrow range of temperatures. While the role of multi-quantum deactivations is very small according to the available experimental data, some believe⁴⁴ that the $v^{2.9}$ scaling law for the HF self-relaxation process may be indicative of open multi-quantum deactivation relaxation pathways, particularly for high v . Direct measurements for the Treanor pumping (reaction [14]) rate constants are also needed, particularly for $HF(v > 1) + HF(v > 1)$, for which no data currently exists. Clarification of these issues would undoubtedly significantly enhance our understanding of the HF laser.

4. ACKNOWLEDGMENTS

GCM wishes to acknowledge the National Research Council for support. The authors are grateful for productive discussions with S. R. Leone, F. F. Crim, M. C. Heaven, M. H. Alexander, M. A. Kwok, D. Lyman, and D. W. Setser, as well as helpful comments from the reviewers.

Table 1: HF Fundamental and Overtone Einstein Emission Coefficients

Transition	Herbelin & Emanuel ²	Sileo & Cool ¹¹⁸	Arunan, Setser & Ogilvie ³	Zemke et. al. ⁴
$\Delta v = -1$				
1-0	188.6	189	194.5	203.5
2-1	319.8	324	333.9	348.4
3-2	398.3	410	422.8	439.9
4-3	429.7	453	467.7	484.1
5-4	421.3	460	477.2	487.2
6-5	381.1	436	459.8	455.9
7-6	318.6	386	425.4	397.7
8-7	243.7	317	354.6	320.9
9-8	166.9	236	269.8	235.2
$\Delta v = -2$				
2-0	23.4	23.6	23.5	24.7
3-1	67.9	66.2	65.9	70.7
4-2	130.5	124	123.5	134.2
5-3	207.0	193	191.2	212.3
6-4	291.9	271	262.3	301.9
7-5	378.3	354	328.0	399.9
8-6	457.8	443	429.1	501.3
9-7	520.9	536	531.9	599.8
$\Delta v = -3$				
3-0	1.2	1.6	1.5	1.6
4-1	4.8	6.1	5.5	5.9
5-2	12.2	14.4	13.1	13.9
6-3	25.0	27.0	25.4	26.1
7-4	44.5	43.9	44.9	43.3
8-5	72.4	64.8	---	66.5
9-6	109.5	89.1	---	96.7

Table 2: Experimentally determined nascent vibrational distributions for H + F₂

v	CFD Kinetics Packages		Experimental Measurements ^a					Recommended ^d
	Cohen & Bott ⁹ (1977)	Cohen & Bott ¹⁰ (1982)	Jonathan et. al. ¹⁵ (1972) ^b	Polanyi et. al. ¹⁴ (1976) ^b	Tardy et. al. ¹⁶ (1988) ^c	Setser et. al. ¹⁹ (1979)	Kaufman et. al. ²⁰ (1982)	
0	0.00	0.00	<0.04 (<0.03)	≤0.10 (≤0.08)	0.00 (0.00)	0.00	0.00	0.04 ± 0.04
1	0.00	0.00	0.09 (0.06)	0.12 (0.07)	0.15 (0.14)	0.07	0.06	0.08 ± 0.03
2	0.00	0.00	0.11 (0.08)	0.13 (0.10)	0.13 (0.12)	0.17	0.12	0.13 ± 0.03
3	0.18	0.21	0.13 (0.10)	0.25 (0.20)	0.27 (0.26)	0.28	0.17	0.20 ± 0.07
4	0.30	0.39	0.45 (0.36)	0.35 (0.30)	0.41 (0.40)	0.59	0.37	0.40 ± 0.11
5	0.80	0.70	0.89 (0.83)	0.78 (0.70)	0.72 (0.70)	0.93	0.76	0.78 ± 0.10
6	1.00	1.00	1.00 (1.00)	1.00 (1.00)	1.00 (1.00)	1.00	1.00	1.00
7	0.00	0.45	0.45 (0.43)	0.40 (0.48)	0.76 (0.80)	0.52	0.62	0.50 ± 0.25
8	0.00	0.36	0.20 (0.19)	0.26 (0.37)	0.46 (0.49)	0.00	0.00	0.30 ± 0.15
9	0.00	0.00	<0.04 (<0.01)	0.16 (0.12)	0.41 (0.43)	0.00	0.00	0.15 ± 0.15
10	0.00	0.00	<0.04 (<0.01)	0.00 (0.00)	0.00 (0.00)	0.00	0.00	0.01 ± 0.01

^a The values in parentheses for Jonathan, Polanyi and Tardy are corrected for the Einstein coefficients of Setser³.

^b The corrected values shown were calculated from the distributions reported by Kaufman²⁰ which were corrected for the Einstein coefficients of Sileo & Cool¹¹⁸.

^c Tardy¹⁶ originally used the Einstein coefficients of Meredith and Smith¹⁷.

^d See text for details

Table 3: HF total self relaxation rate constants

Reference	$k_{300}(\text{HF}(v) + \text{HF}) \rightarrow \text{products}, (10^{-12} \text{ cm}^3 \text{ molecules}^{-1} \text{ s}^{-1})$						
	$v = 1$	$v = 2$	$v = 3$	$v = 4$	$v = 5$	$v = 6$	$v = 7$
Experiments							
Bott & Cohen ⁷¹	1.8 ± 0.3						
Hinchen & Hobbs ⁶⁹	1.8 ± 0.2						
Bina & Jones ⁷⁰	2.3 ± 0.3	5 ± 2					
Kwok & Wilkins ⁷²	1.6 ± 0.6	16 ± 5	26 ± 9	27 ± 10	(58) ^a	(101) ^a	
Osgood, et. al. ⁷⁶	1.7	25 ± 7	49 ± 15	43 ± 18			
Airey & Smith ⁷³		16	17	≥ 44	≥ 65		
Poole & Smith ^{74, 75}		13	19	32	46	52	~ 43
Douglas & Moore ⁷⁷			28 ± 4	72 ± 5			
Lampert et. al. ⁷⁸			32 ± 6	88 ± 11			
Kaufman ^{20, 63-66}	1.8	19	31	73	140	290	450
Copeland, et. al. ⁵⁸	1.46 ± 0.1	19.8 ± 1.0					
Jursich & Crim ⁶²			30.2 ± 3.0	72.8 ± 2.7	151 ± 8		
Calculations							
Wilkins & Kwok ^{79, 80}	1.7	22	29	33	42	51	
Coltrin & Marcus ^{81, 82}	0.2 ± 0.1	19 ± 3	28 ± 4	53 ± 10	69 ± 10	156 ± 11	455 ± 49
Billing & Poulsen ⁸³	0.81	6.2 ± 2.2	10 ± 4	19 ± 7	27 ± 10	43 ± 15	82 ± 29
Standard Kinetics Packages^b							
Cohen & Bott 1977 ⁹	1.66	6.62	9.94	4.97	16.6	23.2	82.8
Cohen & Bott 1982 ¹⁰	1.66	10.0	28.8	60.9	108.8	174.7	260.9
^a M. A. Kwok and N. Cohen, personal communication reported in ⁶³ .							
^b only single quantum deactivation rate constants are listed.							

Table 4: Room Temperature Quenching Rate Constants for HF + H₂

Reference	$k_{300}(\text{HF}(v) + \text{H}_2 \rightarrow \text{HF}(v-1) + \text{H}_2) (10^{-12} \text{ cm}^3 \text{ molecules}^{-1} \text{ s}^{-1})$						
	$v = 1$	$v = 2$	$v = 3$	$v = 4$	$v = 5$	$v = 6$	$v = 7$
Bott & Cohen ^{71, 84}	0.52 ± 0.03						
Poole & Smith ⁷⁵		0.21	0.15	0.21	0.49	0.99	1.6
Douglas and Moore ⁸⁶			$0.31 \pm .06$	$0.47 \pm .12$			
Bott & Heidner ⁸⁵	0.52 ± 0.05		$0.35 \pm .04$				
Kaufman ²⁰					1.7 ± 0.5	3.5 ± 1	9.1 ± 2.7
Jursich, et. al. ⁸⁷			0.38 ± 0.25	0.67 ± 0.10	1.64 ± 0.19		
Cohen & Bott ¹⁰	0.01	0.07	0.21	0.45	0.83	1.35	
Recommended	0.52 ± 0.04	0.20 ± 0.04	0.35 ± 0.04	0.50 ± 0.2	1.6 ± 0.3	3.5 ± 1	9.1 ± 2.7

Table 5: Recommended Rate Constants for the HF laser system

Reaction	Equation	Recommended Rate Constant Expression	References
$F + H_2 \rightarrow HF + H$	$T = 190 - 376 \text{ K:}$ $g(v) * 1.1 \pm 0.1 \times 10^{-10} e^{-(450 \pm 50)/T}$ $T > 376 \text{ K:}$ $g(v) * 2.2 \pm 0.4 \times 10^{-10} e^{-(595 \pm 50)/T}$	$g(0) = 0.00, g(1) = 0.15$ $g(2) = 0.55, g(3) = 0.30$	10, 39, 43
$H + F_2 \rightarrow HF + F$	$g(v) * 5.0 \times 10^{-15} T^{-1.5} e^{-845/T}$	$g(0) = 0.01, g(1) = 0.02, g(2) = 0.04, g(3) = 0.06,$ $g(4) = 0.11, g(5) = 0.22, g(6) = 0.28, g(7) = 0.14,$ $g(8) = 0.08, g(9) = 0.04$	10, 14-16, 19, 20
$H + HF(v) \rightarrow H_2(v') + F$	$v = 3$ $3.0 \times 10^{-11} T^{-0.179} e^{-382/T}$ $v = 4 - 6$ $g(v, v') * 1.0 \times 10^{-10} e^{-252/T}$	$g(4,0) = g(4,1) = 0.5, g(5,0) = 0.5, g(5,1) = 1.0,$ $g(6,0) = g(6,1) = 0.5,$ $g(6,2) = 1.5$	10, 53-55
$HF(v) + H_2 \rightarrow HF(v') + H_2$	$g(v) * 1.0 \times 10^{-12}$	$g(1) = 0.52, g(2) = 0.2, g(3) = 0.35, g(4) = 0.50,$ $g(5) = 1.60, g(6) = 3.5, g(7) = 9.1$	10, 20, 71, 84-87
$HF(v) + H_2(v') \rightarrow HF(v-1) + H_2(1)$	$5.2 \pm 0.4 \times 10^{-13}$	$v = 1 \text{ only}$	10, 20, 71, 84-87
$HF(v) + H \rightarrow HF(v') + H$	$A(v) * 1.7 \times 10^{-8} T^{-1}$ [$\Delta v = -1 \text{ only}$] $B(v) * 1.7 \times 10^{-15} e^{-352/T}$ [$\Delta v \geq 1$]	$A(3) = 1.4, A(4) = 2.0, A(5) = 2.7, A(6) = 3.5$ $B(1) = 0.4, B(2 - 6) = 0.7$	10, 53, 54
$HF(v) + F \rightarrow HF(v-1) + F$	$g(v) * 2.7 \times 10^{-11} e^{-1359/T}$	$g(v) = v$	10, 119-121
$HF(v) + M \rightarrow HF(v-1) + M$	$A(M) * 1.7 \times 10^{-29} * v * T^{4.5}$	$A(Ar) = 2.0$ $A(F_2) = 2.0$ $A(He) = 3.7$	10, 122
$HF(v) + HF \rightarrow HF(v') + HF$	$v = 1 - 5:$ $k_c * A(v) T^{-1.3}$ $v = 6^a, 300 \text{ K:}$ 2.9×10^{-10} $v = 7^a, 300 \text{ K:}$ 4.5×10^{-10}	$k_c = \pi d^2 \sqrt{\frac{8RT}{\pi \mu}}$ $d = 0.25 \text{ nm}$ $A(1) = 12.0, A(2) = 218.0, A(3) = 315.2,$ $A(4) = 764.0, A(5) = 1610.3$	59, 61, 63
$HF(v) + HF(v') \rightarrow HF(v+1) + HF(v'-1)$	$(v+1)^{0.35} 4.5 \times 10^{-9} T^{-1}$		10, 12
$F + F + M \rightarrow F_2 + M$	$M \times 10^{-34}$	$M(He) = 6 \pm 1$ $M(F_2) = 4.7 \pm 1.2$ $M(Ar) \sim 3$	123, 124

^a the temperature dependence of $HF(6-7) + HF$ has not been measured. If the $T^{-1.3}$ dependence and the expression used for $v = 1 - 5$ holds, then $A(6) = 3107$ and $A(7) = 4339$.

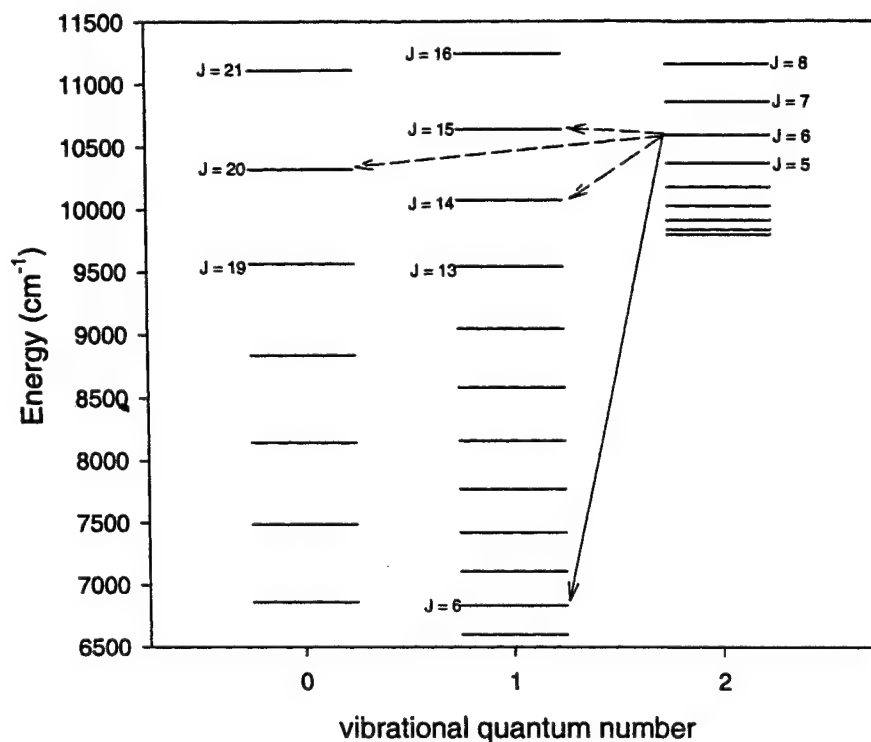


Figure 1: Detailed V-T,R relaxation pathways. The distinction between "true" V-T,R energy transfer and V-R redistribution is shown by the solid and broken lines, respectively. Numerous combinations of HF(1, J) and HF(0, J) states can be populated by HF V-T,R energy transfer. Because of the presence of near-resonant energy levels in $v = 1$ and 0, V-R redistribution can populate high rotational states of $v = 0$ and 1. For example, the near resonant V-R redistribution pathways shown in the figure have energy defects of -46.9 , 519.6 , and 273.7 cm^{-1} , for relaxation to (1,15), (1,14) and (0,20), respectively. On the other hand, if HF(2, 6) is relaxed to HF(1, 6) by HF(0, J), up to 8 quanta of rotational energy can be transferred to the HF($v = 0$) molecule.

5. REFERENCES

1. G. Emanuel, "Numerical Modeling of Chemical Lasers", John Wiley & Sons, New York, 1976.
2. J. M. Herbelin and G. Emanuel, "Einstein coefficients for diatomic molecules", *J. Chem. Phys.*, **60**, 689 - 696, 1974.
3. E. Arunan, D. W. Setser and J. F. Ogilvie, "Vibration-rotational Einstein coefficients for HF/DF and HCl/DCI", *J. Chem. Phys.*, **97**, 1734 - 1741, 1992.
4. W. T. Zemke, W. C. Stwalley, S. R. Langhoff, G. L. Valderrama and M. J. Berry, "Radiative transition probabilities for all vibrational levels in the X1S+ state of HF", *J. Chem. Phys.*, **95**, 7846 - 7853, 1991.
5. J. A. Coxon and P. G. Hajigeorgiou, "Isotopic dependence of Born-Oppenheimer breakdown effects in diatomic hydrides: The B1S+ and X1S+ states of HF and DF", *J. Mol. Spectrosc.*, **142**, 254 - 278, 1990.
6. W. T. Zemke, W. C. Stwalley, J. A. Coxon and P. G. Hajigeorgiou, "Improved potential energy curves and dissociation energies for HF, DF, and TF", *Chem. Phys. Lett.*, **177**, 412 - 418, 1991.
7. J. F. Ogilvie, "The electric dipole moment function of HF", *J. Phys. B*, **21**, 1663 - 1674, 1988.
8. N. Cohen and J. F. Bott, "A Review of Rate Coefficients in the H₂-F₂ Chemical Laser System", SAMSO-TR-76-82, 1976.
9. N. Cohen, "A Review of Rate Coefficients in the H₂-F₂ Chemical Laser System - Supplement (1977)", SAMSO-TR-78-41, 1978.
10. N. Cohen and J. F. Bott, "Review of Rate Data for Reactions of Interest in HF and DF Lasers", SD-TR-82-86, 1982.
11. N. Cohen and K. R. Westberg, "Chemical Kinetic Data Sheets for High Temperature Chemical Reactions", *J. Phys. Chem. Ref. Data*, **12**, 531-590, 1983.
12. S. R. Leone, "Rate coefficients for vibrational energy transfer involving the hydrogen halides", *J. Phys. Chem. Ref. Data*, **11**, 953 - 996, 1982.

13. G. A. Hart Jr., "DF Pulsed Chemical Laser Rotational Nonequilibrium Computer Model (PULSDF) and Data Base", NRL Memorandum Report 5051, 1983.
14. J. C. Polanyi and J. J. Sloan, "Energy distribution among reaction products. VII. $H + F_2$ ", *J. Chem. Phys.*, **57**, 4988 - 4998, 1972.
15. N. Jonathan, S. Okuda and D. Timlin, "Initial vibrational energy distributions determined by infra-red chemiluminescence", *Mol. Phys.*, **24**, 1143 - 1164, 1972.
16. D. C. Tardy and L. L. Feezel, "Chemiluminescence mapping: Pressure-pulse results for $H(D) + F_2 \rightarrow HF(DF) + F$ ", *Chem. Phys.*, **119**, 89 - 93, 1988.
17. R. E. Meredith and F. G. Smith, "Computation of Electric Dipole Matrix Elements for Hydrogen Fluoride", *J. Quant. Spectrosc. Radiat. Transfer*, **13**, 89-114, 1973.
18. J. K. Cashion, *J. Chem. Phys.*, **39**, 1872, 1963.
19. J. P. Sung, R. J. Malins and D. W. Setser, "Comparison of rate constants for reactions of hydrogen atoms with chlorine, fluorine, iodine chloride, and chlorine fluoride", *J. Phys. Chem.*, **83**, 1007 - 1013, 1979.
20. L. S. Dzelzkalns and F. Kaufman, "Vibrational relaxation of highly excited diatomics. III. $HF(v = 5, 6, 7) + H_2, D_2, N_2, HF, CO_2, N_2O, CH_4$, and C_2H_6 ", *J. Chem. Phys.*, **77**, 3508 - 3515, 1982.
21. X. Gimenez, J. M. Lucas, A. Aguilar and A. Lagana, "Calculated versus measured vibrational state specific reactivity of $H + F_2$ ", *J. Phys. Chem.*, **97**, 1993.
22. S. Bittenson, D. C. Tardy and J. Wanna, "Chemiluminescence mapping. I. Experimental method and initial measurements on the $D + F_2$ and $F + D_2$ reactions", *Chem. Phys.*, **58**, 313-323, 1981.
23. K. H. Homann, H. Schweinfurth and J. Warnatz, "Rate measurements for the reaction of H atoms with F_2 ", *Ber. Bunsenges. Phys. Chem.*, **81**, 724 - 728, 1977.
24. N. Cohen, note that Refs 10 and 12 list numerous references to "Westberg and Cohen, Int. J. Chem. Kinet. (to be published)." According to a private communication with N. Cohen (The Aerospace Corp., retired) these transition state theory calculations were, in fact, never published.
25. D. L. Baulch, J. Duxbury, S. J. Grant and D. C. Montague, "Homogeneous gas phase reactions of halogen- and cyanide- containing species", *J. Phys. Chem. Ref. Data*, **10**, 1981.
26. S. W. Rabideau, H. G. Hecht and W. B. Lewis, "A study of the kinetics of the reaction between H_2 and F_2 by EPR methods", *J. Magn. Resonance*, **6**, 384, 1972.
27. G. K. Vasil'ev, E. F. Makarov and Y. A. Chernyshev, "Measurement of the chain propagation and termination rate constants for the reaction $F_2 + H_2(D_2)$ inhibited by O_2 ", *Kinetics and Catalysis*, **16**, 272 - 275, 1975.
28. I. B. Goldberg and G. R. Schneider, "Kinetic study of the reaction of H with H_2 and CF_3H by ESR methods", *J. Chem. Phys.*, **65**, 147 - 153, 1976.
29. J. Han, M. C. Heaven and G. C. Manke II, "Hydrogen Atom Reactions with Molecular Halogens: The Rate Constants for $H + F_2$ and $H + Cl_2$ at 298K", *J. Phys. Chem. A*, **submitted**, 2002.
30. D. M. Neumark, A. M. Wodtke, G. N. Robinson, C. C. Hayden, K. Shobatake, R. K. Sparks, T. P. Schafer and Y. T. Lee, "Molecular beam studies of the $F + D_2$ and $F + HD$ reactions", *J. Chem. Phys.*, **82**, 3067 - 3077, 1985.
31. D. M. Neumark, A. M. Wodtke, G. N. Robinson, C. C. Hayden and Y. T. Lee, "Molecular beam studies of the $F + H_2$ reaction", *J. Chem. Phys.*, **82**, 3045 - 3066, 1985.
32. F. Dong, S. H. Lee and K. Liu, "Reactive excitation functions for $F + p-H_2/n-H_2/D_2$ and the vibrational branching for $F + HD$ ", *J. Chem. Phys.*, **113**, 3633 - 3640, 2000.
33. W. B. Chapman, B. W. Blackmon and D. J. Nesbitt, "State-to-state reactive scattering of $F + H_2$ in supersonic jets: Nascent rovibrational $HF(v,J)$ distribution via direct IR laser absorption", *J. Chem. Phys.*, **107**, 8193 - 8196, 1997.
34. S. A. Nizkorodov, W. W. Harper, W. B. Chapman, B. W. Blackmon and D. J. Nesbitt, "Energy-dependent cross sections and nonadiabatic reaction dynamics in $F(2P_{3/2}, 2P_{1/2}) + n-H_2 \rightarrow HF(v,J) + H$ ", *J. Chem. Phys.*, **111**, 8404 - 8416, 1999.
35. M. Faubel, L. Y. Rusin, S. Schlemmer, F. Sundermann, U. Tappe and J. P. Toennies, *J. Chem. Soc. Faraday Trans.*, **89**, 1475, 1993.
36. M. Faubel, L. Y. Rusin, S. Schlemmer, F. Sundermann, U. Tappe and J. P. Toennies, *J. Chem. Phys.*, **101**, 2106, 1994.
37. F. J. Aoiz, L. Banares, B. Martinez-Haya, J. F. Castillo, D. E. Manolopoulos, K. Stark and H. J. Werner, "Ab initio simulation of molecular beam experiments for the $F + H_2 \rightarrow HF + H$ reaction", *J. Phys. Chem. A*, **101**, 6403 - 6414, 1997.
38. V. M. Azriel, G. D. Billing, L. Yu. Rusin and M. B. Sevryuk, "A test of the semiclassical Wigner method for the reaction $F + H_2 \rightarrow H + HF$ ", *Chem. Phys.*, **195**, 243 - 258, 1995.

39. A. Persky and H. Kornweitz, "The kinetics of the Reaction $F + H_2 \rightarrow HF + H$. A critical review of literature data", *Int. J. Chem. Kinet.*, **29**, 67 - 71, 1997.
40. R. Atkinson, D. L. Baulch, R. A. Cox, Jr. R. F. Hampson, J. A. Kerr, M J. Rossi and J. Troe, *J. Phys. Chem. Ref. Data*, **21**, 1125, 1992.
41. R. Atkinson, D. L. Baulch, R. A. Cox, Jr. R. F. Hampson, J. A. Kerr, M J. Rossi and J. Troe, *J. Phys. Chem. Ref. Data*, **26**, 521, 1997.
42. R. Atkinson, D. L. Baulch, R. A. Cox, Jr. R. F. Hampson, J. A. Kerr, M J. Rossi and J. Troe, "Evaluated kinetic and photochemical data for atmospheric chemistry: Supplement VIII, Halogen species. IUPAC subcommittee on gas kinetic data evaluation for atmospheric chemistry", *J. Phys. Chem. Ref. Data*, **29**, 167 - 266, 2000.
43. R. F. Heidner III, J. F. Bott, C. E. Gardner and J. E. Melzer, "Absolute rate coefficients for $F + H_2$ and $F + D_2$ at $T = 295 - 765^\circ$ ", *J. Chem. Phys.*, **72**, 4815 - 4820, 1980.
44. M. A. Kwok, private communication, 2000
45. D. L. Thompson, "Monte Carlo classical trajectory calculation of the rates of H- and D- Atom vibrational relaxation of HF and DF", *J. Chem. Phys.*, **57**, 4170 - 4173, 1972.
46. R. L. Wilkins, "Monte Carlo calculations of reaction rates and energy distribution among reaction products. II. $H + HF(v) \rightarrow H_2(v') + F$ and $H + HF(v) \rightarrow HF(v') + H^*$ ", *J. Chem. Phys.*, **47**, 3038 - 3046, 1973.
47. M. Baer, "A coplanar quantum mechanical study of the exchange reaction $HF + H$ ", *J. Chem. Phys.*, **65**, 493 - 495, 1976.
48. G. C. Schatz and A. Kuppermann, "Vibrational deactivation on chemically reactive potential surfaces: An exact quantum study of a low barrier collinear model of $H + FH$, $D + FD$, $H + FD$, and $D + FH$ ", *J. Chem. Phys.*, **72**, 2737 - 2743, 1980.
49. G. C. Schatz, "A quasiclassical trajectory study of final state distributions in collisions of fast H(D) atoms with HF(DF)", *J. Chem. Phys.*, **86**, 6738 - 6744, 1987.
50. C. F. Bender, B. J. Garrison and H. F. Schaefer III, "A critical test of semiempirical FH₂ potential energy surfaces: The barrier height for $H + FH \rightarrow HF + H$ ", *J. Chem. Phys.*, **62**, 1188 - 1190, 1975.
51. P. Botschwina and W. Meyer, "PNO-CEPA calculation of collinear potential energy barriers for thermoneutral exchange reactions", *Chem. Phys.*, **20**, 43 - 52, 1977.
52. W. R. Wadt and N. W. Winter, "Accurate characterization of the transition state geometry for the $HF + H' \rightarrow H + HF$ reaction", *J. Chem. Phys.*, **67**, 3068 - 3073, 1977.
53. R. F. Heidner III and J. F. Bott, "Vibrational deactivation of $HF(v = 1)$ and $DF(v = 1)$ by H and D atoms", *J. Chem. Phys.*, **63**, 1810 - 1817, 1975.
54. J. F. Bott and R. F. Heidner III, "The vibrational deactivation of $HF(v = 3)$ and $HF(v = 2)$ by H atoms", *J. Chem. Phys.*, **66**, 2878 - 2882, 1977.
55. J. F. Bott and R. F. Heidner III, "Kinetic study of $H + HF(v = 3)$: Kinetic isotope effect and temperature dependence", *J. Chem. Phys.*, **68**, 1708 - 1714, 1978.
56. M. A. Kwok and R. L. Wilkins, "Flow tube measurements of $H + HF(v)$ deactivation rates", *J. Chem. Phys.*, **60**, 2189 - 2190, 1974.
57. N. Cohen and J. F. Bott, It should be noted that the text of Ref. 10 contains $k(HF(3) + H \rightarrow H_2 + F)$ but the table at the end does not. See pp. 40-42 of Ref. 10.
58. R. A. Copeland, D. J. Pearson, J. M. Robinson and F. F. Crim, "Laser double resonance measurements of vibrational energy transfer rates and mechanisms in $HF(v = 2)$ ", *J. Chem. Phys.*, **77**, 3974 - 3982, 1982.
59. J. M. Robinson, D. J. Pearson, R. A. Copeland and F. F. Crim, "Rates and Pathways of Vibrational Self-Relaxation of $Hf(V=2)$ between 300-K and 700-K", *J. Chem. Phys.*, **82**, 780-788, 1985.
60. J. M. Robinson, K. J. Rensberger and F. F. Crim, "A Direct Determination of the Role of Vibration-to-Vibration Energy-Transfer in $Hf(V=3;4)$ Self-Relaxation", *J. Chem. Phys.*, **84**, 220-226, 1986.
61. T. J. Foster and F. F. Crim, "Vibrational relaxation of $HF(v = 3, 4, 5)$ between 300 and 700 K", *J. Chem. Phys.*, **75**, 3871 - 3875, 1981.
62. G. M. Jursich and F. F. Crim, "Vibrational relaxation of $HF(v = 3, 4, 5)$ ", *J. Chem. Phys.*, **74**, 4455 - 4464, 1981.
63. L. S. Dzelzkalns and F. Kaufman, "Vibrational relaxation of highly excited diatomics. IV. $HF(v = 1 - 7) + CO_2$, N_2O , and HF ", *J. Chem. Phys.*, **79**, 3836 - 3844, 1983.
64. L. S. Dzelzkalns and F. Kaufman, "Vibrational relaxation of highly excited diatomics. V. The V-V channel in $HF(v) + HF(0)$ collisions", *J. Chem. Phys.*, **79**, 3363 - 3366, 1983.

65. L. S. Dzelzkalns and F. Kaufman, "Vibrational relaxation of highly excited diatomics. VI. $\text{DF}(9 \leq v \leq 12) + \text{N}_2$, CO , CO_2 , and N_2O and $\text{HF}(v = 5 - 7) + \text{CO}$ ", *J. Chem. Phys.*, **80**, 6114 - 6121, 1984.
66. L. S. Dzelzkalns and F. Kaufman, "Vibrational relaxation of highly excited diatomics. VII. $\text{DF}(v = 9 - 12)$ and $\text{HF}(v = 5 - 7) + \text{HF}(v = 0)$, $\text{DF}(v = 0)$ in all combinations", *J. Chem. Phys.*, **81**, 4975 - 4978, 1984.
67. J. F. Bott, "Gas-dynamic corrections applied to laser-induced fluorescence measurements of $\text{HF}(v = 1)$ and $\text{DF}(v = 1)$ deactivation", *J. Chem. Phys.*, **61**, 3414 - 3416, 1974.
68. J. J. Hinchey, "Vibrational relaxation of hydrogen and deuterium fluorides", *J. Chem. Phys.*, **59**, 233 - 240, 1973.
69. J. J. Hinchey and R. H. Hobbs, "Rotational relaxation studies of HF using IR double resonance", *J. Chem. Phys.*, **65**, 2732 - 2739, 1976.
70. M. J. Bina and C. R. Iones, "Use of direct overtone excitation in the measurement of the $\text{HF}(v = 2)$ deactivation rate", *Appl. Phys. Lett.*, **22**, 44 - 45, 1973.
71. J. F. Bott and N. Cohen, "Temperature dependence of V-V and V-R,T energy transfer measurements in mixtures containing HF^* ", *J. Chem. Phys.*, **58**, 4539 - 4549, 1973.
72. M. A. Kwok and R. L. Wilkins, "Flow-tube studies of vibrational energy transfer in $\text{HF}(v) + \text{HF}$, $\text{DF}(v) + \text{HF}$, and $\text{DF}(v) + \text{D}_2$ systems", *J. Chem. Phys.*, **63**, 2453 - 2460, 1975.
73. J. R. Airey and I. W. M. Smith, "Quenching of infrared chemiluminescence: Rates of energy transfer from $\text{HF}(v \leq 5)$ to CO_2 and HF , and from $\text{DF}(v \leq 3)$ to CO_2 and HF^* ", *J. Chem. Phys.*, **57**, 1669 - 1676, 1972.
74. P. R. Poole and I. W. M. Smith, "Quenching of infrared chemiluminescence. Part 7. Rates of energy transfer from $\text{HF}(v = 2 - 7)$ and $\text{DF}(v = 3 - 5)$ to a wide range of collision partners", *J. Chem. Soc. Faraday Trans. 2*, **73**, 1447 - 1458, 1977.
75. P. R. Poole and I. W. M. Smith, "Quenching of infrared chemiluminescence. Part 6. Rates of energy transfer from $\text{HF}(v = 2 - 7)$ to $\text{HF}(v = 0)$, H_2 , D_2 , and HD , and from $\text{DF}(v = 3 - 5)$ to $\text{HF}(v = 0)$ ", *J. Chem. Soc. Faraday Trans. 2*, **73**, 1434 - 1446, 1977.
76. R. M. Osgood Jr., P. B. Sackett and A. Javan, "Measurement of vibrational-vibrational exchange rates for excited vibrational levels ($2 \leq v \leq 4$) in hydrogen fluoride gas", *J. Chem. Phys.*, **60**, 1464 - 1480, 1974.
77. D. J. Douglas and C. B. Moore, "Vibrational Relaxation of $\text{HF}(v = 3, 4)$ ", *Chem. Phys. Lett.*, **57**, 485, 1978.
78. J. K. Lampert, G. M. Jursich and F. F. Crim, "Collisional relaxation of $\text{HF}(v = 3, 4)$ by HF , CH_4 , and CD_4 ", *Chem. Phys. Lett.*, **71**, 258 - 263, 1980.
79. R. L. Wilkins, "Mechanisms of energy transfer in hydrogen fluoride systems", *J. Chem. Phys.*, **67**, 5838 - 5854, 1977.
80. R. L. Wilkins and M. A. Kwok, "Temperature dependence of vibrational relaxation from the upper vibrational levels of HF and DF ", *J. Chem. Phys.*, **73**, 3198 - 3204, 1980.
81. M. E. Coltrin and R. A. Marcus, "Cross-correlation trajectory study of vibrational relaxation of $\text{DF}(v = 1 - 7)$ by $\text{DF}(v = 0)$ and of HF by HF ", *J. Chem. Phys.*, **76**, 2379 - 2383, 1982.
82. M. E. Coltrin and R. A. Marcus, "Cross correlation trajectory study of vibrational relaxation of $\text{HF}(v = 1 - 7)$ by $\text{HF}(v = 0)$ ", *J. Chem. Phys.*, **73**, 4390 - 4396, 1980.
83. G. D. Billing and L. L. Poulsen, "Theory of V-V and V-T/R energy transfer for $\text{HF}(v = 1 - 7) + \text{HF}(0)$ ", *J. Chem. Phys.*, **68**, 5128 - 5138, 1978.
84. J. F. Bott, "Vibrational relaxation of $\text{HF}(v = 1)$ and $\text{DF}(v = 1)$ by H_2 and D_2 ", *J. Chem. Phys.*, **61**, 2530 - 2535, 1974.
85. J. F. Bott and R. F. Heidner III, "Vibrational relaxation of $\text{HF}(v = 1 \text{ and } 3)$ in H_2 , N_2 , and D_2 at 200 and 295 K", *J. Chem. Phys.*, **72**, 3211 - 3215, 1980.
86. D. J. Douglas and C. B. Moore, "Vibrational relaxation of $\text{HF}(v = 3, 4)$ by H_2 , D_2 , and CO_2 ", *J. Chem. Phys.*, **70**, 1769 - 1773, 1979.
87. G. M. Jursich, D. R. Ritter and F. F. Crim, "Vibrational relaxation of $\text{HF}(v = 3, 4, \text{ and } 5)$ by H_2 , D_2 , CH_4 , CD_4 , and CO_2 ", *J. Chem. Phys.*, **80**, 4097 - 4104, 1984.
88. N. Cohen, J. F. Bott, M. A. Kwok and R. L. Wilkins, "The status of rotational nonequilibrium in HF chemical lasers", SD-TR-86-26, 1986.
89. M. A. Kwok, R. L. Wilkins, G. I. Segal, E. F. Cross, R. H. Ueunten and K. L. Foster, "In search of high J states in the $\text{HF}(v, J)$ system", SD-TR-85-21, 1985.
90. E. Cuellar and G. C. Pimentel, "Rotational laser emission by HF in the ClF-H_2 chemical laser", *J. Chem. Phys.*, **71**, 1385 - 1391, 1979.

91. E. R. Sirkin and G. C. Pimentel, "HF rotational laser emission through photoelimination from vinyl fluoride and 1,1-difluoroethene", *J. Chem. Phys.*, **75**, 604 - 612, 1981.
92. E. R. Sirkin and G. C. Pimentel, "HF rotational lasers: Enhancement of $V \rightarrow R$ multiquantum energy transfer by CO and CO₂", *J. Chem. Phys.*, **77**, 1314 - 1322, 1982.
93. G. L. Richmond and G. C. Pimentel, "HF rotational laser emission from ClF/H₂ reaction: Time evolution of the gain", *J. Chem. Phys.*, **80**, 1162 - 1170, 1984.
94. J. H. Smith and D. W. Robinson, "Chemical pumping of pure rotational HF lasers", *J. Chem. Phys.*, **74**, 5111 - 5115, 1981.
95. J. H. Smith and D. W. Robinson, "The OH and OD laser: Collision-induced energy transfer pumping", *J. Chem. Phys.*, **68**, 5474 - 5480, 1978.
96. J. H. Smith and D. W. Robinson, "Pure rotational lasing in four electronic states of NH: Impulsive to adiabatic collisional pumping", *J. Chem. Phys.*, **71**, 271 - 280, 1979.
97. E. Arunan, D. Raybone and D. W. Setser, "Vibrational relaxation rate constants for HF($v = 1 - 4$) by CO, CO₂, and HCN with product identification by infrared emission", *J. Chem. Phys.*, **97**, 6348 - 6362, 1992.
98. D. Raybone, S. J. Wategaonkar and D. W. Setser, "Near resonant V-R,T energy transfer in the relaxation of vibrationally excited HF by CO", *J. Chem. Phys.*, **89**, 3384 - 3386, 1988.
99. D. L. Thompson, "A Monte Carlo quasiclassical trajectory study of energy transfer in Ar + HF collisions", *J. Chem. Phys.*, **76**, 5947 - 5967, 1982.
100. D. L. Thompson, "Vibrational-rotational energy transfer in collisions of HF($v = 4, J = 20$) with rare gases", *J. Chem. Phys.*, **78**, 1763 - 1766, 1983.
101. H. K. Haugen, W. H. Pence and S. R. Leone, "Infrared double resonance spectroscopy of V-T,R relaxation of HF($v = 1$): Direct measurement of high-J populations", *J. Chem. Phys.*, **80**, 1839 - 1852, 1984.
102. M. A. Muyskens, Ph.D. Thesis, University of Wisconsin, Madison, 1989.
103. R. A. Copeland, D. J. Pearson and F. F. Crim, "Laser double resonance measurements of rotational energy transfer rates in HF($v = 2$)", *Chem. Phys. Lett.*, **81**, 541 - 546, 1981.
104. R. A. Copeland and F. F. Crim, "Rotational energy transfer in HF($v = 2$): Double resonance measurements and fitting law analysis", *J. Chem. Phys.*, **78**, 5551 - 5563, 1983.
105. R. A. Copeland and F. F. Crim, "Rotational energy transfer in HF($v = 2$): Energy corrected sudden approximation scaling relations applied to double resonance measurements", *J. Chem. Phys.*, **81**, 5819 - 5829, 1984.
106. R. A. Copeland, Ph.D. Thesis, University of Wisconsin, Madison, 1982.
107. C. A. Taatjes and S. R. Leone, "Laser double-resonance measurements of rotational relaxation rates of HF($J = 13$) with rare gases, H₂, and D₂", *J. Chem. Phys.*, **89**, 302 - 308, 1988.
108. C. A. Taatjes and S. R. Leone, "Laser double-resonance studies of low-temperature rotational and vibrational relaxation of HF: Rates for HF($J = 13$) + HF from 225 to 298 K and detection of HF($v = 1$) deactivation by HF clusters at 210 - 240 K", *J. Phys. Chem.*, **95**, 5870 - 5877, 1991.
109. L. A. Bollati, G. A. Arguello and E. H. Staricco, "Dependence on vibrational excitation of energy transfer processes for HF(v, J) + HF($v = 0$)", *J. Chem. Phys.*, **83**, 6050 - 6052, 1985.
110. L. A. Bollati, G. A. Arguello and E. H. Staricco, "HF autorelaxation in $v = 1$ and $v = 2$ ", *J. Chem. Soc. Faraday Trans. 2*, **84**, 599 - 609, 1988.
111. R. L. Wilkins and M. A. Kwok, "Rotational energy transfer in HF", *J. Chem. Phys.*, **78**, 7153 - 7158, 1983.
112. R. L. Wilkins and M. A. Kwok, "Temperature dependence of HF($v = 1$) + HF($v = 2$) vibrational relaxation", *J. Chem. Phys.*, **70**, 1705 - 1710, 1979.
113. D. L. Thompson, N. C. Blais and D. G. Truhlar, "Rotational energy transfer in collisions of internally excited molecules. Effect of initial conditions and potential energy surface", *J. Chem. Phys.*, **78**, 1335 - 1338, 1983.
114. D. L. Thompson, "Vibrational and rotational energy transfer in Ar + HF", *Chem. Phys. Lett.*, **84**, 397 - 400, 1981.
115. G. D. Billing, "Cross-sections for rotational/vibrational transitions in HF-HF collisions: Effect of initial state", *Chem. Phys.*, **112**, 95 - 104, 1986.
116. G. D. Billing, "Semiclassical calculation of cross sections for vibration-rotation energy transfer in HF-HF collisions", *J. Chem. Phys.*, **84**, 2593 - 2603, 1986.
117. L. L. Poulsen and G. D. Billing, "A classical trajectory study of the fate of vibrational energy released in HF", *Chem. Phys.*, **53**, 389 - 401, 1980.
118. R. N. Sileo and T. A. Cool, "Overtone emission spectroscopy of HF and DF: Vibrational matrix elements and dipole moment function", *J. Chem. Phys.*, **65**, 117 - 133, 1976.

119. G. P. Quigley and G. J. Wolga, "The deactivation of HF($v = 1$) and DF($v = 1$) by O, Cl, and F atoms", *J. Chem. Phys.*, **63**, 5263 - 5268, 1975.
120. J. A. Blauer and W. C. Solomon, "Deactivation of vibrationally excited hydrogen fluoride ($v = 2$ and $v = 1$) by atomic fluorine", *Int. J. Chem. Kinet.*, **5**, 553 - 558, 1973.
121. J. F. Bott and N. Cohen, "HF vibrational relaxation by F atoms", *J. Chem. Phys.*, **55**, 5124 - 5125, 1971.
122. J. F. Bott, "Vibrational relaxation of DF by He and Ar", *J. Chem. Phys.*, **63**, 2253 - 2254, 1975.
123. A. A. Vasiliev, V. N. Bezmelnitsyn, V. F. Sinianski and B. B. Chaivanov, "Rate constant for heterogeneous dissociation of fluorine in a temperature range of 700 - 900 K on a nickel surface", *J. Fluorine Chem.*, **95**, 153 - 159, 1999.
124. C. J. Ultee, "The homogeneous recombination rate constant of F atoms at room temperature", *Chem. Phys. Lett.*, **46**, 366 - 367, 1977.

Tunable, Solid State Laser for HF Mirror Metrology

AnnMarie L. Oien^a, Timothy J. Carrig^a, Gregory J. Wagner^a,
Chris J. Urbina^a, Jonathan W. Arenberg^{a,b}, Jennifer A. Keene^a
^aCoherent Technologies, Inc; ^bTRW Space & Technology Division

ABSTRACT

HF mirror metrology is currently costly and time consuming, requiring laser component delivery to an HF laser site, and operation of another HF laser to reach relevant wavelengths. Coherent Technologies, Inc (CTI) has developed a solid state Cr:ZnSe laser pumped by a Tm:YALO laser that provides up to 1.1W of output power with 1.1nm linewidth at 2.64 μ m, an HF laser line. The laser can also tune to other HF laser lines in the wavelength range of 2.64 μ m to 2.8 μ m. The Cr:ZnSe laser was used to measure the reflectivity of HF mirror samples provided by TRW. Examples of other possible applications of this source include beam train alignment and preliminary testing of diagnostic subsystems that measure HF laser output power, wavefronts, and beam profiles. Such a direct laser source is simple and can potentially achieve high intensity stability, allowing for a robust and compact HF laser surrogate. Moreover, power scaling is straightforward.

Keywords: Tunable; infrared; Cr:ZnSe lasers; HF lasers; metrology

1. Cr²⁺ DOPED CHALCOGENIDE LASERS

Three significant advantages of Cr:ZnSe are that (1) the material has an extremely broad absorption band (allows it to be pumped by a variety of sources), (2) the laser has an extremely large emission cross-section (high gain) and (3) the laser material has a near-unity fluorescence quantum efficiency at room temperature (high temperature operation possible). An absorption curve is shown in Figure 1. It is apparent that pump sources in the 1.5 μ m to 2.0 μ m wavelength region can be used to excite the Cr²⁺ ion in the ZnSe host. CTI has demonstrated CW operation of Cr:ZnSe lasers using a NaCl:OH⁻ color center laser operating at 1.58 μ m, a 1.8 μ m diode laser, and a Tm:YALO laser operating at 1.94 μ m as pump sources. For most laser geometries, the optimal pump wavelength is expected to be around 1.8 μ m. However, the broad absorption band provides a means of varying the heat load per unit length in the laser crystal without varying the active ion concentration (i.e. provides another design "knob" to tweak).

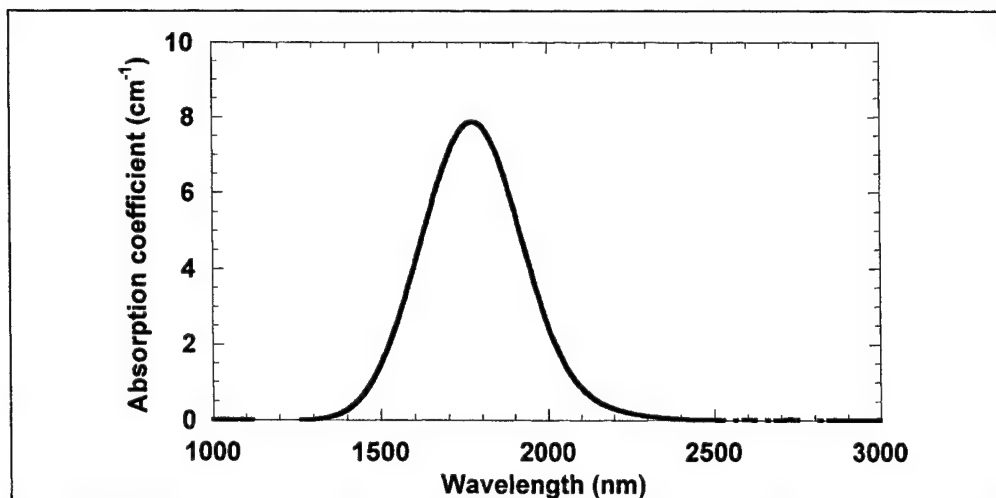


Figure 1. The Cr²⁺:ZnSe absorption spectrum. The sample was prepared by diffusion doping. It is apparent that any pump wavelength in the 1.5 to 2.0 μ m range is suitable.

The Cr²⁺ ion has essentially two electronic states since transitions to higher levels (which coincide with the material's bandgap) are spin-forbidden and, presumably, very weak. In this respect the laser is similar to the Ti:sapphire laser that

has proven to be highly commercially successful. An advantage is the expected absence of loss mechanisms, such as upconversion and excited-state-absorption, that plague many other SWIR and MWIR laser materials. Some advantages of the Cr:ZnSe laser system are listed below.

- Broad tunability (lasing from 2.1-3.1 μm demonstrated)
- Broad absorption bands (relaxed pump wavelength constraints)
- Ability to directly diode pump using strained-layer InGaAsP/InP diode lasers (demonstrated by multiple groups)
- Large gain cross section ($\sigma_{\text{emis}} \sim 9 \times 10^{-19} \text{ cm}^2$)
- Minimal problem of excited state absorption (no spin-allowed excited state transitions from the upper laser level)
- Near unity fluorescence quantum efficiency at 300 K (enables efficient room temperature operation)
- Can produce material by several techniques (diffusion doping and modified Bridgman growth)
- High thermal conductivity – better than YAG (18 W/m•K in ZnSe versus 13 W/m•K in YAG).¹
- High IR (0.6-20 μm) transparency
- Readily available host material (polycrystalline window material works fine)

The main disadvantage of Cr:ZnSe is a higher temperature dependence of refractive index ($\delta n/\delta T$) than other solid-state laser materials, such as YAG. A high $\delta n/\delta T$ (61×10^{-6} at 300 K in ZnSe compared to 7.3×10^{-6} in YAG) means that thermal lensing will be more of a concern in high power ZnSe lasers than in YAG lasers. This problem can be addressed by appropriate laser design (for instance disk, slab, and waveguide designs where thermal lensing is inherently mitigated).

2. Cr:ZnSe LASER TEST RESULTS

CTI has conducted work with Cr:ZnSe lasers concentrating on CW operation, modelocking, and power scaling.² To meet HF laser surrogate requirements, however, CTI concentrated on line narrowing and tuning of a Watt-level Cr:ZnSe laser. The following points summarize achievements to date on this program:

- Constructed a 6W continuous wave (CW) and 3W average power Q-Switched Tm:YALO laser
- Constructed a tunable Cr:ZnSe laser that tunes 0.75 microns Q-Switched and 0.63 microns CW
- Measured emission spectra of the materials Cr:ZnSe, Cr:CdSe, and Cr:Cd_xZn_{1-x}Te, and concluded that Cr:ZnSe was the best thermal candidate and Cr:CdSe may be the best spectral candidate for possible future work

Each of these highlights are described in more detail below.

The laser resonator design for the Tm:YALO laser is shown schematically in Figure 2.

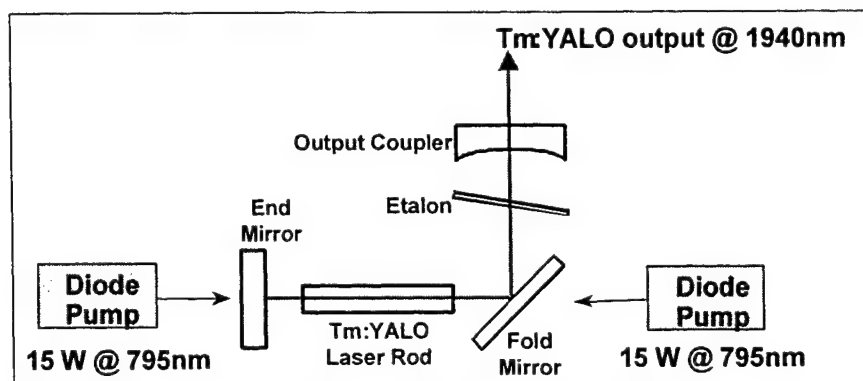


Figure 2: Plan view of the Tm:YALO laser used in the Phase I program's laboratory demonstration.

Since the 3-level Tm:YALO laser increases in efficiency with cooling, the laser head mount incorporates 4 thermo-electric coolers (TEC's). For this work, the laser was run at room temperature and produced sufficient performance for reflectivity survey demonstrations. A copper rod mount is thermally contacted via indium foil to the Tm:YALO rod. A 45 degree incidence dichroic mirror placed in front of the rod reflects the 1940nm Tm:YALO light but passes the 795nm diode pumping light, allowing diode laser end-pumping into the Tm:YALO rod. The Tm:YALO laser can provide up to 6W of power, of which 5W is incident upon the Cr:ZnSe laser after passing through an optical isolator.

The CW Cr:ZnSe laser resonator is shown in Figure 3. It is a folded linear resonator with a waist midway between the two curved mirrors to counteract thermal lensing in the pumped Cr:ZnSe rod. A Brewster plate, prism and two etalons have been used to successfully line narrow and tune the laser. The etalons are 150 and 300 microns thick, and are uncoated fused silica.

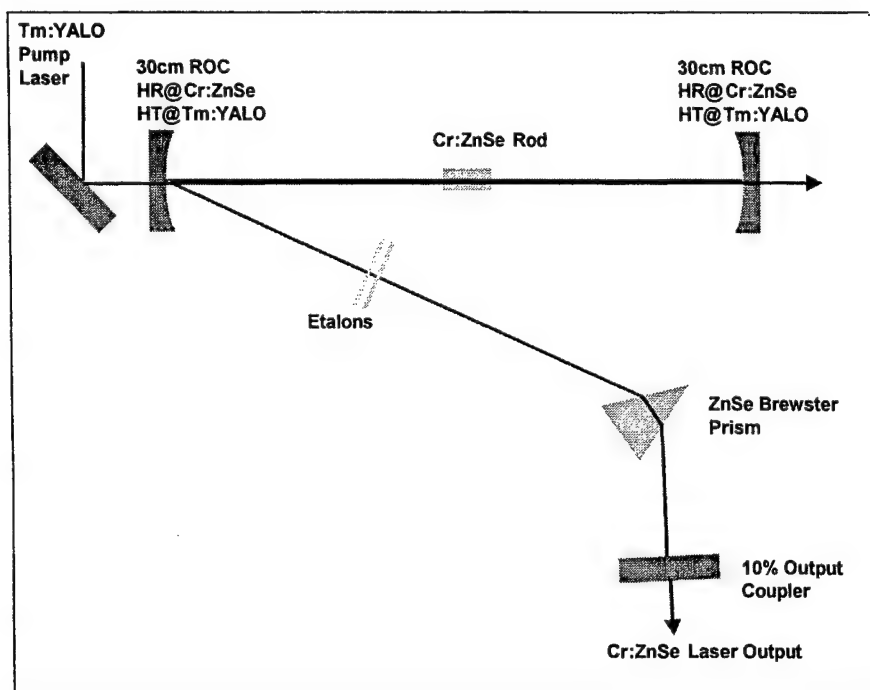


Figure 3: Resonator schematic of the Cr:ZnSe tunable laser, which produced up to 1.4W output power at 2500nm.

The Cr:ZnSe laser rod was 6mm long and absorbed 3W of the 5W maximum pump power incident on the rod. The output power vs wavelength at 5W Tm:YALO pump power is shown in the plot below, Figure 4. The laser had over 600nm continuous-wave tuning range and over 1W output power at the peak of the tuning curve.

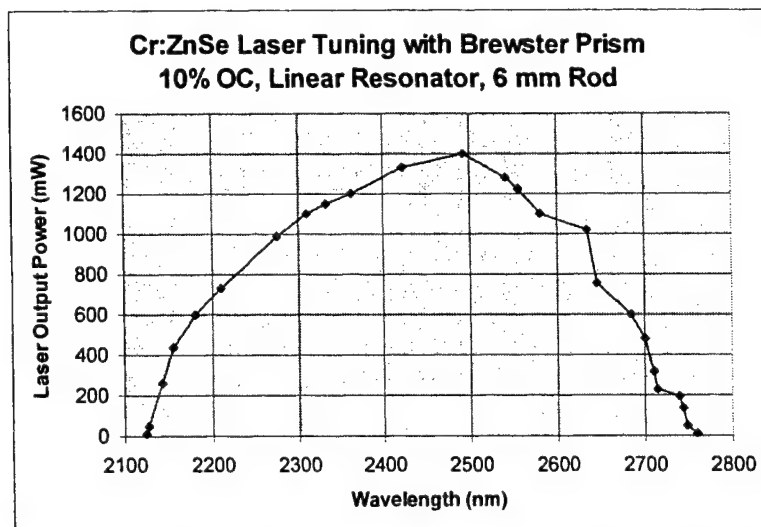


Figure 4: Plot of the output power versus wavelength for the CW Cr:ZnSe laser.

The spectral width of the laser with two etalons and a Brewster prism tuned to one of the HF 1-0 band lines, 2640nm, was measured. The full width half maximum is 1.1nm. The power output at this wavelength is 1.09W. The wavelength tuning range extending only to 2760nm, which is a shorter wavelength than reported by others; for example, CW Cr:ZnSe lasers have been tuned from 2000-3100nm, with appropriate laser design.³ It is therefore possible that longer wavelength tuning is currently limited by cavity optics, crystal coatings, or atmospheric absorption.

CTI has found that the emission spectrum of pumped Cr:ZnSe shows a significant increase in power when the long path of the monochromator is purged with dry nitrogen in the 2600 to 2900nm range. The original detector was replaced with a PbSe detector, which has a flatter spectral response that extends further into the infrared.

The purged and unpurged emission spectrum of the Cr:ZnSe rod which is pumped by Tm:YALO is shown below in Figure 5. The emission spectrum was taken using a PbSe detector, which has a known flat response throughout the 2 to 4 micron wavelength range. This measurement confirmed that the emission is severely affected by atmospheric absorption in the wavelength region of 2.6 to 2.9 microns.

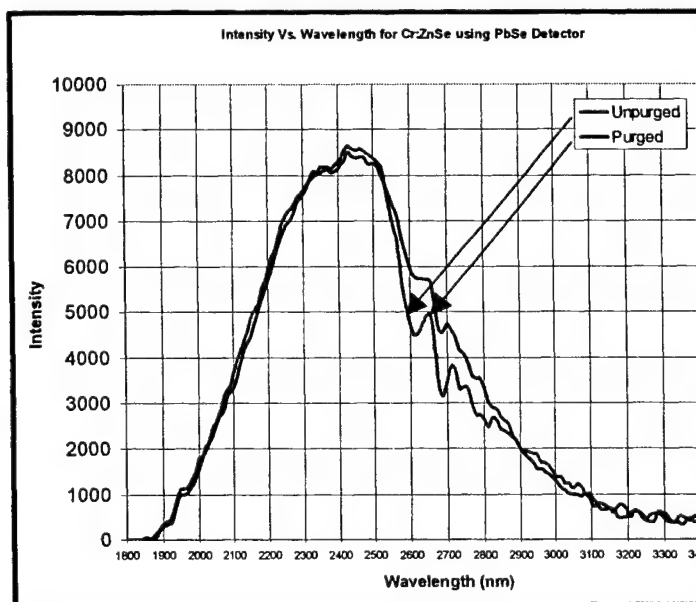


Figure 5 The emission spectrum of Cr:ZnSe with a flat response PbSe detector. Lasing in the 2.6 to 2.8 micron region would be particularly affected by atmospheric absorption lines.

Note that the purging for these emission spectra were not complete and that the path from the pumped crystal to the monochromator (the interior of which is purged with dry nitrogen) remains exposed to air and any residual atmospheric absorption. Therefore this result should be viewed as qualitative.

To investigate pump threshold effects on laser tuning, CTI measured the tuning range of a gain-switched Cr:ZnSe laser, using a 1kHz repetition rate, 3W average power Q-Switched Tm:YALO laser as the pump source. Given the much higher intensities of the Tm:YALO laser, the gain-switched Cr:ZnSe laser was expected to operate much further above threshold, yielding a tuning range that extends further into the infrared. The CW and gain-switched Cr:ZnSe lasers had very similar tuning ranges, indicating that our tuning limitation is probably related to a “non-gain” cause such as optical coatings or atmospheric absorption – both of which can be improved. The cavity used for the measurement is shown in Figure 6.

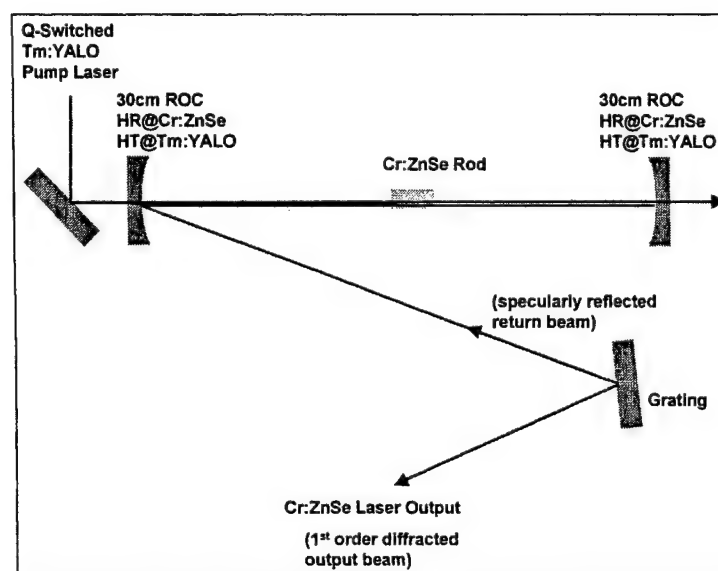


Figure 6: Layout schematic of the grating tuned Cr:ZnSe laser, pumped by a Q-Switched Tm:YALO laser.

The gain-switched laser, which was grating-tuned in the first order Littrow configuration, produced a tuning range of 750nm, which is the largest tuning range demonstrated at CTI. The resonator was tuned by rotating the grating, which changed the wavelength that was diffracted back into the resonator as feedback. The system tuned from 2050nm to 2800nm, and showed an output power that was strongly dependent on the grating diffraction efficiency with wavelength. This result is significant because it showed that the laser can indeed tune further into the infrared, but may still be limited by atmospheric absorption and optical coatings.

The Q-Switched Tm:YALO pump laser increased the gain remarkably, and it is interesting to note that the tuning range in the short range extended well into the region where Cr:ZnSe is absorbant – note that others have used the wavelength of 2013nm to PUMP a Cr:ZnSe laser⁴. Therefore, it is expected that with improvements beyond the scope of the current work, such as a higher power pump laser, improved optical coatings, and reduced cavity loss due to background atmospheric absorption, the tuning range of the CW output format Cr:ZnSe laser can be extended.

3. HF AXICON CONE MIRROR REFLECTIVITY SURVEY RESULTS

HF laser mirrors for metrology experiments were supplied by TRW. Specifically, an aluminum substrate waxicon cone coated with ThF_4 and ZnSe was used, which is a typical mirror shape for an unstable HF laser resonator. CTI has conducted a reflectivity survey of the cone at 2640nm wavelength for comparison to previous TRW measurements, which used a white light source. 2640nm was chosen as it is the wavelength of the P1(4) HF laser line, and the Cr:ZnSe laser could tune to it and provide over 1W output power. The setup used to measure the reflectivity is shown in Figure 8.

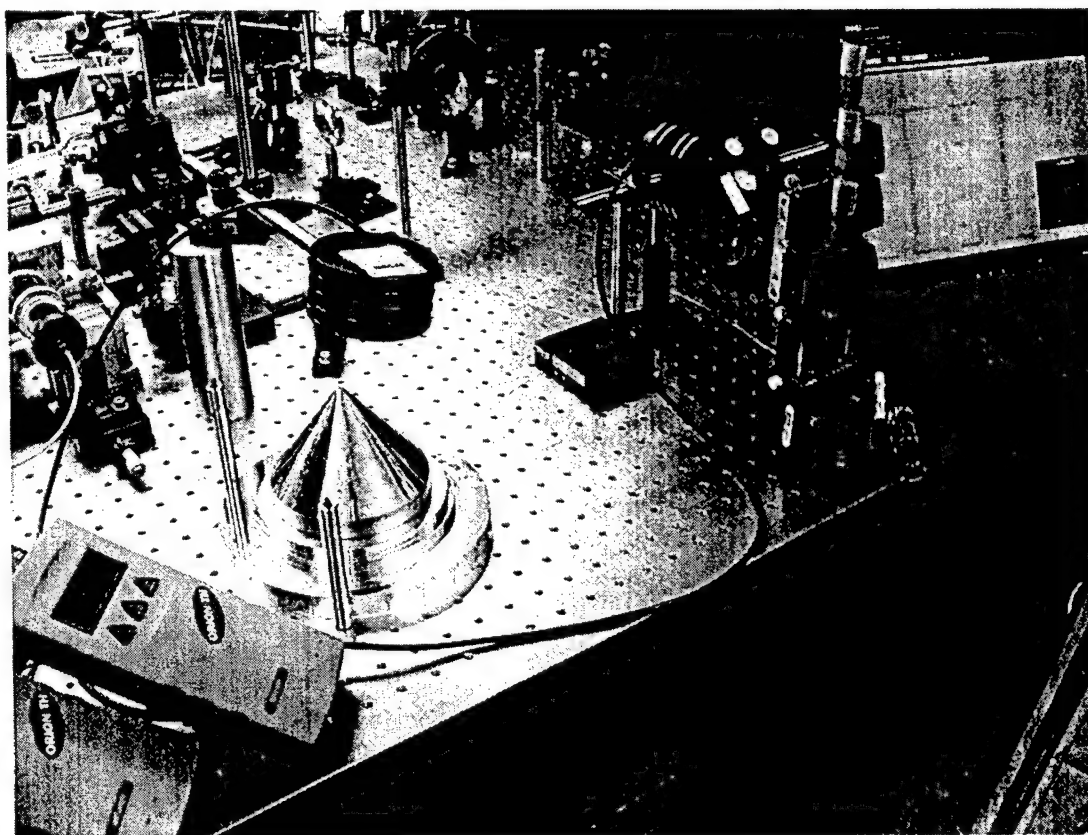


Figure 8: Setup to measure the reflectivity at 2640nm of the HF mirror cone. Two mirrors act as a vertically translatable periscope to send the beam at scanned heights onto the cone. The cone is marked and rotated within locating pins after each vertical scan.

Throughout the axicon cone survey the laser produced $1092\text{mW} \pm 2.5\%$ intensity at 2640nm over the four hour scan. After each reflectivity measurement the incident intensity was measured. The two detectors for incident and reflected intensity were cross-checked for response. The transmission of the laser from the incident intensity detector past the two periscope mirrors was found to be 93.7%, which was used to correct the data.

Figure 9 shows CTI's measurement in the plot format equivalent to that done in the past, except at the HF laser wavelength 2640nm. Only the average reflectivity of the cone as a function of height above the base is shown. The cone was visibly damaged, showing flaking and patchy discoloration, so it was expected that the reflection would not be 100%. No trend in reflectivity is seen with height, but that was not expected given that the measurements were done on the lower 50mm height of the cone, where the reflectivity remained fairly constant in the white-light scan. It was difficult to measure the reflectivity nearer the tip due to the severe curvature of the cone – the tip had a radius of curvature of $\sim 0.5\text{cm}$.

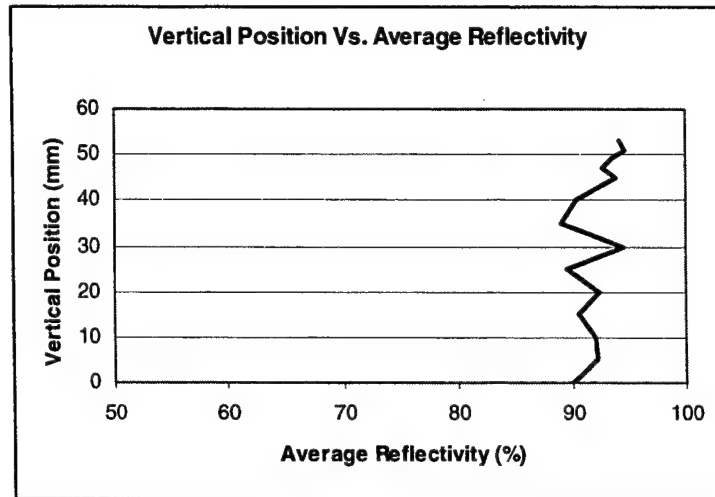


Figure 9: Plot of the average reflectivity around the cone with height.

The reflectivity of the cone as a function of both azimuthal angle and height above the cone base is shown below in Figure 10. The local drops in reflectivity could be quite severe, going to 50% in localized areas, which appeared to visibly correlate to the flaking parts of the cone.

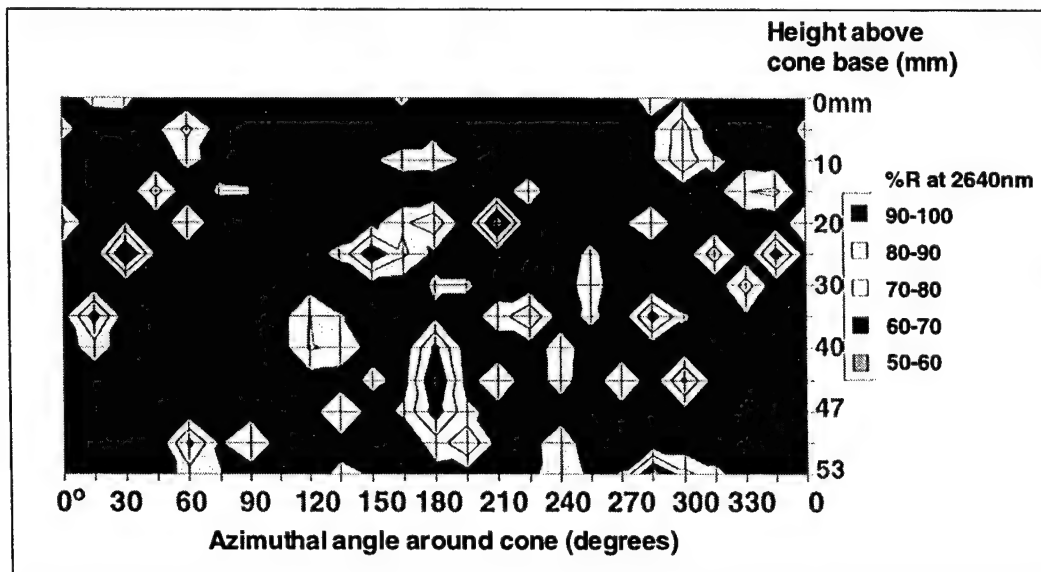


Figure 10: Plot of the measured reflectivity in percent with azimuthal angle and height in mm above the base of the HF mirror cone.

These measurements showed that mirror metrology with extensive spectral and spatial resolution could be conducted with the current Cr:ZnSe laser.

Several attempts were made to detect absorption in the HF mirrors with a focussed Cr:ZnSe laser beam and a coincident green HeNe laser beam. Despite scanning the visible laser beam repeatedly over the area illuminated by the Cr:ZnSe laser, and looking for deflection at a distance calculated to be more than sufficient to see deflection movement, no absorption by deflection was observed.

4. CONCLUSIONS

In conclusion, the results of the Cr:ZnSe laser reflectivity mapping show that the laser is sufficient to conduct spectrally and spatially accurate mirror metrology surveys. As a solid-state laser source it can significantly reduce the cost and time needed to verify a newly-developed mirror's optical properties, accelerating HF laser development. Moreover, for maintenance, beam alignment and diagnostic checking, the laser can be built on a smaller or larger scale, and be used to streamline HF laser operation and preparation procedures. In short, a Cr²⁺ chalcogenide laser is well matched to multiple HF laser surrogate requirements.

ACKNOWLEDEMENTS

We thank the Air Force Research Laboratory, Dr. Gordon Hager, AFRL/DELTC, for funding this work under the Phase I Small Business Innovative Research (SBIR) contract # F29601-01-C-0098.

REFERENCES

1. Material properties of ZnSe are listed in *Optical Crystal Handbook*, Optovac, N. Brookfield, MA. Properties of YAG are given by W. Koechner in *Solid-State Laser Engineering*, third edition, vol. 1. in Springer series in Optical Sciences, Springer-Verlag, Berlin, 1992.
2. See, for example, G. J. Wagner and T. J. Carrig, "Power scaling of Cr²⁺:ZnSe lasers," paper WB1, presented at *Advanced Solid-State Lasers '01*, Seattle, WA, January 31, 2001. Published in the ASSL'01 Proceedings, and T. J. Carrig, G. J. Wagner and A. Burger, "Broadly Tunable Cr²⁺:ZnSe laser," paper SBIR-48, *2001 NSF Design, Service and Manufacturing Grantees and Research Conference*, Tampa, FL, January 9, 2001.
3. Private communication, Dr. I. Sorokina, Technische Universität, Wien, Austria, (submitted to journal 2001).
4. A.V.Podlipensky, V.G. Shcherbitsky, N.V. Kuleshov, V.I.Levchenko, V.N. Yakimovich, A. Diening, M. Mond, S. Kck, and G. Huber, *Advanced Solid-State Lasers*, OSA TOPS Vol. 34, 201, (2000).

* amarie@ctilidar.com, phone +1 303 604 2000; fax +1 303 604 2500; Coherent Technologies, Inc, 655 Aspen Ridge Drive, Lafayette, CO 80026

** jon.arenberg@trw.com; phone +1 310 813 2567; fax +1 310 813 0447; TRW Space & Technology Division, One Space Park, Redondo Beach, CA 90278

Imaging spectroradiometer for HF laser studies

W.T. Rawlins, D.B. Oakes, P.A. Mulhall, and S.J. Davis*
Physical Sciences Inc.

ABSTRACT

We discuss a non-intrusive diagnostic for mixing, species concentration, and optical gain for HF chemical lasers. The instrument is based on hyperspectral imaging using a low order Fabry-Perot interferometer. The basic theory behind this technology is described and several applications to a chemically reacting flowfield are presented

Keywords: chemical laser diagnostics, hyperspectral imaging, reactive flows

1. INTRODUCTION

Certain gas phase chemical reactions form product states that have inverted population distributions. For example, the $F + H_2$ reaction produces $H + HF(v,J)$ where partial inversions exist between many rovibrational levels. Mixing of the reacting gas streams in a chemical laser is a key parameter for producing efficient devices.¹⁻³ This was recognized soon after the first laser demonstrations, but effective diagnostics did not exist that could survive corrosive environments or did not perturb the flows. Measurements of mixing, vibrational and rotational temperatures, small signal gain, and spectral output were difficult and often inaccurate. Even though the HF chemical laser concept is more than 30 years old, there are still important scaling parameters for which there are no effective diagnostics. In 1978 Rapagnani and Davis demonstrated that laser induced fluorescence could be used as a diagnostic for mixing in chemical laser nozzles, and they later developed methods for studying both hot flow and cold flow mixing.^{4,5} In this paper we discuss a new diagnostic for reactive mixing in chemical lasers. Using a device we call the Adaptive Infrared Imaging Spectroradiometer (AIRIS) we have developed methods for examining mixing of F and H_2 flows and for determining spatially resolved maps of population inversions between selected HF rovibrational levels.

1.1 Background

The AIRIS technology was developed at Physical Sciences Inc. (PSI) to address the need for a moderate resolution, rapidly tuned imaging spectrometer for a variety of applications. Our technology is based on Fabry-Perot (F-P) interferometry. Fabry-Perot devices rely upon multiple beam interference between two highly reflecting mirrors to produce an interference pattern that contains spectral information about the light source being probed. If the light source is collimated with a lens, then the resulting interference pattern is usually a series of concentric rings, each representing a different order of the interference. This is illustrated in Fig. 1.

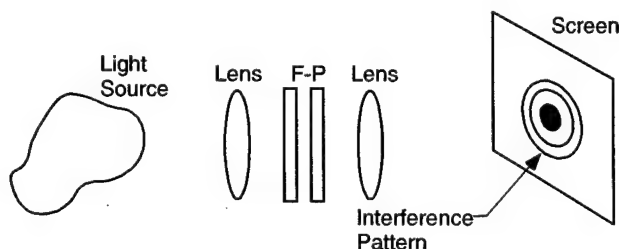


Fig. 1: Typical arrangement for F-P interferometers.

* sdavis@psicorp.com; phone 1 978 689-0003; fax 1 978 689 3232; <http://www.psicorp.com>; Physical Sciences Inc., 20 New England Business Center, Andover, MA, USA 01810-1077

Jacquinet⁶ described an important application of the F-P with the introduction of the center spot technique. He showed that if one placed a pinhole in front of a detector that restricted the detector to view only a small portion of the center spot of the interference pattern, then one could use the F-P as a spectrometer by recording the transmitted light as a function of the distance between the F-P mirrors. Davis and co-workers⁷ used this approach to obtain the first measurements of the collisional broadening coefficient for oxygen on the atomic iodine laser line, crucial data for COIL. This type of spectrometer offers several advantages including: high throughput, high spectral resolution, and compact size.

1.1.1 Basic concepts

The *AIRIS* instrument comprises an IR focal plane array (FPA) coupled to a Fabry-Perot interferometer through imaging optics. In this configuration the interferometer operates as a tunable interference filter, selecting the wavelength viewed by the FPA. In this section we describe the theoretical basis for the development of the interferometer as well as the consequences and advantages of low-order operation.

In a Fabry-Perot interferometer light is selectively transmitted by constructive interference through the faces of two partially-reflecting parallel mirrors. Light is transmitted for wavelengths which satisfy the expression:

$$\lambda_t = \frac{2\ell}{m} \cos \theta \quad (1)$$

where

- ℓ = mirror spacing
- m = order of interference
- θ = incidence angle
- λ_t = transmitted wavelength.

A range of mirror spacings, incidence angles, and orders will all lead to the transmission of a single wavelength. The free spectral range, $\Delta\lambda_{\text{FSR}}$, determines the range of wavelengths transmitted between successive orders of interference:

$$\Delta\lambda_{\text{FSR}} = \frac{\lambda_{\text{max}}}{m_{\text{max}} + 1} \quad (2)$$

where m_{max} is the order in which λ_{max} is transmitted for paraxial rays.

The finesse, F , determines the spectral resolution of the interferometer, which is always a fraction of the free spectral range:

$$\Delta\lambda_{1/2} = \frac{\Delta\lambda_{\text{FSR}}}{F} \quad (3)$$

The elements which define the finesse of the interferometer arise from the reflectivities of the mirrors as well as "defects" in their configuration, such as mirror flatness and parallelism. The total finesse of the interferometer is obtained from the inverse root mean square sum of each finesse component. For practical operation in the infrared, the defect finesse is the limiting factor in determining total finesse. The total finesse can seldom be greater than approximately 30 to 50 due to these limitations.

The interferometer field of view (focal length and detector element size) determines the range of angles incident and detected by the system. Equation (1) shows that a range of incidence angles and interference orders will allow transmission of a common wavelength through the interferometer for a single mirror spacing. The aperture finesse defines the degradation in spectral resolution within a single order due to this effect:

$$F_A = \frac{2}{m(\Delta\theta)^2} \quad (4)$$

As a consequence of Eq. (4), the field of view over which an acceptable finesse can be obtained increases as the interferometer is operated in lower orders. When using IR focal plane arrays, system instantaneous fields-of-view ranging from 6 to 15 deg are generally consistent with an overall finesse of 35.

The short wavelength AIRIS used in this work contains two, custom mirrors with high reflectivity in the 2.0 to 3 micron spectral region. The 38 mm diameter mirrors were fitted with specialized gold pads that form four capacitors that are used to measure and monitor the separation and alignment of the two mirrors in the Fabry-Perot configuration. A photo of the short wavelength AIRIS head is shown in Fig. 2.



Fig. 2: Photo of AIRIS device used to probe HF(v,J) emission.

2. EXPERIMENTS

2.1 Calibrations

Initial testing of the AIRIS system was conducted using a Fourier Transform Infrared (FTIR) spectrometer. The AIRIS head was positioned inside the FTIR, and the FTIR provides a tunable, narrow spectral band of light that can be used as an essentially monochromatic source for AIRIS calibrations. This quasi-monochromatic beam (0.5 to 2 cm^{-1}) passed through the AIRIS and the transmitted intensity was monitored as a function of the wavelength of the source and the mirror separation in AIRIS. Recall that in a Fabry-Perot interferometer the wavelength of the transmitted light is a function of the mirror separation. We performed initial calibration of the AIRIS by systematically setting the mirror separation while recording the transmitted intensity as the wavelength of the light passed by the FTIR was scanned. As the wavelength of the light incident on the AIRIS passed through cavity resonances, transmission peaks of the consecutive orders were observed. A typical spectrum is shown in Fig. 3.

2.2 Chemical HF(v,J) production

We used a high power Microwave Driven Jet (MIDJet™) device to produce the F atoms. MIDJet™ is an electrodeless discharge so that corrosion is not an issue. It has been applied to numerous feedstock gases including SF₆, O₂, He, Cl₂, NF₃, and air. The source gas and diluent are fed into the discharge region of MIDJet™ through a series of sonic injection nozzles. The design of these injectors stabilizes the discharge along the axis of the MIDJet™ chamber and enables the device to operate over a large range of pressures and flow rates. Both sonic and subsonic exit nozzles can be used to cover a wide range of exit conditions. The supersonic exit nozzle isolates the conditions inside the MIDJet™ chamber for flow conditions downstream of the nozzle.

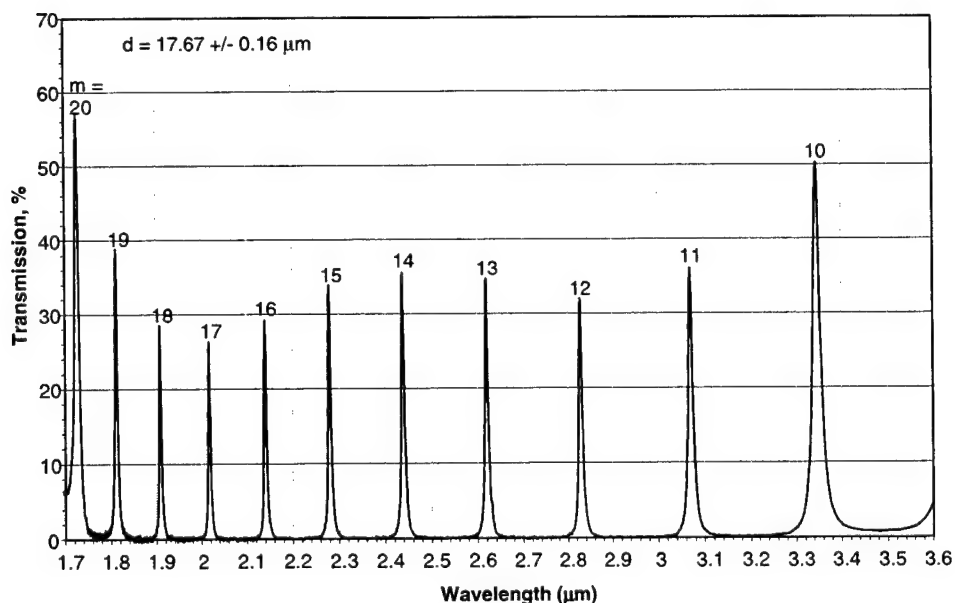


Fig. 3: AIRIS transmission as a function of the wavelength of incident light for a mirror separation of $17.67 \pm 0.16 \mu\text{m}$. The interference order is also indicated. Spectral resolution is 2 cm^{-1} .

The injector was mounted in the MIDJet™ source as indicated in Fig. 4. The HF mixing nozzle for production of HF(v,J) from the $\text{F} + \text{H}_2$ reaction was a 6 mm diameter stainless tube with four holes (0.5 mm diameter) spaced 1.5 cm apart. Hydrogen and He diluent were injected through this arrangement. The four holes produced supersonic flows of H_2 from the exit plane to approximately 2 mm downstream of the holes. Fluorine atoms were produced with a 5 kW MIDJet™ discharge device using SF_6 as the feedstock gas. Details of the water-cooled injector tube are shown in Fig. 5.

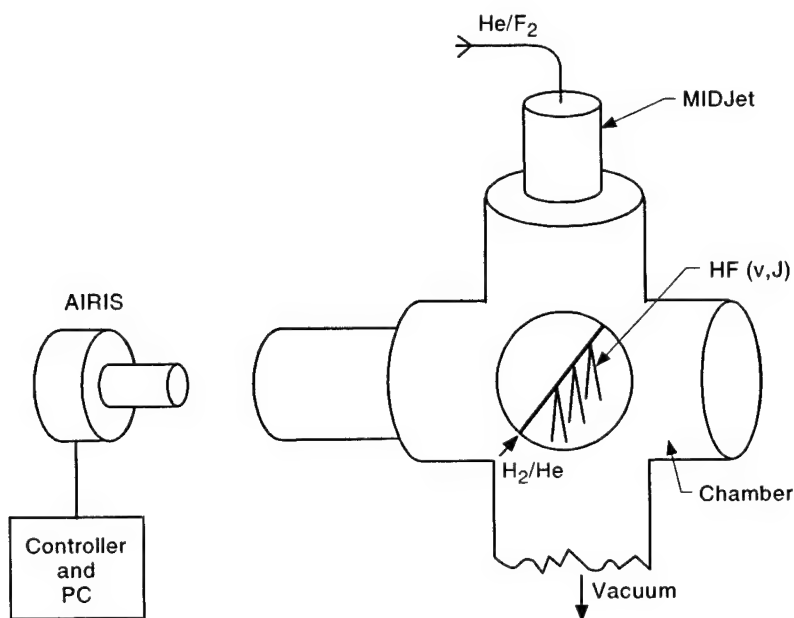


Fig. 4: Block diagram showing injector mounted in MIDJet™ device.

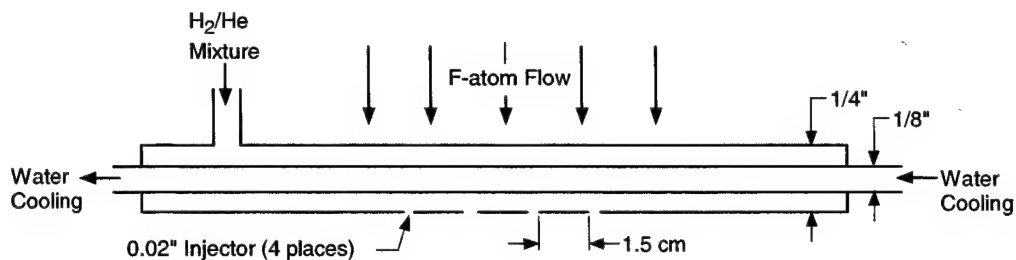


Fig. 5: H₂ injector used in the MIDJet™, HF production chamber.

2.3 Tests of AIRIS on HF flow chamber

The AIRIS device was positioned in front of a Cincinnati Electronics InSb IR camera equipped with a 4.1 μm short-pass cold filter. We also used a bandpass filter to isolate the emission in the 2.6 to 2.9 μm spectral region. The filter was placed directly in front of the camera. A camera zoom lens was used to focus the region of the HF injector, with the camera approximately 60 cm from the HF injector. In order to assure that the HF production chemistry made HF(v,J) we initially viewed the reaction zone with the FTIR spectrometer. The spectral region recorded between 2.65 and 2.9 μm is shown in Fig. 6. Each feature can be assigned to an HF emission line and no other spectral features were observed. Even though the spectra are uncorrected for spectral response, it appears that the vibrational distribution is inverted with $v=2$ having more population than $v=1$. Our source of HF appears to be an excellent surrogate for an actual HF laser reaction zone.

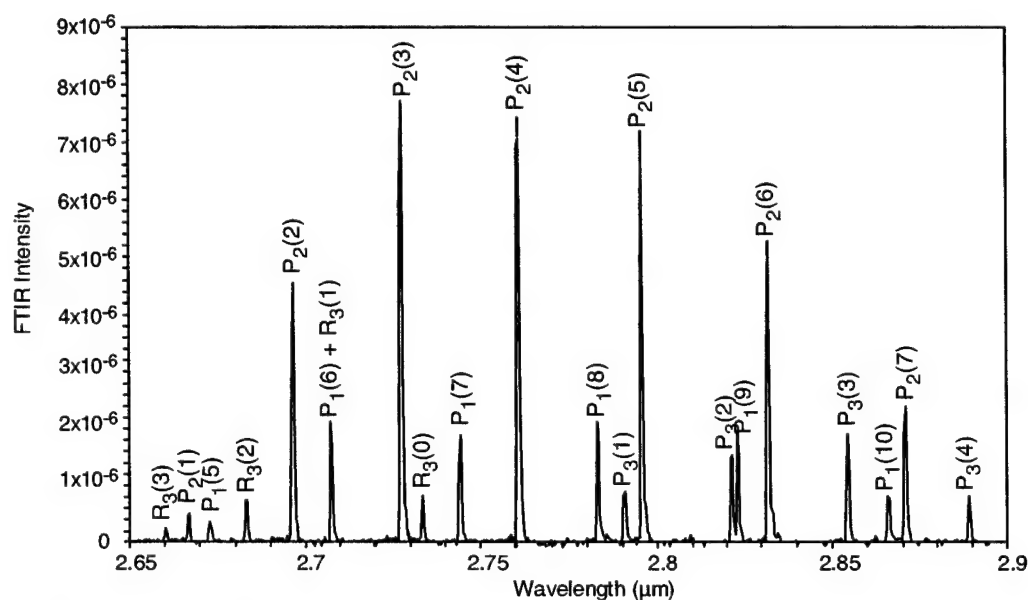


Fig. 6: FTIR spectrum of HF(v,J) emission recorded in our HF production chamber. Spectral resolution is 0.5 cm^{-1} .

Fig. 7 shows an image of the HF flowfield obtained with the AIRIS. The image is emission from the P₂(4) line near 2.76 μm . The mixing of the F and H₂ downstream of the injection points is clearly evident. When the AIRIS is tuned off the P₂(4) line (near the P₁(7) line), the emission disappears, demonstrating the ability of AIRIS to spectrally isolate the HF emission lines. We have collected emission from numerous lines. Each image was also complemented by recording a full field image of a flat black body radiator at each wavelength. This allowed us to subsequently put each image on an absolute intensity basis. We also recorded a background image with the H₂ flow off. The raw images were corrected using the following procedure. First a background image was subtracted from each "raw" image. To correct each pixel for spectral response, each image was divided by the blackbody function at the appropriate wavelength of the image.



Fig. 7: AIRIS image of $P_2(4)$ emission from chemically produced HF.

To further demonstrate that AIRIS can be used to study mixing phenomena in an HF laser, we performed an additional analysis on the flow field images. In Fig. 8 we show a section of the mixing region just downstream of the hydrogen injectors. Four planes: A,B,C, and D are shown. In Fig. 9 we show contours of these four planes and the progression of the mixing is evident as the flow progresses from A to D.

We also developed a strategy to image the population inversion in the flow field. When placed on an absolute scale, one can subtract images of the same scene recorded on sequential emission transitions to obtain these population inversion images. The method is outlined in Fig. 10. We used this approach to produce images of the inversion density of the flow field. Fig. 11 shows an image of the spatially resolved population inversion between the $HF(v,J) = (2,4)$ and $(1,5)$ levels. This key demonstration shows that AIRIS can be used to interrogate the small signal gain, a key parameter in HF lasers.

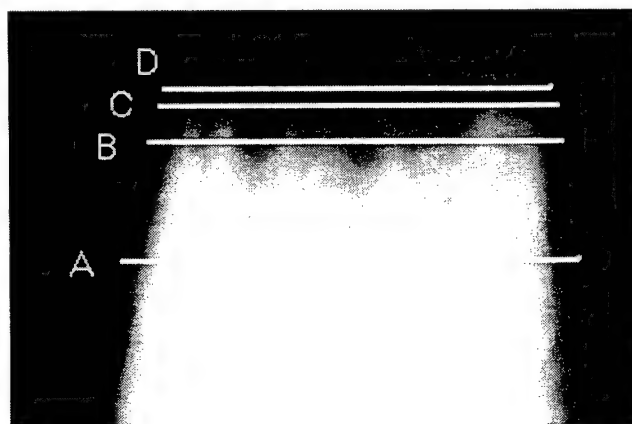


Fig. 8: HF emission from $P_2(5)$ line. Analysis slices are indicated. Flow direction is down.

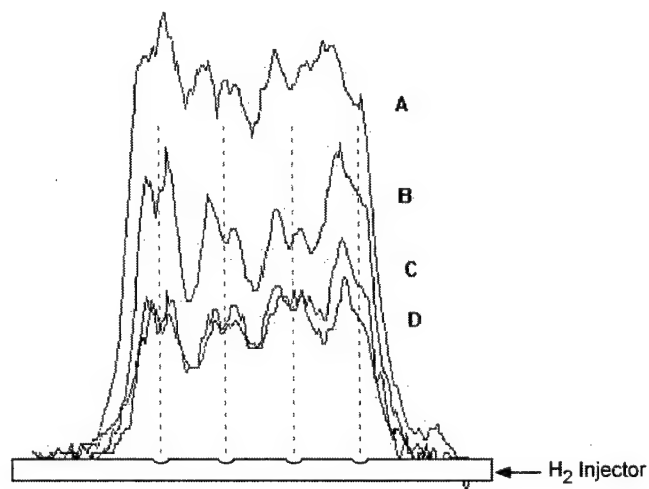


Fig. 9: Intensity profiles from image shown in Fig. 8.
Flow direction is up.

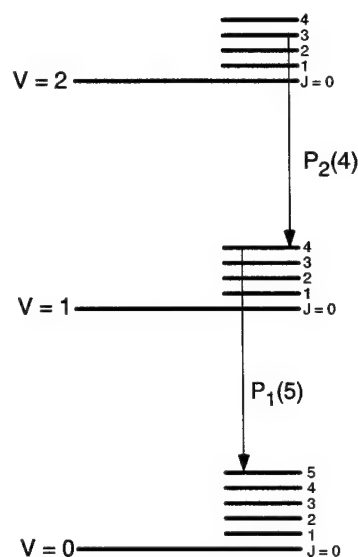


Fig. 10: Strategy for obtaining images of population inversion fields.

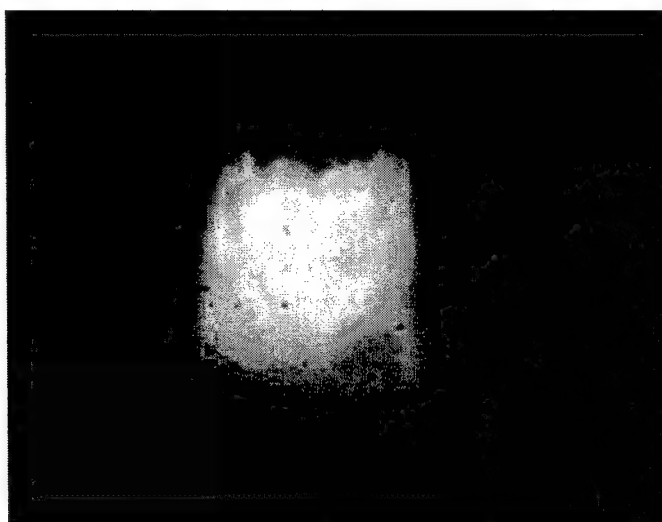


Fig. 11: Image of population inversion in PSI flowfield.

3. SUMMARY

We have described a novel diagnostic capable of probing chemically reacting flows for species concentration maps, mixing, and even population inversion maps. Using a subsonic flow reactor, we have obtained spatially and spectrally resolved maps of emission from excited HF molecules and 2-D images of the population inversion between two adjacent excited states in chemically produced HF. This device will be useful for a investigating a variety of parameters in the development of new, mid-IR chemical lasers.

ACKNOWLEDGMENTS

The authors would like to thank Katie Boates for her assistance in the image data reduction. We also gratefully acknowledge the Air Force Research Laboratory Directed Energy Directorate, Kirtland AFB, NM for support of the effort under Contract #F29601-01-C-0091.

REFERENCES

1. Gross, R.W.F. and Bott, J.F., *Handbook of Chemical Lasers*, John Wiley & Sons, New York, 1976.
2. Kwok, M.A., "Measurement and Analysis of the HF Radiation from a Reacting Supersonic Jet", Technical Report TR-0074(4530)-3, The Aerospace Corporation, Los Angeles, CA (1973).
3. Sentman, L.H., "Mechanisms of HF Laser Performance," *XIII International Symposium on Gas Flow and Chemical Lasers and High-Power Laser Conference*, Vol. 4184, Invited paper, Proceedings, SPIE, Florence, Italy (September 2000).
4. Rapagnani, N.L. and Davis, S.J., "Laser Induced Fluorescence Measurements in a Chemical Laser Flowfield", *AIAA Journ.* **17**, p. 1402, 1979.
5. Rapagnani, N.L. and Davis, S.J., "Laser Induced Fluorescence: A Diagnostic for Fluid Mechanics," *Lasers and Applications* **IV-5**, 127 (1985).
6. Jacquinet, P. and Dufour, C., *CRMS J.Resh.* **61**, p. 91, 1948.
7. Neumann, D.K., Clark, P.K., Shea, R.F., and Davis, S.J., "O₂ Pressure Broadening of the Iodine $^2P_{1/2} \dots ^2P_{3/2}$ Transition", *J.Chem. Phys.* **79**, p. 4680, 1983.

Room Temperature Rate Constant For H + F₂

Jiande Han^a, Gerald C. Manke II^b, and Michael C. Heaven^{a*}

^aDepartment of Chemistry, Emory University, Atlanta, GA 30322

^bAir Force Research Laboratory, Directed Energy Directorate, Kirtland AFB, NM 87117

ABSTRACT

The rate constants for H atom reactions with Cl₂ and F₂ have been measured by monitoring the loss rate of hydrogen atoms in the presence of excess [Cl₂] and [F₂] via time-resolved, laser-induced Lyman- α fluorescence. The rate constants for H + F₂ and H + Cl₂ were found to be 2.4 ± 0.4 (2 σ) $\times 10^{-12}$ and 2.52 ± 0.18 (2 σ) $\times 10^{-11}$ cm³ molecules⁻¹ s⁻¹, respectively. The result for H + F₂ is consistent with the recommendation of Baulch et. al. (J. Phys. Chem. Ref. Data **10** (suppl. 1) (1981)) and our k(H + Cl₂) value is consistent with the majority of previous measurements.

1. INTRODUCTION

A chemical HF laser can be used to produce a high power 2.7 μ m beam. Vibrationally excited HF is generated primarily by the F atom reaction with molecular hydrogen



or via the secondary reaction



The rate constant^{1,2} and nascent HF(v) distribution^{3,4} for reaction [1] are well established, $k_1(T) = 1.1 \pm 0.1 \times 10^{-10} \exp(-450 \pm 50/T)$ cm³ molecules⁻¹ s⁻¹ and 0.0 : 0.15 : 0.55 : 0.30 for P₀:P₁:P₂:P₃. The detailed dynamics of reaction [1] have been exhaustively studied, both theoretically^{5,6} and experimentally⁷⁻¹² by numerous investigators.

Surprisingly, the same cannot be said for reaction [2]. The 1981 kinetics review by Baulch et. al.¹³ lists only 8 previous measurements of the rate constant (compared to 22 for reaction [1]) and recommends $k_2(T) = 1.46 \times 10^{-10} \exp(-1210/T)$ cm³ molecules⁻¹ s⁻¹ and $k_2(298 \text{ K}) = 2.5 \times 10^{-12}$ cm³ molecules⁻¹ s⁻¹. A 1983 review by Cohen & Westberg¹⁴ evaluated the same ensemble of measurements and selected $k_2(T) = 4.8 \times 10^{-15} T^{1.4} \exp(-667/T)$ cm³ molecules⁻¹ s⁻¹ and $k_2(298 \text{ K}) = 1.5 \times 10^{-12}$ cm³ molecules⁻¹ s⁻¹. Both recommendations are based primarily on mass-spectrometric experiments by Dodonov and co-workers.^{15,16} ($k_2(T) = 2.0 \pm 0.2 \times 10^{-10} \exp(-1210 \pm 100/T)$ cm³ molecules⁻¹ s⁻¹ for T = 294 - 565 K) and Homann, et. al.¹⁷ ($k_2(T) = 6.6 \pm 1.7 \times 10^{-11} \exp(-1110 \pm 50/T)$ for T = 224 - 493 K). The activation energies of both expressions are essentially the same but the pre-exponential factors differ by a factor of 3. Additional measurements by Levy & Copeland¹⁸, Rabideau et al.¹⁹, and Sung, et al.²⁰ have also been reported. Levy and Copeland¹⁸ measured F₂ consumption following UV irradiation of a H₂, F₂, N₂ and O₂ mixture. They did not measure k_2 directly; rather, they report the rate constant ratio between reaction [2] and $\text{H} + \text{O}_2 + \text{M} \rightarrow \text{HO}_2 + \text{M}$. Using the accepted value for the reference reaction¹³, their result corresponds to $k_2(298 \text{ K}) = 1.0 \times 10^{-12}$ cm³ molecules⁻¹ s⁻¹. Rabideau, et. al. added molecular fluorine to a fast-flowing mixture of H and H₂ diluted in He, while monitoring the concentration of F and H atoms via EPR. The room temperature rate constants for reactions [1] and [2] were determined to be $6.6 \pm 1.7 \times 10^{-12}$ and $4.2 \pm 0.3 \times 10^{-12}$ cm³ molecules⁻¹ s⁻¹, respectively. Their result for k_1 is approximately a factor of 4 lower than the recommended value of Baulch¹³. Sung et al.²⁰ measured the infrared chemiluminescence from HCl(v) and HF(v) products generated by H atom reactions with Cl₂, F₂, ClF, and ICl. Although they "make no strong claim on the reliability of the H + F₂ rate constant," they report a ratio of $k_2 / k_3 = 0.053$, where k_3 is the rate constant for



If the recommended value for k_3 is used (1.9×10^{-11} cm³ molecules⁻¹ s⁻¹ at 298 K)¹³, $k_2 = 1.0 \times 10^{-12}$ cm³ molecules⁻¹ s⁻¹. Considering the importance of reaction [2], and the scarcity of experimental data, a new direct measurement of k_2 seems timely.

In addition to reaction [2], we have also re-examined the rate constant for reaction [3] which is an important source of HCl(v) in the HCl chemical laser system. Reaction [3] was also used as a reference for competitive H atom reaction studies^{20,21}. Dobis and Benson²² recently applied their very low-pressure reactor (VLPR) technique to this reaction and measured $k_3(298 \text{ K}) = 0.96 \pm 0.04 \times 10^{-11}$ cm³ molecules⁻¹ s⁻¹. This result is a factor of 2 smaller than the generally accepted value given by Baulch, et. al. as $k_3(T) = 1.4 \times 10^{-10} \exp(-590/T)$ for T = 250 - 730 K and $k_3(298 \text{ K}) = 1.9 \times 10^{-11}$ cm³ molecules⁻¹ s⁻¹. Even though Baulch assigns the uncertainty for reaction [3] at $\pm 50\%$, Dobis and

Benson's value seems anomalously small relative to numerous previous measurements, and another measurement of k_3 seems appropriate.

We report the direct measurement of the rate constants for the reaction of H atoms with molecular fluorine and chlorine. We generate low concentrations of H atoms via photolysis of H_2S in the presence of a large excess of F_2 or Cl_2 and monitor the loss rate of $[\text{H}]$ by laser induced fluorescence of the Lyman α transition. Typically, the initial pool of H atoms is consumed in 100 - 200 microseconds or less, and complications related to secondary reactions with products of the primary reaction and wall losses are avoided. Our ability to produce H atoms without H_2 is particularly important for the measurement of k_2 . All previous measurements have used molecular hydrogen as their H atom source. In some cases a discharge is applied to the H_2 directly, while in others a discharge based F atom source and $\text{F} + \text{H}_2$ pre-reactor are used to generate a known flow of H atoms. Undissociated H_2 rapidly reacts with atomic fluorine to regenerate H atoms. This not only complicates the analysis, but also ties the accuracy of the measurement to some assumption about the rate constants for the secondary reactions. Our method eliminates these considerations and simple pseudo first-order kinetics can be applied.

2. EXPERIMENTAL METHODS

Ground state hydrogen atoms were generated by pulsed photolysis of H_2S . To observe the reaction with F_2 or Cl_2 , the H_2S was present as a minor constituent (approximately 6.5×10^{14} molecules cm^{-3} or less) of $\text{H}_2\text{S}/\text{F}_2$ or Cl_2 (in He)/Ar mixtures. Various partial pressures of the halogen/He mixtures were used. Pseudo first-order conditions were achieved by adding 0.5 - 6.0 Torr of a 5% Cl_2 in He mixture (Matheson) or 0.5 - 1.75 Torr of a 10% F_2 in He mixture (Matheson). The main carrier gas was Ar and the total reactor pressure was typically 100 Torr. The flow rates of H_2S and Ar were controlled by needle valves while a mass flow controller was used for F_2 or Cl_2 addition.

Hydrogen sulfide was photolyzed at 193 nm by a Lumonics TE-860-4 excimer laser operating at 10 Hz. The laser emission (~ 60 mJ/pulse) was focused by a 50 cm focal length lens, providing a power density that was sufficient to dissociate all of the H_2S in the focal region. Photodissociation at 193 nm produces translationally hot H and SH fragments^{23,24}. The high pressure of Ar buffer gas was used to thermalize the H atoms and limit their diffusion out of the detection region. Both F_2 and Cl_2 have very weak absorption cross-sections at 193 nm, and were not photodissociated to any significant degree.

LIF detection of H atoms was accomplished by two-photon excitation of the $2s-1s$ transition of atomic hydrogen. Collisions with Ar rapidly quench the $2s$ state to $2p$, which then emits Lyman α radiation as it relaxes back to the ground state. A tunable dye laser (Lambda-Physik EMG-203/FL3002 system) was used to generate 486 nm light. This was frequency doubled using a BBO crystal. A short (20 cm) focal length lens was used to focus the UV in the center of the photolysis cell. The photolysis and LIF lasers were arranged in an overlapping, counter-propagating configuration, see Figure 1. The delays between the photolysis and probe laser pulses were controlled with a precision pulse delay generator (SRS model DG535). A Hamamatsu R6835 solar blind photomultiplier tube and narrow band interference filter (121 nm, 10 nm FWHM) combination was used to detect the vacuum ultraviolet fluorescence while discriminating against scattered UV light from the photolysis and probe lasers. The probe laser was scanned across the Lyman- α spectrum to measure the linewidth, 1.2 cm^{-1} , confirming a thermal H atom translational distribution.

Some difficulty was encountered in finding appropriate conditions for the $\text{H} + \text{F}_2$ reaction. Early on, it was discovered that H_2S and F_2 could not be mixed too far upstream of the photolysis region due to a slow pre-reaction between F_2 and H_2S ($k \leq 6.4 \times 10^{-16} \text{ cm}^3 \text{ molecules}^{-1} \text{ s}^{-1}$)²⁵. This problem was manifested by a total loss of the H atom LIF signal at high $[\text{F}_2]$. To limit the consumption of $[\text{H}_2\text{S}]$, the reaction time was minimized by mixing the reagents just prior to their injection into the photolysis reactor. A second and more troublesome complication for the collection of reliable $\text{H} + \text{F}_2$ data was then discovered. For moderate to high $[\text{F}_2]$ and long delays between the photolysis and probe laser pulses, the LIF signal deviated significantly from single exponential decay. Vibrationally excited HF is produced by $\text{H} + \text{F}_2$. The bond strength of HF is $136.3 \text{ kcal mol}^{-1}$ and a single 243 nm photon can photolyze $\text{HF}(v \geq 2)$. The deviation from single exponential decay was associated with the regeneration of H atoms from probe laser photolysis of vibrationally excited HF. This problem was minimized by considering only the first 50- 100 μs of the decay curve and keeping $[\text{F}_2]$ relatively low.

Measurements for the $\text{H} + \text{Cl}_2$ system were straightforward. We did not see any evidence of a pre-reaction between H_2S and Cl_2 , and the H atom decay curves were single exponentials for all of the conditions investigated.

3. RESULTS AND DISCUSSION

3.1. $\text{H} + \text{F}_2$

A pair of representative H atom decay curves are shown in the upper panel of Figure 2. For our conditions, the slow decay in the absence of added F_2 ($\tau \sim 2700 \text{ s}^{-1}$) was dominated by diffusion out of the small volume sampled by the

probe laser. The addition of $[F_2] = 2.5 \times 10^{15}$ molecules cm^{-3} clearly increased the H atom loss rate. Within the 0 - 100 μs range the decay curves were single exponential and the rate constant was extracted by fitting the data to the expression

$$y = y_0 + Ae^{-bt} \quad [a]$$

where

$$b = k_2[F_2] + \Gamma. \quad [b]$$

and Γ is the loss rate when $[F_2]$ is not present. The baseline intensity, y_0 , was determined from the pre-photolysis pulse signal level. For the case shown in Figure 2, an exponential fit gives $b = 8927 \text{ s}^{-1}$. The decay rate vs. $[F_2]$ data are summarized in Table 1 and plotted in Figure 3. The slope of Figure 3 gives the rate constant, $k_2 = 2.4 \pm 0.4 (2\sigma) \times 10^{-12} \text{ cm}^3 \text{ molecules}^{-1} \text{ s}^{-1}$.

Table 2 summarizes the results from the 8 previous reports of k_2 . Our result compares well with the recommended value of Baulch et al.¹³ and the experimental results of Dodonov et al.¹⁵. The agreement with Homann et al.⁹ is marginal (just inside the combined error bars), and we are in poor agreement with Sung et al.²⁰, Levy and Copeland¹⁸, and Rabideau et al.¹⁹. Interestingly, Baulch et al.¹³ chose a k_2 value that lies halfway between the results of Homann et al.⁹ ($k_2(298 \text{ K}) = 1.6 \pm 0.4 \times 10^{-12} \text{ cm}^3 \text{ molecules}^{-1} \text{ s}^{-1}$) and Dodonov et al.^{7,8} ($k_2(298 \text{ K}) = 3.0 \pm 0.4 \times 10^{-12} \text{ cm}^3 \text{ molecules}^{-1} \text{ s}^{-1}$). Although Dodonov et al.'s method has been criticized for its poor definition of the reaction time and the unknown role of mixing¹⁷, the results appear to be accurate not only for the H + F_2 reaction but also for H + Cl_2 , see Table 4 and the discussion below.

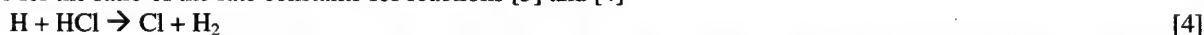
3.2. H + Cl_2

We tested the reliability of our method by applying it to the well-studied H + Cl_2 reaction. As the rate constant for H atom removal is large, this system should be less sensitive to variations in Γ , the baseline decay rate. Representative temporal profiles of the [H] dependent VUV fluorescence signal with and without added Cl_2 are shown in the upper panel of Figure 4. The addition of $[\text{Cl}_2]$ (~50 mTorr) dramatically increased the H atom decay rate and the entire time history was consistent with a single exponential decay. Clearly, the reaction does not yield products that, on photolysis by the probe laser, produce H atoms.

A sample exponential fit is shown in the lower panel of Figure 4. For the sake of comparison, a simulated curve for $k_3 = 9.6 \times 10^{-12} \text{ cm}^3 \text{ molecules}^{-1} \text{ s}^{-1}$ is also shown. Figure 5 and Table 3 summarize the conditions and results for reaction [3]. The slope of the plot in Figure 5 gives $k_3 = 2.52 \pm 0.18 (2\sigma) \times 10^{-11} \text{ cm}^3 \text{ molecules}^{-1} \text{ s}^{-1}$ and the intercept is consistent with the measured decay rate in the absence of Cl_2 .

Our result is in good agreement (i.e. within the combined error bars) with the recommended value of Baulch et al.¹³, and other previous measurements, see Table 4. The difference between Dobis and Benson's²² value and ours is outside of the combined uncertainty.

Table 4 shows that the results from previous measurements of k_3 can be roughly separated into two groups. A majority of the previous studies report $k_3 = 2 \pm 1 \times 10^{-11} \text{ cm}^3 \text{ molecules}^{-1} \text{ s}^{-1}$, while a smaller number give $k_3 \leq 1 \times 10^{-11} \text{ cm}^3 \text{ molecules}^{-1} \text{ s}^{-1}$. A more detailed examination of this second group of experiments shows that nearly all were performed under conditions where secondary reactions were important and the primary data must be carefully processed to extract k_3 . For example, the experiments of Klein and Wolfsberg²⁶ and Armstrong and co-workers^{27,28} provided estimates for the ratio of the rate constants for reactions [3] and [4]



by measuring the yield of H_2 following long-term irradiation (i.e. many minutes of reaction time) of a variety of gaseous mixtures containing HCl. Their results^{26,28} range from $k_4/k_3 = 1.07 \pm 0.15 \times 10^{-2}$ to $8.8 \pm 0.5 \times 10^{-3}$. If the Baulch et al.¹³ recommendation for k_4 is adopted ($k_4(298 \text{ K}) = 4.25 \times 10^{-14} \text{ cm}^3 \text{ molecules}^{-1} \text{ s}^{-1}$), then k_3 ranges from $4.1 \pm 0.6 \times 10^{-12}$ to $4.8 \pm 0.3 \times 10^{-12} \text{ cm}^3 \text{ molecules}^{-1} \text{ s}^{-1}$. Because of the long reaction times and the chemical complexity of the system, a complicated mechanism must be deconvoluted to extract the ratio k_4/k_3 . In addition, the role of wall reactions could not be determined and considerable error can occur if the model is not complete.

The present result is also in disagreement with the k_3 value reported by Whytock and co-workers^{29,30} ($k_3(298) = 0.7 \pm 0.22 \times 10^{-11} \text{ cm}^3 \text{ molecules}^{-1} \text{ s}^{-1}$). The accuracy of this measurement has been examined on several occasions^{22,31,32}. Most attribute the disagreement with their results to the lack of pseudo first-order conditions in Whytock's experiments and the fact that Whytock was working in an extremely difficult H atom detection regime for his electron spin resonance instrument.

The most recent measurement of k_3 by Dobis and Benson²² gives $k_3 = 0.96 \pm 0.04 \times 10^{-11} \text{ cm}^3 \text{ molecules}^{-1} \text{ s}^{-1}$. In their experiment, a phosphoric acid coated discharge tube was used to create a small $[\text{H}]$ ($\sim 10^{10} \text{ atoms cm}^{-3}$) to which Cl_2 was added. Mass spectrometry was used to monitor $[\text{Cl}_2]$, $[\text{Cl}]$, and $[\text{HCl}]$. Dobis and Benson attribute the difference between their result and the larger k_3 values listed in Table 4 to unaccounted for wall reactions that remove H atoms. The difference between our result, which is unaffected by wall effects, and Dobis and Benson's is not entirely clear. We note that Dobis & Benson's^{33,34} application of their VLPR apparatus to the $\text{Cl} + \text{HBr}$ reaction also resulted in a rate constant that was a factor of two smaller than the majority of previous results³⁵⁻³⁷.

4. SUMMARY

The $\text{H} + \text{F}_2$ and $\text{H} + \text{Cl}_2$ reactions were examined under pseudo first order conditions. Pulsed photolysis of low concentrations of H_2S was used to generate H atoms. The subsequent removal of H atoms was monitored by two-photon laser induced fluorescence. For $\text{H} + \text{Cl}_2$, simple exponential decay curves were observed, and a rate constant of $2.52 \pm 0.18 (2\sigma) \times 10^{-11} \text{ cm}^3 \text{ molecules}^{-1} \text{ s}^{-1}$ was obtained. This value was in good agreement with several earlier determinations.

Study of the reaction $\text{H} + \text{F}_2$ was complicated by the production of vibrationally excited HF, which could be photodissociated by the probe laser. Measurements were made under conditions that minimized the influence of this secondary process. The initial H atom decay rate as a function of $[\text{F}_2]$ defined a rate constant of $2.4 \pm 0.4 (2\sigma) \times 10^{-12} \text{ cm}^3 \text{ molecules}^{-1} \text{ s}^{-1}$. This result is in good agreement with the value obtained by Baulch et al.¹³ from a critical review of previous determinations. We recommend continued use of the Baulch et al.¹³ Arrhenius parameters in computational models of HF chemical lasers.

5. ACKNOWLEDGMENTS

We gratefully acknowledge support of this work by AFOSR under grant F49620-01-1-0070.

6. REFERENCES

- (1) A. Persky and H. Kornweitz, *Int. J. Chem. Kinet.* **1997**, 29, 67.
- (2) G. C. Manke II and G. D. Hager, *J. Phys. Chem. Ref. Data* **2001**, 30, 713
- (3) M. J. Berry, *J. Chem. Phys.* **1973**, 59, 6229.
- (4) D. S. Perry and J. C. Polanyi, *Chem. Phys.* **1976**, 12, 419.
- (5) F. J. Aoiz, L. Banares, B. Martinez-Haya, J. F. Castillo, D. E. Manolopoulos, K. Stark, and H. J. Werner, *J. Phys. Chem. A* **1997**, 101, 6403.
- (6) V. M. Azriel, G. D. Billing, L. Yu. Rusin, and M. B. Sevryuk, *Chem. Phys.* **1995**, 195, 243.
- (7) D. M. Neumark, A. M. Wodtke, G. N. Robinson, C. C. Hayden, and Y. T. Lee, *J. Chem. Phys.* **1985**, 82, 3045.
- (8) F. Dong, S. H. Lee, and K. Liu, *J. Chem. Phys.* **2000**, 113, 3633.
- (9) W. B. Chapman, B. W. Blackmon, and D. J. Nesbitt, *J. Chem. Phys.* **1997**, 107, 8193.
- (10) S. A. Nizkorodov, W. W. Harper, W. B. Chapman, B. W. Blackmon, and D. J. Nesbitt, *J. Chem. Phys.* **1999**, 111, 8404.
- (11) M. Faubel, L. Yu. Rusin, S. Schlemmer, F. Sondermann, U. Tappe, and J. P. Toennies, *J. Chem. Phys.* **1994**, 101, 2106.
- (12) M. Faubel, L. Yu. Rusin, S. Schlemmer, F. Sondermann, U. Tappe, and J. P. Toennies, *J. Chem. Soc. Faraday Trans.* **1993**, 89, 1475.
- (13) D. L. Baulch, J. Duxbury, S. J. Grant, and D. C. Montague, *J. Phys. Chem. Ref. Data* **1981**, 10 (Suppl. 1).
- (14) N. Cohen and K. R. Westberg, *J. Phys. Chem. Ref. Data* **1983**, 12, 531.
- (15) R. G. Albright, A. F. Dodonov, G. K. Lavrovskaya, I. I. Morosov, and V. L. Tal'roze, *J. Chem. Phys.* **1969**, 50, 3632.
- (16) A. F. Dodonov, G. K. Lavrovskaya, I. I. Morozov, R. T. Ulbright, V. L. Tal'roze, and A. K. Lyubimova, *Kinetics and Catalysis* **1970**, 11, 677.
- (17) K. H. Homann, H. Schweinfurth, and J. Warnatz, *Ber. Bunsenges. Phys. Chem.* **1977**, 81, 724.
- (18) J. B. Levy and B. K. W. Copeland, *J. Phys. Chem.* **1968**, 72, 3168.
- (19) S. W. Rabideau, H. G. Hecht, and W. B. Lewis, *J. Magn. Resonance* **1972**, 6, 384.
- (20) J. P. Sung, R. J. Malins, and D. W. Setser, *J. Phys. Chem.* **1979**, 83, 1007.
- (21) G. C. Manke II and D. W. Setser, *J. Phys. Chem. A* **2000**, 104, 11013.
- (22) O. Dobis and S. W. Benson, *J. Phys. Chem. A* **2000**, 104, 777.
- (23) W. G. Hawkins and P. L. Houston, *J. Chem. Phys.* **1980**, 73, 297.

- (24) P. A. Berg and J. J. Sloan, *J. Chem. Phys.* **1994**, *100*, 1075.
- (25) A. A. Turnipseed, and J. W. Birks, *J. Phys. Chem.* **1991**, *95*, 6569.
- (26) F. S. Klein and M. Wolfsberg, *J. Chem. Phys.* **1961**, *34*, 1494.
- (27) D. K. Jardine, N. M. Ballash, and D. A. Armstrong. *Can. J. Chem.* **1973**, *51*, 656.
- (28) D. S. Davidow, R. A. Lee, and D. A. Armstrong. *J. Chem. Phys.* **1966**, *45*, 3364.
- (29) P. F. Ambidge, J. N. Bradley, and D. A. Whytock. *J. Chem. Soc. Faraday Trans. 1* **1976**, *72*, 1157.
- (30) P. F. Ambidge, J. N. Bradley, and D. A. Whytock. *J. Chem. Soc. Faraday Trans. 1* **1976**, *72*, 2143.
- (31) P. P. Bemand and M. A. A. Clyne, *J. Chem. Soc. Faraday Trans. 2* **1977**, *73*, 394.
- (32) H. G. Wagner, U. Welzbacher, and R. Zellner. *Ber. Bunsenges. Phys. Chem.* **1976**, *80*, 902.
- (33) O. Dobis and S. W. Benson, *J. Phys. Chem. A* **1997**, *101*, 1305.
- (34) O. Dobis and S. W. Benson, *J. Phys. Chem.* **1995**, *99*, 4986.
- (35) C. C. Moore, and C. B. Moore, *J. Chem. Phys.* **1977**, *67*, 3636.
- (36) D. A. Dolson and S. R. Leone, *J. Phys. Chem.* **1987**, *91*, 3543
- (37) R. Rubin and A. Persky, *J. Chem. Phys.* **1983**, *79*, 4310.
- (38) D. H. Stedman, D. Steffenson, and H. Niki. *Chem. Phys. Lett.* **1970**, *7*, 173.
- (39) J. V. Michael and J. H. Lee, *Chem. Phys. Lett.* **1977**, *51*, 303.
- (40) S. Jaffe and M. A. A. Clyne, *J. Chem. Soc. Faraday Trans. 2* **1981**, *77*, 531.
- (41) D. Kita and D. H. Stedman, *J. Chem. Soc. Faraday Trans. 2* **1982**, *78*, 1249.
- (42) J. V. Seely, J. T. Jayne, M. J. Molina. *Int. J. Chem. Kinet.* **1993**, *25*, 571.

Table 1: Conditions and Results for H + F₂ measurements

[F ₂] 10 ¹⁵ molec cm ⁻³	H atom decay rate ^a 10 ⁵ s ⁻¹	[F ₂] 10 ¹⁵ molec cm ⁻³	H atom decay rate 10 ⁵ s ⁻¹
1.063	0.044	3.928	0.114
1.578	0.070	3.928	0.117
1.578	0.038	3.928	0.119
2.318	0.067	4.540	0.141
2.415	0.088	4.991	0.164
2.512	0.074	5.120	0.189
2.512	0.089	5.152	0.150
3.252	0.092	5.571	0.145
3.928	0.084		

^a These are the raw observed decay rates, uncorrected for the decay rate (Γ) in the absence of F₂

Table 2: Comparison of measured rate constants for H+F₂ at 298 K

Reference	k ₂ (298 K) (x 10 ⁻¹² cm ³ molecules ⁻¹ s ⁻¹)
Experiments	
Homann, et. al. ¹⁷	1.6 ± 0.4
Albright, et. al. ^{15,16}	3.0 ± 0.4
Sung, et. al. ²⁰	1.0 ^a
Levy & Copeland ¹⁸	1.0 ± 0.15 ^b
Rabideau, et. al. ¹⁹	4.2 ± 0.3
This work	2.4 ± 0.4
Reviews	
Cohen & Westberg ¹⁴	1.5 ^c
Baulch, et. al. ¹³	2.5 ^c

^a authors reported k₂ / k₃ = 0.053, absolute value calculated using k₃ = 1.9 x 10⁻¹¹ from ref. 13. ^b authors reported k₂ / k(H+O₂+M)[M] = 4.6 ± 0.7, absolute value calculated using k(H+O₂+M)[M] from ref. 13. ^c recommendation based on literature review.

Table 3: Conditions and Results for H + Cl₂ measurements^a

¹⁰ ¹⁵ [Cl ₂] molec cm ⁻³	Fluorescence decay rate 10 ⁵ s ⁻¹	¹⁰ ¹⁵ [Cl ₂] molec cm ⁻³	Fluorescence decay rate 10 ⁵ s ⁻¹
0.74	0.32	4.81	1.27
1.66	0.40	5.02	1.11
1.66	0.50	5.23	1.56
1.98	0.56	5.47	1.53
2.11	0.60	5.55	1.67
2.11	0.64	5.59	1.50
2.13	0.59	6.44	1.83
2.29	0.79	6.50	1.77
2.83	0.71	7.12	2.06
2.83	0.88	7.28	1.74
3.22	0.90	7.53	1.56
3.27	0.89	7.63	1.98
3.75	0.64	8.60	2.47
4.06	1.28	8.63	2.22
4.31	1.32	9.05	2.34
4.35	1.15	10.55	2.79
4.73	0.87		

^a These are the raw observed decay rates, uncorrected for the decay rate (Γ) in the absence of Cl₂

Table 4: Comparison of measured rate constants for H+Cl₂ at 298 K

Reference	k ₃ (298 K) (10 ⁻¹¹ cm ³ molecules ⁻¹ s ⁻¹)
Klein & Wolfsberg ²⁶	0.46 ± 0.19 ^{a,b}
Davidow, Lee, & Armstrong ²⁸	0.49 ± 0.03 ^{b,c}
Jardine, Ballash, & Armstrong ²⁷	0.43 ± 0.04 ^{b,d}
Ambidge, Bradley, & Whytock ²⁹	0.70 ± 0.14
Dobis & Benson ²²	0.96 ± 0.04
Dodonov, et. al. ^{15,16}	2.97 ± 0.89
Stedman, Steffenson, and Niki ³⁸	3.5 ± 1.2
Wagner, Welzbacher and Zellner ^{9,32}	1.91 ± 0.25
Bemand & Clyne ³¹	2.19 ± 0.32
Michael & Lee ³⁹	1.6 ± 0.1
Jaffe and Clyne ⁴⁰	2.13 ± 0.78
Kita and Stedman ⁴¹	1.7 ± 0.26
Seeley, Jayne, and Molina ⁴²	1.8 ± 0.5 ^c
This work	2.52 ± 0.18

^a authors reported k₄ / k₃ = 0.143 ± 0.033 exp(-(1540 ± 130)/RT).

^b k₃(298 K) calculated from k₄(298 K)¹³ = 4.25 × 10⁻¹⁴ cm³ molecules⁻¹ s⁻¹.

^c authors reported k₄ / k₃ = 0.0088 ± 0.0005 at 298 K.

^d authors reported k₄ / k₃ = 0.01 ± 0.001 at 298 K.

^e authors do not give a numerical result, value in table is estimated from Figure 16 of reference 42.

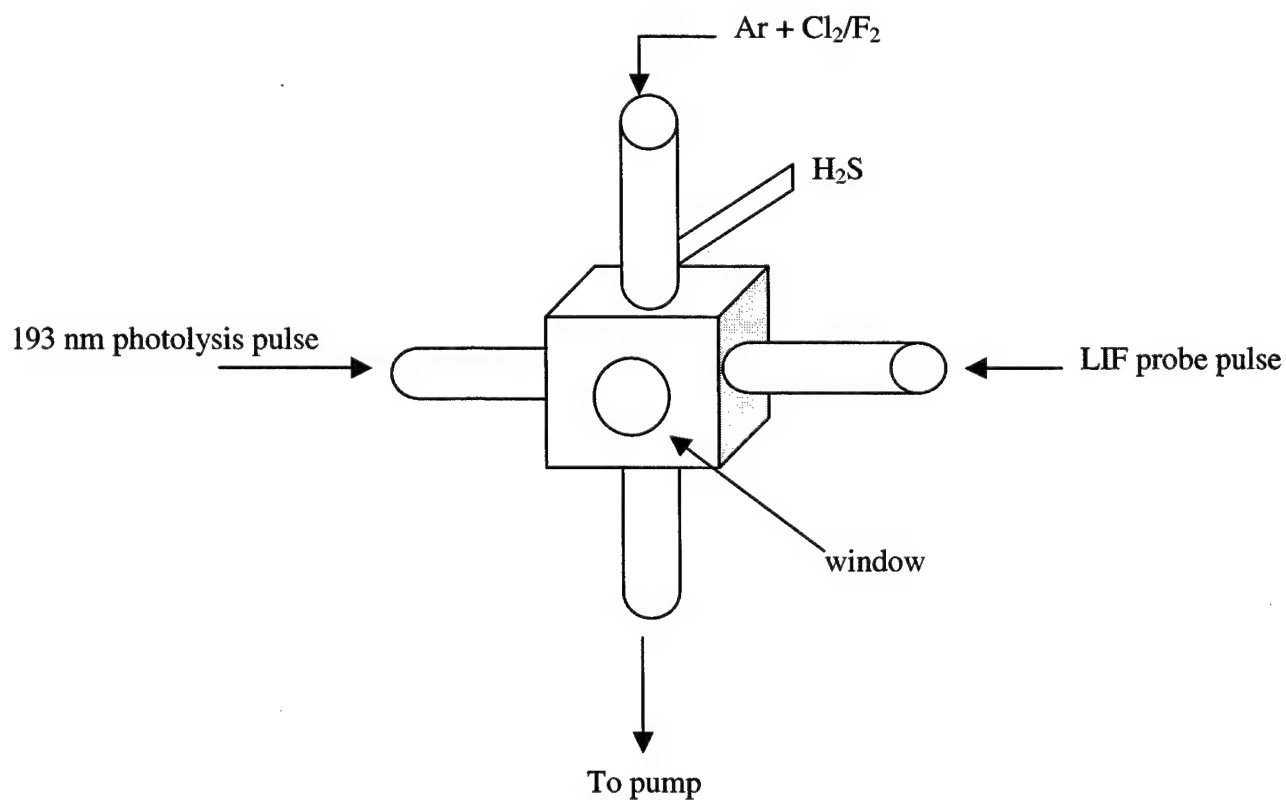


Figure 1. Schematic diagram of the experimental apparatus. The reaction between hydrogen atoms and molecular F₂ or Cl₂ was pulse initiated by 193 photolysis of a H₂S/Cl₂(F₂)/Ar mixture. The time history of the H atoms was monitored by laser induced fluorescence of the Lyman- α transition.

Figure 2. Representative $\text{H} + \text{F}_2$ data is shown. The slow decay in the absence of F_2 in the upper panel is attributed to diffusion and H atom loss via reactions with photoproducts. The lower panel demonstrates the quality of the fit to a single exponential decay. The best least squares fit gives $k_2 = 2.47 \pm 0.11 \text{ cm}^3 \text{ molecules}^{-1} \text{ s}^{-1}$. For the sake of comparison, the background-corrected decay curve for $k_2 = 1.0 \times 10^{-12} \text{ cm}^3 \text{ molecules}^{-1} \text{ s}^{-1}$ is shown.

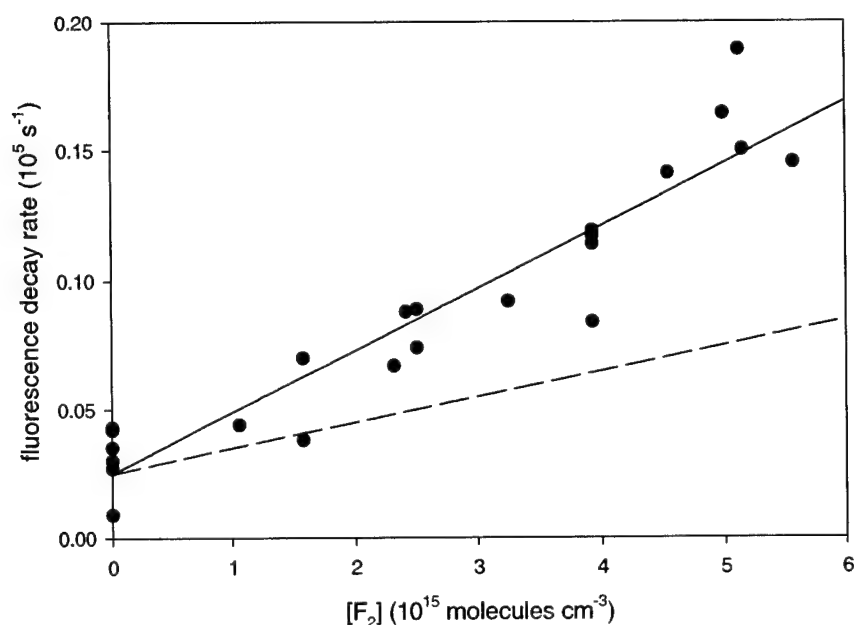
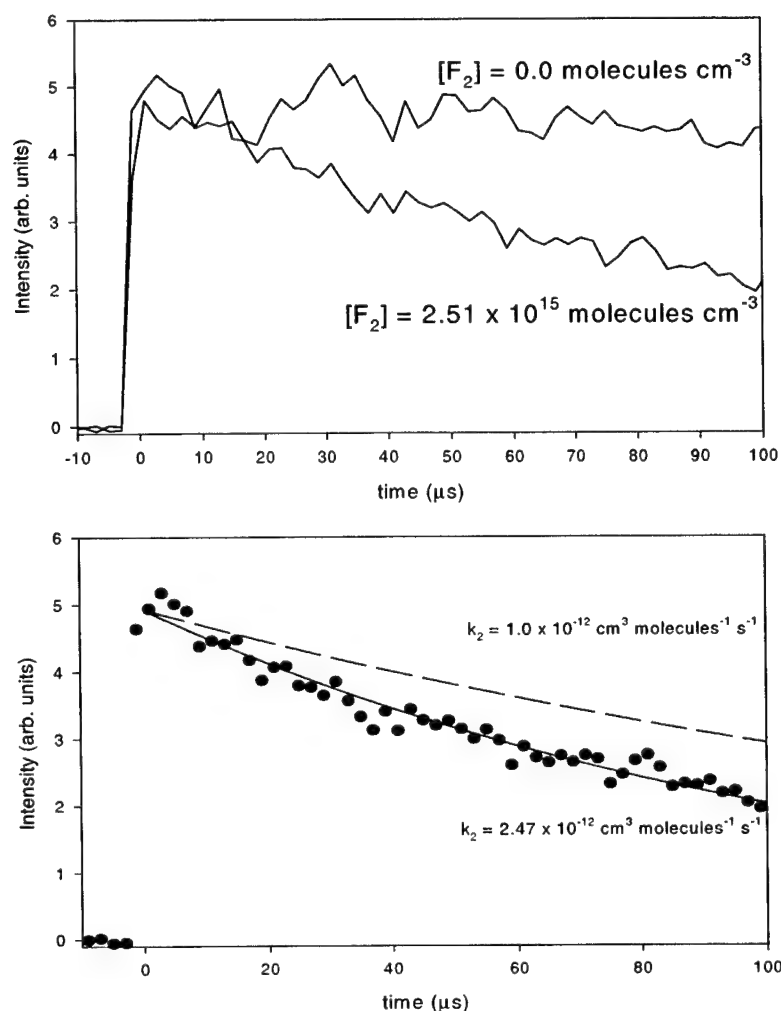


Figure 3. H atom decay rate vs. $[\text{F}_2]$. The rate constant for reaction [2] is given by the slope, $k_2 = 2.4 \pm 0.4 (2\sigma) \times 10^{-12} \text{ cm}^3 \text{ molecules}^{-1} \text{ s}^{-1}$. This result agrees with the previous measurements by Dodonov and co-workers^{15,16} and the recommended value of Baulch, et. al.¹³. The broken line represents $k_2 = 1.0 \times 10^{-12} \text{ cm}^3 \text{ molecules}^{-1} \text{ s}^{-1}$.

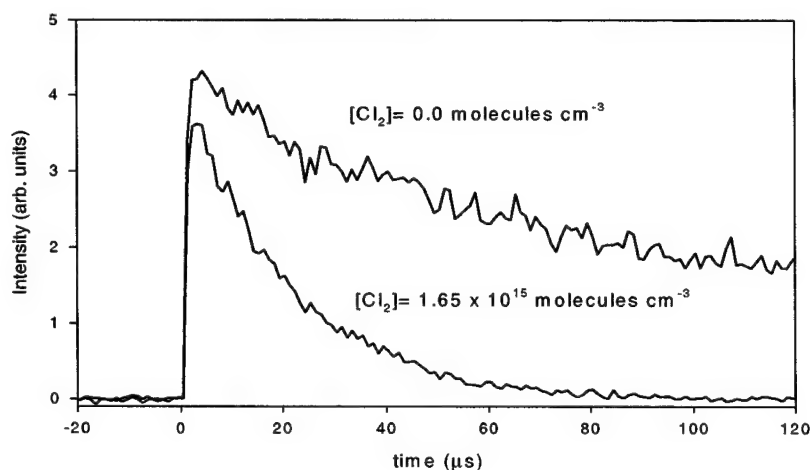


Figure 4. Representative H + Cl₂ data is shown. The slow decay in the absence of Cl₂ in the upper panel is attributed mainly to diffusion out of the observation zone with a minor amount of H atom loss via reactions with photoproducts. The lower panel demonstrates the quality of the fit to a single exponential decay. The corresponding rate constant is $2.47 \pm 0.04 \text{ cm}^3 \text{ molecules}^{-1} \text{ s}^{-1}$.

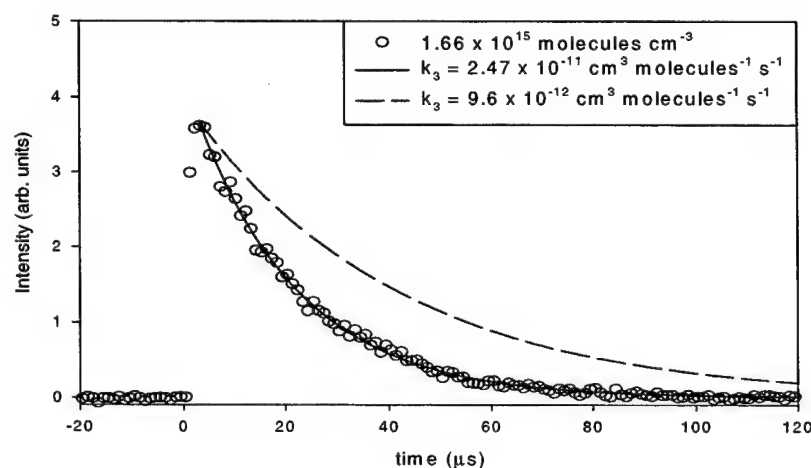
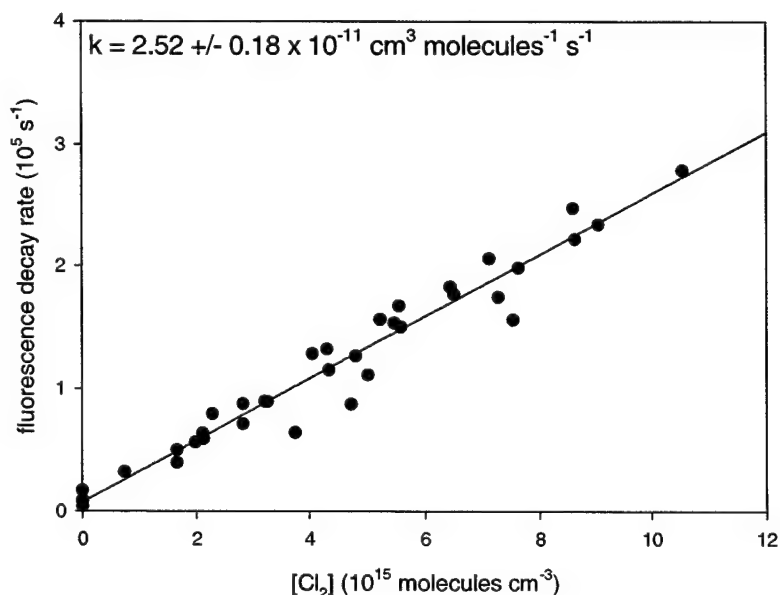


Figure 5 H atom decay rate vs. [Cl₂]. The rate constant for reaction [3] is given by the slope, $k_3 = 2.52 \pm 0.18 (2\sigma) \times 10^{-11} \text{ cm}^3 \text{ molecules}^{-1} \text{ s}^{-1}$. This result agrees with many previous measurements and the recommended value of Baulch, et. al.¹. Our result does not agree with the recent result of Dobis and Benson²², who reported $k_3 = 0.96 \pm 0.04 \times 10^{-12} \text{ cm}^3 \text{ molecules}^{-1} \text{ s}^{-1}$.



Study on IR and UV - lasers interaction with metal surfaces

Victor F. Tarasenko*, Sergey B. Alekseev, Andrey V. Fedenev, Igor' M. Goncharenko,
Nikolay N. Koval', Konstantin V. Oskomov, Victor M. Orlovskii,
Nikolay S. Sochugov, Mikhail A. Shulepov

High Current Electronics Institute, Siberian Division of the Russian Academy of Sciences
(HCEI SB RAS)

ABSTRACT

The complex of experimental installations for studying of laser radiation interaction with surface of metals has been established. At titanium surface irradiating depending on the accumulated laser radiation energy, the surface color might be changed from bright yellow to red and deep-blue colors. The presented results testify to the possibility to use the change of titanium surface color at heating by laser irradiation in the open air to obtain dot raster images (even colored ones). Presently, from the world data available on interaction of laser radiation with metal and dielectric surfaces and development of experimental diagnostics techniques by itself it is allowed to raise a reverse question, i.e., restoration of laser radiation energy spatial distribution through surface imprint. Using imprints, it is also possible to make an express diagnostics of multi-layer surface coatings. With this in mind, we have made the detailed morphology of imprint of the pulsed HF-laser interaction with carbon steel surface through atomic force microscope.

Keywords: titanium oxide, laser treatment, laser interaction with surface

1. INTRODUCTION

The harnessing of laser irradiation for surface treatment has been practically made at once as the first lasers were developed. Both the gas discharge IR lasers on CO₂ molecule transitions and solid-state Nd:YAG lasers have gained major application in this field¹. CO₂-based laser with high efficiency and specific output parameters has a comparatively big wavelength and limited gas mixture lifetime. The Nd:YAG laser also has a high efficiency and it provides operation both in continuous and pulsed repetition modes (up to 100 kHz), but active medium scaling is rather poor. In this paper, preliminary results on lasers interaction with metal surfaces for recently developed lasers, i.e. non-chain gas discharge HF laser and Xe laser pumped by e-beam preionized electric discharge are presented. As objects for study, thin titanium foils and carbon steel samples (0.4% C, 0.8 – 1.0 % Cr, 4140(USA)) were taken.

Titanium oxide coatings attract particular interest in a row of applications such as optical coatings, decorative coatings, catalysts, medical implantates and gas sensors. A good technique to produce such coatings is laser irradiation of metallic titanium surface in reactive atmosphere². As it is presented by authors², at titanium plate surface melting depending on the accumulated laser radiation energy, the surface color might be changed from bright yellow to red and deep-blue colors. In the paper², the data on titanium surface oxidation in atmospheric pressure air at pulsed Nd:YAG lasing are presented. The laser operated at the wavelength of 1,064 nm, average radiation output of 60 W at 30 kHz. Several samples were treated by accumulation of different laser pulses per unit of square. The experiments were carried out at accumulated laser energy from 54 up to 294 J/cm². The characteristics of the treated samples and different colors appeared were studied using various measurement techniques. Morphology analysis by scanning electron microscopy has revealed that melting and second solidification occurs during laser beam action in the whole range of exposure values. Moreover, at more high values of the accumulated fluxes the craters are forming. Measurements of spectral reflection allowed to determine chromatic coordinates corresponding to different

* VFT@loi.hcei.tsc.ru; phone: (+7 382-2) 258685; fax: (+7 382-2) 259410; http:// www.hcei.tsc.ru; High Current Electronics Institute, 4, Akademicheskoy Ave., Tomsk 634055, Russia

colors observed on the samples. X-ray diffractometry has shown that at low exposure values no oxidation occurs but crystallites orientation change to the characteristic of powders distribution takes place. Diffractograms at higher accumulated fluences reveal the formation of basically Ti_2O and TiO crystalline phases among the oxides, which show a monotonic increase in their content with increase of irradiation rate. Other phases such as TiO_2 either in rutile or anatase crystalline structures, or Ti_2O_3 were identified through Raman spectroscopy. The low Raman signal levels and absence of those phases in most of the diffractograms points to that their contents is essentially smaller than that of Ti_2O and TiO . Besides that, the change of signal levels as a function of the accumulated laser fluence is non-monotone. The comparison of the compositional analyses with color distribution observed shows that there is some correlation between the onset of the different colors and changes in the composition of samples².

The above presented results testify to the possibility to use the change of titanium surface color at heating by laser irradiation in the open air to obtain dot raster images (even colored ones). For this, as an image carrier either a thin titanium layer (silver color) or titanium dioxide (white) at the paper surface can be used. From this reasoning, we have carried out experiments on determination of color change conditions for thin titanium foils irradiated by pulsed IR laser.

Presently, from the world data available on interaction of laser radiation with metal and dielectric surfaces and development of experimental diagnostics techniques by itself it is allowed to raise a reverse question, i.e., restoration of laser radiation energy spatial distribution through surface imprint. Using imprints, it is also possible to make an express diagnostics of multi-layer surface coatings. With this in mind, we have made the detailed morphology of imprint of the pulsed HF-laser interaction with carbon steel surface through atomic force microscope.

2. EXPERIMENTAL EQUIPMENT AND TECHNIQUES

Based on the developed at the HCEI e-beam accelerators and powerful electrical schemes, a succession of lasers based on high pressure gases was created³⁻⁸. For the experiments on laser radiation interaction with matter from the point of view of high power, high energy and high efficiency, the XeCl^* , CO_2 and HF molecules based lasers and lasers on atomic transitions of Xe were chosen. Radially convergent and planar e-beam based accelerators and set-ups with self-sustained discharge and e-beam-initiated discharge were used as excitation sources. Maximal radiation output energy in UV spectral range of up to 2 kJ has been obtained at $\lambda=308$ nm for 600-l e-beam pumped XeCl -laser^{6,7}. Using the same experimental set-up but with Ar-Xe ($\lambda=1.73$ μm) and He-Ar-Xe ($\lambda=2.03$ μm) mixtures, the output lasing as 100 and 50 J, correspondingly, has been achieved. Laser radiation output energy of 110 J at $\lambda=308$ nm and of 90 J at $\lambda=249$ nm were demonstrated using the set-up with a radially convergent e-beam and active volume of 30 liters and laser radiation aperture of 20 cm^3 . Choice of radially convergent e-beam pumping appeared to be successful for excitation of non-chain HF laser. The output energy of generation up to 200 J with efficiency up to 10 % in reference to the loaded into the gas e-beam energy has been obtained at the HF molecule transition at $\lambda \sim 2.8$ μm ^{3,4}. The average output laser radiation up to 1 kW was realized using CO_2 – laser pumped by e-beam preionized discharge at pulsed repetition rate (p.r.r.) of 50 Hz⁷. The use of inductive energy storage for pumping of non-chain discharge HF laser allowed to obtain lasing with the efficiency up to 5.5 % in reference to the input energy in gas, and use of zeolite absorber allowed to increase the gas mixture lifetime up to 1000 pulses^{7,8}. Use of the generator based on inductive energy storage in order to form a prepulse in the gas discharge XeCl laser allowed to form a high homogeneity discharge and to increase duration of oscillation up to 450 ns at output energy up to 1.1 J and total efficiency of 2.2 %. The main parameters of the experimental laser set-ups are presented in the Table 1.

In our experiments we used two laser set-ups. The set-up № 1 was based on the e-beam preionized discharge laser⁷. Active gas volume of 72.3-2.4 cm^3 was bounded by a copper electrode and a steel mesh protecting the electron accelerator exit foil window. The e-beam parameters were as follows: duration of 4 ns, total current behind the foil of 6 kA, and average energy of electrons behind the foil was of ~ 150 keV. The bank of capacitors with total capacitance of 0.2 μF was situated directly in the gas chamber being charged up to 10-12 kV. The resonator consisted of a flat mirror with aluminum coating and a parallel-plane plate KRS-5 as output window. The parallel-plane resonator provided laser radiation divergence of about 1,6 mrad. Water cooling systems of the output foil window and operating mixture circulation at flow velocity of about 10 m/s allowed operation at p.r.r. of up to 50 Hz. The mixture Ar:Xe=100:1 at pressure of 1 atm was used. The main part of laser energy was radiated at $\lambda = 1.73$ μm .

The laser provided an impulse energy as 10-15 mJ at duration ~ 320 ns and average power of 70 and 300 mW at p.r.r. of 10 and 25 Hz, correspondingly.

As the second set-up we used HF discharge non-chain chemical laser^{5,8}. The active volume was $60.2.3.1 \text{ cm}^3$ pumped through the two-circuit scheme preionized by the surface discharge from under the mesh which is one of the electrodes. The bank of capacitors with total capacitance of 64 nF charged up to 40 kV was the main storage, with this the peaking capacitor was 23 nF. The laser resonator consisted of a flat steel mirror and a parallel-plane plate either KRS-5 or CaF_2 as an output window. Laser pulse energy was of 1.5 – 2.0 J at pulse duration of ~ 350 ns. HF-laser could also be operated in a pulsed repetition mode with frequency of up to 5 Hz. Zeolite used as an absorbent for HF molecules produced in discharge allowed to achieve stable energy parameters of laser pulses with decrease for 10-15% at 10^3 turns on at 1-2 Hz.

Laser radiation energy and average power were measured by a calorimeter IMO-2N and pyroelectric sensor PE-25 (OPHIR Opt.) calibrated in the measured optical range with an accuracy of 5%.

In order to investigate the irradiated surface we used optical microscopes of MBS-10 type (maximal magnification is 100x) and MMR-4 type (maximal magnification is 1300x). For morphology analysis of the samples a scanning probe microscope "Solver P47" (produced by NT-MDT, Russia) was used. Relief imaging of the surface was obtained in the mode of contacting atomic-force microscopy. The probe force affected the sample was equal to $1.7 \cdot 10^{-7} \text{ N}$, and the curvature radius of the probe was about 10 nm. The sample was continuously scanned along X-axis with a velocity of $4.77 \cdot 10^{-4} \text{ m/s}$ and moved discretely along the Y-axis with frequency of 2 Hz and lead of $4.751 \cdot 10^{-8} \text{ m}$.

3. INTERACTION OF IR RADIATION WITH TITANIUM FOIL SURFACE

In the experiments the titanium foils of 8, 13 and 50 μm in thickness were used. Focusing was realized using the lens made of BaF ($F=123 \text{ mm}$), the diameter of the focal spot made about 300 μm . In the pulsed repetition mode (pulse frequency was 25 Hz, average laser power was 250 mW) the thin foils of 8 and 13 μm in width had been destroyed in about 5 s (accumulated energy density was $q = 1,063 \cdot 10^3 \text{ J/cm}^2$) or 300 pulses in a single mode ($q = 1,786 \cdot 10^3 \text{ J/cm}^2$) and 4 min ($q = 51.02 \cdot 10^3 \text{ J/cm}^2$), correspondingly. The rupture occurred in the area of the maximal energy of the focal spot due to titanium foil heating up to temperatures enough for plastic deformation and foil break-through, obviously, due to laser plasma pressure in the pulse-repetition mode. With this, the foil broken edges turned around away from the laser radiation. The more thick foil of 50 μm had not been heating up downward totally and it was destroyed. Such a mechanism of the foil break-through can explain reasons for absence of effect at low-frequency operation in the case of using the foil of 13 μm in thickness and in the case of 50 μm -foil. At low-frequency operation (p.r.r. was $\leq 1 \text{ Hz}$) the impulse energy within the time between pulses had been dissipated (re-emission, heat conduction) and the foil was not heated up to the temperature needed.

The surfaces of all the samples at change of accumulated laser energy due to exposure time and p.r.r. variation were observed to change color. Figure 1 presents photos of the titanium foil surface at different irradiation regimes. With not high energies accumulated by titanium foil surfaces (both in single mode and at not high p.r.r.) the foil surface remelting occurs. In certain conditions (50 mW output power, 25 Hz, 4 min, 50 μm -foil), after cooling the remelt surface was observed as cracked areas that points to the fact that internal stress forces occurred in the foil. With increasing of accumulated energy ($q = 2,125 \cdot 10^3 \text{ J/cm}^2$ at 25 Hz, or $q = 1,45 \cdot 10^3 \text{ J/cm}^2$ at 10 Hz), Fig. 1(a,d), the surface of the titanium 13 μm -foil becomes yellow. Further increase of energy value ($q = 4,25 \cdot 10^3 \text{ J/cm}^2$ at 25 Hz and $q = 1,78 \cdot 10^3 \text{ J/cm}^2$ at 10 Hz) brought to color change from yellow to dark-blue in the imprint center, Fig. 1,(b,e). And lastly, at accumulated energy of $q = 6,38 \cdot 10^3 \text{ J/cm}^2$ the whole imprint surface gains dark-blue color, Fig. 1(c,f). The basic data are presented in the Tab.2. Here the data on oxide film composition obtained by A. Perez del Pino, et al.² are also shown.

For comparison purposes, an experiment on UV laser radiation effect on titanium foil of 50 μm in thickness was made. A discharge exciplex laser "Foton"⁷ with the wavelength of 222 nm (KrCl), pulse duration of 20 ns and pulse energy of 35 mJ was taken. In some experiments the energy of lasing decreases up to 3 mJ due to using a

diaphragm. The laser could operate in a single pulse regime or at p.r.r. of 1 Hz. The radiation focusing was realized using quartz lens with focal distance of 10 cm. In those regimes tried (single pulse regime, pulsed repetition regime with frequency of 1 Hz) there was a crater followed after on the titanium foil surface with melt bottom of the silver color. At multiple irradiation (over 5 pulses) there the bands of yellow-orange and blue colors appeared around the crater. The melt surface of the crater represented by itself a wavy structure, most clearly expressed at multiple laser action (10-15 pulses). The colored bands around the crater are probably determined by deposition of titanium oxides, having been evaporated by laser radiation from the crater and reacted with oxygen from air. It must be noted that those colored bands repeated in shape the areas radiated by the part of UV radiation with greater divergence.

4. TOPOLOGY OF STEEL SURFACE AFTER INTERACTION WITH POWERFUL IR LASER RADIATION

The carbon steel sample 4140 was placed in the focal plane of lens ($F = 123$ mm). After irradiation by 10 pulses from HF-laser (p.r.r. is 0.5 Hz) a crater with the area of 1×0.5 mm² formed on the steel surface (see Fig. 2). Figure 2 also presents the photos made using optical microscope of the 5 separate crater zones differed in surface topology. Surfaces of the far zones № 4 and 5 represent by itself solidified metal splashes carried away from the central zones melt by laser irradiation. The splashes are directed outward the center of crater, their sizes being decreased as moving away from the center. Measurements were carried out by reweighing of the sample, which had many not overlapping single pulse imprints. It was shown that within a single laser impulse about $4 \cdot 10^{-4}$ g/cm² of metal was removed from the sample surface. Zones №2 and 3 are situated closer to the crater center and present by itself the areas of solidified metal with wavy surface. Figure 3(a,b) shows the scanning results obtained in those areas using atomic force microscope. Heights of irregularities (waves and drops of solidified metal) in zone №3 made up to 650 nm that is the most high value for all the crater areas. There are separate drops seen which have transversal sizes of 2–3 μ m. In zone №2, irregularities height does not exceed 250–300 nm and separate drops are practically absent. Besides, on the image obtained by scanning the surface in zone №2 using atomic force microscope there is a fine grain structure, see Fig. 3(b). Transversal sizes of grains are 400–800 nm, they vary above the metal surface by 15–30 nm. In the central crater zone, i.e. zone №1, irregularities also do not exceed the height of 300 nm and the grain structure is observed. Differed from zone №2, these grains are somewhat smaller in size (transversal size is 200–500 nm, the height above the surface is 10-15 nm). Big grains are also observed, see Fig. 3(c). Figure 4 presents a surface profilogramme of zone №1 showing a part of coarse grains. Height of the coarse grain decreases from the center to edges for about 40 nm overlaying metal surface totally for 100–120 nm. Cross-section size of such a coarse grain is well seen in Fig. 4 (zone №1) and makes 50 – 60 μ m.

5. DISCUSSION AND CONCLUSION

While comparing our results obtained for thin foils with experimental results obtained for 1-mm width plates², the following conclusions may be done. Effect of titanium surface modification is determined by temperature and is dependent on supply heating rate and the heat dissipation rate of the sample. The values of the specific laser energy accumulated by surface at which modification occurs in our experiments exceed by several orders the values reported by A. Perez del Pino, et al.². It may be explained that in the experiments², at high p.r.r. (30 kHz) the surface temperature becomes increased with each following impulse, and though the major thickness of the sample as compared with foil provides a high heat removal rate, the heating up occurs more efficiently. Other fact was that the reflection factor of laser radiation by the metal surface becomes lower with increase of temperature of the sample. Moreover, in our experiments, the laser radiation pulse energy exceeded the value taken by A. Perez del Pino, et al. by 3-5 factors that led to much higher absorption of laser radiation in the plume of laser plasma and evaporated target matter.

In order to produce colored oxide film on a thin titanium foil through one laser radiation impulse we need to have longer pulse duration, such as, to have (at energy enough) the surface heating up to necessary temperatures and keeping such temperature within a certain time needed for chemical reactions to take place. For determination optimal parameters of laser impulse it is necessary to carry out additional experiments and calculations.

Surface structure formation in zone №2 occurs following two mechanisms: 1) melting and solidification of the metal resided in the given zone directly; 2) cooling and solidification of the metal removed under influence of hydrodynamic forces from zone №1 due to intensive boiling. In distinction to zones №3 and №4, where the melt metal removed out the crater center is being cooled down at a comparatively cold surface, in zone №2 the initial surface temperature and evaporated metal correlate, owing to which much slower metal cooling down occurs resulting in fine grained structure formation. The similar fine-grained structures identified as grains of γ -iron were obtained at carbon steel surface melting by pulsed high-energy electron beam⁹. In zone №1, the surface temperature during a laser radiation pulse is the highest one and the main processes occurred are intensive boiling and metal evaporation. In this case an initial ferropearlite structure develops with a characteristic morphology of solidification for each phase. It is supposed that the large smooth grain in the Fig. 2(a) is a ferrite one. There are other pearlite grains possessing typical fine-grained structure resided around it.

A more accurate identification of the structures formed on the carbon steel surface affected by laser radiation pulse demand further additional experiments.

ACKNOWLEDGEMENTS

The work has been fulfilled being supported by ISTC, the Project No 1206.

REFERENCES

1. V.S. Kovalenko, *Lazernaja tekhnika i tekhnologija*. – K.: Vishcha shkola. Golovnoje izdatel'stvo, 280 p., 1989 (in Russian).
2. A. Perez del Pino, P. Serra, J.L. Morenza, "Oxidation of titanium through Nd:YAG laser irradiation", *Abstracts of the 6-th Intern. Conf. on Laser Ablation COLA'01*, October 1-5, 2001, Tsukuba, Japan, p. 228.
3. E.N. Abdullin, A.M. Efremov, B.M. Koval'chuk, V.M. Orlovskii, A.N. Panchenko, V.V. Ryzhov, E.A. Sosnin, V.F. Tarasenko, I.Yu. Turchanovskii, "Laser based on an SF₆-H₂ mixture pumped by a radially converging electron beam", *Quantum Electronics*, **24**, №9, pp. 761-765, 1997.
4. E.N. Abdullin, A.M. Efremov, B.M. Koval'chuk, V.M. Orlovskii, A.N. Panchenko, E.A. Sosnin, V.F. Tarasenko, A.V. Fedenev, "Powerful HF laser pumped by e-beam initiated non-chain chemical reaction", *Pis'ma v JTF*, **23**, № 5, pp.58-64, 1997 (in Russian).
5. V.F. Tarasenko, S.B. Alekseev, M.V. Erofeev, V.M. Orlovskii, *Proc. of the Int. Conf. LASERS 2000*, Ed. By V.J. Corcoran and T.A. Corcoran, STS Press, McLean, VA, pp.317-322, 2001.
6. E.N. Abdullin, S.P. Bugaev, A.M. Efremov, V.B. Zorin, B.M. Koval'chuk, V.V. Kremnev, S.V. Loginov, G.A. Mesyats, V.S. Tolkachev, P.M. Shanin, "Electron accelerators based on Marx generator with vacuum insulation", *Pribori i Tekhnika Eksperimenta*, № 5, pp.138-141, 1993 (in Russian).
7. V.F. Tarasenko, E.H. Baksht, A.V. Fedenev, V.M. Orlovskii, A.N. Panchenko, V.S. Skakun, E.A. Sosnin, "Ultraviolet and infrared lasers with high efficiency", *Proc. of the Int. Conf. High Power Laser Ablation, SPIE Vol. 3343*, pp.715-724, 1998.
8. V.F. Tarasenko, S.B. Alekseev, M.V. Erofeev, V.M. Orlovskii, "Electrodischarge HF-lasers on H₂-SF₆ mixture", *Proc. of the Intern. Conf. LASERS-2000*, Albuquerque, New Mexico, Dec. 4-8, 2000, STS Press, McLEAN, VA, pp. 317-323, 2001.
9. V.B. Markov, V.P. Rotshtein, "Thermal and strain-wave mechanism of hardening of carbon steel at effect of high-energy high-current e-beam", *Fizika i Khimija Obrabotki Materialov*, **6**, pp. 37-41, 1997 (in Russian).

Table 1. Characteristics of laser set-ups.

Set-ups	Pumping technique, Active medium, P.r.r.	Transitions, Wavelengths, Gas mixture, pressure	Pulse duration, Energy, Efficiency	Notes
"DM"	Electron beam, $j = 40 \text{ A/cm}^2$, 600 l, aperture $D = 60 \text{ cm}$ single pulse regime	XeCl, 308 nm, Ar-Xe-HCl, $p=2.5 \text{ atm}$	300 ns, 2000 J,	[6], [7]
		Xe, 1.73 μm , 2.03 μm , Ar-Xe, He-Ar-Xe	300 ns, 100 J, 50 J, 1-2 %	[7]
"Coaxial"	Electron beam, $I = 5 - 500 \text{ A}$, 200 kV 20 l, aperture $D = 20 \text{ cm}$ 0.1 – 50 Hz	Xe, 1.73 μm , 2.03 μm , Ar-Xe, He-Ar-Xe $p = 1.0 - 1.5 \text{ atm}$	10 – 1000 μs 6 J, 2 %	Water cooling of the foil [7]
"ELON - 1M"	Electron beam, $j = 40 \text{ A/cm}^2$, 30 liters, aperture $D = 20 \text{ cm}$ single pulse regime	XeCl, 308 nm, Ar-Xe-HCl, $p=2.5 \text{ atm}$	300 ns, 110 J, 5.5 %	[7]
		Xe, 1.73 μm , 2.03 μm , Ar-Xe, He-Ar-Xe	700 ns, 16 J, ~ 2 %	
		HF, (non-chain) ~ 2.8-3 μm , SF ₆ -H ₂	700 ns, 200 J, 11 %	[3,4]
"Cascade"	E-beam initiated discharge, 72x3x2.4 cm ³ , 0.1 – 50 Hz	CO ₂ , 10.6 μm , N ₂ -CO ₂ -H ₂	50 ns – 8 μm , 30 J, 1 kW	Gas cooling and circulation system [7]
"LIDA-T"	Discharge, 3.5x1.5x60 cm ³ , 5 Hz	XeCl, 308 nm, Ar-Xe-HCl, $p=2.0 \text{ atm}$	100-450 ns, 0.2 – 1.0 J,	Inductive energy storage generator [7]
		HF, (non-chain) ~ 2.8-3 μm , SF ₆ -H ₂	350 ns, 2 J, 2.9 %	[5,8]

Table 2. Characteristics of titanium foil surface modification (foil thickness is 13 μm) with dependence on the laser radiation energy accumulated at different regimes. Composition of oxide coatings was taken from [2] for similar experimental conditions.

Surface modification	P.r.r.	Time of treatment	Laser radiation energy accumulated, J/cm ²	Composition of the surface coating [2]	Notes
Remelting	10 Hz	10 s	~ 0,6·10 ³	Crystallites orientation similar to that of powders	On treatment at low average power the surface is being cracked
Remelting	1 Hz	10 pulses	~ 0,059·10 ³	The same	
Yellow color	10 Hz	20 s	1,45·10 ³		Probably due to titanium nitride
Reddish-yellow color	25 Hz	10 s	2,13·10 ³	a-Ti ₂ O ₃ + TiO ₂ (rutile)	
Appearance of dark blue color traces	10 Hz	30 s	1,78·10 ³	a-Ti ₂ O ₃ + TiO ₂ (rutile)	In the spot center against a background of yellow
Appearance of dark blue color	25 Hz	20 s	4,25·10 ³	a-Ti ₂ O ₃ + TiO ₂ (rutile)	In the spot center against a background of yellow
Dark blue color	25 Hz	30 s	6,38·10 ³	c-Ti ₂ O ₃ + TiO ₂ (rutile)	The spot is uniform in color
Hole break-through	25 Hz	4 min	51.02·10 ³		Edges of hole are melt and forced apart

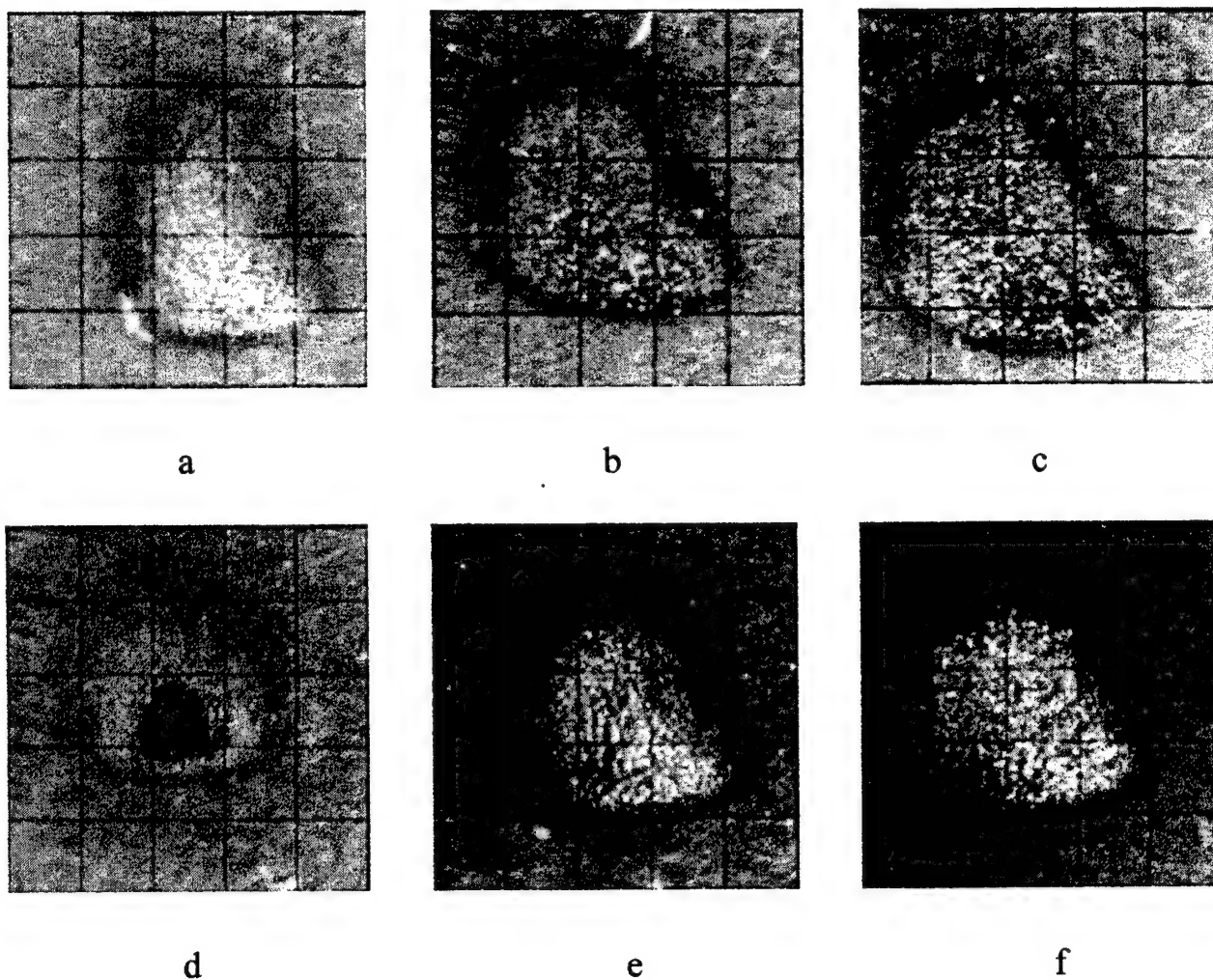


Fig.1. Photo of the titanium foil surface (thickness of foil is 13 μm) after irradiation by Ar-Xe laser. (a,b,c) – an average power of 250 mW at p.r.r. of 25 Hz, (d,e,f) – an average power of 70 mW at p.r.r. of 10 Hz. Time of treatment is 10 s (a,d), 20 s (b,e), 30 s (c,f). The side of the grid square is equal to 140 μm .

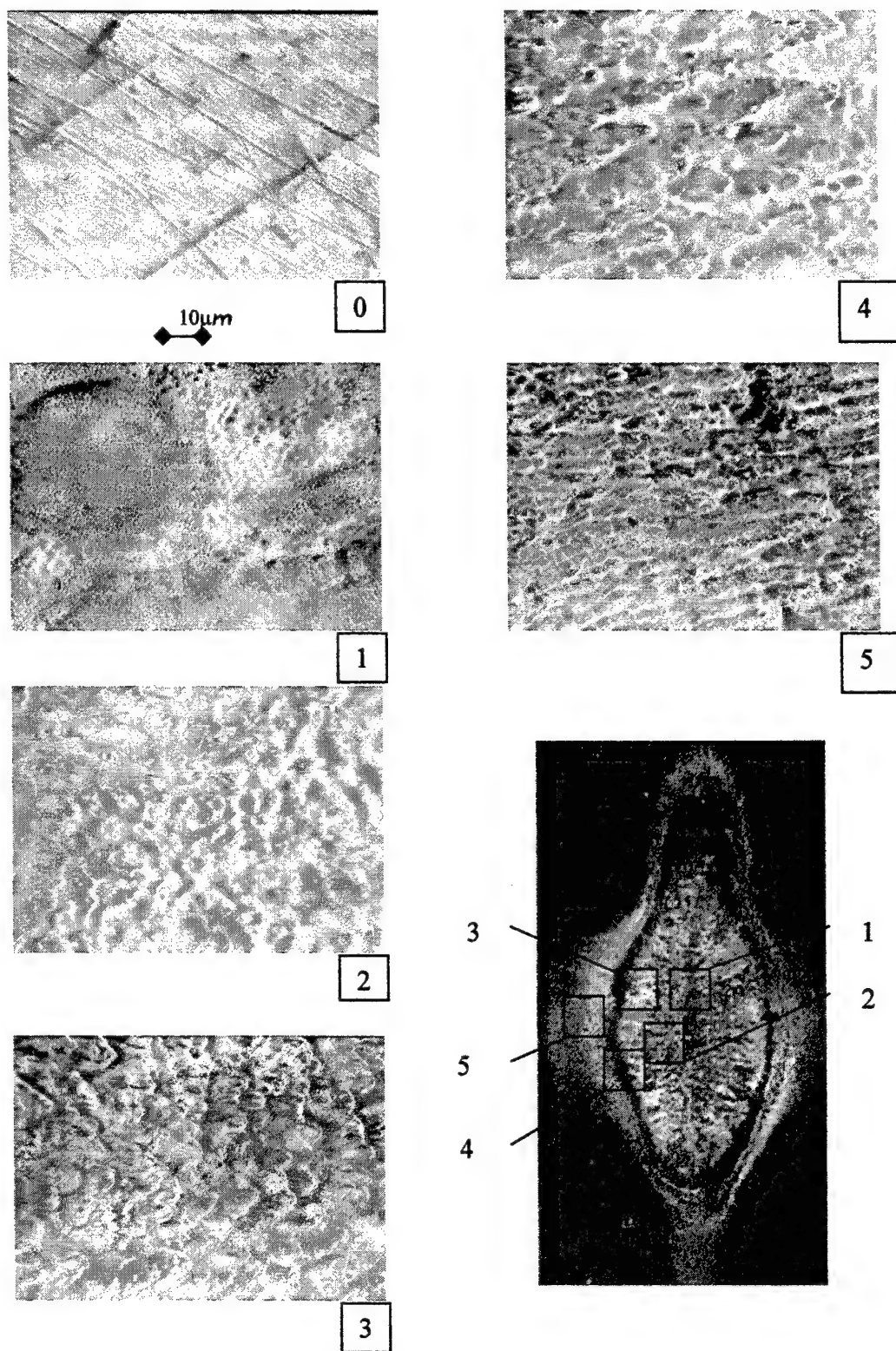


Fig.2. HF-laser print on the 4140-steel surface (10 pulses) and magnified images of distinguished zones.

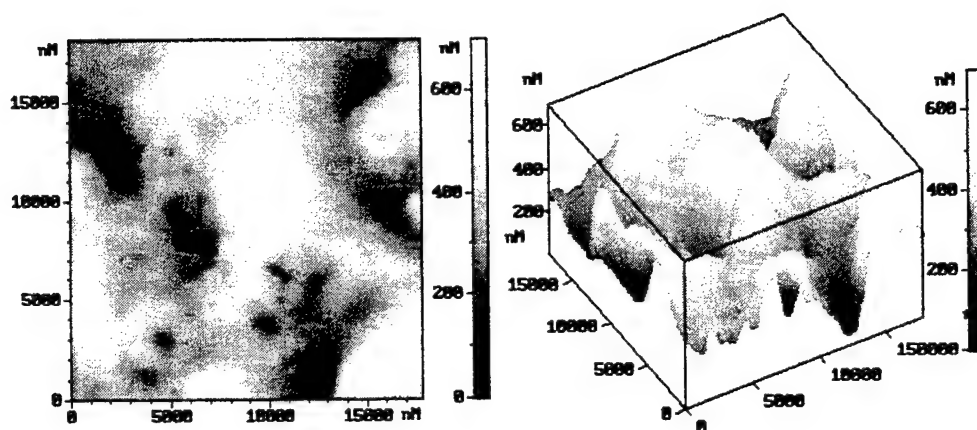


Fig. 3(a). The metal surface observed after laser action (zone №3).

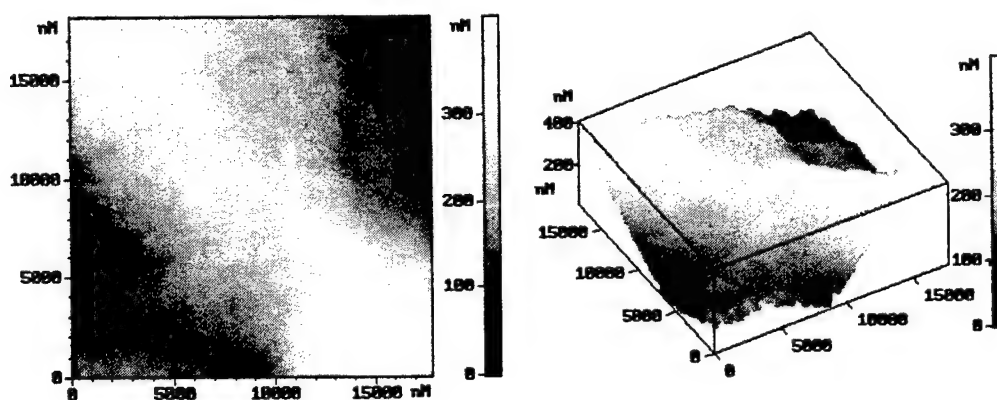


Fig. 3(b). The metal surface observed after laser action (zone №2).

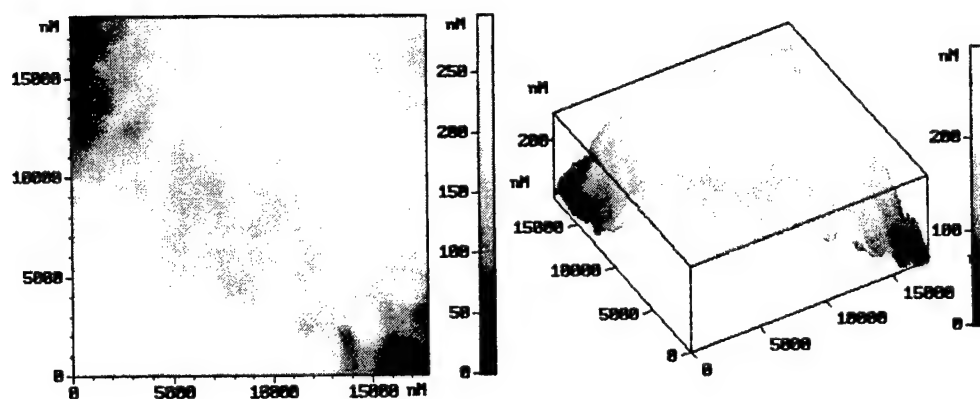


Fig. 3(c). The metal surface observed after laser action (zone №1).

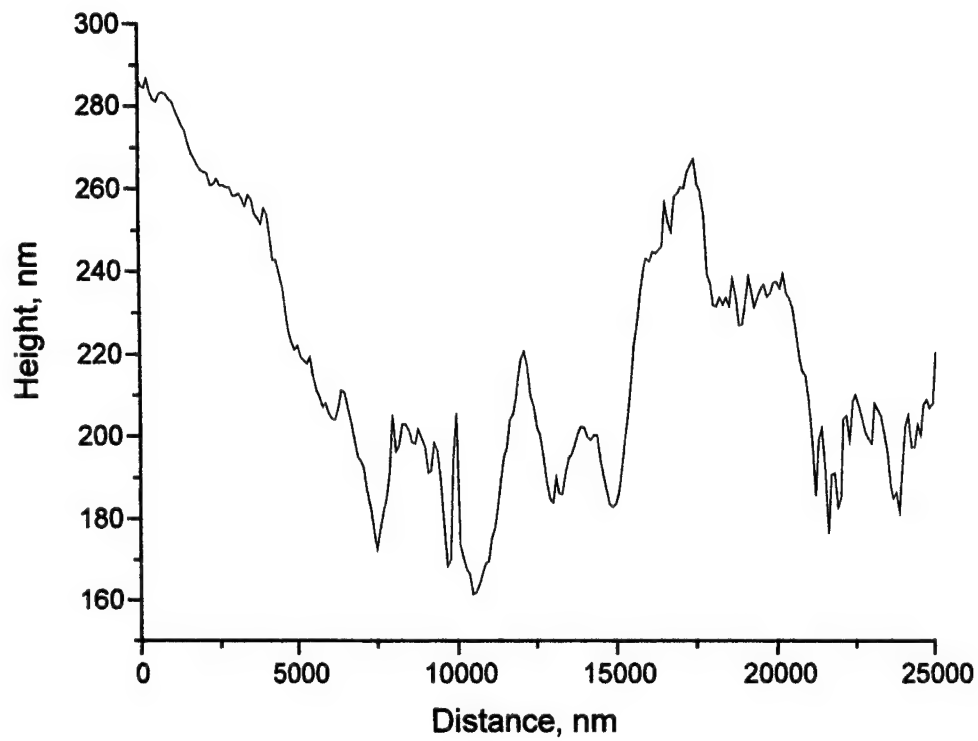


Fig. 4. Profilogramme of the crater surface in zone № 1 (along the diagonal line of Fig. 3(c) from the left to right, from the down to top) obtained using the software of the atomic force microscope.

Energy transfer dynamics in the $A(0_u^+)$ state of Bi_2

Joseph L. Cox,¹ Michael W. Dolezal,² Robert E. Franklin,³ and Glen P. Perram⁴
Air Force Institute of Technology

ABSTRACT

Laser induced fluorescence, pulsed and CW, techniques have been used to study energy transfer within the $A(0_u^+)$ state of Bi_2 . In particular, electronic quenching in the vibrational levels near predissociation, $v'=18-25$, have been examined for rare gas and nitrogen collision partners. The quenching from non-predissociated levels is independent of vibrational state and are rather rapid, $2.3 - 8.5 \times 10^{-11} \text{ cm}^3/\text{molecule-s}$ for $v'=22$. The quenching from the first significantly predissociated level, $v'=23$, is even faster with rate coefficients ranging from $7.4 - 15.7 \times 10^{-11} \text{ cm}^3/\text{molecule-s}$. Heterogeneous predissociation is very rapid for $21 \leq v' \leq 39$, with rates, $\Gamma = k_{\text{pd}}(v') J(J+1)$, of k_{pd} as large as $1.5 \times 10^5 \text{ s}^{-1}$. Vibrational-to-translational energy transfer probabilities for the lowest vibrational levels, $v'=0-4$, range from 0.75 – 1.75% per collision, considerably lower than would be anticipated for these highly non-adiabatic collisions. Spectrally resolved emissions from collisionally populated rotational levels of $\text{Bi}_2(A, v'=1)$ were observed for helium, neon and argon collision partners after laser excitation of the high rotational levels $J'=171, 201$, and 231. Total rotational removal rates from the initially prepared state range from $2.8 - 8.9 \times 10^{-10} \text{ cm}^3/\text{molecule-s}$. Collisional population of rotational states with $|\Delta J| \leq 56$ was observed at pressures of 0.09 – 1.4 torr. The state-to-state rates are adequately modeled by the energy based statistical power gap law.

Keywords: bismuth dimer, spectroscopy, predissociation, quenching, vibrational energy transfer, rotational energy transfer, laser induced fluorescence

1. INTRODUCTION

Several optically pumped Bi_2 (A-X) lasers were demonstrated in the late 1970's and early 1980's with photon efficiencies approaching 20%.¹⁻² Bismuth dimers also play an important role in the $\text{NF}(a^1\Delta) - \text{BiF}$ laser system.³ The current work reports on the collisional dynamics of the $\text{Bi}_2 A(0_u^+)$ state from a series of laser induced fluorescence experiments.⁴⁻⁶

The bismuth dimer is the heaviest stable diatom and offers a unique opportunity to study the collisional dynamics of states with high angular momentum, as well as vibrational energy transfer in strongly coupled systems. The vibrational frequency is low, $\omega_e \approx 132 \text{ cm}^{-1}$, and the $\text{Bi}_2 - \text{He}$ collision involves a high relative speed at room temperature, yielding a ratio of collision time to the vibrational period of ~ 0.06 . The very low rotational constant for Bi_2 offers significant populations in rotational states above $J=200$ even at modest temperatures ($T \approx 300 \text{ K}$).

The spectroscopy of the $\text{Bi}_2 A(0_u^+) - X(0_g^+)$ system is well characterized, particularly for the low lying vibrational levels.⁷⁻⁹ The radiative lifetime of $\text{Bi}_2(A)$ is 272 - 595 ns for $v' < 20$, and a strong predissociation is observed near $v'=27$.¹⁰⁻¹¹ However, the collisional dynamics of $\text{Bi}_2(A)$ is less studied. The radiative rates,^{5,10-11} quenching from a few (v', J') levels,¹¹ and vibrational energy transfer in the lowest vibrational levels¹² have previously been reported. In addition, several $\text{Bi}_2(A-X)$ lasers have been demonstrated.¹⁻²

¹joseph.cox@eglin.af.mil; phone 1 850 8821724 x 117; Fax 1 850 882 1717; <http://www.afrl.af.mil>; Air Force Research Laboratory/MNGS, 101 West Eglin Blvd Suite 287, Eglin AFB, FL 32542-6810 ²michael.dolezal@aftac.patrick.af.mil; phone 321 494-9610; <http://www.aftac.gov>; Air Force Technical Applications Center/TAT-A, 1030 S Highway A1A, Patrick AFB, FL 32925; ³robert.franklin@wpafb.af.mil; phone 937 674 8035x3903; <https://www.asc.wpafb.af.mil/asc/>; Aeronautical Systems Center/GRI, 2145 Monahan Way, Wright-Patterson AFB, OH 45433; ⁴glen.perram@afit.edu; phone 1 937 255 3636 x 4504; Fax 1 937 255 2921; <http://www.afit.edu>; Air Force Institute of Technology/ENP, 2950 P Street, Wright-Patterson AFB, OH 45433-7765

2. EXPERIMENT

The steady-state laser induced fluorescence apparatus is depicted in Figure 1. A Coherent model 899-29 ring dye laser with Rhodamine 590 dye was used to selectively excite the $A(0_v^+)$ state. Laser excitation spectra were recorded,^{4,8} indicating the excitation of a pure (v', J') state. The dye laser was operated with a power of 0.3 – 0.9 mW and the laser linewidth was less than 100 MHz. A McPherson 1.3m monochromator with a Princeton Instruments model 1024 SR/B optical multichannel analyzer (OMA) was used to resolve the laser induced fluorescence with a resolution of 0.5 cm^{-1} and a bandwidth of 225 cm^{-1} . The spectral response of the OMA was calibrated with a blackbody source at 1266 K.⁴

The bismuth dimer was generated by heating a small sample of granular bismuth (Mallinckrodt, 99.8%) in a 1 cm aluminum oxide crucible and tungsten basket heater to 900 – 1000 K. Such an apparatus typically produces about 33% atomic bismuth and 66% bismuth dimer.¹¹ The fluorescence cell consisted of a 6-way (3.8 cm diameter x 20 cm length) stainless steel cross with quartz windows along the laser axis and for viewing the laser induced fluorescence. The fluorescence cell could be evacuated to 8×10^{-6} Torr via an oil diffusion pump, and exhibited a room temperature leak rate of less than 3 mTorr/hour. Typically, the cell was operated with 0.1 – 12.0 Torr of rare gases (99.996%) added to induce energy transfer. The rate of out-gassing with the basket heater on was 1-2 mTorr/min. The cell pressure was monitored with MKS model 390 10 Torr and model 122A 100 Torr capacitance manometers.

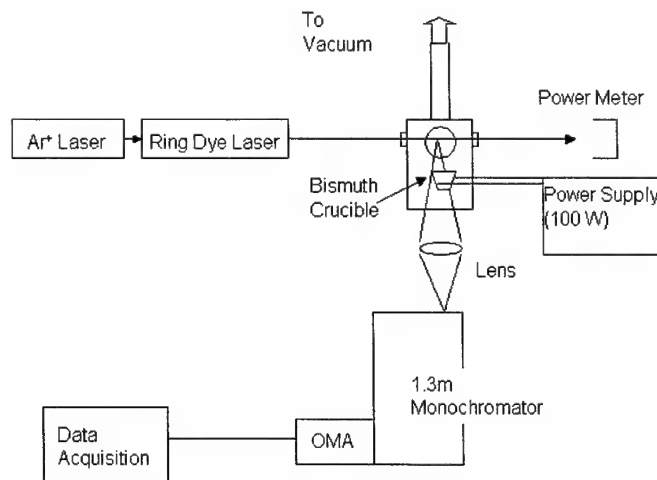


Figure 1. CW laser induced fluorescence apparatus.

For the pulsed laser induced fluorescence experiments, a Nd:YAG pumped dye laser using Coumarin 460, 480 and 500 dyes with typical pulses energies of 10-25 mJ was used to excite $\text{Bi}_2(A)$ in a similar vacuum apparatus. The side fluorescence was detected with an RCA C30134 photomultiplier tube and recorded on a LeCroy 940 350 MHz digital oscilloscope.

3. RESULTS

The experiments are grouped into four sections: (1) pulsed Laser Induced Fluorescence (LIF) lifetimes to study predissociation, (2) electronic quenching rates from time-resolved emission profiles, (3) CW LIF studies of vibrational energy transfer, and (4) CW LIF rotational energy transfer for high J within $v'=1$.

3.1 Predissociation

The laser excitation spectrum from 18,725 to $21,950\text{ cm}^{-1}$ was recorded with a Nd:YAG pumped dye laser at 0.3 cm^{-1} spectral resolution. A segment of the spectrum is provided in Figure 2. The sudden onset of predissociation is seen for $v' \geq 22$ as a dramatic decrease in the extent of the rotational distribution. The red shaded bands are reduced to narrow features near the band head. In fact, for most of the predissociated levels, no resolved rotational structure can be identified.

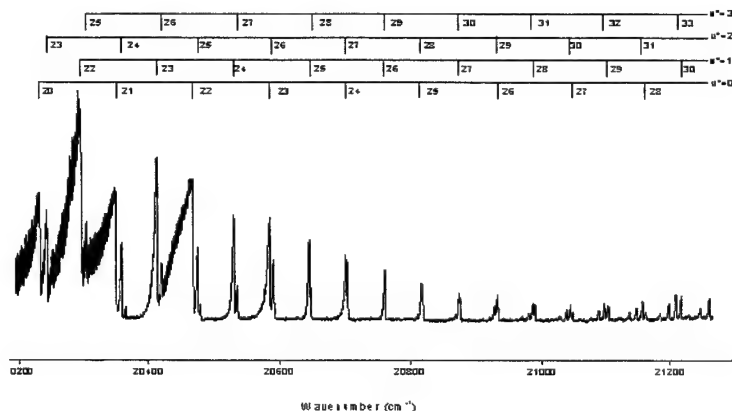


Figure 2. Pulsed laser excitation spectrum with (v', v'') band heads indicated.

The fluorescence intensity as a function of time for $v'=21$ -22 decays exponentially, as shown in Figure 3. The logarithmic plot illustrates single exponential behavior for at least 6 e-folds. By examining the dependence of the decay rates on pressure, the collisionless decay rates were determined. A plot of these collisionless decay rates as a function of rotational state is shown in Figure 4. The transition rates for heterogeneous predissociation are given by $\Gamma_0 = 1/\tau_r + k_{pd}(v')J(J+1)$, where τ_r is the radiative lifetime and $k_{pd}(v')$ is a measure of the strength of the predissociation and is dependent on vibrational level.

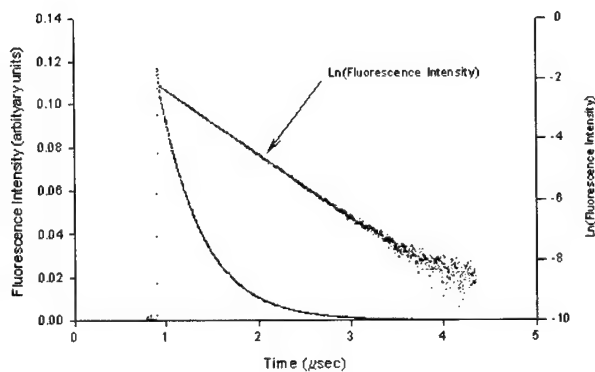


Figure 3. Decay lifetime for $v'=21$, $J'=50$ at 100 mTorr.

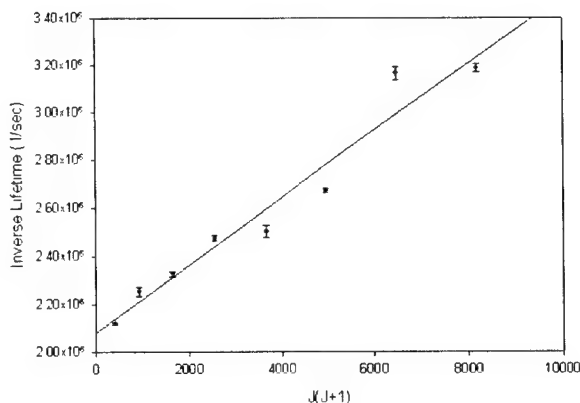


Figure 4. Rotational dependence to predissociation in $v'=21$.

For $v' > 22$, the predissociation is sufficiently strong that only rotational states near the band head have significant emission intensity, and these rotational levels cannot be isolated by the pump laser. To extract predissociation rates, k_{pd} , for these states, we have employed a spectral simulation.⁵ Briefly, the intensity of each rotational line is modeled, including the effects of predissociation, and convolved using the laser linewidth to simulated the laser excitation spectra. By comparing the synthetic and observed spectra, a best estimate for the predissociation rate is determined. A summary of the resulting predissociation rates is provided in Figure 5.

The predissociation in $\text{Bi}_2(\text{A})$ is very strong, exhibits a broad dependence of vibrational level and yields no stable vibrational levels above $v'=22$.

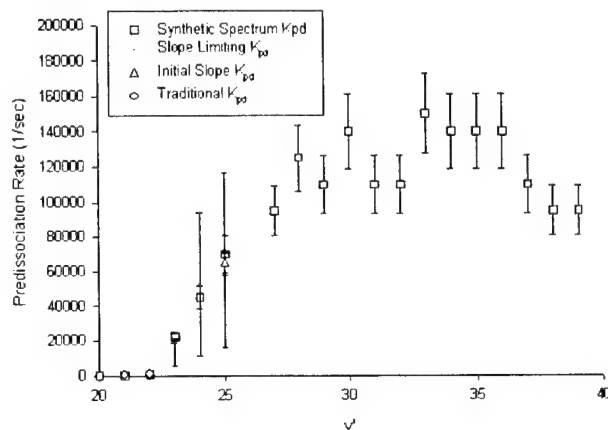


Figure 5. Predissociation rate constant, k_{pd} , as a function of vibrational level.

3.2 Electronic Quenching

The pressure dependence of the total fluorescence decay rates establish the electronic quenching rates, $\Gamma = \Gamma_0 + k_q[M]$, where $[M]$ is the concentration of the added buffer gas. For the vibrational levels below the onset of predissociation, $v'=18$ -22, the electronic quenching rates for helium are independent of vibrational level, as shown in the Stern-Volmer plot of Figure 6. The probability for quenching, defined as the ratio of the observed quenching rate to the gas kinetic rate, depends linearly on reduced mass of the collision pair, as shown in Figure 7.

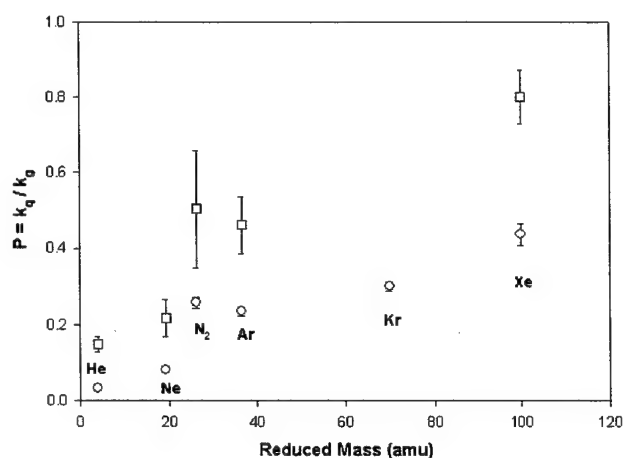
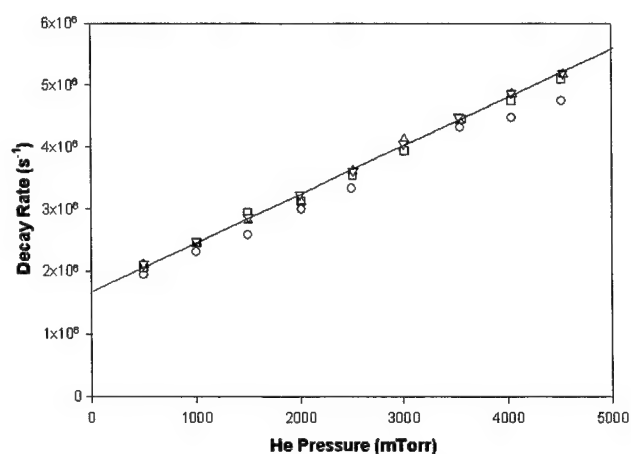


Figure 6. Electronic quenching for $v'=18$ (o), 19 (\square), 20 (Δ) and 21 (∇). Figure 7. Quenching probability for $v'=22$ (o) and $v'=23$ (\square).

The quenching from $v'=23$ are about twice the rates for $v'' \leq 22$. Vibrational ladder climbing to higher, strongly predissociated vibrational states and rotational energy transfer to higher J within $v'=23$ likely contributes to the increased total quenching.

Table I.
Electronic Quenching for $v'=22$

Buffer Gas, M	Reduced Mass (amu)	Quenching Rate, k_q ($10^{-11} \text{ cm}^3 / \text{molecule-s}$)	Gas Kinetic Rate ($10^{-10} \text{ cm}^3 / \text{molecule-s}$)	Probability, P
He	3.96	$2.27 \pm .16$	7.03	0.0323 ± 0.0023
Ne	19.3	$2.80 \pm .19$	3.41	0.0822 ± 0.0056
Ar	36.5	$6.65 \pm .35$	2.84	0.2340 ± 0.0123
Kr	69.8	$6.39 \pm .25$	2.13	0.2998 ± 0.0115
Xe	99.9	$8.51 \pm .55$	1.95	0.4362 ± 0.0282
N ₂	26.2	$8.03 \pm .45$	3.12	0.2574 ± 0.0145

Quenching rates for $v' > 23$ were not reliably obtained, due to the very fast predissociation. Figure 8 illustrates the decay waveforms for $v' = 22 - 25$. The very fast decay rates for $v' = 24 - 25$ exceed $5 \times 10^7 \text{ s}^{-1}$, or $\tau \leq 20 \text{ ns}$. The pulsed dye laser has a pulse width of about 10 ns, and does not allow for sufficient temporal resolution to extract reliable quenching rates.

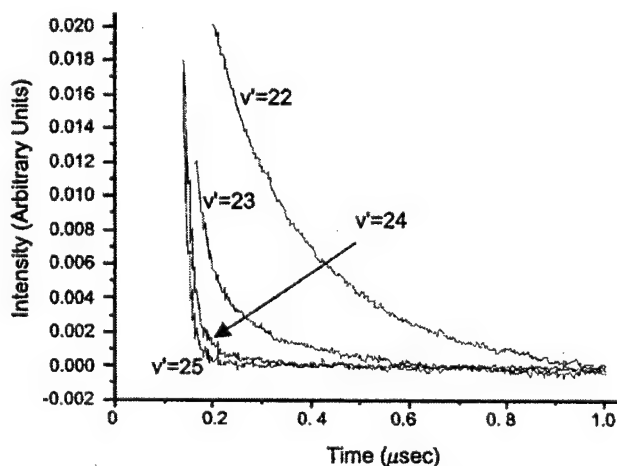


Figure 8. Lifetimes for He at 3 Torr.

3.3 Vibrational Energy Transfer

A spectrum showing the effects of vibrational energy transfer after laser excitation of $v'=3$ is shown in Figure 9. Band heads are labeled (v',v'') for some of the more prominent features. The spectrum was recorded for a neon buffer gas at 4.76 Torr and significant populations are observed in $v'=0-2$, indicating rapid vibrational energy transfer. The P-R doublet emission from the laser excited $v'=3$, $J'=104$ level is evident in the (3,8) band. This P-R doublet structure is not clearly evident in the other two bands originating from $v'=3$ due to low Franck-Condon factors. A spectral region with low Franck-Condon factors from the laser excited, or parent, state is desirable for quantifying the population in collisionally populated, or satellite states. Similar spectra were recorded for He, Ne, Ar, Kr, and Xe buffer gases at pressures of 0.1 – 12.0 torr. In order to determine the populations in various vibrational levels, synthetic spectra were fit to the observed spectra. The comparison between the observed and fit spectra, as shown in Figure 9, is generally adequate. The differences are largely attributed to vibrational bands excluded from the spectral simulation.

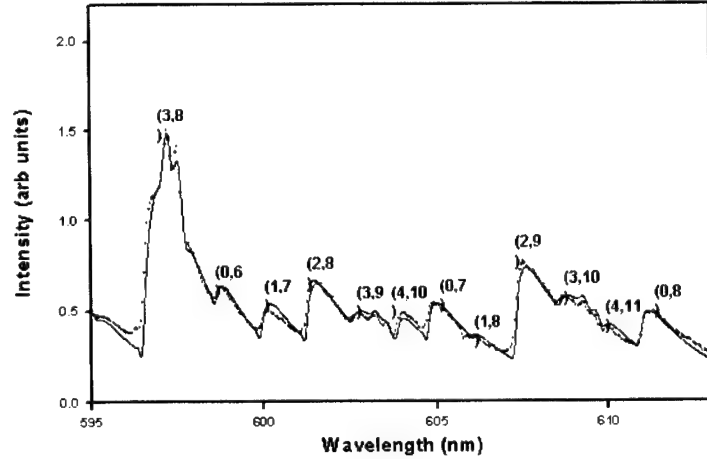


Figure 9. CW LIF vibrationally resolved spectrum and simulation. Band heads are indicated (v',v'') .

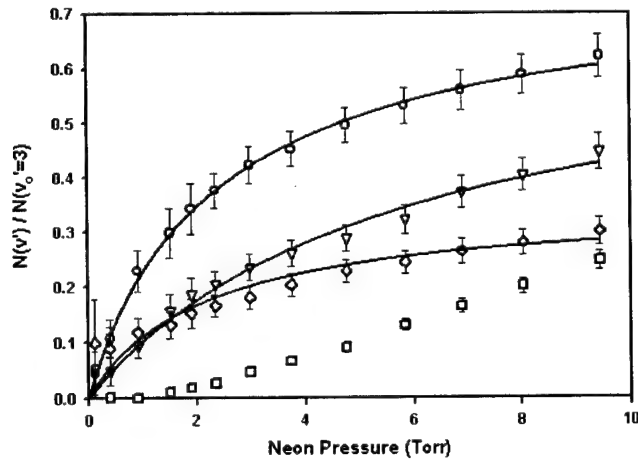


Figure 10. Vibrational population distributions as a function of neon buffer gas pressure after laser excitation of $v'=3$. The observed populations for: (O) $v'=2$, (∇) $v'=1$, (\diamond) $v'=4$, and (\square) $v'=0$ are fit to: (—) equation (4), and (---) the constrained rate matrix of equation (2).

In order to extract state-to-state vibrational transfer rate coefficients from data similar to that shown in Figure 10, a steady-state analysis of the master rate equation is required. The master rate equation for the population in vibrational level v is:^{4,6}

$$\frac{dN_v}{dt} = S\delta_{v,v_0} + \sum_w R_{vw}N_w \quad (1)$$

where w is the quantum number for other vibrational levels of $\text{Bi}_2(\text{A})$, S is rate for laser excitation of the parent level v_0 , and R_{vw} denotes the rate coefficient matrix:

$$R_{vw} = k_{vT}(w \rightarrow v)[M] - \delta_{vw} \left\{ \Gamma_r + k_Q(v)[M] + \sum_w k_{vT}(v \rightarrow w)[M] \right\} \quad (2)$$

The goal of this work was to extract the rate coefficients for vibrational transfer from state w to state v , $k_{vT}(w \rightarrow v)$, from the rate matrix, R_{vw} . The radiative decay rate for $\text{Bi}_2(\text{A}, v' \leq 3)$ is $\Gamma_r = 1.6 - 2.3 \times 10^6 \text{ s}^{-1}$.¹¹ For a given rate matrix, R_{vw} , the relative steady-state populations can easily be determined as:

$$\frac{N_v}{N_{v_0}} = \frac{k_{vT}(v_0 \rightarrow v)[M]/\Gamma_r}{1 + [k_Q(v)[M] + \sum_w k_{vT}(v \rightarrow w)[M]/\Gamma_r - \sum_w k_{vT}(w \rightarrow v) \left(\frac{N_w}{N_v} \right) [M]/\Gamma_r]} \quad (3)$$

The third term in the denominator of equation (3) represents multiple collisions that populate the observed vibrational level. In general, this term possesses a complicated pressure dependence. However, at moderate pressures where multiple collisions are not dominant, equation (3) reduces to the form:

$$\frac{N_v}{N_{v_0}} = \frac{Ax}{1 + Bx} \quad (4)$$

where $A = k_{vT}(v)/\Gamma_r$, $B = (k_Q(v) + \sum_w k_{vT}(v \rightarrow w))/\Gamma_r$, and $x = [M]$.

Figure 10 illustrates a least-square fit of equation (4) to the data, providing an initial estimate of the state-to-state V-T rate coefficients, as reported for neon in Table II. The data for $v' = 0$ can not be adequately represented by equation (4), since single collision transfer involving $\Delta v = -3$ is insignificant. Similar data were recorded for laser excited states $v' = 1-4$ and for He, Ne, Ar, Kr, and Xe buffer gases.

Table II.
Vibrational transfer rate coefficients for neon.
($10^{-12} \text{ cm}^3/\text{molecule-s}$)

v	$k_{vT}^{\text{Ne}}(v \rightarrow v-1)$ (from fit to equation (4))	$k_{vT}^{\text{Ne}}(v \rightarrow v-1)$ (from rate matrix model)	k_{eq}	f
1	6.3 ± 0.7	6.2 ± 0.7	< 0.9	0.16
2	9.6 ± 0.7	9.6 ± 0.7	< 2.9	0.10
3	15.1 ± 1.4	14.1 ± 1.4	< 3.3	0.12
4	19.6 ± 3.5	19.2 ± 3.5	< 3.3	0.05

In order to refine the determination of the vibrational transfer rate coefficients, the full rate matrix of equation (2) is utilized. To reduce the number of independent matrix elements, detailed balancing is used to specify transitions that increase vibrational energy, linear scaling of the vibrational transfer rate coefficients with vibrational quantum number as predicted for harmonic oscillators is applied, transfer involving multi-quanta is assumed to be a fixed fraction, f , of the $\Delta v = -1$ rate, and the rates for $|\Delta v| \geq 3$ are neglected. The electronic quenching and radiative rates are assumed independent of vibrational level. By varying the quantities $k_{vT}(v \rightarrow v-1)$, k_q and f , a single rate matrix which best represents the full set of spectrally-resolved laser induced fluorescence data can be established. The corresponding predictions for $v'=4,2$, and 1 are quite similar to the fits from equation (4). The resulting rate parameters for neon collisions are provided in Table I. Collisions with the remaining rare gases were studied in somewhat less detail. The vibrational levels examined and resulting rate coefficients are reported in Table III.

Table III.
Fundamental vibrational transfer rate coefficients for rare gases.
(10^{-12} cm³/molecule-s)

Gas	v_0'	$k_{VT}(v \rightarrow v-1)$	$k_{VT}(1 \rightarrow 0)$	$\sigma_v(1,0) / \sigma_g$
He	2	10.6 ± 1.5	5.3 ± 0.7	0.0075
Ne	1-4	(see Table I)	4.8 ± 0.9	0.0142
Ar	3	7.6 ± 1.2	2.5 ± 0.4	0.0089
Kr	2	4.8 ± 0.7	2.4 ± 0.4	0.0112
Xe	2	6.8 ± 1.3	3.4 ± 0.7	0.0175

The Schwartz, Slawsky, and Herzfeld (SSH) theory¹³ successfully predicts the probability for vibrational transfer (V-T), particularly the scaling with mass and vibrational frequency, under a wide range of conditions.¹⁴ The SSH theory depends on the first-order Born approximation, models a harmonic oscillator perturbed by an exponential interaction potential, and assumes a relatively non-impulsive, or near adiabatic, collision. The SSH theory predicts the probability for vibrational transfer as:¹⁴

$$P(1,0) = \frac{\sigma(1,0)}{\sigma_g} = M \left(\frac{\Theta'}{\Theta} \right) \left(\frac{\Theta'}{T} \right)^{1/6} \exp \left[-3/2 \left(\frac{\Theta'}{T} \right)^{1/3} + \left(\frac{\Theta}{2T} \right) + \left(\frac{\epsilon}{kT} \right) \right] \quad (5)$$

where

$$M = \sqrt{\frac{2\pi}{3}} \frac{2m_A^2 m_B m_C}{(m_B + m_C)(m_A + m_B)^2 \mu}$$

$$\mu = \text{collision pair reduced mass} = m_A(m_B + m_C)/(m_A + m_B + m_C)$$

$$\Theta' = 4\pi^2 L^2 (2\pi c \omega_e)^2 \mu / kT$$

$$\Theta = hc \omega_e / kT$$

$$\omega_e = \text{fundamental vibrational frequency (cm}^{-1}\text{)}$$

$$\epsilon = \text{potential well depth}$$

$$L = \text{potential interaction length}$$

$$\sigma_g = \text{gas kinetic or hard sphere cross-section}$$

Surveying the existing database of V-T transfer for the diatomic halogens indicates a deficiency of the SSH theory for highly impulsive collisions.¹⁵ By converting the observed V-T transfer rate coefficients to a transition probability, using the specified masses, vibrational frequency, and translational temperature, and assuming a small well depth, $\epsilon/kT \approx 0$, the interaction lengths, L , required to satisfy equation (5) are specified displayed in Figure 11. For adiabaticity, $\xi = c\omega_e L (\pi\mu/8kT)^{1/2} > 0.5$, the interaction lengths are in the range $L = 0.25$ - 0.10 , which is typical for V-T transfer.¹⁴ However, the most impulsive collisions, particularly the $\text{Bi}_2(\text{A}) - \text{He}$ interaction, require unreasonably large interaction lengths. In other words, the SSH theory over-predicts the probability for V-T transfer involving highly impulsive conditions. A large interaction length artificially reduces the prediction to generate agreement with the observed rates.

There are several approximations made in the SSH theory that depend on near adiabatic conditions: (1) the first-order Born approximation is used to compute the transition probability, (2) the matrix elements for the exponential interaction potential are approximated by a first-order Taylor series, and (3) when averaging over the velocity distribution, the approximation $\text{csch}^2(2\pi^2 c\omega_e L/v) \approx 4 \exp(-4\pi^2 c\omega_e L/v)$ is employed. The latter two approximations can be improved,¹⁶⁻¹⁷ but the differences are not sufficiently large to account for the interaction lengths computed in Figure 7. The large interaction lengths for the most impulsive collisions ($\xi < 0.3$) appear to result from the failure of the first-order Born approximation.

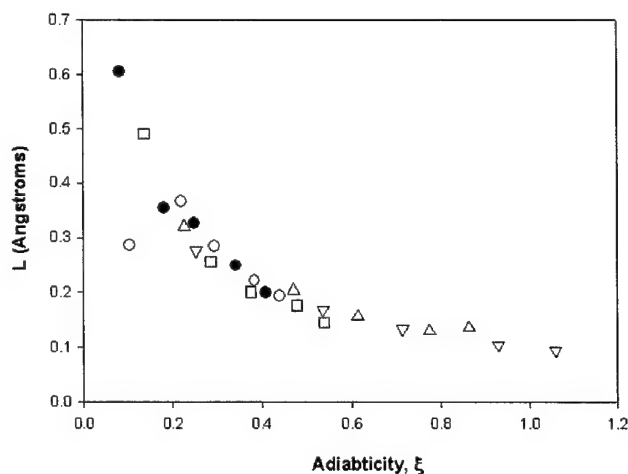


Figure 11. The interaction length derived using the SSH theory of equation (15) from V-T rate coefficients observed for: (●) $\text{Bi}_2(\text{A})$ (present work), (○) $\text{Br}_2(\text{B})$ (ref 21), (□) $\text{BrCl}(\text{B})$ (ref 18), (△) $\text{BrF}(\text{B})$ (ref 21), and (▽) $\text{IF}(\text{B})$ (ref 19). To evaluate the adiabaticity, a constant value for the interaction length was chosen, $L = 0.02 \text{ nm}$.

3.4 Rotational Energy Transfer

Similar experiments have been performed with rotational state resolution. The spectrally resolved emission from the $v'=1 \rightarrow v''=5$ band after excitation of $v'=1, J'=171$ in the presence of 0.855 torr of helium is shown in Figure 12. The strong P-R doublet emission from the laser populated state is clearly evident. The weaker satellite transitions are from the collisionally populated rotational states. Emission is observed only from even rotational levels because the nuclear spin is not readily altered by collisions.²² For $J' < 140$, a near coincidence of the P(J) and R(J+14) lines precludes complete spectral isolation. The rotational transfer rates are quite rapid, with significant population in the satellite states even at low buffer gas pressures.

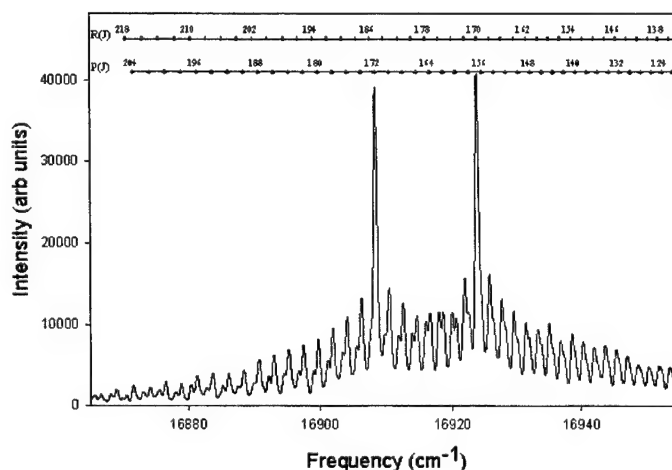
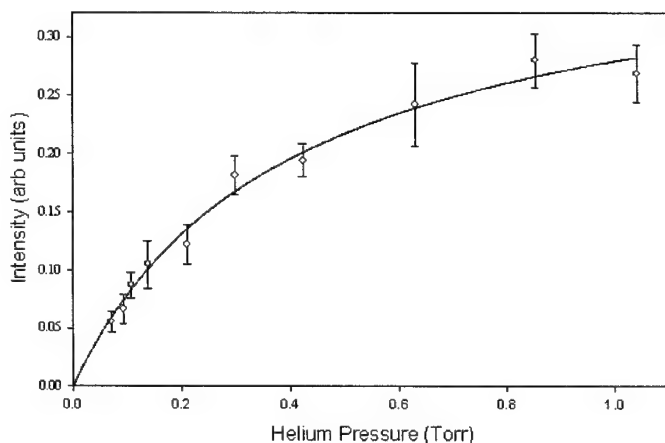


Figure 12. Spectrally resolved $\text{Bi}_2(\text{A-X})$ laser induced fluorescence from the $v'=1$ to $v''=5$ band in the presence of 855 mTorr of helium buffer gas after laser excitation of $v'=1, J'=171$.

A plot of the population in the satellite level $J'=165$ relative to the population in the parent level, $J'=171$, is shown as a function of helium buffer gas pressure in Figure 13. The error bounds indicated in Figure 13 are obtained from the



uncertainties in the amplitudes from the spectral fits. Similar data were obtained for initially pumped states $J'_0=171, 201$ and 231 and satellite states $-56 < \Delta J < +44$. This data was analyzed with a steady-state analysis similar to that described above for vibrational energy transfer and typical rate constants are provided in Figure 14.

Figure 13. Plot of the population of the satellite $J'=165$ rotational level relative to the parent state ($J'=171$) for collisions with helium buffer. The solid line is a least-squares fit to the data using an analysis similar to equation (4).⁴

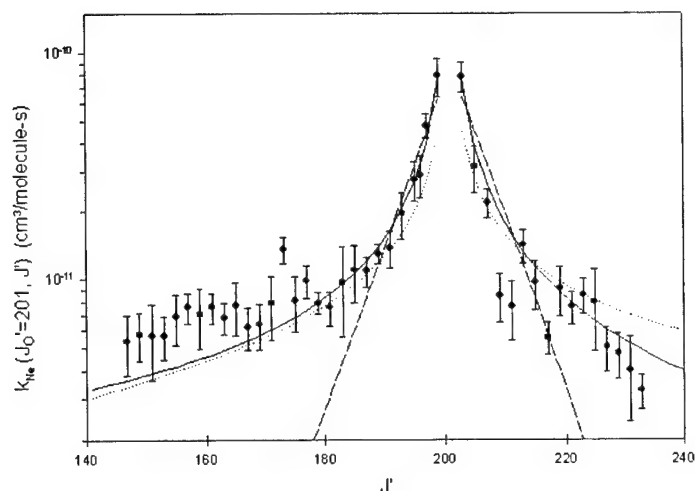


Figure 14. State-to-state rotational energy transfer rate constants for Ne after laser excitation of $v'=1$, $J'=201$. Three scaling law fits are also shown: (—) SPG1, (....) SPG2 and (---) EGL1.

Several empirical relationships have been proposed to describe the scaling of the state-to-state rotational energy transfer rate constants with rotational quantum number.²³⁻²⁴ A variety of these fitting laws have been applied to the current data in an attempt to evaluate those which adequately represent the data. In Figure 14, a fit of the SPG1, SPG2 and EGL1 fitting laws are shown.⁴ The exponential gap law fails for all the initially

prepared J_0 levels and buffer gas studies observed in the present work. The EGL1 and EGL2 fitting laws can be made to represent either the rotational levels near the pumped state, or for larger ΔJ , but not both. The statistical power gap laws do provide an adequate representation of the data for all J_0 and all three collision partners. The M_J conserving form of the statistical factor $f(J)$ (SPG1) provides a fit standard error of 20-50% less than the completely randomized factor (SPG2) and in all cases provides a better fit. Fit parameters for the statistical power gap law (SPG1) are summarized for each of the collision partners in Table II.

Table II.
Fit parameters for the statistical power gap scaling law, SPG1.

Collision Partner	(v', J_0')	B (10^{-8} cm ³ /molecule-s)	γ
He	(1,171)	5.45 ± 1.17	0.944 ± 0.030
He	(1,201)	3.85 ± 0.59	0.902 ± 0.021
He	(1,231)	2.79 ± 0.50	0.834 ± 0.025
Ne	(1,201)	5.00 ± 1.23	0.968 ± 0.034
Ar	(1,201)	1.25 ± 0.50	0.786 ± 0.042

4. CONCLUSIONS

A systematic study of predissociation in $\text{Bi}_2(\text{A})$ has been completed, indicating a curve crossing at $v'=23$. The predissociation is very strong, exhibits a broad dependence of vibrational level and yields no stable vibrational levels above $v'=22$. Electronic quenching is rapid, with rates 0.03 – 0.8 time the limiting gas kinetic value. Quenching is independent of vibrational level to the predissociation limit, but increase significantly at $v'=23$. Vibrational energy transfer in the lowest vibrational levels of $\text{Bi}_2(\text{A})$ is rapid, although somewhat less than predicted by the SSH theory. The $\text{Bi}_2(\text{A})$ potential is nearly harmonic, leading to a linear scaling of the vibrational transfer rates with vibrational quantum number and a low probability for multi-quantum transfer. Interaction lengths for bismuth dimer – rare gas collisions are consistent with those derived for the diatomic halogens when the collision pair exhibits the same adiabaticity. Rotational energy transfer within $\text{Bi}_2(\text{A})$ is rapid, constrained to $\Delta J = \text{even}$ by parity conservation, and best represented by the statistical power gap scaling law with M_J conservation. Single collision population of rotational levels with $|\Delta J| \leq 52$, $\Delta E > 300$ cm⁻¹, is readily apparent. Even for these very high rotational states, with large angular momentum, the energy based scaling laws appear to provide a better representation of the rates than the energy corrected sudden with a power law for the angular momentum scaling.

REFERENCES

1. W.P. West and H.P. Broida *Chem. Phys. Lett.* **56** 283 (1978).
2. S. Drosch and G. Gerber *J. Chem. Phys.* **77** 123 (1982).
3. D.J. Benard *J. Appl. Phys.* **74** 2900 (1993).
4. R.E. Franklin "Spectroscopic and Kinetic Studies of Bismuth Dimers", PhD Dissertation, Air Force Institute of Technology, AFIT/DS/ENP/97-04 (1997).
5. Michael W. Dolezal *Spectroscopic Constant, Lifetimes and Predissociation Rates for $Bi_2 A(0_u^+)$* , Ph.D. Dissertation, Air Force Institute of Technology, AFIT/DS/ENP/01-01 (2001).
6. Joseph L. Cox, *Electronic Quenching of the $A(0_u^+)$ State of Bi_2* , M.S. Thesis, Air Force Institute of Technology, AFIT/GAP/ENP/01M-02 (2001).
7. R.F. Barrow, F. Taher, J.D. Incani, C. Effantin, A.J. Ross, A. Topovzkhanian, G. Wannous, and J. Verges, *Molecular Physics* **87** 725 (1996).
8. R.E. Franklin and G.P. Perram, *J. Molec. Spectrosc.* **194** 1 (1999).
9. G. Gerber, Honinger, and J. James *Chem. Phys. Lett.* **85** 415 (1982).
10. J.M. Blondeau, G. Gandara, P. Carette and J. Messelyn *Chem. Phys. Lett.* **71** 246 (1980).
11. G. Ehret and G. Gerber *Chem. Phys.* **66** 27 (1982).
12. Robert E. Franklin and Glen P. Perram, "Collisional Dynamics of $Bi_2 A(0_u^+)$. I. Quantum-Resolved Vibrational Energy Transfer for $v'=0-4$ ", *Journal of Chemical Physics*, **111**, 5757 (1999).
13. R.N. Schwartz, Z.I. Slawsky, and K.F. Herzfeld, *J. Chem. Phys.* **20** 1591 (1952).
14. J.T. Yardley *Introduction to Molecular Energy Transfer* (Academic, New York, 1980).
15. C.D. Holmberg, G.S. Williams, and G.P. Perram *J. Chem. Phys.* **102** 6481 (1995).
16. J. Keck and G. Carrier *J. Chem. Phys.* **43** 2284 (1965).
17. D. Rapp and T.E. Sharp *J. Chem. Phys.* **38** 2641 (1963).
18. G.P. Perram and S.J. Davis *J. Chem. Phys.* **98** 373 (1993).
19. P.J. Wolf and S.J. Davis *J. Chem. Phys.* **87** 3492 (1987).
20. J.I. Steinfeld *J. Chem. Phys.* **46** 4550 (1967).
21. G.P. Perram, D.W. Melton, T.L. Thompson, and W.B. Roh *J. Chem. Phys.* **97** 3258
22. C.W. McCurdy and W.H. Miller, *J. Chem. Phys.*, **67** 463 (1977).
23. T.A. Brunner and D. Pritchard, "Fitting Laws for Rotationally Inelastic Collisions" in *Advances in Chemical Physics, Volume 50: Dynamics of the Excited State*, edited by K.P. Lawley (John Wiley and Sons, 1982)
24. J.I. Steinfeld, P. Rittenberg, G. Millot, G. Fanjoux, and B. Lavorel, *J. Phys. Chem.* **95**, 9638 (1991).

Numerical testbed for laser materials processing

M.S. Gross^a, I. Black^a and W.H. Müller^b

^aHeriot-Watt University,
Department of Mechanical and Chemical Engineering,
Riccarton Campus,
Edinburgh, UK, EH14 4AS

^bTU-Berlin, Institut für Mechanik,
Fachgebiet Kontinuumsmechanik und Materialtheorie,
Sekt. MS 2, Einsteinufer 5, Berlin, Germany, 10587

ABSTRACT

Current numerical simulations of laser materials processing usually simplify any process model to a great extent in order to allow for short computation times. This significantly decreases their flexibility and ability to simulate the great variation of today's processes with their subtle but important differences. The simulation presented in this paper can be said to be truly three dimensional as opposed to other reported work that uses symmetric boundary conditions. This enables the investigators to simulate real laser beams. In contrast to the (well-documented) Marangoni flow profile, the authors will show results that do not use the usual simplifying assumptions of flat surfaces. Preliminary output from the simulation deals with the transient coupled velocity and pressure profile and temperature distribution and hence the heat affected zone (HAZ). From this, conclusions can be drawn with regard to improving process efficiency, especially in laser cutting. It will be shown that the traditional perception of equating higher processing speeds with better processing efficiency does not hold in all cases. In fact, the opposite may well hold true. However, to demonstrate this the actual process of producing a part needs to be fully understood. A process may influence the workpiece material properties beneficially when it is performed at reduced speeds (material hardening or softening). The investigators contend that numerical modeling of the above can only be achieved credibly using high performance computing methods.

Keywords: laser materials processing, laser sources, numerical simulation, numerical modeling, fluid flow, Marangoni, free surfaces

1. INTRODUCTION

Laser machine tools have found a secure place for a variety of materials processing techniques such as drilling, cutting, welding, heat-treating and alloying. Their unique capacities can also give rise to novel manufacturing approaches.¹ The application of lasers spans such diverse fields of engineering as welding of parts, heat treatment, surface coating, cutting and drilling and even medical applications like surgical cutting, welding of wounds, modification of tissue and many more. The range of materials to which the laser can be applied to is similarly diverse including ceramics, plastic, metals, biological tissue and wood.

2. NUMERICAL TESTBED - A DEFINITION

Materials processing by the means of lasers is a complex field. The vast amount of literature available concerned with the modeling of laser materials processing highlights the need for unbiased predictive tools. However, Sargent *et al*² point out that:

"... many projects, while successful in their own narrow areas, never produce general, useful results."

Further author information: (Send correspondence to M.S.Gross)

E-mail: m.s.gross@hw.ac.uk

This is the main motivation for building a simulation framework which addresses exactly this shortcoming. A testbed has to be versatile and the amount of pre-analysis assumption has to be reduced to the maximum extent possible. With respect to laser materials processing, this holds for the laser source as well as the assumptions made concerning the workpiece. It would be of little use for the practitioner, who is confronted with a decision to be made about the quality of the laser source to be used in practice, if the numerical model assumed a perfect source. With regard to the model of the workpiece, it would be equally disadvantageous if the experimentalist had to decide *a priori* if the melt flow is of significance or not, or even if the velocities within the melt are above or below a certain threshold value for which the simulation is understood to be valid or not. Obviously, in order to achieve a simulation that addresses these issues, certain simplifications have to be made. The main challenge is to reduce these to an acceptable minimum. In order to fully appreciate the need for a numerical testbed, the main features of laser material processing are outlined as follows.

2.1. Process features

Copley *et al*³ presented the topography of regions melted by a continuous wave (cw) CO₂ laser beam and developed a theory to explain phenomena due to convective processes related to epitaxial regrowth and surface relief in laser melted regions. At the point of impingement of the laser beam, the temperature increases and, because the temperature coefficient of the surface tension is positive for most materials, the surface tension increases along a line from the impingement point to the edge of the melt pool. Thus any volume element of the surface experiences a net force parallel to the surface causing it to move from the center to the edge of the melt pool. In the case of a moving melt pool the convection pattern becomes unsymmetrical. In Figure 1 the origin of ripples and other topographical features associated with travelling melt pools (such as laser melted regions) is illustrated. Similar effects have been reported by Moore *et al*⁴ and the striking resemblance of laser surface melts to welds is pointed out. The most dominant feature is the *chevron pattern* formed by the isolines of temperature and hence the melt pool. Laser surface melts often exhibit a central crest which runs the length of the melt and which is flanked on each side by a trough as shown in Figure 2. The resulting surface roughness due to the ripples is reported to be between 5-15 μm . In laser welding these can easily add up to 0.01 times the width of the weld.⁵

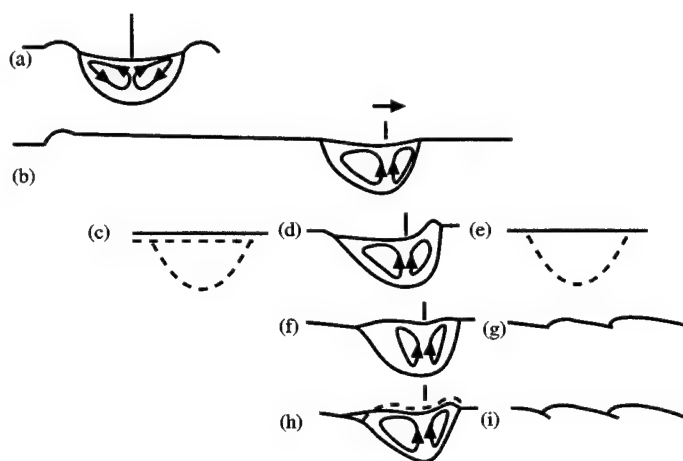


Figure 1. Mechanism of ripple formation: (a) laser translational velocity equals zero; (b) and (d) velocity not equal to zero; projected area of back side of pool (c) less than that at front edge of pool (e); (f) and (g) ripples without back flow; (h) and (i) ripples with back flow³

The appearance of humps on the surface of the weld bed is usually referred to as humping phenomena. A sketch of a typical shape of the cross section is shown in Figure 3. The deep depression of the material at the former solid-liquid interface, called undercut, is experimentally found to be associated with the humping phenomenon. In general, these humps occur periodically along the weld bead.⁶ The undercut phenomena

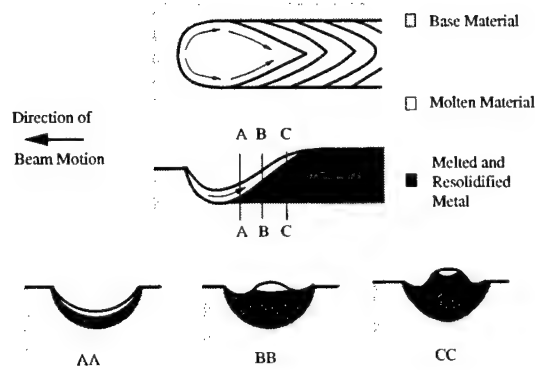


Figure 2. Schematic diagram of the laser surface melting process showing a top view (top), lengthwise cross section (middle), and various transverse cross sections (bottom)⁴

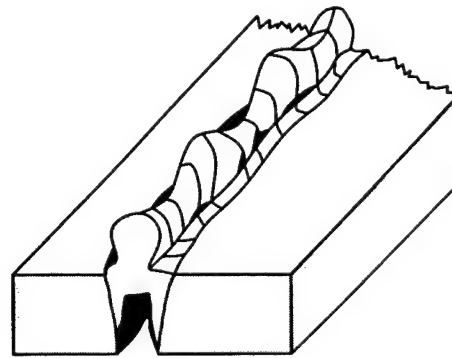


Figure 3: Humping phenomena in laser welding. Sketch of the weld bead based on a microscopic study.⁶

shown in the Figure 3 may lead to stress risers during service life of the manufactured part and is addressed in Atwa *et al.*⁷ Additionally these authors point towards problems concerning lack of penetration, root undercut, inclusions and burn-through in the context of premature failure of pipelines.

2.1.1. Laser cutting

Salient features of the laser cutting process are depicted in Figure 4. Process parameters can be adjusted and tuned to provide the quality of cut desired, but this procedure consumes exhaustive amounts of time and effort, without the optimal cutting conditions being found. If a different type of material is to be cut, then this procedure has to be repeated. This has been recognized as a major shortcoming in laser machining set-up.⁹ Furthermore the optimum process parameter may well be a transient set of parameters, depending on the path of cut (may be three dimensional), the material (composition) or the cutting condition (cutting speed, sheet thickness, etc.). The effects of melt flow over an edge (refer to Figure 5) have been studied in an extensive manner by Brown and Davis¹⁰ but so far no generic simulation includes these factors.

Regular spaced ripples or “striations” along the cut edge as shown in Figure 6 can be observed during laser cutting. In thin sections these may be clear and regular from the top of the cut edge to the bottom. However, on thicker sections, the striations may be clear towards the top of the edge but are replaced towards the bottom by more random ripples associated with the flow of liquid out of the cut zone.¹¹ Di Pietro and Yao⁹ comment thoroughly on the state of the knowledge concerning the formation of striations:

“... the mechanisms affecting the forming of stria are not well understood. Striations will result to some extent due to the non-steady nature of laser cutting.”

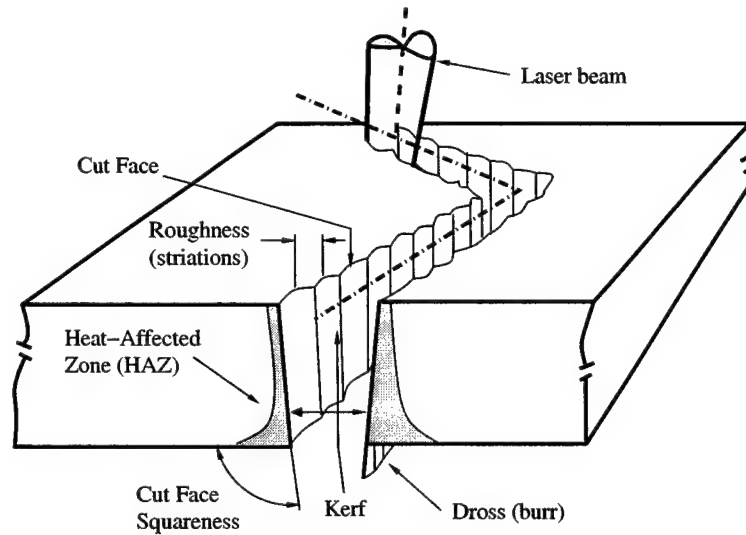


Figure 4: Factors in Laser Cutting⁸

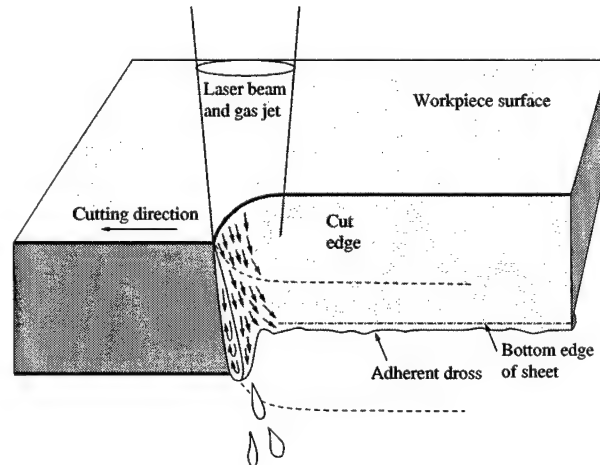


Figure 5. A schematic of the cut zone. The high surface tension of the melt and its adhesion to the workpiece results in dross adhering to the lower edge of the cut.¹¹

A similar scatter of theories and the limited predictive capabilities of current simulations prevails in context with other features in laser materials processing such as humping, rippling and dross formation.

The ambiguity in process parameters becomes obvious in the following example reported by Klocke *et al.*¹² For a 3 mm thick sheet PRMMC (particle reinforced metal matrix composites) - such as SiC-Al with 20% SiC, a cutting speed of 600 mm/min can be achieved. Increasing the laser power or decreasing the cutting speed can increase the cut width. When cutting pure aluminum a smaller width of cut is achieved. The dross for pure aluminum with similar cutting parameters is shorter and the cut face squareness is larger with a reduced cutting speed. Usually the surface roughness is reduced by increasing the cutting speed or laser power. The reverse is true for pure aluminum. A relationship between HAZ and dross has been reported.

Laser cutting of ceramics is still a problem due to their low thermal shock resistance. Sometimes the cutting performance with ceramics is increased when the focal spot is above the material surface. This results in a wider cut and the shield gas can be used more effectively for melt removal. For 10mm thick ZrO₂ an optimum focal

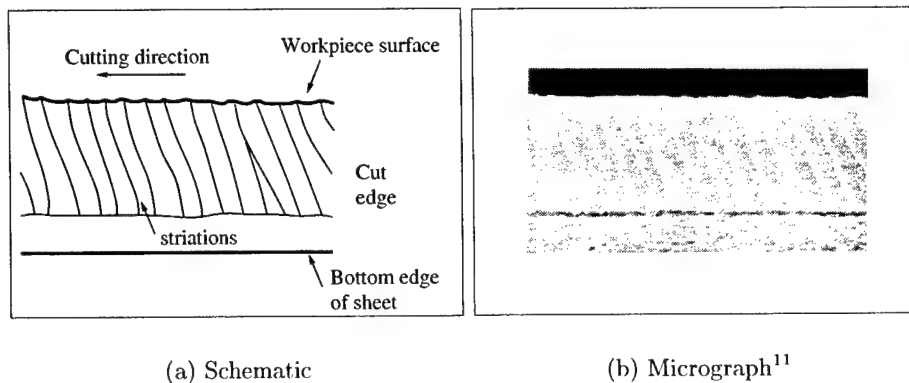


Figure 6: Striations in laser cutting

spot position is 5mm above the surface, and cutting speeds of up to 500 mm/min in cw mode are reported.¹² When cutting Al_2O_3 an optimum speed of 50 mm/min has been reported¹² and attributed to the smaller amount of melt generated. An occurrence of macroscopic crevice formation was observed due to the high brittleness of the material. Improvement was reported when using a Nd:YAG as supposed to a CO_2 laser. Cutting without cracking was achieved, and this was attributed to the smaller focal spot and higher intensity. All the previous examples highlight the need for a versatile and precise simulation.

3. MODELING STRATEGY

This paper will not provide a detailed discussion of the physical/mathematical modeling strategies used by the authors. The underlying physical model and its mathematical modeling will be published elsewhere. Here the authors wish to focus on the main principle, rather than the implementation. From the definition of a numerical testbed given above, two main features are immediately apparent. The model has to be three-dimensional in the spatial discretization, and the flow of the molten material must be included in the model. The first feature is due to the fact that a symmetry assumption would a) infer a perfect source and b) reduce the applicability to straight lines, which in practice represent only a fraction of the work to be performed. The fluid flow is important, because we can only discard it sensibly if the simulation clearly shows that it is of no significance. Doing so beforehand involves a sound complex physical reasoning which is extremely difficult, especially as today the scientific community as a whole is not in agreement on the explanation of certain phenomena as dross, stria and ripples. From studying the literature available it becomes obvious that modeling the physics involved is extremely complex and indeed justifies a separate numerical analysis. For example Chen *et al*¹³ modeled oxidation effects in laser cutting, the assist gas flow in a kerf was studied by Vicanek *et al*¹⁴ and Kar *et al*¹⁵ developed a gas-dynamical model in order to describe the plasma formation, velocity and particle size distributions in the plasma during laser ablation. On their own though, as mentioned before, the published work does not contribute significantly towards a comprehensive simulation of the process itself. Rather, it has to be incorporated on a phenomenological basis into a numerical testbed. This will be done in this paper and in future work. The main strategy is depicted in Figure 7 and shall be outlined below in the example of the incorporation of the stagnation pressure of a shield (or shroud) gas into the current testbed.

A unique set of unrestricted parameters is input to the numerical testbed. No restrictions that would result from previous assumptions in the model itself (e.g. neglecting the fluid flow) are present in the testbed. Certain phenomena can, at present, only be incorporated on a knowledge basis. This means that the explicit treatment in terms of discrete differential equations would increase the computational effort beyond current capabilities. Rather, these phenomena are studied beforehand parametrically, and by identifying the respective parameters during the simulation in the testbed, the output knowledge of prior simulations can be retrieved. In other words, for the example of the shroud gas stagnation pressure, a large quantity of simulations of the stagnation pressure field would be performed beforehand on varying surface profiles. For certain surface profiles

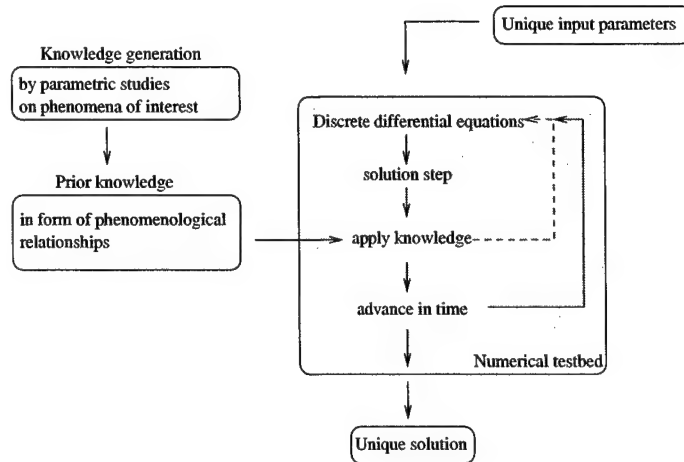


Figure 7: Strategy for the numerical testbed

the stagnation pressure distribution will be close to the analytically exact solution of the Navier-Stokes equation for a stagnation flow targeting a flat plate. Hence this can be utilised as “knowledge”. If this is not the case, characteristic parameters of the surface will be extracted and the pressure distribution will then be reconstructed from the parameterized solution of the shroud gas simulation and subsequently incorporated into the testbed at that time step. For the subsequent time step, a new set of parameters will be identified and a new gas flow profile profile retrieved.

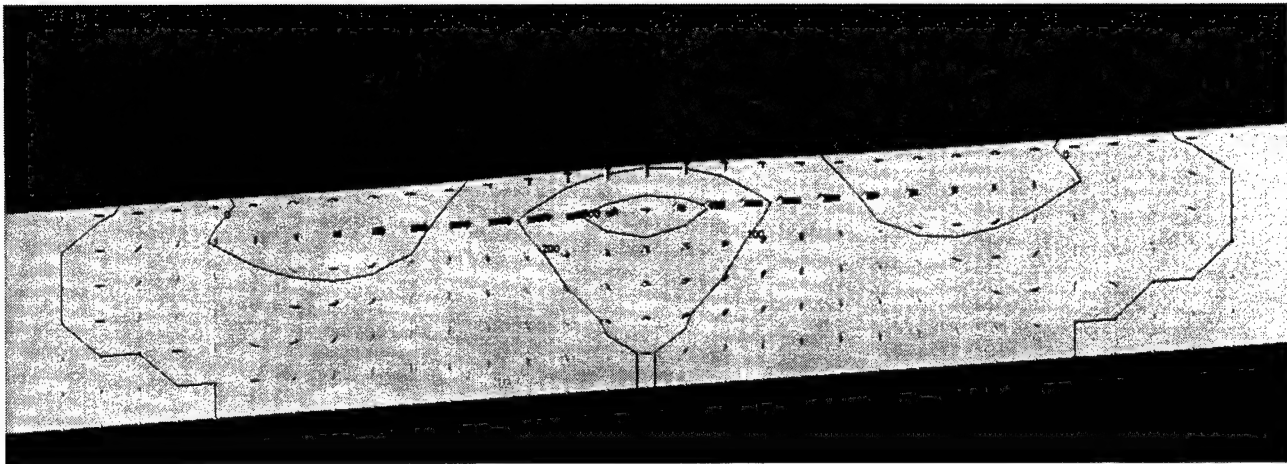
4. ROAD-MAP

The time frame for the development for the numerical testbed is set for three years. In this paper the authors have presented the work and results of the first year. During that year, a model has been developed for the solution of the incompressible Navier-Stokes equations with free surfaces, surface pressure due to the curvature of the surface and Marangoni surface tension driven flow with energy balance. Preliminary results from this work are presented. In the forthcoming year, the model will be extended significantly. Knowledge based modules will be incorporated to allow for shield (shroud) gas pressures, evaporation at the surface and melt outflow will be incorporated and hence the cutting process will be captured. This has to go along with full parallelization of the code, since for a realistic simulation the discretization needs a significant increase in density of discrete points. During the third year, the incorporation of knowledge modules is expected to continue, with application to case studies.

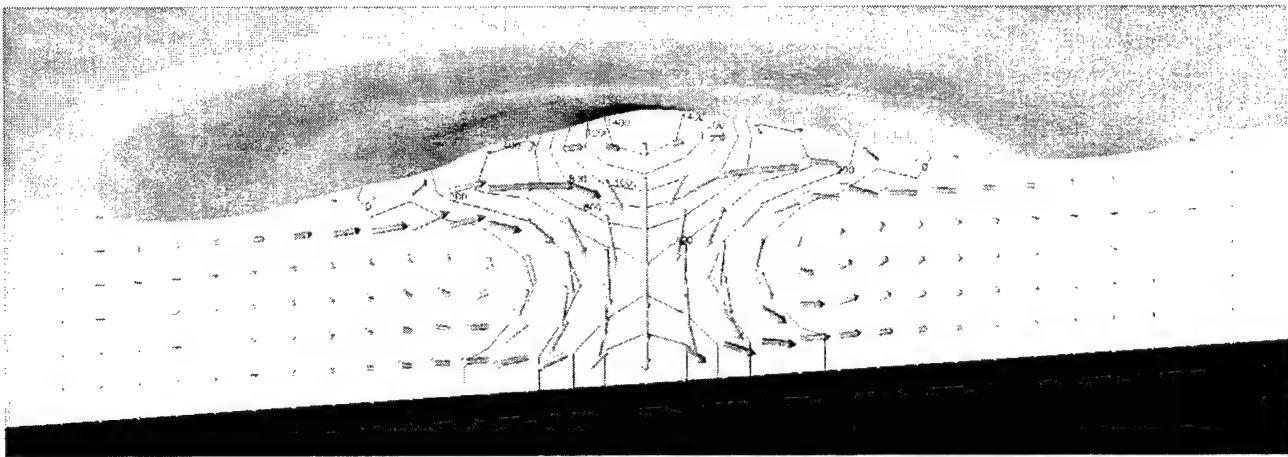
4.1. Preliminary results

The preliminary results from this simulation are concerned with computing the dynamic behaviour of a weld pool subject to Marangoni surface driven flow. In Figures 8 and 9 a time sequence simulation is shown. Initially the surface is flat, evolving through a set of dynamic oscillations during time. Isolines of pressure in the melt pool are plotted and the velocities are indicated by their respective vectors, with the magnitude of velocity represented by their length. The trace of the height of the central point of the free surface is plotted over time in Figure 10.

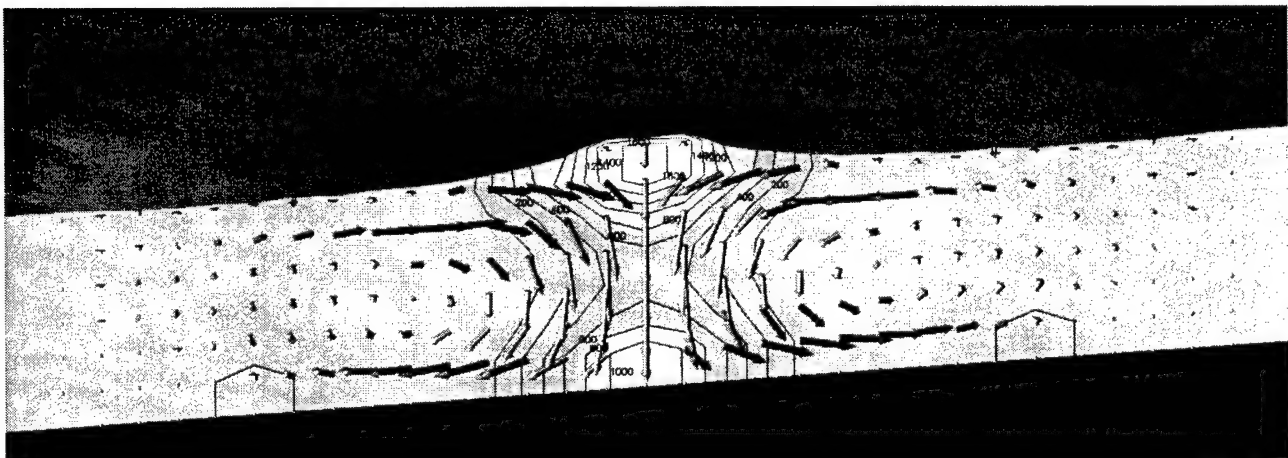
The time step of the simulation is 0.5×10^{-4} s and hence the time interval between the first and second maxima is $(333 - 135) \times \Delta t \approx 0.01$ s. This leads to a frequency of about 100 Hz. As this is a solution to a very coarsely discretised general problem, the results can certainly only be interpreted in a qualitative manner. It shows clearly the complex interplay of different physical forcing and oscillation phenomena.



(a) $1 \times \Delta t$

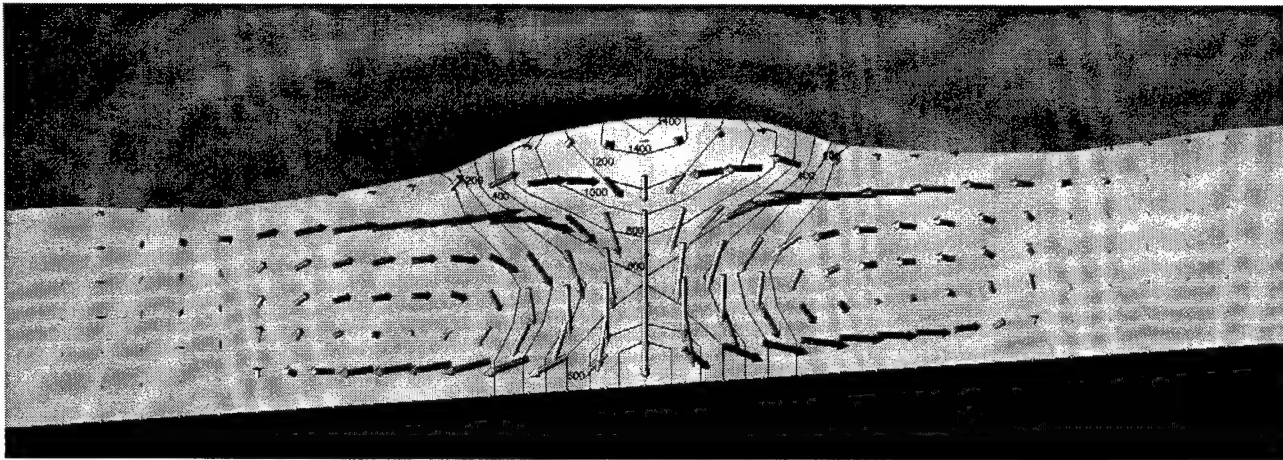


(b) $100 \times \Delta t$

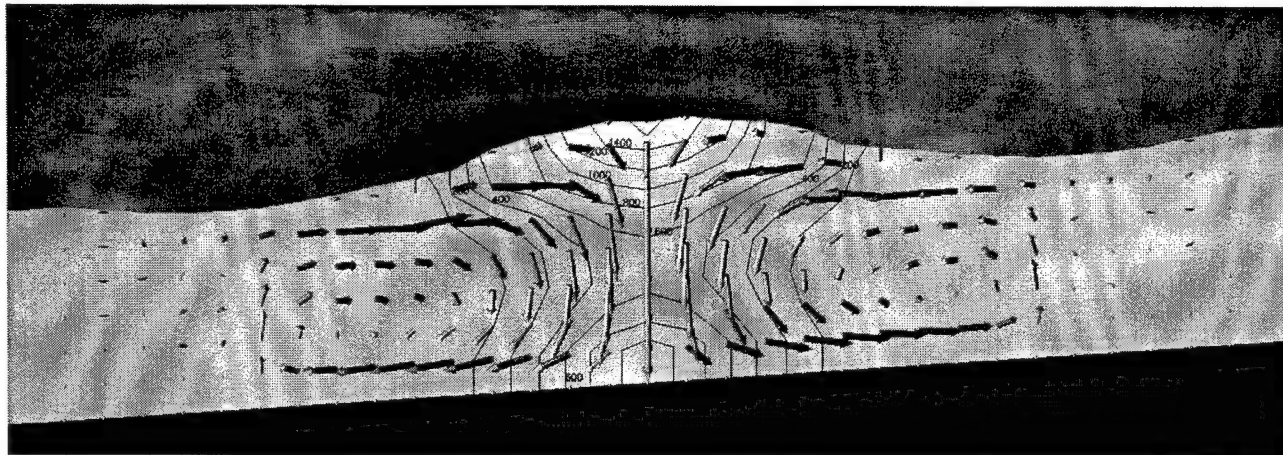


(c) $200 \times \Delta t$

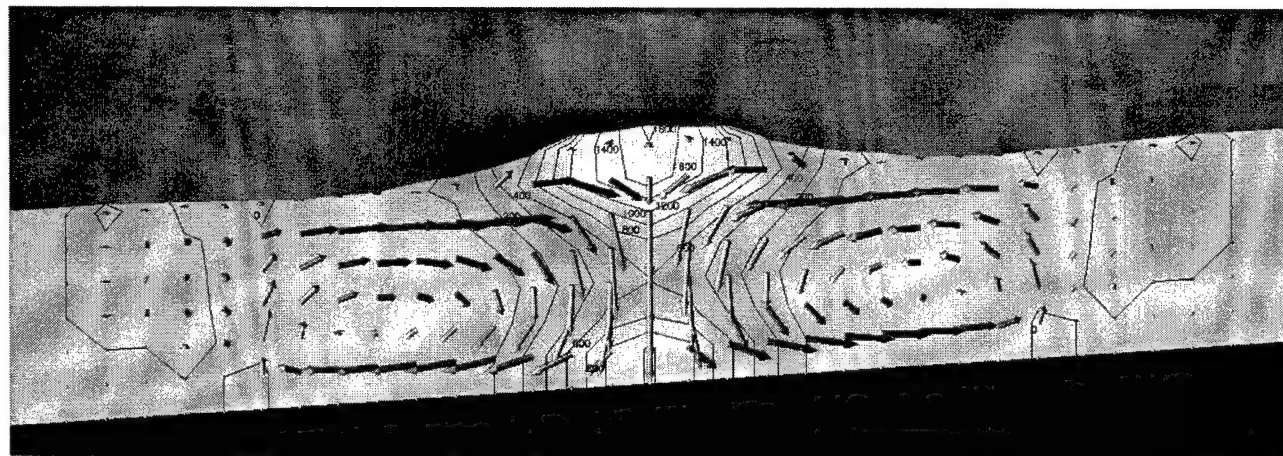
Figure 8: Time sequence of surface, pressure and velocity distribution



(a) $300 \times \Delta t$



(b) $400 \times \Delta t$



(c) $500 \times \Delta t$

Figure 9: Time sequence of surface, pressure and velocity distribution

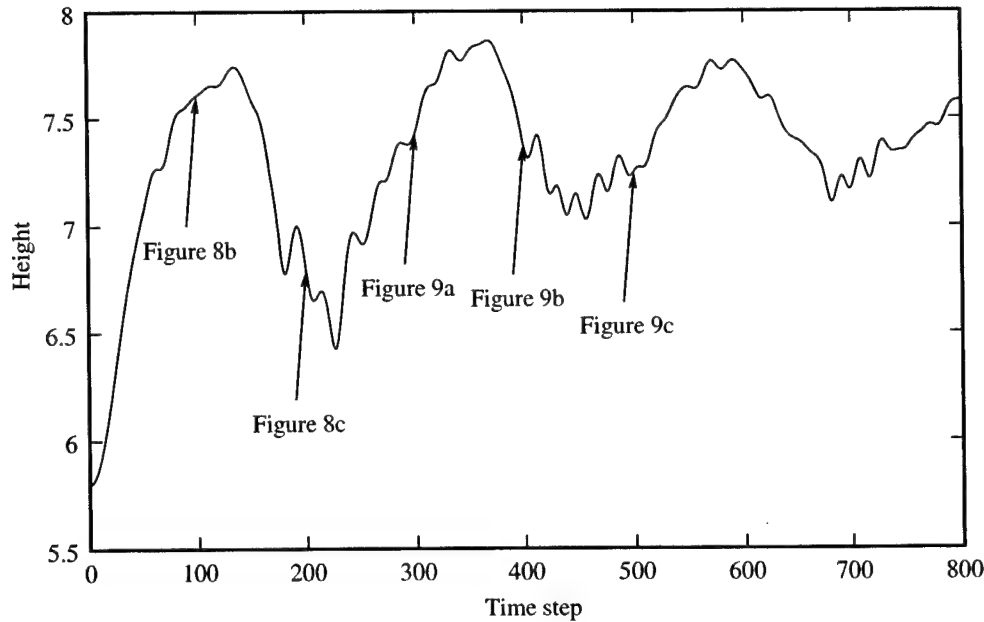


Figure 10: Time sequence of the evolution of the height of the central point of the free surface

Initially the flow is confined to the volume immediately underneath the surface, with the velocities aiming towards the center of the weld pool surface. In consequence a stagnation pressure builds up. Since initially less energy is required to lift the surface, rather than to initiate a recirculation flow field, the surface moves upward. The build-up of liquid in the center is counteracted by gravity and surface tension. This leads to a build-up of recirculation that eventually reduces the surface height in the center. Since this is a dynamic process, several oscillations are observed before a steady state profile is assumed.

5. DERIVATION OF SECONDARY INFORMATION FROM A NUMERICAL TESTBED

The authors believe that the full scale testbed will provide significant findings for the practitioner. With respect to the laser cutting process, this could involve the precise prediction of the heat affected zone. Most simulations available to date are not capable of capturing the extent of the HAZ at the outflow edge (shown in Figure 11), since the fluid flow is often neglected.

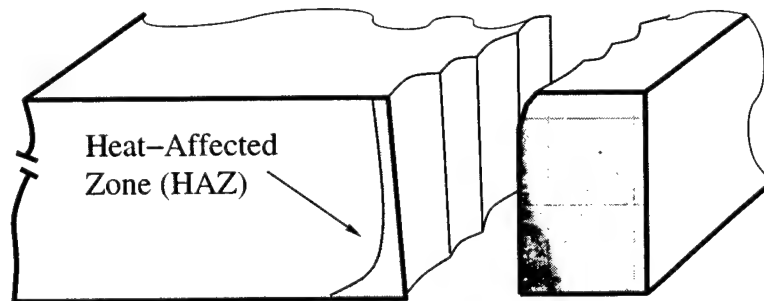


Figure 11. Schematic and micrograph of the HAZ when cutting a ceramic tile. The microstructural change in the HAZ is clearly visible due to its darker shading.

Predicting the size and cooling rate of the HAZ is of major importance since this can impact on the mechanical properties of the finished product, when phase transformations due to the temperature distribution

are considered (e.g. tempering, hardening). Hence reduced cutting speeds (as opposed to the optimum speed, usually defined as being the speed associated with best quality results) may enhance properties of the workpiece in the proximity of the cut. Predicting dross distribution has a direct benefit during part manufacture, since the build up of dross usually requires further processing steps to remove it, with associated quality issues.

6. CONCLUSION

The authors are optimistic that the final result will be a versatile tool for the applied scientist and engineer. It is expected that the numerical testbed can be used in a diverse manner, ranging from evaluation of the applicability of certain simplified simulations to gaining insight into ripple, stria and dross formation with a predictive capability with respect to the HAZ. The authors contend that, in order to achieve these aims, a significant computational resource is needed, and this may not always be justified. With regard to usability on the shopfloor, this is a serious limitation. As experience shows, though, computational resources are getting more and more accessible at significantly less cost, and hence the investigators envisage that this will ultimately broaden the use of this tool at the shopfloor as well.

REFERENCES

1. A. V. La Rocca, "Laser applications in manufacturing," *Sci. Am.* **246**(3), pp. 80–87, 1982.
2. P. Sargent, H. Shercliff, and B. Wood, "Modelling materials processing: An overview," in *Proceedings of International Conference on Computer-Assisted Materials Design and Process Simulation, COMMP'93*, pp. 474–479, Iron and Steel Institute of Japan, Sept 1993.
3. B. D. Copley S.M., "Laser melt quenching and alloying," in *Laser-Solid Interactions and Laser Processing, AIP Conference Proceedings* **50**, AIP, 1978.
4. K. C. Moore P., "Topographical characteristics of laser surface melted metals," in *Laser-Solid Interactions and Laser Processing, AIP Conference Proceedings* **50**, AIP, 1978.
5. T. R. Anthony and H. E. Cline, "Surface rippling induced by surface tension gradients during laser surface melting and alloying," *Appl. Phys.* **48**, pp. 3888–3894, 1977.
6. U. Gratzke, P. D. Kapadia, J. Dowden, J. Kroos, and G. Simon, "Theoretical approach to the humping phenomenon in welding processes," *Journal of Physics D: Applied Physics* **25**(11), pp. 1640–1647, 1992.
7. H. Atwa, N. M. Mawsouf, and M. Y. Younan, "Study of the effect of defects on the fatigue behavior and the fracture-toughness for low-carbon steel (api 5l grade b) gas transmission pipelines," *Engineering Fracture Mechanics* **44**, pp. 921–, APR 1993.
8. R. E. Green, ed., *Machinery's Handbook 25*, Industrial Press, 25 ed., 1996.
9. P. Di Pietro and Y. L. Yao, "An investigation into characterizing and optimizing laser cutting quality - a review," *International Journal of Machine Tools & Manufactur* **34**, pp. 225–243, FEB 1994.
10. R. A. Brown and S. H. Davis, *Free boundaries in viscous flows. Workshop. Program on phase transitions and free boundaries. Papers*, vol. 61 of *The IMA volumes in mathematics and its applications*, Springer-Verlag, 1994.
11. J. Powell, *CO₂ Laser Cutting*, Springer, second ed., 1998.
12. F. Klocke, O. Auer, and M. Hamers, "Laser treatment of advanced materials," *wt Werkstattstechnik* **1**, 2000.
13. K. Chen, Y. L. Yao, and V. Modi, "Numerical simulation of oxidation effects in the laser cutting process," *International Journal of Advanced Manufacturing Technology* **15**(11), pp. 835–842, 1999.
14. M. Vicaneek, G. Simon, H. M. Urbassek, and I. Decker, "Hydrodynamical instability of melt flow in laser cutting," *Journal of Physics D: Applied Physics* **20**(1), pp. 140–145, 1987.
15. A. Kar and J. Mazumder, "Mathematical-model for laser-ablation to generate nanoscale and submicrometer-size particles," *Physical Review E* **49**, pp. 410–419, JAN 1994.

High power gas-discharge and laser-plasma based EUV sources

Frank Flohrer, Kai Gäbel, Diethard Klöpfel, Peter Köhler
XTREME technologies GmbH, Göschwitzer Str. 25, D-07745 Jena, Germany

Imtiaz Ahmad, Sven Götze, Jürgen Kleinschmidt, Vladimir Korobotchkov, Jens Ringling,
Guido Schriever, Uwe Stamm
XTREME technologies GmbH, Hans-Böckler-Str. 27, D-37079 Göttingen, Germany
Phone +49-551-6938-261, Fax +49-551-6938-260, email secretary@xtremetec.de

ABSTRACT

In this paper we discuss new results from investigations on high power EUV sources for micro-lithography based on gas discharge produced plasmas and laser produced plasmas. The EUV development is performed at XTREME technologies GmbH, a joint venture of Lambda Physik AG, Göttingen, and Jenoptik LOS GmbH, Jena.

For gas discharge EUV sources we report data based on Xenon filled Z-pinches. Prototypes of the EUV source achieve an EUV output power of 10 W in-band in continuous operation. Repetition rates of 1 kHz are possible with liquid cooling of the discharge head. The spectral distribution of the EUV radiation shows a maximum around 13.5 nm and matches the reflection characteristics of silicon/molybdenum multilayer mirrors. Conversion efficiencies between 0.25% and 0.7% into a solid angle of 2π sr were achieved with the Z-pinch source depending the discharge geometry. The total EUV average power in the spectral range between 5 nm and 50 nm is about 200 W in 1.8 sr. Pulse energy stability data show standard deviation between 1-4 %. Spatial and temporal emission characteristics of the discharge source in dependence on the discharge geometry are discussed.

The laser plasma investigations are performed with an experimental setup consisting of a diode pumped laser system coupled to a liquid jet target. Since the conversion efficiency into EUV-power depends critically on the emitter density in the interaction region, we use a Xenon-jet, which is cryogenically liquefied and injected under high pressure into the vacuum vessel. Thus the laser is impinging on a target of solid-state density, which allows the generation of EUV-radiation with high conversion efficiencies of 0.5 % into a solid angle of 2π sr.

Keywords: gas-discharge, z-pinch, laser-produced plasma, EUV, lithography

1. INTRODUCTION

Next generation lithography exposure tools for semiconductor chip manufacturing are expected to be based on extreme ultraviolet (EUV) technologies. Current approaches of the optical system are designed to use an illumination wavelength of 13.5 nm. The mirrors used in the illumination system will reflect a spectral portion of 0.27 nm of the radiation from the EUV source (2% bandwidth).

Currently two different kinds of EUV sources are under investigation worldwide for commercialization of EUV related technology: Gas discharge produced plasmas and laser produced plasmas. The output power of the EUV radiation and source lifetime of state of the art EUV sources are the most critical parameters. Up to now they are still orders of magnitude below those parameters, which are expected as the requirements of sources for EUV-lithography mass-production. Based on current knowledge both concepts, gas-discharge sources or laser-plasma sources, have their own, specific advantages and drawbacks. Scientists at XTREME technologies are investigating both source concepts to fulfill the source requirements. The gas discharge based sources are aimed to match the specifications needed during the development phase for EUV lithography, whereas the achievement of specifications for production tools is a high technical risk. The laser produced plasma source is considered as a backup development for high EUV output power for production tools. This technology suffers from the high cost of ownership caused by the high power laser system.

Critical issues limiting the lifetime of the sources are the strong plasma wall interaction, which leads to sputtering effects and wall material erosion. In case of gas discharge produced plasma sources these are the electrodes and the

ceramics separating them, in case of the laser produced plasma sources the nozzle providing the target material is the part closest to the plasma. Gas-discharge produced plasma sources operate with small plasma-wall separation which implies limitations due to heat removal. Laser-plasma sources offer a potentially larger plasma-wall separation while the reliable operation of the plasma at a large distance from the nozzle at a high power level has to be demonstrated. Both concepts are currently investigated by XTREME technologies.

2. GAS-DISCHARGE PRODUCED PLASMA EUV-SOURCE

We report data from gas discharge EUV sources based on Xenon filled Zpinches [1]. A wide field of discharge parameter is accessible with this setup. This includes geometrical parameter (e.g. electrode distance, insulator diameter and electrode shapes) as well as electrical parameter (e.g. voltage, capacity and inductivity) to achieve highest conversion efficiencies (schematic see figure 1). The electrical circuit including magnetic compression stages are matched to the discharge unit to achieve short discharge current rise-times and to minimize losses in the circuit. The capacitor storage bank allow for electrical input energies up to 40 J/pulse.

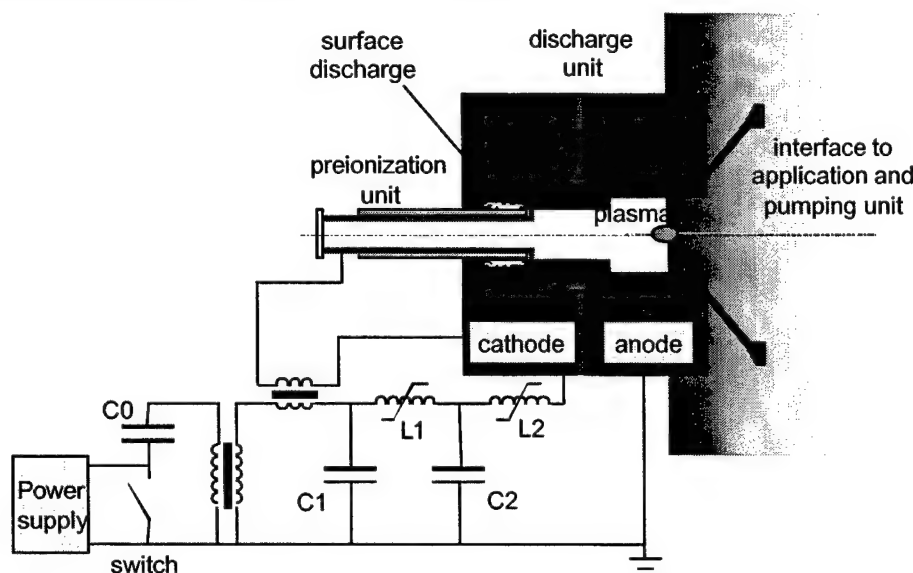


Figure 1 Schematic of the Z-pinch gas discharge device with surface pre-ionization.

The emission power of the gas discharge based source has been determined by using calibrated standard metrology tools. The energy monitoring tool comprising two multi-layer mirrors to select the proper EUV band, a metal filter to reject "out of band" radiation, and an EUV sensitive photodiode. A calibration factor is applied to account for the slightly wider EUV band of our particular measurement tool. These tools enable the absolute measurement of the EUV output power. The calibration of the measurement tools was performed in collaboration with AIXUV, Aachen, Germany. For this cross calibration the used metrology tools were compared to tools, which were calibrated before by using synchrotron radiation at PTB in Berlin.

The gas discharge prototype source achieves an EUV output power of 10 W at 13.5 nm wavelength in 2 % bandwidth and the usable angle of 1.8 sr working with a repetition rate of 1000 Hz. Assuming an isotropic emission distribution this corresponds to an output power of 35 W into a solid angle of 2π sr. Using a fast photodiode behind the described optical filters the emission duration was determined to 180 ns (FWHM). The measured output energy leads to conversion efficiencies between 0.25 and 0.7 % in 2 % bandwidth and 2π sr solid angle from electrically stored energy into usable in-band EUV power, depending on the discharge geometry.

The surface discharge pre-ionization in the design allows for homogenous ignition conditions of the plasma yielding reproducible results and good pulse-to-pulse energy stability (measured between $\sigma = 1\%$ and $\sigma = 4\%$) of the emitted pulses (figure 2).

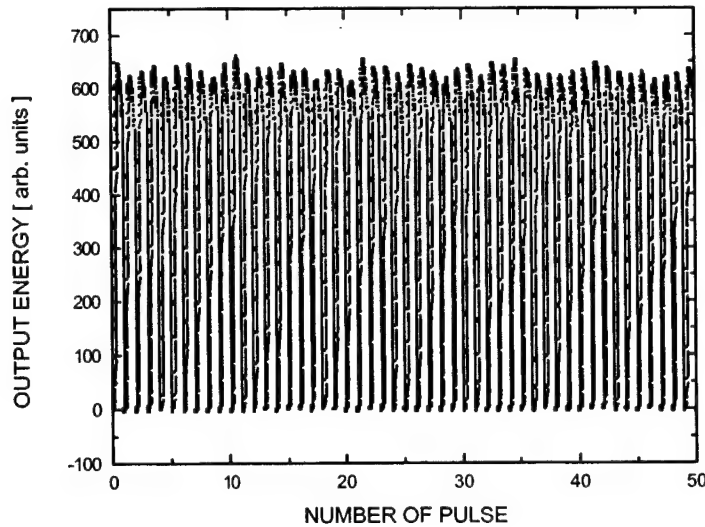


Figure 2 Pulse to pulse stability of the EUV emission. At 400 Hz repetition rate the energy emission was measured to $\sigma < 2\%$.

The emission spectrum of the radiation was measured with a reflection grating spectrograph including a flat-field grating and a CCD detector. Using Xenon as working gas the spectrum shows a maximum of intensity around 13.5 nm in adaptation to the reflection characteristic of a molybdenum silicon multilayer mirror (figure 3). The reflection band of 2% bandwidth of a multilayer system is shown as a bar in the background. Oxygen as working gas was used for the emission of small freestanding lines for the wavelength calibration and the determination of the spectral resolution of the spectrograph. Assuming delta shaped emission lines from oxygen the spectral resolution of the spectrograph could be measured to $\lambda/\Delta\lambda \approx 100$.

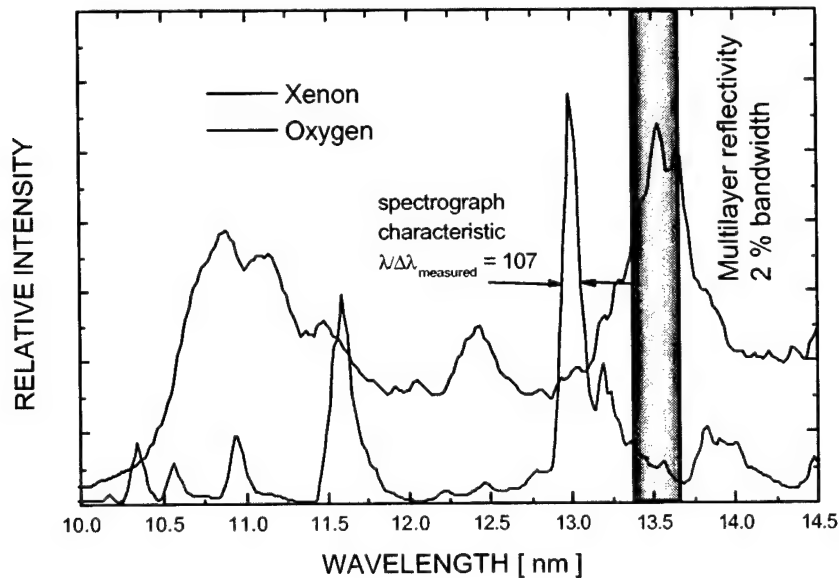


Figure 3 Emission characteristic of the Z-pinch EUV source filled with xenon in comparison to oxygen. The 2 % bandwidth of a multilayer system at 13.5 nm is shown as bar in the background.

The Xenon emission spectrum (figure 3) shows a large amount of radiation in the EUV spectral range outside of the bandwidth of 2 % around 13.5 nm wavelength. Only radiation within the bandwidth, which is marked in the spectrum, can be reflected by a stack of multilayer mirrors used for imaging in future lithography tool. All other radiation is absorbed inside the mirror layers and heats the optics. The use of grazing incidence optics with broad reflection characteristics could make this radiation utilizable for applications requiring broadband radiation as e.g. material research or micro machining.

3. LASER-PRODUCED PLASMA EUV-SOURCE

Figure 4 shows the principal setup of a laser-produced plasma EUV-source and an additional EUV optics to collect the emission and re-direct it into an intermediate focus. A similar scheme can be expected when the laser-produced EUV-plasma is employed as the source in a lithography scanner. Several diagnostics of the emission characteristics, radiative and particulate, are employed for optimization and source monitoring.

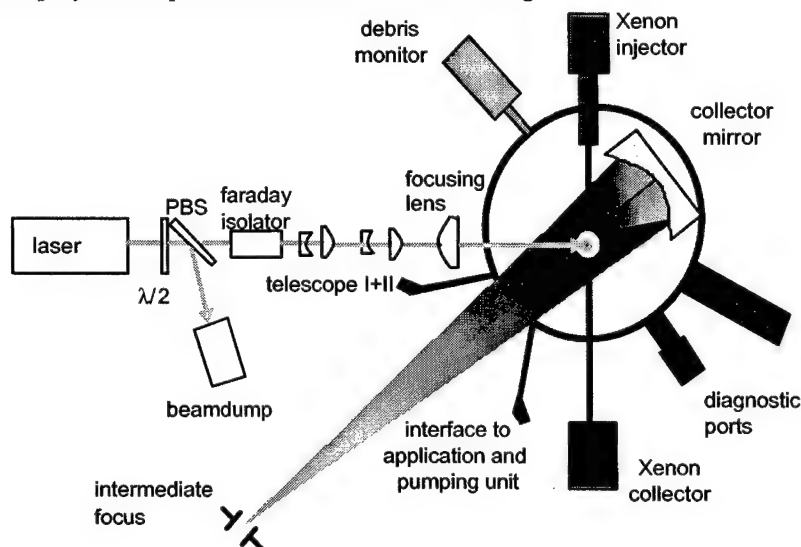


Figure 4 schematic of a laser-produced plasma EUV-source unit

Laser radiation is converted into EUV in a hot plasma with temperature $T \sim 10^6$ K, which is formed by the interaction of the laser beam with a high density target. Apart from the requirement of high conversion efficiency into EUV-radiation additional constraints are imposed by minimized particle-bombardment (debris) of surrounding optics.

The requirements onto the target can be summarized as follows:

- (1) A volume of high target density at the laser focus to supply a large number of emitters \Rightarrow liquid or solid modification
- (2) An interaction region at a large distance from surrounding components to minimize the heat load density at these components \Rightarrow high pointing stability of the target stream
- (3) A benign material which converts laser radiation into EUV efficiently \Rightarrow Xe

The inert gas Xenon seems currently the best compromise of intense EUV-emission into a 2% bandwidth at 13.5 nm and minimal optics contamination / damage.

A first experimental setup of a laser produced plasma EUV source was built up consisting of a Xe-jet-target coupled to a pulsed 40 W laser with 100Hz repetition rate. This system was used to acquire data on the spatial stability of the jet-target and on the conversion efficiency.

Jet-targets of different liquids coupled to intense laser beams are published to generate radiation in several spectral regions, some of them covering the relevant EUV-band [2]. In our setup Xenon is cryogenically liquefied and injected under high pressure through a nozzle of several 10 μ m diameter into the vacuum vessel. A 2nd cryogenic pump serves as the collector of the target material, and pumps the chamber to a pressure below 10^{-3} mbar. A photograph of the target

assembly is shown in figure 5. The jet enters the chamber from the top and is collected in the cryogenic pump at the bottom. The laser beam enters the chamber normal to the plane of the figure and hits the jet in the center of the chamber.

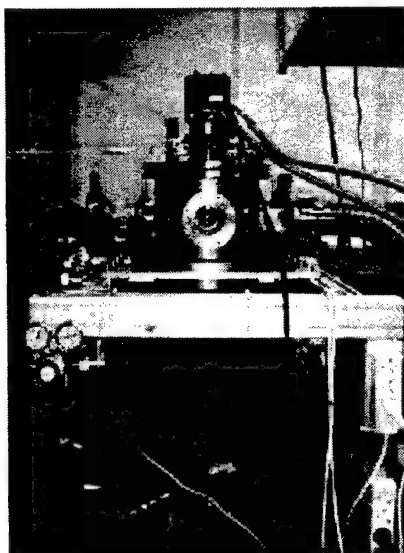


Figure 5 photograph of the interaction chamber

The spatial stability of the jet allows for plasma generation up to a distance of 1cm from the nozzle-tip. Typical experiments were performed at a distance of about 5 mm, which results in reduced fluctuations of the EUV-yield.

Figure 6 shows a photograph of the liquid Xe-jet and of the plasma generated by interaction of the laser beam with the jet respectively. The plasma picture was taken with a CCD-camera, which was sensitive in the VIS region.



Figure 6 photograph of the liquid Xenon jet (left) and of the laser plasma generated on the jet (right)

The EUV energy was measured with a calibrated energy monitoring tool as used for the gas discharge produced plasma EUV sources and described above. Figure 7 shows an EUV energy monitor signal averaged over 128 shots. The measured EUV-yield corresponds to a conversion efficiency exceeding 0.5% in 2π sr and 2% bandwidth. The current conversion efficiency corresponds to an average EUV power of 200 mW, which can be generated with 40 W laser power.

It is noteworthy that the current conversion efficiency was obtained with alignment of the laser focus relative to the Xe-jet only. Improvements are expected by optimization of laser and target parameters.

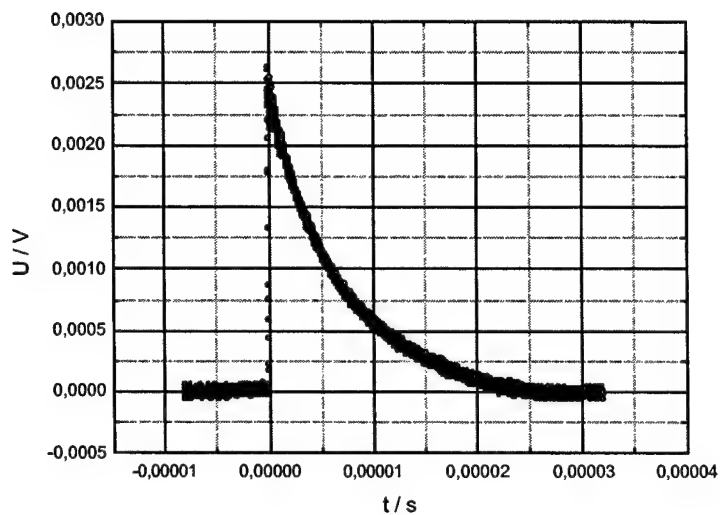


Figure 7 detector signal of the EUV-monitor averaged over 128 shots

A higher power EUV-system is currently under development, which will employ a 500 W laser coupled to an improved target injector. Figure 8 shows a CAD drawing of the complete system comprising the laser, a beam delivery unit, and the target vessel. The high power laser is based on commercially available oscillator and amplifier modules today used in industrial applications as laser machining and micro-machining. In current development status the laser driver delivers pulses of 20 ns duration at 2kHz repetition frequency at an average power of 200 W. The laser produced plasma EUV source is expected to generate an average power of 2.5 W in 2π sr and 2 % bandwidth.

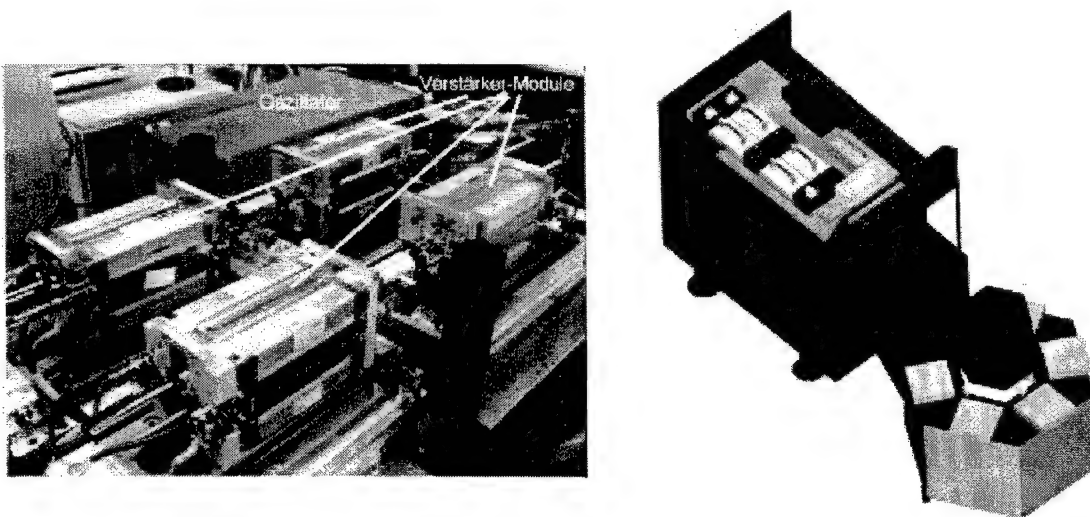


Figure 8 photograph of the high power laser (left) and CAD drawing of the laser-plasma EUV-source, employing a pulsed 500 W laser (right)

4. CONCLUSIONS / SUMMARY

EUV sources based on gas discharge produced plasmas as well as laser produced plasmas have been investigated as potential sources for EUV lithography exposure tools. For gas discharge produced plasmas conversion efficiencies of 0.3-0.7% into 2% bandwidth at 13.5 nm and in a solid angle of 2π sr have been measured. For laser produced plasmas conversion efficiencies under same conditions of 0.5 % have been achieved. As the conversion efficiencies are of the same order of magnitude, the generation of a certain output power requires a similar energy input into the plasma for both concepts. While the gas discharge produced plasma EUV sources require high voltage power supplies as driver, laser produced plasma EUV sources have to use laser drivers of the same average power. With gas discharge we generated an EUV output power of 10 W at 13.5 nm wavelength in 2% bandwidth. The usable angle was 1.8 sr. With the laser produced plasma we achieved 200mW EUV output power in 2π sr and 2% bandwidth.

Due to the broad emission characteristics of Xenon plasmas generated by both described methods, the output power of the sources is much higher if the useable spectral range is not limited by multilayer optics. This can be used for other applications working with broadband optics, e.g. grazing incidence mirrors.

5. ACKNOWLEDGEMENT

We acknowledge the research work by K. Nicklaus, R. Meyer, L. Becks, Ch. Warias, and D. Hoffmann of the Fraunhofer Institut für Lasertechnik performed on the development of a pulsed high power laser and V. Borisov, A. Ivanov, O. Khristoforov and A. Vinokhodov from State Research Center of Russian Federation, Troitsk Institute for Innovation and Fusion Research (TRINITI) for the support of the gas discharge plasma development.

6. REFERENCES

- [1] G. Schriever, M. Rahe, U. Stamm, D. Basting, O. Khristoforov, A. Vinokhodov, V. Borisov, „Compact Z-pinch EUV source for photolithography”, Proc. SPIE **4343**, 615 – 620 (2001)
- [2] Hertz, H.M., Bergland, M., Hansson, B.A.M., Rymelli, L.: SPIE **3767**, No. 01, 2-9 (1999)

Phone +49-551-6938-261, Fax +49-551-6938-260, email: secretary@xtremetec.de

Pulsed COIL with Volume Generation of Iodine Atoms in Electric Discharge.

Nikolai N. Yuryshev, Nikolai P. Vagin, Aleksei F. Konoshenko, Vladimir S. Paziuk
P.N. Lebedev Physical Institute, Moscow, Russia 119991

ABSTRACT

The method of volume generation of iodine atoms to obtain the pulsed mode of COIL is the most effective by the ratio of pulsed power to cw one at the same flowrate of chemicals. The electric discharge is a very convenient tool to produce iodine atoms in an active medium. The electrical efficiency close to 100% was obtained when longitudinal glow discharge was used.

The investigation of both influence of the discharge gap length on the performance of pulsed COIL initiated with longitudinal discharge and transverse discharge initiated pulsed COIL based on the Jet Singlet Oxygen Generator were performed. The lasing of Jet SOG based pulsed COIL has been obtained for the first time. The operation pressure of 17 Torr at oxygen partial pressure of 7 Torr in the laser cavity has been obtained

The temperature parameters of active medium being under electric discharge initiation were analyzed. The active medium temperature growth was shown to be responsible for decrease of specific output energy in discharge initiated COIL unlike that for photolytic initiation.

Keywords: gas laser, chemical oxygen-iodine laser, pulsed mode, singlet oxygen generator, iodide

1. INTRODUCTION

Application of the transverse self-sustained electric discharge to initiate pulsed chemical oxygen-iodine laser (COIL) with volume generation of iodine atoms was successfully demonstrated in [1]. This kind of electric discharge makes it possible to work at higher active medium pressure but at the same time it requires significant efforts to make this discharge to be uniform. In its turn, longitudinal glow discharge, having limitation by operation pressure, is a very simple in realization and provide the laser to have high electrical efficiency. The value of close to 100% efficiency (ratio of laser output energy to that stored in capacity) was reported [2].

The goal of this work is investigation of the influence of the length of the longitudinal discharge gap on the pulsed COIL output parameters. The results obtained can be useful for designing the pulsed COIL with electric discharge initiation. Unlike that for transverse initiation geometry the longitudinal one reserve the degree of freedom which can be used, for example, to mount the Q-switch system based on the Zeeman effect.

Saying on longitudinal discharge we have in mind the discharge geometry where the distance between the electrodes significantly exceed the electrode size. So one can see that shortening the discharge gap results in discharge geometry more close to transverse one.

As it was shown in the works carried out in Lebedev Physical Institute the application of such a discharge to initiate the pulsed COIL with volume generation of iodine atoms makes it possible the laser to operate with a high electrical efficiency close to 100 % at specific output energy of 0.5 J / l per 1 Torr of O₂. The laser operation at a length of discharge gap of 60 cm was demonstrated. The application of a glow discharge to generate iodine atoms in the gas mixture containing the singlet oxygen to form COIL active medium is not a trivial task. Indeed, the electrical discharge produces electrons, ions, and molecular fragments. The sort and concentration of these components, in general, depend on discharge parameters - mainly discharge energy and reduced strength of electric field E/N. Besides, the length of the discharge gap determines the resistance of plasma channel and, hence, the energy deposition into the active medium. Thus the optimization of discharge parameters to improve the energy parameters of the laser is a crucial task and variation of the length of the discharge gap allows one to vary latter parameter keeping the voltage constant.

2. EXPERIMENTAL

The schematic diagram of experiment with longitudinal discharge is shown in a Fig.1. The discharge chamber is mounted in one of the shoulders of experimental facility used in investigations of a pulsed COIL initiated with a longitudinal discharge [2]

The discharge chamber, 39-mm i.d., is made of PMMA. The chamber has 5 electrode holes. The electrode section of typical flash lamp, 20-mm o.d., is chosen as a cathode. These sections are inserted into electrode holes and sealed. The annular electrode is a common anode. To eliminate the influence of near electrode regions the electrodes are carried out the laser cavity area. Thus, the discharge positive column processes only form the laser active medium. The discharge chamber with a moving annular cathode was investigated too. But this design was abandon due to instability of results obtained.

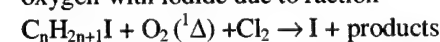
The electrical discharge fed by a capacitor bank is triggered with a thyatron TGI-25/1000 operating at a voltage up to 25 kV. The capacitor bank is assembled of several disk ceramic capacitors. Variation of both the voltage and the number of capacitor makes it possible to change the discharge energy.

The singlet oxygen is produced in the sparger type SOG packed with Rushig rings to, firstly, intensify the mass-transfer and, secondly, to prevent ejection of BHP from SOG. The buffer gases (N_2 , Ar, SF_6) is fed trough the SOG in a mixture with chlorine. The typical pump capacity in experiment is 80 l / s. The previously made measurements of the dependence of singlet oxygen yield on pump capacity allow us to evaluate the value of SO yield under different experiment conditions.

The laser operation at different length of the discharge gap is compared by output specific energy and efficiency, i.e. ratio of output specific energy to specific deposition energy. But output laser energy depends on the level of threshold exceeding, which, in its turn, depends on the gain length, i.e. length of the discharge gap. The 0.8 % transmission of the output spherical mirror of laser cavity is chosen to minimize this effect (the transmission of about 4 % is optimal for majority of experimental conditions). The 0.05 % transmission spherical mirror is chosen as a totally reflecting one. The laser output energy is limited with an external 30-mm diameter diaphragm installed 45 cm from output mirror.

The output laser energy emitted from aperture of 30 mm is measured with IMO – 2N, the pulse shape is recorded with a store oscilloscope and then is recorded with a digital camera Kodak DC-240.

The traditional design counter flow jet singlet oxygen generator of 4 cm internal diameter was used in experiments with pulsed COIL initiated with transverse discharge (Fig.2). The jets were formed with an assembly of 120 tubes of 0.7 mm i.d. The length of jets or reaction zone (distance from jets injector edge to the point of chlorine injection) was as long as 14 cm. The calculated value of specific surface area for smooth jet was 2 cm^{-1} . The working BHP solution was prepared in a separate vessel providing mixture cooling during the dilution process. Before utilization the working mixture was cooled down to -10^0 C . Medicine purity hydrogen peroxide of 38 % concentration and 12 N water solution of high purity KOH were used to prepare 4 l of working BHP. The jets were driven with atmospheric pressure. This volume was enough to provide the runtime of 17 s. The operation parameters of jet SOG were optimized to minimize the content of residual chlorine in the SOG effluents. It was necessary to avoid instability of the mixture of singlet oxygen with iodide due to raction



The discharge chamber made of PMMA has a gain length 5 cm. The laser is initiated by a discharge occurring between the bulk anode and 34 pins cathode. To stabilize the discharge each of pins is loaded with an active resistor $R = 150 \Omega$. The electrodes are 2 cm spaced. So the active medium volume is 20 cm^3 . The capacitor bank consist of ceramic $C = 4.7 \text{ nF}$ capacitors. The necessary capacitance and operation voltage of the bank is obtained by connecting several units in parallel or in series. The investigated region of capacitance is from 2.3 to 7 nF. Operation voltage is 16 kV. The trigger generator provided the discharge repetition frequency of about 1 Hz.

The laser optical cavity is formed with spherical and plane mirrors spaced by 70 cm. The generation parameters are detected with calorimeter IMO-2N and Ge-photodetector.

Singlet oxygen produced in the jet SOG is fed to laser chamber through the transport section of 20x50 mm cross-section and 160 mm length. The pump rate in the SOG is controlled via injection of necessary flow of buffer gas N_2 through the tube injector. 8mm o.d placed near the inlet of transport section. Iodide is injected into $N_2 - O_2$ mixture 60 mm downstream of N_2 injector. The iodide mixing length is 105 mm.

3. RESULTS AND DISCUSSION

3.1. Pulsed COIL initiated with longitudinal discharge

All experiments were carried out with an operation mixture of 1 Torr O₂ and 0.5 Torr CF₃I. Helium, nitrogen and sulfur hexafluoride are used as buffer gases. The experimental parameters were varied within 10 – 58.5 cm for discharge gap, from 10 to 20 kV for discharge voltage and from 2 to 8 Torr for partial buffer gas pressure.

Unlike photolysis, which is a very selective tool for iodide decomposition, the electric discharge interacts with all components of active medium. Forming electrons, ions and different molecular fragments, electric discharge modifies the active medium composition. In its turn, the initial composition of an active medium is a factor determining the discharge parameters: breakdown voltage, electron distribution by energy, discharge resistance, etc. Thus, the interpretation of the results obtained is a very difficult task. Nevertheless, we tried to evaluate the general rules in the behavior of the pulsed COIL with longitudinal discharge initiation.

The term "transverse" usually applies to the discharge geometry when discharge gap is appreciably less the cross-size. In this case the discharge resistance is low. When resistant loaded pins electrode is used for discharge stabilization the energy stored in capacitor bank is distributed between the plasma and load proportionally to their resistance. So, the variation of plasma resistance due to buffer gas, for example, results in change of energy deposition into active medium.

In the case of longitudinal geometry, when electrode separation is long enough, the capacitor energy is wholly deposited into active medium. So, the energy deposition is governed by capacitor only. It results in less influence of buffer gas pressure on laser output energy and pulse duration as compared with that for transverse excitation. This effect is most strongly marked for He as a buffer gas.

Another situation takes place when nitrogen N₂ is used as a buffer gas. In this case the pattern of buffer gas influence depends on the length of the discharge gap. Considering only the situations when the laser operates highly over the threshold one can see that for short discharge length the increase of nitrogen partial pressure results in initially weak and then sharp drop of output energy. At longer discharge length the sharp drop of output energy arrives at less nitrogen pressure. It means the buffer gases not only increases the heat capacity of active medium but also significantly change the plasma parameters and, may be, the discharge uniformity.

This effect is more demonstrated for sulfur hexafluoride. Being very electronegative, SF₆ affects very strongly even at low concentration. Nevertheless, at short discharge length longitudinally excited COIL can operate with SF₆ as a buffer gas and, hence, chemical generation of iodine atoms due to reaction of fluorine atoms produced in a discharge with hydrogen iodide as an iodine donor is possible.



It was observed in the first experiments with electric discharge initiated pulsed COIL the output specific energy of such a laser is at disadvantage in relation to photolytically initiated one. The different factors can be the reason of such a phenomenon. They are decrease of the singlet oxygen yield, forming the effective quenchers of excited states, heating of active medium and, hence, decrease of extractable fraction of energy stored in singlet oxygen. As it was shown the latter reason is the most possible.

The typical value of energy required to break the bond C-I in alkyl iodides or perfluoro-alkyl iodides is about 210 kJ/mol (53 kkal/mol for CF₃I, 54 kkal/mol for CH₃I). When photolysis is used to produce iodine atoms from these species which have a maximum absorption at the wavelength of about 270 nm the energy absorbed to produce one iodine atom is $7.4 \cdot 10^{-19}$ J (446 kJ/mol). Thus, the photo dissociation process is 225 kJ/mol exothermic. In fact the reaction is somewhat less exothermic because the fraction of iodine atoms is produced in excited state I (²P_{1/2}) (92 kkal/mol). The yield of excited state strongly depends on the sort of iodine donor and assumed to be zero in this consideration. If one produces the iodine concentration of $1 \cdot 10^{18}$ l⁻³ that corresponds to the COIL pulse duration of about 10 μs, the UV energy absorbed in the active medium is 0,74 J/l. But only half of this quantity of energy (0.37 J/l) is transferred to translation degrees of freedom i.e. to heat.

Another situation takes place when electric discharge is used instead of photolysis. In this case the comparable pulse duration is obtained when specific energy stored in the capacitor bank exceeds 8 J/l. When longitudinal discharge without ballast resistor is used, all energy stored in the capacitor bank is deposited into active medium. Thus, subtracting the energy consumed for breaking the CF₃–I bond, one can evaluate the value of energy to be transferred to heat (7.63 J/l) twenty times as much as that in photolysis.

As soon as the active medium is practically immovable during the short pulse its temperature is governed by heat capacity C_v. The values of C_v for different components of the mixture at partial pressure 1 Torr are:

CF ₃ I	$3.3 \cdot 10^{-3}$ J / l K
O ₂	1.12
Ar, He	0.67

N ₂	1.11
SF ₆	4.72

Thus, for the typical mixture composition O₂ : CF₃I : He = 1 : 0.5 : 3 Torr one has C_v = 4.78 · 10⁻³ J / l K. The energy that can be theoretically transferred to heat is 8,23 J/l. Being wholly transferred to translation degrees of freedom this energy results in ΔT = 1722 K of temperature growth. This value is an upper limit of temperature growth. In fact, the real value of temperature is somewhat less because of excitation of rotation and vibration degrees of freedom of mixture components and formation of ions and different fragments. Such a great growth of temperature results in growth of threshold yield of singlet oxygen and, thus, in significant decrease of extractable energy. Indeed, the value of threshold yield

$$Y_{th} = 1 / 1.5 \exp(401/T) + 1, \quad (1)$$

has a limit Y_{th} = 0,4 when temperature tends to infinity. Thus, at the temperature T = 2022 K (T₀ + ΔT) the value of threshold yield is Y_{th} = 0,35 instead of Y_{th} = 0,15 at room temperature. A previously made investigations of sparger SOG used in experiments shows the yield of singlet oxygen Y = 0,5 ± 0.05. One can derive that the extractable energy E_{extract} under discharge initiation is E_{extrac} = (0.10 – 0.20)[O₂]hν_{laser} instead of E_{extrac} = (0.3 – 0.4)[O₂]hν_{laser}. Having in mind that the real temperature growth is not so high one can conclude this effect is a primary reason of output energy drop when discharge is used instead of photolysis to initiate.

The special experiments were performed to evaluate the threshold yield and, thus, the real temperature of active medium. Unexcited oxygen was admixed to the active medium up to the concentration resulting in quenching of lasing. It is easy to show

$$Y_{th} = Y_0 / (1 + \Phi_{O_2} / \Phi_{Cl_2}), \quad (2)$$

where Y₀ is an initial singlet oxygen yield, Φ_{Cl₂} is a chlorine flowrate, Φ_{O₂} is an additional oxygen flowrate resulting in quenching of lasing. It is obvious, these experiments were carried out with totally reflecting mirrors of laser resonator. The mixture composition O₂ : CF₃I : N₂ = 1 : 0.5 : 3 Torr and discharge length of 40 cm were used. For the cases of 20.4 nF capacitor bank, 20 kV of operation voltage and Φ_{Cl₂} = 83.2 Torr l/s the value Φ_{O₂} = 62 Torr l/s was obtained.

Thus, assuming Y₀ = 0.45 – 0.55 one can evaluate Y_{th} = 0.26 – 0.31. Such values of Y_{th} correspond to the growth of temperature due to initiation energy deposition within the range of 326K – 716K. The conditions of experiments correspond to that of run 56.4, where the specific energy deposition is as large as 8.6 J/l. At the heat capacity of active medium C_v = 6.1 · 10⁻³ J / l K this value of energy deposition corresponds to the temperature growth of ΔT = 1410K. This value is twice as much as that obtained via threshold yield. It may signify that not all energy deposited into active medium is transferred to translation degrees of freedom. Note, that energy consumed to produce iodine atoms is too small to be account.

The similar experiment made for the energy stored in capacitor bank of 1.4J (C = 3.4 nF, U = 20 kV) gives the growth of temperature ΔT = 280K. The same parameter evaluated from deposited energy and heat capacity is ΔT = 240K. It is seen both values are in a good agreement.

Note, that because of a weak dependence of threshold yield on temperature at high values of temperature the accuracy of temperature measurement via threshold yield drops with temperature increase.

As it follows from aforesaid, at high energy deposition the chemical efficiency has a theoretical limit of about 20% (Y₀ = 0.45 – 0.55, Y_{th} = 0.26 – 0.31). But it was shown in experiments with transverse discharge the specific output energy of 0.5 J/l is obtainable at oxygen pressure 1 Torr. This value of specific energy corresponds to 10% of chemical efficiency. This fact demonstrates a very high efficiency of laser energy extraction from active medium.

Thus, the electric discharge initiation of pulsed COIL creates specific conditions of its operation. Unlike CW supersonic mode of COIL operation when the active medium temperature is low, the pulsed COIL with discharge initiation works under high temperature (close to 1000K) of active medium. This situation requires the new kinetic information on rate constants of processes which are critical for laser operation. The first of them is temperature dependence of energy exchange between singlet oxygen and iodine atom. In application to supersonic cw operation this process was under deep investigation for temperatures below room ones. As to temperature region above 300K, it is not investigated so deeply. The different temperature dependences are reported in literature, K(T) = 2.3 · 10⁻⁸/T [3], K(T) = 5.12 · 10⁻¹² · √T [4]. The correct temperature dependence of rate constant is necessary for adequate modeling of laser operation. Our evaluations of iodine atom concentration from duration of a laser pulse were made using the room temperature value for energy transfer constant. One can see the real concentration can be several times higher.

The high temperature active medium being produced in the electric discharge initiated COIL, is a model of active medium which, one can expect, can be produced in Electric COIL, i.e. oxygen-iodine laser with electrical SOG. Indeed, production of 40% yield of singlet oxygen in pure oxygen with concentration of 10²¹ cm⁻³ (corresponds to 30 Torr at

room temperature) requires the energy deposition of 125 J/l. At the efficiency of the excitation process of 50% [5] the energy transferred to translation degrees of freedom is 62 J/l. The heat capacity of oxygen at pressure 30 Torr is about $34 \cdot 10^{-3}$ J/l K. Thus, the growth of active medium temperature can achieve $\Delta T = 1823$ K. To drop this high temperature the adiabatic expansion in supersonic nozzle is used. But even Mach number $M=3$ makes it possible to drop temperature to only $T=764$ K. Note, the density of oxygen at this Mach number drops to $8 \cdot 10^{16} \text{ cm}^{-3}$.

The output energy is one of the key parameters defining laser operation. Figures 3 – 6 demonstrate the influence of initiation length (discharge gap length) on the laser output energy for He as a buffer gas and for different initiation conditions (voltage, bank capacity). One can see the output energy grows proportionally with initiation length, at least for lengths over the threshold one. It means, as a first approximation, the output energy doesn't depend on initiation energy and reduced electric field strength. These parameters can be more essential for iodine atom generation. The influence of initiation energy on laser output brings mainly via heat effects i.e. grows of a threshold yield and gain drop. The fact the dependence falls off linear for initiation length of 600 mm can be explained as a mutual influence of singlet oxygen relaxation, low specific initiation and, may be, discharge nonuniformity. (Note, the uncontrolled breakdown to the flange of the discharge cell can be the source of possible error for the 60 cm gap length.)

The temporary laser pulse behavior is governed by mainly the specific energy deposited into active medium. The comparison of results obtained for discharge length 20 cm and 60 cm shows the pulse durations of 38 μs and 44 μs are obtained for specific deposition energy of 8.6 J/l. Note, the values of reduced electric field strength differs about three times (521 Td and 178 Td, respectively).

Like that observed under initiation with transverse electric discharge, the pulse duration depends on deposition energy. At the case of investigated earlier transverse resistively stabilized discharge the energy stored in capacitor bank shared between resistors and plasma. Having no information on volt-ampere characteristic of discharge, it is impossible to determine the value of energy deposited into active medium. In longitudinal discharge practically all energy is deposited into active medium. This fact makes it possible to evaluate the energy cost of iodine atom produced by discharge. Thus for the pulse duration of 10 μs energy deposition is $8.6 \text{ J/l} = 53 \cdot 10^{18} \text{ eV/l}$ and iodine atom concentration determined through pulse duration is $1.3 \cdot 10^{18} \text{ l}^{-3}$. So the energy cost of iodine atom in experiment is about 41 eV/atom. Note, this value is one-fifth as large as that reported for transverse discharge initiation at the same pulse duration.

The same energy deposition into active medium with SF_6 resulted in pulse duration as short as 5 μs . This fact shows the influence of plasma parameters on process of iodine atom formation.

3.2. Pulsed COIL based on the Jet SOG

The motivations for investigation of the pulsed chemical oxygen-iodine laser based on the jet singlet oxygen generator are the promising results obtained in investigation of the features of pulsed COIL initiation with transverse discharge [1], as well as results of numerical analysis and experimental study of COIL with generation of singlet oxygen via photolytic ozone decomposition [6]. It was shown that pulsed COIL output energy increased linearly with the growth of the oxygen pressure.

The value of specific energy, that is energy obtained from the unit of the volume of the active medium, is a crucial factor, which governs the mass and dimension of laser. Thus the trend to increase the operation pressure is motivated. Recently, Japanese scientists attempted to get COIL operation using the porous high pressure SOG and method of volume generation of atomic iodine from CH_3I [7]. The experiments made at the pressure over 30 Torr results in 2.8 J/l of specific output energy and 2 ms of pulse duration. The results obtained are far from that one could expect. By the way, the similar result was obtained earlier when molecular iodine was used as iodine donor. It means, the authors failed to realize the method of volume iodine generation completely. The most possible reason why the low result was obtained, is a low efficiency of chlorine utilization and, hence, relatively high chlorine concentration. It was shown in works carried out earlier in LPI [8], the chlorine being mixed with singlet oxygen decompose molecules of alkyl iodide and release the free iodine atoms thus forming the active medium one has when singlet oxygen is mixed with I_2 . Note, the long pulse duration is evidence of more of cw operation than pulsed one.

The jet SOG is a source of high-pressure singlet oxygen too. The special preliminary experiments showed the operation conditions when chlorine utilization is rather high. So, one can expect the influence of release of free iodine atoms will be negligible.

When BHP jets are injected into low pressure medium of SOG the gas saturated liquid comes to the boil, thus producing the drops. The drops are carried out by gas flow from SOG to laser chamber thus resulting in experiment break-down. To avoid this effect the buffer gas is fed to the pressure of 10 Torr and then the chlorine flow is fed. The

oxygen pressure in the SOG is a sum of that for chlorine, nitrogen and iodide. At the same time, the oxygen partial pressure in the laser chamber is equal to total pressure divided by ratio of nitrogen flowrate to that of oxygen. As the flow velocity is subsonic the total pressure in the laser chamber is equal to that in the SOG.

Because of large idle volume of experimental set-up and low chlorine flowrate the transient period for gas flow is too long. One can assume this effect is responsible for degradation of laser pulse parameters during the run. The pulse amplitude decreases with time and, hence, with increase of oxygen pressure. Iodide methyl CH_3I was used as an iodine atom donor. As it was shown [9], this iodide provides the better energy parameters of laser. But its merit takes place when active medium is free of chlorine. The experiments show that in spite the SOG operates under conditions when the chlorine utilization is maximal, the concentration of residual chlorine is enough to cause the active medium to be unstable. It is a reason why we could not increase the CH_3I pressure and make a laser to work over the threshold.

The laser chamber used was previously designed to work in joint experiments with Samara branch of LPI and comparison of CW and pulsed modes of COIL operation. It governed the dimensions of laser chamber. But, as it follows from the analysis of the temperature working conditions of active medium in the case of discharge initiation, the chosen dimension of laser chamber is not enough to provide the laser operation over threshold. Indeed, the typical iodine atom concentration in supersonic cw COIL is about 10^{15} cm^{-3} . It follows from the experiments on the pulsed COIL initiated by the longitudinal electric discharge to create such a concentration needs to deposit into active medium energy of 10 J/l. The specific heat capacity of the mixture of oxygen and nitrogen under 15 Torr is $C_v = 16,8 \cdot 10^{-3} \text{ J/K}$. Thus the temperature increase is $\Delta T = 600 \text{ K}$. It means the temperature of active medium can achieve the value of 900K. Under such a temperature the small signal gain is $G_0 = 7,8 \cdot 10^{-4} \text{ cm}^{-1}$ at singlet oxygen yield $Y=50\%$. So the total gain at the double pass length $L=10 \text{ cm}$ is $G = 7,8 \cdot 10^{-3} = 0,78\%$.

The temperature of active medium in the case of supersonic cw COIL is but 150K. This value at the similar operation condition corresponds to the small signal gain of $G_0 = 5,4 \cdot 10^{-3} \text{ cm}^{-1}$ and total gain of $G = 5,4\%$. Thus, pulsed laser with discharge initiation has a gain one order of magnitude less. So, the laser operation needs application of mirrors with high reflection. Such mirrors, as a rule, have relatively high level of losses.

It is not correct to say about any energy parameter when the laser operates with a totally reflecting mirrors. Nevertheless, we succeeded to get the laser operation under oxygen pressure in laser cavity of 7 Torr, iodide pressure of 1.8 Torr and total pressure of 17 Torr. Note the pulse duration obtained was as short as 5 μs .

4. CONCLUSION

The experiments with pulsed COIL initiated with a longitudinal electric discharge showed the initiation length up to 60 cm is available in the active medium conditions close to that of cw laser.

It is shown the active medium temperature growth after discharge can be responsible for the specific output energy drop as compared to photolytic initiation.

The laser effect is obtained for the first time with the pulsed COIL based on the jet singlet oxygen generator. The laser operation is obtained under the total pressure of 17 Torr and oxygen partial pressure of 7 Torr. The laser operation under the high pressure makes it possible to reduce the pump rate and, thus, to minimize the weight and size of the laser.

ACKNOWLEDGEMENTS

This work was partially supported by EOARD through the ISTC contract #1864P

REFERENCES

1. P. Vagin and N.N. Yuryshv, *Quantum Electronics* **31**(2), pp.127-131, 2001
2. N.P. Vagin, V.S. Pazyuk and N.N. Yuryshv, *Quantum Electronics* **25**(8), pp. 746-748, 1995
3. D.A. Copeland, A.H. Bauer, *IEEE J. Quant. Electron.*, **29**, p. 2525, 1993
4. T. Marter, M.C. Heaven and D. Plummer, *Chem. Phys. Lett.*, **260**, p. 201 1996

5. D. M. King, D. L. Carroll, J. K. Laystrom, J. T. Verdeyen, M. S. Sexauer, W. C. Solomon. *Proc. Int. Conf. LASERS 2000*, Dec. 4-8, 2000, Albuquerque, NM, USA, Ed. by V.J. Corcoran & T.A. Corcoran, STS Press, McLEAN, VA, p.265, 2001
6. V.A. Zolotarev, P.G. Kryukov, et al. *Kratk. Soobshch. Fiz.* (3) p. 24, 1990
7. K. Suzuki, K. Minoshima, D. Sugimoto et al, *Proc. SPIE* vol. 4184, pp. 124-127, 2001
8. N.P. Vagin, P.G. Kryukov, V.S. Pazyuk and N.N. Yuryshev, *Sov. J. Quantum Electronics* **18**, pp. 1114-1117, 1988
9. N.P. Vagin., V.A. Zolotarev et al. *J.Sov.Las.Res.*, **13**, p. 60, 1992.

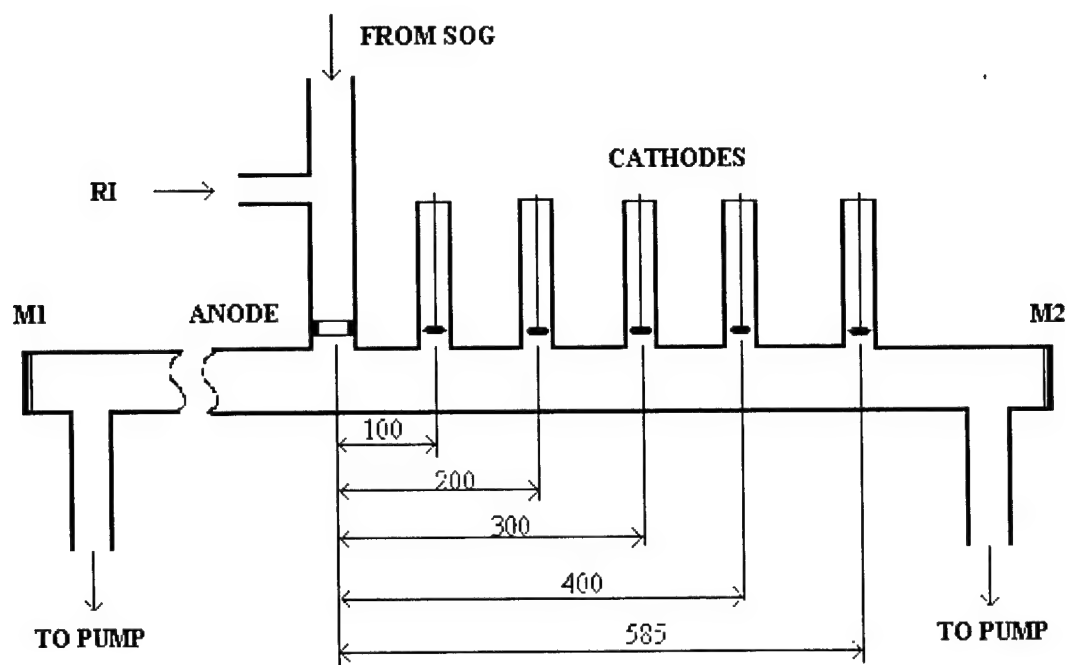


Fig.1. Schematic diagram of the discharge chamber used in investigation of a pulsed COIL initiated with a longitudinal glow discharge.

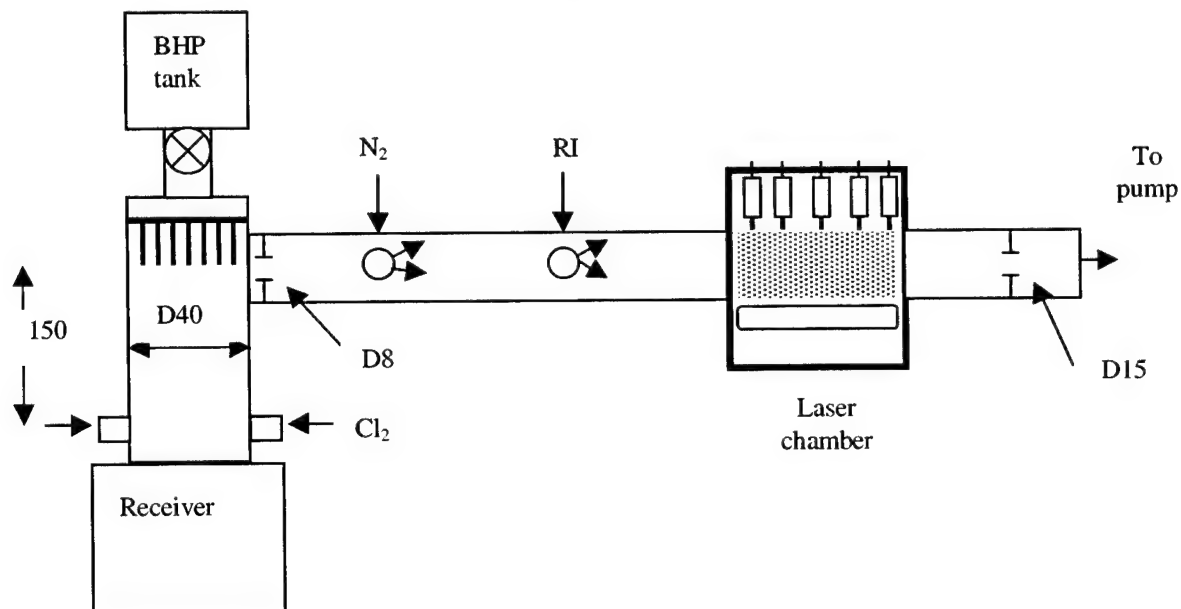


Fig.2. Schematic diagram of experiment with pulsed COIL based on a jet SOG

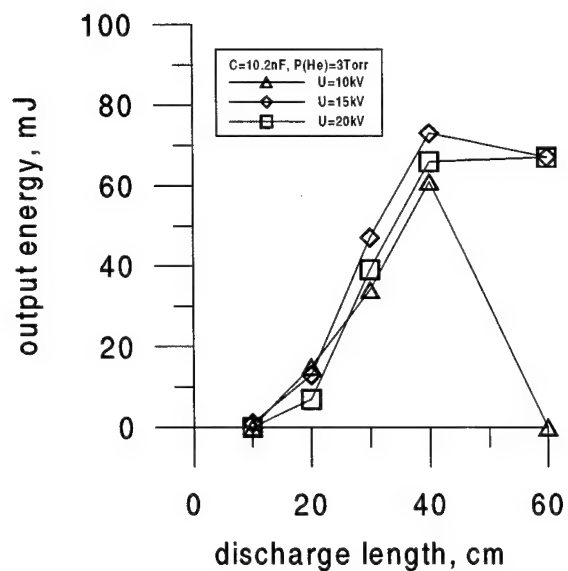


Fig.3.

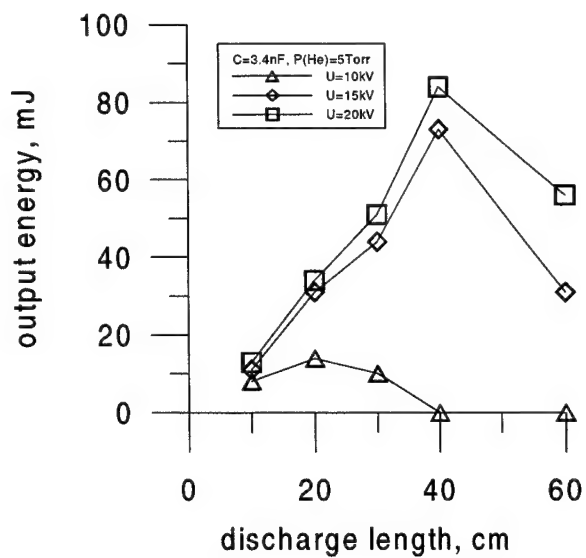


Fig.4.

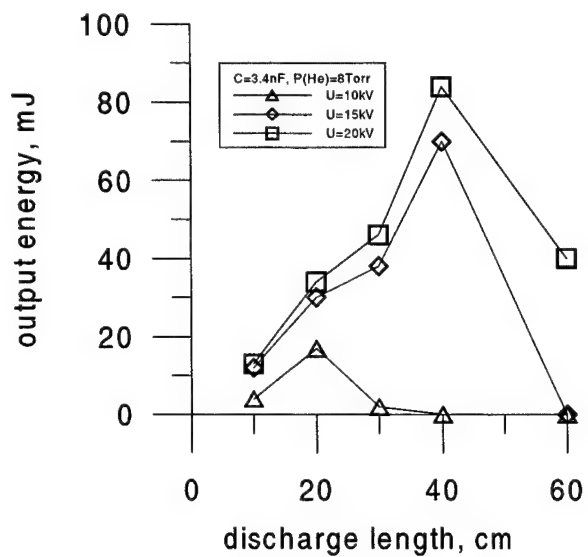


Fig.5.

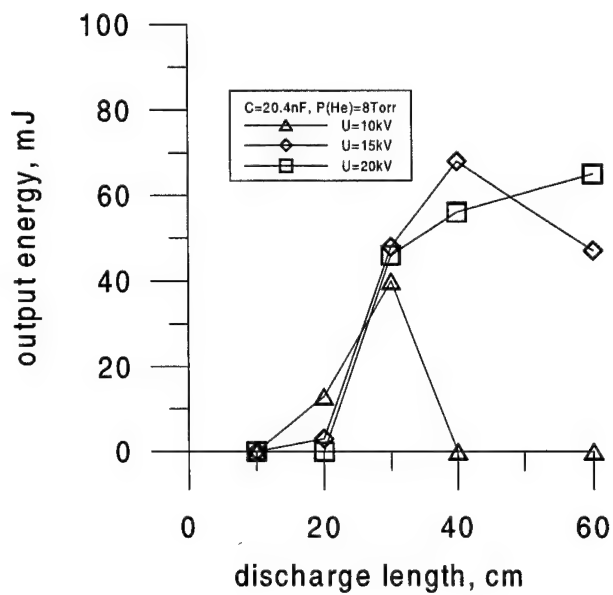


Fig.6.

Observation on laser induced lens effect in sound generation under water using high power ultrashort pulse laser

Huijuan He ^{*a}, Saosong Feng ^b, ^a Shanghai Institute of Optics and Fine Mechanics; ^b Shanghai Acoustics Lab

ABSTRACT

The ultrashort pulse of Nd:YAG laser system is used to generate the sound in water. The picosecond laser beams are focused at two points in experiments. This effect implies that the time response is inherent due to the changes of index of refraction of water induced by laser beam intensity.

Keywords: Ultrashort pulse, mode-locked laser, train pulse, single pulse, laser induced lens, index of refraction of water, shock wave, focusing spots, sound wave, bifocus effect

1. INTRODUCTION

Since Bell¹ discovered the photoacoustic effect in 1880, the generation of sound in water by photoacoustic effect has been proposed again hundred years later². Generation photoacoustic effect using laser beam with very high intensity is an attractive method. According to the energy emitted by the laser, three mechanisms fall under the generation of sound: (1) thermoacoustic, (2) evaporation and (3) optical breakdown. In this paper, the ultrashort pulse laser has been used to generate the sound under water. An effect of laser induced lens has been observed obviously. There are two focusing spots in water. One of them is the convex lens used for focusing laser beam to produce focusing spot. Other is laser energy induced lens, which produces induced focus spot. The time process occurs when the index of refraction of water is changed, the variety of index of refraction is induced by laser beam. This phenomenon can be used to estimate the response time of the changes of index of refraction of water.

2. EXPERIMENT RESEARCH

The ultrashort pulse laser is a Nd:YAG mode-locked laser³, which consists of oscillator and two stages amplifiers. Passive mode-locking dye cell for short pulse duration and active acousto-optics modulation for stabilization are combined in the oscillator. It is possible to generate extremely reproducible mode-locked pulses with Gaussian temporal and spatial profile. The transverse mode structure is TEM₀₀. Usually the output of ultrashort pulse is a train of 10 pulses as shown in Figure 1. A single pulse selector is used to select one pulse from the train for amplification. The train pulse and single pulse laser beam are used for research the photoacoustic effect respectively. The duration of single pulse is 40 picosecond. The envelope of train pulse is 100 nanosecond contains 10 pulses with pulse duration 40 picosecond. The separation between two pulses is 10 nanosecond. The power intensity of laser pulse is more than 10^{10} W/cm².

The set-up of the experiment is shown in Figure 2. The laser beam is splitting into two beams by an optical splitter. One of them is focused by a convex lens. The focusing spot is located under the water surface at 2cm. Other beam is going to photodiode for monitor the energy of laser beam. The sound induced by laser beam in water is detected by a Hydrophone (piezoelectric transducer). The frequency response is straight in the frequency band 1-10MHz and the sensitivity is about $0.5 \mu \text{ v/Pa}$.

When the laser beam is focused by the convex lens at 2cm under water surface, the hydrophone is located at the 4cm under the water surface and 1.5cm apart the laser beam. The waveform of the sound pulses have been detected by hydrophone. The results are shown in Figures 3-5 with pulse duration 40 picosecond. In figures 3 and 4 the waveform is induced by train pulse of laser. The waveform in figure 3 is the case of lower intensity $6 \times 10^{10} \text{ W/cm}^2$, the shock wave does not be excited on the water surface. In figure 4 the intensity of laser beam is stronger as $25 \times 10^{10} \text{ W/cm}^2$, in this case the shock wave is excited on water surface. The waveform induced by a single pulse is shown in Figure 5. For this case the laser beam intensity is $6.4 \times 10^{10} \text{ W/cm}^2$, similar to that for the case of figure 3, but the shocks excited on the water surface, likes that in figure 4. For the case of figure 3, the laser beam intensity for every pulse in train pulses is about ten times lower than the single pulse of laser beam in the case of figure 5. While for the case of figure 4, the laser beam intensity of some pulses in train pulse is alike that of single pulse in the case of figure 5. For the case of figure 3, the detected sound waves come from the focus spot 2cm below the water surface. For the case of figure 4 and 5, the detected sound waves come from two different points. One focus spot is located at 2cm below the water surface, and another is 3.3cm below the water surface. It is interesting to note that the sound waves generated from two focusing spots a and b in figures 4 and 5. The sound waves are reflected by water surface as a' and b' in figures 3-5.

3. ANALYSIS OF RESULTS

The phenomenon can be interpreted by nonlinear effect of high power laser beam in water. The induced lens is produced by changes of index of refraction of water. When the intensity of laser beam is low, the beam is focused at the focus spot of optical lens. While the intensity of laser beam is high, the index of refraction of water will be changed by nonlinear effect of high power beam in water. This nonlinear effect produces induced lens in water. Therefore when the intensity of laser beam is high enough to excite the effect of induced lens, the laser beam would not be focused at the focus spot of optical lens, but at the focus spot of induced lens. If the time-width of laser pulse is far longer than the response time, in which the change of index of refraction Δn of water is taken place, the laser beam would be focused at focus spot by induced lens. If these two times are comparable, but the time of the laser pulse is somewhat longer than the response time, then the head of the laser pulse would be focused at the focus spot of optical lens, because Δn could not be established. The tail of laser pulse would be focused at the focus spot of induced lens, because the Δn has been taken place. If the change of index of refraction of water Δn is negative, the focus spot of induced lens is behind the focus spot of optical lens. If the Δn is positive, the focus spot of induced lens is before that of optical lens. It means

that the self-induced focus would be caused. The change of index of refraction of water Δn is negative, therefore, when the intensity of ultrashort pulse from laser is high, the head of the laser pulse would be focused at the focus spot of optical lens, then the tail of laser pulse would be focused at the focus spot of induced lens. It means that the bifocus effect occurs.

The bifocus effect may be used to estimate the time response for the change of index of refraction of water Δn . The acoustical energy induced by the head of laser pulse focused at the focus spot of optical lens is proportional to the laser beam energy in the head part of laser pulse; while the acoustical energy induced by the tail part of the laser pulse focused at the focus spot of induced lens is proportional to the beam energy in the tail part of the laser pulse. The ratio of the acoustical energy which comes from the focus spot of optical lens and from the focus of induced lens respectively corresponds to the ratio of the beam energy in the head of laser pulse and in the tail of laser pulse, if the laser pulse is approximately rectangular pulse. So this ratio is equivalent to the ratio of duration occupied by the head and by the tail. Therefore, the time response for the change of index of refraction Δn can be estimated roughly using this ratio. The ratio is 0.15 / 0.85 given by our experiments. It implies that the first 15% of laser pulse is focused at the focus spot of optical lens, when the index of refraction of water has not been changed by the laser beam. So the response time for the change of index of refraction of water Δn equals to $40\text{ps} \times 0.15 = 6\text{ps}$. It is interesting to point out that the acoustical method to estimate the response time of Δn is simple.

4. Conclusions

The mechanism of the generation of sound in water by ultra-short laser pulse is mainly the optical breakdown. As the optical breakdown is caused in water by high power intensity ultrashort laser pulse, the bifocus effect is produced. For train pulse of laser beam, if the intensity is insufficient to excite the induced lens, the optical breakdown occurs at the focus spot of optical lens. For single pulse or train pulse of laser beam, if the intensity is sufficient to excite the induced lens, the optical breakdown mainly occurs at the focus spot of induced lens. This bifocus effect shows the time process in the change of index of refraction Δn in water. So the bifocus effect can be used to estimate the time response of Δn .

REFERENCES

1. A. G. Bell, Phil. Mag. Ser. 5, pp. 32-34, 1881.
2. P. J. Westervelt, R. S. Larson, J. Acoust. Soc. Am. **54**, pp. 121-123, 1973.
3. Huijuan He, Acta Optica Sinica, **12**, pp.1092-1096, 1986.

*hehuij@online.sh.cn; Phone 0086-21-59911863; fax 0086-21-59528812; Shanghai Institute of Optics and Fine Mechanics, Shanghai 201800, China.

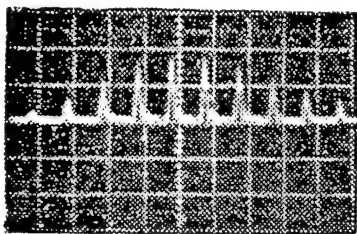


Fig. 1. Mode-locked train of pulse
Time scale: 10ns/cm

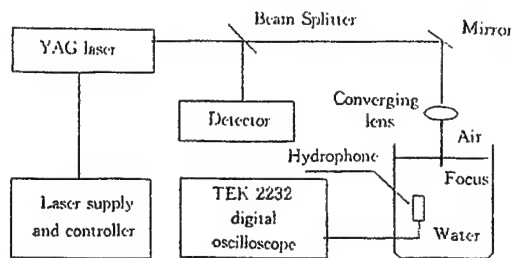


Fig. 2. Set-up of the experiment

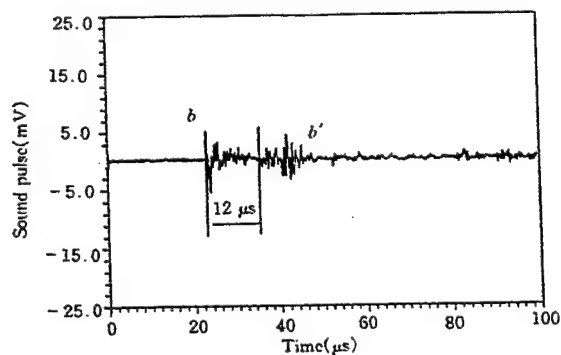


Fig. 3. Sound generated by train of pulse
with lower intensity

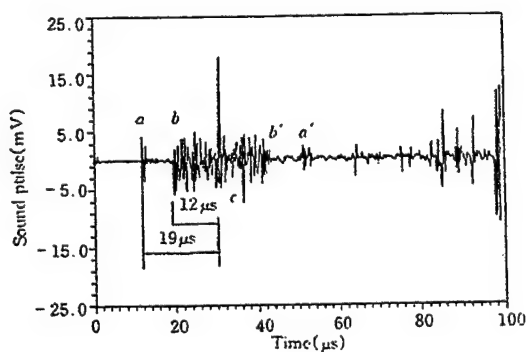


Fig. 4. Sound induced by train of pulse
with higher intensity

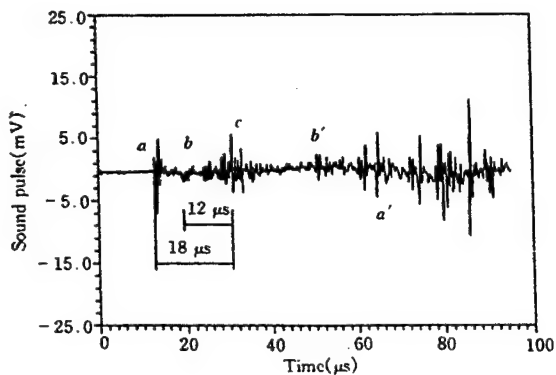


Fig. 5. Sound induced by a single pulse
with duration 40 ps

Plasma-Chemical Oxygen-Iodine Laser: Problems of Development

A.A.Ionin, A.P.Napartovich*, N.N.Yuryshev

P.N.Lebedev Physics Institute of Russian Academy of Sciences,
Leninsky pr. 53, 119991 Moscow, Russia; phone/fax: 7(095)132 0425,
e-mail: aion@mail1.lebedev.ru; yuryshev@mail1.lebedev.ru

* TRINITI, Troitsk, Moscow Region, phone:7(095)334 0450, e-mail: apn@triniti.ru

ABSTRACT

Great success has been obtained in the R&D of a chemical oxygen-iodine laser (COIL) operating on the electronic transition of the iodine atom, which gets an excitation from the energy donor -singlet delta oxygen (SDO). The latter is normally produced in a chemical SDO generator using very toxic and dangerous chemicals, which puts a limit for civilian applications of COIL that is still a very unique apparatus. Totally new non-chemical SDO generator is needed to allow oxygen-iodine laser to achieve its full potential as a non-hazardous efficient source of high-power laser radiation. There was interest in producing SDO in electric discharge plasma since the 50's long before COIL appearing. The idea of using SDO as a donor for iodine laser was formulated in the 70's. However, the injection of iodine molecules into a low- pressure self-sustained discharge did not result in iodine lasing. One of the main factors that could prevent from lasing in many experiments is a rather high threshold yield ~15% at 300K, which is needed for obtaining an inversion population. An analysis of different attempts of producing SDO in different kinds of electric discharge plasma has been done which demonstrates that high yield at gas pressure of practical interest ($p > 10$ Torr) for modern COIL technology can be obtained only in non-self sustained electric discharge plasma. The reason is that the value of relatively low reduced electrical field strength $E/N \sim 10^{-16}$ V.cm², which is an order of magnitude less than that for the self-sustained discharge, is extremely important for the efficient SDO production. Although different kinds of non-self sustained discharges can be used for SDO production, we got started experiments with e-beam sustained discharge in gas mixtures containing oxygen. High specific input energy up to ~3 - 5 kJ/l. atm [O₂] has been experimentally obtained. Theoretical calculations have been done for different experimental conditions indicating a feasibility of reasonable SDO yield. Experimental and theoretical research of self-sustained electric discharge in SDO produced in a chemical generator, which is very important for getting plasma-chemical kinetic data needed for an estimation of SDO yield, is also discussed.

Keywords: COIL, iodine laser, singlet delta oxygen, electric discharge plasma

1. INTRODUCTION

Great success has been obtained in the research and development (R&D) of a chemical oxygen-iodine laser (COIL) [1] over the last 20 years, the best progress being obtained in the development of COIL for military applications such as the high-power airborne laser [2]. The potential of civilian applications of a COIL was claimed [3] to be very high because of its high-power output and the opportunity of using low loss optical fibers for delivery of the laser radiation at the lasing wavelength $\lambda = 1.315 \mu\text{m}$. Despite successful experiments on applications of COIL for construction materials cutting [4; 5], rock drilling [6], etc., COIL is still a very unique apparatus. The active medium of COIL is atomic iodine emitting photons when changing its electronic state: $I^*(^2P_{1/2}) \rightarrow I(^2P_{3/2}) + h\nu$. Atomic iodine in the excited state $I^*(^2P_{1/2})$ is produced by energy transfer from the singlet delta oxygen (SDO) O₂(¹Δ) molecule: $O_2(^1\Delta) + I(^2P_{3/2}) \rightarrow O_2(^3\Sigma) + I(^2P_{1/2})$ (1). SDO is obtained in COIL in a chemical generator through the following chemical reaction running in liquid phase: $Cl_2 + 2 KOH + H_2O_2 \rightarrow O_2(^1\Delta) + 2 KCl + 2 H_2O$ (2). Very toxic and dangerous chemicals are used in the reaction, which put a limit for civilian applications of COIL. Thus, a totally new non-chemical SDO generator is needed to allow oxygen-iodine laser to achieve its full potential as a non-hazardous efficient source of high-power laser radiation. Quite a different method of SDO production can be used, namely, generation of SDO in electric discharge. The advantages of such a method of SDO production are the absence of dangerous chemicals, the feasibility of a development of a gas phase oxygen-iodine laser and other ones such as atomic iodine production through I₂ dissociation by O₂(¹Σ) [7]. The problems of SDO production in electric discharge and development of an oxygen-iodine laser using SDO produced in electric discharge plasma, i.e. plasma-chemical oxygen-iodine laser (PlasmaCOIL), are discussed in the paper.

2. SDO PRODUCTION IN ELECTRIC DISCHARGE

There was interest in producing SDO in electric discharge since the 50's long before the first laser was launched. "A fraction of $O_2(^1\Delta)$ between 5-25% of the total flow" was claimed to be observed in several papers [8] at gas pressure <1 Torr under RF or MW discharge excitation. For the first time the idea of using SDO as a donor for iodine laser was formulated in [9] a few years before the laser effect under chemical pumping, i.e. before COIL lasing was obtained. However, the injection of iodine molecules into a low-pressure self-sustained discharge ($O_2:I_2$; $p \leq 1$ Torr) did not result in iodine lasing. One of the main factors which could prevent from lasing in this and other experiments is a particular high threshold yield Y_{th} , which is needed for obtaining an inversion population $2[I(^2P_{1/2})] - [I(^2P_{3/2})] > 0$, $Y_{th} = [O_2(^1\Delta)] / \{[O_2(^1\Delta)] + [O_2(^3\Sigma)]\} > (1 + 2 K_{eq})^{-1}$, where $K_{eq} = [I(^2P_{1/2})][O_2(^3\Sigma)] / \{[O_2(^1\Delta)][I(^2P_{3/2})]\} = 0.75 \exp(\Delta E/T)$ is an equilibrium constant for the reaction (1); $\Delta E = 402$ K is the energy difference between $O_2(^1\Delta)$ and $I(^2P_{1/2})$ [10]. At $T = 300$ K, $K_{eq} = 2.84$ and $Y_{th} = 0.15$; at $T = 100$ K, $K_{eq} = 40$ and $Y_{th} = 0.012$. Another attempt of producing SDO by using non-self-sustained discharge [11] also failed, because the authors were unable to load any notable specific energy into the high pressure (1.18 bar) gas mixture of noble gas and electro-negative oxygen. DC self-sustained electric discharge was used for obtaining SDO in a set of papers (see [12,13], for instance), ~30% yield being claimed in the 80's [12] and ~10% at the end of the 90's [13]. No any attempt was made to get iodine lasing in these papers. There was quite recently demonstrated 21% yield under a MW discharge [14] and 32% yield under RF discharge excitation [15,16]. Iodine threshold lasing was claimed to be observed in the latter paper when mixing SDO with iodine, which looked more probably like iodine luminescence because there was no notable spectral line narrowing. However, the level of SDO partial pressure (< 1 Torr) in these [14-16] experiments seems to be of little any practical interest because the gas pressure should be ~10 Torr or higher for modern COIL technology. Moreover, for these experiments, estimation gives an energy efficiency for production of the SDO under conditions of maximum yield of about 2%. The reduced energy loading was about 50 J scm^{-3} (scm^{-3} means at unit gas volume at standard conditions, gas pressure 1 bar and temperature 300 K) that is 50 kJ/atm at the same temperature. This is an enormous amount of energy almost completely released into useless gas heating.

Thus, up to now, there has not been any answer to the question, is there the possibility for efficient electrical excitation of SDO with a yield and partial pressure reasonable for development of a Plasma- Chemical Oxygen-Iodine Laser (PlasmaCOIL).

3. NON-SELF SUSTAINED DISCHARGE AS A POTENTIAL PRODUCER OF SDO

Quite recently it was claimed [7,17] that the value of reduced electrical field strength E/N (where E is electrical field strength, N is gas density) is extremely important for efficient SDO excitation. The parameter E/N must be ~ 10^{-16} V cm^2 (~2.7 kV/cm atm), which is an order of magnitude less than that for the self-sustained discharge used in most of the previous experiments.

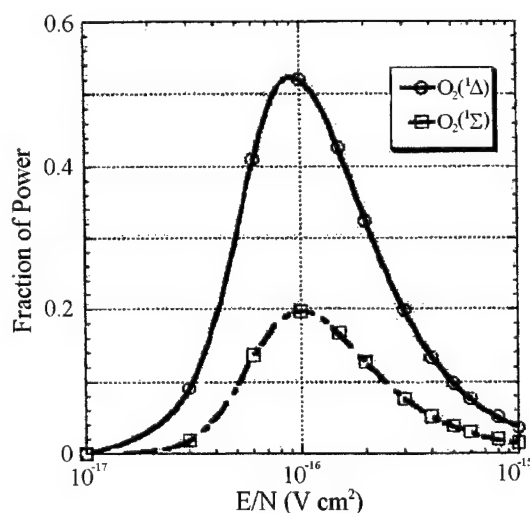


Fig.1. Fraction of power going into $O_2(^1\Delta)$ and $O_2(^1\Sigma)$ versus E/N [7]

This fact is illustrated by Fig.1 [7] that demonstrates a quasi-resonance dependence of fraction of electric discharge power going to production of SDO and $O_2(^1\Sigma)$. Therefore a non-self-sustained discharge that operates at low value of E/N parameter ~ 10^{-16} V cm^2 must be used for SDO production. A variety of non-self-sustained discharge can be used for such a purpose. A pulsed controlled avalanche discharge is used in Texas A&M University [17], SDO yield 16% being claimed to be obtained. A combined CW AC/RF discharge operating at low E/N parameter, in which RF electric field is applied to plasma generated by AC discharge, is used in the University of Illinois in Urbana-Champaign [7]. On the other hand, well-known e-beam sustained discharge (EBSD) lasers such as CO_2 , CO and N_2O lasers, some of which use electronegative gases as an active medium, do operate at the same parameter E/N [18]. A feasibility of using EBSD for SDO production was discussed in [19-21]. Having very rich experience in R&D of such lasers and in study of EBSD in electronegative gases, our research team consisting of experimentalists of Gas Lasers Lab and Chemical Lasers Lab of the Lebedev Institute and theoreticians of TRINITI has started its activity to study both

experimentally and theoretically the best way of producing SDO with a high yield and at oxygen pressure adequate for development of Plasma COIL and to attempt to get PlasmaCOIL lasing.

4. EXPERIMENTAL AND THEORETICAL STUDY OF SDO PROPERTIES AND SDO PRODUCTION IN ELECTRIC DISCHARGE

To properly evaluate the concept of SDO production in EBSD it is necessary to perform experiments in conjunction with theory and modeling of the complex plasma discharge. Therefore, there should be performed following tasks: study of influence of SDO on electric discharge to get important kinetic data and development of EBSD generated plasma for oxygen-iodine laser.

4.1. Effects of SDO on electric discharge properties

Information about processes involving SDO and other excited states of oxygen molecule is rather scarce. A simple idea exploited by us is to place the self-sustained discharge chamber at the exit of traditional chemical SDO generator, which allowed us to vary the concentration of the SDO within a very wide range and study the influence of it on the discharge characteristics (Fig.2).

EFFECTS OF $O_2(^1\Delta)$ ON ELECTRIC DISCHARGE PROPERTIES

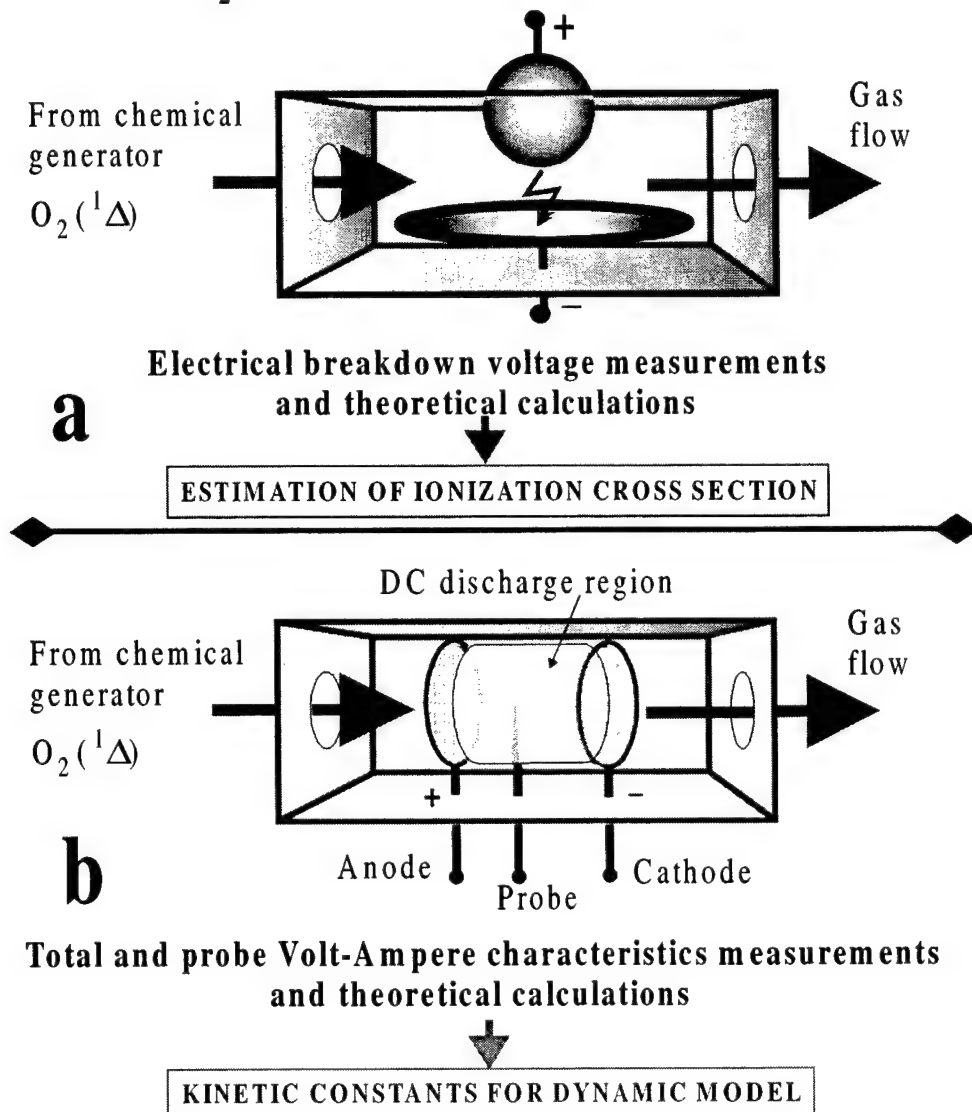


Fig.2. Experimental layout for electric discharge breakdown and volt-ampere characteristic measurements

4.1.1. Electric breakdown in SDO

Breakdown characteristics of a low-pressure self-sustained discharge in oxygen with 50% of SDO content were measured and compared with the breakdown characteristics of pure oxygen. The breakdown voltage as a function of the composition, temperature, and pressure of the gas mixture was measured in the discharge chamber connected to the gas duct downstream of SDO chemical generator. The electric field was directed perpendicularly to the gas flow (Fig.2a). The experimental results obtained were compared with the results of numerical modeling for adequate description of

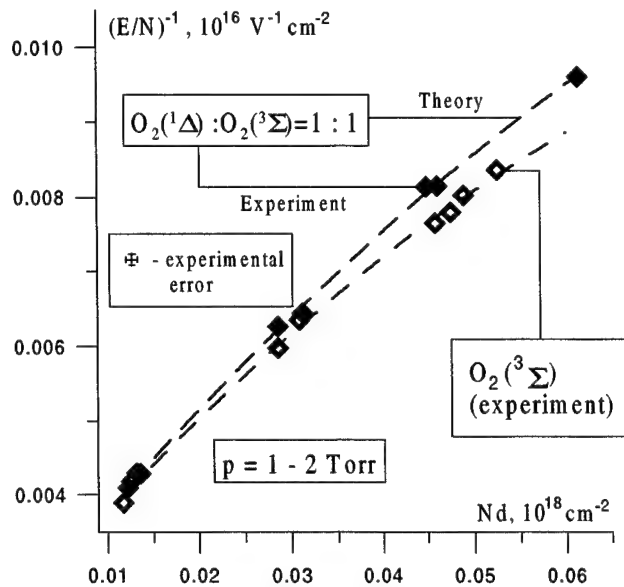


Fig.3. Inverse E/N versus Nd (N - density, d - electrode spacing) for electric discharge breakdown in oxygen and SDO (experiment and theory)

decreases when oxygen is excited on the singlet delta level. Good agreement between the experimental and theoretical data justifies the procedure of calculating σ_{ion}^{SDO} . A decrease in the breakdown voltage in the presence of $\text{O}_2(^1\Delta)$ is due to the increase in the ionization rate because of a lower ionization potential for the $\text{O}_2(^1\Delta)$ compared to $\text{O}_2(^3\Sigma)$.

4.1.2. Volt-ampere characteristics of electric discharge in SDO

The first results of experimental research of glow discharge in gas mixtures with high SDO content were obtained. Electric discharge chamber was incorporated into a gas duct going out of SDO chemical generator (Fig. 2b). An electric field being longitudinal relative to gas flow was produced with electrode system consisted of upstream anode and downstream cathode. The cathode was cooled by water. Electric potentials of plasma column in different points were measured with a metal needle probe. Experiments were carried out with pure oxygen going directly to the discharge chamber from a cylinder and gas mixture of oxygen containing 50% SDO going from SDO chemical generator through a water vapor trap to the discharge chamber. Probe and total volt-ampere characteristics of the electric discharge for pure oxygen and gas mixture $\text{O}_2 : \text{SDO} = 1:1$ at gas pressure of $\sim 1 \text{ Torr}$

glow discharge in oxygen. A comparison of breakdown electric field strengths for $\text{O}_2(^3\Sigma)$ and gas mixture $\text{O}_2(^3\Sigma) : \text{O}_2(^1\Delta) = 1:1$ was done (Fig.3). The ionization cross-section appears to be of the most importance for calculations of electric breakdown parameters. The direct data on the ionization cross-section for SDO are absent. However, the position of the molecular terms for $\text{O}_2(^1\Delta)$ and $\text{O}_2(^3\Sigma)$ allows us to say that a simple downward shift along the energy axis gives satisfactory ionization cross-section for SDO.

$$\sigma_{ion}^{SDO}(E) = \sigma_{ion}^{O_2 \text{ ground}}(E - \Delta E)$$

$$\Delta E = E_{SDO} - E_{O_2 \text{ ground}} = 0.98 \text{ eV}$$

As one can see from Fig.3 threshold breakdown voltage

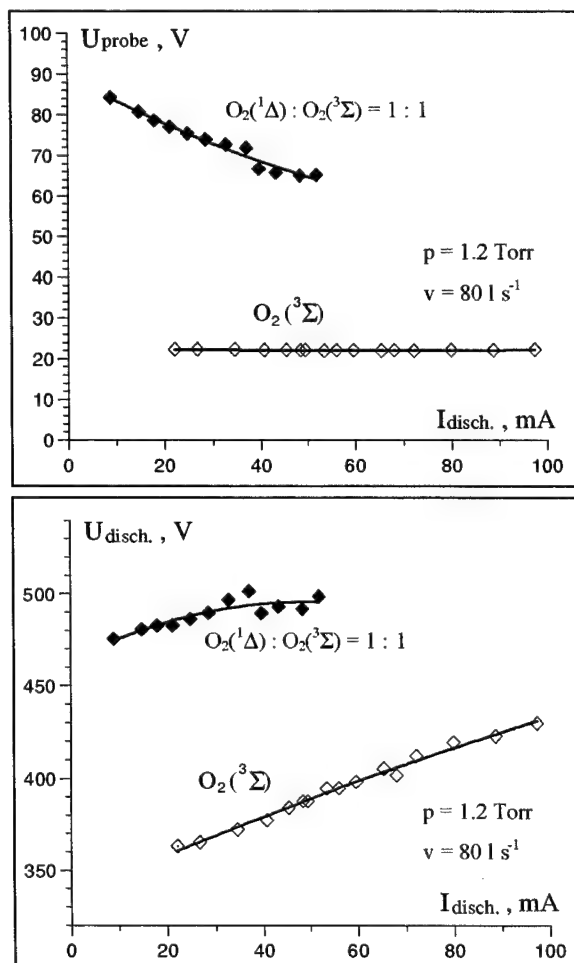


Fig.4. Volt-ampere probe and total characteristics of electric discharge in oxygen and SDO

are presented in Fig.4. As one can see in the figure, there is a big difference between the characteristics for pure oxygen and SDO, which indicates the fact that the two substances have different electrical features. It should be noted that the experimental results were obtained for relatively short electric discharge chamber, which did not permit to have a positive column of the electric discharge plasma. Although we did observe the big difference between the volt-ampere characteristics for pure oxygen and SDO, experiments should be done for longer discharge tube with a positive column, which makes it easy to calculate electric discharge characteristics. A simplified mathematical model for a description of a transitional space in electric discharge in oxygen was formulated. Diffusion coefficients, electron mobility and constants of ionization, attachment and detachment were calculated as a function of reduced electric field E/N . A comparison of the theoretical data with the experimental results is supposed to give new information about kinetic processes in electric discharge with SDO.

4.2. Electron beam sustained discharge in oxygen containing mixtures

ELECTRICALLY GENERATED PLASMA FOR PLASMACOIL

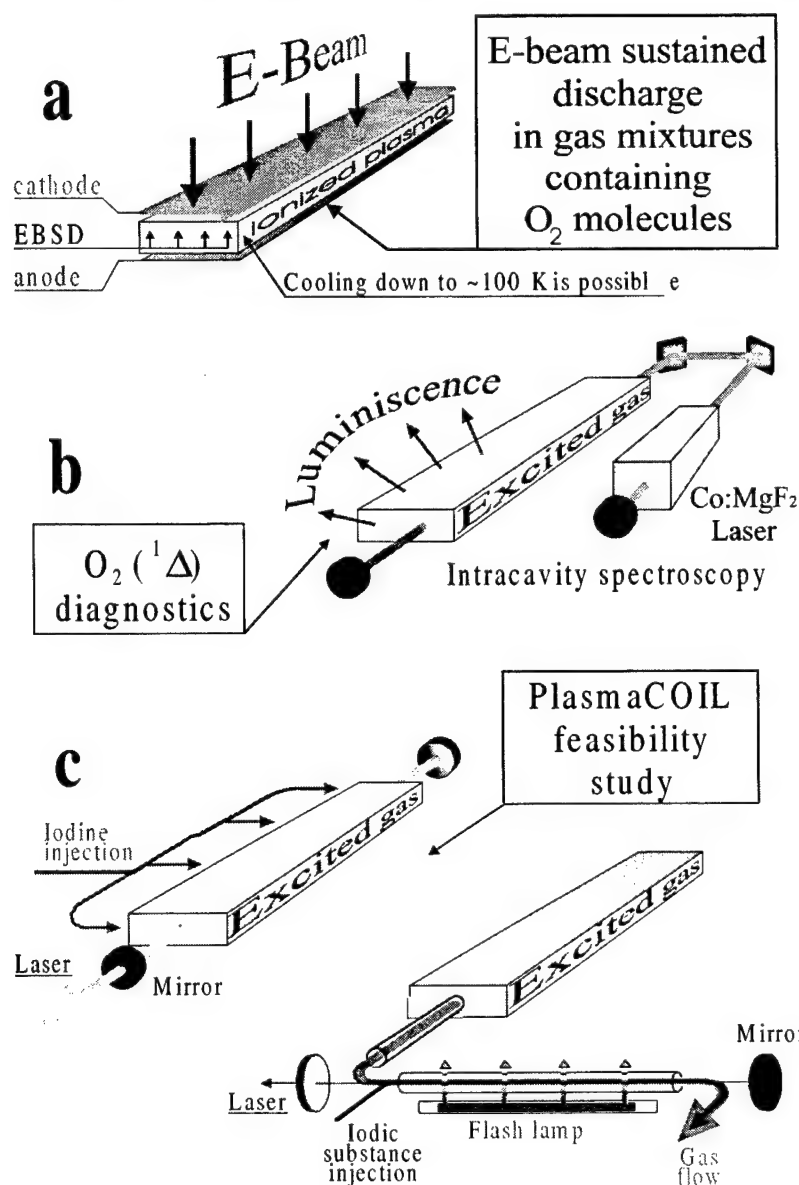


Fig.5. Schematic diagrams of EBSD application for SDO production and plasma-chemical oxygen-iodine lasing

One of the principal advantages of the EBSD approach (Fig.5a) is that it is possible to control E/N parameter within the E/N range most optimal for effective SDO production. However, there is an important question if it is possible at all to load much energy into electronegative oxygen in EBSD. Previously EBSD characteristics were studied both for electric discharge in pure oxygen [22] and its mixture with noble gases [11]. Taking into account a cathode voltage drop specific input energy into oxygen can be indirectly estimated as ~ 90 J/l atm [O_2] in [22] (active volume $V=60$ cm³) and ~ 150 J/l atm [O_2] in [11] ($V=150$ cm³; Ne: O_2 =96:4; $P=1.18$ bar). It should be pointed out that minimal specific energy formally needed for transformation of all oxygen (with efficiency of 100%) from its ground state $O_2(^3\Sigma)$ into SDO state with energy of 0.98 eV is 94 kJ/mole [O_2] \approx 4.2 kJ/l atm [O_2]. If one even assumes the efficiency of SDO production to be 100%, only 2-3% of oxygen is transformed into SDO in [11,22], which is an order of magnitude less than it is needed for oxygen-iodine laser. Quite recently we demonstrated experimentally [20,21] that far more specific energy up to ~ 3 -5 kJ/l atm [O_2] can be loaded into EBSD with active volume of ~ 15 l (Fig.6). A fraction of total power going to SDO production taken from Fig.1 is also presented in Fig.6, which allows

one to estimate specific input energy going to SDO production ~ 1 kJ/atm $[O_2]$ corresponding to SDO yield up to $\sim 25\%$. Of course, only experimental measurement of SDO concentration can give a final answer to the question if the EBSD is the best way of SDO production.

4.3. SDO diagnostics

The measurements of SDO concentration and gas temperature are the key elements of the measurement procedure.

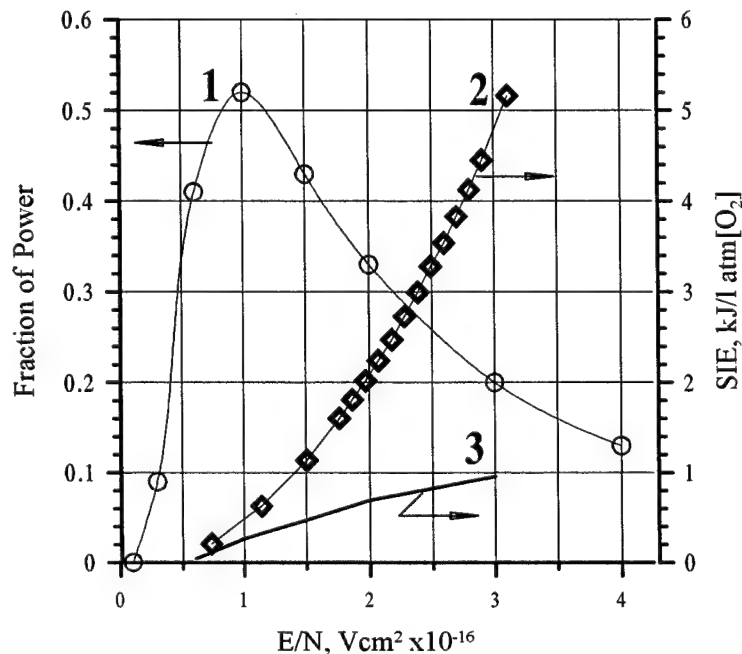


Fig.6. Fraction of power and specific energy going to oxygen and production of SDO. 1 - fraction of total power going to production of $O_2(^1\Delta)$ [7]; 2 - specific input energy (SIE) going to O_2 (experimental data); 3 - SIE going to production of $O_2(^1\Delta)$

Different methods to measure the SDO concentration exist [8]. They are mass spectrometry, electron paramagnetic resonance, isothermal calorimetry, photoionization, "chemical" methods and optical spectroscopy [8]. Each of these techniques has limitations. For the pulsed discharge facility, the optical methods seem to be more preferable. Being strongly forbidden the $O_2(^1\Delta) \rightarrow O_2(^3\Sigma)$ transition emits very weak radiation with the wavelength $1.27 \mu m$. So, the very sensitive intrinsic germanium detectors cooled with liquid nitrogen or photon counting apparatus are needed to detect $1.27 \mu m$ radiation. These methods are applicable for a continuous process, but its application can be problematic when a pulsed process is under investigation. One of the problems is electric discharge interference. Nevertheless, it may be possible to use a liquid nitrogen cooled germanium detector with high sensitivity for measuring SDO concentration. However, intracavity laser spectroscopy (ILS) appears to be a very useful technique for measuring SDO and other

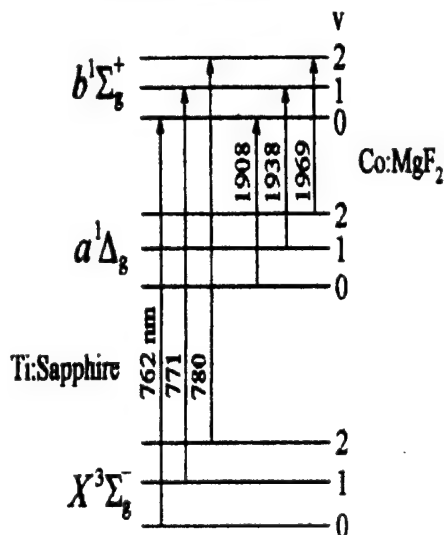


Fig.7. Schematic diagram of intracavity laser spectroscopy measurement of $O_2(^1\Delta)$ and $O_2(^1\Sigma)$ by Ti:Sapphire and Co:MgF₂ lasers [23,24].

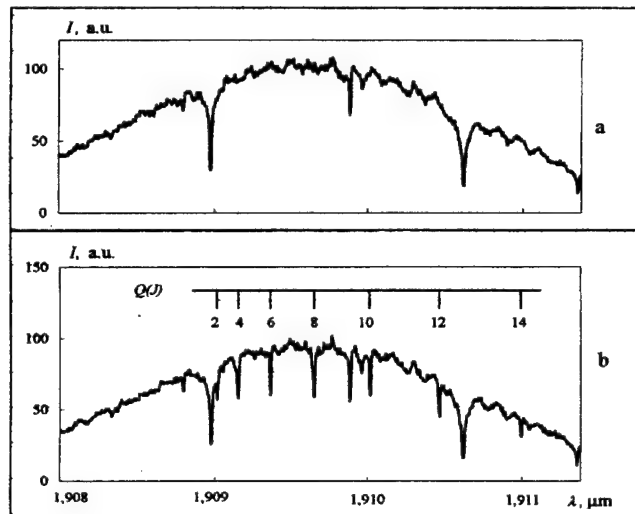


Fig.8. Output spectra of the broad band Co:MgF₂ laser (oxygen pressure in the laser cavity is 1.9 Torr): (a)- the discharge is turned off (absorption lines belong to water vapor); (b) - the discharge is turned on (additional absorption lines belong to the Q-branch of the 0-0 band of a $^1\Delta_g \rightarrow b^1\Sigma_g^+$ transition of molecular oxygen) [24].

species concentrations. The apparatus developed at the Lebedev Institute allows one to measure the concentration of the key components $O_2(^3\Sigma)$, $O_2(^1\Sigma)$, and $O_2(^1\Delta)$ [23,24] (Fig.5b). It was shown that ground state oxygen can be measured using a Ti: sapphire laser-based intracavity spectrometer operable near the 760 nm $O_2(^3\Sigma) \rightarrow O_2(^1\Sigma)$ absorption lines [23]. A sensitivity of $\sim(2-5) 10^{14} \text{ cm}^{-3}$ was obtained when a Co:MgF₂ laser (1.6-2.5 μm tuning range) was used in the ILS method for direct measurement of $O_2(^1\Delta)$ produced in MW discharge [24]. The concentration of $O_2(^1\Delta, v=0,1,2)$ can be determined via absorption measurements at 1.91 μm (0,0), 1.94 μm (1,1) and 1.97 μm (2,2 bands of $O_2(^1\Delta) \rightarrow O_2(^1\Sigma)$ system) (Fig.7). Many rotational lines are recorded simultaneously in the ILS method due to the broad-band laser spectrum (Fig.8). Consequently, the gas temperature can be measured using the dependence of the absorption coefficients of molecular lines on the rotational quantum number.

Another approach is to inject iodine atoms to SDO and then detect the iodine luminescence at the wavelength 1.315 μm . As soon as iodine is in equilibrium with singlet oxygen due to the fast energy exchange process $O_2(^1\Delta) + I(^2P_{3/2}) \rightleftharpoons I(^2P_{1/2}) + O_2(^3\Sigma)$ the intensity of iodine luminescence can serve as a criteria of SDO yield (titration techniques). A calibration of this method can be made using a traditional chemical SDO generator with a known value of yield. The Einstein coefficient for iodine transition $I(^2P_{1/2}) \rightarrow I(^2P_{3/2})$ is more than four orders of magnitude larger than that of the $O_2(^1\Delta) \rightarrow O_2(^3\Sigma)$ transition. Thus, even at lower iodine concentrations of about 1% of that of oxygen the luminescence intensity can be three orders of magnitude higher. To avoid the problems of dissociating iodine molecules we suggest to mix oxygen extracted from the discharge region with iodide CF₃I, CH₃I and then decompose iodide molecules by photolysis. Photolysis is preferable to a discharge because of its high selective interaction with the active medium. As a final step of the experiments, atomic iodine can be mixed with the SDO produced in a pulsed EBSD plasma and small-signal gain and/or lasing if any can be measured (Fig5c).

4.4. Theoretical calculations of EBSD generated plasma

Electron energy balance as a function of the reduced electric field strength E/N is illustrated in Fig.9. It was calculated from solving the steady-state electron Boltzmann equation with the set of cross sections. Calculations were made for pure oxygen, all molecules in ground state. One can see that the energy fraction going into direct excitation of $O_2(^1\Delta_g)$ is fairly high approaching maximum 0.43 at $E/N = 0.87 \cdot 10^{-16} \text{ V cm}^2$.

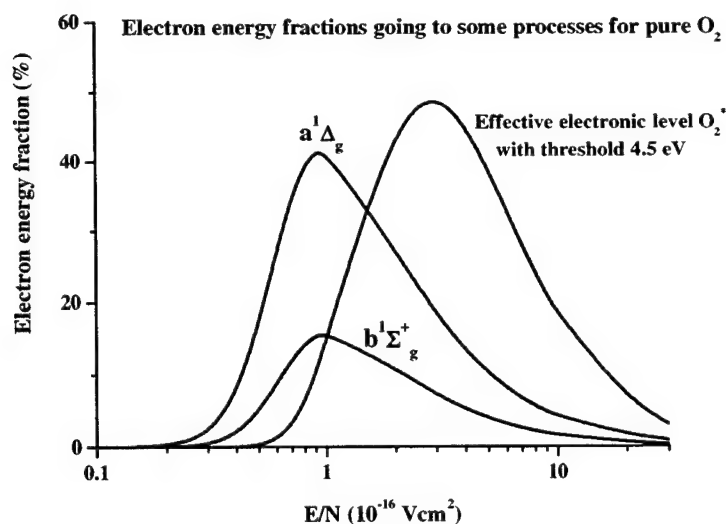


Fig.9. Electron energy fraction going to some processes for pure O_2

immediately draw two conclusions: it is necessary to cool the gas flow; it is necessary to take special measures for discharge stabilization. Let us note that these evaluations may over-estimate gas heating (we neglect the energy contained in atoms and other excited states). From the other side, the total efficiency of SDO production may be higher

For the plasma with external source of ionization (e-beam, ionizing high-voltage pulses, etc.) the value of E/N can be controlled independently of electric current. Then, assuming that optimum conditions for production of the SDO are realized in a discharge plasma, we can take as an upper limit for SDO production efficiency, for a final concentration of 30%, the value $\eta_{SDO}^{max} = 0.21$, which is roughly an average of initial and final (set equal to zero) efficiencies of direct excitation of $O_2(^1\Delta_g)$. The minimum energy loading for such an efficiency and SDO yield of 30% is easily evaluated: $\epsilon_{min} = 6.5 \text{ J/scm}^3$. Assuming that the fraction of energy $(1 - \eta_{SDO})$ is released into gas heating, the increment of gas temperature can be estimated as 5500 K.

The above estimations allow us to

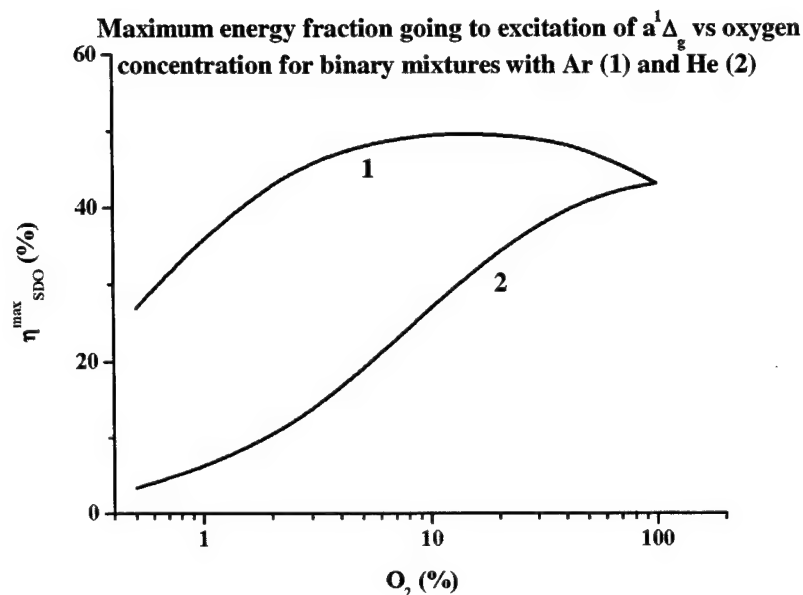


Fig.10. The maximum energy fraction going to excitation of SDO versus oxygen concentration for binary mixtures with Ar (1) and He (2)

denote the oxygen molecule number density) for which $\eta_{SDO}^{\max} = 0.497$. For comparison, in Fig.10 a similar dependence of the maximum energy fraction going to excitation of $O_2(^1\Delta_g)$ on oxygen percentage in the binary mixture $O_2:He$ is shown. For this mixture, η_{SDO}^{\max} is a monotonously growing function of oxygen content. Use of the gas mixture $O_2:Ar$ may be advantageous due to some increase in discharge efficiency and lowering of the gas temperature for the same energy load into singlet oxygen.

5. CONCLUSIONS

Breakdown and volt-ampere characteristics of self-sustained electric discharge in SDO studied both experimentally and theoretically indicate the fact that SDO and pure oxygen have different electric features. A comparison of the experimental and theoretical results justifies the procedure of calculating SDO ionization cross-section, the latter being that of ground state oxygen shifted 0.98 eV toward the lower energies. A difference between volt-ampere characteristics can give the opportunity of obtaining kinetic constants for SDO.

An analysis of different attempts of producing SDO in different kinds of electric discharge plasma has been done which demonstrates that high yield at gas pressure of practical interest ($p > 10$ Torr) for modern COIL technology can be obtained only in non-self sustained electric discharge plasma. The reason is that the value of relatively low reduced electrical field strength $E/N \sim 10^{-16}$ V.cm², which is an order of magnitude less than that for the self-sustained discharge, is extremely important for the efficient SDO production.

High specific energy up to 3- 5 kJ /l atm[O₂] has been demonstrated to be loaded into a pulse non-self-sustained (e-beam sustained) discharge in oxygen containing mixtures, which together with theoretical calculations brings a hope of obtaining SDO yield in EBSD up to 20-30% with a high efficiency.

In case of positive results on mixing iodine with products of e-beam sustained discharge containing SDO, i.e. iodine lasing, well developed technology of EBSD CO₂ and CO lasers can be used in future for designing SDO generators for PlasmaCOIL. The latter laser technology being cryogenic can diminish demand in high SDO yield.

than it was assumed (cascade excitation processes were neglected in making the estimations). Therefore, more detailed simulations may give more optimistic predictions.

Using mixtures of oxygen with some gases results in a variation of the electron energy balance. Generally, one may expect a decrease of the electron energy fraction going into direct excitation of $O_2(^1\Delta_g)$ when molecular or atomic additives appear. Let us note an interesting effect observed in gas mixture $O_2:Ar$. The results of Boltzmann calculations of η_{SDO}^{\max} for this mixture in dependence on oxygen content are shown in Fig. 10. It is seen that an optimum mixture composition exists ($[O_2] = 0.1 N$, where N is the total gas density and the brackets

ACKNOWLEDGMENTS

The authors are very grateful to G.Hager, W.Solomon,D.Carroll and.A.Hill for helpful discussions and to.A.Kotkov, I.Kochetov, N.Vagin,D.Sinitzyn,L.Seleznev, A.Deryugin and.Yu.Klimachev for their experimental and theoretical efforts on study of EBSD in oxygen containing mixtures and electric discharge in SDO.

The research has been supported by the Russian Foundation of Basic Research (grant 02-02-17452), the Russian Federal Program "Integration" (Project AO 155) , EOARD and AFRL.

REFERENCES

- 1.McDermott, W.E., Pchelkin, N.R. et al. (1978). *Appl. Phys. Lett.*, **32**, 469
- 2.Lambertson, S. (2001) *Proc. SPIE* ,**4184** ,1
- 3.Hallada, M., Seiffert, S., Walter, R., Vetrovec, J. (2000). *Laser Focus World*, **5**, 205
- 4.Kar, A., Scott, J.E., Latham, W.P. (1996). *J. Laser Applications*, **8**, 125-133
- 5.Carroll, D. and Rothenflue, J. (1997). *J. of Laser Applications*, **9**, 3, 119.
- 6.Graves, R., et al. (2000). *Int. Conf. LASERS '2000*, Albuquerque, NM, USA, Technical Digest, p.13
- 7.King, D., Carroll, D., Laystrom, J., Verdeyen, J., Sexauer, M. and Solomon, W. (2001). *Proc. Int. Conf. LASERS '2000*, Ed. by V. Corcoran and T. Corcoran ,STS Press, McLean ,VA, p.265
- 8.Wayne,R.P., (1969) "Singlet Molecular Oxygen" in "Advances in Photochemistry", **7**, p.311
- 9.Zalessky V., (1974) *J. Experimental and theoretical physics*, **67**, 30 (in Russian)
- 10.Yuryshchev, N.N. (1996). *Quantum Electronics*, **26** (7), 567
- 11.Fournier, G., Bonnet, J., Pigashe, D. (1980). *Journal de Physique*, Colloque C9, **41**, 449
- 12.Vasil'eva A., Grishina,I., Klopovsky K., Rakhimov A. et al, (1989) *Physics of plasma*,**15**, 190 (in Russian)
13. Ivanov, V, Klopovsky, K., Rakhimov ,A. et al, (1999) *IEEE Transactions on plasma science*, **27**, 1279
14. Itami, S., Nakamura, Y., Shinagawa, K., Okamura, M., Fujii, H. et al (1999). *Proc. SPIE*, **3889**, 503.
- 15.Fujii, H., Itami, S., Schmiedberger, J., et al (2000)., *Proc. SPIE*, **4065**, 818.
- 16.Schmiedberger, J., Hirahara, S , Fujii, H. et al (2000). *Proc. SPIE* ,**4184**, 32
- 17.Hill, A.,(2001), *Proc.Int.Conf. LASERS '2000*, Ed. by V.Corcoran and T.Corcoran ,STS Press, McLean ,VA, p.249
- 18.Basov, N., Ionin, A., Suchkov, A. (1990). *Proc. SPIE*, **1225**, 389
- 19.Napartovich, A. ,Deryugin, A., Kochetov,I.,(2001) *J.Phys.D:Appl.Phys*, **34**, 1827
- 20.Ionin, A. ,(2001) *Int. COIL R&D Workshop*, Prague, Czech. Rep., 28-29 May 2001, CD-ROM
- 21.Ionin A., Napartovich, A, Yuryshchev, N.(2001), *Int. Workshop on High Energy Lasers Including Novel Pumping Schemes driven by Chemical Reactions or Explosives*, French-German Res. Inst Saint-Louis, France, Nov 13-14, 2001
- 22.Londer, Ya., Menakhin, L., Ul'yanov,K.,(1981), *Thermophysics of high temperatures*, **4**, 720 (in Russian)
- 23.Podmar'kov, Yu., Frolov M., (1996), *Quantum Electronics*,**26**,595
- 24.Pazyuk, V.S., Podmar'kov, Yu.P., Raspopov, N.A., Frolov, M.P. (2001)., *Quantum Electronics*,**31**,363

Addendum

The following papers were announced for publication in these proceedings but have been withdrawn or are unavailable.

- [4631-13] **Comparing the efficiency of supersonic oxygen-iodine laser with different mixing designs**
B. A. Vyskubenko, A. A. Adamenkov, V. V. Bakshin, V. I. Efremov, S. P. Ilyin, Y. V. Kolobyenin, I. M. Krukovsky, E. A. Kudryashov, V. B. Moiseyev, Russian Federal Nuclear Ctr.
- [4631-18] **Modeling of DF chemical laser flowfields with HYLTE nozzle array**
S. Yuan, Z. Jiang, W. Hua, Y. Zhao, National Univ. of Defense Technology (China)
- [4631-26] **Application of vortex-flow dc glow discharge for atomic iodine production**
P. A. Mikheyev, A. A. Shepelenko, P.N. Lebedev Physical Institute (Russia)
- [4631-34] **Discharge in InI vapor as a lasing medium for indium 451.1-nm laser**
Y. O. Shpenik, V. A. Kelman, Y. V. Zhmenyak, Institute of Electron Physics (Ukraine)
- [4631-35] **TEA-N₂ and TEA-Xe lasers with increased average radiation power**
B. A. Kozlov, R. I. Ashurkov, A. V. Belikov, O. N. Gulaeva, V. K. Darymov, S. V. Gidkov, A. V. Folomkin, D. V. Kizlitsin, Radio-Engineering Academy (Russia)
- [4631-36] **Programmable power supply for multikilowatt CO₂ laser**
R. Thekkeppat, Ctr. for Advanced Technology (India); P. Choudhary, Science Research Lab., Inc. (USA); M. O. Ittoop, A. K. Nath, Ctr. for Advanced Technology (India)
- [4631-37] **Resource characteristics of small-sized sealed-off TEA-CO₂ lasers with pulse repetition rate of 25 Hz**
B. A. Kozlov, P. A. Anisiforov, O. Y. Boiko, N. I. Egoshkin, A. S. Fomin, O. N. Shamshina, P. V. Trubitsin, Radio-Engineering Academy (Russia)
- [4631-39] **Experimental study and optimization of the iodine gas and singlet oxygen mixing in a supersonic oxygen-iodine laser**
Y. V. Kolobyenin, A. A. Adamenkov, V. V. Bakshin, V. V. Buzoverya, L. A. Vdovkin, B. A. Vyskubenko, Y. N. Deryugin, V. I. Efremov, S. P. Ilyin, V. V. Kalinovskiy, V. V. Konovalov, E. A. Kudryashov, I. M. Krukovsky, V. B. Moiseyev, Russian Federal Nuclear Ctr.
- [4631-40] **Numerical simulation of supersonic oxygen-iodine laser**
B. A. Vyskubenko, Y. N. Deryugin, D. A. Zelensky, S. P. Ilyin, Y. V. Kolobyenin, E. A. Kudryashov, Russian Federal Nuclear Ctr.

- [4631-42] **Visible and near-IR luminescence of microwave discharge products in oxygen and nitrogen mix**
Y. V. Savin, L. V. Goryachev, A. A. Adamenkov, V. V. Bakshin, V. V. Buzoverya, B. A. Vyskubenko, V. V. Egorov, S. P. Ilyin, Y. V. Kolobyatin, E. A. Kudryashov, Russian Federal Nuclear Ctr.
- [4631-44] **Novel wavelength tunable mode-locked fiber ring laser using a FP LD as a modulator and a comb filter**
C. Zhao, N. Ma, S. Yuan, W. Gao, Z. Li, S. Yang, X. Dong, Nankai Univ. (China)
- [4631-45] **Development of time-of-flight x-ray photoelectron spectrometer**
T. Harada, T. Iwamoto, Y. Morihisa, Y. Nagumo, S. Fujita, S. Hayashi, Shimadzu Corp. (Japan)
- [4631-47] **Physics of overtone CO₂ laser operating on highly excited vibrational transitions**
A. A. Ionin, P.N. Lebedev Physical Institute (Russia); A. P. Napartovich, Troitsk Institute for Innovation and Fusion Research (Russia)
- [4631-48] **Energy transfer and reaction kinetics of the NCE(a)-driven iodine laser**
M. C. Heaven, Emory Univ. (USA)

Author Index

- Adamenkov, Anatoliy A., Addendum
 Ahmad, Imtiaz, 264
 Alekseev, Sergey B., 234
 Anisiforov, Pavel A., Addendum
 Arenberg, Jonathan W., 209
 Ashurkov, Roman I., Addendum
 Bakshin, Victor V., Addendum
 Barmashenko, Boris D., 23, 74
 Belikov, Andrei V., Addendum
 Benard, David J., xi
 Black, Ian, 254
 Bohn, Willy L., 53
 Boiko, Olga Y., Addendum
 Bousek, Ronald R., xi
 Bruins, Esther, 23, 74
 Buzoverya, V. V., Addendum
 Carrig, Timothy J., 209
 Carroll, David L., 154
 Čenský, Miroslav, 34, 43
 Chen, Fang, 161
 Choudhary, Praveen, Addendum
 Cox, Joseph L., 244
 Crowell, Peter G., 167
 Darymov, Vladislav K., Addendum
 Davis, Steven J., 60, 178, 217
 Deryugin, Yuri N., Addendum
 Dolezal, Michael W., 244
 Dong, Xiaoyi, Addendum
 Duo, Liping, 161, 184
 Efremov, Valentin I., Addendum
 Egorov, Vladimir V., Addendum
 Egoshkin, Nikolay I., Addendum
 Endo, Masamori, 116
 Fang, Benjie, 161
 Fedenev, Andrey V., 234
 Feng, Saosong, 280
 Flohrer, Frank, 264
 Folomkin, Alexander V., Addendum
 Fomin, Alexander S., Addendum
 Franklin, Robert E., 244
 Fujioka, Tomoo, 116
 Fujita, Shin, Addendum
 Furman, Dov, 23, 74
 Gäbel, Kai, 264
 Gao, Weiqing, Addendum
 Gelb, Alan H., 178
 Gidkov, Sergey V., Addendum
 Goncharenko, Igor M., 234
 Goncharov, Vasily, 13
 Goryachev, L. V., Addendum
 Götze, S., 264
 Gross, Markus S., 254
 Gulaeva, Olga N., Addendum
 Hager, Gordon D., 167, 192
 Han, Jiande, 225
 Harada, Takahiro, Addendum
 Hayakawa, Akiyoshi, 128
 Hayashi, Shigeki, Addendum
 He, Huijuan, 280
 Heaven, Michael C., Addendum, 13, 225
 Hua, Weihong, Addendum
 Hurlock, Stephen, 101
 Ilyin, Sergei P., Addendum
 Ionin, Andrei A., Addendum, 284
 Ittoop, Melappuram O., Addendum
 Iwamoto, Takashi, Addendum
 Jakubec, Ivo, 34
 Jiang, Zhongfu, Addendum
 Jirásek, Vít, 34, 43
 Kalinovsky, V. V., Addendum
 Katz, Arje, 23
 Keene, Jennifer A., 209
 Kelman, Vladimir A., Addendum
 King, Darren M., 154
 Kizlitsin, Dmitry V., Addendum
 Kleinschmidt, Jürgen, 264
 Klöpfel, Diethard, 264
 Kodymová, Jarmila, 34, 43, 86
 Köhler, Peter, 264
 Kolobyatin, Yuriy V., Addendum
 Komissarov, Anatoly V., 13
 Konoshenko, Aleksei F., 271
 Kononov, V. V., Addendum
 Korobotchko, Vladimir, 264
 Koval, Nikolai N., 234
 Kozlov, Boris A., Addendum
 Krukovsky, Ivan M., Addendum
 Kudryashov, Evgeniy A., Addendum
 Li, Jian, 184
 Li, Zhaohui, Addendum
 Ma, Ning, Addendum
 Manke, Gerald C., II, 167, 192, 225
 McDermott, William E., xi, 1
 Mikheyev, Pavel A., Addendum
 Min, Xiangde, 184
 Moiseyev, V. B., Addendum
 Morihisa, Yuji, Addendum
 Mulhall, Phillip A., 217
 Müller, Wolfgang H., 254
 Nagumo, Yuzo, Addendum
 Nakabayashi, Tokuhiko, 128
 Nanri, Kenzo, 116
 Napartovich, Anatoly P., Addendum, 284
 Nath, Ashish K., Addendum
 Oakes, David B., 178, 217
 Oien, AnnMarie L., 209
 Orlovskii, Victor M., 234
 Oskomov, Konstantin V., 234
 Paziuk, Vladimir S., 271
 Pchelkin, Nicholas R., xi

Perram, Glen P., 145, 244
 Phillips, Grady T., 145
 Rawlins, W. Terry, 217
 Read, Michael J., 178
 Ringling, Jens, 264
 Roh, Won B., 145
 Rosenwaks, Salman, 23, 74
 Rybalkin, Victor, 23, 74
 Sang, Fengting, 161, 184
 Savin, Yuri V., Addendum
 Schriever, Guido, 264
 Shamshina, Olga N., Addendum
 Shepelenko, Alexander A., Addendum
 Shpenik, Yuriy O., Addendum
 Shulepov, Mikhail A., 234
 Sochugov, Nikolay S., 234
 Solomon, Wayne C., 154
 Špalek, Otomar, 34, 43, 86
 Stamm, Uwe, 264
 Suzuki, Sachio, 128
 Takada, Tomohito, 137
 Takeda, Shuzaburo, 116
 Tang, Shukai, 184
 Tarasenko, Victor F., 234
 Thekkeppat, Reghu, Addendum
 Trubitsin, Pavel V., Addendum
 Truman, C. Randall, 167
 Uchiyama, Taro, 116
 Urbina, Chris J., 209
 Vagin, Nikolai P., 271
 Vdovkin, L. A., Addendum
 Verdeyen, Joseph T., 154
 Vyskubenko, Boris A., Addendum
 Wagner, Gregory J., 209
 Wani, Fumio, 128, 137
 Wisniewski, Charles F., 167
 Yang, Bailing, 184
 Yang, Shiquan, Addendum
 Yasuda, Kozo, 128, 137
 Yuan, Shengfu, Addendum
 Yuan, Shuzhong, Addendum
 Yuryshchev, Nikolai N., 271, 284
 Zelensky, D. A., Addendum
 Zhang, Yuelong, 161
 Zhao, Chunliu, Addendum
 Zhao, Weili, 161
 Zhao, Yijun, Addendum
 Zhmenyak, Yuriy V., Addendum